Pradeep L. Menezes
Pradeep K. Rohatgi
Emad Omrani *Editors*

Self-Lubricating Composites

MATERIALS.SPRINGER.COM

Springer

Self-Lubricating Composites

Pradeep L. Menezes • Pradeep K. Rohatgi
Emad Omrani
Editors

Self-Lubricating Composites

With 170 Figures and 17 Tables

Springer

Editors
Pradeep L. Menezes
Department of Mechanical Engineering
University of Nevada Reno
Reno, Nevada, USA

Pradeep K. Rohatgi
Department of Materials Science and Engineering
University of Wisconsin-Milwaukee
Milwaukee, WI, USA

Emad Omrani
Department of Materials Science and Engineering
University of Wisconsin-Milwaukee
Milwaukee, WI, USA

ISBN 978-3-662-56527-8 ISBN 978-3-662-56528-5 (eBook)
https://doi.org/10.1007/978-3-662-56528-5

Library of Congress Control Number: 2018937891

Printed on acid-free paper

This Springer imprint is published by Springer Nature, under the registered company Springer-Verlag GmbH, DE
The registered company address is: Heidelberger Platz 3, 14197 Berlin, Germany

Preface

Solid lubricant materials have become the necessity for present engineering innovation in the field of aerospace, automobile, bioimplants, etc. Solid lubricating materials have been replacing the liquid lubricants due to their superior stability at extreme conditions such as high temperature and high pressure. Understanding of lubrication mechanism for various solid lubricant materials has been the key factor for their reliable application. This book emphasizes on various solid lubricant materials, their application in the form of a coating, self-lubricating composites, and as an additive in the oil.

► Chapter 1 details the fundamentals of solid surfaces, contact mechanism, and fundamental of solid lubricants. The application and mechanism of solid lubricant as the coating material is emphasized to control the tribological properties. Further, various solid lubricant materials are discussed as the chemistry of solid lubricants play an important role in the formation of a lubricating film (tribo-film) during sliding. Along with coating, various other applications of solid lubricant materials are highlighted.

► Chapter 2 presents the application of solid lubricant materials in metal matrix composites that includes material selection, processing techniques, and tribological performance. The tribological performance is explained through the third body approach as well as the parent materials where the mechanical, structural, and chemical interactions between the matrix and reinforcement play a key role. Based on the current status of metal matrix composites, this chapter also emphasizes the development of new materials and new processing techniques for further improving the tribological properties.

► Chapter 3 describes various self-lubricating polymer matrix composites for both types of the polymers, such as thermoplastics and thermosets. Polymer matrix has been used with multiphase reinforcement materials, such as fibers and textiles for strength, and solid lubricant materials for lubricating properties. A detailed description of lubrication mechanism and various factors affecting polymer composites is presented followed by nanostructured self-lubricating polymer composites in ► Chap. 4. The current state of the art is presented on lubricant nanomaterials that give a deep insight to readers about the interaction between filler and matrix materials, modern technologies, and hybrid nanostructures to achieve high-demanding tribological applications.

► Chapter 5 addresses the self-lubricating ceramic matrix composites that signify the applicability of ceramic composites at extreme environmental condition due to their high-temperature resistance and chemical inertness. This chapter presents the processing and mechanism for two new types of self-lubricating ceramic composites which are functionally graded materials and core-shell structured composite powders in ceramic matrix. The mechanical and tribological properties of these new composites are also compared with traditional self-lubricating composites.

► Chapter 6 deals with the polymeric solid lubricant transfer film. The transfer film is essential for lower friction and wear rates, and measurement of these transfer film has been the critical part to control tribological performance. In this chapter, recent advances in characterization of polymeric transfer film are focused that includes topographical, adhesive, mechanical, and chemical properties.

Graphite is one of the promising reinforcement for self-lubricating composites, and the formation of in-situ 2D graphite in composites is the latest development in the field of self-lubricating composites. A detailed processing, characterization, and characterization of in-situ generated turbostratic 2D graphite are described in ► Chap. 7. The superior lubrication performance of in-situ 2D graphite is also compared with other forms of graphite.

In the field of tribology, surface engineering plays an important role in controlling the friction and wear phenomena. The significance of surface engineering in self-lubricating alumina matrix composites is shown in ► Chap. 8. This chapter brings out the relationship between surface microstructure and properties (mechanical and tribological) in the presence of three-dimensional self-lubricating materials.

► Chapter 9 focuses on various theories and available models on self-lubricating materials for molecular dynamics (MD) simulation. This chapter provides a basic understanding of MD simulation and also the need of MD simulation for self-lubricating composites. This chapter is aimed to improve the understanding of lubrication mechanism on molecular level using available models.

The ubiquitous negative effects of different materials on ecosystems are outlined in ► Chap. 10, along with the recent efforts to develop eco-friendly lubricant materials. This chapter provides a deep environmental analysis of self-lubricating composites that gives a clear picture of environmental benefits by using self-lubricating composites, such as aluminum/graphite composites.

This book is intended for professionals as well as university students to provide basic understating as well as the recent development in the field of self-lubricating materials. We have added an extensive listing of results of different concerning fields that are mechanical, chemical, materials and manufacturing, and environment safety. Professionals connected with development and applications of self-lubricating materials will find this book very useful in understanding the multidisciplinary knowledge. We have also added the extensive list of references at the end of each chapter, and it makes this book as an excellent source of references in the field of self-lubricating composites.

Comprehensive knowledge of self-lubricating materials through this book has been possible with the collective efforts of various research groups around the world.

Contents

About the Editor

Pradeep L. Menezes (corresponding author) is an Assistant Professor in the Department of Mechanical Engineering at the University of Nevada, Reno, Nevada. Before joining this university, he worked as an Adjunct Assistant Professor at the University of Wisconsin–Milwaukee (UWM), Wisconsin, and as a Research Assistant Professor at the University of Pittsburgh, Pennsylvania. Dr. Menezes's productive research career has produced more than 70 peer-reviewed journal publications (citations more than 2000, h-index–24), 25 book chapters, and two books related to tribology. Pradeep K. Rohatgi is a UWM Distinguished Professor. He has coedited and coauthored 12 books and more than 400 scientific papers and has 19 US patents. He is considered as a world leader in composites and materials policy for the developing world. He has served on committees of governments of United States and India in the areas of materials, especially those related to automotive sector, to promote collaboration. His research includes advanced manufacture of lightweight, energy absorbing, self-lubricating, and self-healing materials and components including micro- and nanocomposites and syntactic foams. He is the founder chief technology officer (CTO) of Intelligent Composites, LLC, Milwaukee, Wisconsin. Emad Omrani is a graduate student of Dr. Rohatgi at the UWM. He has coauthored 2 book chapters and 7 peer-reviewed scientific papers. At UWM, Dr. Menezes collaborated with Dr. Rohatgi and Mr. Omrani in the areas of tribology and self-lubricating materials and published several research papers on the tribology of self-lubricating materials. Dr. Menezes and Dr. Rohatgi are well-known tribologists and self-lubricating materials scientists. These editors are therefore well known and well connected in this field to put forth an excellent book on this topic.

This book is intended for professionals as well as university students to provide basic understanding as well as the recent development in the field of self-lubricating materials. An extensive listing of results of different concerning fields that are mechanical, chemical, materials and manufacturing, and environment safety are included in this book. Professionals connected with development and applications of self-lubricating materials will find this book very useful in understanding the multidisciplinary knowledge. Due to the extensive lists of references at the end of each chapter, this book makes an excellent source of references in the field of self-lubricating composites.

Contributors

Ali Bakhshinejad University of Wisconsin-Milwaukee, Milwaukee, WI, USA

Mohammad Hasan Balali Department of Industrial and Manufacturing Engineering, College of Engineering & Applied Science, University of Wisconsin-Milwaukee, Milwaukee, WI, USA

Cristiano Binder Laboratório de Materiais, Departamento de Engenharia Mecânica, Universidade Federal de Santa Catarina, Florianópolis, SC, Brazil

David Burris Department of Mechanical Engineering, University of Delaware, Newark, DE, USA

Richard R. Chromik Department of Mining and Materials Engineering, McGill University, Montreal, QC, Canada

Roshan M D'Souza University of Wisconsin-Milwaukee, Milwaukee, WI, USA

Hengzhong Fan State Key Laboratory of Solid Lubrication, Lanzhou Institute of Chemical Physics, Chinese Academy of Sciences, Lanzhou, China

University of Chinese Academy of Sciences, Beijing, China

Yuan Fang State Key Laboratory of Solid Lubrication, Lanzhou Institute of Chemical Physics, Chinese Academy of Sciences, Lanzhou, China

Diana Haidar Department of Mechanical Engineering, University of Delaware, Newark, DE, USA

Litian Hu State Key Laboratory of Solid Lubrication, Lanzhou Institute of Chemical Physics, Chinese Academy of Sciences, Lanzhou, China

Chang-Soo Kim University of Wisconsin-Milwaukee, Milwaukee, WI, USA

Aloisio Nelmo Klein Laboratório de Materiais, Departamento de Engenharia Mecânica, Universidade Federal de Santa Catarina, Florianópolis, SC, Brazil

Jose Daniel Biasoli de Mello Laboratório de Materiais, Departamento de Engenharia Mecânica, Universidade Federal de Santa Catarina, Florianópolis, SC, Brazil

Pradeep L. Menezes Department of Mechanical Engineering, University of Nevada Reno, Reno, Nevada, USA

Marjan Nezafati University of Wisconsin-Milwaukee, Milwaukee, WI, USA

Narjes Nouri Lubar School of Business, University of Wisconsin-Milwaukee, Milwaukee, WI, USA

Emad Omrani Department of Materials Science and Engineering, University of Wisconsin-Milwaukee, Milwaukee, WI, USA

Wilkistar Otieno Industrial and Manufacturing Engineering Department, University of Wisconsin-Milwaukee, Milwaukee, WI, USA

Ajay Kumar Prajapati Department of Materials Science and Engineering, University of Wisconsin-Milwaukee, Milwaukee, WI, USA

Sonia Maria Hickel Probst Laboratório de Materiais, Departamento de Engenharia Mecânica, Universidade Federal de Santa Catarina, Florianópolis, SC, Brazil

Pradeep K. Rohatgi Department of Materials Science and Engineering, University of Wisconsin-Milwaukee, Milwaukee, WI, USA

Junjie Song State Key Laboratory of Solid Lubrication, Lanzhou Institute of Chemical Physics, Chinese Academy of Sciences, Lanzhou, China

University of Chinese Academy of Sciences, Beijing, China

Andrea Sorrentino Institute for Polymers, Composites and Biomaterials (IPCB), National Research Council (CNR), Lecco, Italy

Guangyong Wu School of Mechanical Engineering, Shandong University, Jinan, China

Guangchun Xiao School of Mechanical and Automotive Engineering, Qilu University of Technology, Jinan, China

Key Laboratory of Advanced Manufacturing and Measurement and Control Technology for Light Industry in Universities of Shandong, Qilu University of Technology, Jinan, China

Chonghai Xu School of Mechanical Engineering, Shandong University, Jinan, China

School of Mechanical and Automotive Engineering, Qilu University of Technology, Jinan, China

Key Laboratory of Advanced Manufacturing and Measurement and Control Technology for Light Industry in Universities of Shandong, Qilu University of Technology, Jinan, China

Jiaxin Ye Institute of Tribology, Hefei University of Technology, Hefei, China

Mingdong Yi School of Mechanical and Automotive Engineering, Qilu University of Technology, Jinan, China

Key Laboratory of Advanced Manufacturing and Measurement and Control Technology for Light Industry in Universities of Shandong, Qilu University of Technology, Jinan, China

Yinyin Zhang Department of Mining and Materials Engineering, McGill University, Montreal, QC, Canada

Yongsheng Zhang State Key Laboratory of Solid Lubrication, Lanzhou Institute of Chemical Physics, Chinese Academy of Sciences, Lanzhou, China

RETRACTED CHAPTER: Fundamentals of Solid Lubricants

1

Ajay Kumar Prajapati, Emad Omrani, Pradeep L. Menezes, and Pradeep K. Rohatgi

Contents

The original version of this chapter was revised. An erratum of the original chapter can be found under https://doi.org/10.1007/978-3-662-56528-5_11

A. K. Prajapati (✉) · E. Omrani · P. K. Rohatgi
Department of Materials Science and Engineering, University of Wisconsin-Milwaukee, Milwaukee, WI, USA
e-mail: Kumar38@uwm.edu

P. L. Menezes
Department of Mechanical Engineering, University of Nevada Reno, Reno, Nevada, USA

corrected publication 2020, P. L. Menezes et al. (eds.), *Self-Lubricating Composites*,
https://doi.org/10.1007/978-3-662-56528-5_1

Abstract

Solid lubricants technology is a flourish field that deserves the attention of the designer of machines and devices that will operate in ordinary as well as in extreme environments. This chapter describes solid lubrication processes, the mechanisms by which solid lubricants function, the properties of solid lubricants, and the materials involved in solid lubrication and techniques for their application. Reliability of solid lubrication and wear life of solid-film lubricants are being improved by designing machine elements specifically to employ solid lubricants and by careful matching of the solid lubricant with the substrate bearing material. Solid lubricants are applied either as surface coatings or as fillers in self-lubricating composites. Tribological (friction and wear) contact with solid lubricant coatings typically result in transfer of a thin layer of material from the surface of the coating to the counterface, commonly known as a transfer film or tribofilm. The wear surfaces can exhibit different chemistry, microstructure, and crystallographic texture from those of the bulk coating due to surface chemical reactions with the surrounding environment. As a result, solid lubricant coatings that give extremely low friction and long wear life in one environment can fail to do so in a different environment. Most solid lubricants exhibit non-Amontonian friction behavior with friction coefficients decreasing with increasing contact stress. The main mechanism responsible for low friction is typically governed by interfacial sliding between the worn coating and the transfer film. Strategies are discussed for the design of novel coating architectures to adapt to varying environments.

1.1 Introduction

Solid lubricants are solid materials which reduce coefficient of friction and wear of rubbing parts preventing direct contact between their surfaces even under high loads. Solid lubricants are of particular interest under conditions where oils and greases by their very nature cannot be used. Solid lubricants and coatings are needed for lunar and Martian applications also, where liquid lubricants are ineffective and undesirable, and these lubricants must perform well in the extreme environments of the Moon, Mars, and space, as well as on Earth, where they will be assembled and tested. Solid lubricants are key ingredients in high-performance anti-seize pastes and anti-friction coatings, used as additives in some greases and oils [1], and can be provided as free-flowing powders. These special lubricant powders and additives fill in and smooth surface asperity peaks and valleys as they adhere to the substrate and cohere to each other. The solids provide effective boundary lubrication, optimizing friction and reducing wear under extreme operating conditions.

Most mechanical components in moving mechanical assemblies (e.g., bearings and gears) are fabricated from metallic materials. Surface interactions between two flat metal surfaces, as they are brought into atomic contact, were analyzed by Tabor [2]. It was depicted that bonds first form due to long-range van der Waals forces, and

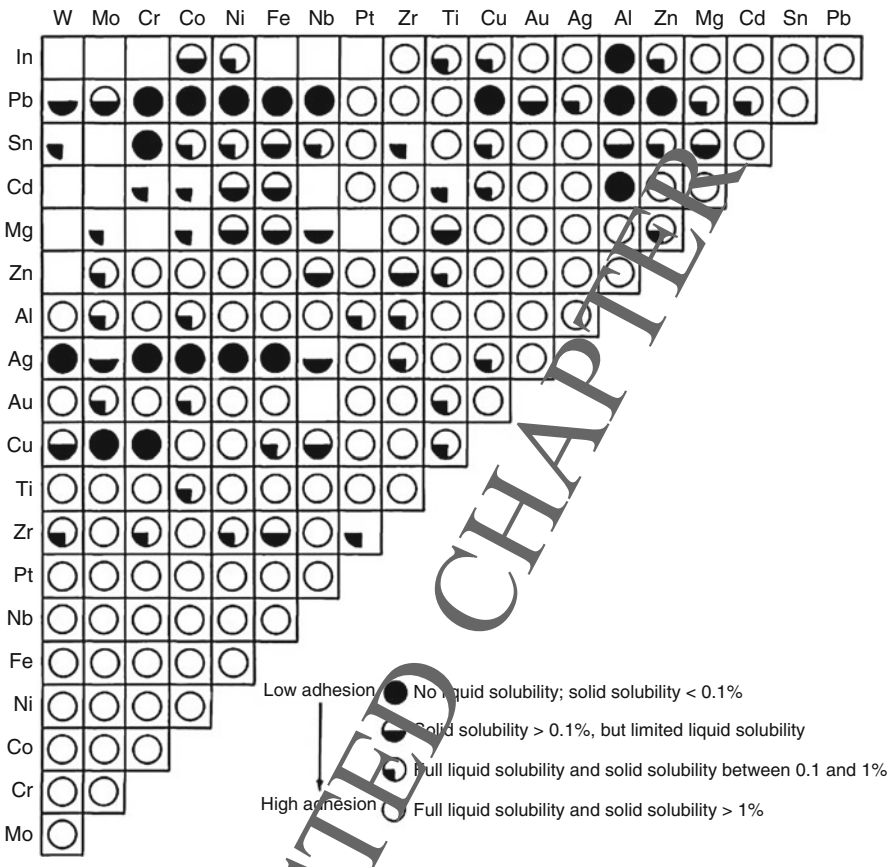

Fig. 1.1 Compatibility chart developed by Rabinowicz for selected metal combinations derived from binary equilibrium diagrams. Chart indicates the degree of expected adhesion (and thus friction and wear) between the various metal combinations [4]

as separation distances approach the interatomic distances, strong metallic bonds would result. The bonding between similar and dissimilar metals has been discussed in terms of mutual solubility [3]. Implicit is the assumption that mutually soluble pairs exhibit strong adhesive bonding and hence high friction, while insoluble pairs show weak adhesive bonding and hence low friction. This approach has been extended by Rabinowicz [4] to develop a generalized compatibility chart (Fig. 1.1) based on equilibrium binary phase diagrams. According to Rabinowicz, adhesion and friction should decrease as one progresses from couples of the same material and those that form solid solutions to insoluble couples and to metal-nonmetal pairs. However, this approach should be regarded as a general guideline and not as an ultimate design rule for the selection of materials involving moving contacts. Materials designed for friction and wear mitigation, commonly referred to as

tribological materials, must meet mechanical and physical property requirements: strength, stiffness, fatigue life, thermal expansion, and damping. From a practical design perspective, it becomes almost impossible to balance these diverse requirements and mitigate friction from bulk materials which are used to build tribological components. Friction and wear mitigation is typically accomplished by introducing a shear-accommodating layer (e.g., a thin film of liquid) between contacting surfaces. When the operating conditions are beyond the liquid realm (e.g., high temperature or vacuum), or in situations where liquids cannot be introduced, attention turns to *solid lubricant* coatings. The solid lubricating behavior of naturally occurring materials, such as graphite and molybdenite, is well known. However, the development of modern coating technologies (e.g., physical vapor, chemical vapor, and plasma-enhanced chemical vapor depositions) has greatly expanded the use of solid lubricant materials. Some of the more commonly used solid lubricant materials include the diamond-like carbons (DLCs), transition metal dichalcogenides (TMD), and polymeric composite coatings. The emergence of surface and subsurface analytical techniques (e.g., X-ray photoelectron spectroscopy, scanning Auger microscopy, time-of-flight secondary mass spectroscopy, and focused ion beam (FIB) microscopy) has significantly facilitated the fundamental understanding of the synthesis-structure tribology relationships in solid lubricant materials.

Solid lubrication has emerged as an integral part of materials science and engineering. In this chapter, we briefly discuss the nature of solid surfaces, contact mechanics, and the area of contact between engineering surfaces that are important prerequisites in the design and application of solid lubricant coatings. We then discuss the fundamental mechanisms of solid lubrication processes with emphasis on the role of tribochemistry, contact load, and counterface material on the formation and attrition of transfer films. Frictional contact also induces microstructural evolution in the surface and subsurface regions. Therefore, material lubrication also depends on the loading conditions.

Boundary films formed by solid lubricants can maintain a steady thickness that is unaffected by load, temperature, or speed, unlike oil or grease fluid films for hydrodynamic lubrication. Solid lubricants are applied either as surface coatings or as fillers in self-lubricating composites. Tribological (friction and wear) contacts with solid lubricant coatings typically result in transfer of a thin layer of material from the surface of the coating to the counterface, commonly known as a transfer film or tribo-film. The wear surfaces can exhibit different chemistry, microstructure, and crystallographic texture from those of the bulk coating due to surface chemical reactions with the surrounding environment. Thus, solid lubricant coatings that give extremely low friction and long wear life in one environment can fail to do so in a different environment.

The specific aim of this chapter is to compile information on the following:

- Selection of lubricant type
- Advantages and disadvantages of solid lubricants
- Ranges of application of solid lubricants
- Suppliers of advanced solid lubricants and coatings

- State-of-the-art coatings research
- Designing for solid lubricants and coatings
- Tribological and surface characterization

1.2 Surfaces and Contact Area

Engineering surfaces exhibit various types of layers and are "rough" on multiple size scales, shown in Fig. 1.2a, irrespective of how they were manufactured, e.g., machined, ground, and/or polished. The real area (A_r) of contact at the asperity level is much smaller, in the order of 10^{-2} to 10^{-6}, than the apparent area (A_a) of the contacting bodies (Fig. 1.2b, c). The A_r is a function of the surface topography, material properties, and interfacial loading conditions. It is a very difficult parameter to experimentally measure or visualize without the use of optically transparent bodies because it is at the buried interface. The magnitude of A_r generally needs to be minimized (lower degree of interaction) for low adhesion. Even when the apparent contact stresses are elastic, the localized stresses can exceed the elastic limit at the tips of asperities where actual contact occurs, resulting in localized plastic deformation. Thus, adhesion is thought to be a component of the plastic deformation of asperities, which strongly influences the amount and the nature of the overall deformation [6, 7]. The Greenwood and Williamson theory developed for contacting

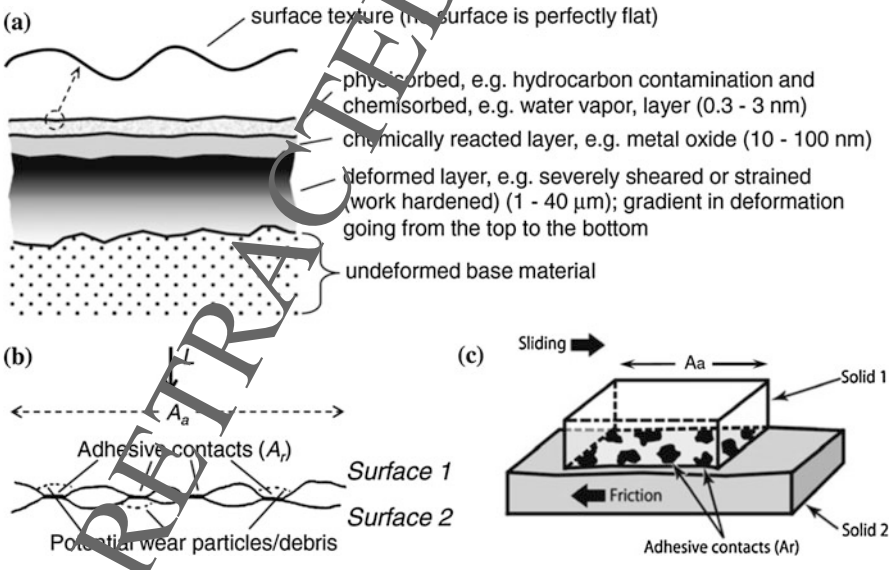

Fig. 1.2 Schematics (not to scale) of (**a**) typical polished metal surface and subsurface layers with approximate thicknesses, (**b**) Metal–metal adhesive contact between two solid surfaces showing A_r versus the A_a under L. (**c**) Adhesion and friction can lead to the generation of third bodies: wear particles (debris) at the asperity contacts, and transfer films that are detached from the softer solid and adhered to the harder solid [5]

rough surfaces under static (normal) loads modeled the condition at which change-over from elastic to plastic contact takes place [8]. Their theory assumes that the tips or summits of these asperities are spherical, have the same characteristic radius of curvature R_s, and follow a random or Gaussian distribution. They found that no matter what the shape of the Gaussian distribution, it is only the most prominent asperities (large vertical height values) that will take part in surface interactions. Based on their theory, a plasticity index (Ψ) can be calculated:

$$\Psi = \frac{E^*}{H}\sqrt{\frac{\sigma_s}{R_s}} \tag{1.1}$$

where the composite or reduced Young's modulus E^* is

$$\frac{1}{E^*} = \frac{1-\nu_1^2}{E_1} + \frac{1-\nu_2^2}{E_2} \tag{1.2}$$

where $E_{1,2}$ and $\nu_{1,2}$ are the respective elastic modulus and Poisson's ratio of contacting materials 1 and 2, respectively, H is the hardness of the material that plastically deforms first (softer), σ_s is the standard deviation of peak heights ($\sigma_s^2 = \sigma_1^2 + \sigma_2^2$), and R_s is the composite peak radius ($1/R_s = 1/R_1 + 1/R_2$). The square root term in Eq. 1.1 is related to the mean slope of the surface and can be obtained from profilometry data. The plasticity index, a nondimensional value, determines the likely deformation (elastic or plastic) of a rough surface. When Ψ is <0.6 l elastic deformation dominates; when Ψ is >1, a large portion of the contact involves plastic deformation. Furthermore, the A_r can be estimated from the Greenwood and Williamson model for elastic contacts (based on Ψ calculation):

$$\frac{A_r}{A_a} \cong \frac{3.2\ P_H}{E^*\left(\sigma_s/R_s\right)^{1/2}} \tag{1.3}$$

where P_H is the mean Hertzian contact pressure (stress). For plastic contacts (based on Ψ calculation), A_r can also be estimated:

$$\frac{A_r}{A_a} \cong \frac{P_H}{H} \tag{1.4}$$

because A_r is (a) inversely proportional to H, (b) proportional to normal load (L), and (c) independent of A_a. Other variations to the Greenwood and Williamson plasticity index model include the Whitehouse and Archard [9] and Bower and Johnson [10] plasticity indices. In general, these indices suggest how the adhesive forces can be minimized (an important contribution to the overall friction discussed below) by lowering A_r and increasing H and E.

Contact mechanics modeling of surfaces which come into sliding contact can be more complex with the introduction of frictional forces. In addition to static (normal) contact stresses, dynamic (frictional) contact stresses are generated below

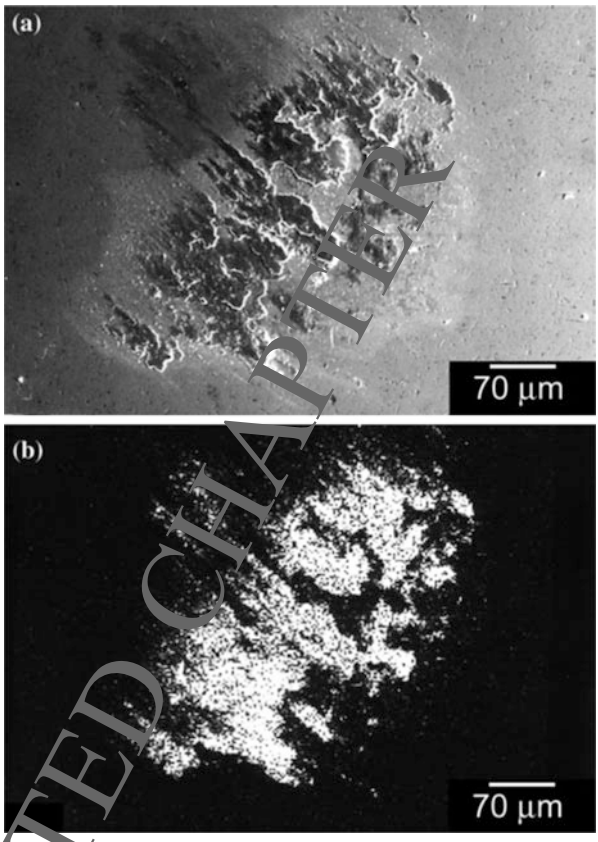

Fig. 1.3 Smearing of Al on a steel ball during a ball-on-disk friction and wear test. (**a**) SEM image of Al adhesive transfer on steel ball, and (**b**) corresponding Al X-ray dot map [5]

the interface with different values of the principle (σ_x, σ_z) and maximum shear (τ) stresses at a given ratio of depth (z) to contact area (a). The main changes going from static (indentation) to dynamic (sliding) are that the stress fields ahead of the counter body (ball) are compressive, while those behind are tensile, and the introduction of friction increases the maximum subsurface shear stress and moves its position closer to the surface. Besides friction, a coating-substrate interface introduces an additional complexity in contact mechanics modeling of coated surfaces. However, the most important consideration is to ensure that any local plastic deformation in the substrate material does not adversely affect the coating-substrate integrity.

Surfaces also consist of several zones having physical and chemical properties that are different from those of the bulk, shown schematically in Fig. 1.2a. Frictional adhesive contacts (Fig. 1.2b, c) can result in significant microstructural changes in the subsurface regions. In the case of metal–metal contacts, the native oxides can be worn away during the initial run-in period resulting in an unwanted metal-to-metal contact. In the example shown in Fig. 1.3, aluminum was transferred to a harder steel ball during a ball-on-disk friction and wear test through adhesive friction and wear processes, shown schematically in Fig. 1.2c. In the absence of external fluid or solid

lubrication, aluminum can flow and adhere to the hard counterface, creating an interface of lower shear strength that results in the reduction of friction. The binary alloy compatibility chart in Fig. 1.1 shows that Al and Fe (steel) exhibit solid solubility of >1%, and therefore high adhesion, which supports the large amount of adhesive transfer shown in Fig. 1.3.

1.3 Fundamentals of Solid Lubrication

According to the classical theory of Bowden and Tabor [14], friction force, F, is a product of the real contact area and the shear strength of the lubricant material, $A_r.\tau$ (see Fig. 1.4). Thus, the friction coefficient, μ, can be expressed by

$$\mu = \frac{F}{L} = \frac{A_r.\tau}{L} = \frac{\tau}{P_H} = \frac{\tau_o}{P_H} + \alpha \tag{1.5}$$

where τ_o is the interfacial shear strength, a "velocity accommodation parameter" which is a property of the interface, and α represents the pressure dependence of the shear strength. The constant α is the lowest attainable friction coefficient for a given friction couple. According to Eq. 1.5, the friction coefficient is the ratio of friction force to applied normal force, or the ratio of shear strength to pressure, if both forces are divided by the contact area. In principle, a hard material with a soft "skin" ought to provide a low friction coefficient by reducing so and increasing P_H (low A). The Bowden and Tabor concept is schematically illustrated in Fig. 1.5a for the general case of a soft versus hard metal contacts. Bowden and Tabor validated their model by demonstrating that indium metal when applied as a thin film on a much harder steel substrate can indeed act as a solid lubricant, as shown in Fig. 1.5b. It is also interesting to note from their study that while the friction coefficients for the unlubricated steel (top curve) and for the steel lubricated with mineral oil (middle curve) obeyed Amonton's first law of friction (μ is independent of L), the friction coefficient of indium film on steel substrate decreased considerably with increasing normal load. Here, the increased deformation of the underlying steel resulting from an increase in normal load produced only a small increase in the real contact area.

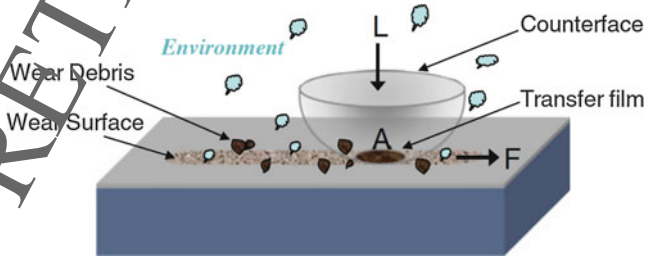

Fig. 1.4 Schematic illustration of a hemispherical ball sliding on a solid lubricant coated substrate with the wear surface in contact with the transfer film on the counterface ball [5]

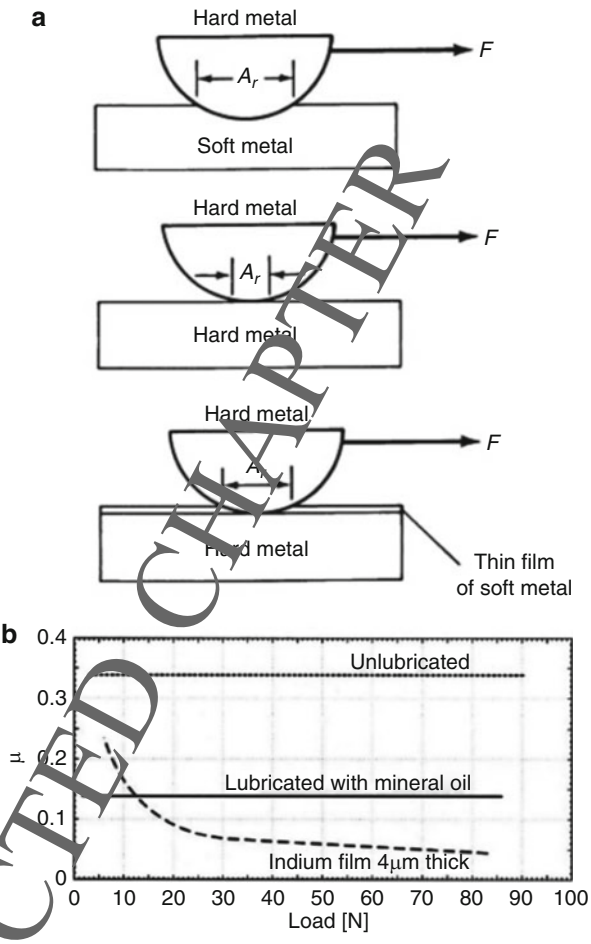

Fig. 1.5 (**a**) Relation of friction force ($F = A_r.\tau$) to metal substrate hardness. Top hard metal in contact with soft metal (small τ and large A_r). Middle two hard metals of comparable hardness in contact with each other (large τ and small A_r). Bottom two hard metals of comparable hardness separated by a thin film of soft metal deposited on one metal surface (both A_r and τ are small). (**b**) Experimental proof for the case of steel–indium sliding contacts (friction coefficient as a function of normal load) [11]

Thus, there is only a slight increase in frictional force as the load is increased, which results in a corresponding decrease in friction coefficient according to Eq. 1.5. This behavior can also be explained if we consider a "sphere-on-flat" elastic contact, which is known as the Hertzian elastic contact model, where the friction coefficient can be expressed as

$$\mu = \tau_o.\pi\left(\frac{3R}{4E^*}\right)^{2/3} L^{-1/3} + \alpha \tag{1.6}$$

where R is the sphere radius. In contrast to Amonton's first law of friction, the Bowden and Tabor analysis for Hertzian contacts predicts,

$$\mu \propto L^{-1/3} \tag{1.7}$$

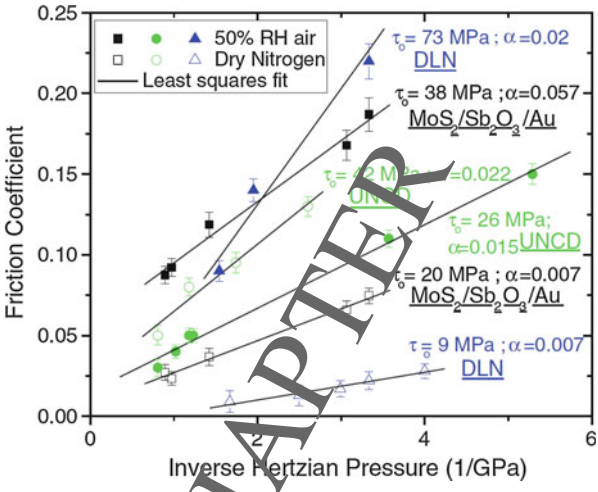

Fig. 1.6 Linear regression fits for sliding friction coefficients as a function of inverse mean Hertzian pressure fitted to $\mu = (\tau_o/P_H) + \alpha$ with values of shear strength (τ_o) shown for three solid lubricant, environmentally robust coatings: Si_3N_4 on DLN, Si_3N_4 on $MoS_2/Sb_2O_3/Au$, and UNCD coated Si_3N_4 on UNCD, in both dry nitrogen and humid air [5]

Thus, when contact deformation is elastic, the friction coefficient will decrease with increasing normal load (or mean Hertz pressure), as shown in Fig. 1.5b, for the indium film. The linear relationship between $L^{-1/3}$ and μ has also been experimentally verified for a number of low friction (solid lubricant) coatings (see Fig. 1.6). For thin and soft coatings, the pressure is primarily supported by the substrate, and increasing the substrate elastic modulus and hardness will decrease the contact area for a given normal load (pressure), which is in accordance with Eqs. 1.3 and 1.4 (Greenwood and Williamson model) respectively. Thus, the ideal scenario for achieving low friction according to the Bowden and Tabor concept is to have an elastically stiff and hard substrate to support the normal load and keep the contact area small, while the surface coating provides shear accommodation and reduces junction strength, until the substrate begins to yield and plastically deform. Deviations in Bowden and Tabor analysis for Hertzian contacts have been determined to occur under lightly loaded contacts. As examples, solid lubricant coatings MoS_2, Au-MoS_2, and Ti-MoS_2 [12, 13] and diamond-like nanocomposite (DLN) [14] do not follow $\mu \propto L^{-1/3}$ behavior in the microscopic load range.

The above scenario is necessary, but not totally sufficient, condition for most low friction and low wear solid lubricant coatings. In addition, transfer films or tribofilms (third bodies) that adhere to the counterface (Fig. 1.2) can lower so further and provide long wear life by accommodating interfacial shear. The role of the transfer film is twofold. First, a mixture of inference and in situ friction and wear testing evidence [15–17] suggests that the transfer film covers the area of contact preventing direct contact between the sliding surfaces. Second, and more importantly, the low friction and long wear life rely on the transfer film to provide low shear at or near the sliding interface. If the transfer film wears away, then the friction coefficient increases and the contacting surfaces can eventually seize or gall, unless of course the transfer film is replenished. Therefore, solid lubricants do not necessarily have to exhibit low inherent shear strength to impart low friction. While necessary, the

material's low shear strength cannot account for either the Hertzian behavior (Eq. 1.6) or the long wear life of a solid lubricant coating. Though most solid lubricants function by transfer film processes, there are a few notable exceptions, like the near frictionless carbon (NFC) and ultrananocrystalline diamond (UNCD) that do not appear to form observable transfer films, as discussed in later sections.

In addition to adhesive friction and wear, other mechanisms can be involved in contacts to varying degrees, such as abrasion – plowing of one surface by asperities on the other, or cutting action of harder particles on a softer surface, which can result in the formation of permanent grooves in the surface of the softer material. If the particles become bonded to one of the contacting surfaces, the process is referred to as two-body or fixed abrasion. In three-body abrasion, the abrasive is in the form of loose particles between the two contacting materials. Deformation and/or fracture of surface layers, such as oxides, can also occur in contacts.

Friction and wear do not just rely on physical and mechanical properties of individual materials that come into contact; instead, they are systems' properties involving interactions within pairs of contacting surfaces and between them and the environment. Many tribological contacts result in the aforementioned transfer of material from the coating surface to the counterface, plus surface chemical reactions with the surrounding environment (Fig. 1.2), known as tribochemical reactions, resulting in wear surfaces whose chemistry is significantly different from that of the bulk. In addition to the chemistry of the transfer films, or tribofilms, the chemistry/composition of the sliding counterface can influence the friction and wear behavior especially during the run-in stage when the transfer film begins to adhere to the counterface.

As can be seen from the following classes of solid lubricant materials, environment, load, counterface material, sliding speed, etc., play a significant role in determining their tribological behavior. For instance, coatings that give extremely low friction and long wear life in one environment can fail to do so in a different environment. In addition, no single material can act as a solid lubricant in all environments and under all operating conditions.

1.4 Solid Lubricant Coatings and Lubrication Mechanisms

Solid lubricant coatings are primarily used to control friction and wear under severe application conditions (such as high vacuum, aerospace, high-speeds, high loads, and very low or high temperatures), where conventional materials and lubricants cannot provide the desired levels of performance or durability. During the past two decades or so, remarkable progress has been made in the design, development, and uses of solid lubricant films. The current trend in modern tribology is to limit or reduce the use of liquid lubricants as much as possible (mainly because of environmental concerns), but increase the use of solid materials and coatings with self-lubricating properties. However, in the near term, the best compromise may be to consider a combination of solid and liquid lubricants to meet emission or

Table 1.1 Major shortcomings of solid lubricant films and corresponding requirements to overcome the present limitations [18]

Shortcomings	Requirements
Adherence	Interface optimization
Fluctuation in friction coefficient	Run-in control and wear debris removal
Finite wear life	Difficulty of replenishment
Tribo reactivity	Effect of temperature and environments
Poor thermal conductivity	How to carry away heat?
Complex deposition procedures	Lowering costs

environmental requirements of future tribological systems while providing the levels of desired friction and wear performance.

Solid lubricant coatings have come a long way in recent years, and they are now capable of providing extremely low friction and wear coefficients under certain or highly controlled test conditions. However, as depicted in Table 1.1, solid lubricant films still have shortcomings, in spite of considerable progress made during the past 15 years. At present, no single coating can provide both low friction and high wear resistance over very broad use conditions, temperatures, and environments. Furthermore, solid lubricant coatings have problems with limited lifetime, difficulty in replenishment, and oxidation and aging-related degradation (in the case of certain lamellar solid lubricants, such as MoS_2).

Solid lubricants vary widely in terms of composition and properties. Solid lubricants may be present in the friction area in forms of either dispersed particles or surface films:

- Coating (film) of a solid lubricant applied on the part surface.
- Composite coating consisting of particles of a solid lubricant dispersed throughout a matrix.
- Particles of a solid lubricant dispersed throughout the bulk of the part material (composite material).
- Powder of a solid lubricant delivered to the rubbing area (dry lubrication).
- Additives in lubricating oils or greases.

1.5 Classification of Solid Lubricants

There are four distinct classes of solid lubricant materials: (1) carbon-based materials (e.g., graphite, DLCs, and nanocrystalline diamond); (2) transition metal dichalcogenide compounds (MoS_2 and WS_2); (3) polymers (PTFE); and (4) soft metals like silver, tin, indium, and gold. Barring a few exceptions, such as PTFE and its composites, most of these materials can be applied as thin films and coatings on tribological components (bearings, seals, magnetic hard drives, etc.) to reduce friction, wear, and debris generation. Solid lubricant coatings can be both single

Table 1.2 Types of lubricating films [18]

Type	Lubricating films
Solid films	Nanotubes, nano-onions, and other nanoparticles (C, BN, MoS_2, and WS_2)
	Nanocomposite coatings (WC/C, MoS_2/C, WS_2/C, TiC/C, and nanodiamond)
	Diamond and diamond-like carbon coatings (diamond, hydrogenated carbon (a-C:H), amorphous carbon (a-C), carbon nitride (C_3N_4), and boron nitride (BN) films)
	Superhard or hard coatings (VC, B_4C, $A1_2O_3$, SiC, Si_3O_4, TiC, TiN, TiCN, A1N, and BN)
	Lamellar film (MoS_2 and graphite)
	Nonmetallic film (titanium dioxide, calcium fluoride, glasses, lead oxide, zinc oxide, and tin oxide)
	Soft metallic film (lead, gold, silver, indium, copper, and zinc)
	Self-lubricating composites (nanotubes, polymer, metal-lamellar solid, carbon, graphite, ceramic, and cermets)
	Lamellar carbon compound film (fluorinated graphite and graphite fluoride)
	Carbon
	Polymers (PTFE,[a] nylon, and polyethylene)
	Fats, soap, wax (stearic acid)
	Ceramics and cermets
Fluid films	Hydrodynamic film:
	Thick hydrodynamic film
	Elastohydrodynamic film
	Hydrostatic film
	Squeeze film
Thin films	Mixed lubricating film
	Boundary lubricating film
Gas films	Hydrodynamic film
	Hydrostatic film

[a]Polytetrafluoroethylene

phase (elements or compounds) materials and multiphase composites. Table 1.2 summarizes many characteristics of solid lubricant coatings.

1.5.1 Inorganic Lubricants with Lamellar Structure

The crystal lattice of these materials has a layered structure consisting of hexagonal rings forming thin parallel planes. Within the plane each atom is strongly bonded (covalent bonding) to other atoms. The planes are bonded to each other by weak Van der Waals forces. The layered structure allows sliding movement of the parallel planes. Weak bonding between the planes determines low shear strength and lubricating properties of the materials.

The most commonly used inorganic solid lubricants with lamellar structure are graphite, molybdenum disulfide (MoS_2), and boron nitride (BN). Other examples of such materials are sulfides, selenides, and tellurides (chalcogenides) of molybdenum, tungsten, niobium, tantalum, titanium (e.g., WS_2, $MoSe_2$, $TaSe_2$, $TiTe_2$), monochalcenides (GaS, GaSe, SnSe), chlorides of cadmium, cobalt, lead, cerium, zirconium (e.g., $CdCl_2$, $CoCl_2$, $PbCl_2$, CeF_3, PbI_2), and also some borates (e.g., $Na_2B_4O_7$) and sulfates (Ag_2SO_4).

1.5.2 Oxide

The examples of oxides are B_2O_3, MoO_2, ZnO, Re_2O_7, TiO_2, $CuO\text{-}MoO_2$, $NiO\text{-}Mo_2$, $PbO\text{-}B_2O_3$, and $CuO\text{-}Re_2O_7$.

1.5.3 Soft Metals

Due to their low shear strength and high plasticity, some soft metals possess lubrication properties. Examples are lead (Pb), tin (Sn), bismuth (Bi), indium (In), cadmium (Cd), and silver (Ag).

Soft metals are used in pure form or as alloys, in the form of coatings (Lead based engine bearing overlays, Tin based engine bearing overlays) as the second phase in Metal Matrix Composites (Copper based bearing materials, Aluminum based bearing materials). Coatings from soft metal lubricants are produced by the methods of electroplating, vapor deposition, and thermal spraying. Composites containing soft metal lubricants are prepared by casting or sintering methods. Soft metal is widely used as solid lubricants in engine bearing materials.

1.5.4 Organic Lubricants with Chain Structure of the Polymeric Molecules

Polytetrafluoroethylene (PTFE) and polychlorofluoroethylene are the typical examples of such materials. The molecular structure of the materials consists of long-chain molecules parallel to each other. The bonding strength between the molecules is weak; therefore, they may slide past one other at low shear stresses. The strength of the molecules along the chains is high due to strong bonding between the atoms within a molecule. Such anisotropy of mechanical properties provides good lubrication properties of the materials. Chain structure lubricants are used in form of coatings (films) applied on the substrate surfaces (polymer based engine bearing overlays).

1.5.5 Soaps

Soaps are metal (lithium, calcium, sodium, potassium) salts of fatty acids. Soaps are prepared by chemical treating of oils and fats by strong alkaline solutions. A soap molecule is composed of a long nonpolar hydrocarbon tail, which is hydrophobic

(repelled by water), and the salt polar end, which is hydrophilic (water soluble). The soap molecules attached to the substrate surface provide good adhesion of the soap lubricant and low coefficient of friction.

1.5.6 Graphite

Graphite is a classic example of carbon-based material that is well known for its solid lubricating behavior. Of more relevance are the various types of DLC coatings, which have been synthesized specifically for friction and wear reduction. Unlike graphite, the DLCs are amorphous in nature. Schmellenmeier [19] and later Eisenberg and Chabot [20] were the first researchers to deposit DLC coatings. Diamond being intrinsically hard was not originally thought of as a solid lubricant material; however, when the grains are nanocrystalline, solid lubricity is observed under certain operating conditions, e.g., in the presence of oxygen and water vapor.

Graphite, shown in Fig. 1.7a, is a layered solid with a hexagonal lattice (space group 194 $P6_3/mmc$) and high c/a ratio ($c = 6.70$ A°, $a = 2.46$ A°) [23]. The carbon atoms in its basal planes are held with strong covalent bonds, while the basal planes themselves are held together by weak Van der Waals cohesive forces, resulting in interplanar mechanical weakness. Thus, it is traditionally thought that under a shearing force the basal planes slide over one another by intracrystalline slip, often referred to as "deck of-cards" shear. The presence of water vapor and oxygen in the environment is believed to facilitate the interlamellar shearing of graphite crystals. These close packed basal planes exhibit low surface energies and have little adhesion between them [24, 25]. This was confirmed by Buckley [26] who determined that when clean, metallic surfaces, e.g., iron and tantalum, were in sliding contact with the basal planes of pyrolytic graphite in ultrahigh vacuum, no adhesive transfer of metal was observed, resulting in lower friction coefficients. However, there was significant adhesive transfer of metal to the graphite surface when sliding on the chemically more active prismatic planes that resulted in higher friction coefficients because shear took place in the metal. However, when the basal plane becomes damaged, high energy edge sites of the lamellae are exposed and bond strongly to other edge sites causing increased adhesion. Low friction is maintained when these reactive edge sites are neutralized (passivated) by the adsorption of water or other condensed vapors [23, 27]. This is true for many carbon-based solid lubricants. Unlike MoS_2 and WS_2 (discussed later), graphite needs moisture, or adsorbed gases, in the environment (>100 ppm) to passivate the dangling covalent bonds and the edges of the basal planes in order to lubricate [28]. In vacuum and in dry environments, graphite without additives exhibits high friction, a phenomenon known as "dusting" that was first observed in aircraft during the late 1930s when graphite in brushes experienced accelerated wear at high altitudes [29]. A recent report refutes the traditional claim that the interlamellar weakness in graphite results from chemisorption or intercalation of vapor molecules near the surface leading to an increase in the interlayer spacing between near-surface basal planes [30]. Raman spectroscopy is an excellent technique to probe the various structures of graphite, such as

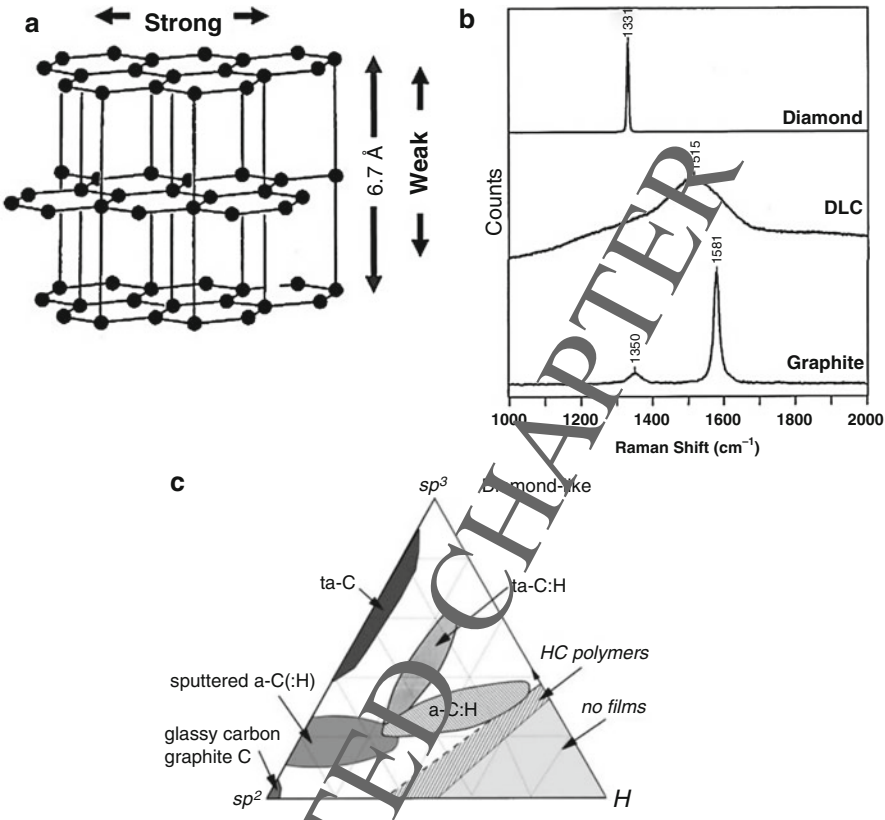

Fig. 1.7 (**a**) Lamellar crystal structure of graphite. (**b**) Typical Raman spectra of graphite, DLC coating, and diamond taken with k = 458 nm [21]. (**c**) Ternary phase diagram of bonding in amorphous carbon–hydrogen alloys [22]

single crystal, polycrystalline (nanocrystalline and microcrystalline grains), and highly ordered pyrolytic graphite (HOPG), due to the enhanced Raman sensitivity of C–C bonding [31].

Figure 1.7b shows the Raman spectrum for microcrystalline graphite [21]. Graphite has two fundamental Raman modes, both of E_{2g} symmetry, occurring near 47 and 1581 cm^{-1}, the latter denoted as the G-peak. Another Raman peak that often occurs in graphite is located near 1350 cm^{-1}, referred to as the D-peak, which has been associated with disorder in the graphite lattice (domain edge effects, small graphite crystallites, and oxide species). The values of the D and G-peak intensities, peak positions, and full width at half maxima are very sensitive to changes in the structure of carbon and its allotropes, and thus are very useful in studying chemical and structural changes that result during sliding contact. The most widespread use of graphite (besides electrical contact brushes) in anti-friction applications is in metal and polymer-matrix self-lubricating composites as a "built-in" solid lubricant. Sometimes graphite is also applied as a resin-bonded coating.

1.5.7 Diamond-like Carbon (DLC)

DLC coatings are typically amorphous with short range ordered phases of mixed sp^3-type tetrahedral bonding (diamond hybridization) and sp^2-type trigonal bonding (graphitic hybridization). These are known to exhibit an unusual combination of tribological and mechanical properties: low friction coefficients and low wear rates, relatively high hardness, and high elastic modulus [22, 32, 33].

DLC can provide both high hardness and low friction. Thus, it is an exception to the previously discussed Bowden and Tabor concept, which associates low friction with low shear strength materials like graphite, not high hardness materials like DLC. Early formulations of DLCs have two drawbacks: the coatings exhibited relatively large residual compressive stresses that result in delamination, and they were not mechanically tough (high H/E ratios, analogous to the Greenwood-Williamson plasticity index, Ψ, in Eq. 1.1). To alleviate these two issues, DLCs are typically doped with metals or lightweight elements, and thus have found several applications on a commercial scale. DLCs doped with hydrogen (~10–50 at.%) are commonly referred to as hydrogenated DLCs (a-C:H). Alternatively, DLCs can be doped with other lightweight elements, such as nitrogen, silicon, and silicon oxide, as well as transition metals, such as Cr, W, and Ti, which form nanoscale hard metal carbide phases and improve their mechanical strength, hardness, and wear resistance. Fig. 1.7b shows a Raman spectrum of a typical DLC coating. The broad, asymmetric G-peak, typically between 1500 and 1560 cm^{-1}, is a characteristic of DLC coatings produced by most deposition techniques [21]. A small intensity D-peak around ~1350 cm^{-1} is often observed as well. In comparison to graphite, the D and G peak broadening is indicative of the structural disorder of these amorphous coatings.

Figure 1.7c is a ternary diagram that shows the specific domains of various carbon-based coatings with respect to their sp^2-, sp^3-type bonding and hydrogen contents [22]. Most of the coatings on the diagram are inherently hard and lubricious under typical sliding conditions. The diagram consists of three main regions. The first region along the left axis is H-free amorphous carbon (a-C). There are three main coating types along this axis. The first, glassy carbon is sp^2 a-C made by pyrolysis of hydrocarbon polymers or by evaporation and is not considered DLC. The second is an a-C of higher sp^3 content, but still without H, is typically made by sputtering, and is a DLC. Other sputtering-based techniques, such as unbalanced magnetron sputtering, can create DLC with increased sp^3 contents. At even higher sp^3 content, the last type of a-C coating is designated as tetrahedral amorphous carbon or ta-C which is deposited from ion or plasma beams with a high ion fraction including mass selected ion beam (MSIB) deposition, filtered cathodic vacuum arc (FCVA), and pulsed laser ablation deposition (PLD) [34]. The second region of the phase diagram is the bottom right of the figure, where no films are formed (just gas molecules) because the H content is so large that the material cannot form a fully connected network [22]. Just above this region lies the a-C:H coatings which are typically deposited by plasma-enhanced chemical vapor deposition (PECVD) of hydrocarbon molecules, or by the reactive sputtering of graphite in an atmosphere

including H, or by ion beam deposition from a hydrocarbon gas precursor [35–37]. In this a-C:H region, the hydrogen content in the coating can vary over a wide range of ~10 to 50 at. % of the total number of atoms. The last region contains coatings that are denoted as tetrahedral amorphous hydrogenated carbon or ta-C:H. These coatings are deposited in the presence of hydrogen with very high density plasmas generated by electron cyclotron resonance or inductively coupled plasma sources [38].

The friction coefficients of DLC coatings vary widely from 0.01 to 0.5 depending upon the test conditions (i.e., contact stress, sliding velocity, temperature, and counterface material) and the environment, as listed in Table 1.1. In addition, the chemical bonding and hydrogen content of the coatings profoundly influence the friction coefficient. For instance, hydrogen-free DLC coatings perform best in humid air where low friction coefficients (~0.1) can be achieved for long durations, while hydrogenated coatings perform better in dry or inert gas environments. Another class of DLC coatings, known as near friction-less carbon (NFC), can provide what may be the lowest friction coefficients of any known material, $\mu \sim 0.005$, in self-mated sliding contact [39]. NFC coatings, in contrast to most DLCs, do not appear to form adherent transfer films on the sliding counterface to achieve low friction and wear. Instead, it has been determined that super low friction is due to hydrogenated carbon atoms passivating the contacting surfaces [33, 40]. In addition, DLCs also often exhibit non-Amontonian behavior with friction coefficient decreasing with increasing Hertzian contact stress, according to Eq. 1.6, and shown in Fig. 1.6, for a diamond-like nanocomposite (DLN) coating. The DLN interfacial shear strength values τ_o, computed from these plots, are 9 MPa in dry nitrogen and 78 MPa in humid air [41].

Synthesizing one single DLC material to achieve low friction in both dry and humid environments is a challenging task. Recent research shows promise for environmentally robust tribological nanocomposite coatings, such as DLN, the structure of which has been conjectured to consist of two amorphous interpenetrating networks, a diamond-like (a-C:H) network and a quartz-like (a-Si:O) network, with minimal bonding between the two networks [41]. The mutual stabilization of these networks prevents the growth of graphitic carbon at high temperatures, as well as serves to enhance the adhesion and reduce the coating residual stress to approximately −0.5 GPa. The composition of DLN can vary but is typically around $(CH_{0.15})_{0.7}(SiO_{1.3})_{0.3}$. Figure 1.8a shows the Raman spectra from a DLN coating [41]. Like the DLC coating in Fig. 1.7b, there are similar D and G peak features characteristic of an amorphous structure. The Raman spectra from transfer films on Si_3N_4 counterfaces generated in both dry nitrogen and humid air clearly exhibited peak shifts compared to those from the DLN coating. The narrowing and increasing Raman shift of these peaks indicates a transformation to a more graphitic structure albeit with nanometer-scale domain sizes. This transformation of DLC-like amorphous carbon to nanocrystalline graphite is well documented for thermal treatment [21] and frictional rubbing [34, 40, 42]. Comparing the transfer film spectra as a function of environment, the film generated in humid air showed a very slight narrowing at 1605 cm^{-1}, but no peak shift, compared to the dry nitrogen transfer

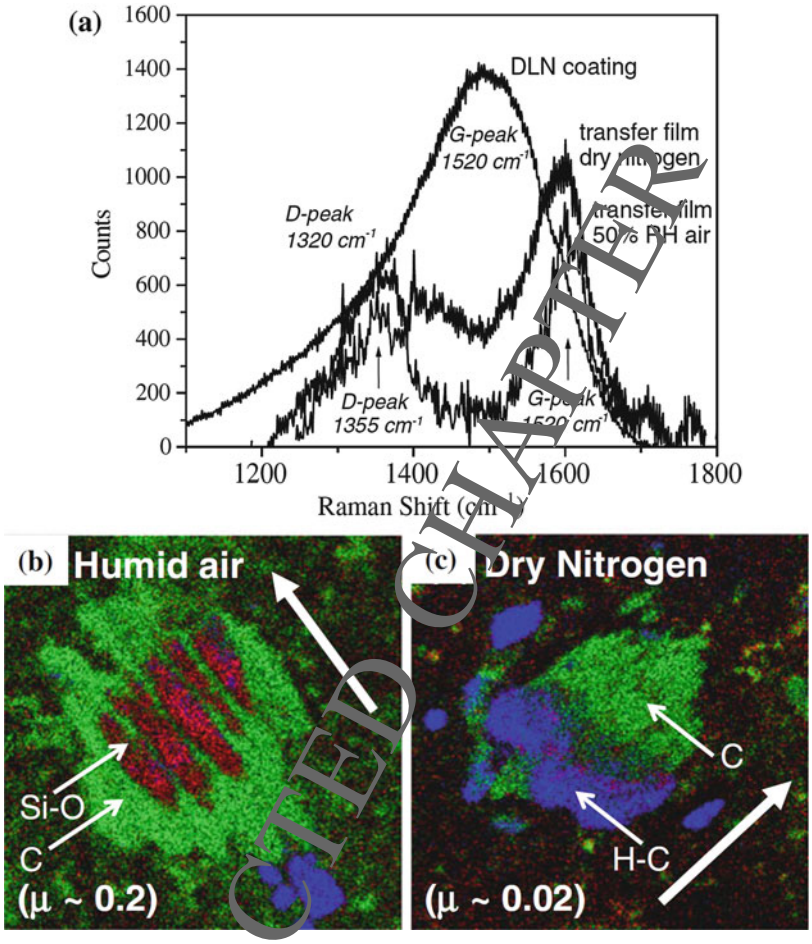

Fig. 1.8 (**a**) Raman spectra collected in spot mode of unworn DLN coating and transfer films generated in dry nitrogen and humid air. Time-of-flight SIMS (negative secondary ion image) maps of silicon oxide ($O + Si + SiO_2 + SiO_3$), long range carbon (C_1–C_4), and hydrogenated carbon ($CH + CH_2 + C_2H$) fragments on the counterfaces generated in (**b**) humid air and (**c**) dry nitrogen. The thicker arrows indicate the sliding direction with corresponding friction coefficients (l). The image size is 100 × 100 μm^2 [41]

film. As opposed to a modification in carbon structure, this slight width change may be indicative of a thicker transfer film formed in air than in dry conditions, which has been reported for DLN transfer films generated in humid versus dry air [15, 43].

Thus, in this particular case, Raman spectroscopy analyses were determined to be insensitive to near surface differences in the transfer film tribochemical products. Chemical mapping of the transfer films in Fig. 1.8b and c by time-of-flight secondary ion mass spectroscopy (ToF–SIMS) revealed differences in the tribochemistry of the transfer films. Long range ordered and more importantly hydrogenated carbon-

containing species are responsible for very low friction coefficients ($\mu \sim 0.02$) and interfacial shear strengths in dry nitrogen, while silicon and silicon oxide species lead to higher, but reasonable, value of $\mu \sim 0.2$, in humid air. Thus, it appears that DLN is able to adapt itself to both dry and humid environments, thus becoming an environmentally robust low friction coating. This link between interfacial tribochemsitry and the pressure-induced transfer film shear strength provided the chemical–mechanical mechanism for explaining friction and wear differences in different environments. These types of combined analyses are needed to unequivocally determine processing–structure–property interrelationships in solid lubricants.

1.5.8 Molybdenum Disulfide (MoS_2)

MoS_2 has a lamellar structure, easily sheared in the direction direction. Particle size and film thickness can be matched to surface roughness. MoS_2 solid lubricants offer:

- High load-carrying capacity
- Wide service-temperature range
- Excellent adhesion
- Protection against fretting corrosion
- Decreased friction with increasing loads
- Stick-slip prevention

Precaution: MoS_2 should not be used in wet environments; moisture can increase friction.

MoS_2 is a mined material found in the thin veins within granite and highly refined in order to achieve a purity suitable for lubricants. Just like graphite, MoS_2 has a hexagonal crystal structure with the intrinsic property of easy shear. MoS_2 lubrication performance often exceeds that of graphite and is effective in vacuum as well whereas graphite does not. The temperature limitation of MoS_2 beyond 300 °C is restricted by oxidation. The particle size and film thickness are important parameters that should be matched to the surface roughness of the substrate. Large particles may result in excessive wear by abrasion caused by impurities in the MoS_2; small particles may result in accelerated oxidation.

1.5.9 TMD and Adaptive Nanocomposites

Among the various members of the TMD family of compounds, MoS_2 and WS_2 are well known for their solid lubricating behavior and are widely used in several applications (Table 1.2). Their lubricating behavior stems from their intermechanical weakness, which is intrinsic to their crystal structure. Similar to graphite, MoS_2 crystallizes in the hexagonal structure where a sheet of molybdenum atoms is sandwiched between two hexagonally packed sulfur layers with a high c/a ratio ($c = 12.29$ A°, $a = 3.16$ A°), schematically shown in Fig. 1.9a [23, 46]. The bonding

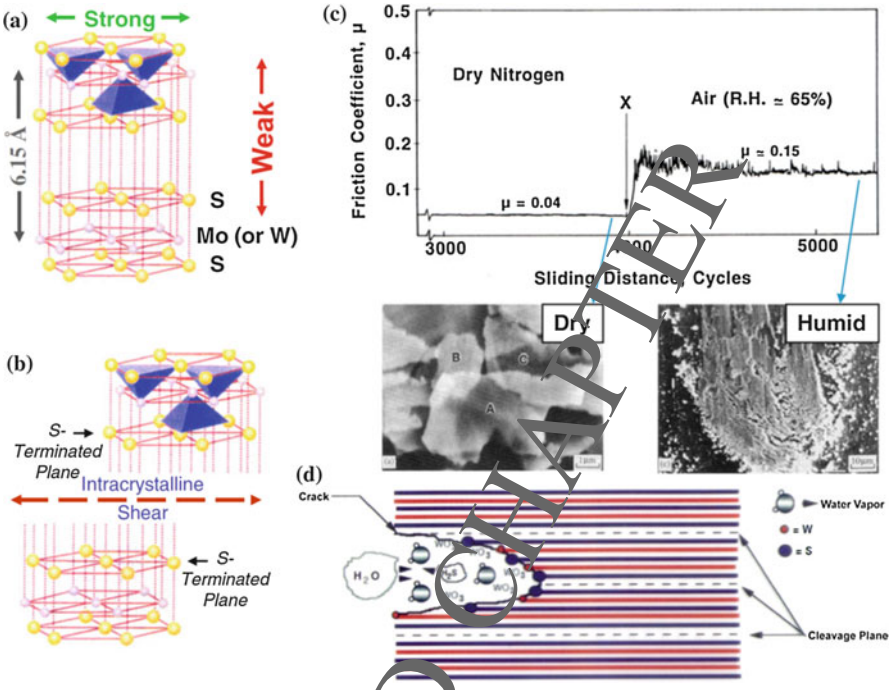

Fig. 1.9 (**a**) Lamellar crystal structure of Mo (or W) disulfide. (**b**) The weak VDW forces give rise to interlamellar mechanical weakness and hence easy shear (slip) between the planes. (**c**) Transition in friction coefficient of WS_2 from dry nitrogen to humid air accompanied by their transfer films on 440C SS counterface. In dry nitrogen, the weak VDW forces give rise to intracrystalline shear shown in b, while in humid air, WS_2 oxidizes and loses its ability to lubricate shown in (**d**) [44, 45]

within the S–Mo–S sandwich is covalent, while weak Van der Waals forces hold the sandwich together resulting in interlamellar mechanical weakness. Thus, under a shearing force the basal planes slide over one another by intracrystalline slip (same "deck-of-cards" shear as graphite), schematically shown in Fig. 1.9b; this leads to transfer film formation on the rubbing counterface. Therefore, the main mechanisms for imparting low interfacial shear in TMD are (a) creation of (0002) basal planes and subsequent (re)orientation parallel to the sliding direction and (b) the development of a transfer film on the counterface to accommodate interfacial sliding [47]. Both MoS_2 and WS_2 coatings exhibit extremely low friction coefficients ($\mu \sim 0.05$ or less) and long wear life (several million sliding cycles) when employed in either dry inert gas or in ultrahigh vacuum such that the coatings do not oxidize and/or react with water vapor, thereby preserving their intrinsic solid lubrication [23, 48, 49]. However, when sliding in humid air, higher friction coefficients (0.15–0.2) and extremely short wear life (typically less than a few thousand cycles) result, which is likely due to dangling or unsaturated bonds on the edge of basal planes reacting with moisture and oxygen in the environment to form tribooxidation products, such as MoO_3 and WO_3 [44, 48, 49]. For example, Fig. 1.9c shows the

friction behavior of a 1-μm thick pulse laser deposited (PLD) WS_2 coating in dry nitrogen and humid air [45, 50]. The transfer film shown in Fig. 1.9c (formed in dry nitrogen) consists of a stack of plate-like crystallites that lie flat on the steel ball. These platelets are thin enough (<60 nm) to be transparent to the electron beam and the features of the platelets B and C lying underneath the platelet A are partially resolved. The other transfer film shown in Fig. 1.9c (formed in humid air) is significantly different than the transfer film formed in dry nitrogen. It appears patchy and powdery in nature with portions of uncovered steel surface in the center. Analyses of the transfer films and wear scars by X-ray photoelectron and laser Raman spectroscopies indicate that oxidation of WS_2 to WO_3 during sliding in air, schematically shown in Fig. 1.9d, is a strong possibility, as is MoS_2 to MoO_3 [50, 51]. The same oxidation tribochemical reaction was shown for the transition metals in metal-doped DLC coatings [17, 52].

The ability of MoS_2 and WS_2 to form transfer films on the counterface implies that it is not necessary to coat both surfaces of the sliding couple; coating one contacting surface would suffice to generate low friction after the initial run-in period. In addition, it is not necessary to start with fully crystalline TMD coatings or with coatings that exhibit the preferred crystallographic texture of (0002) basal planes parallel to the sliding direction. Several experimental studies have confirmed that frictional stresses can induce crystallinity into MoS_2-based coatings that initially lack long-range order [53, 54] or result in reorientation of the TMD (0002) planes parallel to the sliding direction in as-deposited crystalline coatings [55]. Figure 1.10 shows these scenarios where the unworn coating has (a) crystallinity (basal planes perpendicular and/or parallel to the substrate) or (b) amorphous structure. Two structural evolution processes during friction are shown in Fig. 1.10 to achieve the same result. In sequence a → c → d, there is shear (sliding)-induced reorientation of perpendicular (or randomly oriented) basal planes parallel to the sliding direction to achieve low friction for a randomly orientated crystalline MoS_2/Au coating. While in sequence b → c → e there is an amorphous to crystalline transformation to basal planes parallel to the sliding direction to achieve low friction in an amorphous MoS_2/Sb_2O_3/Au coating [54].

Similar to the friction behavior trends (Fig. 1.9c), lower wear rates/factors are typically observed in dry conditions and higher values in humid conditions. As examples, wear factors of MoS_2 and MoS_2/Sb_2O_3/Au coatings are plotted as a function of sliding cycles in Fig. 1.11. The wear factors were computed on a cumulative basis. For example, the wear factors at 1000 cycles were calculated based on the volume of wear generated for 1000 cycles. Wear factors, although normalized for unit sliding distance, are not independent from the number of sliding cycles. For instance, the wear factor (in mm^3/Nm) of pure MoS_2 in dry nitrogen decreased from 2×10^{-6} at 1000 cycles to 7×10^{-7} at 10,000 cycles, implying that the initial wear rate was significantly higher than the steady state wear. In air, the wear factors for pure MoS_2 are higher than those in dry nitrogen (4×10^{-6} at 1000 cycles), and the data could not be extended for the entire 10,000 cycles since the pure MoS_2 coatings failed at ~4500 cycles. By comparison, the MoS_2/Sb_2O_3/Au composite coatings showed significantly improved wear factors in both dry nitrogen

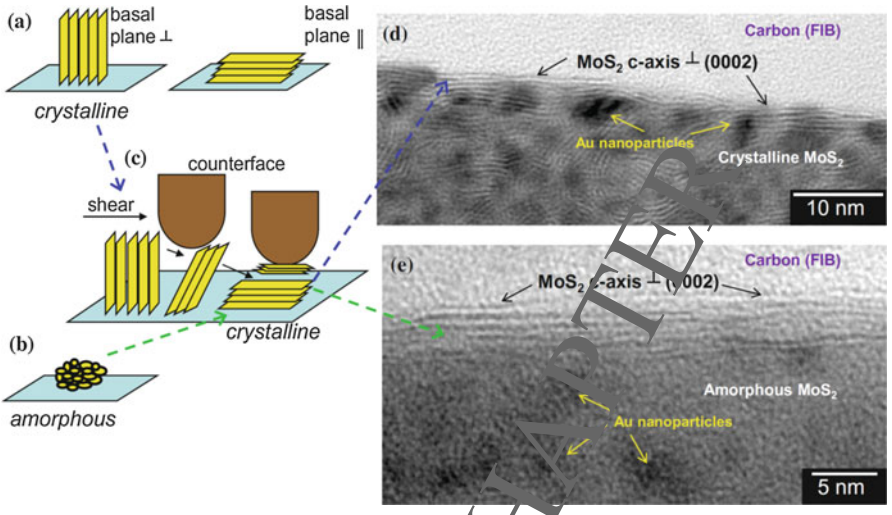

Fig. 1.10 Schematic representations of (**a**) two crystallographic growth textures with basal planes perpendicular or parallel (preferred) to the substrate, and (**b**) amorphous structure. The process of shear (sliding)-induced (a → c → d) reorientation of perpendicular (or randomly orientated) basal planes parallel to the sliding direction to achieve low friction, or (b → c → e) amorphous to crystalline transformation to achieve low friction. Corresponding cross-sectional TEM images inside the wear track of (**d**) crystalline MoS_2/Au coating (1000 sliding cycles, $P_m = 0.3$ GPa) and (**e**) amorphous MoS_2/Sb_2O_3/Au coating (10,000 sliding cycles $P_m = 0.7$ GPa) [5]

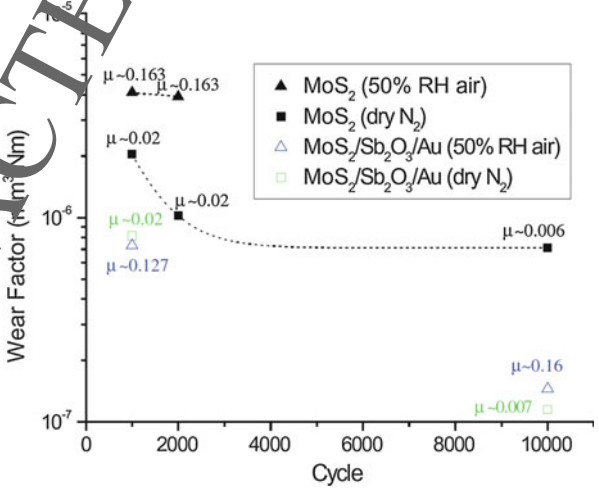

Fig. 1.11 Wear factor (and corresponding steady-state friction coefficients) of MoS_2/Sb_2O_3/Au and pure MoS_2 coatings on Si in dry nitrogen and air at 50% RH at a mean Hertzian contact stress of 1.03 GPa [54]

and air (50% RH) environments. For instance, the initial wear factor for the composite in dry nitrogen is 8×10^{-7}, which is roughly an order of magnitude lower than the pure MoS_2. A far more significant finding is that the steady-state wear factor for the composite in humid air is only marginally higher than in dry nitrogen at

10,000 cycles, confirming the environmental robustness of the composite compared to pure MoS_2.

In term of high temperature solid lubrication, TMD as single compounds do not exhibit low friction and wear for extended periods of time or thermal cycling due to formation of oxidation products, as discussed previously. In general, WS_2 is thermally stable to ~400 °C, while MoS_2 begins to oxidize above ~300 °C [48, 49]. Thus, composite coatings are being developed with other phases to decrease high temperature friction and wear. Other TMDs, such as diselenides and ditellurides of molybdenum and tungsten, have similar structure to MoS_2 and WS_2, but have not proved to be good solid lubricants and are of little technological interest.

There is an increasing demand for environmentally robust solid lubricant coatings that can adapt themselves to different environments [54, 56]. For instance, even if the targeted application is friction and wear mitigation in space, often the satellites and satellite launch vehicles wait for extended periods of time in humid coastal environments before launch, potentially exposing the moving mechanical assemblies to humidity. In view of this, there have been major studies aimed at developing multiphase, nanocomposite materials known as adaptive lubricants and chameleon coatings [56] because graphite, DLC, UNCD, and TMD cannot provide solid lubrication by themselves under varying degrees of humidity. Several metal or oxide dopants in MoS_2 have been successfully tried. Notable examples of dopants include: Ti, Al, Ni, Au, Pb, PbO, and Sb_2O_3. The presence of these dopants can lead to increased coating density, hardness, and oxidation resistance in humid environments compared to pure MoS_2. Among these, the previously discussed Sb_2O_3- and Au-doped MoS_2 nanocomposite coatings [55, 57, 58], shown in Figs. 1.6, 1.10, and 1.11, and other doped MoS_2 [59, 60] and WS_2 [61, 62] coatings are gaining acceptance as robust coatings for commercial use, including for satellite applications. Table 1.1 summarizes many of these characteristics.

1.5.10 Polytetrafluoroethylene (PTFE)

PTFE consists of carbon and fluorine atoms. Low surface tension makes this one of the most slippery manmade materials known. PTFE solids provide:

- Colorless film lubricity
- Low load-carrying capacity
- Low coefficient of friction at low loads
- Good chemical resistance
- Good sliding-friction reduction

PTFE is widely used as an additive in lubricating oils and greases. Due to the low surface energy of PTFE, stable unflocculated dispersions of PTFE in oil or water can be produced. Contrary to the other solid lubricants discussed, PTFE does not have a layered structure. The macromolecules of PTFE slip easily along each other, similar

to lamellar structures. PTFE shows one of the smallest coefficients of static and dynamic friction, down to 0.04. Operating temperatures are limited to about 260 °C.

1.5.10.1 Boron Nitride

Boron Nitride is a ceramic powder lubricant. The most interesting lubricant feature is its high temperature resistance of 1200 °C service temperature in an oxidizing atmosphere. Further, boron has a high thermal conductivity. Boron is available in two chemical structures, i.e., cubic and hexagonal where the last is the lubricating version. The cubic structure is very hard and used as an abrasive and cutting tool component.

1.6 Requirements to Solid Lubricants Properties

- Low shear strength in the sliding direction. This property provides low coefficient of friction due to easy shear movement of the lubricant material.
- High compression strength in the direction of the load (perpendicular to the sliding direction). A solid lubricant possessing high compression strength is capable to withstand high loads without sufficient direct contact between the rubbing surfaces.
- Good adhesion of the solid lubricant to the substrate surface. This property provides a presence of the solid lubricant on the part surface even at high shear stresses.

The best combination of the first two properties possess anisotropic materials like graphite, molybdenum disulfide, or boron nitride having lamellar crystal structure.

1.7 Characterization of Solid Lubricants

Advantages of solid lubricants:

- Ability to work under high loads
- High thermal stability
- Diversity of the application forms

Disadvantages of solid lubricants:

- Higher coefficient of friction and wear as compared to hydrodynamic regime
- Low stability of the lubrication film
- Less convenient system of the lubricant delivery to the friction surfaces. In contrast to solid lubricants fluid lubricants are continuously supplied, filtered, and cooled (Table 1.3)

Table 1.3 The most commonly used solid lubricants and their characteristics [18]

Solid lubricant	Characteristics
MoS_2	MoS_2 has a low coefficient of friction both in vacuum and atmosphere, and it does not rely on adsorbed vapors or moisture. Its thermal stability in nonoxidizing environments is acceptable to 1373 K, but in air the temperature limitation of MoS_2 may be reduced to a range of 623–673 K by oxidation. Adsorbed water vapors and oxidizing environments may actually result in a slight, but insignificant, increase in friction. MoS_2 has greater load-carrying capacity than other commonly used lubricants, such as graphite and PTFE. MoS_2 has a hexagonal crystal structure with the intrinsic property of easy shear. The lubrication performance of MoS_2 often exceeds that of graphite, and MoS_2 is effective in vacuum where graphite is not
Graphite	Graphite has a low coefficient of friction and very high thermal stability (2273 K and above). Graphite has a hexagonal crystal structure with the intrinsic property of easy shear, although graphite relies on adsorbed moisture or water vapors to achieve low friction. Use in dry environments, particularly in vacuum, may be limited. At temperatures as low as 373 K, the amount of water vapor adsorbed may be reduced to the point that low friction cannot be maintained, so sufficient water vapor may be deliberately introduced to maintain low friction. Practical application at high temperatures is limited to a range of 773–873 K because of oxidation. When necessary, additives composed of inorganic compounds may be added to enable use at temperatures to 823 K
PTFE[a]	PTFE has a low coefficient of friction both in vacuum and in atmosphere because of a lack of chemical reactivity. PTFE does not rely on adsorbed vapors or moisture. It possesses low surface energy and does not have a layered structure. The macromolecules of PTFE slip easily along each other, similar to lamellar structures. Practical application temperatures range from 173 to 523 K. PTFE does not have greater load-carrying capacity and durability than other alternatives. The low thermal conductivity of PTFE inhibits heat dissipation, which causes premature failure due to melting and limits use to low-speed sliding applications where MoS_2 is not satisfactory. PTFE shows one of the smallest coefficients of static and dynamic friction, down to 0.04. Operating temperatures are limited to about 523 K
Soft metals	Lead, gold, silver, copper, indium, and zinc possess relatively low coefficients of friction both in vacuum and in atmosphere because of their low shear strengths. These metals are extremely useful for high-temperature applications up to 1273 K and for rolling element applications, such as roller bearings, where sliding is minimal

[a]Polytetrafluoroethylene

1.8 Typical Applications

- Solid lubricants are useful for conditions when conventional lubricants are inadequate like reciprocating motion. A typical application is a sliding or reciprocating motion that requires lubrication to minimize wear as for example in gear and chain lubrication. Liquid lubricants will have squeezed out while solid lubricants do not escape and prevent for fretting corrosion and galling.

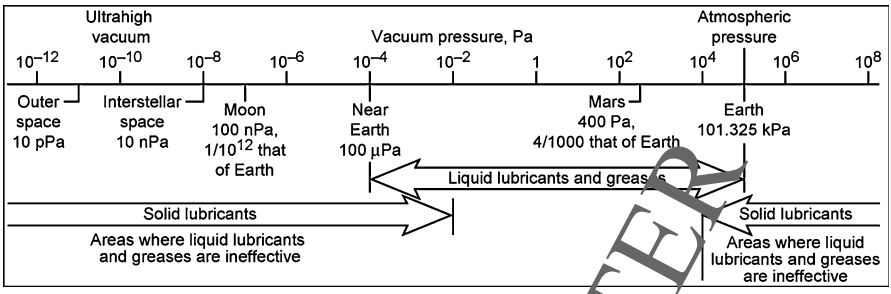

Fig. 1.12 Ranges of application of various lubricants in vacuum environments. (Figure has both solid and liquid lubricants) [18]

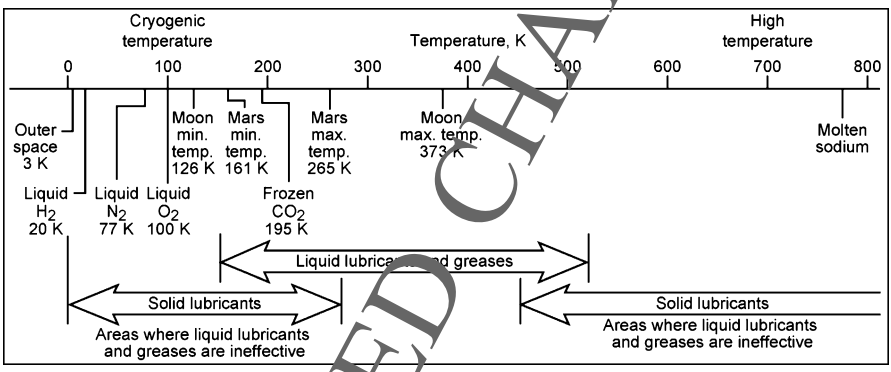

Fig. 1.13 Ranges of application of various lubricants in cryogenic and high-temperature environments. (Figure has both solid and liquid lubricants) [18]

- Another application is for the cases where chemically active lubricant additives have not been found for a particular surface, such as polymers and ceramics.
- Graphite and MoS_2 exhibit high temperature and oxidizing atmosphere environments, whereas liquid lubricants typically will not survive. A typical application includes fasteners which are easily tightened and unscrewed after a long stay at high temperatures.
- The lamellar structure orient parallel to the sliding surface resulting in high bearing-load combined with a low shear stress. Most applications in metal forming that involve plastic deformation will utilize solid lubricants (Figs. 1.12, 1.13, and 1.14, Table 1.4).

1.9 Solid Lubricant in Additive Oils

Nanoparticles as additives in base oil have been investigated widespreadly for tribology applications. It has been found that when the nanoparticles were added to base oil, the extreme-pressure property and load-carrying capacity are improved

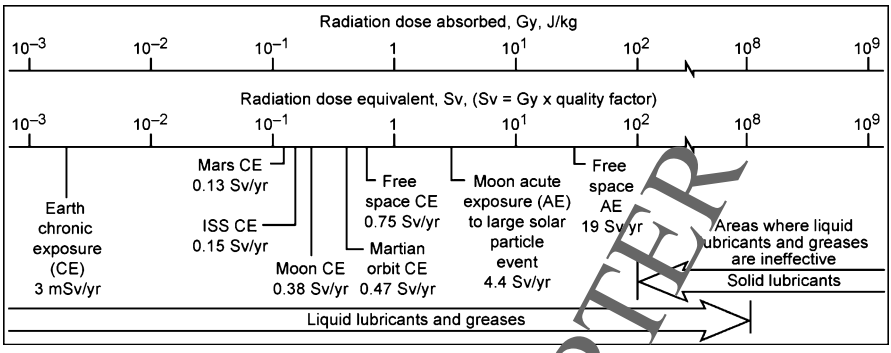

Fig. 1.14 Ranges of application of various lubricants in radiation environments. (Figure has both solid and liquid lubricants) [18]

Table 1.4 Advantages and disadvantages of solid lubricants [18]

Advantages	Disadvantages
Are highly stable in high-temperature, cryogenic temperature, vacuum, and high-pressure environments	Have higher coefficients of friction and wear than for hydrodynamic lubrication
Have high heat dissipation with high thermally conductive lubricants, such as diamond films	Have poor heat dissipation with low thermally conductive lubricants, such as polymer-base films
Have high resistance to deterioration in high-radiation environments	Have poor self-healing properties so that a broken solid film tends to shorten the useful life of the lubricant (However, a solid film, such as a carbon nanotube film, may be readily reapplied to extend the useful life.)
Have high resistance to abrasion in high-dust environments	May have undesirable color, such as with graphite and carbon nanotubes
Have high resistance to deterioration in reactive environments	
Are more effective than fluid lubricants at intermittent loading, high loads, and high speeds	
Enable equipment to be lighter and simpler because lubrication distribution systems and seals are not required	
Offer a distinct advantage in locations where access for servicing is difficult	
Can provide translucent or transparent coatings, such as diamond and diamondlike carbon films, where desirable	

and friction coefficient is decreased. At present, the viewpoint about mechanisms of nanoparticle additives is as follow: (1) ball effect [63, 64]; (2) tribochemical reactions [65–67], and (3) adsorption film theory [68]. Nanoparticles using as lubricating oil additive can improve the tribological properties of base oils. Commercially layered compound powders, usually as solid lubricants, dispersed in oil are also included [69–73]. The solid lubricants, such as MoS_2, dispersed in oil exhibited

beneficial effects by reducing the friction and wear [69, 70, 74]. Chu et al. [75] found that graphite existed on the rubbing surfaces stably and formed composition film with the oil-soluble additives. Bartz [72] found that an "optimal concentration" existed, and the wear rate actually increased with increasing the concentration over the optimal point of the solid lubricant dispersed in oil under heavily loaded conditions, and the larger the size of the solid lubricant particles, the larger the wear rate of surface. With fine particles at heavily loaded conditions, the lubricating effectiveness was improved. Bartz [72, 73] have found that the addition of solid lubricant to mineral oil can have beneficial or detrimental effects on the antiwear performance of these oils depending on the other types of additives in oils, particle hardness, and particle size of the solid lubricant.

1.10 Conclusion

Solid lubricants are critically important for safe and smooth operations of numerous tribological systems. Lamellar solids, soft metals, diamond and DLC films, lubricious oxides, and certain polymers are well-known solid lubricants. Their uses are expected to further increase in coming years, mainly because the operating conditions of future tribosystems are becoming more and more demanding and liquid and grease-type lubricants are undesirable due to environmental concerns. In modern applications, most solid lubricants are produced as thin solid films on sliding surfaces. Several PVD and CVD techniques are now available for the deposition of strongly bonded solid lubricant films on various kinds of substrates, including metallic, ceramic, and polymeric types. These techniques produce solid lubricant films in gradient, duplex, multiplex, and nanostructured or composite forms, resulting in better performance and durability under severe applications. In recent years, researchers have also prepared coatings that are designed to adapt to the changing conditions of tribological applications. These are called "adaptive" or "chameleon" solid lubricant coatings. As a novel approach, researchers have recently coupled solid lubricant films with smart surface engineering strategies (such as micro-texturing and/or micro-patterning) and thus achieved even higher levels of performance and durability under severe tribological conditions. For applications involving high temperatures, most layered solid lubricants appear ineffective. Certain lubricious oxides and fluorides may be used to combat friction and wear at high temperatures. A new generation of adaptive solid lubricant films was also shown to be effective in achieving lubrication at broader temperature ranges. Certain polymers are also used as solid lubricants because the attractive properties they combine are unavailable in other solid lubricants. Polymers are particularly favored for applications where cost, weight, corrosion, and biocompatibility are the major considerations. In short, solid lubricants have been around for a long time, and they have been meeting some very important and critical tribological needs. They are expected to be in high demand for many more years to come.

References

1. Rohatgi, P.K., Menezes, P.L., Lovell, M.R., Kailas, S.V.: Addition of solid lubricants to metal matrices and liquid lubricants to improve tribological performance. ASIATRIB (2014)
2. Tabor, D.: Friction – the present state of our understanding. J. Lubr. Technol. **103**(2), 169–179 (1981)
3. Rabinowicz, E.: Friction and Wear of Materials, 3rd edn, p. 34. Wiley, New York (1995)
4. Rabinowicz, E.: The determination of the compatibility of metals through static friction tests. ASLE Trans. **14**(3), 198–205 (1971)
5. Scharf, T.W., Prasad, S.V.: Solid lubricants: a review. J. Mater. Sci. **48**, 511–531 (2013). https://doi.org/10.1007/s10853-012-7038-2
6. Gao, G.T., Mikulski, P.T., Harrison, J.A.: Molecular-scale tribology of amorphous carbon coatings: effects of film thickness, adhesion, and long-range interactions. J. Am. Chem. Soc. **124**(24), 7202–7209 (2002)
7. Johnson, K.L.: Contact Mechanics. Cambridge University Press, Cambridge (1985)
8. Larsen-Basse, J.: ASM Handbook, Vol 18: Friction, Lubrication, and Wear Technology, p. 30. (1992)
9. Greenwood, J.A., Williamson, J.B.P.: Contact of nominally flat surfaces. Proc. R. Soc. Lond. A. **295**(1442), 300–319 (1966)
10. Whitehouse, D.J., Archard, J.F.: The properties of random surfaces of significance in their contact. Proc. R. Soc. Lond. **A316**(1524), 97–121 (1970)
11. Bower, A.F., Johnson, K.L.: The influence of strain hardening on cumulative plastic deformation in rolling and sliding line contact. J. Mech. Phys. Solids. **34**(4), 471–493 (1989)
12. Bowden, F.P., Tabor, D.: The Friction and Lubrication of Solids, pp. 112–120. Clarendon Press, Oxford (1986)
13. Stoyanov, P., Chromik, R.R., Goldbaum, D., Lince, J.R., Zhang, X.: Microtribological performance of Au–MoS2 and Ti–MoS2 coatings with varying contact pressure. Tribol. Lett. **40**(1), 199–211 (2010)
14. Stoyanov, P., Strauss, H.W., Chromik, R.R.: Scaling effects between micro- and macro-tribology for a Ti–MoS2 coating. Wear. **271–275**, 149–161 (2012)
15. Chromik, R.R., Wahl, K.J.: World Tribology Congress III, pp. 829–830. American Society of Mechanical Engineers, New York (2005)
16. Singer, I.L., Dvorak, S.D., Wahl, K.J., Scharf, T.W.: Role of third bodies in friction and wear of protective coatings. J. Vac. Sci. Technol. A. **21**(5), S232–S240 (2003)
17. Wahl, K.J., Sawyer, W.G.: Observing interfacial sliding processes in solid–solid contacts. MRS Bull. **33**(12), 1159–1167 (2008)
18. Miyoshi, K.: Solid Lubricants, and Coatings for Extreme Environments: State-of-the-Art Survey. NASA/TM – 2007-214668
19. Strauss, H.W., Chromik, R.R., Hassani, S., Klemberg-Sapieha, J.E.: In situ tribology of nanocomposite A–Si–C–H coatings prepared by PE-CVD. Wear. **272**(1), 133–148 (2011)
20. Schmellenmeier, H.: Exp. Tech. Phys. **1**, 49 (1953)
21. Robertson, J.: Amorphous carbon. Adv. Phys. **35**(4), 317–374 (1986)
22. Erdemir, A., Donnet, C. (eds.): Tribology of Diamond-like Carbon Films: Fundamentals and Applications. Springer, New York (2008)
23. Eisenberg, S., Chabot, R.: Ion-beam deposition of thin films of diamondlike carbon. J. Appl. Phys. **42**(7), 2953–2958 (1971)
24. Braithwaite, E.R.: Solid Lubricants and Surfaces, p. 139. Clarendon Press, Oxford (1964)
25. Deacon, R.F., Goodman, J.F.: Lubrication by lamellar solids. Proc. R. Soc. Lond. A. **243**(1235), 464–482 (1958)
26. Roselman, I.C., Tabor, D.: The friction of carbon fibres. J. Phys. D. **9**(17), 2517 (1976)
27. Buckley, D.H.: Surface Effects in Adhesion, Friction, Wear and Lubrication. Elsevier, Amsterdam (1981)
28. Skinner, J., Gane, N., Tabor, D.: Micro-friction of graphite. Nature. **232**(35), 195 (1971)

29. Savage, R.H.: Graphite lubrication. J. Appl. Phys. **19**(1), 1–10 (1948)
30. Ramadanoff, D., Glass, S.W.: High-altitude brush problem. Trans. Am. Inst. Electr. Eng. **63**(11), 825–829 (1944)
31. Yen, B.K., Schwickert, B.E., Toney, M.F.: Origin of low-friction behavior in graphite investigated by surface x-ray diffraction. Appl. Phys. Lett. **84**(23), 4702–4704 (2004)
32. Tallant, D.R., Parmeter, J.E., Siegal, M.P., Simpson, R.L.: The thermal stability of diamond-like carbon. Diam. Relat. Mater. **4**(3), 191–199 (1995)
33. Robertson, J.: Diamond-like amorphous carbon. Mater. Sci. Eng. R. **37**(4–6), 129–281 (2002)
34. Grill, A.: Review of the tribology of diamond-like carbon. Wear. **168**(1–2), 143–153 (1993)
35. Erdemir, A., Donnet, C.: Tribology of diamond-like carbon films: recent progress and future prospects. J. Phys. D. Appl. Phys. **39**(18), R311 (2006)
36. Koidl, P., Wagner, C., Dischler, B., Wagner, J., Ramsteiner, M.: Plasma deposition, properties and structure of amorphous hydrogenated carbon films. Mater. Sci. Forum. **52**, 41 (1990)
37. Tamor, M.A., Vassell, W.C., Carduner, K.R.: Atomic constraint in hydrogenated "diamond-like" carbon. App. Phys. Lett. **58**(6), 592–594 (1991)
38. Donnet, C., Fontaine, J., Lefevre, F., Grill, A., Patel, V., Jahnes, C.: Solid state 13 C and 1 H nuclear magnetic resonance investigations of hydrogenated amorphous carbon. J. App. Phys. **85**(6), 3264–3270 (1999)
39. Weiler, M., Sattel, S., Giessen, T., Jung, K., Ehrhardt, H., Veerasamy, V.S., Robertson, J.: Preparation and properties of highly tetrahedral hydrogenated amorphous carbon. Phys. Rev. B. **53**(3), 1594 (1996)
40. Erdemir, A., Eryilmaz, O.L., Fenske, G.: Synthesis of diamondlike carbon films with superlow friction and wear properties. J. Vac. Sci. Technol. A. **18**(4), 1987–1992 (2000)
41. Erdemir, A.: Friction and wear of diamond and diamond-like carbon films. Proc. Inst. Mech. Eng. J. **216**(6), 387–400 (2002)
42. Scharf, T.W., Ohlhausen, J.A., Tallant, D.R., Prasad, S.V.: Mechanisms of friction in diamondlike nanocomposite coatings. J. Appl. Phys. **101**(6), 063521 (2007)
43. Donnet, C.: Recent progress on the tribology of doped diamond-like and carbon alloy coatings: a review. Surf. Coat. Technol. **100**, 180–186 (1998)
44. Sliney, H.E.: Solid lubricant materials for high temperatures – a review. Tribol. Int. **15**(5), 303–315 (1982)
45. Prasad, S.V., Zabinski, Tribology of tungsten disulphide (WS_2): characterization of wear-induced transfer films. J.S. J. Mater. Sci. Lett. **12**(18), 1413–1415 (1993)
46. Scharf, T.W., Singer, I.L.: Quantification of the thickness of carbon transfer films using Raman tribometry. Tribol. Lett. **14**(2), 137–145 (2003)
47. Prasad, S.V., Zabinski, J.S.: Lubricants: super slippery solids. Nature. **387**(6635), 761 (1997)
48. Singer, I.L.: In: Singer, I.L., Pollock, H.M. (eds.) Fundamentals of Friction: Macroscopic and Microscopic Processes, p. 237. Kluwer, Dordrecht (1992)
49. Brainard, W.A.: The thermal stability and friction of the disulfides, diselenides, and ditellurides of molybdenum and tungsten in vacuum. NASA TN D5141 (1969)
50. Prasad, S.V., Zabinski, J.S., McDevitt, N.T.: Friction behavior of pulsed laser deposited tungsten disulfide films. Tribol. Trans. **38**(1), 57–62 (1995)
51. Zabinski, J.S., Donley, M.S., Prasad, S.V., McDevitt, N.K.: Synthesis and characterization of tungsten disulphide films grown by pulsed-laser deposition. J. Mater. Sci. **29**(18), 4834–4839 (1994). https://doi.org/10.1007/BF00356530
52. Chromik, R.R., Strauss, H.W., Scharf, T.W.: Materials phenomena revealed by in situ tribometry. J. Manag. **64**(1), 35–43 (2012)
53. Muratore, C., Bultman, J.E., Aouadi, S.M., Voevodin, A.A.: In situ Raman spectroscopy for examination of high temperature tribological processes. Wear. **270**(3–4), 140–145 (2011)
54. Wahl, K.J., Dunn, D.N., Singer, I.L.: Wear behavior of Pb–Mo–S solid lubricating coatings. Wear. **230**(2), 175–183 (1999)
55. Scharf, T.W., Kotula, P.G., Prasad, S.V.: Friction and wear mechanisms in MoS2/Sb2O3/Au nanocomposite coatings. Acta Mater. **58**(12), 4100–4109 (2010)

56. Hu, J.J., Wheeler, R., Zabinski, J.S., Shade, P.A., Shiveley, A., Voevodin, A.A.: Transmission electron microscopy analysis of Mo–W–S–Se film sliding contact obtained by using focused ion beam microscope and in situ microtribometer. Tribol. Lett. **32**(1), 49–57 (2008)
57. Muratore, C., Voevodin, A.A.: Chameleon coatings: adaptive surfaces to reduce friction and wear in extreme environments. Ann. Rev. Mater. Res. **39**, 297–324 (2009)
58. Hilton, R., Fleischauer, P.D.: Applications of solid lubricant films in spacecraft. In: Metallurgical Coatings and Thin Films, 435–441 (1992)
59. Zabinski, J.S., Donley, M.S., Walck, S.D., Schneider, T.R., McDevitt, N.T.: The effects of dopants on the chemistry and tribology of sputter-deposited MoS2 films. Tribol. Trans. **38**(4), 894–904 (1995)
60. Teer, D.G.: New solid lubricant coatings. Wear. **251**(1–12), 1068–1074 (2001)
61. Fox, V.C., Renevier, N., Teer, D.G., Hampshire, J., Rigato, V.: The structure of tribologically improved MoS2–metal composite coatings and their industrial applications. Surf. Coat. Technol. **116**, 492–497 (1999)
62. Scharf, T.W., Prasad, S.V., Dugger, M.T., Kotula, P.G., Goeke, R.S., Grubbs, R.K.: Growth, structure, and tribological behavior of atomic layer-deposited tungsten disulphide solid lubricant coatings with applications to MEMS. Acta Mater. **54**(18), 4731–4743 (2006)
63. Tarasov, S., Kolubaev, A., Belyaev, S., Lerner, M., Tepper, F.: Study of friction reduction by nanocopper additive to motor oil. Wear. **252**, 63–69 (2002)
64. Xu, T., Zhao, J., Xu, K., Xue, Q.: Study on the tribological properties of ultradispersed diamond containing soot as an oil additive. Tribol. Trans. **40**(2), 178–182 (1997)
65. Dong, J.X., Hu, Z.S.: A study of the anti-wear and friction-reducing properties of the lubricant additive, nanometer zinc borate. Tribol. Int. **31**(5), 219–223 (1998)
66. Liu, W., Chen, S.: An investigation of the tribological behaviour of surface-modified ZnS nanoparticles in liquid paraffin. Wear. **238**, 120–124 (2000)
67. Chen, S., Liu, W., Yu, L.: Preparation of DDP coated PbS nanoparticles and investigation of the antiwear ability of the prepared nanoparticles as additive in liquid paraffin. Wear. **218**, 153–158 (1998)
68. Xue, Q., Liu, W., Zhang, Z.: Friction and wear properties of a surface-modified TiO_2 nanoparicle as an additive in liquid paraffin. Wear. **213**, 29–32 (1997)
69. Gansheimer, J., Holinski, R.: Molybdenum disulfide in oils and greases under boundary conditions. ASME J. Lubr. Technol. **95**, 242–248 (1973)
70. Wo, H., Hu, K., Hu, X.: Tribological properties of MoS_2 nanoparticles as additive in a machine oil. Tribology. **24**(1), 33–37 (2004)
71. Bartz, W.J.: Solid lubricant additive-effect of concentration and other additives on antiwear performance. Wear. **17**, 421–432 (1971)
72. Bartz, W.J.: Some investigation on the influence of particle size on the lubrication effectiveness of molybdenum disulfide. ASLE Trans. **15**, 207–215 (1972)
73. Bartz, W.J., Oppelt, J.: Lubricating effectiveness of oil-soluble additives and molybdenum disulfide dispersed in mineral oil. Lubr. Eng. **36**(10), 579–585 (1980)
74. Cusano, C., Sliney, H.E.: Dynamics of solid dispersions in oil during the lubrication of point contacts. Part I. Graphite. ASEM Trans. **25**(2), 183–189 (1982)
75. Chu, S., Jin, Z., Xu, Q.: Study of the interaction between natural flake graphite and oil soluble additives. Tribology. **17**(4), 340–347 (1997)

Tribology of Self-Lubricating Metal Matrix Composites

2

Yinyin Zhang and Richard R. Chromik

Contents

Abstract

Self-lubricating metal matrix composites (SLMMCs) are a class of materials that have potential to help engineers meet the demands of global initiatives for green

Y. Zhang · R. R. Chromik (✉)
Department of Mining and Materials Engineering, McGill University, Montreal, QC, Canada
e-mail: Richard.chromik@mcgill.ca

P. L. Menezes et al. (eds.), *Self-Lubricating Composites*,
https://doi.org/10.1007/978-3-662-56528-5_2

manufacturing and sustainability. While SLMMCs have existed for many decades with traditional lubricant materials like graphite and other lamellar solids, such as MoS_2, WS_2, h-BN and CaF_2, BaF_2, scientists have recently incorporated nano-structured versions of the materials (e.g., carbon nanotubes and graphene). At the same time, new manufacturing and processing techniques have come online, such as additive manufacturing techniques that may provide significant innovation for SLMMCs. In this chapter, the current state of SLMMC research is reviewed, including materials, processing methods, and tribological performance. Processing and property relationships are described, such as influence of testing parameters and content of solid lubricants on friction and wear. Improvements in tribological behavior, as much as possible, are interpreted through third-body approach, which emphasizes materials phenomena at the sliding interface – including mechanical, structural, and chemical changes to the parent materials. Based on the review of SLMMCs and their tribology, recommendations for future research are made that emphasize the use of new materials, new processing routes, and research approaches that seek to reveal more completely the mechanisms by which these materials form tribofilms that are effective at lowering friction and reducing wear.

2.1 Introduction

Modern technology has placed materials into increasingly demanding and harsh environments. To meet the needs of next-generation applications, scientists and engineers are tasked with designing new materials with sufficient life cycle and reliability. Higher forces, temperatures, and exposure to environmental corrosion and mechanical wear lead to the need for various design strategies involving increased mechanical properties both in the bulk and at the surface. One such strategy that can be used for both surface and bulk enhancement of properties is use of composite materials.

Composite materials make use of more than one material class with one acting as the matrix and the other as a reinforcing component. Historically, composites have been used for thousands of years, with the very first examples being mud and straw composites used for housing in Egypt and Mesopotamia (circa 1500 BC) [1]. Modern engineering composites can be found nearly everywhere in our daily life, with the most common variety being polymer matrix composites (PMC) used, for example, as bicycle frames, hockey sticks, and airframe materials. More often than not, modern composites are designed from a mechanical properties perspective, where the matrix alone does not have adequate strength and/or stiffness for the design requirements. The reinforcing component, which in the PMC example is often a glass or ceramic material, enhances mechanical properties by a load transfer or load-sharing mechanism. Alongside the development of PMCs, scientists and engineers developed metal-matrix composites (MMCs). Technologies to fabricate MMCs were developed in the 1970s with increasing adoption of these materials in various

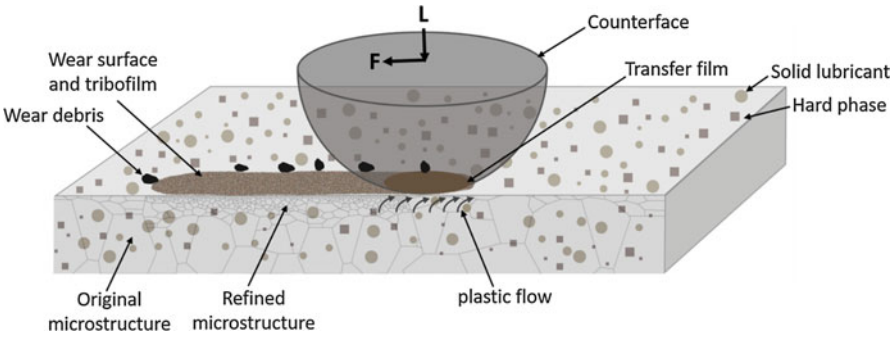

Fig. 2.1 A schematic of a bulk SLMMC that are under service. Solid lubricant–related tribofilms and, in some cases, transfer films are formed. Sliding usually generates refined microstructure on the subsurface of the wear track, and the plastic flow, shown as arrows underneath the counterface, promotes solid lubricant particles squeezing out to replenish the tribofilm and the transfer film

applications in the following decades [2, 3]. Reinforcing components in MMCs can take the form of hard materials such as ceramics or glasses, but may also be materials for enhancement of the surface properties, known as solid lubricants.

Composite materials are often employed for tribological applications, where wear resistance and control of friction are important. Self-lubricating metal matrix composites (SLMMCs) may be in the form of bulk composites [4, 5], thick coatings or claddings [6], or thin nanocomposite coatings [7, 8]. Figure 2.1 depicts the scenarios of a bulk SLMMC that contains solid lubricants to modify friction and hard phases to support load and reduce wear. Common hard ceramic phases are Al_2O_3 and SiC and common solid lubricants are graphite (Gr), MoS_2, h-BN, and many others. The latter impart "self-lubricating" (sometimes "auto-lubricating") properties to the MMC by the formation of lubricating tribofilms and, in some cases, transfer films at the contact that can be regenerated during in-service wear of the component. Here, tribofilm refers to a surface modified layer on the material being tested and transfer films refer to a modified layer attached to the counterface (as depicted in Fig. 2.1). SLMMCs are an important class of materials for future green manufacturing and engineering sustainability. Use of SLMMCs reduces the need for oil lubrication and reduces friction and thus the energy consumption in the systems where they are used. They can also mitigate wear and increase the lifetime of components.

2.2 Selected Tribology Concepts for Metals, Solid Lubricants, and SLMMCs

2.2.1 Third Bodies for Metals and Solid Lubricants

When two surfaces are brought together to form a sliding contact, mechanical and chemical interactions lead to the formation of what tribologists commonly refer to as "third bodies" [9, 10]. The characteristics of third bodies are dictated by the

parent materials (the two "first bodies" sliding against one another), the ambient environment and parameters such as load and sliding velocity. Once the third bodies form, their behavior in the tribological system often has a significant role in determining the friction and wear performance. As shown in Fig. 2.1, transfer films may form on the ball (i.e., "countersurface" or "counterface" material) due to adhesive wear processes. Tribofilms may form on the test material of interest. They may be due to mechanical and chemical modification of the parent material but may also be due to redeposition of transfer film material to the worn surface. Wear debris is third body material that leaves the contact and no longer participates in the sliding process. There are many other names given to third bodies in the open literature, including but not limited to mechanically mixed layers (MML), tribologically transformed structures (TTS), tribomaterial, transfer layer, fragmented layer, highly deformed layer, glaze layer, white-etching layer, and nanocrystal layer [11]. MML is a common terminology in metals tribology where work-hardened, nanocrystalline, and other transformed microstructures are found at the surface [12]. TTS is a terminology used to describe nascent materials that are about to leave the first body to become part of the third bodies in the contact [13, 14]. For this chapter, we restrict discussion to "transfer films," "tribofilms," and "wear debris" – three distinct types of third bodies as labeled in Fig. 2.1.

For decades, third bodies were studied primarily by ex situ methods, where after a laboratory scale test the first bodies were separated and the nature of these materials was examined with a variety of material characterization techniques [15]. More recently, scientists developed in situ methods that are capable of directly examining third bodies during the wear test. These techniques and the history of their development were recently reviewed by Chromik et al. [16] and Wahl and Sawyer [17]. Here we mention these techniques as they were key in demonstrating the importance of examining third body "processes" or third body "flows" and the concept of velocity accommodation [18]. This is especially true for solid lubricants [19–24], such as MoS_2 and DLC. More recently, the techniques have been used to study metals tribology [25–29], which also demonstrated the importance of third bodies in determining the performance of metals in sliding contact. The manner in which third bodies modify how velocity is accommodated between two surfaces in relative motion was described by Berthier et al., where 20 velocity accommodation mechanisms (sometimes "modes") were defined or identified based on experimental evidence [18, 30].

For the context of SLMMCs, understanding of third bodies and their formation is crucial. These materials are designed specifically to form and replenish tribofilms from the self-lubricating fillers within their matrix. The effectiveness of this process and the mechanisms by which it occurs are not always fully explored in the literature. In fact, it is only until recently that in situ tribology techniques have been applied to composite materials for nanocomposite PVD coatings [8] and MMCs [28, 29, 31]. Researchers have, however, used ex situ methods to investigate tribofilm formation on SLMMCs which have demonstrated their importance and role in lubrication and enhancement of the tribological properties [32–36]. It is also true that the nature of self-lubrication for an SLMMC is related to the same processes that occur for solid lubricant applied as coatings. However, the source flow of lubricating material is

potentially much less for an SLMMC and the third bodies that form, and their flows are expected to be substantially altered. As such it is worthwhile to have a short review of what is expected for self-lubrication when solid lubricants are applied as blanket films.

2.2.2 Solid Lubricants

Solid lubricants are a class of materials that provide a lower friction in comparison to standard tribological couples found in engineering systems, where the vast majority are metal-metal or metal-alloy type contacts [15, 37, 38]. The most popular solution is the use of oil lubrication, but in cases where this is not possible (e.g., space applications, open system), one may resort to the use of solid lubrication. The most common solid lubricants are lamellar type solids, such as Gr and a set of metal dichalcogenides (e.g., MoS_2, WS_2). However, there are many others [15] and it is also the case that soft metals (e.g., Pb, In, Au) are considered solid lubricants at elevated temperatures. All solid lubricants typically have a narrow range of effectiveness in term of environmental conditions such as temperature, humidity, and ambient pressure.

The mechanisms by which solid lubricants provide low friction are always a topic of debate. However, scientists do agree on the basic concept of an interfacial shear strength. Figure 2.2 shows schematically the concept of modifying the friction by an interfacial film with lower shear strength than the bulk solid to which it is applied. Velocity is accommodated by the solid lubricant, which could be in the form of a coating or a tribofilm formed from a SLMMC. The velocity accommodation mode (VAM) can be: (i) interfacial sliding between a transfer film and tribofilm; (ii) the counterface material and the tribofilm (absent of transfer film); (iii) interfilm shearing of the transfer film, tribofilm, or both; or (iv) interfacial sliding between the counterface and wear track (absence of tribofilm and transfer film). For a blanket

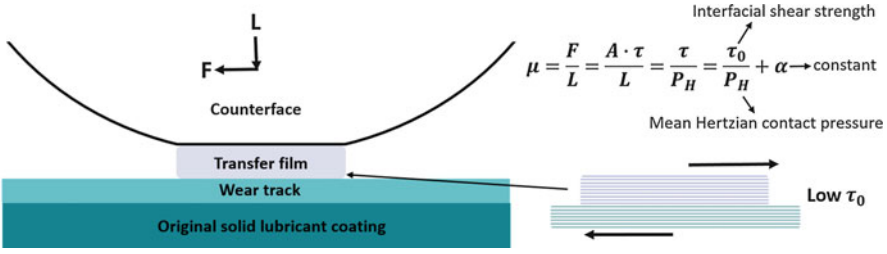

Fig. 2.2 A schematic of interfacial sliding along transfer film and wear track interface and how solid lubricants modify the friction by an interfacial film with low interfacial shear strength. The above expression for the friction coefficient is based on the classical theory of Bowden and Tabor, where friction force can be expressed as a product of real contact area (A) and shear strength of the lubricant material (τ). τ_0 is the interfacial shear strength, a "velocity accommodation parameter" which is a property of the interface, and α is the lowest attainable friction coefficient for a given friction couple [16, 38, 39]

coating of solid lubricants, the most common VAMs are (i) and (iii). For SLMMCs, where there is incomplete coverage of the wear track, all four can occur, but (ii) and (iv) are most common. Interfacial sliding of counterface versus the tribofilm is the mechanism of lubrication for SLMMCs. In the absence of solid lubricant in the tribofilm, interfacial sliding leads to higher friction, and adhesive and/or plowing wear, which provides a mechanism to release more solid lubricant materials from the subsurface of the SLMMCs.

For lubrication by carbonaceous species, there is extensive literature on diamond-like carbon coatings, which was recently summarized in [40, 41]. Carbonaceous films are quite common and also from other species such as oils, varnishes, and greases, as pointed out by Hoffman and Marks [42]. Historically, tribologists explained the lubricating effect from diamond-like carbon coatings as a "graphitization" process by which the initially amorphous coating formed tribofilms that transformed to Gr due to the temperatures and/or pressures induced by the sliding [43, 44]. Work by Scharf and Singer demonstrated the importance of formation of transfer films for a specific Si doped DLC [19, 21]. However, it is not the case that all DLC coatings behave the same way and in some cases one observes that transfer films are less important and tribofilms on the worn surface dominate the process [45]. Sometimes it is even the case that the dominant mechanism determining friction is near surface passivation state of the DLC. Recent computational simulations by Pastewka et al. [46] demonstrated that it is not always a graphitic structure that provides low friction. Sometimes it is sufficient to form sp^2 hybridized carbon from the sp^2/sp^3 matrix of the DLC coating. They also concluded that a passivation process was important for realizing low friction. Experimental observations of superlubricity in some DLC coating support these observations, where the surface termination is highly important for realizing the ultralow friction [47]. Other carbon species, such as graphene (G) or carbon nanotubes (CNTs), have been added as surface layers and resulted in lowered friction an improved tribological performance. Work by Berman et al. [48–51] has demonstrated outstanding lubricating effects by deposition of G onto metallic surfaces.

Coatings made from MoS_2 and WS_2 have been applied for many decades as solid lubricants, having been developed in the early days of the development of space technology [52]. This lamellar solid is most effective for low friction in vacuum or in the absence of humidity. Ambient conditions lead to a rise in friction and more rapid removal of the coating. The mechanism of the effect of humidity is debated in the literature, with some researchers showing evidence of the formation of Mo-oxides [53] and others demonstrating that friction between pristine MoO_3/MoS_2 interfaces is extremely small along the channel direction, which is formed by S atoms at the sliding surface, even smaller than that of MoS_2. The friction rise is due to the high energy barrier of MoO_3 (001) interlayer sliding that leads to an increase in the shear strength [54, 55]. The formation of transfer films is critical for the performance of these materials [8, 56, 57]. Recent work by Hoffman and Marks [58] demonstrated the mechanism for transfer film formation. It is also the case that even after wearing through an MoS_2 coating, low friction can persist by the presence of tribofilms and recirculation of MoS_2 debris back into the tribosystem [59]. Recent work by Lince

et al. demonstrated that other Mo-S compounds that have green manufacturing processes have promise to be as effective as MoS_2 [60]. Similar to carbon materials, MoS_2 and WS_2 have seen an evolution of their structure to make two-dimensional structure (e.g., like G) and nanoparticles/nanotubes [7, 61]. These materials have the possibility to be placed on surfaces for lubrication or added as filler materials in SLMMCs.

2.2.3 Incorporation of Solid Lubricants in MMCs

There is a long history of incorporation of solid lubricant materials into metal matrices. Graphite inclusions are the most extensively studied, with Rohatgi and coworkers carrying out much of the early work on Al-Gr composites fabricated by casting routes [2, 62–66]. Researchers have also incorporated MoS_2, WS_2, and h-BN into metals by powder metallurgy or other techniques [67–69]. Since the early years of manufacture of SLMMCs, which was primarily with casting and powder metallurgy methods, there have been significant advances in both alternative processing technologies and the materials themselves (e.g., Gr replaced by CNTs or G). In the end, regardless of processing route or material system, the fabrication of any SLMMC has a few key goals in mind. Firstly, the solid lubricant should be dispersed as homogeneously as possible and be unmodified by the processing. The actual volume fraction of the solid lubricant included is often a function of the application itself. This is because as the volume fraction of the solid lubricant increases, there is inevitably a detriment to the bulk mechanical properties. Often there may be some benefit to mechanical properties at low volume fractions, but at higher concentrations, the solid lubricant will result in softening. Thus, the second main goal is finding a balance of the lubricant content. Ideally, one requires a sufficient amount that there can be a sustainable lubricating tribofilm at the material's surface throughout its lifetime, but not so much lubricant that there is an unacceptable debit in mechanical properties. This is why one often finds SLMMCs that also include hard phases. The load-supporting nature of hard inclusions helps to overcome the debit in mechanical properties introduced by the solid lubricant. Many of the newly developed processing routes also seek to incorporate higher content of lubricant with better maintainability of mechanical properties. The remainder of this chapter will address the tribology of carbon-based and MoS_2/h-BN/WS_2/CaF_2/BaF_2 SLMMCs with special attention to the role of third bodies in determining the performance of these materials.

2.3 Synthesis of SLMMCs

Historically, Gr has been incorporated in metal matrices for many decades. This is especially true for Al and its alloys, where these materials have found applications as bearing surfaces, fan bushings and pistons and liners of internal combustion engines [4]. These materials can be fabricated in a relatively low-cost casting process [65, 70–73], infiltration techniques [63], or by powder metallurgy routes [74, 75]. More recently, newer processing methods have been developed including friction

Table 2.1 Summary of some fabrication methods for SLMMCs containing Gr, CNTs, or G

Carbon species	Fabrication method	Matrix materials	References
Gr	Stir casting	Al or Al alloy	[65, 70–73]
	Infiltration	Al or Al alloy	[63]
	Powder metallurgy	Al or Al alloy	[74, 75]
	Friction stir welding	Al or Al alloy	[76–82]
	Microwave sintering	Cu	[95]
CNTs	Powder metallurgy	Cu, Al	[99–101]
	Friction stir welding	Al or Al alloy	[76]
	Microwave sintering	Cu	[96]
	Cold spray	Cu, Al	[86–91, 102]
	Laser AM technique	Ni	[98, 103]
	Infiltration	Al	[104]
G	Sintering (spark plasma, semisolid, or laser)	Ni_3Al, Al alloy, Ti	[105–107]
	Powder metallurgy	Al	[108]
	Friction stir welding	Al or Al alloy	[76]

stir techniques [76–82], electrodeposition [83–85], thermal spray, cold spray [86–94], microwave sintering [95–97], and laser melting/additive manufacturing methods [98]. Some of these fabrication methods are more directed as fabrication of coatings (i.e., electrodeposition and thermal spray), while the remainder are directed at fabricating a bulk material. Cold spray is capable of producing coatings and also can be used as an additive manufacturing method to create near-net shape bulk parts. The manufacturing methods and materials for carbon-based lubricants were summarized in Table 2.1 according to the most recent literature, while Table 2.2 listed the most recent main techniques used for synthesis of MoS_2-, h-BN-, WS_2-, CaF_2-/BaF_2-SLMMCs. One may notice that manufacturing methods have a significant influence on material selection, microstructure of the matrix, stability of the solid lubricant reinforcement(s), as well as bonding mechanism between the matrix and the reinforcement(s). Powder metallurgy has been applied to a wide range of matrix materials such as Cu, Mg, steel, and Ni base alloy. Plasma spray and laser cladding can be used to fabricate superalloy–based composites because of high temperatures they are able to achieve. However, cold spray, due to its bonding mechanism (discussed in details later), while has been widely used for ductile metals deposition, is still under development for manufacturing superalloy coatings [119].

2.3.1 Powder Metallurgy

Powder metallurgy basically includes three steps: mixing, compacting, and sintering of mixtures consisting of matrix and reinforcement powders [64]. The current primary problems and challenges regarding fabrication of SLMMCs using powder

Table 2.2 Summary of most recent main synthesis of SLMMCs containing MoS_2, WS_2, h-BN, CaF_2, and BaF_2

Technique of synthesis	Processing temperature (°C) or material state	Matrix material	Solid lubricant(s)	Reference
Powder metallurgy	1200	Ni base alloy	Ag + h-BN	[109]
Powder metallurgy	600 and 1200	SS316L	h-BN, MoS_2	[36]
Powder metallurgy	530	Mg-TiC	MoS_2	[110]
Powder metallurgy	800	Cu-Sn	MoS_2	[111]
Plasma spray	Semi-liquid	NiCr-Cr_3C_2	h-BN	[112]
Plasma spray	Semi-liquid	WC-Co-Cu	MoS_2	[113]
Laser cladding	Liquid	Ni base alloy	WS_2	[114]
Laser cladding	Liquid	Co base alloy-TiC	CaF_2	[115]
Cold spray	Solid	Cu	MoS_2	[32, 116]
Cold spray	Solid	Ni	h-BN	[117, 118]

metallurgy are decomposition of solid lubricants due to high processing temperature, high porosity and poor bonding strength of the matrix and reinforcement(s), and manufacturing of self-lubricating MMCs for high temperature applications.

Decomposition of solid lubricants occurs because sintering temperatures are higher than oxidation or dissociation temperatures of commonly used solid lubricants, as shown in Table 2.3 [38, 120, 121]. For Cu-MoS_2 composites, sintering temperature above 780 °C causes decomposition of MoS_2 and formation of a brittle phase $CuMo_2S_3$ that is detrimental to tribological behavior [111, 122]. Figure 2.3 exhibits typical microstructure of SS316L-15 vol.% MoS_2 composite fabricated by powder metallurgy [36]. During sintering (1200 °C), MoS_2 phase was replaced by iron sulfide due to decomposition of MoS_2 and interaction with 316L. As the newly formed sulfides are not as lubricious as MoS_2 [123], some strategies have been employed to improve maintenance of solid lubricants. Adding alloying elements, i.e., phosphorus (admixed and pre-alloyed) and molybdenum (admixed), into steel matrix delayed, yet did not avoid, MoS_2 decomposition and reaction [123]. Moreover, h-BN or metal-coated h-BN was used to withstand high sintering temperature because of its high thermal and chemical stability [36, 124, 125]. However, due to the low wettability and poor sinterability, incorporation of h-BN into metal matrix led to slight decrease in mechanical property, i.e., hardness [36, 124–126]. Other solid lubricants exhibiting higher oxidation resistance could be potentially applied to stand high sintering temperatures.

Porosity and bonding strength between metal matrix and solid lubricant reinforcements are important material properties that have to take into account. Inadequate bonding occurs when sintering temperature is below melting point of

Table 2.3 Oxidation or decomposition temperatures of selected solid lubricants

	Gr	MoS_2	WS_2	h-BN	(Ca, Ba)F_2
Oxidation/°C	325	370	539	>700	~600

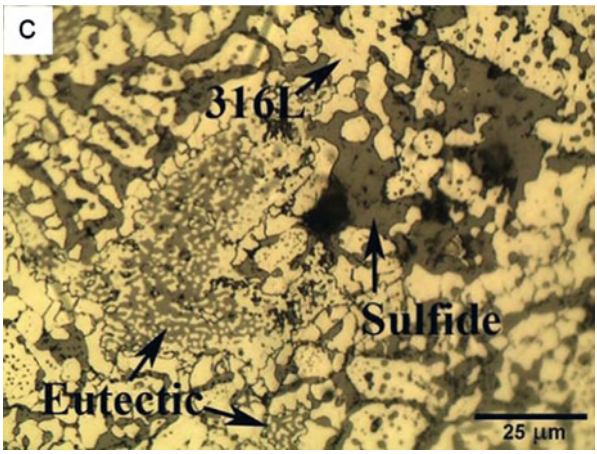

Fig. 2.3 An optical micrograph of cross section of SS316L-15 vol.% MoS_2 composite fabricated by powder metallurgy. Reprinted from [36], with permission from Elsevier

metals. In order to improve it, hot pressing, which performed sintering under a high pressure, and spark plasma sintering, which produced a high heating rate (up to 100 °C/min), were used to effectively decrease porosity and improve bonding strength [64, 127]. Glow discharge sintering is a relatively new technique that uses abnormal glow discharge plasma to generate a rapid and accurate heating process and reduce porosity [128]. Finally, post-treatment such as extrusion improved density and hardness of Cu-Sn-MoS_2 composites [123].

2.3.2 Laser Surface Cladding (LSC)

Due to a recent reduction in cost of laser equipment, researchers have devoted efforts on research and development on laser cladding process [129]. During LSC, an alloy or a composite layer is fused onto the surface under a coherent and high intensity laser beam irradiation [129]. The melt pool temperature can achieve as high as 2000 °C by using extremely high power density [129]. Critical processing parameters include mixing of the feedstock powders, heating rates, convection, diffusion, and cooling rates [129]. A significant difference between LSC and other coating techniques is its strong bond between coating and substrates due to the fact that substrate is partially melted into melt pool and participate in coating development. Therefore, there is no significant interface visible between the substrate and coating. For fabrication of self-lubricating MMCs, LSC has recently been employed to produce superalloy–based composites for high temperature applications [33, 114]. A major problem of LSC applied to solid lubricants is decomposition and

vaporization during the high temperature laser processing. It has been observed that MoS_2 dissociated and interacted with matrix materials in the melting pool [130, 131]. Xu et al. fabricated Ni-TiC-MoS_2 composite on 1045 low carbon steel using laser cladding. MoS_2 was found to be decomposed to Mo and S, resulting in the formation of $Ni_{2.5}Mo_6S_{6.7}$, intermetallic $Mo_{0.84}Ni_{0.16}$, and binary element sulfides (Ni_3S_4, NiS_2, Ni_3S_2, NiS) [130]. Generally, there are two methods to improve the decomposition. First of all, solid lubricants having higher oxidation resistance and melting points such as h-BN, WS_2, CaF_2, and BaF_2 have been observed to have a higher recovery in the final composites [33, 115, 127, 132–134]. Moreover, feedstock pretreatments such as encapsulation solid lubricants with metal by high energy milling or electroless plating reduced effectively decomposition and vaporization of solid lubricants [132, 135–137].

2.3.3 Thermal Spray

In this method, melting or semi-melting metal particles are co-sprayed with solid lubricants. Ni base alloys and WC-Co have recently been sprayed with MoS_2, h-BN, as well as (Ca, Ba)F_2 [112, 113, 139–142]. Figure 2.4 shows typical gas temperature and particle velocity of thermal spray techniques and cold spray [138]. The biggest challenge of the current thermal spray techniques is to prevent solid lubricant from decomposition and interaction to the matrix material during high temperature processing. Metal-coated solid lubricant prepared by ball milling or hydrogen reduction followed by alloying method helped to retain MoS_2 and h-BN in the composite coating [112, 113]. However, due to poor wettability of h-BN with melt metals, real interparticle contact surface and bonding strength decreased with h-BN, and 10 wt% of h-BN was found to destroy the continuity of Ni_3Al matrix [142]. Detonation gun spray, due to its relatively lower heat input and higher particle speed, could potentially minimize MoS_2 decomposition [140].

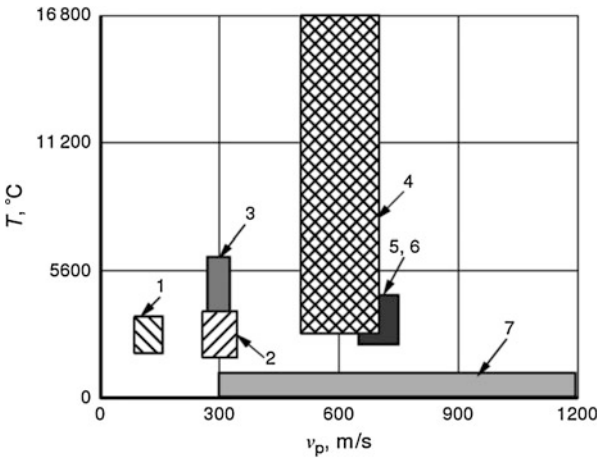

Fig. 2.4 Diagram of jet temperatures (T) and particle velocities (*v*p) used in thermal spray and cold spray methods. *1* low velocity gas plasma; *2* high velocity gas plasma; *3* electric arc; *4* plasma; *5*, *6* detonation and high velocity oxy-fuel (HVOF); and *7* cold spray. Reprinted from [138], with permission from Elsevier

2.3.4 Friction Stir Processing (FSP)

Friction stir processing (FSP) is a solid state process aiming to modify microstructures of a single or multiple workpieces and to fabricate MMCs [81, 143]. A specially designed rotating pin is inserted into the material with a proper tilt angle, and moving along the designed path. Rotation of the pin stirs the metallic surface and generate friction and plastic deformation heat, leading to a mix of the surface material (i.e., coated powder) and the metallic matrix [76, 81]. The mix then flows to the back of the pin, where it is extruded and forged behind the tool, and eventually consolidates and cools down under hydrostatic pressure conditions [81]. FSP is an excellent method to fabricate MMCs showing well-dispersed solid lubricant and/or ceramic reinforcements and improved mechanical properties [76–82]. Gr, G, CNTs, and MoS_2 have been incorporated into aluminum alloy by FSP and these composites exhibited improved mechanical property and tribological performance [76–82, 144]. Hybrid composites including solid lubricant and ceramics such as SiC and Al_2O_3 have been developed successfully by FSP on aluminum alloy surface [76–82, 144]. However, FSP has been mainly applied for aluminum MMCs so far. New applications of FSP to other metallic materials are under development [81].

2.3.5 Cold Spray

Cold spray, or cold gas-dynamic spray, is a solid state deposition process by exposing a suitable substrate to a high velocity (300–1200 m/s) jet of particles, which are generally metals or blends of metals and other materials [119, 146, 147]. The powders are accelerated by a high pressure gas jet through a de Laval nozzle [119, 146, 147]. Upon impact, the metallic particles that achieve a critical velocity undergo adiabatic shear instability, leading to metallurgical bonding, and consequently buildup of a coating [146–148]. The impact phenomenon and comparison with a wide range of other types of impact is summarized in Fig. 2.5, that points out the cold spray deposition possibly occurs within a typical particle size range of 5–150 μm at an impact velocity of 300–1200 m/s, which forms the cold spray regime [145]. Low temperature and high speed deposition make it very attractive for oxidation and heat sensitive materials and to fabricate high density composites [138, 149]. Even though cold spray has been discovered early in 1980s and successfully used for metals and metal-ceramic composites, its application to SLMMCs has just begun [146, 147, 150]. Currently, there are two main research groups including Penn State University and McGill University that have investigated cold sprayability of solid lubricants with metals. Figure 2.6 shows an optical micrograph of cold sprayed Cu-MoS_2 composite using admixed Cu and MoS_2. MoS_2 was distributed along Cu particles, and it was demonstrated that under the optimized spraying condition, average MoS_2 content in the composite was around 2–3 wt%, lower than those fabricated by some of the other techniques, e.g., around

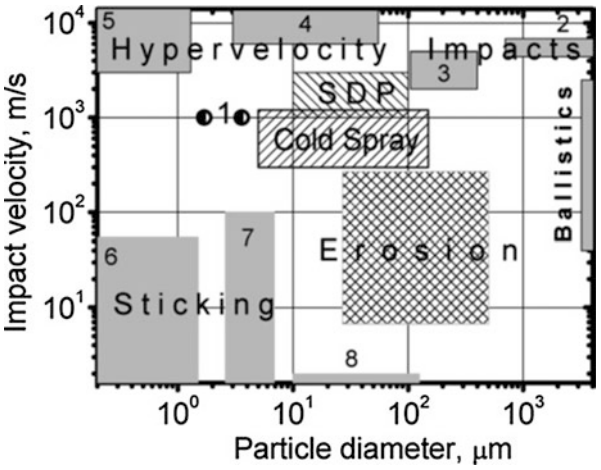

Fig. 2.5 Influence of impact velocity and particle size on material interaction upon impact of ductile metals or alloys with plane solid surfaces. Regions characteristic of impact phenomena are shown: *1*: no adhesion; *2, 3, 4,* and *5*: hypervelocity impacts; *6* and *7*: low-velocity impact; *8*: rebound; *SDP* super-deep penetration. Reprinted from [145], with permission from Elsevier Masson SAS. All rights reserved

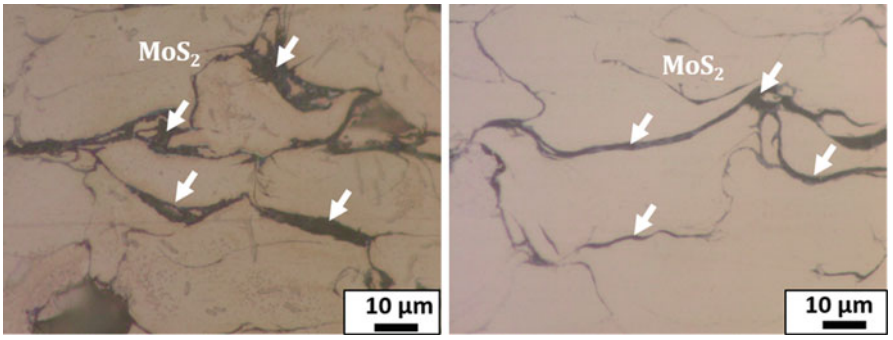

Fig. 2.6 Typical optical micrographs of cold sprayed Cu-MoS_2 composite using admixed Cu and MoS_2. Reprinted from [116], with permission from Springer

30 wt% MoS_2 can be achieved by powder metallurgy [32, 116, 133]. Deposition mechanism of Cu and MoS_2 composite during cold spray was proposed by Zhang et al. [116]. Presence of MoS_2 hindered extensive adiabatic shear instability of Cu occurring, leading to inadequate bonding between Cu particles, and therefore reduced mechanical property e.g., hardness of the composite [116]. Adding ceramic phase, e.g., WC to form hybrid composite Cu-MoS_2-WC could potentially improve mechanical property. Moreover, Ni-coated h-BN was fabricated by electroless process and used as feedstock to develop Ni-matrix h-BN composite. The size of solid lubricant core was found to play an important role on recovery of solid lubricant and bonding between particles. Nano-h-BN (100 nm) encapsulated with Ni helped to achieve around 10 vol.% h-BN retained in the composite [118, 151]. However, they observed 1 vol.% h-BN composite produced the best combination of friction and wear behavior [118, 151]. More extensive observation on bonding mechanism of the solid lubricant and metal particles, as well as its influence on tribological performance, is required.

2.4 Metal-Graphite, CNTs, Graphene SLMMCs

2.4.1 Advances in Materials (Gr → CNTs → G)

An aspect of the carbon-based SLMMCs that has changed over the years is the nature of the carbon species that is impregnated into the composite. In the early days, researchers were limited to Gr flakes as the only commercially available material. With the invention of carbon nanotubes in the 1980s followed by graphene in 2000s, there is now the possibility of including other forms of carbon in place of Gr flakes. The tribology of composites with carbon nanotubes is well researched, having been studied nearly since their invention with a recent review article published on the topic by Moghadam et al. [152]. Research on graphene-containing composites have only recently been demonstrated and carried out [82, 102, 107, 108, 153–156]. Limited information on the tribology of these materials has been published [76, 84, 85, 157–159]. However, for all of these additions, the intention is still that the carbon species will develop a tribofilm on the surface upon sliding.

2.4.2 Tribological Behavior of SLMMCs Containing Graphite, CNTs, and Graphene

The tribological behavior of Gr, CNTs, and G containing SLMMCs has been the subject of recent reviews by Omrani, Moghadam, and coworkers [4, 5, 152, 160]. Some general trends of friction and wear with material and test parameter for MMCs containing Gr are well understood, especially for Al matrices. With increasing Gr content in the composite, there is a reduction in friction coefficient. Figure 2.7a presents friction results versus Gr content for two separate studies by Akhlaghi et al. [161, 162]. Variation in the friction among the studies is related to changes in applied load and sliding velocity, but in general there is a consistent trend to lower friction with increasing Gr content. The trend is observed for the vast majority of literature on Al-Gr MMCs regardless of their method of manufacture. Similarly, for wear of the composite (see Fig. 2.7b), there is a decrease in wear with increase in the Gr content for a set of studies by Ravindran et al. and Suresha et al. [163, 164]. It should be noted that this trend is not always respected. That is, many authors have reported that as the Gr content is increased, eventually wear will increase. There is some optimum content of Gr to obtain both low friction and wear, above which wear will increase even if the low friction is maintained. This is generally related to a reduction in the mechanical properties of the composite with the increased Gr content, which can lend itself to enhance mechanical properties at low inclusion content but with large content, leads to a softening of the composite. In general, the effect can be more pronounced for composites produced by powder metallurgy as compared to those prepared by stir casting. Liu et al. prepared stir cast Al-50%Gr composites and saw a relatively good performance for both friction and wear [63]. However, for composites produced by powder metallurgy, Akhlaghi et al. observed an increasing trend in wear with increasing Gr content [4, 75].

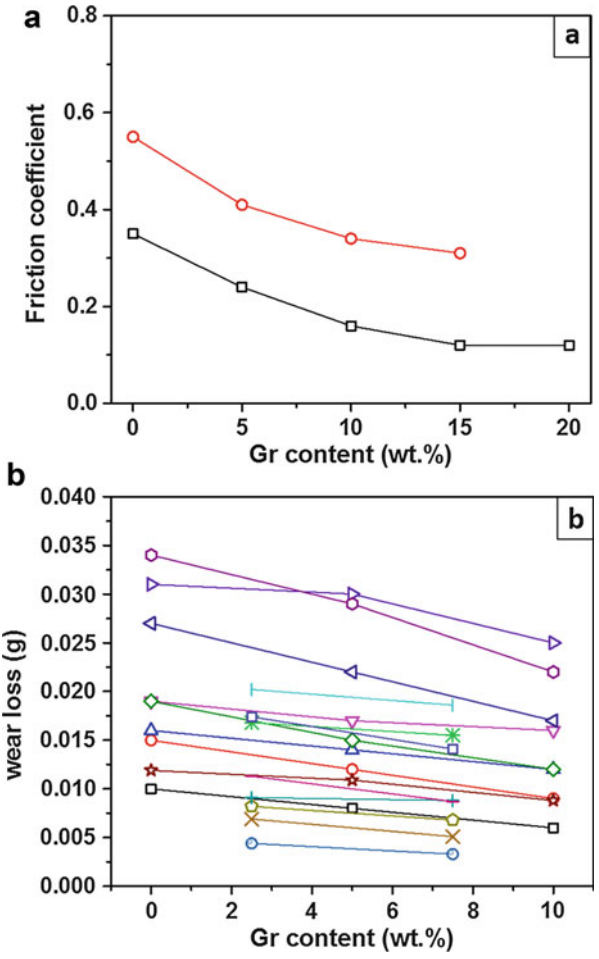

Fig. 2.7 The trends of (**a**) friction [161, 162] and (**b**) wear loss [163, 164] with Gr content in Al SLMMCs

To overcome this trend, they included SiC reinforcements to enhance the mechanical properties of the composite. This is a common strategy that can maintain acceptable wear rates at higher Gr concentrations.

More recently, researchers have mixed CNTs and G into MMCs. The remarkable mechanical properties of CNTs and friction properties of G led naturally to the research question of whether these carbonaceous reinforcements would lead to even better self-lubricating properties than Gr. Zhou et al. [104] studied the tribology of CNT in Al-Mg MMCs. Figure 2.8 demonstrated the reduction in friction and wear they observed with CNT. Similar reductions were also observed by Choi et al. on a CNT-Al composite [165]. One aspect of the inclusion of CNTs that is often not fully explored by all researchers is the state of the CNTs post-processing. Poirier et al. studied Al-CNT composites made by a mechanical milling process and discovered that nearly all of the CNTs were destroyed and had reacted to form carbides with the

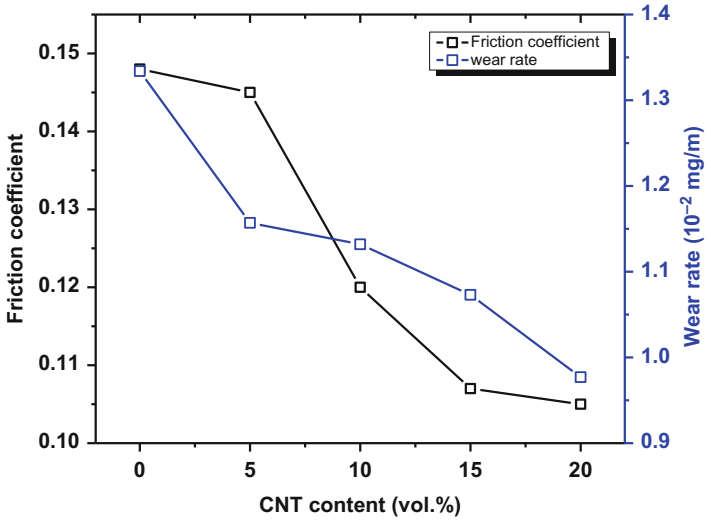

Fig. 2.8 Trends with CNT content in an Al composite made by powder metallurgy methods [104]

Al matrix [166]. Depending on the aggressiveness of the processing steps taken to create the composites, one may find retention of CNT as a distinct phase in the microstructure or instead the formation of carbides. Both Zhou et al. [104] and Choi et al. [165] showed evidence with transmission electron microscopy that nanotubes were retained in their composite in an unreacted state.

Only recently have researchers studied the inclusion of G in MMCs [76, 84, 108, 158, 167]. Ghazaly et al. [108] studied the tribology of Al-G composites and discovered the wear performance was not significantly improved. On the other hand, research on Ni-G composites showed a reduction in both friction and wear of the composite with an increase in G content [84]. Sometimes it is difficult to ascertain the effectiveness of a new materials due to differences in processing, matrix material, and test parameters. As such, it is very difficult at these early stages of G-based SLMMCs to determine whether the form of the carbon introduced in the composite affects significantly the tribological performance. However, a recent paper by Maurya et al. [76] provides a side-by-side comparison of Gr, CNT, and G reinforcements in a friction stir processed Al alloy. In Fig. 2.9, the friction trends they observed are presented. Gr and CNT additions had a similar reduction in the friction coefficient to about 0.4, while G lowered the friction to around 0.25. For the wear of the composite, they observed that all reinforcements reduced wear compared to the friction stir alloy without carbon additions. There was also a trend in wear depending on the carbon species, where G reduces the wear most followed by CNT and the least effective being Gr. While the authors conducted ex situ analysis of their wear scars, the precise mechanism of the differences in the performance of the three carbonaceous species was not identified. Future research on carbon-containing SLMMCs should certainly focus on more side-by-side comparisons between Gr, CNTs, and G.

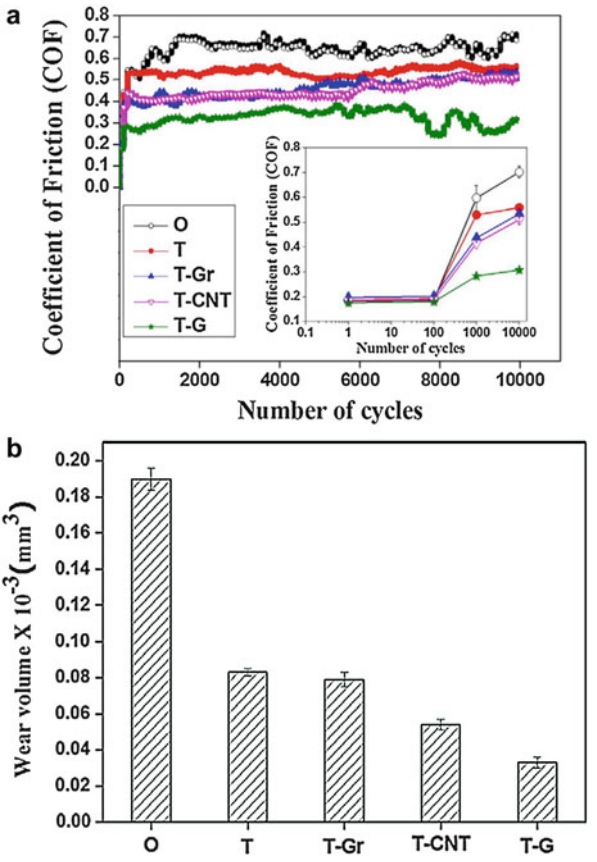

Fig. 2.9 Friction and wear trends with Gr, CNTs, and G composites made with Al6061 alloy with friction stir processing. Reprinted from [76], with permission from Elsevier

2.4.3 Tribofilms Observed for SLMMCs Containing Graphite, CNTs, or Graphene

Examination of worn surfaces after tribology testing can help to determine the wear mechanisms. In the case of SLMMCs, the comparisons between the composite and a pure version of the matrix material can explain the effectiveness of the solid lubricant in reducing friction and wear. Figure 2.10 are secondary electron images of worn surfaces on Al7075/Gr composites with increasing Gr concentration [168]. With no Gr, there is evidence of adhesive wear and plastic deformation on the worn surface. As Gr is introduced to the composite, evidence of this wear mechanism is reduced and instead a smoother worn surface with grooved features is observed. Many authors have explored the characteristics of the graphitic tribofilms formed on Al-Gr composites [63, 161, 163, 169–173]. General trends observed are that with increased Gr content in the composite, there is an enhancement of the tribofilm coverage of the surface that correlates with the reduction in friction. Interestingly, there is a significant lack of observation of the counterface materials in tribological

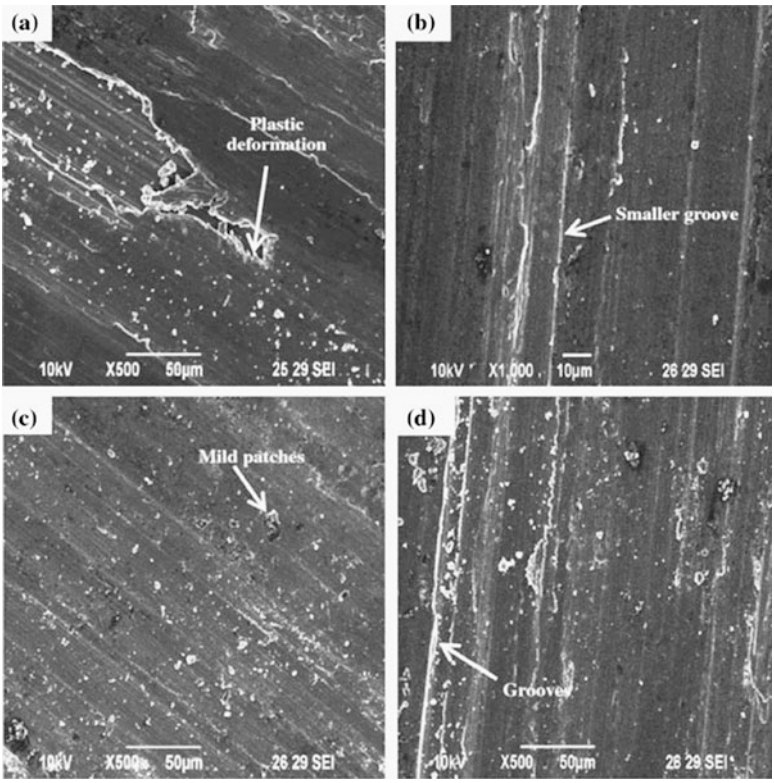

Fig. 2.10 Worn surfaces for an Al-Gr composites (**b**–**d**) with increasing Gr content, compared to the matrix alloy (**a**). Reprinted from [168], with permission from Elsevier

studies of these materials. Without information on transfer films, it makes it problematic to fully understand the third body flows and the mechanisms for replenishment of the graphitic tribofilm. Authors theorize that the replenishment comes from the subsurface of the composite, but tribofilms can also be replenished by recirculation flows between the counterface and wear track.

Similar trends in the appearance of the wear track morphology are also observed for CNT composites (see Fig. 2.11). As Zhou et al. [104] increased the CNT content in their composites, they observed a smoother wear surface. For only 5% CNT content, the wear track was rough and there was evidence of ploughed materials. For 10% and 20% addition of CNTs, the worn surface became smoother, with less evidence of ploughing. This was accompanied by reduction in friction and wear, as was presented above.

Carbon nanotubes can also be incorporated into a composite with cold spray methods. Bakshi et al. [89], using a composite powder, created Al-CNT composites and studied their tribology with a scratch tester. As can be seen in Fig. 2.12, the total wear volume of the scratch was decreased for all normal loads by the introduction of

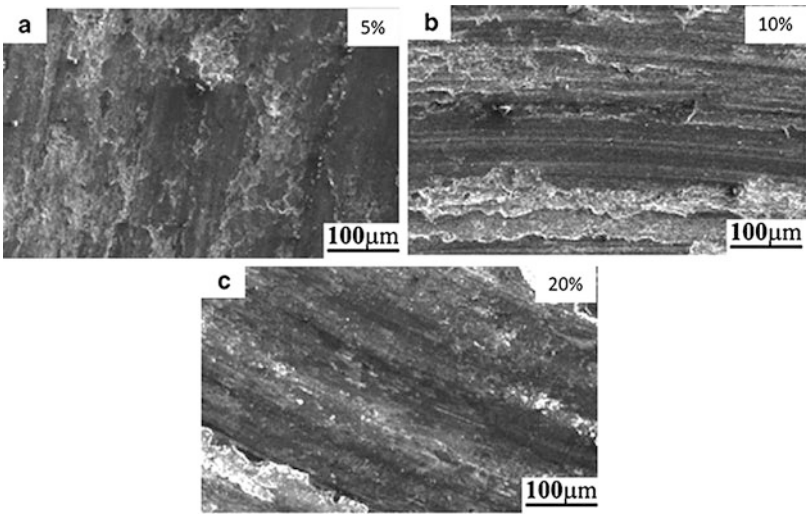

Fig. 2.11 Typical tribofilms observed for Al-CNT composites containing (**a**) 5%, (**b**) 10%, and (**c**) 20% CNTs made by powder metallurgy methods. Reprinted from [104], with permission from Elsevier

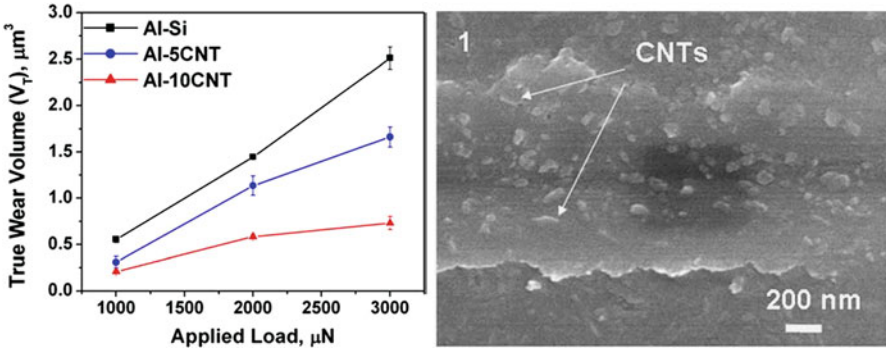

Fig. 2.12 Scratch testing wear results for an Al-CNT composite made by cold spray and corresponding observation of the worn surface with CNTs. Reprinted from [89], with permission from Elsevier

CNTs. The scratch track observed by SEM was found to have CNTs on the surface, which may have aided in the composite to resist wear during the scratch experiment.

Wear tracks can also be examined in cross sections, which can often give significant additional information on the exact nature of the material transformations in the tribofilms. These can be done as mechanical cross sections [169] but more recently can also be examined with focused ion beam (FIB) cross sectioning [98, 174, 175]. Figure 2.13 is an example of a mechanical cross-section of a wear track created on an Al alloy composite with 10% SiC and 4% Gr. In this study by Riahi

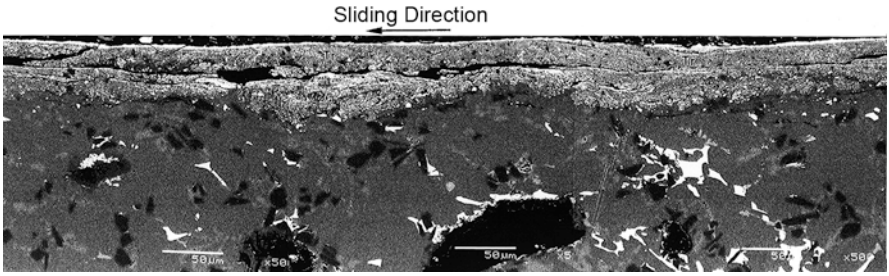

Fig. 2.13 Tribolayer observed on Al-10%SiC-5%Gr composite run against a steel-bearing material. The tribolayer in this case is primarily iron oxide with Al_3Ni and SiC particulates. Reprinted from [169], with permission from Elsevier

and Alpas [169], the composite was run in a block-on-ring test with a bearing steel, a tribo-test that more closely replicates the contact conditions the composite would encounter in service. Rather than high coverage of a carbonaceous tribofilm, the authors found that a thick tribofilm is formed that is composed of a mixture of iron and aluminum oxides, fractured SiC and intermetallic Ni_3Al, which is from the base alloy. Graphite did exist in these tribofilms, but clearly the mechanisms for lubrication and wear of this alloy are significantly more complicated than one can determine from observation of top-down wear track morphology, as was reviewed above.

Use of FIB microscopy in recent years allowed for high resolution observation of the cross section of worn surfaces and also provided the utility of being able to prepare TEM foils when desired. Use of these methods can better reveal the mechanisms for lubrication in SLMMCs. Figure 2.14 are cross sections prepared by FIB from a wear track on a Ni-3Ti-20C composite that was manufactured by laser additive manufacturing methods [98]. Each view is a region within the near surface of the wear track. Once can clearly observe an MML and distinct C tribofilm at the surface of all images. Also, striking is the observation of the mechanism of combined plastic deformation near surface and "wicking" of the carbon within the composite towards the surface to become part of the tribofilm. This observation is particularly interesting as the carbon can be brought to the surface without significant wear occurring but instead by simply the plastic deformation.

2.5 Metal-MoS_2, WS_2, h-BN, CaF_2, and BaF_2 SLMMCs

2.5.1 Tribological Behavior of SLMMCs Containing MoS_2, WS_2, h-BN, CaF_2, and BaF_2

Figures 2.15 and 2.16 summarized coefficient of friction observed in a number of different metal matrices of Cu, steel, Ni, and Ni-based alloy reinforced with MoS_2 and h-BN, respectively. The composites were fabricated by different manufacturing

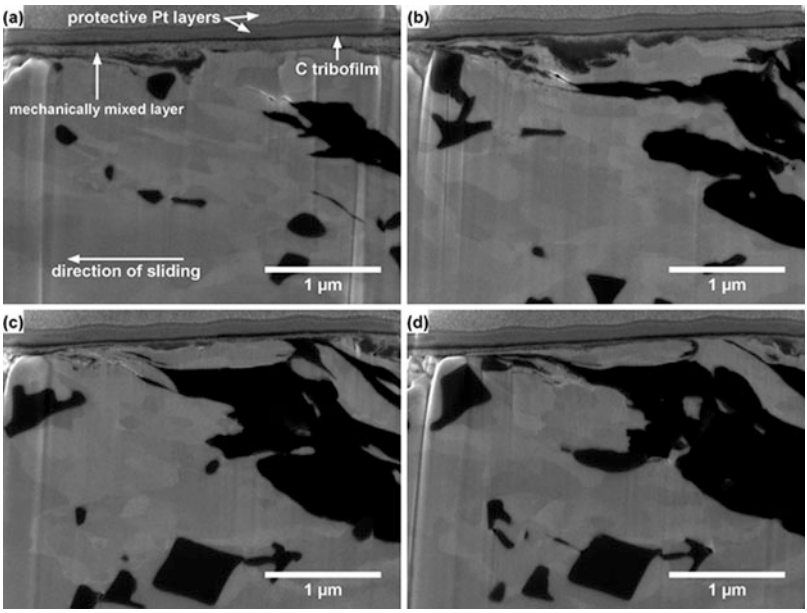

Fig. 2.14 Example of tribofilm formation in a Ni-3Ti-20C composite made by laser additive manufacturing methods. Reprinted from [98], with permission from Springer

methods such as powder metallurgy [34, 35, 122, 176], thermal spray [112, 142], cold spray [32], and laser cladding [132]. The tests were carried out with different tribometer configurations, mainly pin-on-disk and ball-on-plate, different normal loads, sliding speeds, and different counterface materials, e.g., different types of steels, Si_3N_4, alumina. Even though it is difficult to compare the absolute values due to the above variables, all the composites show some common trends. First of all, their coefficient of friction decreased with increasing solid lubricant content and then tended to keep constant or, in some cases, increased slightly. Early research carried out by Tsuya et al. demonstrated that in cold pressed Cu-MoS_2 composites, a minimum friction was reached at a MoS_2 concentration of 7–10% and remained fairly constant up to a concentration of close to 90% [179]. Similar trend was also observed in Gr reinforced SLMMCs by other researchers [64]. However, for the majority of the composites listed in Figs. 2.15 and 2.16, the lowest friction coefficient was around 0.4 or even higher. That is much higher than that sliding against blanket films of solid lubricants fabricated by physical vapor deposition and chemical vapor deposition, indicating metal matrix at the contact plays an important role. The effect of metal matrix component on friction coefficient has been analyzed theoretically by Rohatgi et al. [64]. The friction of an SLMMC can be written as

$$f = \left(1 - A_f\right) f_m + A_f f_f \tag{2.1}$$

Matrix	Cu	Cu	Ni-20Cr+W+Fe+C	Ni-20Cr+W+Al+Ti	316L
	◻	▷ ⬡	△ ○	▽	◁ ◇
Normal load (N)	5	40, 80	5	5	PV=1.1, 1.8
Sliding speed (m/s)	0.002	0.15	0.8	0.8	

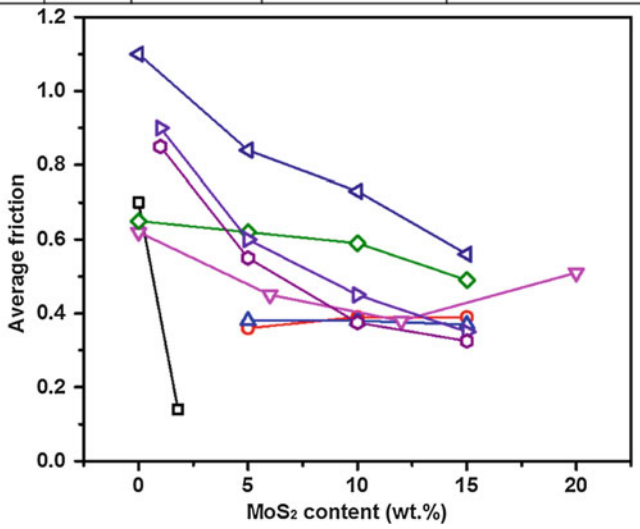

Fig. 2.15 Variation of average friction with content of MoS_2 for composites with different matrix materials and corresponding brief tribology testing parameters [32, 34, 35, 122, 176]

where A_f is fraction of lubricating tribofilm in the contact, f_f, f_m are friction coefficients of the lubricating tribofilm and matrix, respectively. Therefore, the coefficient of friction of composites may vary between f_m and f_f depending on solid lubricant content and ability of development and stability of lubricating film over sliding.

WS_2, BaF_2, and CaF_2 have been used as high temperature solid lubricants and incorporated with metals, e.g., Ni and Ni alloy using powder metallurgy techniques, plasma spray, and laser cladding. The coefficient of friction reduced significantly with even a small amount of solid lubricant in the composites, and this effect was even more pronounced at elevated temperatures [33, 114, 121, 135, 141]. The same trend was observed in wear rates. In general, BaF_2 and CaF_2 exhibit excellent wear resistance at a broad temperature range between room temperature and 1000 °C [112, 121], while WS_2 shows the lowest wear rate at 300 °C [33]. Strong matrix, combined with sulfides and fluorides, sometimes oxides formed at high temperature, are responsible for low friction and high wear resistance at high temperatures [121, 133]. It is worth to note that as the materials have to experience high temperature during fabrication, decomposition of solid lubricants are inevitable, even completely decomposed under some circumstances [114, 135]. However, some high temperature products, e.g., $CaCrO_4$ and $CaMoO_4$ (CaF_2 added

Matrix	Ni_3Al+Ag	Ni_3Al	Ni-20Cr+W+Mo+Al+Ti	Ni-20Cr+W+Mo+Al+Ti+Ag	NiCr+Cr_3C_2	Ni	Ni
	□	◇	△	▽	◁	○	▷
Normal load (N)	5	4.9	20	100	9.8	100	50
Sliding speed (m/s)	0.132	0.188	1	0.5	0.188	0.226	-

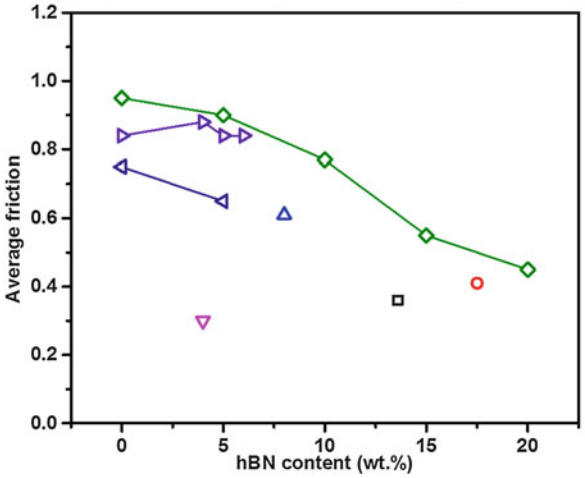

Fig. 2.16 Variation of average friction with content of h-BN for composites with different matrix materials and corresponding brief tribology testing parameters [109, 112, 118, 132, 142, 177, 178]

to Ni_3Al matrix), are lubricious and lead to improved tribological behavior at elevated temperatures [133].

Figure 2.17 shows wear rate evolution with solid lubricant content for composites with various matrix materials and fabricated by different manufacturing processes. Again, even though the absolute values cannot be compared because of different testing conditions and insufficient characterization on the composites, the general trends of wear rate with solid lubricant concentration are revealed. In Fig. 2.17a, the wear rates decreased more rapidly with increasing only a small amount of solid lubricants, and then tended to keep constant with further increase in MoS_2 or h-BN. However, as observed in the Gr SLMMCs, there was an opposite trend where wear rates increased with solid lubricant after a certain amount, as seen in Fig. 2.17b, c. Cold sprayed Cu-MoS_2 composites using admixed feedstock show continuous increase in wear track depth with increase in MoS_2 content (Fig. 2.17c right). The increase in wear rates was mainly due to degraded mechanical property induced by poor bonding strength between solid lubricant and metal matrix [32, 64, 116, 142]. In order to improve wear resistance, adding hard phase like ceramics to increase load-bearing capacity of the matrix was an effective method [3, 95, 130, 164]. Moreover, in the case of powder metallurgy route, increasing sintering temperature to get adequate bonding strength and low porosity was able to reduce significantly wear rate at higher h-BN content, as shown in Fig. 2.17b [126]. Post-plastic deformation, e.g., extrusion, was also able to decrease porosity effectively

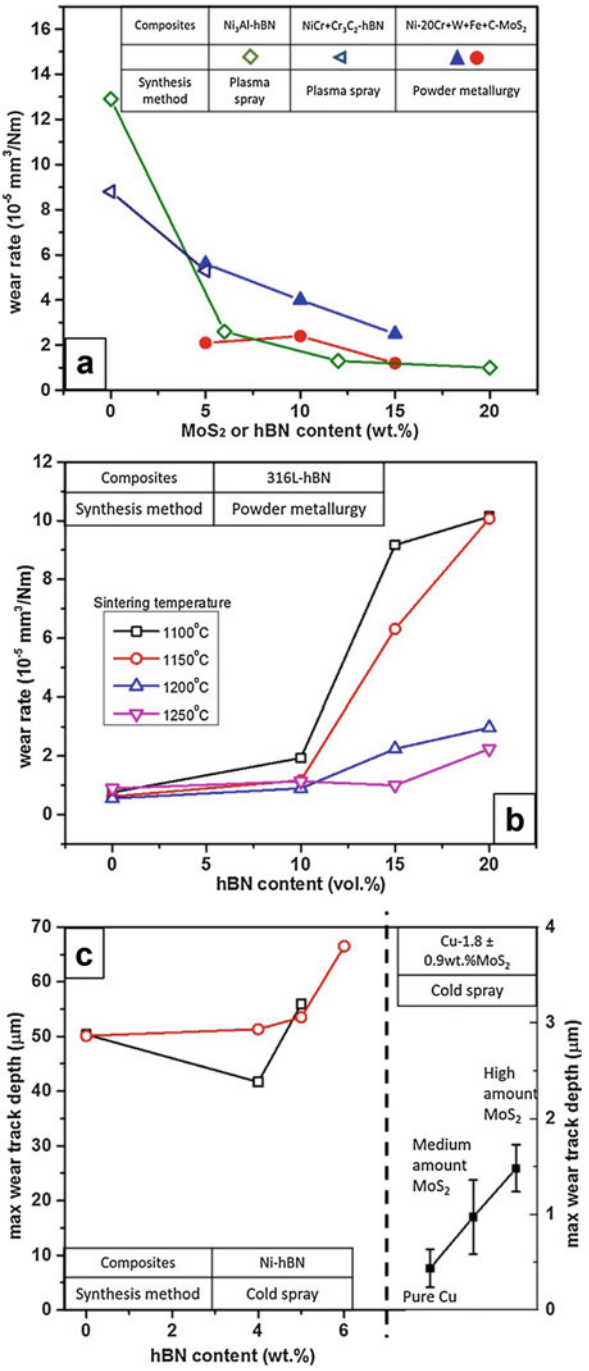

Fig. 2.17 Variation of wear rates with MoS_2 or h-BN content for composites with different metal matrix materials and various synthesis methods. (**a**) Wear rates of Ni alloys reinforced by MoS_2 or h-BN fabricated by plasma spray or powder metallurgy [35, 112, 142], (**b**) wear rates of 316L-h-BN composites developed using different sintering temperatures [125], and (**c**) wear rates of cold sprayed Ni-h-BN (left) [118] and Cu-MoS_2 (right) [32] composites

and therefore improve wear resistance [180]. As described in the Sect. 2.4.2, the transition point based on solid lubricant content above which wear rate starts climbing varies with manufacturing routes. In general, composites made by the liquid methods such as laser cladding and plasma spraying exhibit higher transition point than those fabricated by semisolid and solid methods, e.g., powder metallurgy and cold spray. As shown in Fig. 2.17a, c, plasma sprayed Ni_3Al-h-BN composites showed continuous decrease in wear rate up to 20 wt% h-BN, while for cold sprayed Ni-h-BN composites, wear rate started increasing at around 5 wt% h-BN.

Except for materials, there are some testing parameters that affect wear rate evolution and they are normal load and sliding speed. The influence of those two factors on friction and wear of SLMMCs have been studied extensively and well summarized by Omrani et al. and Rohatgi et al. [4, 5, 64, 181].

2.5.2 Third Bodies Observed for SLMMCs Containing MoS_2, WS_2, h-BN, CaF_2, and BaF_2

As described in Sect. 2.2.1, friction and wear mechanisms are conventionally examined by observation of sliding contact, i.e., worn surfaces using ex situ methods. Even though the design of SLMMCs, as shown in Fig. 2.1, is to form a full solid lubricating film on the wear track or contact, the role of metal matrix has to be taken into account. In general, for metal-metal contact, incorporation of solid lubricants reduced adhesive wear to some extent depending on the solid lubricant concentration and the testing condition [34, 122]. For Cu-MoS_2 composites sliding against Cu, powdery particles of solid lubricant, not a full film, in the contact were responsible for reduced friction and adhesion and was the main wear mechanism [122]. Mahathanabodee et al. [36, 125] proposed a wear model for a 316L-h-BN and a 316L-h-BN-MoS_2 composites sliding against high-chromium steel counterfaces. They observed adhesive wear, abrasive wear, oxidation, formation of a compact layer, as well as delamination. The compact layer consisting of metal, sulfides, h-BN, and oxide helped to reduce friction and wear. However, this layer tended to be detached and caused delamination due to cyclic loading over sliding. WS_2 is used as a high temperature solid lubricant, and the mechanism of improving tribological behavior is presented in Fig. 2.18 [33]. Without WS_2, large pits were found at 300 °C wear track, therefore abrasive and adhesive wear played a role. However, for NiCr/Cr_3C_2/WS_2 coating, WS_2 and newly formed CrS generated transfer films in the contact, leading to a smoother wear track and lower friction coefficient. Moreover, as degradation of mechanical property at 300 °C was minor due to presence of Cr_7C_3, laser clad NiCr/Cr_3C_2/WS_2 composite coating exhibited a good combination of friction and wear at 300 °C. In addition, ceramic phase additives alter wear mechanism of self-lubricating composites as well. Xu et al. [130] reported adhesion, delamination, and plastic deformation were the main wear mechanisms in a Ni-MoS_2 composite, while incorporation of TiC helped to generate a smoother worn surface and eliminated adhesive wear. Although wear mechanisms seem to be identified through observation of worn surfaces by ex situ approach, more detailed information

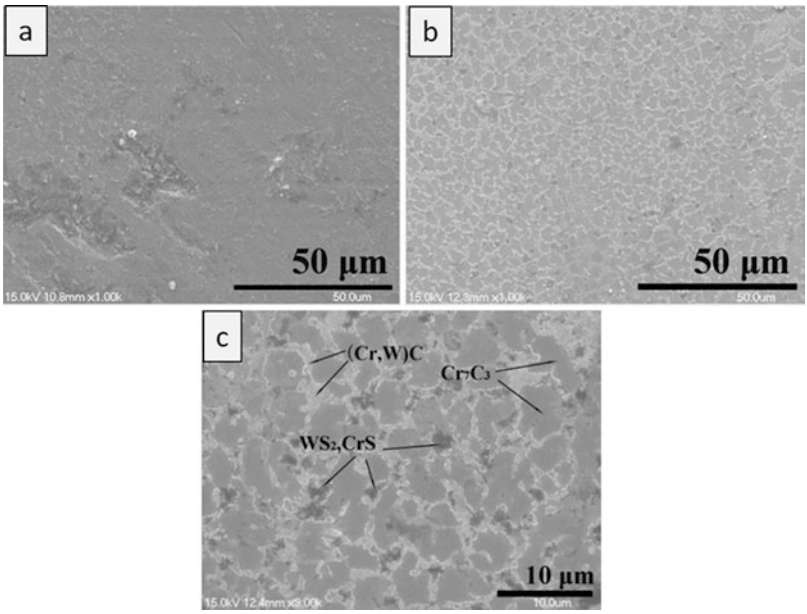

Fig. 2.18 Wear tracks of (**a**) laser clad NiCr/Cr_3C_2 coating and (**b**, **c**) laser clad NiCr/Cr_3C_2/WS_2 coating at 300 °C. Reprinted from [33], with permission from Elsevier

on dynamics of third bodies in the contact, e.g., initiation of tribofilms and transfer films, as well as their evolution, is helpful to better understand friction and wear behavior. That is the design purpose of in situ tribometry, as discussed in the Sect. 2.2.1. A combination of ex situ and in situ method has been applied on cold sprayed Cu-MoS_2 composites, and the results will be presented in the remainder of this section.

Zhang et al. [32] reported recently that when Cu-1.8 wt% MoS_2 composite rubbing against alumina, how MoS_2 smeared out forming discontinuous tribofilms, and their evolution with sliding. Spatial friction was extracted to link local coverage of MoS_2 tribofilms. As shown in Fig. 2.19, at 100 cycles, MoS_2 was smeared out and formed MoS_2-rich patches in the wear track. The local friction distribution combined with chemical analysis demonstrated that higher MoS_2 content zones generated lower local friction. The MoS_2 patches were expanded and tended to distribute more homogenously as sliding continued (see MoS_2 distribution of the 1000 cycle wear track in Fig. 2.20). Inside the patches, MoS_2 was found to be powdery and mixed with Cu_2O and/or Cu (Figs. 2.19d, 2.20d, and 2.21e). The mechanism for low friction in a metal-MoS_2 composite was expected to be different from that found in blanket films of MoS_2 made by physical vapor deposition (PVD) or similar methods, which was discussed in Sect. 2.2.2 [59, 182, 183]. The main feature of these latter coatings was to form transfer films on the counterfaces, which led to MoS_2 sliding versus MoS_2 and friction coefficients in the range of 0.02–0.06 in dry air at similar test conditions to those performed here [59]. Thus, while there is

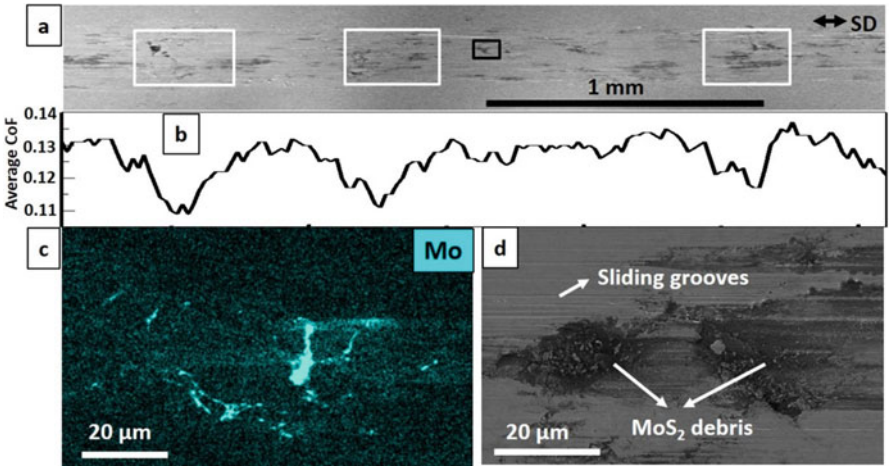

Fig. 2.19 Top-down view of the Cu-MoS_2 wear track after a 100 cycle test. (**a**) Overall morphology; (**b**) spatial friction along the wear track at the 100th cycle; (**c**) an EDX map of the black rectangle in (**a**); (**d**) a closer view of the wear track morphology. Reprinted from [32], with permission from Springer

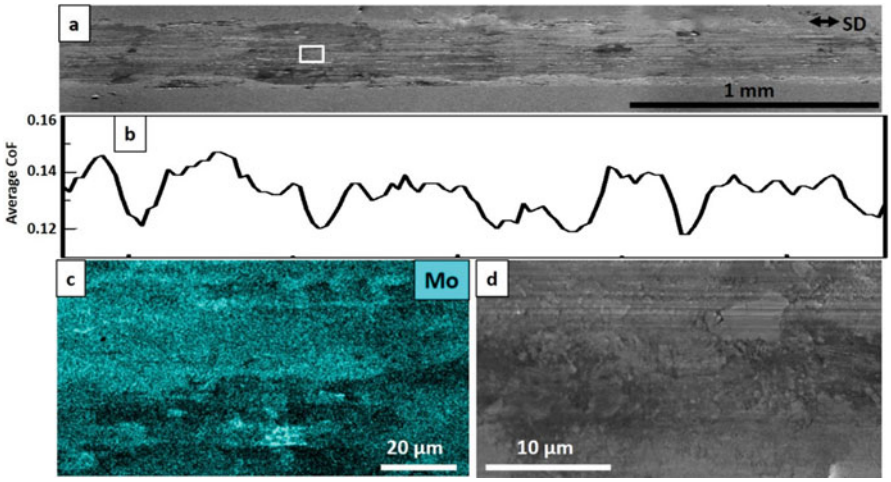

Fig. 2.20 Top-down view of the Cu-MoS_2 wear track after a 1000 cycle test. (**a**) Overall morphology; (**b**) spatial friction along the wear track at the 100th cycle; (**c**) an EDX map of the black rectangle in (**a**); (**d**) a closer view of the wear track morphology. Reprinted from [32], with permission from Springer

a significant friction reduction due to the presence of MoS_2, the mechanisms for this reduction were modified due to the presence of the Cu. The first noticeable difference was the lack of a transfer film observed at 100 and 1000 cycle tests (Fig. 2.21a, b). With only 1.8 wt% MoS_2 in the coating, any transfer films that did form were readily

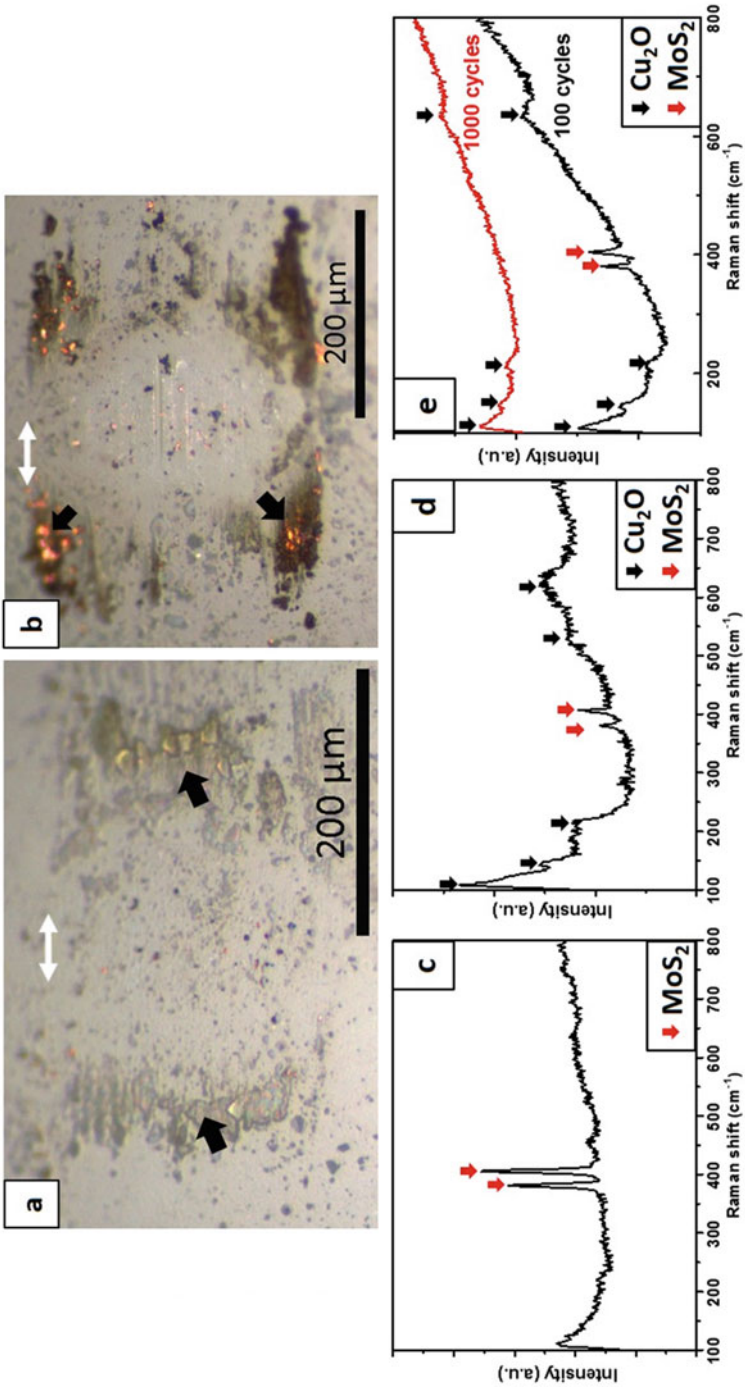

Fig. 2.21 Micrographs of the counterfaces mating with the Cu-MoS_2 coating after (**a**) 100 cycles and (**b**) 1000 cycles. Transferred patches and/or debris were found outside the contact, indicated as black arrows. Their Raman spectra were shown in (**c**) and (**d**), respectively. (**e**) Raman spectra taken from the wear tracks. White arrows indicate sliding direction. Reprinted from [32], with permission from Springer

removed and redeposited onto the wear track. This was due to the interactions of MoS_2 with the wear track, which was primarily Cu – a very different contact condition compared to sliding on a PVD coating with a constant source of MoS_2. With the interactions of the metal, the transfer films were unstable and continuously removed, ultimately resulting in MoS_2 patches on the wear track that were expanded over sliding (Figs. 2.19d and 2.20d).

The VAM within MoS_2-rich tribofilms was also explored briefly in this study [32]. Using the two-term friction model that is commonly employed to combine two velocity accommodation modes with an assumption that interaction between the friction mechanisms is negligible [39], the total friction can be written as

$$\mu = \mu_{int} + \mu_{fracture} \tag{2.2}$$

where μ_{int} is friction from interfacial sliding and $\mu_{fracture}$ is the friction from fracture. Dvorak et al. [8, 56, 57] proposed a similar model for taking account of two friction mechanisms in MoS_2. For Cu-1.8 wt% MoS_2, the low MoS_2 content in the coating and the absence of a persistent MoS_2 transfer film on the counterface indicate that interfacial sliding between MoS_2 and MoS_2 did not occur to any great extent. The process by which the transfer films were removed and deposited back to the wear track as powdery MoS_2 was primarily related to the fracture of MoS_2. So the velocity difference was mostly accommodated by fracturing of MoS_2 third bodies. Therefore, $\mu_{int} \cong 0$, and $\mu \cong \mu_{fracture}$. Uemura et al. [184] demonstrated that fracture dominated friction was three to four times higher than interfacial sliding (i.e., $\mu_{fracture} \cong 3.5*\mu_{int}$). Also, Dvorak et al. [8, 56, 57] showed that the friction induced by interfacial sliding in dry air (i.e., $\mu \cong \mu_{int}$) under a wide range of contact pressure (0.41–1.39 GPa) was below 0.05. Thus, based on the results of Uemura and Dvorak, an estimate of fracture-induced friction indicated it should be roughly 0.18 or below. This estimate was in a good agreement with the present study, where the friction of the high MoS_2 zones was 0.11–0.12. This analysis helped to understand how low friction can be observed with MoS_2 through a primarily fracture-based process instead of interfacial shearing. However, the elevated friction compared to an interfacial sliding mechanism must also partly be due to the occurrence of some metallic friction, evidenced by sliding grooves at the zones with little/no MoS_2 (Fig. 2.19d) and oxidation (Fig. 2.21e).

Cross-sectional microstructures of the wear tracks exhibit influence of solid lubricants on tribologically modified microstructure and therefore permit a better understanding of tribological behavior of SLMMCs. As shown in Fig. 2.22, in the Cu-MoS_2 wear track, sliding induced a cohesive mechanically mixed layer (MML) with fine cracks and a shallow dynamic recrystallized (DRX) layer 3–5 μm deep, where a decrease in defect density was observed but no significant grain growth. However, for the Cu wear track, sliding introduced large cracks within the MML. The DRX layer penetrated into the coating as deep as 10–30 μm and substantial grain growth was found in the DRX layer. The minor changes in subsurface microstructure and phase transformation in the Cu-MoS_2 wear track compared to Cu wear track probably resulted from a much minder stress field generated underneath the

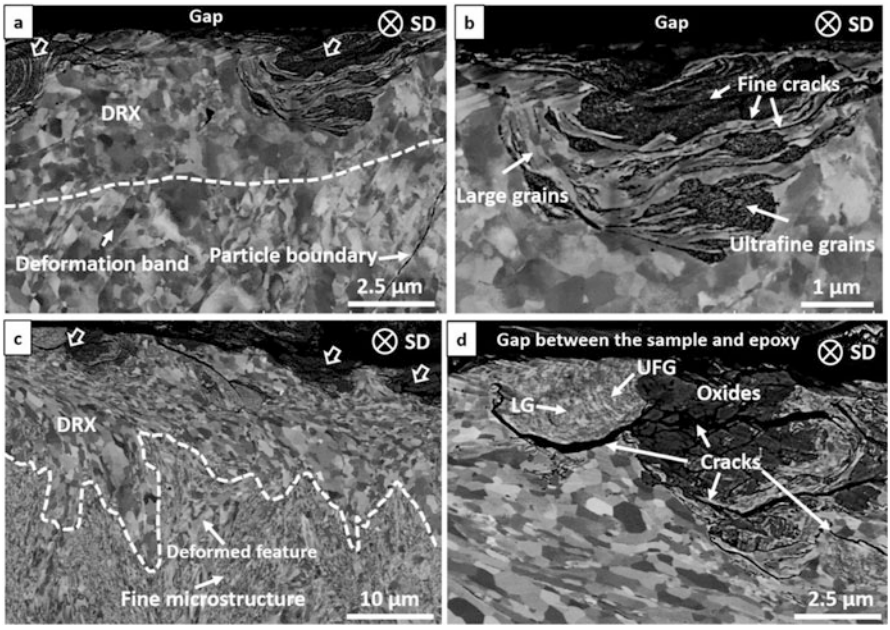

Fig. 2.22 (**a**) Micrograph of cross section of the Cu-MoS_2 wear track after a 3000 cycle test. The hollow arrows denote MML, and the dashed line the border of the sliding-induced microstructure and as-sprayed microstructure. (**b**) A closer view of the sliding-induced microstructure. (**c**) Micrograph of cross section of the Cu wear track after a 3000 cycle test. The hollow arrows denote MML, the dashed line the border of the sliding-induced microstructure and the as-sprayed microstructure. (**d**) A closer view of the sliding-induced microstructure. SD indicates sliding direction. Reprinted from [32], with permission from Springer

Cu-MoS_2 wear tracks [32, 185–187]. There is a chance that frictional heating might play a role on the microstructural modification [188].

As discussed in Sect. 2.2.1, for SLMMCs, even though traditional ex situ techniques have been used extensively to observe third body behaviors, e.g., formation and evolution of lubricating tribofilms and transfer films, the effectiveness of replenishment process and the mechanisms have not been fully understood. In situ tribology technique is capable of capturing third body "processes" over the whole testing, which provides generation and dynamics of lubricating films at the contact. Here we present formation of MoS_2 tribofilms and transfer films at the very beginning and how they were depleted with sliding. More details on in situ tribometer setup can be found in [16] and sliding wear testing parameters in [32]. As shown in Fig. 2.23, once sliding commenced, patchy MoS_2 transfer film was formed. Where and how much of the transfer film can be generated largely depent on local MoS_2 content. The transfer films were then deposited onto the wear track when rubbing against pure Cu, and were consumed completely eventually, as shown in Fig. 2.23b–d. This process continued with sliding. At 20 cycles (see Fig. 2.24a), more MoS_2 tribofilms were developed, indicating MoS_2 was expanded more

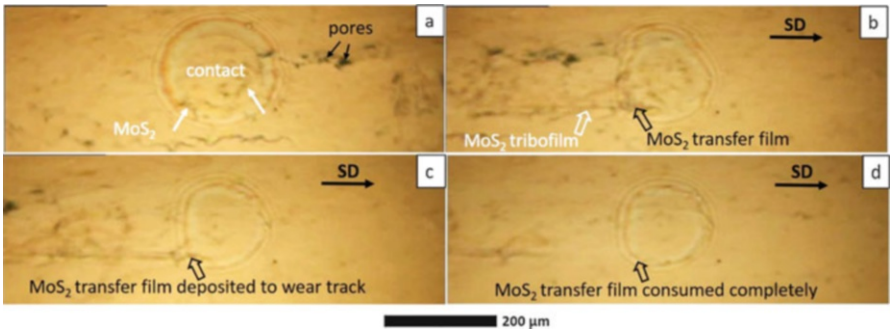

Fig. 2.23 In situ micrographs of Cu-MoS_2 composite during the first half cycle. (**a**) Right before sliding, followed by (**b**–**d**) where sliding commenced. SD indicates sliding direction. (Mining and Materials Engineering, McGill University, Montreal, Canada)

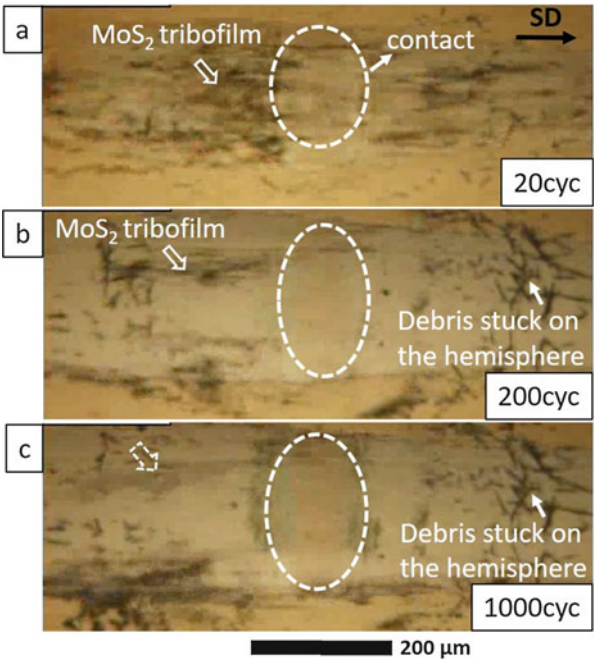

Fig. 2.24 In situ micrographs of Cu-MoS_2 composite at (**a**) 20 cycles, (**b**) 200 cycles, and (**c**) 1000 cycles. The same spot was taken to investigate evolution of the lubricating film. Dashed lines of ellipses indicate contact, while the arrow with dashed lines denotes the MoS_2 tribofilm become barely visible through optical microscope. (Mining and Materials Engineering, McGill University, Montreal, Canada)

extensively and in the meantime MoS_2 was replenished as wearing through the top surface. The MoS_2 tribofilms were then depleted gradually as seen in Fig. 2.24b, c. They could become wear debris deposited onto the counterface or outside the wear track. It is worth noting that even though only a few visible patchy MoS_2 tribofilms over the majority of sliding, the presence of MoS_2 eliminated metal oxidation comparing to the pure Cu case (not shown). These results are consistent with wear track morphology observation by ex situ techniques (Fig. 2.22). Even though higher

resolution micrographs and in situ chemical/phase composition analysis, e.g., in situ Raman spectroscopy, are required to better understand third body generation and evolution over sliding, we believe combination of ex situ and in situ methods are able to reveal third body behavior of SLMMCs more comprehensively.

2.6 Applications, Challenges, and Future Directions

SLMMCs remain an important class of engineering materials, especially considering global initiatives for green manufacturing and increased sustainability in engineering design. These materials find applications in aerospace, automotive, marine, and other sectors where tribological contacts are made that require low friction, such as bearings, bushings, and piston liners. Many different metal matrices have been studied (e.g., Cu, Mg, Al, Ni, Ti, and their alloys) with a range of solid lubricants (e.g., Gr, CNTs, G, MoS_2, WS_2, h-BN, and others). One also finds SLMMCs manufactured by a wide range of methods that have been reviewed here, from the mature stir casting method for Al alloys with Gr to the more recent techniques of cold spray, friction stir processing, and laser additive manufacturing methods. Thus, there is a significant body of scientific literature and knowledge base for SLMMCs. However, based on this review, we have identified some areas of future research that could make significant impact on understanding of the lubrication mechanisms for SLMMCs and also the development of SLMMCs with optimized properties.

The basic understanding of the lubrication mechanisms of SLMMCs consists of tribofilm formation, which is the formation of a surface layer that consists of lubricating material that reduce the fraction of metal-to-metal junctions in the sliding contact. However, as shown in this review the structure of a tribofilm can be considerably more complex than this. In the work of Riahi and Alpas [169], they observed a tribofilm that was composed of many components with a small fraction of the graphite lubricant. Researchers should devote more efforts on describing the exact nature of the tribofilms for SLMMCs as their formation is key for the function of the composite, but the mechanism and the nature of their formation are not always fully elucidated.

Generally, third body flows and lubrication mechanisms for SLMMCs deviate significantly from blanket films of solid lubricants. For blanket films, there is a large volume fraction of solid lubricant available; the VAM is solid lubricant vs. solid lubricant or interfacial shearing of the solid lubricant, as depicted in Fig. 2.2. For SLMMCs, the total volume fraction of lubricant is lower. Often one finds that transfer films do not persist in the sliding contact, as was shown by in situ tribometry above in the work of Zhang et al. (McGill University). Any transfer film material formed generally flows back to the wear track in recirculation flow or out of the contact as debris. This means the mechanisms observed by Mogonye et al. [98] are more important. An understanding of the replenishment mechanisms for the tribofilms from the near surface solid lubricant particles would be key in better design of SLMMCs. The flow of solid lubricant materials toward the surface can naturally occur by wear or by plastic deformation, but the process must have a dependence on the fabrication

methods of the composite, lubricant content and morphology, and the microstructure of the matrix itself. Researchers have already described these as being key variables for the performance of the composites, but these links are not as strong as they could be without more detailed information on the mechanisms of near surface lubricant flow, tribofilm formation and structure, and the recirculation flow of lubricants.

SLMMCs have an opportunity to undergo a significant revolution in both materials and processing/manufacturing. In terms of materials, researchers are actively exploring incorporation of newer forms, often nanostructured, of popular lubricants. Recent excitement on graphene and before that CNTs have translated to their use in SLMMCs. Similarly, 2D versions of MoS_2 are becoming readily available and can be utilized for making SLMMCs. Challenges of course remain for these materials. Researchers must focus as best they can on side-by-side comparisons [76] between these newer materials and traditional forms of the lubricants. Otherwise, the understanding of performance differences becomes lost in the cloud of tribological test parameters. Also, it is critical that the lubricants be examined with electron microscopy and other spectroscopic methods to quantify the state of the lubricant in the SLMMC postprocessing.

On the manufacturing side, new processing routes provide new possibilities for SLMMCs. In particular additive manufacturing provides a new vista. While most additive manufacturing researchers are focused on making bulk parts from metals and alloys, there is a real possibility for using these techniques to tailor the properties for SLMMCs, including but not limited to a more precise control of the lubricant content and morphology in the composite. However, many of these techniques are laser based, and challenges on control of lubricant state in the composite would be a key issue. Similarly, cold spray, which is currently a method primarily focused on metals and coatings, has the potential to become an additive manufacturing method utilized for SLMMCs. Even though cold spray eliminates or avoids decomposition of the solid lubricants that is inevitable for most of the other manufacturing processes, challenges for this technique are precise control of powder delivery systems and development of optimized feedstocks that are suitable for cold spray. The feedstocks can be conceivably modified to composite powders using dryer spraying technique, metal-coated solid lubricant powders made by deposition or ball milling, and even combination of them, i.e., metal-coated composite powders. These pretreatments could improve cold sprayability of the materials according to deposition mechanism described in Sect. 2.3.5. Moreover, due to poor sprayability of solid lubricants, in situ formation of solid lubricants during post spraying treatment, e.g., heat treatment, could avoid spraying solid lubricant directly. This could promote a new route to fabricate SLMMCs using cold spray. In addition, several alternatives of conventional lamellar solid lubricants are some oxides, e.g., TiO_2, and soft metals, e.g., Sn, which could be used as solid lubricants at elevated temperature. In fact, TiO_2 ceramic coating has been sprayed by high pressure cold spray system and low pressure cold spray system [189, 190]. Even though there are some challenges, cold spray provides an interesting opportunity to develop a next generation of SLMMCs.

References

1. Daniel, I.M., Ishai, O.: Engineering Mechanics of Composite Materials. Oxford University Press, New York (1994)
2. Prasad, S., Asthana, R.: Aluminum metal-matrix composites for automotive applications: tribological considerations. Tribol. Lett. **17**(3), 445–453 (2004)
3. Miracle, D.B.: Metal matrix composites – from science to technological significance. Compos. Sci. Technol. **65**(15–16), 2526–2540 (2005)
4. Omrani, E., et al.: Influences of graphite reinforcement on the tribological properties of self-lubricating aluminum matrix composites for green tribology, sustainability, and energy efficiency – a review. Int. J. Adv. Manuf. Technol. **83**(1–4), 325–346 (2016)
5. Omrani, E., et al.: New emerging self-lubricating metal matrix composites for tribological applications. In: Davim, P.J. (ed.) Ecotribology: Research Developments, pp. 63–103. Springer International Publishing, Cham (2016)
6. Dellacorte, C., Fellenstein, J.A.: The effect of compositional tailoring on the thermal expansion and tribological properties of PS300: a solid lubricant composite coating. Tribol. Trans. **40**(4), 639–642 (1997)
7. Zhang, X., et al.: Carbon nanotube-MoS_2 composites as solid lubricants. ACS Appl. Mater. Interfaces. **1**(3), 735–739 (2009)
8. Chromik, R.R., et al.: In situ tribometry of solid lubricant nanocomposite coatings. Wear. **262** (9–10), 1239–1252 (2007)
9. Godet, M.: The third-body approach: a mechanical view of wear. Wear. **100**(1), 437–452 (1984)
10. Godet, M.: Third-bodies in tribology. Wear. **136**(1), 29–45 (1990)
11. Rigney, D.A., Karthikeyan, S.: The evolution of tribomaterial during sliding: a brief introduction. Tribol. Lett. **39**(1), 3–7 (2010)
12. Biswas, S.K.: Wear of metals: a material approach. In: Stachowiak, G.W. (ed.) Wear: Materials, Mechanisms and Practice, pp. 21–36. Wiley, West Sussex (2005)
13. Descartes, S., Busquet, M., Berthier, Y.: An attempt to produce ex situ TTS to understand their mechanical formation conditions – the case of an ultra high purity iron. Wear. **271**(9–10), 1833–1841 (2011)
14. Tumbajoy-Spinel, D., et al.: Assessment of mechanical property gradients after impact-based surface treatment: application to pure α-iron. Mater. Sci. Eng. A. **667**, 189–198 (2016)
15. Singer, I.L.: Solid lubrication processes. In: Singer, I.L., Pollock, H.M. (eds.) Fundamentals of Friction, pp. 237–261. Kluwer, Dordrecht (1992)
16. Chromik, R., Strauss, H., Scharf, T.: Materials phenomena revealed by in situ tribometry. JOM. **64**(1), 35–43 (2012)
17. Wahl, K.J., Sawyer, W.G.: Observing interfacial sliding processes in solid – solid contacts. MRS Bull. **33**(12), 1159–1167 (2008)
18. Berthier, Y., Godet, M., Brendle, M.: Velocity accommodation in friction. Tribol. Trans. **32**(4), 490–496 (1989)
19. Scharf, T.W., Singer, I.L.: Role of third bodies in friction behavior of diamond-like nanocomposite coatings studied by in situ tribometry. Tribol. Trans. **45**(3), 363–371 (2002)
20. Scharf, T.W., Singer, I.L.: Quantification of the thickness of carbon transfer films using Raman tribometry. Tribol. Lett. **14**, 137–146 (2003)
21. Scharf, T.W., Singer, I.L.: Monitoring transfer films and friction instabilities with in situ Raman tribometry. Tribol. Lett. **14**, 3–8 (2003)
22. Scharf, T.W., Singer, I.L.: Role of the transfer film on the friction and wear of metal carbide reinforced amorphous carbon coatings during run-in. Tribol. Lett. **36**(1), 43–53 (2009)
23. Strauss, H.W., et al.: In situ tribology of nanocomposite Ti-Si-C-H coatings prepared by PE-CVD. Wear. **272**, 133–148 (2011)
24. Wahl, K.J., Chromik, R.R., Lee, G.Y.: Quantitative in situ measurement of transfer film thickness by a Newton's rings method. Wear. **264**(7–8), 731–736 (2008)

25. Shockley, J.M., et al.: The influence of Al_2O_3 particle morphology on the coating formation and dry sliding wear behavior of cold sprayed Al-Al_2O_3 composites. Surf. Coat. Technol. **270**, 324–333 (2015)
26. Sriraman, K.R., et al.: Tribological behavior of electrodeposited Zn, Zn-Ni, Cd and Cd-Ti coatings on low carbon steel substrates. Tribol. Int. **56**, 107–120 (2012)
27. Stoyanov, P., et al.: Combining in situ and online approaches to monitor interfacial processes in lubricated sliding contacts. MRS Commun. 6(3), 301–308 (2016)
28. Shockley, J.M., et al.: Third body behavior during dry sliding of cold-sprayed Al-Al_2O_3 composites: in situ tribometry and microanalysis. Tribol. Lett. **54**(2), 191–206 (2014)
29. Shockley, J.M., et al.: In situ tribometry of cold-sprayed Al-Al_2O_3 composite coatings. Surf. Coat. Technol. **215**, 350–356 (2013)
30. Berthier, Y.: Experimental evidence for friction and wear modelling. Wear. **139**(1), 77–92 (1990)
31. Alidokht, S.A., et al.: Role of third-bodies in friction and wear of cold-sprayed Ti and Ti-TiC composite coatings. Tribol. Lett. 65, 114 (2017)
32. Zhang, Y., et al.: Tribological behavior of a cold-sprayed Cu–MoS_2 composite coating during dry sliding wear. Tribol. Lett. **62**(1), 1–12 (2016)
33. Yang, M.-S., et al.: Microstructure and wear behaviors of laser clad NiCr/Cr_3C_2–WS_2 high temperature self-lubricating wear-resistant composite coating. Appl. Surf. Sci. **258**(8), 3757–3762 (2012)
34. Raadnui, S., Mahathanabodee, S., Tongsri, R.: Tribological behaviour of sintered 316L stainless steel impregnated with MoS_2 plain bearing. Wear. **265**(3), 546–553 (2008)
35. Li, J.L., Xiong, D.S.: Tribological properties of nickel-based self-lubricating composite at elevated temperature and counterface material selection. Wear. **265**(3), 533–539 (2008)
36. Mahathanabodee, S., et al.: Dry sliding wear behavior of SS316L composites containing h-BN and MoS_2 solid lubricants. Wear. **316**(1), 37–48 (2014)
37. Scharf, T.W.: Low friction coatings. In: Bruce, R. (ed.) Handbook of Lubrication and Tribology. CRC Press, Boca Raton (2012)
38. Scharf, T.W., Prasad, S.V.: Solid lubricants: a review. J. Mater. Sci. **48**(2), 511–531 (2012)
39. Bowden, F.P., Tabor, D.: The Friction and Lubrication of Solids, vol. 1. Oxford University Press, New York (2001)
40. Erdemir, A., Fontaine, J., Donnet, C.: An overview of superlubricity in diamond-like carbon films. In: Donnet, C., Erdemir, A. (eds.) Tribology of Diamond-Like Carbon Films: Fundamentals and Applications, pp. 237–262. Springer US, Boston (2008)
41. Fontaine, J., Donnet, C., Erdemir, A.: Fundamentals of the tribology of DLC coatings. In: Donnet, C., Erdemir, A. (eds.) Tribology of Diamond-Like Carbon Films: Fundamentals and Applications, pp. 139–154. Springer US, Boston (2008)
42. Hoffman, E.E., Marks, L.D.: Graphitic carbon films across systems. Tribol. Lett. **63**(3), 32 (2016)
43. Liu, Y., Erdemir, A., Meletis, E.I.: An investigation of the relationship between graphitization and frictional behavior of DLC coatings. Surf. Coat. Technol. **86**, 564–568 (1996)
44. Liu, Y., Erdemir, A., Meletis, E.I.: A study of the wear mechanism of diamond-like carbon films. Surf. Coat. Technol. **82**(1), 48–56 (1996)
45. Fontaine, J., et al.: Tribological behaviour of metal-DLC nanocomposite coatings: the critical role of tribofilm build-up. In: World Tribology Congress 2009 – Proceedings (Kyoto, Japan) (2009)
46. Pastewka, L., Moser, S., Moseler, M.: Atomistic insights into the running-in, lubrication, and failure of hydrogenated diamond-like carbon coatings. Tribol. Lett. **39**(1), 49–61 (2010)
47. Al-Azizi, A.A., et al.: Surface structure of hydrogenated diamond-like carbon: origin of run-in behavior prior to superlubricious interfacial shear. Langmuir. **31**(5), 1711–1721 (2015)
48. Berman, D., et al.: Macroscale superlubricity enabled by graphene nanoscroll formation. Science. **348**(6239), 1118–1122 (2015)
49. Berman, D., et al.: Nanoscale friction properties of graphene and graphene oxide. Diam. Relat. Mater. **54**(1), 91–96 (2015)

50. Berman, D., et al.: Extraordinary macroscale wear resistance of one atom thick graphene layer. Adv. Funct. Mater. **24**(42), 6640–6646 (2014)
51. Berman, D., Erdemir, A., Sumant, A.V.: Few layer graphene to reduce wear and friction on sliding steel surfaces. Carbon. **54**, 454–459 (2013)
52. Spalvins, T.: Lubrication with sputtered MoS_2 films: principles, operation, and limitations. J. Mater. Eng. Perform. **1**(3), 347–351 (1992)
53. McDevitt, N.T., Donley, M.S., Zabinski, J.S.: Utilization of Raman spectroscopy in tribochemistry studies. Wear. **166**(1), 65–72 (1993)
54. Liang, T., et al.: First-principles determination of static potential energy surfaces for atomic friction in MoS_2 and MoO_3. Phys. Rev. B Condens. Matter Mater. Phys. **77**(10), 104105 (2008)
55. Liang, T., et al.: Energetics of oxidation in MoS_2 nanoparticles by density functional theory. J. Phys. Chem. C. **115**(21), 10606–10616 (2011)
56. Dvorak, S.D., Wahl, K.J., Singer, I.L.: In situ analysis of third body contributions to sliding friction of a Pb-Mo-S coating in dry and humid air. Tribol. Lett. **28**(3), 263–274 (2007)
57. Wahl, K.J., Belin, M., Singer, I.L.: A triboscopic investigation of the wear and friction of MoS_2 in a reciprocating sliding contact. Wear. **214**(2), 212–220 (1998)
58. Hoffman, E.E., Marks, L.D.: Soft interface fracture transfer in nanoscale MoS_2. Tribol. Lett. **64**(1), 1 (2016)
59. Wahl, K.J., Singer, I.L.: Quantification of a lubricant transfer process that enhances the sliding life of a MoS_2 coating. Tribol. Lett. **1**(1), 59–66 (1995)
60. Lince, J.R., et al.: Tribochemistry of MoS_3 nanoparticle coatings. Tribol. Lett. **53**(3), 543–554 (2014)
61. Spear, J.C., Ewers, B.W., Batteas, J.D.: 2D-nanomaterials for controlling friction and wear at interfaces. Nano Today. **10**(3), 301–314 (2015)
62. Rohatgi, P.K.: Metal matrix composites. Def. Sci. J. **43**(4), 323 (1993)
63. Liu, Y., Rohatgi, P.K., Ray, S.: Tribological characteristics of aluminum-50 vol pct graphite composite. Metall. Trans. A. **24**(1), 151–159 (1993)
64. Rohatgi, P.K., Ray, S., Liu, Y.: Tribological properties of metal matrix-graphite particle composites. Int. Mater. Rev. **37**, 129 (1992)
65. Rohatgi, P.K., et al.: A surface-analytical study of tribodeformed aluminum alloy 319-10 vol. % graphite particle composite. Mater. Sci. Eng. A. **123**(2), 213–218 (1990)
66. Jha, A., et al.: Aluminium alloy-solid lubricant talc particle composites. J. Mater. Sci. **21**(10), 3681–3685 (1986)
67. Bowden, F., Shooter, K.: Frictional behaviour of plastics impregnated with molybdenum disulphide. Res. Appl. Ind. **3**, 384 (1950)
68. Lancaster, J.: Composite self-lubricating bearing materials. Proc. Inst. Mech. Eng. **182**(1), 33–54 (1967)
69. Prasad, S., Mecklenburg, K.R.: Self-lubricating aluminum metal-matrix composites dispersed with tungsten disulfide and silicon carbide. Lubr. Eng. **50**(7), 511 (1994)
70. Das, S., Prasad, S.V., Ramachandran, T.R.: Tribology of Al-Si alloy-graphite composites: triboinduced graphite films and the role of silicon morphology. Mater. Sci. Eng. A. **138**(1), 123–132 (1991)
71. Das, S., Prasad, S.V., Ramachandran, T.R.: Microstructure and wear of cast (Al-Si alloy)-graphite composites. Wear. **133**(1), 173–187 (1989)
72. Gibson, P.R., Clegg, A.J., Das, A.A.: Wear of cast Al-Si alloys containing graphite. Wear. **95**(2), 193–198 (1984)
73. Biswas, S.K., Bai, B.N.P.: Dry wear of Al-graphite particle composites. Wear. **68**(3), 347–358 (1981)
74. Jha, A.K., Prasad, S.V., Upadhyaya, G.S.: Sintered 6061 aluminium alloy – solid lubricant particle composites: sliding wear and mechanisms of lubrication. Wear. **133**(1), 163–172 (1989)

75. Akhlaghi, F., Mahdavi, S.: Effect of the SiC content on the tribological properties of hybrid Al/Gr/SiC composites processed by in situ powder metallurgy (IPM) method. Adv. Mater. Res. **264–265**, 1878–1886 (2011)
76. Maurya, R., et al.: Effect of carbonaceous reinforcements on the mechanical and tribological properties of friction stir processed Al6061 alloy. Mater. Des. **98**, 155–166 (2016)
77. Sarmadi, H., Kokabi, A., Reihani, S.S.: Friction and wear performance of copper–graphite surface composites fabricated by friction stir processing (FSP). Wear. **304**(1), 1–12 (2013)
78. Soleymani, S., Abdollah-Zadeh, A., Alidokht, S.: Microstructural and tribological properties of Al5083 based surface hybrid composite produced by friction stir processing. Wear. **278**, 41–47 (2012)
79. Dolatkhah, A., et al.: Investigating effects of process parameters on microstructural and mechanical properties of Al5052/SiC metal matrix composite fabricated via friction stir processing. Mater. Des. **37**, 458–464 (2012)
80. Alidokht, S.A., et al.: Microstructure and tribological performance of an aluminium alloy based hybrid composite produced by friction stir processing. Mater. Des. **32**(5), 2727–2733 (2011)
81. Gan, Y., Solomon, D., Reinbolt, M.: Friction stir processing of particle reinforced composite materials. Materials. **3**(1), 329 (2010)
82. Chen, L.-Y., et al.: Novel nanoprocessing route for bulk graphene nanoplatelets reinforced metal matrix nanocomposites. Scr. Mater. **67**(1), 29–32 (2012)
83. Nickchi, T., Ghorbani, M.: Pulsed electrodeposition and characterization of bronze-graphite composite coatings. Surf. Coat. Technol. **203**(20), 3037–3043 (2009)
84. Algul, H., et al.: The effect of graphene content and sliding speed on the wear mechanism of nickel-graphene nanocomposites. Appl. Surf. Sci. **359**, 340–348 (2015)
85. Uysal, M., et al.: Structural and sliding wear properties of Ag/Graphene/WC hybrid nanocomposites produced by electroless co-deposition. J. Alloys Compd. **654**, 185–195 (2016)
86. Pialago, E.J.T., Kwon, O.K., Park, C.W.: Cold spray deposition of mechanically alloyed ternary Cu–CNT–SiC composite powders. Ceram. Int. **41**(5), 6764–6775 (2015)
87. Pialago, E.J.T., Park, C.W.: Cold spray deposition characteristics of mechanically alloyed Cu-CNT composite powders. Appl. Surf. Sci. **308**, 63–74 (2014)
88. Cho, S., et al.: Multi-walled carbon nanotube-reinforced copper nanocomposite coating fabricated by low-pressure cold spray process. Surf. Coat. Technol. **206**(16), 3488–3494 (2012)
89. Bakshi, S.R., et al.: Nanoscratch behavior of carbon nanotube reinforced aluminum coatings. Thin Solid Films. **518**(6), 1703–1711 (2010)
90. Bakshi, S.R., et al.: Deformation and damage mechanisms of multiwalled carbon nanotubes under high-velocity impact. Scr. Mater. **59**(5), 499–502 (2008)
91. Bakshi, S.R., et al.: Carbon nanotube reinforced aluminum composite coating via cold spraying. Surf. Coat. Technol. **202**(21), 5162–5169 (2008)
92. Chen, Y., Bakshi, S.R., Agarwal, A.: Correlation between nanoindentation and nanoscratch properties of carbon nanotube reinforced aluminum composite coatings. Surf. Coat. Technol. **204**(16), 2709–2715 (2010)
93. Pialago, E.J.T., et al.: Ternary Cu–CNT–AlN composite coatings consolidated by cold spray deposition of mechanically alloyed powders. J. Alloys Compd. **650**, 199–209 (2015)
94. Pialago, E.J.T., Kwon, O.K., Park, C.W.: Nucleate boiling heat transfer of R134a on cold sprayed CNT–Cu composite coatings. Appl. Therm. Eng. **56**(1), 112–119 (2013)
95. Rajkumar, K., Aravindan, S.: Tribological performance of microwave sintered copper–TiC–graphite hybrid composites. Tribol. Int. **44**(4), 347–358 (2011)
96. Rajkumar, K., Aravindan, S.: Tribological studies on microwave sintered copper–carbon nanotube composites. Wear. **270**(9), 613–621 (2011)
97. Rajkumar, K., Aravindan, S.: Tribological behavior of microwave processed copper–nanographite composites. Tribol. Int. **57**, 282–296 (2013)

98. Mogonye, J.E., et al.: Solid/self-lubrication mechanisms of an additively manufactured Ni–Ti–C metal matrix composite. Tribol. Lett. **64**(3), 37 (2016)
99. Esawi, A.M.K., et al.: Fabrication and properties of dispersed carbon nanotube–aluminum composites. Mater. Sci. Eng. A. **508**(1–2), 167–173 (2009)
100. Kim, K.T., Cha, S.I., Hong, S.H.: Hardness and wear resistance of carbon nanotube reinforced Cu matrix nanocomposites. Mater. Sci. Eng. A. **449–451**, 46–50 (2007)
101. Dong, S.R., Tu, J.P., Zhang, X.B.: An investigation of the sliding wear behavior of Cu-matrix composite reinforced by carbon nanotubes. Mater. Sci. Eng. A. **313**(1–2), 83–87 (2001)
102. Tjong, S.C.: Recent progress in the development and properties of novel metal matrix nanocomposites reinforced with carbon nanotubes and graphene nanosheets. Mater. Sci. Eng. R. Rep. **74**(10), 281–350 (2013)
103. Scharf, T., et al.: Self-lubricating carbon nanotube reinforced nickel matrix composites. J. Appl. Phys. **106**(1), 013508 (2009)
104. Zhou, S.-m., et al.: Fabrication and tribological properties of carbon nanotubes reinforced Al composites prepared by pressureless infiltration technique. Compos. A Appl. Sci. Manuf. **38** (2), 301–306 (2007)
105. Hu, Z., et al.: Laser sintered single layer graphene oxide reinforced titanium matrix nanocomposites. Compos. Part B Eng. **93**, 352–359 (2016)
106. Zhai, W., et al.: Investigation of mechanical and tribological behaviors of multilayer graphene reinforced Ni_3Al matrix composites. Compos. Part B Eng. **70**, 149–155 (2015)
107. Bastwros, M., et al.: Effect of ball milling on graphene reinforced Al6061 composite fabricated by semi-solid sintering. Compos. Part B Eng. **60**, 111–118 (2014)
108. Ghazaly A., Seif B., Salem H.G.: Mechanical and Tribological Properties of AA2124-Graphene Self Lubricating Nanocomposite. In: Sadler B.A. (ed.) Light Metals 2013. The Minerals, Metals & Materials Series. Springer, Cham (2013)
109. Tyagi, R., et al.: Elevated temperature tribological behavior of Ni based composites containing nano-silver and hBN. Wear. **269**(11), 884–890 (2010)
110. Selvakumar, N., Narayanasamy, P.: Optimization and effect of weight fraction of MoS_2 on the tribological behaviour of Mg-TiC-MoS_2 hybrid composites. Tribol. Trans. **59**(4), 733–747 (2016)
111. Kato, H., et al.: Wear and mechanical properties of sintered copper–tin composites containing graphite or molybdenum disulfide. Wear. **255**(1), 573–578 (2003)
112. Du, L., et al.: Preparation and wear performance of NiCr/Cr_3C_2–NiCr/hBN plasma sprayed composite coating. Surf. Coat. Technol. **205**(12), 3722–3728 (2011)
113. Yuan, J., et al.: Fabrication and evaluation of atmospheric plasma spraying WC–Co–Cu–MoS_2 composite coatings. J. Alloys Compd. **509**(5), 2576–2581 (2011)
114. Liu, X.-B., et al.: Development and characterization of laser clad high temperature self-lubricating wear resistant composite coatings on Ti–6Al–4V alloy. Mater. Des. **55**, 404–409 (2014)
115. Yan, H., et al.: Laser cladding of Co-based alloy/TiC/CaF_2 self-lubricating composite coatings on copper for continuous casting mold. Surf. Coat. Technol. **232**, 362–369 (2013)
116. Zhang, Y., et al.: Cold-sprayed Cu-MoS_2 and its fretting wear behavior. J. Therm. Spray Technol. **25**(3), 473–482 (2016)
117. Neshastehriz, M., et al.: On the bonding mechanism in cold spray of deformable hex-BN-Ni clusters. J. Therm. Spray Technol. **25**(5), 982–991 (2016)
118. Smid, I., et al.: Cold-sprayed Ni-hBN self-lubricating coatings. Tribol. Trans. **55**(5), 599–605 (2012)
119. Moridi, A., et al.: Cold spray coating: review of material systems and future perspectives. Surf. Eng. **30**(6), 369–395 (2014)
120. Hou, X., et al.: Preparation and properties of hexagonal boron nitride fibers used as high temperature membrane filter. Mater. Res. Bull. **49**, 39–43 (2014)
121. Bi, Q., S. Zhu, and W. Liu, High Temperature Self-Lubricating Materials. In: Pihtili H. (ed.) Tribology in Engineering, pp.109–134. InTech, Rijeka (2013)

122. Kovalchenko, A., Fushchich, O., Danyluk, S.: The tribological properties and mechanism of wear of Cu-based sintered powder materials containing molybdenum disulfide and molybdenum diselenite under unlubricated sliding against copper. Wear. **290**, 106–123 (2012)
123. Furlan, K.P., et al.: Influence of alloying elements on the sintering thermodynamics, microstructure and properties of Fe–MoS_2 composites. J. Alloys Compd. **652**, 450–458 (2015)
124. Mahathanabodee, S., et al.: Comparative studies on wear behaviour of sintered 316L stainless steels loaded with h-BN and MoS_2. Adv. Mater. Res. **747**, 307 (2013). Trans Tech Publ
125. Mahathanabodee, S., et al.: Effects of hexagonal boron nitride and sintering temperature on mechanical and tribological properties of SS316L/h-BN composites. Mater. Des. **46**, 588–597 (2013)
126. Mahathanabodee, S., et al.: Effect of h-BN content on the sintering of SS316L/h-BN composites. Adv. Mater. Res. **410**, 216–219 (2012)
127. Shi, X., et al.: Tribological behavior of Ni_3Al matrix self-lubricating composites containing WS_2, Ag and hBN tested from room temperature to 800 °C. Mater. Des. **55**, 75–84 (2014)
128. Cardenas, A., et al.: Effect of glow discharge sintering in the properties of a composite material fabricated by powder metallurgy. J. Phys. Conf. Ser. **687**(1), p. 012025 (2016)
129. Quazi, M., et al.: A review to the laser cladding of self-lubricating composite coatings. Lasers Manuf. Mater. Process. **3**(2), 67–99 (2016)
130. Xu, J., Liu, W., Zhong, M.: Microstructure and dry sliding wear behavior of MoS_2/TiC/Ni composite coatings prepared by laser cladding. Surf. Coat. Technol. **200**(14–15), 4227–4232 (2006)
131. Lei, Y., et al.: Microstructure and phase transformations in laser clad CrxSy/Ni coating on H13 steel. Opt. Lasers Eng. **66**, 181–186 (2015)
132. Zhang, S., et al.: Friction and wear behavior of laser cladding Ni/hBN self-lubricating composite coating. Mater. Sci. Eng. A. **491**(1), 47–54 (2008)
133. Zhu, S., et al.: Ni_3Al matrix high temperature self-lubricating composites. Tribol. Int. **44**(4), 445–453 (2011)
134. Liu, X.-B., et al.: Effects of temperature and normal load on tribological behavior of nickel-based high temperature self-lubricating wear-resistant composite coating. Compos. Part B Eng. **53**, 347–354 (2013)
135. Wang, A., et al.: Ni-based alloy/submicron WS_2 self-lubricating composite coating synthesized by Nd: YAG laser cladding. Mater. Sci. Eng. A. **475**(1), 312–318 (2008)
136. Liu, X.-B., et al.: Microstructure and wear behavior of γ/Al_4C_3/TiC/CaF_2 composite coating on γ-TiAl intermetallic alloy prepared by Nd:YAG laser cladding. Appl. Surf. Sci. **255**(11), 5662–5668 (2009)
137. Liu, W.-G., et al.: Development and characterization of composite Ni–Cr–C–CaF_2 laser cladding on γ-TiAl intermetallic alloy. J. Alloys Compd. **470**(1), L25–L28 (2009)
138. Papyrin, A.: 2 – The development of the cold spray process A2. In: Champagne, V.K. (ed.) The Cold Spray Materials Deposition Process, pp. 11–42. Woodhead Publishing, Cambridge, England (2007)
139. Du, H., et al.: Structure, mechanical and sliding wear properties of WC–Co/MoS_2–Ni coatings by detonation gun spray. Mater. Sci. Eng. A. **445**, 122–134 (2007)
140. Du, H., et al.: Fabrication and evaluation of D-gun sprayed WC–Co coating with self-lubricating property. Tribol. Lett. **23**(3), 261–266 (2006)
141. Du, L., et al.: Effect of NiCr clad $BaF_2{\cdot}CaF_2$ addition on wear performance of plasma sprayed chromium carbide-nichrome coating. J. Therm. Spray Technol. **19**(3), 551–557 (2010)
142. Du, L., et al.: Preparation and characterization of plasma sprayed Ni_3Al–hBN composite coating. Surf. Coat. Technol. **205**(7), 2419–2424 (2010)
143. Sahraeinejad, S., et al.: Fabrication of metal matrix composites by friction stir processing with different particles and processing parameters. Mater. Sci. Eng. A. **626**, 505–513 (2015)
144. Aruri, D., et al.: Wear and mechanical properties of 6061-T6 aluminum alloy surface hybrid composites [(SiC + Gr) and (SiC + Al_2O_3)] fabricated by friction stir processing. J. Mater. Res. Technol. **2**(4), 362–369 (2013)

145. Klinkov, S.V., Kosarev, V.F., Rein, M.: Cold spray deposition: significance of particle impact phenomena. Aerosp. Sci. Technol. **9**(7), 582–591 (2005)
146. Champagne, V.K.: 1 – Introduction. In: The Cold Spray Materials Deposition Process, pp. 1–7. Woodhead Publishing, Cambridge, England (2007)
147. Papyrin, A.N.: Preface. In: Cold Spray Technology, pp. x–xii. Elsevier, Oxford (2007)
148. Assadi, H., et al.: Bonding mechanism in cold gas spraying. Acta Mater. **51**(15), 4379–4394 (2003)
149. Papyrin, A., et al.: Chapter 1 – Discovery of the cold spray phenomenon and its basic features. In: Cold Spray Technology, pp. 1–32. Elsevier, Oxford (2007)
150. Botef, I., Villafuerte, J.: Overview. In: Villafuerte, J. (ed.) Modern Cold Spray: Materials, Process, and Applications, pp. 1–29. Springer International Publishing, Cham (2015)
151. Stark, L., et al.: Self-lubricating cold-sprayed coatings utilizing microscale nickel-encapsulated hexagonal boron nitride. Tribol. Trans. **55**(5), 624–630 (2012)
152. Moghadam, A.D., et al.: Mechanical and tribological properties of self-lubricating metal matrix nanocomposites reinforced by carbon nanotubes (CNTs) and graphene – a review. Compos. Part B Eng. **77**, 402–420 (2015)
153. Wang, J., et al.: Reinforcement with graphene nanosheets in aluminum matrix composites. Scr. Mater. **66**(8), 594–597 (2012)
154. Bartolucci, S.F., et al.: Graphene–aluminum nanocomposites. Mater. Sci. Eng. A. **528**(27), 7933–7937 (2011)
155. Stankovich, S., et al.: Graphene-based composite materials. Nature. **442**(7100), 282–286 (2006)
156. Rafiee, M.A., et al.: Enhanced mechanical properties of nanocomposites at low graphene content. ACS Nano. **3**(12), 3884–3890 (2009)
157. Xue, B., et al.: Microstructure and functional mechanism of friction layer in Ni_3Al matrix composites with graphene nanoplatelets. J. Mater. Eng. Perform. **25**(10), 4126–4133 (2016)
158. Chmielewski, M., et al.: Tribological behaviour of copper-graphene composite materials. Key Eng. Mater. **674**, 219–224 (2016)
159. Chen, F., et al.: Effects of graphene content on the microstructure and properties of copper matrix composites. Carbon. **96**, 836–842 (2016)
160. Moghadam, A.D., et al.: Functional metal matrix composites: self-lubricating, self-healing, and nanocomposites-an outlook. JOM. **66**(6), 872–881 (2014)
161. Akhlaghi, F., Zare-Bidaki, A.: Influence of graphite content on the dry sliding and oil impregnated sliding wear behavior of Al2024–graphite composites produced by in situ powder metallurgy method. Wear. **266**(1–2), 37–45 (2009)
162. Akhlaghi, F., Pelaseyyed, S.A.: Characterization of aluminum/graphite particulate composites synthesized using a novel method termed "in-situ powder metallurgy". Mater. Sci. Eng. A. **385** (1–2), 258–266 (2004)
163. Ravindran, P., et al.: Investigation of microstructure and mechanical properties of aluminum hybrid nano-composites with the additions of solid lubricant. Mater. Des. **51**, 448–456 (2013)
164. Suresha, S., Sridhara, B.K.: Wear characteristics of hybrid aluminium matrix composites reinforced with graphite and silicon carbide particulates. Compos. Sci. Technol. **70**(11), 1652–1659 (2010)
165. Choi, H.J., Lee, S.M., Bae, D.H.: Wear characteristic of aluminum-based composites containing multi-walled carbon nanotubes. Wear. **270**(1–2), 12–18 (2010)
166. Poirier, D., Gauvin, R., Drew, R.A.L.: Structural characterization of a mechanically milled carbon nanotube/aluminum mixture. Compos. A Appl. Sci. Manuf. **40**(9), 1482–1489 (2009)
167. Venkatesan, S., Anthony Xavior, M.: Investigation of aluminum (Al7050) metal matrix composites reinforced with graphene nanoparticles using stir casting process. Int. J. Appl. Eng. Res. **10**(15), 35778–35783 (2015)
168. Baradeswaran, A., Perumal, A.E.: Wear and mechanical characteristics of Al 7075/graphite composites. Compos. Part B Eng. **56**, 472–476 (2014)

169. Riahi, A.R., Alpas, A.T.: The role of tribo-layers on the sliding wear behavior of graphitic aluminum matrix composites. Wear. **251**(1–12), 1396–1407 (2001)
170. Basavarajappa, S., et al.: Influence of sliding speed on the dry sliding wear behaviour and the subsurface deformation on hybrid metal matrix composite. Wear. **262**(7), 1007–1012 (2007)
171. Guo, M.L.T., Tsao, C.Y.A.: Tribological behavior of self-lubricating aluminium/SiC/graphite hybrid composites synthesized by the semi-solid powder-densification method. Compos. Sci. Technol. **60**(1), 65–74 (2000)
172. Ravindran, P., et al.: Tribological behaviour of powder metallurgy-processed aluminium hybrid composites with the addition of graphite solid lubricant. Ceram. Int. **39**(2), 1169–1182 (2013)
173. Shanmughasundaram, P., Subramanian, R.: Wear behaviour of eutectic Al-Si alloy-graphite composites fabricated by combined modified two-stage stir casting and squeeze casting methods. Adv. Mater. Sci. Eng. **2013**, 8 (2013)
174. Goldbaum, D., et al.: Tribological behavior of TiN and Ti (Si,C)N coatings on cold sprayed Ti substrates. Surf. Coat. Technol. **291**, 264–275 (2016)
175. Li, J., et al.: FIB and TEM characterization of subsurfaces of an Al–Si alloy (A390) subjected to sliding wear. Mater. Sci. Eng. A. **421**(1–2), 317–327 (2006)
176. Li, J.L., Xiong, D.S., Huo, M.F.: Friction and wear properties of Ni–Cr–W–Al–Ti–MoS_2 at elevated temperatures and self-consumption phenomena. Wear. **265**(3), 566–575 (2008)
177. Zhang, S., et al.: Preparation and characterization of reactively sintered Ni_3Al–hBN–Ag composite coating on Ni-based superalloy. J. Alloys Compd. **473**(1), 462–466 (2009)
178. Tyagi, R., Xiong, D., Li, J.: Effect of load and sliding speed on friction and wear behavior of silver/h-BN containing Ni-base P/M composites. Wear. **270**(7), 423–430 (2011)
179. Tsuya, Y., Umeda, K., Kitamura, M.: Optimum concentration of solid lubricant in compact. Lubr. Eng. **32**(8), 402–407 (1976)
180. Kumar, P.S., Manisekar, K., Vettivel, S.C.: Effect of extrusion on the microstructure and tribological behavior of copper-tin composites containing MoS_2. Tribol. Trans. **59**(6), 1016–1030 (2016)
181. Rohatgi, P.K., et al.: Tribology of metal matrix composites. In: Menezes, L.P., et al. (eds.) Tribology for Scientists and Engineers: From Basics to Advanced Concepts, pp. 233–268. Springer, New York (2013)
182. Lince, J.R.: Tribology of co-sputtered nanocomposite Au/MoS_2 solid lubricant films over a wide contact stress range. Tribol. Lett. **17**(3), 419–428 (2004)
183. Stoyanov, P., Strauss, H.W., Chromik, R.R.: Scaling effects between micro-and macro-tribology for a Ti–MoS_2 coating. Wear. **274**, 149–161 (2012)
184. Uemura, M., et al.: Effect of friction mechanisms on friction coefficient of MoS_2 in an ultrahigh vacuum. Lubr. Eng. **43**(12), 937–942 (1987)
185. Rupert, T.J., Schuh, C.A.: Sliding wear of nanocrystalline Ni–W: structural evolution and the apparent breakdown of Archard scaling. Acta Mater. **58**(12), 4137–4148 (2010)
186. Rupert, T., et al.: Experimental observations of stress-driven grain boundary migration. Science. **326**(5960), 1686–1690 (2009)
187. Hamilton, G.M.: Explicit equations for the stresses beneath a sliding spherical contact. Proc. Inst. Mech. Eng. C J. Mech. Eng. Sci. **197**(1), 53–59 (1983)
188. Yao, B., Han, Z., Lu, K.: Dry sliding tribological properties and subsurface structure of nanostructured copper at liquid nitrogen temperature. Wear. **301**(1), 608–614 (2013)
189. Kliemann, J.-O., et al.: Formation of cold-sprayed ceramic titanium dioxide layers on metal surfaces. J. Therm. Spray Technol. **20**(1–2), 292–298 (2011)
190. Yamada, M., et al.: Cold spraying of TiO_2 photocatalyst coating with nitrogen process gas. J. Therm. Spray Technol. **19**(6), 1218–1223 (2010)

RETRACTED CHAPTER: Self-Lubricating Polymer Composites

3

Ajay Kumar Prajapati, Emad Omrani, Pradeep L. Menezes, and Pradeep K. Rohatgi

Contents

The original version of this chapter was revised. An erratum of the original chapter can be found under https://doi.org/10.1007/978-3-662-56528-5_11

A. K. Prajapati (✉) · E. Omrani · P. K. Rohatgi
Department of Materials Science and Engineering, University of Wisconsin-Milwaukee, Milwaukee, WI, USA
e-mail: Kumar38@uwm.edu

P. L. Menezes
Department of Mechanical Engineering, University of Nevada Reno, Reno, Nevada, USA

corrected publication 2020, P. L. Menezes et al. (eds.), *Self-Lubricating Composites*, https://doi.org/10.1007/978-3-662-56528-5_3

Abstract

Friction and wear during sliding or rolling of solid surfaces are universal phenomena, and they reflect the tendencies of energy to dissipate material to deteriorate. In general, solid surfaces in relative motion require lubrication, which dramatically reduces the extent of friction and wear. The situation when no external lubrication is required is called self-lubrication. Self-lubricating polymer composite materials are two-phase system that contain soft second-phase particles in the polymer matrix. The soft phase exposed to the surface during sliding. So the properties of both the hard matrix and the soft second-phase particles, as well as the shape and size of the particles, control the processes of deformation and flow of the soft phase. This chapter details polymer matrix structures, self-lubricating polymer composites, mechanisms of polymer composite lubrication, transfer film mechanisms, factor affecting polymer composites on friction, and wear and application of polymer composites.

3.1 Introduction

Lubrication in automobiles and aircrafts presents most of the problems that are encountered in terrestrial applications. In some instances, though, liquids cannot be utilized. For example, they would not be used when (a) contamination by a liquid is a problem, (b) in cold temperatures where liquids freeze or become too viscous to pour, and (c) in high temperatures where they thermally breakdown. In these cases, solid lubricants must be employed. The most common way to utilize solid lubricants is to apply them as films to metallic surfaces. The solid lubricant can be (a) burnished (rubbed) onto the surface, (b) vapor deposited by techniques such as sputtering or ion plating, and (c) incorporate into a binder system which contains a liquid carrier and then applied as a film by spraying, dipping, etc. The binder material does not necessarily have to be a lubricant, and its principle purpose is to bind solid lubricant particles to the metallic surface after the liquid carrier is removed. Another way to utilize solid lubricants is to make the sliding mechanism or a component of the mechanism into a self-lubricating composite. Among various reinforcements, recent emerging material, carbonous materials, is found to have many favorable attributes such as high thermal conductivity, low coefficient of thermal expansion, high damping capacity, and good self-lubricant property [1, 2]. Considerable amount of research has been made to study the influences of embedding graphite particles into the metal matrix on the tribological properties of aluminum alloys [3–5]. Metal matrix composites embedded by graphite or carbon fibers have self-lubricating behavior since graphite act as a solid lubricant [6–8]. In this regard, solid lubricant as reinforcement tends to decrease the friction coefficient of MMCs and improve tribological properties of self-lubricating composite compared to composites reinforced by ceramic particles. The graphite sizes, which is commonly used in MMCs fabrication and obtaining desired mechanical and self-lubricating properties, are in the micron range [9–16]. Authors have also reported polymer matrix composites reinforced with natural fibers in the green materials world are showing a good potential for employing in several applications due to their positive economic and

environmental aspects, as well as their good tribological properties [17]. It has been found that the graphene nanoplatelets reinforced nano-composites showed superior tribological properties and demonstrated the ability of the self-lubricating nature of the composite during tribological conditions [18]. Authors have brought self-lubricating composites into different operating systems to reduce the use of external toxic petroleum-based lubricants in sliding contacts in a way to help the environment and reduce energy dissipation in industrial components for strategies toward sustainability and energy efficiency [19]. Authors have developed Al-16Si-5Ni-5Graphite composite successfully synthesized as a substitute material for steel in piston ring materials [14].

A self-lubricating composite is a material that consists of a reinforcing matrix, one or more reinforcements including solid lubricant additives, and various other constituents which are added for binding components together, for environmental stabilization, etc. An example of where a self-lubricating composite might be used is in the case of a rolling element bearing. The most common solid lubricants employed in terrestrial applications are the layer lattice compounds, graphite and molybdenum disulfide and the polymer, polytetrafluoroethylene (PTFE). Graphite usually is not used for space applications since it needs absorbed vapor to be a good lubricant. Molybdenum disulfide on the other hand works much better in the absence of absorbed vapors; thus, it is a widely used solid lubricant in space. It does have a couple of problems and those are: (a) its life can be shortened if it slides too long in air before it is used in vacuum and (b) longtime storage can sometimes induce decomposition to molybdenum oxide.

In general, PTFE works well both in presence of vapors and in a vacuum environment. However, PTFE also has a problem in that it tends to cold flow under load and must be incorporated into some sort of a binder system to keep it in place. To date, there have not been many other polymer materials widely utilized for various applications. However, some recent work by Fusaro [20] indicated that some of the polyimide polymers also possess excellent lubrication properties in a vacuum environment, but they must be properly conditioned first. More research needs to be conducted on these materials before they will become qualified, however, since there is vast potential for the greater use of polymers in lubrication, it is the purpose of this chapter to review the current understanding of polymer lubrication. This will be done by looking at the properties of polymers and the environmental factors that can affect their friction, wear, and transfer performance due to film formation. Some different polymers, fillers for polymers, and means of incorporating polymers or polymer composites into sliding mechanisms will be discussed. In addition, the chapter will review the current use of polymers and polymer composites as space lubricants.

3.2 Polymer Structure

In order to understand the physical properties of polymers, considerable research has been conducted on their molecular structure. Nearly all polymers used today for lubrication or mechanical purposes are organic polymers. They consist of very

large molecules which contain carbon atoms as the main component in their backbone. Polymers tend to grow into long chains which are built up of repeating small chemical units called monomers. A polymer can grow to a molecular weight of several million, depending on polymerization conditions. The length of the chain can affect the mechanical properties of the polymer.

Polymers can be classified as being thermoplastics or thermosets. Thermoplastics have a lack of cross-linking between the long-chain molecules, while thermosets are highly cross-linked. Polymers may also be classified as being either amorphous or crystalline; however, even in well-crystallized polymers, amorphous regions have been found to exist. Likewise, in amorphous polymers, crystalline regions have been observed. Undoubtedly, the interaction of these regions, as well as the transformation from one phase to another, can influence the physical properties of a polymer. In order to explain the various physical properties of polymers, several models of polymer structure have been proposed. Some of the most prominent models are (l) random coil, (2) fringed micelle, (3) folded chain, (4) extended chain, and the (5) molecular domain. The model that is most widely accepted for crystalline polymers is the folded chain. It is based on the fact that complex aggregates of molecules, called spherulites, exist throughout the entire mass of solid polymers. X-ray diffraction studies have shown these spherulites to be composed of plate like lamellae. These lamellae are characterized by a rather uniform thickness, of the order of 5–100 nm.

Scanning electron microscopy and X-ray diffraction studies have shown that the lamellae consist of regularly folded chains which are perpendicular to the lamellae surface; thus, the reason for the model has been designated as folded-chain. Figure 3.1 gives a schematic representation of a polymer which has been crystallized under different conditions and has attained different degrees of order [21]. Folded chains, extended chains, and the amorphous nature of the polymer can also be seen in the figure. If the distance between the folds becomes greater than 200 nm, the crystal is then designated as an extended chain crystal. When no folds are present, the term fully extended-chain crystal is applied.

There are several ways that the extended-chain crystals can form. They can be formed from the melt by regulating crystallization conditions, they can be formed in a polymer solid by annealing it at temperatures above the crystallization temperature, or they can be formed by applying a mechanical stress to a polymer so as to induce chain unfolding.

Two models for chain unfolding by mechanical deformation of lamellae have been proposed [22]. The first proposes that by plastic deformation, the chains simply unfold in the direction of the applied force. The second proposes that by shearing deformation, the chains gradually become tilted by twisting and slipping and thus become progressively oriented in the direction of the force. Whichever the case, it appears that the extended chain structure is the preferred structure when low friction and wear are desired.

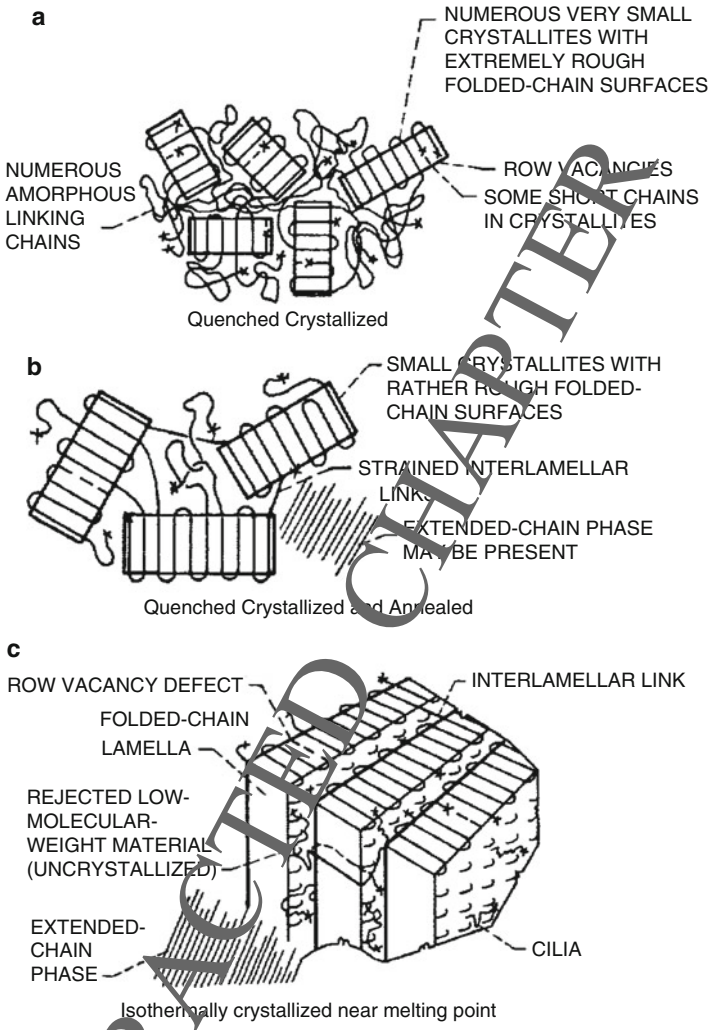

Fig. 3.1 Schematic representation of fine structure of a polymer prepared under different crystallization conditions [21]

3.3 Self-Lubricating Polymer Composites

There are several reasons for adding other materials to polymers to make composites. One reason is to increase the polymer's load carrying capacity. Fibers or particulates can be used to accomplish this. In general, fiber composites tend to have better load carrying capacity than particulate composites. A second reason for

Table 3.1 Plastics and fillers for self-lubricating composites [23]

Thermoplastics	Max useful temp, °C
Polyethylene (high MW and UHMW)	80
Polyacetal (homo- and co-polymer)	125
Nylons (types 6, 6.6, 11)	130
Poly (phenylene sulfide)	200
Poly (tetrafluoroethylene)	260
Poly (p-oxybenzoate)	300
Thermosetting	
Phenolics	~150
Cresylics	~150
Epoxies	~200
Silicones	~250
Polyimides	~300
Reinforcements	
Glass fibers	–
Asbestos fibers	–
Textiles (polyester, "Nomex," cotton)	–
Mica	–
Friction and wear reducing additives	
Graphite	–
Molybdenum disulfide	–
Polytetrafluoroethylene (PTFE)	–
Metal oxides	–
Silicon fluids	–
Thermal conductivity adjunctives	
Bronze	–
Graphite	–
Sliver	–

making a composite is to include lubricating additives to help lower the friction coefficient and the wear rate. One must be careful with these additives though, since they can also lower the load carrying capability because of the lubricating additives have easy slip planes. This is true especially when particulate lubricating additives are used. When higher load carrying capacity and good lubrication are desired, composites are often formulated using both reinforcing fibers and lubricating particulate additives, or sometimes with a combination of nonlubricating and lubricating fibers. Fibers can be chopped into short pieces and randomly dispersed throughout the polymer matrix or continuous. Fibers can be used to form two- or three-dimensional mats which are then filled with the polymer. A third reason for using additives is to increase the composite's thermal conductivity. Polymers in general are not good thermal conductors; thus, to reduce the heat build-up in sliding contacts, a thermally conductive material may be added. Some possible polymers

Table 3.2 Some self-lubricating composites and their possible uses in space [23]

Composite type	Uses
PTFE/glass fiber	Bearing cages
PTFE/glass fiber/MoS_2	Bearings, cages, gears
Polyacetal homopolymer/co-polymer	Bearings, cages, gears
Reinforced phenolics	Bearings, cages, gears
Polyimide/MoS_2	Bearing cages, gears
PTFE/Woven glass fiber/resin	Bushings
PTFE/Bronze sinter	Bushings, rotating nuts

and additives commonly incorporated into the making of polymer composites as given by *The CRC Handbook of Lubrication* [23] are listed in Table 3.1.

Polymers are classified as thermoplastics or as thermosets. Additives are classified as reinforcement, friction and wear reducing, or thermal conducting. Some particulate additives, such as graphite, are classified both as friction and wear reducing and as thermal conducting additives, but one would not want to use graphite as a friction and wear reducing additive for space applications since graphite needs absorbed vapors to be a good lubricant. Similarly, in air, graphite (carbon) fibers work very well to lower the friction and wear characteristics and to increase the load carrying capability; but one would not want to use these fibers in vacuum for lubrication purposes because of the absorbed vapor requirements. Some polymer composites and their use in space applications are listed in Table 3.2.

3.4 Mechanisms of Polymer Composite Lubrication and Wear

In order for a solid body polymer or polymer composite to provide lubrication, it must be able to support the dynamic stresses induced by the applied load and the tangential friction stresses. If the polymer/polymer composite cannot support these stresses, it will wear rapidly (plastically deform, brittle fracture, etc.). In some cases, this will cause catastrophic failure. In other cases, the composite may wear rapidly only until the contact area increases to the point where the polymer will support the decreased dynamic stresses and then transformation to a milder form of wear will occur. Stress is probably the most important parameter to consider with self-lubricating composites. A part must be designed so that the self-lubricating composite will be able to support the dynamic stress of sliding.

In the cases where a polymer or polymer composite have adequate load carrying capability, different types of wear can occur depending on the polymer and additives used and the conditions of sliding. It has been observed by Fusaro [24] that in order to provide the best lubrication, some sort of a "shear layer" must develop between the sliding surfaces. This shear layer is necessary to reduce the adhesive and the "plowing" interactions that takes place between relatively moving surfaces. In addition to reducing friction, this layer can also reduce the stresses in bulk of the

polymer body. In general, it has been observed that the thinner the shear layer the better.

Some polymer materials have the ability to form a shear layer on their own. PTFE chains can be drawn out on the surface to form an extended chain type of crystal structure which is conducive to low shear and thus low friction [25]. However, bulk PTFE does not have good load carrying capability, and thus in order to achieve long life, PTFE must be incorporated into a composite, both as a solid body and as a coating or film.

Some polyimides (a class of long chain polymers with repeating imide groups as an integral part of the chain) also can form thin shear layers at the surface but can only do so under vacuum conditions or at temperatures above 100 °C in air [20, 26]. The reason appears to be that water molecules can form hydrogen bond to the polymer chains and inhibit their ability to be drawn out on the surface into an extended chain molecule. When run under vacuum conditions or at high temperatures, friction coefficients of less than 0.02 have been obtained with these polyimides and the wear rates have been extremely low [26]. The advantage of the polyimides over PTFE is that the load carrying capability remains very high even though the friction drops to very low values. Thus, additives are not often necessary, especially for space applications. A problem with polyimide is that it is like a sponge in air and absorbs copious amounts of water vapor. The absorbed water vapor tends to cause the polyimides to give higher friction coefficient values. Merely putting the polyimide in vacuum does not remove the water vapor. The water has to be driven out by heating in vacuum, or the high friction (a friction coefficient of 0.2 or higher occurs

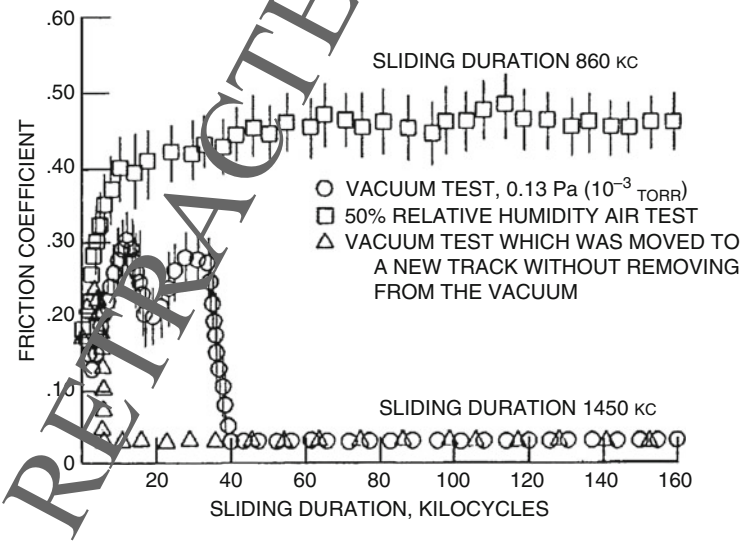

Fig. 3.2 Comparison of the friction properties of a commercially available polyimide solid body in vacuum and in 50% relative humidity air [26]

with absorbed water) must be endured until the surface layer containing the water is worn away. Currently it is not known how thick this water containing layer is or how much water vapor is involved. This is an area for research if polyimide is to become a viable lubricant in space.

Figure 3.2 Fusaro [26] plots the friction coefficient as a function of sliding distance in air and in vacuum for a commercially available polyimide (Vespel SP 1). In air, the friction coefficient starts out at about 0.20 and increases to an average value of about 0.47. In vacuum, the friction also starts off at 0.20 but eventually decreases to a value less than 0.02 after 40 kilo cycle of sliding. At 100 rpm this represents 400 min of sliding time to wear away the absorbed moisture layer and obtain low friction.

Ultra-High-Molecular-Weight-Polyethylene (UHMWPE) is another important polymer which possesses good load carrying capability, and it can shear on the surface via a very thin shear layer. However, UHMWPE does not have good high temperature stability (begins to melt at 101 °C). It does have excellent potential for lower temperature use. This material is the prevalent material used in artificial hip joints today. The quality of the shear layer formed determines how well the composite will provide lubrication. In order for it to endure it must remain bonded to the bulk of the polymer and it must have a quality which the author has designated "flowing into itself," i.e., as the counter face passes over the layer, molecules in the layer move, but they slide over one another in such manner that no apparent differences in the layer occur. Failure of the layer can occur by fatigue (debonding) of a small area of the layer from the bulk or by the gradual flow of a small portion of the layer out of the contact area.

Usually the formation of this lubricative surface layer promotes the formation of a transfer film to the counter face. As long as the transferred layer remains thin, shear will take place either within or between the two layers. If the transfer tends to build up into too thick a layer, there is a tendency for higher adhesive forces and localized stresses to occur which can increase the friction and cause the wear processes at the surface of the composite to change. Instead of the shear within the layer, larger wear particles are produced at the surface of the composite and more severe wear occurs.

3.5 Transfer Film Lubricating Mechanisms

In the lubrication mechanism mentioned above, shear takes place within the shear layer on the surface of the polymer/polymer composite, the transfer film on the counter face, or between the two. A mechanism involving a double transfer lubricating film has been devised to lubricate ball bearings. In this mechanism, the cage of the ball bearing is made out of the polymer composite material; the rest of the bearing is made of metal. The assumption behind this lubrication process is that the cage transfers material to the balls, which in turn transfers material to the inner and outer races. Figure 3.3 shows a sketch of how this transfer film mechanism operates.

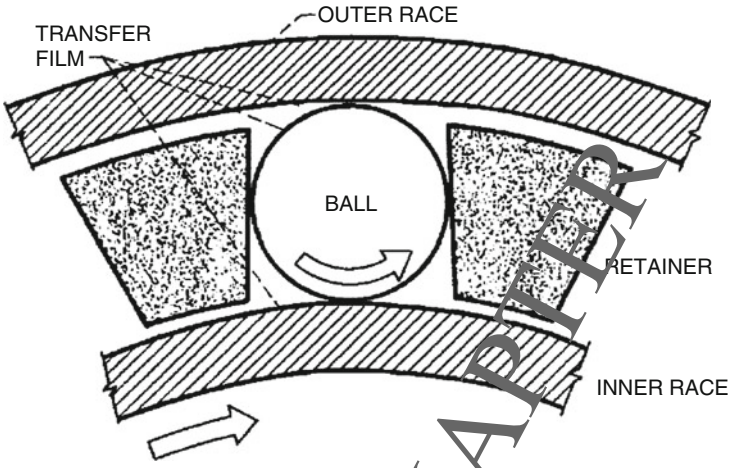

Fig. 3.3 Schematic illustration of ball bearing film transfer mechanism [27]

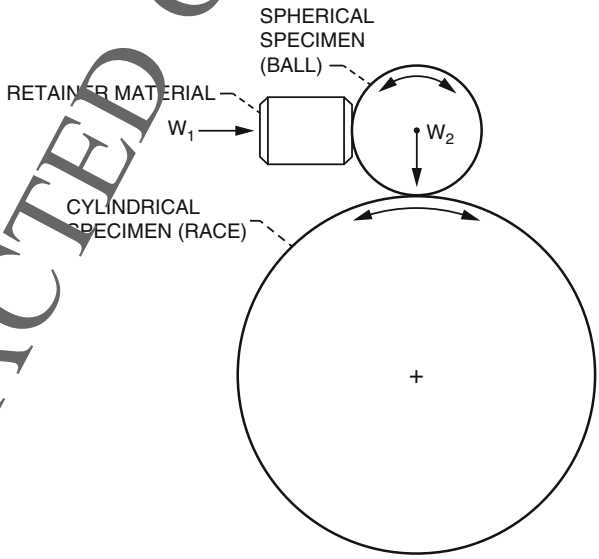

Fig. 3.4 Schematic drawing of apparatus for transfer analysis [28]

Kamal and Dufrane [28] have studied the effect of load in an ambient air atmosphere on the double transfer of a PTFE composite (Rulon-A and 5% MoS_2) in a device like that is shown in Fig. 3.4. They found that as the load (contact stress) between the ball and the ring (race) was increased, the roughness of the wear track decreased slightly. They also found that at a mean stress level of 1.38 GPa, the transfer film was insufficient to prevent roughening of the surfaces (Fig. 3.5). Their

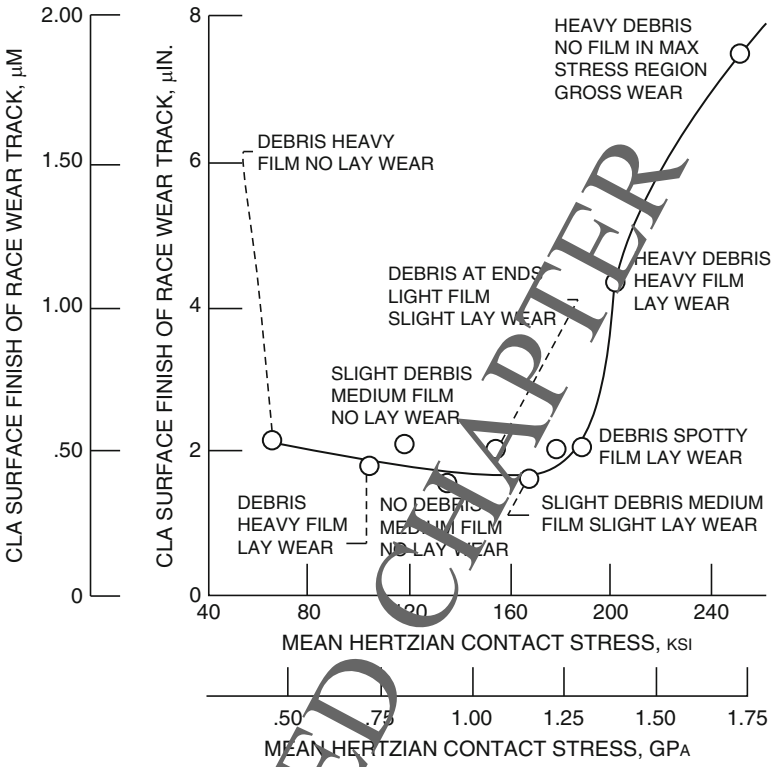

Fig. 3.5 Relationship between race wear track surface finish and ball-race contact stress for a race lubricated with a Rulon-a + 5% MoS$_2$ transfer film [28]

experiments imply that there is a limiting stress for effective transfer film lubrication with PTFE composites, at least in an air environment.

Because of the load limitations, this double transfer film lubrication process ordinarily has only been used to lubricate lightly loaded, low speed ball bearings. However, it has also been used to lubricate the bearings of the Space Shuttle Main Engines (SSME) turbopumps, where it has been only minimally successful.

3.6 Factors Affecting Polymer Composite Wear and Transfer

3.6.1 Load/Stress

As mentioned previously, in order for a polymer composite to function as a solid body lubricant, it must be able to support the load and the tangential stresses induced by sliding. It has been observed that there are two regimes of polymer film wear and

composite wear dependent on load/stress [29]. Some might indicate these regimes mild and severe wear. Essentially low loads lead to mild wear, but high loads can cause severe wear. The severe wear regime is characterized by brittle fracture or severe plastic deformation.

The mild wear regime is characterized by the formation of the "shear layer" at the composite surface, the formation of a thin transfer film, and a delamination type of wear process of the shear layer. It has been shown [30] that a polyamide-bonded graphite fluoride film (0.0025 cm thick) was able to support the load and act like a solid body. Mild wear was characterized by the spallation of very thin surface layers (<1 μm thick), while severe wear was characterized by brittle fracture of the surface 1 to 6 μm deep. The depth of brittle fracture was dependent on load, area of contact, and the build-up of thick transfer films. In the mild wear regime, wear rate (wear per unit sliding distance) was found to increase linearly as a function of increasing load, while in the severe wear regime, wear rate was found to increase exponentially as a function of load and could at some point even be catastrophic.

3.6.2 Contact Area

Contact area is important from two points of view. First, the contact area will determine the projected contact stress. If the load cannot be reduced, one way of reducing the contact stress is to increase the projected contact area, which lowers the

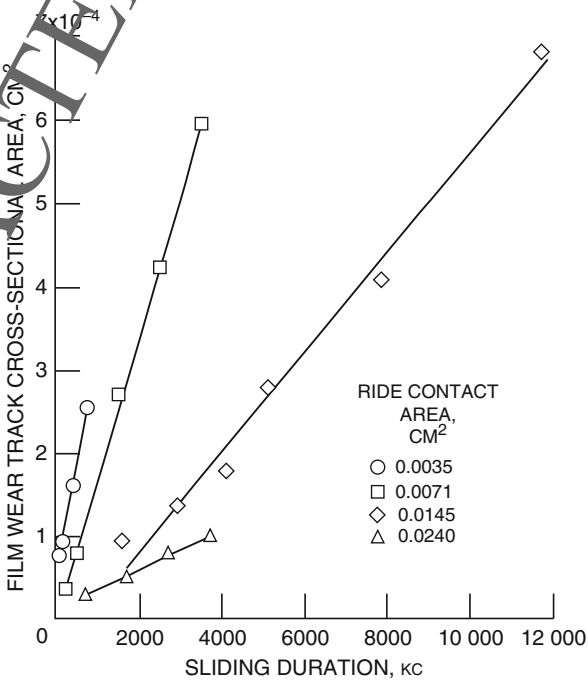

Fig. 3.6 Polyimide-bonded graphite fluoride film wear rate as a function of sliding duration for four different counterface contact areas sliding against the film under constant load [31]

stress and promotes sliding in the mild regime of wear. Figure 3.6 shows the variation of polyimide-bonded graphite fluoride film wear rate as a function of sliding duration for four different counter face contact areas sliding against the film under constant load. The figure shows that as contact area increased (and the resulting stresses decreased) the wear decreased [29]. However, a larger contact area and lower stresses can cause other problems as mentioned below.

The second effect of contact area is on transfer film formation. The contact area can affect the amount and type of transfer taking place. As mentioned previously what is desired is a very thin "plastically flowing" transfer film. If the area of contact becomes too large, instead of the transfer flowing across the metallic counter face surface, it will have a tendency to build up and form ridges which can cause high localized stresses and higher adhesion. This will lead to higher friction and severe wear. Thus, it is important to design a part with the optimum condition of load and contact area.

3.6.3 Sliding Speed

The sliding speed can have a couple of effects on polymer composites. First, high sliding speeds can produce high temperatures due to frictional heating. This may cause the polymer or the polymer composite additives to degrade. However, in some cases higher temperatures might be beneficial to the lubricating process. It could help drive out absorbed water vapor or increase the temperature above some molecular relaxation temperature which in turn could provide greater mobility to the polymer molecules.

Second, polymers are composed of molecular chains. In order to develop a surface shear film and a transfer film, the molecular chains must have time to reorient. If one slides too fast over these unoriented chains, instead of reorienting, they will fracture, leading to the production of large wear particles and high wear. Thus, it is important to appropriately choose the sliding speed for each particular polymer to ensure the best results. Absorbed gases/vapors solid lubricants are very sensitive to the atmosphere in which they are slid. Graphite needs absorbed gases or vapors to make it a good lubricant, while molybdenum disulfide functions much better in absence of absorbed gases or vapors, which makes it an excellent lubricant in vacuum. Polymer composites can be even more affected by the atmosphere in which they slide. This is partly because they may contain solid lubricant additives that are sensitive to atmospheric vapors and also because they themselves can be affected by atmospheric vapors.

PFTE seems to be the best in this regard as it is not highly affected by atmospheric conditions. But polyimides, polyamides, epoxies, and in general any polymer which has a free hydrogen bond in its structure are highly affected by absorbed vapors, especially water vapor. It is postulated that the water, which forms hydrogen bonds to the polymer chains, restricts the molecules ability to flow on the surface to form an extended chain crystal structure and consequently the thin lubricating surface layer does not form. Thus, these types of polymers, especially the polyimides, tend to lubricate much better in a vacuum [26].

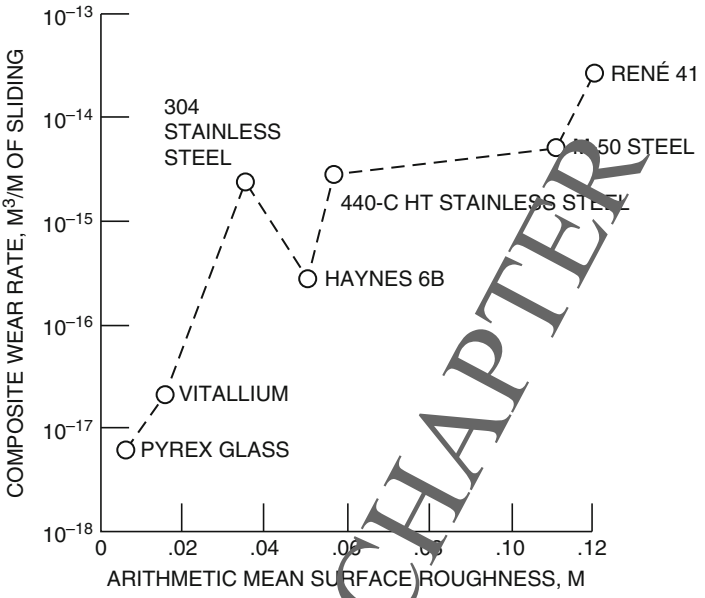

Fig. 3.7 Composite pin wear rate as a function of arithmetic mean surface roughness and material type [31]

3.6.4 Counter Face Topography

The material counter face that slides against a polymer composite is very important in determining the friction and wear characteristics of that composite. For example, if the counter face is too rough, it can abrade the composite and not allow a shear film or transfer film to form. The effect of counter face material type and surface roughness on the wear rate (Fig. 3.7) and friction coefficient (Fig. 3.8) of graphite-fiber-reinforced polyimide composites sliding against different materials with different surface roughness was studied by Fusaro [31]. All the materials, except the glass and vitallium, were given surface finishes using the same procedure. A wide variety of surface roughnesses were obtained. It was evident that to obtain a very smooth surface with a given material, a specific surface treatment needs to be developed for a particular material. Thus, from this study, it could not be ascertained whether or not the material type had an effect on the friction and wear properties. The study did demonstrate that the smoother the counter face, the lower the wear rate.

In addition, it was found that there are some factors to watch out for. A root mean square (rms) or a centerline average (CLA) low value of roughness does not always mean the surfaces are smooth. It was found that over-polishing the 440C HT stainless steel tended to polish away the softer matrix material of the metal and left hard carbide particles protruding above the surface. When the polymer composite slid against this surface, it was severely abraded.

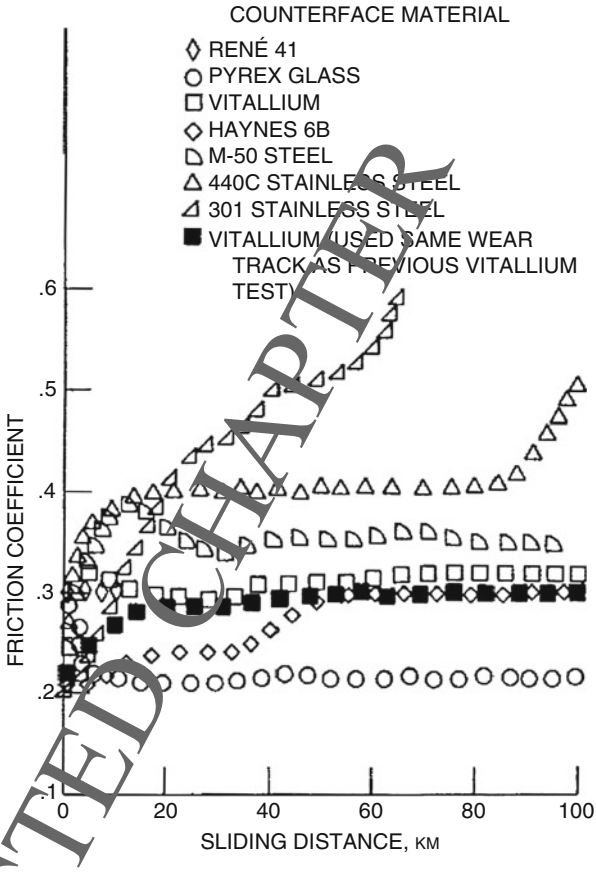

Fig. 3.8 Friction coefficient as a function of sliding distance for graphite fiber reinforced polyimide pins sliding against various counter faces in 50% relative humidity air at 25 °C [31]

Surface finish or material type did not initially affect the friction coefficient. Friction tended to start out at the same value; but as sliding distance increased, transfer characteristics changed and so did the friction coefficients. The best results were obtained with Pyrex glass which was the smoothest surface and produced extremely thin transfer films. It should be pointed out that these tests were done in air and equivalent results may not occur in vacuum for this composite material since graphite is involved, but it is believed that the basic principles about surface roughness and transfer do apply.

3.6.5 Cleanliness

Cleanliness is an extremely important parameter in dealing with polymer composites. As mentioned previously, absorbed gases and vapors can affect polymer friction and wear, likewise adsorbed liquids can have similar deleterious effects. Dirt can even have more disastrous effects. Dirt can embed into the surface of the composite

Fig. 3.9 Shows a surface profile of the Sliding contact areas illustrating the wear caused by an embedded hard particle in the UHMWPE disk [29]

and turn it into abrasive material instead of a lubricant. Figure 3.9 shows a small hard inclusion which got imbedded into an UHMWPE polymer solid [29]. The particle acted like an abrasive and wore a groove in the 440C stainless steel (Rockwell C-60) counter face.

3.6.6 Temperature and Molecular Relaxations

Most polymers possess molecular relaxations, i.e., at certain temperatures various molecular segments are freed up and give the capability for movement. For example, the glass transition temperature is the temperature above which the movement of the main chain in the polymer obtains its greatest degree of freedom (or conversely the temperature below which the motion is frozen) and thus the polymer obtains a great deal of plasticity above this temperature. Other relaxations can occur at lower temperatures in polymers which relate to movements of molecular segments, side chains, etc. These movements or restrictions of movements can seriously affect the tribological properties of a polymer. They can restrict small movement in the chains which can restrict the formation of the thin "shear layer."

One method for determining the temperatures at which relaxations occur in polymers is a technique called torsional braid analysis (TBA). Fusaro [22] attempted to correlate the relaxations as determined by TBA techniques to the friction properties of a commercially available polyimide (PI 4701). The results of that study are shown in Fig. 3.10 where the logarithmic decrement as determined by TBA and friction coefficient is plotted as a function of sliding distance. Essentially four TBA relaxation peaks were found. The most pronounced peak was the peak which correlated to the glass transition temperature. When the friction coefficient values were compared to these peaks, it was found that there was a significant friction change correlating to a α-peak (the glass transition temperature) and one correlating to the B-H20 peak (due to absorbed water vapor). It was interesting that heating the polyimide to 500 °C in dry argon increased the glass transition temperature to 500 °C and decreased the friction coefficient in this temperature region (300–500 °C) also. Later studies have shown that if the absorbed water vapor can be removed from this polyimide, low friction coefficients can also be obtained below 50 °C [26].

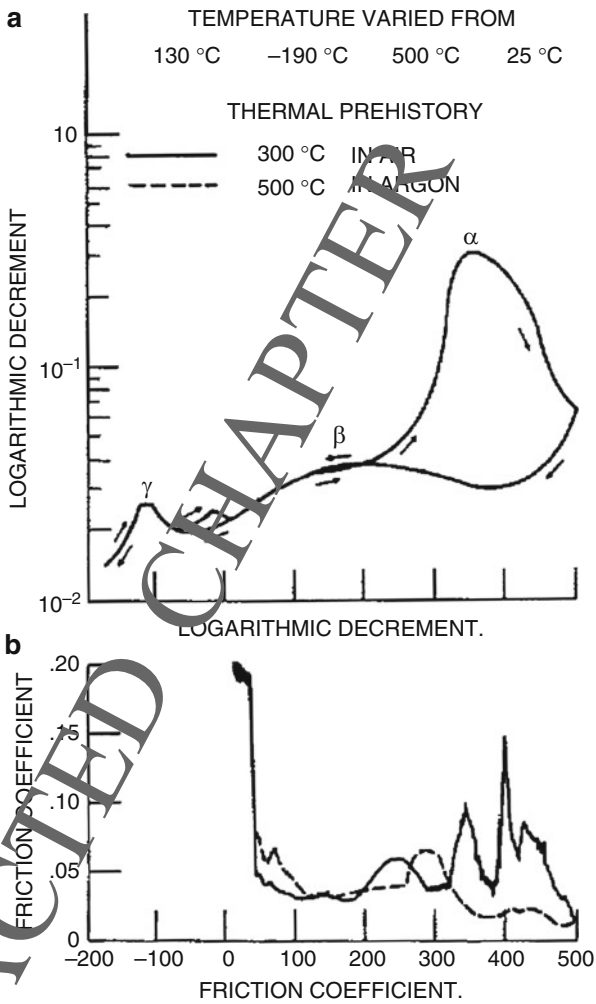

Fig. 3.10 Comparison of logarithmic decrement (a ratio of the energy dissipated to the maximum energy stored during mechanical deformation) and the friction coefficient as a function temperature in dry argon for a commercially available polyimide film [22]

Another example of molecular relaxation effects occurs with PTFE. PTFE has a couple of relaxations that occur below ambient temperature. It is known that at lower temperatures, the friction and wear properties of PTFE are not as exceptional as they are at or above ambient (~25 °C) temperature. The most likely cause of decreased friction and wear properties is the restriction of motion of molecular segments of the PTFE chain.

In addition to relaxation effects which occur at various temperatures in polymers, temperature can affect the lubricating properties of the additives in polymer composites. Additives might desorb gases at certain temperatures or even decompose. Temperature can also affect the bonding between the additives and the polymer matrix. These are some of the ways that temperature can affect polymer composite friction and wear. Very few polymer materials, if any, have friction and wear properties independent of temperature.

Table 3.3 Tribological behavior of plastic gears [32]

Test	Materials		Tooth load, N/mm	Pinion speed, rpm	Lubricant	Total pinion revs	Tooth flank wear rate, mm depth per encounter	
	Pinion	Wheels					Pinion	Wheels
1	Carbon fibre inpoly-acetal	Stain-less steel	[a]21 (60)	50	Dry	5×10^4	1×10^{-7}	Zero
2			21	50	Dry	3×10^5	7×10^{-8}	
3			21	50		5×10^5	7×10^{-8}	
4			21	100		7×10^5	7×10^{-8}	
5			21	200		16×10^5	5×10^{-9}	
6			21	500		30×10^5	5×10^{-9}	
7			21	1000		60×10^5	5×10^{-9}	
8			7(35)	1000		30×10^5	[b]3.5×10^{-9}	
9			3(23)	1000		30×10^5	[b]2×10^{-9}	
10			1(13)	1000		30×10^5	[b]1×10^{-9}	
11	Vespel SP31	Stain-less steel	21 (50)	50	Dry	1×10^4	1×10^{-8}	Zero
12			21	50		3×10^5	7×10^{-9}	
13				50		5×10^5	7×10^{-9}	
14				100		7×10^5	9×10^{-9}	
15				200		16×10^5	6×10^{-9}	
16				500		30×10^5	5×10^{-9}	
17				1000		60×10^5	4×10^{-9}	
18			7(30)	1000		30×10^5	3×10^{-9}	
19			3(20)	1000		30×10^5	2×10^{-9}	
20			1(10)	1000		30×10^5	1×10^{-9}	
21	Vespel SP8	Stain-less steel	7	200	Dry	1×10^5	4×10^{-8}	Zero
22				200	Dry	40×10^5	4×10^{-9}	
23				200	BP110	1×10^5	8×10^{-8}	
24				200	BP110	40×10^5	4×10^{-9}	

[a]Tooth contact stress in N/mm^2
[b]Steady state wear rate after running-in wear completed

3.7 Polymer Composite Tribology Applications

3.7.1 Gear

In general, currently polymer composite gears are only considered for use in light load, precision space applications. The composite gears are run in dry condition against stainless steel or against anodized aluminum alloys. For gears, there is a need for stiffness and hardness as well as low friction and wear. This limits the choice of composites. For example, PTFE must be heavily reinforced to be usable as a gear material. Other polymers considered for gears are polyimides, polyamides (nylons), polyamide-imides, and polyacetals. Glass fibers are used for reinforcement, and

MoS_2 is often added to lower the friction coefficient. On occasion, a polyimide with MoS_2 powder additive has been used to make gears for use in space. This material is easy to machine and very good surface finishes can be obtained; thus, it has been found suitable for fine-pitch gears.

Another material that seems to be well suited for gears is a high-pressure laminate of cotton fabric and a phenolic polymer. This material has been found to be particularly tough and resilient when used to make gears. A problem with it though is that it must be machined from sheet and thus the surface quality is not as good as desired [32]. The tribological behavior of some plastic gears as determined by Steven [32] are shown in Table 3.3.

Good results have been reported by the European Space Tribology Lab (ESTL) for both polyimide and polyacetals with lightly loaded gears running against stainless steel, titanium, or aluminum [35]. Their work indicates that polyimide gives the lowest wear rate of all polymers they tested. They also demonstrated that by incorporating carbon fibers into the polyacetal polymer, lower wear rates could be obtained as compared to the next polymer; the wear rate was still not as low as that obtained with polyimide. They also indicate that the maximum load for these materials should be limited to 10 N/mm tooth width.

Vest [34] evaluated a composite consisting of PTFE + MoS_2 + glass fibers as a retainer material for oscillating bearings and found that the bearings were still in good condition after 10,000 h (1×10^6 cycles) of testing. The author also evaluated them at 100 rpm under full circular motion and found that the bearings also to be in reasonably good shape after 12,600 h (7.6×10^7 cycles). Both tests used a 7 N (1–1/2 lb) radial load. Increasing the load to 23 N (5 lb) in the unidirectional test produced considerably more wear debris over the same running period as the 7 N loaded bearing, and the bearing surfaces were rated as poor, indicating the load carrying capacity of the bearing had been exceeded.

Christy [33] has reported that some PTFE-MoS_2 composite cages, which are used in gimbal ball bearings that dither over a 4° rotation angle, have produced transfer material to the balls in the form of lumps. When these gimbals have to slew in 50° steps, this transfer produces high torque peaks. This points out the importance of using cage materials that produce uniform transfer films.

The European Space Agency (ESA) has been using PTFE/glass fibers/MoS_2 self-lubricating composite for many years with much success as a cage material in small, lightly loaded, slow speed rotary motion ball bearings [35]. They have determined that this composite performs well as long as the Hertzian contact stress does not exceed 1200MN/m^2 at 20 °C. They have tried the composite without MoS_2, but found it works better with the MoS_2 additive. The MoS_2 appears to prevent the transfer from becoming too thick. As mentioned previously, thick transfer (especially lumpy) produces erratic torque. As Vest found, the failure in these tests was associated with the wearing-out of the cage, creating large quantities of debris.

Table 3.4 Torque results from bearing tests conducted in vacuum using metallic cages coated with sputtered MoS_2 or ion-plated lead and with PTFE-composite cages [17]

Lubricant	Axial preload	Range of average torque, Nm $\times 10^{-4}$	Range of peak-to-peak torque, Nm $\times 10^{-4}$	Remarks
None (degreased)	40 N	12–43	105–144	Torque failure after 1340 revs
Sputtered MoS_2	40 N	6–10 (20 initially)	50–100 (up to 220 initially)	Low dc torque noise, but torque failures between 0.7 and 3.6 $\times 10^6$ revs
	40 N	16–26	80–150	No torque failures
	100 N	40–50	150–250	
Ion-plated lead	250 N (after 100 N)	100–180	400–1100	
	250 N (no run in)	80–160	500–1300	dc torque steadier than for PTFE but peak-to-peak torque (noise) greater
PTFE-composite cage				No torque failures
	40 N	6–50	34–160	Stress below limit
	100 N (after 40 N)	10–60	75–250	Stress below limit (1×10^6 revs only)
	250 N (after 40/100 N)	50–500	250–1050	Stress below limit. Periods of high dc torque
	250 N (no run in)	40–500	150–700	Stress above limit. Initially high dc torque

Table 3.4 compares some torque results from bearing tests using metallic cages coated with sputtered MoS_2 or ion-plated lead, and for PTFE-composite cages [35]. The sputtered MoS_2 bearing failed between 0.7 and $3.6x10^6$ revolutions but provided low torque noise. The ion-plated lead cage and PTFE-composite cage provided approximately equivalent results except that the torque was slightly steadier and the peak-to-peak torque (noise) was greater for ion-plated lead. Roberts [36] has compared the torque properties of ion-plated lead cages, PTFE-composite cages, and PTFE-composite cages which were sputtered with MoS_2. Figure 3.11 summarizes the results of that work. Plotted here are typical "torque bands" for 20 mm bore angular-contact ball bearings lubricated with each of the above-mentioned lubricants. The values represent ambient temperature tests on bearings axially loaded to 40 N and rotated at speeds up to 200 rpm in high vacuum. Torque values were presented in bands since performance has been observed to vary from component to component. The figure indicates that the sputtered MoS_2 film dramatically lowered the torque and torque noise for the PTFE-composite cage under these test conditions.

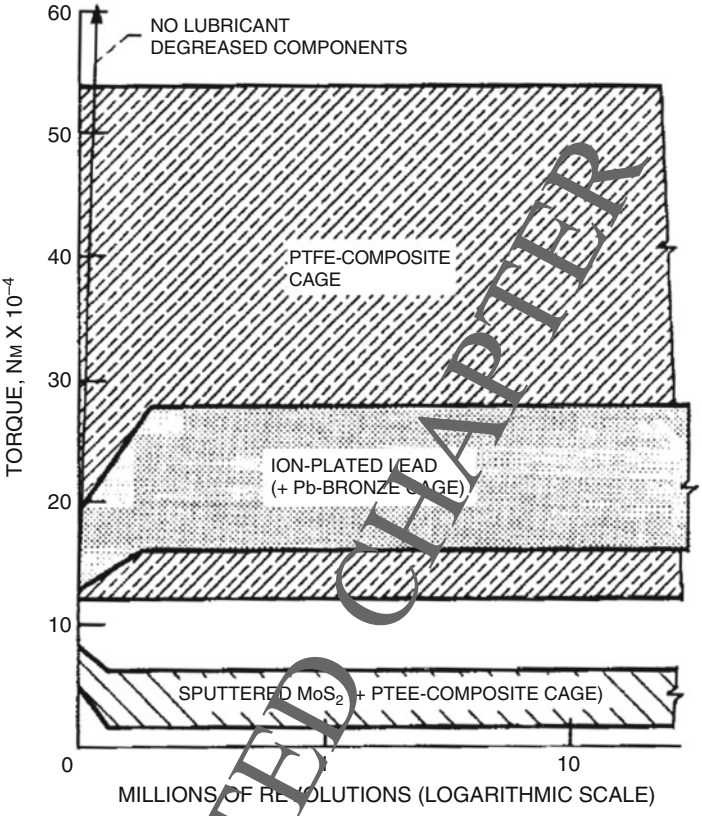

Fig. 3.11 Mean torque bands from repeated tests of solid lubricated ball bearing pairs in vacuum [36] (bearing type: ED20: 40 N preload)

3.7.2 Cryogenic Ball Bearings

There are many current and future space missions which will require instruments that must be cooled to cryogenic temperatures. These include infrared detectors, superconducting devices, and several telescopes (infrared, X-ray, gamma-ray, and high energy) [37]. In addition, high speed turbopumps, like those used on the Space Shuttle Main Engines (SSME), operate with the cryogen passing directly through the bearings. Oils and greases solidify at these temperatures; therefore, the only viable alternative is solid lubrication.

NASA has been interested in developing self-lubricating composite materials for cryogenic applications since the late 1950s/early 1960s [38, 39]. In addition, NASA has spent considerable effort at the same time developing the bearing technology necessary for utilizing these self-lubricating composite materials in a cryogenic environment [27, 40–43].

Table 3.5 Properties of PTFE formulated composite bearing cages evaluated in early NASA cryogenic bearing tests [27]

Bearing designation	Cage material	Composition, wt %	Cage construction
A	Laminated-glass cloth with PTFE binder	38% glass cloth laminates with 62% PTFE binder	One-piece body with riveted aluminum side plates
B			
C	Glass-fiber-molybdenum disulfide filled PTFE	15% glass fibers, 5% molybdenum disulfide, 80% PTFE[a]	One piece body with no external support
D			
E	Glass-fiber-filled PTFE	15–20% glass fibers, balance PTFE	One-piece body with one-piece riveted aluminum shroud
F			
G	Bronze-filled PTFE	30% bronze powder, 70% PTFE	One-piece body with no external support
H			

Ball bearings used in liquid cryogen turbopumps have several basic material and design requirements. Among them are the selection of: (l) the ball-race material, (2) the self-lubricating cage material (that provides lubricant to the load carrying surfaces by a transfer mechanism and that provides a long wear life), (3) a cage design that has adequate strength and sufficient clearances at cryogenic temperatures, and (4) the internal design and geometric factors that minimize heat generation with the bearing due to ball spin.

The best lubricant found in these early studies for use at cryogenic temperatures (and it is still the predominantly used material today) was polytetrafluoroethylene (PTFE). It was found however that PTFE had poor strength properties and tended to cold flow even under the lightest loads. It also had poor thermal conductivity which is a problem for high speed bearings, where heat generation can be detrimental to successful bearing operation. Thus, the need was established to compound it with other materials to give it more desirable properties. Some of the early formulations used were laminated glass cloth with a PTFE binder, glass-fiber-filled PTFE, glass-fiber-molybdenum disulfide-filled PTFE, and bronze-filled PTFE [27]. Table 3.5 lists some properties of those composites.

The above four composite cages were evaluated in 40-mm ball bearings. The bearings were operated in 33 K gaseous hydrogen at 20,000 rpm under a 200 lb thrust load for running times up to 10 h A profile tracing technique was used to study the formation and life histories of the transfer films provided from the cages to the bearing's inner races. Figure 3.12 shows typical surface profiles (obtained at various times during the life of the bearing) from tests using the glass cloth-filled PTFE composite cage.

It can be seen after 284 min a fairly good film of lubricant has been deposited on the inner race. However, some scratches can be seen in the profile. These were

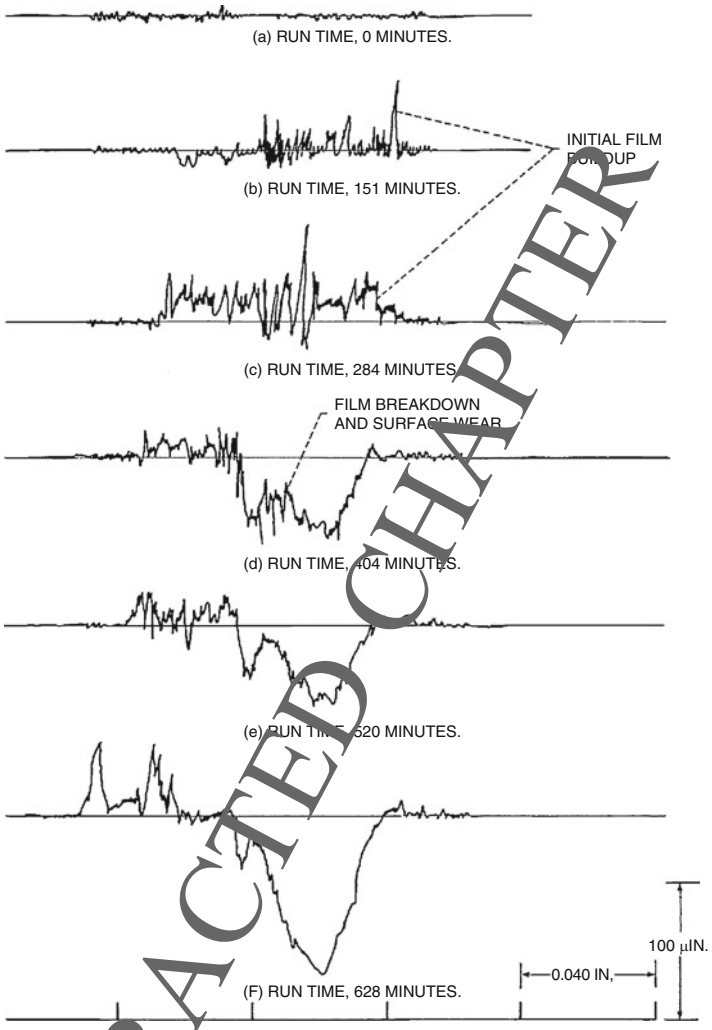

Fig. 3.12 Progressive profile traces of inner-race groove of bearing a with a laminated-glass cloth with PTFE binder cage material. Shaft speed, 20,000 rpm; thrust load, 200 pounds; coolant, hydrogen gas at 60 °R [27]

believed to have been caused by abrasion of the glass fibers in a cage material. With continued running, the film tended to break down and the wear of the inner race surface accelerated. Race wear increased with time and after l0 h the bearing was near failure. It was believed that the cause of the film breakdown and large amount of race wear was caused by the abrasion of the glass fibers which become shredded from the cage material. A postulated abrasive-wear process is illustrated in Fig. 3.13.

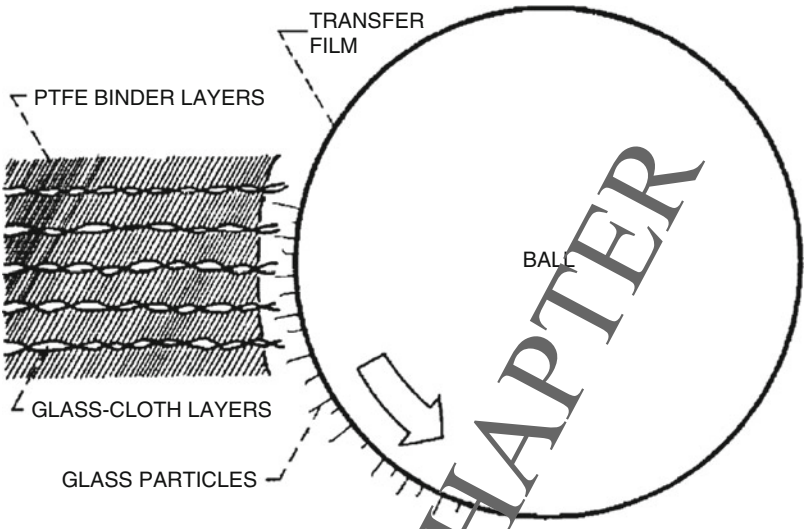

Fig. 3.13 Postulated wear process of how glass fibers from a laminated glass-cloth with PTFE binder retainer wear the races of a ball bearing [27]

The figure shows an alternate layer of glass cloth and PTFE. The ball rotates and wears away the softer PTFE material. After a short time, the PTFE is worn away exposing the glass fibers to the rubbing action of the balls.

Continued rubbing caused the glass fibers to shred and embed into the transferred PTFE film. This makes the film an abrasive and soon wears away any protecting PTFE transfer film on the race with resultant high wear of the race. The other three PTFE composites provided good transfer film production and adequate lubrication for the 10 h test duration. Although some scratches were found on the inner races with the composite that contained MoS_2, no severe wear occurred as was found in the previously mentioned case. The bronze-PTFE cage provided very thin transfer and no scratches were observed on the races.

Percent weight loss of the four PTFE composite cages is plotted as a function of time in Fig. 3.14. All four cages showed very low weight loss. The maximum weight loss was 0.89% for one of the bronze cages. This wear was attributed to the fact that it had an eccentric shape and rubbed heavily on the inner-race. The maximum weight loss for the rest of the cages was 0.25%.

Cunningham and Anderson [41] experimentally evaluated the same PTFE composite retainer materials under radial loads of 450 to 2700 N (100–600 lb) and at speeds of up to 30,000 rpm in 40-mm-bore ball bearings. The DN values (bearing bore in millimeters times shaft speed in rpm) was up to 1.2 million. Some of the results of that work are given in Fig. 3.15, where retainer wear is plotted as a function of retainer sliding distance for three of the PTFE composite materials. In these tests, the laminated glass cloth-PTFE binder exhibited the best wear resistance. Based

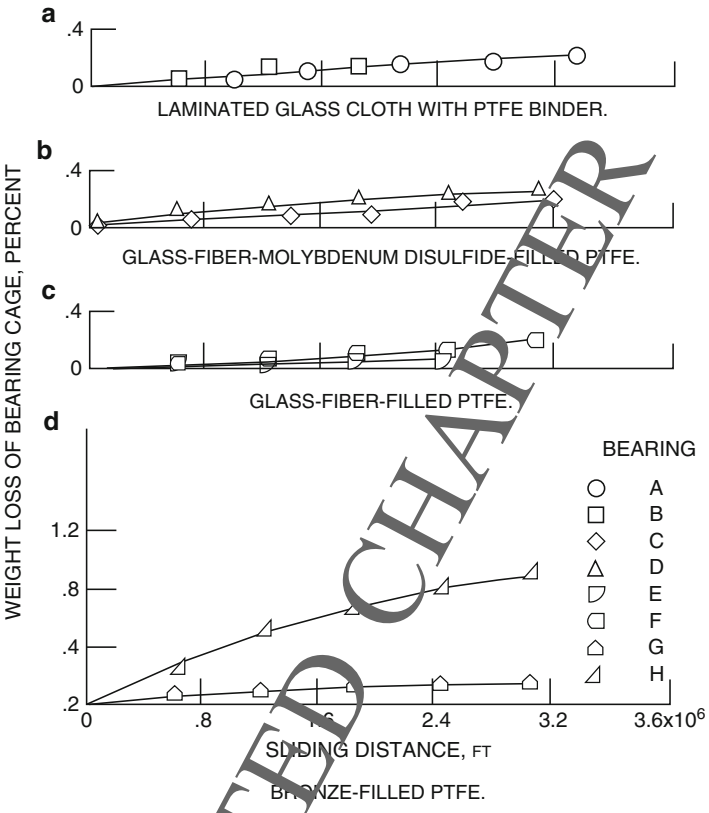

Fig. 3.14 Bearing cage weight loss as a function of sliding distance relative to the inner race for tests gun in gaseous hydrogen at 33 K. shaft speed, 20,000 rpm, thrust load, 900 N (200 lb) [27]

upon these experiments and previous work, this material was chosen as the SSME bearing cage material. The material seems to work well in the liquid hydrogen pumps, but not as well in liquid oxygen (LOX) pumps. Problems have occurred with the LOX pump bearings in that after a few launches the bearings have experienced excessive wear and must be replaced. Since it is desired that the SSME turbopumps be able to operate for multiple launches between overhauls, better cage materials are being sought [44, 45]. One of the problems encountered is developing a cage material that will provide the strength of the laminated glass cloth-PTFE binder cage, yet not be abrasive.

The European Space Tribology Laboratory (ESTL) has been evaluating the torque produced by various cage materials in vacuum (but not in the cryogenic media itself) from 300 K down to 20 K [37]. They found that the mean torque and the torque noise of bearings lubricated with composite cages containing either PTFE or MoS_2 increases with cryogenic cooling down to 20 K. Bearings fitted with lead-

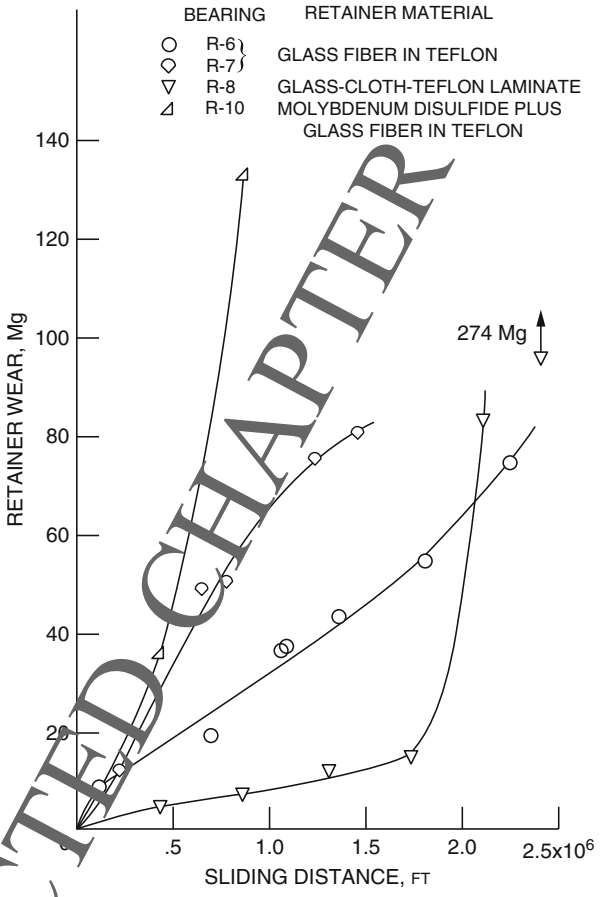

Fig. 3.15 Bearing cage weight loss as a function of sliding distance relative to the inner race for tests run in liquid oxygen. Shaft speed, up to 30,000 rpm, radial loads 450 to 1350 N (100 to 300 lb) and thrust Loads of 110 n (25 lb) [41]

containing ball retainer cages and lubricated with an ion-plated lead film showed torque levels that remained unaffected on decreasing temperature.

3.8 Concluding Remarks

The current state-of-the-art of self-lubricating polymer composites and polymer transfer film lubrication has been summarized. The chapter discusses many of the factors that affect polymer and polymer composite friction, wear, and transfer. However, many of the factors stated here which influence the tribological properties of these materials have only been evaluated in air environments. The results may not be exactly the same in a vacuum environment. Similarly, accelerated testing machines give an indication of how certain parameters affect friction and wear, but again the results achieved may be different when the lubricants are incorporated into

the real end-use device. Certainly, more work needs to be done on these materials in a vacuum environment and in end-use mechanisms to ascertain their suitability for space use.

In addition, work needs to be done on new concepts of bearing design which utilizes the special properties that polymers possess. New bearing and self-lubricating composite materials need to be assessed, especially in relation to transfer film formation and growth. While the transfer film mechanism for the lubrication of rolling element bearings has been successful for lightly loaded bearings, it seems reasonable to speculate that this may not necessarily be the best way to utilize self-lubricating polymer materials for space lubrication. The potential is there for low friction, long life self-lubricating polymer composite bearings, and the problem is to develop the technology for properly employing them and for space qualifying them.

References

1. Moghadam, A.D., Omrani, E., Menezes, P.L., Rohatgi, P.K.: Mechanical and tribological properties of self-lubricating metal matrix nanocomposites reinforced by carbon nanotubes (CNTs) and graphene: A review. Compos. Part B. **77**, 402–420 (2015)
2. Dorri-Moghadam, A., Schultz, B.F., Ferguson, J., Omrani, E., Rohatgi, P.K., Gupta, N.: Functional metal matrix composites: self-lubricating, self-healing, and nanocomposites-an outlook. JOM. **66**(6), 872–881 (2014)
3. Baradeswaran, A., Perumal, E.: Wear and mechanical characteristics of Al 7075/graphite composites. Compos. Part B. **56**, 472–476 (2014)
4. Baradeswaran, A., Perumal, A.E.: Study on mechanical and wear properties of Al 7075/Al_2O_3/graphite hybrid composites. Compos. Part B. **56**, 464–471 (2014)
5. Iacob, G., Ghica, V.G., Buzatu, M., Buzatu, T., Petrescu, M.I.: Studies on wear rate and microhardness of the Al/Al_2O_3/Gr hybrid composites produced via powder metallurgy. Compos. Part B Eng. **69**, 603–611 (2015)
6. Liu, X.-B., Liu, H.-Q., Liu, Z.-F., He, X.-M., Sun, C.-F., Wang, M.-D., et al.: Effects of temperature and normal load on tribological behavior of nickel-based high temperature self-lubricating wear-resistant composite coating. Compos. Part B Eng. **53**, 347–354 (2013)
7. Rohatgi, P.K., Tabandeh-Khorshid, M., Omrani, E., Lovell, M.R., Menezes, P.L.: Tribology of metal matrix composites. In: Tribology for Scientists and Engineers, pp. 233–268. Springer, New York, NY (2013)
8. Kestursatya, M., Kim, J., Rohatgi, P.: Wear performance of copper-graphite composite and a leaded copper alloy. Mater. Sci. Eng. A. **339**(1), 150–158 (2003)
9. Liu, Y., Rohatgi, P., Ray, S.: Tribological characteristics of aluminum-50 vol pct graphite composite. Metall. Trans. A. **24**(1), 151–159 (1993)
10. Rohatgi, P., Ray, S., Liu, Y.: Tribological properties of metal matrix-graphite particle composites. Int. Mater. Rev. **37**(1), 129–152 (1992)
11. Liu, Y., Lim, S., Ray, S., Rohatgi, P.: Friction and wear of aluminium-graphite composites: the smearing process of graphite during sliding. Wear. **159**(2), 201–205 (1992)
12. Krishnan, B., Raman, N., Narayanaswamy, K., Rohatgi, P.: Performance of an AleSi-graphite particle composite piston in a diesel engine. Wear. **60**(1), 205–215 (1980)
13. Badia, F.A., Rohatgi, P.K: Dispersion of Graphite Particles in Aluminum Castings through Injection of the Melt. Trans. AFS **76**, 402–406 (1969)

14. Menezes, P.L., Rohatgi, P.K., Lovell, M.R.: Self-lubricating behavior of graphite reinforced metal matrix composites. In: Green Tribology Biomimetics, Energy Conservation and Sustainability, pp. 445–480. Springer, Berlin/Heidelberg (2012)
15. Menezes, P.L., Reeves, C.J., Rohatgi, P.K., Lovell, M.R.: Self-lubricating behavior of graphite-reinforced composites. In: Tribology for Scientists and Engineers, pp. 341–389. Springer (2013)
16. Omrani, E., Menezes, P.L., Rohatgi, P.K.: State of the art on tribological behavior of polymer matrix composites reinforced with natural fibers in the green materials world. Eng. Sci. Technol. Int. J. **19**, 717–736 (2016)
17. Tabandeh-Khorshid, M., Omrani, E., Menezes, P.L., Rohatgi, P.K.: Tribological performance of self-lubricating aluminum matrix nanocomposites: role of graphene nanoplatelets. Eng. Sci. Technol. Int. J. **19**, 463–469 (2016)
18. Omrani, E., Moghadam, A.D., Menezes, P.L., Rohatgi, P.K.: Influences of graphite reinforcement on the tribological properties of self-lubricating aluminum matrix composites for green tribology, sustainability, and energy efficiency – a review. Int. J. Adv. Manuf. Technol. **83**, 325 (2016). https://doi.org/10.1007/s00170-015-7528-x
19. Omrani, E., Moghadam, A.D., Algazzar, M., Menezes, P.L., Rohatgi, P.K.: Effect of graphite particles on improving tribological properties Al-16Si-5Ni-5 Graphite self-lubricating composite under fully flooded and starved lubrication conditions for transportation applications. Int. J. Adv. Manuf. Technol. **87**, 929 (2016). https://doi.org/10.1007/s00170-016-8531-6
20. Fusaro, R.L.: Effect of atmosphere and temperature on wear, friction, and transfer of polyimide films. ASLE Trans. **21**(2), 125–133 (1978)
21. Hoffman, J.D., Williams, G., Passaglia, E.: Analysis of the alpha, beta, and gamma relaxations in polychlorotrifluorethylene and polyethylene: dielectric and mechanical properties. In: Boyer, R.F. (ed.) Transitions and Relaxations in Polymers. J. Polym. Sci: .Pt. C, Polym. Symp. **14**, 173–235 (1966)
22. Fusaro, R.L.: Friction Transition in Polymide Films as Related to Molecular Relaxations and Structure. NASA TN D-7954 (1975). www.ntrs.nasa.gov
23. Booser, R.E. (ed.): CRC Handbook of Lubrication, Vol. 2, Theory and Design. CRC Press, Boca Raton (1984)
24. Fusaro, R.L.: Self-Lubricating Polymer Composites and Polymer Transfer Film Lubrication for Space Application. NASA TM 102492 (1990)
25. Pooley, C.M., Tabor, D.: Friction and molecular structure: the behavior of some thermoplastics. Proc. Roy. Soc. (Lond.) A. **A329**, 251–274 (1972)
26. Fusaro, R.L.: Evaluation of several polymer materials for use as solid lubricants in space. STLE Tribol. Trans. **31**(2), 174–181 (1988)
27. Brewe, D.E., Scibbe, H.W., Anderson, N.J.: Film-Transfer Studies of Seven Ball-Bearing Retainer Materials in 60 °R (33 °K) Hydrogen Gas at 0.8 Million DN Value. NASA TN D-3730 (1966)
28. Kannel, J.W., Dickinson, J.K.F.: Rolling Element Bearings in Space. The 20th Aerospace Mechanisms Symposium, NASA CP-2423, pp. 121–132. National Aeronautics and Space Administration, Washington, DC (1986)
29. Fusaro, R.L.: Effect of load, area of contact and contact stress on the wear mechanisms of a bonded solid lubricant film. Wear. **75**, 403–422 (1982)
30. Fusaro, R.L.: Mechanisms of lubrication and wear of a bonded solid-lubricant film. ASLE Trans. **24**(2), 191–204 (1981)
31. Fusaro, R.L.: Counterface effects on the tribological properties of polyimide composites. Lubr. Eng. **42**(11), 668–675 (1986)
32. Stevens, K.T.: The tribology of gears for satellite applications. In: Guyenne, T.D., Hunt, J.J. (eds.) First European Space Mechanisms and Tribology Symposium, ESA-SP-196, pp. 131–146. European Space Agency, Paris (1983)
33. Todd, M.J.: Solid lubrication of ball bearings for spacecraft mechanisms. Tribol. Int. **15**(6), 331–337 (1982)

34. Vest, C.E., Ward Jr., B.W.: Evaluation of space lubricants under oscillatory and slow speed rotary motion. Lubr. Eng. **24**(4), 163–172 (1968)
35. Briscoe, M., Todd, M.J.: Considerations on the Lubrication of Spacecraft Mechanisms. The 17th Aerospace Mechanisms Symposium, NASA CP-2273, pp. 19–37. National Aeronautics and Space Administration, Washington, DC (1983)
36. Roberts, W.H.: Some current trends in tribology in the UK and Europe. Tribol. Int. **19**(6), 295–311 (1986)
37. Gould, S.G., Roberts, E.W.: The In-Vacuum Torque Performance of Dry Lubricated Ball Bearings at Cryogenic Temperatures. The 23rd Aerospace Mechanisms Symposium, NASA CP-3032, pp. 319–333. National Aeronautics and Space Administration, Washington, DC (1989)
38. Wisander, D.N., Maley, C.E., Johnson, R.L.: Near and friction of filled polytetrafluoroethylene compositions in liquid nitrogen. ASLE Trans. **2**(I), 58–66 (1959)
39. Wisander, D.N., Ludwig, L.P., Johnson, R.L.: Wear and Friction of various Polymer Laminates in Liquid Nitrogen and In Liquid Hydrogen. NASA TN D-3706 (1966)
40. Scibbe, H.W., Anderson, W.J.: Evaluation of ball-bearing performance in liquid hydrogen at DN values to 1.6 million. ASLE Trans. **5**(I), 220–232 (1962)
41. Cunningham, R.E., Anderson, W.: Evaluation of 40-mm Bore Ball Bearings Operating in Liquid Oxygen at DN Values to 1.2 Million. NASA TN D-2637 (1967)
42. Zaretsky, E.V., Scibbe, H.N., Brewe, D.E.: Studies of Low and High Temperature Cage Materials. NASA TM X-52262 (1967)
43. Scibbe, H.W., Brewe, D.E., Coe, H.H.: Lubrication and Wear of Ball Bearings in Cryogenic Hydrogen. NASA TM X-52476 (1968)
44. Kannel, J.N., Dufrane, K.F., Barber, S.A., Gleeson, J.: Development of improved self-lubricating cages for SSME HPOTP bearings. In: Richmond, R.J., Wu, S.T. (eds.) Advanced Earth-to-Orbit Propulsion Technology 1988, Vol. l, NASA CP-3012-VOL-I, pp. 175–189. National Aeronautics and Space Administration, Washington, DC (1988)
45. Poole, W.E., Bursey Jr., R.M.: Pratt and Whitney cryogenic turbopump bearing experience. In: Richmond, R.J., Wu, S.T. (eds.) Advanced Earth-to-Orbit Propulsion Technology 1988, Vol l, NASA CP-3012-VOL-I, pp. 190–199. National Aeronautics and Space Administration, Washington, DC (1988)

Tribology of Self-Lubricating Polymer Nanocomposites

4

Andrea Sorrentino

Contents

Abstract

In the last few years, polymeric materials filled with different kinds of nanomaterials have attracted particular attention as useful alternatives in structural components subjected to severe friction and wear loading conditions. The intention of this chapter is to give a comprehensive picture of these nanofillers and to show their ability to improve friction and wear behavior of polymer composites.

A. Sorrentino (✉)
Institute for Polymers, Composites and Biomaterials (IPCB), National Research Council (CNR), Lecco, Italy
e-mail: andrea.sorrentino@cnr.it

P. L. Menezes et al. (eds.), *Self-Lubricating Composites*,
https://doi.org/10.1007/978-3-662-56528-5_4

The aim is to organize the current state-of-the-art knowledge on these nanomaterials and point out on the key mechanisms governing their reinforcing effects. Despite the existing differences between literature results, there is a general agreement on the crucial role played by size, shape, concentration, and distribution of these fillers within the polymer matrix. The compatibility/interaction between filler and matrix is another important aspect in determining good filler dispersion and effective load transfer between the phases. As a consequence, the development of polymer nanocomposites showing high tribological features requires a deep selection of the nanofiller type and dimension along with its possible surface modification. Fortunately, modern technologies allow the design and the preparation of complex hybrid nanostructures able to put together the benefit of several structural factors. Although the state of the art demonstrates the potential of these materials, further researches are, however, necessary in order to definitely reach all possible improvements attainable for future high-demanding tribological applications.

4.1 Introduction

Nanotechnology promises breakthroughs in many areas such as materials and manufacturing, nanoelectronics, medicine and healthcare, energy, biotechnology, and food [1–3]. In the area of tribology, nanotechnology is expected to have a profound impact on design, friction reduction, wear resistance, and lubrication of moving/sliding surfaces [4–6]. The use of nanomaterials can offer a number of benefits for extending the systems lifetime, preventing their chemical and/or mechanical degradation and controlling temperature and moisture transmission [7, 8]. The key characteristic of nanomaterial is its enormous surface area-to-volume ratio, which in turn is the main responsible for the surprizing physical and chemical properties showed by these materials [9, 10]. When properly controlled, these features can be used to enhance efficiency and resistance of existing materials [11, 12]. Nanoparticles are already introduced in commercial liquid and semi-liquid lubricants for obtaining advanced capabilities and functionalities [13, 14]. Improved antiwear performances, thermal and chemical stability, as well as controlled fluidity and heat transfer, are some of the declared benefits [15, 16]. In several lubricant formulations, the aptitude of nanoparticles to carry a wide variety of additives, antioxidants, anticorrosion, and antifungal agents has been reported [17, 18].

Self-lubricant polymeric materials are normally used in applications where lightness, safety, versatility, and low cost are necessary [19]. Some examples of these applications include gears, bearing cages, artificial human joint bearing surfaces, food industry, aviation, or aerospace [20, 21]. Nanometric filler addition is a simple route to obtain a fine tuning of the mechanical and thermal properties of polymeric materials [7, 22]. In fact, a huge literature on the polymer/nanoparticles composites generally termed as “nanocomposites” reports excellent performance [23–25]. The reinforcing effects of these fillers depend on their dimensions, shape, dispersion,

distributions, and compatibility with the matrix [26, 24]. When all these factors are carefully controlled, materials with impressive properties are obtained [27, 28]. Among the other factors, the filler dimensions have attracted particular interest in recent years [10, 29, 30]. The growing commercial availability of materials with controlled nanometric dimensions open the possibility to develop a plethora of new polymer-based composites [20]. Nanomaterials are generally classified according to the number of dimensions outside the range from 1 to 100 nm. Accordingly, the 0D-materials are particles with all the three dimensions below 100 nm, the 1D-materials have two dimensions below 100 nm, and the 2D-materials have only one dimension in the nanometer scale. Among the 0D-materials there are carbon nanomaterials, Al_2O_3, $CaCO_3$, CuO, SiO_2, SiC, Si_3N_4, ZnO, ZrO_2, and TiO_2. Classical examples of 1D-materials are the carbon nanotubes and carbon nanofibers. 2D-materials include the wide class of the layered materials such as natural cationic clays, graphene, and molybdenum disulfide.

Despite the actual availability, up to now, only a limited number of these nanomaterials have been tested in polymeric materials for tribological applications [7]. When properly combined, these nanomaterials strengthen the polymer matrix and increase its load-bearing capacity [10, 29, 31]. Such improvements can expand the use of polymer materials to the applications where the control of the chemistry and morphology occurring within a few nanometers are a critical factor determining friction, wear, and stick-slip [4, 8, 32]. A correct choice of the filler-matrix pair is a complex task [33]. The filler size, shape, concentration, and, of course, the materials itself influence the lubrication performance of a specific system [34, 35]. Experimental results on the tribology characterization of nanoparticle-filled polymers have shown interesting but sometimes contradictory results. In some cases, filler contributes to enhanced wear resistance, while in other cases they have contributed to the properties deterioration of the composite [36]. Sometimes the same filler shows opposite trends when was reduced in size or when was chemically changed its affinity with the polymer matrix. In literature, particular attention was devoted to the effect of the nanofiller on the transfer film formation [4, 8]. Often, the presence of nanoparticles renders the transfer film more thin and tenacious [37]. Dispersion is another important factor in order to yield a good property profile. The natural tendency to agglomerate of the nanoparticles is considered to be a common problem, especially at higher filler contents. Some of the gains in wear resistance was also attributed to an increase in the thermal conductivity of the nanocomposite. High thermal conductivity facilitates the dissipation of the heat generated during friction and thus lowers the working temperature of the system [38].

In Fig. 4.1 the wear rates found in the literature for several polymer composites are reported [23]. In order to make a direct comparison between the different systems, results are normalized to that of the respective neat matrix. Obviously, better filler improvement is denoted by lower wear rate values at minimum filler additions [23]. It is quite evident from the plot that microcomposites require at least 10 wt% of loading for obtaining a reduction of 1 order of magnitude in the wear rate. Nanocomposites systems show a more complex behavior. In one case, filler concentrations lower than 1 wt% is sufficient for obtaining reductions greater than 1000

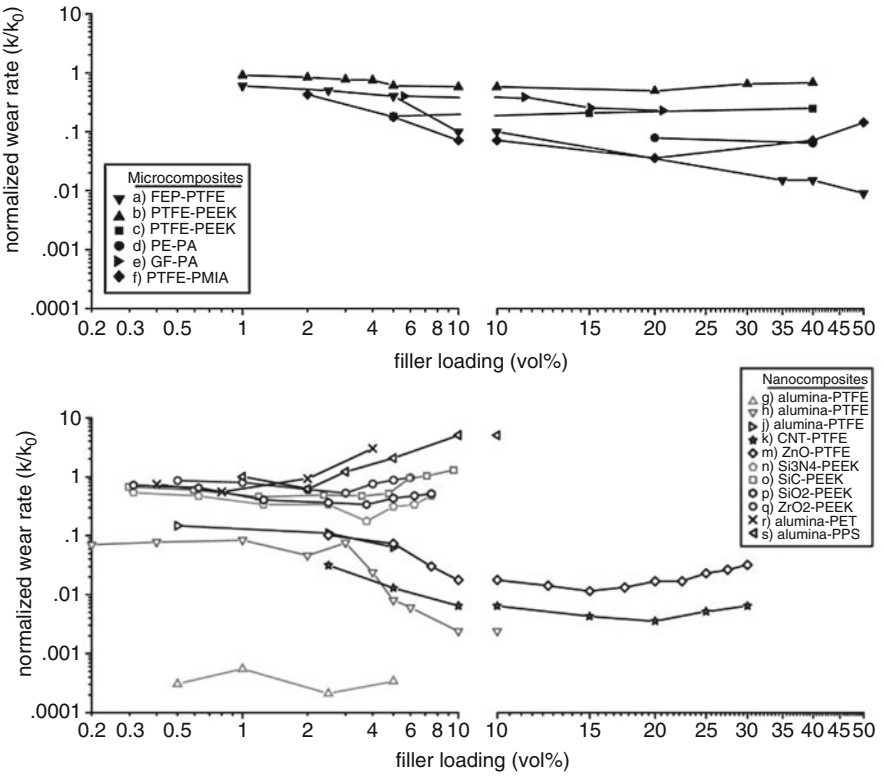

Fig. 4.1 Normalized wear rate plotted versus filler loading reported in the following references: (**a**) [39, 40]; (**b**) [41]; (**c**) [42]; (**d**) [43]; (**e**) [44]; (**f**) [45]; (**g**) [46]; (**h**) [47]; (**j**) [48]; (**k**) [49]; (**m**) [50]; (**n**) [51]; (**o**) [41]; (**p**) [52]; (**q**) [51]; (**r**) [53]; (**s**) [34]. (Reproduced from [23])

times. Evidently, nanofillers have the potential to impart new and outstanding properties to the materials for tribological applications. However, there are several aspects of these systems that must be analyzed before to obtain a complete control of their improving mechanisms [8].

This chapter presents an overview of the principal nanometric fillers actually under investigations. They were grouped into filler dimensions and are analyzed with emphasis to their tribological behavior.

4.2 0-D Fillers

The well-known metallic, ceramic, or polymeric "nanoparticles" represent the broad class of zero dimensional fillers [54]. They can be hard or soft, composed of single or multichemical elements, and exhibit various shapes and forms [55]. Up to now, several types of such nanoparticles have been incorporated into polymer matrices to improve their wear performances. In general was found that they became effective in

change the matrix wear properties at very low concentrations. It generally means that the resulting composite can be improved while retaining other properties such as density or color. Probably, the most interesting and used of these nanoparticles are those inorganic and hard. The interest in this type of nanoparticles is related to their ability to improve the mechanical modulus and the impact resistance of the polymer matrix [1].

Soft polymeric nanoparticles are also used as filler for reducing the friction [18]. Even if, in this case, the composite material becomes somewhat less tough in comparison to the pristine polymer and thus more prone to wear, a proper optimization can avoid these problems.

Current technologies allow to synthesize nanoparticles with any type of shape or dimension, either immobilized or coated onto different surface types [7, 54]. A complete and updated list of all available nanoparticles is really hard to compile [8, 18]. In the following are reported, some of the most important along with exemplary experimental results found in the literature.

4.2.1 Alluminia Oxide

Probably the alumina nanoparticles are the class of nanofiller more investigated and utilized in tribological applications [47, 56]. Lower concentrations of nanometric Al_2O_3 in polyamide produce a significant reduction in wear rates [57]. Similar results were found in polyimide nanocomposites, where reduction in friction coefficient and wear volume is observed at very low filler concentrations. In both cases, the filler addition changes the rate in transfer film formation and modifies its morphology. The wear resistance has been found to increase also in other thermoplastic materials such as poly(ethylene terephthalate) (PET) and PTFE [53]. In both cases, filler content up to 5 vol% was found to enable the deposition of thin uniform transfer films on the counterface. Higher concentrations in Al_2O_3 generally results in filler agglomeration with a resulting degradation of the transfer film. The wear rate of polyphenylene sulphide (PPS) filled with Al_2O_3 nanoparticles was studied by Schwartz and Bahadur [34]. Also in this case, the formation of the transfer film and thus the steady state wear rate resulted strongly influenced by the concentration of the filler addition. However, the coefficient of friction results almost unaffected. The reduction in wear rate was related to the increase in bond strength between the transfer film and the counterface [34].

The roughness of the counterface has a strong effect on the wear resistance of the Al_2O_3/PPS nanocomposites [58]. For the counterface with the lower roughness, the addition of Al_2O_3 nanoparticles did not have an effect on the wear rate. A morphological investigation revealed that by decreasing the roughness of the counterface the transfer film becomes nonuniform with much of the metal surface exposed. As the percentage of uncovered metal is the main responsible for the wear rate, the filler resulted less active in the case of the smoothest counterface [58].

The effect of the filler size on PTFE wear resistance was studied by Mcelwain in his master thesis [59]. α phase alumina particles with different sizes were used as

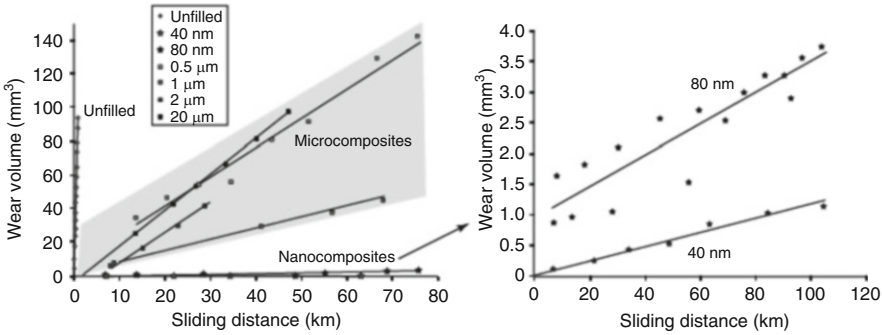

Fig. 4.2 Effect of the particle size on the wear volume of PTFE filled with 5 wt% of α phase alumina filler. (Reproduced from [59])

filler for the PTFE matrix. In Fig. 4.2 is reported the evolution of the wear volume with the sliding increase obtained with a three-pin-on-disk tribometer (speed of 10 mm/s and contact pressure of 3.1 MPa). It is clear from the Fig. 4.2 that the wear resistance progressively increases with the reduction in the filler dimension.

The effects of Al_2O_3 nanoparticles on tribological properties of polyoxymethylene (POM) nanocomposites have been investigated under dry and oil lubricated sliding conditions [56]. Polymeric coatings containing Al_2O_3 nanoparticles showed enhanced abrasive and scratch resistance compared to that of the neat polymer [60]. The improvement was attributed to the hardening effect of Al_2O_3 nanoparticles on the polymer matrix.

For phenolic composites, an optimal Al_2O_3 filler content was found to be less than 3 wt% [61]. The detrimental effects of the agglomeration of Al_2O_3 nanoparticles in the transfer film of epoxy composites have been reported [35]. The same authors [62] report that the combination of nano- Al_2O_3 (13 nm) and micro-$CaSiO_3$ (4-15 μm) induced some kind of synergistic effect and improved both the wear resistance and the stiffness of epoxy.

In summary, the existence of an optimum filler concentration has been explained by the formation of abrasive agglomerates within the protective transfer films [63]. In all cases analyzed, the transfer film was reported to become discontinuous and poorly bonded to the counterface with increasing the filler concentration. It has been showed that the chemical grafting of the Al_2O_3 nanoparticles prevents agglomeration of the particles at the sliding interface and increase the abrasive wear resistance of the composite [35, 64].

4.2.2 Copper Nanoparticles

Copper-based particles in both micro- and nano sizes have been extensively investigated as polymer filler in tribological applications. CuO in micrometer size was added to high-density polyethylene [65, 66], polyamide [67], PEEK [68],

polyphenylene sulfide (PPS) [69], and thermosetting polyester [70]. In all cases, a good enhancement in the wear resistance was obtained. Similar results were obtained by adding micrometric CuS to PTFE [71], polyamide [72], PEEK [73], and PPS [74, 75] systems. Several investigations have pointed out that the same benefits of microsize Cu-based fillers can be obtained by using the same filler in nanometric dimensions. In this case, however, the best results are obtained at extremely smaller volume fractions [76]. The addition of 1–4 vol% of CuO nanoparticles to a PPS matrix leads to a strong reduction of the wear rate in the transient stage. The improvement is maintained also in the steady state where the wear volume per unit sliding distance reduces from 0.291 mm^3/km of the unfilled PPS to 0.047mm^3/km of the sample added with 2 vol% of CuO [76]. The reduction in wear rate was attributed to the development of a more uniform and better-bonded transfer film over the counterface [76].

4.2.3 Zinc Oxide

The addition of nanometric ZnO to polyurethane (PU) coatings has proven to decrease the friction coefficient and the wear rate of these materials [77]. Results showed that the presence of ZnO nanoparticles can help the adhesion of the transfer films to the counterface. In contrast, the addition of ZnO nanoparticles to a PPS matrix strongly decreases its wear resistance during sliding against a tool steel counterface [78]. In this case, a discontinuous and poorly bonded transfer film was produced during sliding. Li et al. [50] have shown that the addition of nanometric ZnO to a PTFE matrix lead to an increase in wear resistance. Probably, the contradictory results found with ZnO nanoparticles are due to their abrasive properties. Different filler sizes, as well as changes in the test conditions, are responsible for the different tribological behavior showed by these nanocomposites.

4.2.4 Titanium Dioxide

The addition of 1–5 wt% of TiO_2 nanoparticles in the range 30–50 nm to a PPS matrix was effective in reducing the composite wear rate [78]. Similarly to that found for other nanoparticles, lower filler additions ensure the formation of a uniform transfer film on the counterface. With the increase in TiO_2 concentrations, the transfer film became thick and lumpy, and it also did not cover the counterface completely. As a result, wear rate increased considerably up to exceed that of the unfilled PPS. The effects of the particle dimensions on the wear resistance of epoxy resin have been investigated [79]. TiO_2 particle in nanometric dimensions was found more effective in wear reduction than that in the micrometer dimensions [79]. Increasing the bond between the filler and the matrix has also been shown to have positive effects on the wear resistance. Chang et al. [80] showed that the addition of 5 vol% TiO_2 nanoparticles to poly(etherimide) (PEI) containing short carbon fibers and graphite flakes increased the wear resistance of the composite.

Also in the case of polyamide 66 (PA66) containing short carbon fibers and graphite flakes, the addition of TiO_2 nanoparticles produces a strong increase in the wear resistance [81, 82]. Similar synergisms were found with epoxy matrix filled with short carbon fibers, graphite flakes, and TiO_2 nanoparticles [79, 83].

4.2.5 Silica Nanoparticles

The use of SiO_2 nanoparticles as fillers in polymer matrices has shown mixed results on wear. The tribological characterization of PEEK filled with SiO_2 nanoparticles has shown a positive effect of this filler on the wear rate and friction coefficient of the composite [52]. Opposite effects were found for a poly(phthalazine ether sulfone ketone) (PPESK) matrix [84]. In that case, both micro- and nano SiO_2 particles induce a significant abrasive wear loss. For an epoxy matrix, SiO_2 nanoparticles were shown to increase the wear resistance with the increase of bond strength between the particles and the matrix [85]. Polycarbonate (PC) filled with nanometric SiO_2 showed high hardness and stiffness with respect to the polymer matrix [86]. Smaller scratch depth and lower frictional coefficient were found by tests carried out on the PC/SiO_2 nanocomposites. The wear mechanism of polyamide-1010 (PA-1010) filled with nanometric SiO_2 showed lower friction and better wear resistance with respect to the pure PA-1010 [87].

Also for the nanometric SiO_2, filler dimensions, as well as particles agglomeration, are the key factors for the nanocomposites improvement.

4.2.6 Carbon Nanomaterials

Carbon nanomaterials (CN) such as carbon black, fullerenes, and its derivate have been investigated as fillers for tribological applications. They have high surface area, are chemically and thermally stable, have relatively low cost, and generally are environmentally friendly. Melt compounding is generally sufficient to achieve a good distribution of carbon nanomaterials in the bulk of thermoplastics polymers [88–91]. However, the dispersion of these nanomaterials can be optimized by applying combined processes, such as chemical and mechanical pretreatments of the polymer and nanofiller [7, 92–94]. The addition of CN to a PTFE matrix results in a both compressive strength and hardness increase [95, 96]. The wear rate was found to decrease up to 150 times for PTFE containing 2 wt% of carbon nanomaterials [96]. Small quantities (<1 wt%) of C_{60} fullerene added to a natural rubber caused great variations in the friction coefficient [97]. Different types of fluorocopolymers added with 10–15 wt% of carbon nanomaterials increased resistance to abrasive surfaces.

Figure 4.3 shows the wear rate and the friction coefficient of nylon 1010 and its composites filled with MoS_2 (SL) microparticles and chopped carbon fiber

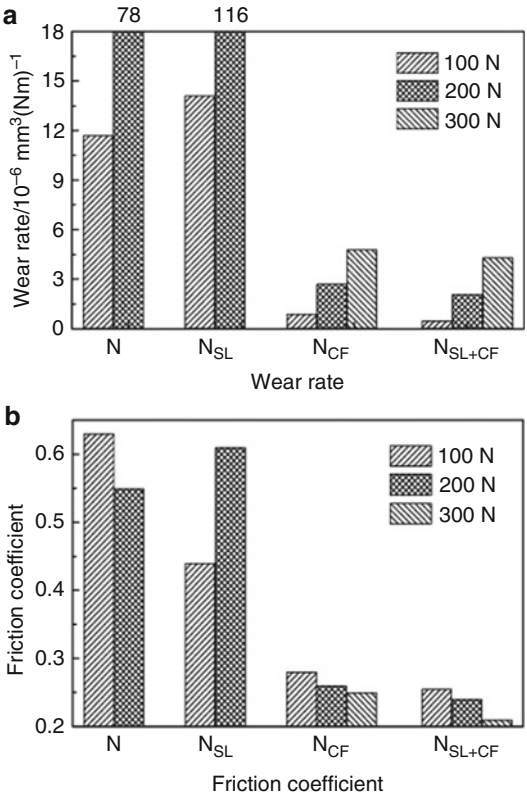

Fig. 4.3 Wear rate and Friction coefficient of Nylon 1010 and its composites filled with MoS_2 (SL) microparticles and chopped carbon fiber under various loads in dry sliding friction. (Reproduced from [98])

(CF) under various loads in dry sliding friction [98]. Unfilled nylon sample showed excessive wear probably due to the melting process taking place during the frictional process. Similar results were found by adding 10 wt% of MoS_2 microparticles. On the opposite, by adding 10 wt% of chopped carbon fiber, the wear rate was approximately reduced by a factor of 10. More interesting, the reduction in wear was greater when chopped carbon fiber and MoS_2 microparticles were combined. The authors found that the combination of the two fillers helps the formation of thin, uniform, and continuous transfer film [98].

The wear behavior of epoxy matrices in the presence of glass fibers and graphite was investigated by Suresha et al. [99]. The authors reported a pronounced reduction in wear rate as well as in frictional coefficient. A similar behavior was found for composites of PEI, carbon fibers, and graphite [80]. The incorporation of graphite particles (GPs) significantly reduces friction of polymer composites [100, 101]. It was proposed that the nanoparticles removed from the matrix debris act as third body elements in the contact region. Thus, they can reduce the shear stress in the contact region and accordingly enhance the matrix damage [102].

4.2.7 Other Nanoparticles

Schwartz and Bahadur [75] identified two opposite behaviors in polymeric composites filled with inorganic fillers. They found that AgS and CuS fillers contribute to increasing the wear resistance of a PPS matrix, whereas the same addition of ZnF_2 and SnS particles strongly reduced wear resistance. The authors suggested that this opposite behavior is due to the different mechanical properties of the filler [75]. In particular, the AgS and CuS particles are more prone to be deformed during flow with respect to the hard and abrasive ZnF_2 and SnS particles. Similar conclusions were reached using copper particles added to polyoxymethylene (POM) [103]. Also in this case, results have been explained by a predominantly plastic deformation mechanism of Cu particles [103]. However, the abrasive properties are strongly depended by the particle size used [15, 34, 53, 104, 105]. Wang et al. [51] investigated the influence of several ZrO_2 nanoparticles, varying from 10 to 100 nm, in reducing the wear of a PEEK matrix. Effective reduction of the wear rate was monitored only when the particles were less than 15 nm in size. Xing and Li [106] evaluated the wear properties of an epoxy matrix filled with spherical particle varying from 120 to 510 nm. They also found that the smaller the particles used as fillers, the better was the wear resistance of the composites.

Si_3N_4 and SiC nanoparticles grafted with polyacrylamide (PAAM) were used as filler for epoxy matrix [105]. Experimental results show that the compatibilization of the filler contributes to increased wear resistance of the epoxy composite. Inorganic nanoparticles such as $CaCO_3$ were added to several self-lubricating composites containing glass fibers with the aim to improve the adhesion between the reinforcing fibers and the matrix [107]. The resulting materials were able to operate under more severe sliding conditions than the composites with nanoparticles alone.

4.3 1-D Fillers

Filler with one dimension outside the nanometric range includes nanotubes, nanorods, nanofibers, and nanowires. They can be metallic, ceramic, or polymeric and can be amorphous or crystalline. The addition of these fillers to a polymer matrix has shown interesting results in terms of load-bearing capacity and toughness. These fillers can promote the formation of a tenacious and thin transfer film on the counterface and reduce the wear of the composites.

4.3.1 Carbon Nanotubes

Carbon nanotubes (CNT) are excellent filler for reinforcing polymers. They are exceptionally stiff and strong with a Young's modulus in the order of TPa and a tensile strength 100 times stronger than that of steel [29, 108]. Also, the nanometer size ensures extremely large interface and potentially excellent bonding [109, 110]. CNT-based nanocomposites are expected to have excellent tribological

properties [111, 112]. For that reason, several investigations have focused on the friction properties of thermoplastic and thermosetting composites filled with carbon nanotubes [113–115]. Results show that the experimental factors that are the main responsible for the tribological behavior of the CNT-nanocomposites are [116–118]:

(a) The preparation and purification method of the nanotubes
(b) The dispersion method
(c) The filler concentration in the nanocomposites
(d) Compatibilization with the polymer matrix

The effect of the addition of CNT on the wear life and load-bearing capacity of common polymers in tribological applications, such as polyethylene (HDPE and UHMWPE), has been analyzed by several authors [119–122]. The wear resistance of the composites is generally improved by the addition of low CNT concentrations [123]. It was explained by the reinforcement effect of CNT. However, CNTs are not easily dispersed in the polymer matrix and, especially at high concentrations (>5%), they tend to form large agglomerates. For this reason, poor mechanical and tribological properties are sometimes observed [119]. Low friction coefficient was obtained for nanocomposite reinforced with amino-functionalized CNT [124]. The conclusion was that a uniform distribution of CNTs in the matrix is a prerequisite for lowering friction.

A decrease in the wear rates of PTFE sliding over steel can be achieved by adding CNTs [49, 125]. The friction coefficient was observed to increase for the same CNT concentration [49]. The effect of the CNT on the friction coefficient on different polyamides (PA) was analyzed under dry and lubricated wear conditions [126–128]. In these cases, CNTs were able to reduce both the friction coefficients and the wear rates. The decrease in friction coefficients is ascribed to the improved strength properties of the polymer along with the lubricating action of CNT [49]. CNTs were also able to increase the wear resistance of epoxy resin [117, 129] and high resistant composites such as PEEK reinforced with carbon fibre [130]. In this case, the favorable effect of CNT was explained by the enhanced resistance of the matrix to the shear stresses [131].

4.3.2 Carbon Nanofibers

Carbon nanofibers (CNFs) are morphologically differentiated from carbon nanotubes by the orientation of the graphene planes [132]. They can be imagined as stacked graphitic discs, truncated cones, or planar layers along the filament length. These nanostructures have an outer diameter in the range 50–100 nm. However, commercial CNF fibers are slightly larger (100–200 nm) in diameters. This particular micrometric structure confers to the carbon nanofibers a semi-conducting behavior [133]. These fillers also have chemically active end planes on both the inner and outer surfaces [134]. CNFs are particularly suitable as reinforcing fillers in polymeric composites [135] and as an additive in carbon fiber reinforced plastics

[136, 137]. The addition of CNFs to a PEEK matrix strongly reduces unlubricated wear over alloy steel [138]. They result effective also when were added to a ternary composite such as PEEK reinforced with ordinary carbon fibers or PTFE. It was suggested that CNFs reduce to small graphitic debris particles during shear stress. These nanoparticles can anchor to the counterface and reduce its roughness [139, 140]. In addition, CNFs are able to reinforce the transfer film [107].

4.4 2-D Fillers

Two-dimensional nanomaterials such as clay, graphene, metal chalcogenides, and transition metal oxides are a broad range of materials that cover a variety of different properties. They have a layered structure with weak van der Waals interactions between them. Typically, the single layers of these materials are few nanometers thick with extraordinary electronic, magnetic, and thermal properties. The use of 2D nanomaterials for controlling friction and wear has received increased attention over the past few years [141, 142].

4.4.1 Clays

The most common clay materials are that identified as 2:1 phyllosilicates (montmorillonite, saponite). They are diffuse in nature as micron-size multilayered tactoids [143]. The individual layers having thicknesses of about 1 nm and surface lengths on the order of 100–1000 nm [144]. The layered structure of silicate makes it possess good solid lubrication [145]. Exfoliation and dispersion of natural clay in the polymer matrix are the necessary prerequisite for the nanocomposite formation [146, 147]. Several modification procedures were developed for expands the spacing between the individual clay layers and improves their compatibility with polymers [148, 149]. The effectiveness of these methods is found strongly dependent on the processing conditions as well as the polymer characteristics [26, 94, 150]. The clay sheets act like impermeable obstacles for gases or vapor diffusing through the matrix [30]. Good dispersion and surface interaction between filler and polymer are necessary for the mechanical and barrier improvements [24, 31, 144]. Dispersion is also responsible for the increase in wear resistance of several polymer nanocomposites [151, 152]. Yuan et al. [153] studied the scratch resistance of a polypropylene (PP) reinforced with an organo-modified montmorillonites. Figure 4.4 shows the surface deformation morphology of neat PP and PP modified with 4 wt% of nanoclay under identical scratch test conditions. Both samples showed periodic multiple ripple-type deformation tracks. However, nanoclay reinforcement decreases the susceptibility of the system to micro- and nanoscale deformation. It was attributed to the increased in modulus and yield strength of the composite [153].

Polyamide 6 (PA6) modified with neat or organically modified clay show different behaviors. Increased wear resistance was observed only for nanocomposites containing organically modified clays [151]. The authors suggest that the increase

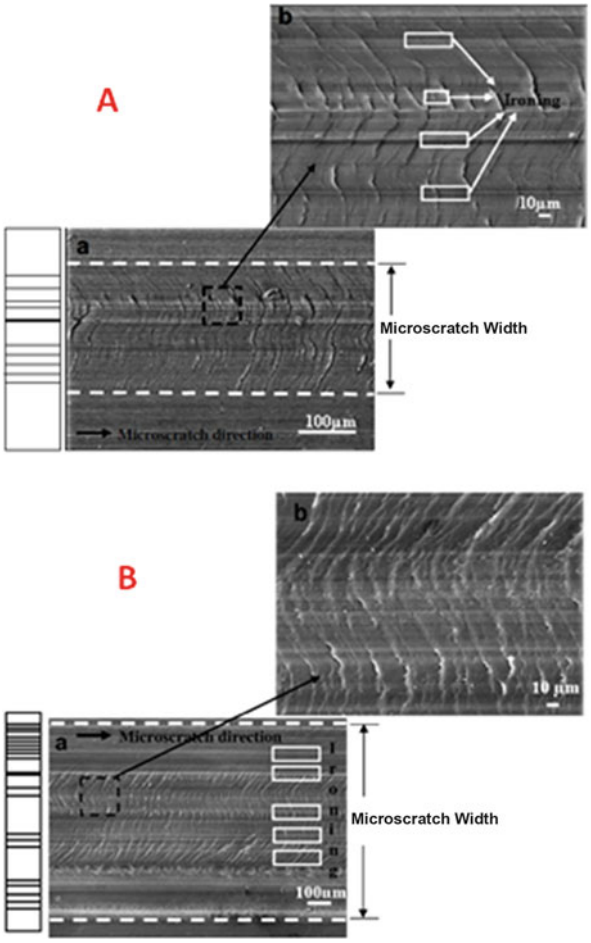

Fig. 4.4 Surface deformation morphology of microscratches: (**a**) Pure PP and (**b**) PP-4 wt% clay nanocomposite. (Reproduced from [153])

is achieved only if a good dispersion of the clay platelets in the polymer matrix is combined with a high level of compatibility between the clay and the polymer matrix. Similar results were found for PA nanocomposites systems filler with different types of organically modified clays [154, 155]. The addition of these nanomaterials also affects tribo-chemical processes taking place in friction contact zone. The dispersion of clay particles in a PI matrix was found to inhibit the degradation of macromolecules. As a result, wear resistance of the PI nanocomposite is enhanced. However, at higher clay concentrations the formation of large clay aggregates was observed on the counterface [92]. This was associated with high wear degradation rate. Nanoclay fillers were reported to increase the wear resistance of many thermoplastic polymers such as polycarbonate, polyester, polyamide, and polyvinylidenefluoride (PVDF) [156]. Tribological tests indicate that the addition of organo-modified montmorillonite enhanced wear resistance, antifriction property, and better fabric integrity of self-lubricating liners [157].

4.4.2 Graphene

Graphene sheets formally are two-dimensional layers of sp2-bonded carbon. The one-atom thick structure is expected to have a range of unusual properties [158]. High-quality graphene can be synthesized by chemical-vapor deposition [159]. It has been used in transparent conductors, flexible electronics, field-effect transistors, fuel cells, batteries, solar cells, biomaterials, biosensors, and water purifiers [160–162].

Graphene has been proposed as an alternative to conventional filler in the fields of transportation and electronics. Unfortunately, its cost and the difficulty to obtain as free single layers have limited its applications. Two derivates of graphene materials, namely, graphene oxide (GO) and reduced GO (rGO), have been proposed as substitutes [163, 164]. They are formally derived from low-cost graphite by chemical oxidation or electrochemical exfoliation and can be easily dispersed into polymeric materials [165–167]. The unique physical, mechanical, and chemical properties of graphene-like make it an attractive candidate for many tribological applications [168, 169].

Graphene oxide has been added to UHMWPE and characterized with a microhardness tester and high speed reciprocating tribometer [170]. Results show that the wear resistance and hardness of the composites are improved significantly, while the coefficient of friction increases rapidly. GO/polyimide (PI) nanocomposites were prepared by in situ polymerization techniques. The GO/PI exhibited better mechanical and thermal properties. Also the wear resistance of PI was found to increase [171]. Pan et al. [172] analyzed the tribological performance of graphene modified PI coatings. They found a sensible increase in the wear resistance of the coating. Better performances were found by increasing the interaction between the graphene filler and polyimide matrix [173]. PI/GO nanocomposites have demonstrated good tribological properties also under seawater-lubricated conditions [171]. Song et al. [174] prepared Cu nanoparticles decorated on polydopamine (PDA) functionalized graphene oxide (GO) nanosheets. Tests with sliding steel surfaces showed that the soybean oil with 0.1 wt% Cu/PDA/GO nanocomposites had the lowest friction coefficient under all of the sliding conditions. Kalin M et al. [175] investigated the effect of solid lubricant nanoparticles on poly-ether-ether-ketone (PEEK) composites. In the PEEK matrix, different types of nanoparticles were added, like graphene, WS_2 needle-like, WS_2 fullerene-like, and CNT. The results obtained under dry sliding conditions show that the morphology of the nanoparticles has an important effect on the friction coefficient and the wear behavior [175].

4.4.3 Molybdenum Disulfide

Molybdenum disulfide (MoS_2) is a naturally mined inorganic material that occurs as the mineral Molybdenite. Molybdenum disulfide has many unique properties, which makes it one of the most popular solid lubricants on the market [176, 177]. Similar to

graphite, these materials possess layered structures that can be exfoliated into small thicknesses containing mono- or multilayers [178, 179]. Among the 2D materials, molybdenum compounds are probably the most interesting for tribological applications. In particular, the interest for the molybdenum disulfide (MoS_2) in nanometric dimensions has increased exponentially due to their impressive chemical and physical properties [180, 181]. Nanometric MoS_2 have shown better lubrication performance than bulk MoS_2 [98]. Thus, considerable attention has been given to the preparation of MoS_2-based nanocomposites. Even if the MoS_2 can be easily dispersed and exfoliated in polymers [182–188], its tendency to re-organize in large agglomerate is still a big problem. Several synthetic routes were suggested to obtain 2D crystals of MoS_2 on a stable nanometric scale [189, 190]. Intercalation-exfoliation methods in common liquid solvents [191] and micromechanical exfoliation of natural molybdenite crystals were also proposed [192]. A simple and versatile method for the production of 2D nanosheet crystals of MoS_2 was proposed [5, 193, 194]. The nanosheets covered by a protective oleylamine coating were successfully tested as additives for high-performance liquid and solid lubricants [5]. Moreover, hybrid organic-inorganic oleylamine@MoS_2-CNT nanocomposites were obtained and successfully tested as nanoadditive for grease lubricant [195].

The introduction of MoS_2@oleylamine into a Polystyrene matrix was found to reduce its mechanical properties [196, 197]. A noticeable reduction of both the glass transition temperature and the elastic modulus was observed. The friction coefficient, as well as the wear resistance of PS nanocomposites, was found to decrease [196, 197].

Several polymeric matrices were proposed as a matrix for MoS_2 nanocomposites. They include polyoxymethylene (POM) [198, 199] and high-density polyethylene (HDPE) [200].

MoS_2 as micro- and nano-platelet and sphere were added to POM and HDPE matrices [200, 201]. Results show that the two structures exhibited a similar performance in friction reduction under dry friction. However, in the case of HDPE matrix, the nano-platelet MoS_2 showed lower friction coefficients than both microplatelets and nano-spheres. Chemical intercalation of MoS_2 can help its dispersion during the mechanical mixing [202]. However, the chemical intercalation can destroy the crystal structure of MoS_2 and negatively affect its lubrication performance [199].

Xin et al. [203] prepared a self-lubricating and antiwear polyimide composites by adding different percentages of graphene oxide/nano-MoS_2 hybrid. Figure 4.5a shows the friction coefficient of the various composites analyzed in the paper. The hybrid addition was found to reduce the friction coefficient. However, a fluctuation phenomenon appears in the curves when the filler concentration became higher than 0.5 wt%. The authors suggested [203] that at high concentrations the self-lubricating effect receded, due to the stacking of the nano-hybrid sheets. The effect of various additives on the friction coefficient is shown in Fig. 4.5b. A combination of the protective effect of graphene sheets, rolling friction effect of the detached nano-MoS_2 particles, and a transfer film composed of MoS_2 were proposed as a synergic mechanism for the enhancement of the tribological properties.

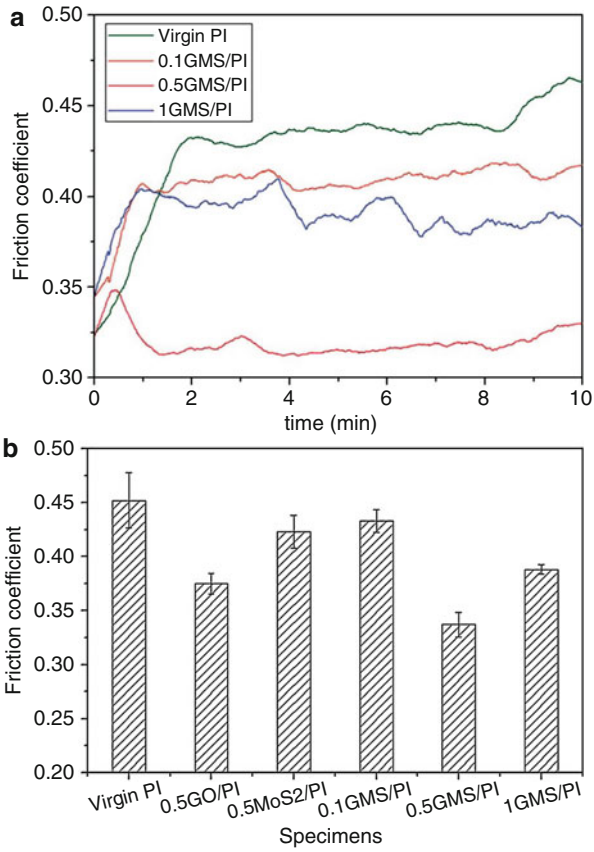

Fig. 4.5 (**a**) Friction coefficients of neat polyimide (PI), 0.1 wt% of graphene oxide/nano-MoS_2 in PI matrix (0.1GMS/PI), 0.5 wt% of graphene oxide/nano-MoS_2 in PI matrix (0.5GMS/PI), and 1 wt% of graphene oxide/nano-MoS_2 in PI matrix (1GMS/PI) specimens as a function of sliding time. (**b**) Friction coefficients of virgin PI, 0.5 wt% of graphene oxide in PI matrix (0.5GO/PI), 0.5 wt% of MoS_2 in PI matrix (0.5MoS_2/PI), 0.1 wt% of graphene oxide/nano-MoS_2 in PI matrix (0.1GMS/PI), 0.5 wt % of graphene oxide/nano-MoS_2 in PI matrix (0.5GMS/PI), and 1 wt% of graphene oxide/nano-MoS_2 in PI matrix (1GMS/PI) specimens. (Reproduced from [203])

4.5 Trends and Perspectives

The trend in the area of polymers composites for tribological applications is quickly moving towards multifunctional materials and coatings. Materials that can sustain high pressure and velocity with low wear rate are needed for the incoming high-tech applications. Nanomaterials offer new and intriguing possibility to design and develop innovative materials with these advanced properties. They will positively affect the quality, safety, and security of the polymer composites. The main advantage of these materials over traditional fillers is in its ability to improve mechanical, electrical and chemical properties at very low concentrations. As a matter, several examples of nanotechnology-based composites materials are already present on the market. The actual limitation to the definitive diffusion of these materials is the lack of information about their tribology performance. In fact, the tribological research on these systems is still at a relatively early stage. Additional experimental results and innovative research works are thus necessary. New chemical and physical approach

are necessary for improving the compatibility of the nanofillers with the matrix. Attention must be devoted to the development of new methods for achieving controlled in situ structuring of particles in three-dimensional structure. Researchers are called to further improve the performances of these materials and expand their use in newer tribological applications.

Acknowledgments The author acknowledges the financial support from the "VINMAC" (INNOVATIVO SISTEMA INTEGRATO DI VENTILAZIONE INDUSTRIALE IN MATERIALI COMPOSITI) project Regione Lombardia POR FESR 2014-2020 ASSE 1 – AZIONE I.1.B.1.3 BANDO LINEA R&S PER AGGREGAZIONI, ID 139455 CUP: E67H16000980009.

References

1. Gorrasi, G., Sorrentino, A.: Mechanical milling as a technology to produce structural and functional bio-nanocomposites. Green Chem. **17**, 2610–2625 (2015). https://doi.org/10.1039/C5GC00029G
2. Rogers, B., Adams, J., Pennathur, S.: Nanotechnology: Understanding Small Systems. CRC Press, Boca Raton (2014)
3. Reddy, B. (ed.): Advances in Diverse Industrial Applications of Nanocomposites. InTech (2011). https://doi.org/10.5772/1931
4. Briscoe, B.J., Sinha, S.K.: Tribological applications of polymers and their composites – past, present and future prospects. In: Tribology of Polymeric Nanocomposites, pp. 1–22. Elsevier, Amsterdam (2013). https://doi.org/10.1016/B978-0-444-59455-6.00001-5
5. Gnerre, C., Ciambelli, P., Altavilla, C., Sarno, M., Siraw, Y., Petrone, V., Senatore, A., Nobile, M.R., Somma, E.: Tribological and rheological properties of tungsten disulphide nanosheets as additive in lubricant mineral oil. In: Veneto Nanotech (ed.) International Conference Nanotechnology Nanomaterials, Venezia, pp. 177–178. (2010)
6. Menezes, P.L., Ingole, S.P., Nosonovsky, M., Kailas, S.V., Lovell, M.R.: Tribology for Scientists and Engineers. Springer, New York (2013)
7. Delogu, F., Gorrasi, G., Sorrentino, A.: Fabrication of polymer nanocomposites via ball milling: present status and future perspectives. Prog. Mater. Sci. **86**, 75–126 (2017). https://doi.org/10.1016/j.pmatsci.2017.01.003
8. Davim, J.P.: Tribology of Nanocomposites. Springer, Berlin (2013)
9. Caseri, W.: Nanocomposites of polymers and inorganic particles. In: Hybrid Materials, pp. 49–86. Wiley-VCH Verlag GmbH & Co. KGaA, Weinheim (2007). https://doi.org/10.1002/9783527610495.ch2
10. Sinha Ray, S., Okamoto, M.: Polymer/layered silicate nanocomposites: a review from preparation to processing. Prog. Polym. Sci. **28**, 1539–1641 (2003). https://doi.org/10.1016/j.progpolymsci.2003.08.002
11. Yin, Y., Talapin, D.: The chemistry of functional nanomaterials. Chem. Soc. Rev. **42**, 2484 (2013). https://doi.org/10.1039/c3cs90011h
12. Sorrentino, A.: Nanocoatings and ultra-thin films for packaging applications. In: Makhlouf, A. S.H., Tiginyanu, I. (eds.) Nanocoatings Ultra-Thin Film, pp. 203–234. Elsevier, Oxford (2011). https://doi.org/10.1533/9780857094902.2.203
13. Huang, H.D., Tu, J.P., Gan, L.P., Li, C.Z.: An investigation on tribological properties of graphite nanosheets as oil additive. Wear. **261**, 140–144 (2006)
14. Kim, D., Archer, L.A.: Nanoscale organic– inorganic hybrid lubricants. Langmuir. **27**, 3083–3094 (2011)
15. Stachowiak, G., Batchelor, A.W.: Engineering Tribology. Butterworth-Heinemann, Oxford (2013)

16. Czichos, H.: Chapter: 1 Introduction and background. In: Tribology a Systems Approach to the Science and Technology of Friction, Lubrication and Wear, pp. 1–13. Elsevier, Berlin (1978). https://doi.org/10.1016/S0167-8922(09)70004-5
17. Rudnick, L.R.: Lubricant Additives: Chemistry and Applications. CRC press, Boca Raton (2009)
18. Wang, Q., Chung, Y.: Encyclopedia of Tribology. Springer, New York (2013)
19. Menezes, P.L., Kailas, S.V., Lovell, M.R.: Fundamentals of engineering surfaces. In: Tribology for Scientists and Engineering, pp. 3–41. Springer, New York (2013). https://doi.org/10.1007/978-1-4614-1945-7_1
20. Friedrich, K., Schlarb, A.K., Bahadur, S., Schwartz, C.: Tribology of Polymeric Nanocomposites. Elsevier, Amsterdam (2013). https://doi.org/10.1016/B978-0-444-59455-6.00002-7
21. Guadagno, L., De Vivo, B., Di Bartolomeo, A., Lamberti, P., Sorrentino, A., Tucci, V., Vertuccio, L., Vittoria, V.: Effect of functionalization on the thermo-mechanical and electrical behavior of multi-wall carbon nanotube/epoxy composites. Carbon N. Y. **49**, 1919–1930 (2011)
22. Baillie, C.: Green Composites, Polymer Composites and the Environment. CRC Press, Cambridge (2004)
23. Burris, D.L., Boesl, B., Bourne, G.R., Sawyer, W.G.: Polymeric nanocomposites for tribological applications. Macromol. Mater. Eng. **292**, 387–402 (2007). https://doi.org/10.1002/mame.200600416
24. Sorrentino, A., Tortora, M., Vittoria, V.: Diffusion behavior in polymer-clay nanocomposites. J. Polym. Sci. Part B Polym. Phys. **44**, 265–274 (2006). https://doi.org/10.1002/polb.20684
25. Sorrentino, A., Vertuccio, L., Vittoria, V.: Influence of multi-walled carbon nanotubes on the β form crystallization of syndiotactic polystyrene at low temperature. Express Polym Lett. **4**, 339–345 (2010). https://doi.org/10.3144/expresspolymlett.2010.43
26. Pavlidou, S., Papaspyrides, C.D.: A review on polymer–layered silicate nanocomposites. Prog. Polym. Sci. **33**, 1119–1198 (2008). https://doi.org/10.1016/j.progpolymsci.2008.07.008
27. Gorrasi, G., Attanasio, G., Izzo, L., Sorrentino, A.: Controlled release mechanisms of sodium benzoate from a biodegradable polymer and halloysite nanotube composite. Polym. Int. **66**, 690–698 (2017). https://doi.org/10.1002/pi.5309
28. Liparoti, S., Landi, G., Sorrentino, A., Speranza, V., Cakmak, M., Neitzert, H.C.: Flexible poly (amide-imide)-carbon black based microheater with high-temperature capability and an extremely low temperature coefficient. Adv. Electron. Mater. **2**, 1600126 (2016). https://doi.org/10.1002/aelm.201600126
29. Gorrasi, G., Di Lieto, R., Patimo, G., De Pasquale, S., Sorrentino, A.: Structure–property relationships on uniaxially oriented carbon nanotube/polyethylene composites. Polymer (Guildf). **52**, 1124–1132 (2011). https://doi.org/10.1016/j.polymer.2011.01.008
30. Sorrentino, A., Gorrasi, G., Vittoria, V.: Environmental Silicate Nano-Biocomposites. Springer, London (2012). https://doi.org/10.1007/978-1-4471-4108-2
31. Ajayan, P.M., Schadler, L.S., Braun, P.V. (eds.): Nanocomposite Science and Technology. Wiley-VCH Verlag GmbH & Co. KGaA, Weinheim (2003). https://doi.org/10.1002/3527602127
32. Bhushan, B.: Micro/Nanotribology and Its Applications. Springer Netherlands, Dordrecht (1997). https://doi.org/10.1007/978-94-011-5646-2
33. Chand, N., Fahim, M.: Introduction to tribology of polymer composites. In: Tribology of Natural Fiber Polymer Composites, pp. 59–83. Elsevier, Cambridge (2008). https://doi.org/10.1533/9781845695057.59
34. Schwartz, C.J., Bahadur, S.: Studies on the tribological behavior and transfer film–counterface bond strength for polyphenylene sulfide filled with nanoscale alumina particles. Wear. **237**, 261–273 (2000)
35. Wetzel, B., Haupert, F., Qiu Zhang, M.: Epoxy nanocomposites with high mechanical and tribological performance. Compos. Sci. Technol. **63**, 2055–2067 (2003). https://doi.org/10.1016/S0266-3538(03)00115-5

36. Bhushan, B.: Fundamentals of Tribology and Bridging the Gap Between the Macro- and Micro/Nanoscales. Springer Netherlands, Dordrecht (2001). https://doi.org/10.1007/978-94-010-0736-8
37. Chang, L., Zhang, Z., Ye, L., Friedrich, K.: Tribological properties of epoxy nanocomposites: III. Characteristics of transfer films. Wear. **262**, 699–706 (2007)
38. Hutchings, I., Shipway, P.: Design and selection of materials for tribological applications. In: Tribology Friction and Wear of Engineering Materials, pp. 283–302. Elsevier, Oxford (2017). https://doi.org/10.1016/B978-0-08-100910-9.00008-8
39. Blanchet, T.A., Peng, Y.-L.: Wear resistant irradiated FEP/unirradiated PTFE composites. Wear. **214**, 186–191 (1998). https://doi.org/10.1016/S0043-1648(97)00254-8
40. Menzel, B., Blanchet, T.A.: Effect of particle size and volume fraction of irradiated FEP filler on the transfer wear of PTFE. Tribol. Lubr. Technol. **58**, 29 (2002)
41. Wang, Q.-H., Xue, Q.-J., Liu, W.-M., Chen, J.-M.: The friction and wear characteristics of nanometer SiC and polytetrafluoroethylene filled polyetheretherketone. Wear. **243**, 140–146 (2000)
42. Lu, Z.P., Friedrich, K.: On sliding friction and wear of PEEK and its composites. Wear. **181**, 624–631 (1995)
43. Palabiyik, M., Bahadur, S.: Mechanical and tribological properties of polyamide 6 and high density polyethylene polyblends with and without compatibilizer. Wear. **246**, 149–158 (2000)
44. Bahadur, S., Polineni, V.K.: Tribological studies of glass fabric-reinforced polyamide composites filled with CuO and PTFE. Wear. **200**, 95–104 (1996)
45. Liu, X., Li, T., Tian, N., Liu, W.: Tribological properties of PTFE-filled PMIA. J. Appl. Polym. Sci. **74**, 747–751 (1999)
46. Burris, D.L., Sawyer, W.G.: Tribological sensitivity of PTFE/alumina nanocomposites to a range of traditional surface finishes. Tribol. Trans. **48**, 147–153 (2005)
47. Sawyer, W.G., Freudenberg, K.D., Bhimaraj, P., Schadler, L.S.: A study on the friction and wear behavior of PTFE filled with alumina nanoparticles. Wear. **254**, 573–580 (2003)
48. Burris, D.L., Sawyer, W.G.: Improved wear resistance in alumina-PTFE nanocomposites with irregular shaped nanoparticles. Wear. **260**, 915–918 (2006)
49. Chen, W.X., Li, F., Han, G., Xia, J.B., Wang, L.Y., Tu, J.P., Xu, Z.D.: Tribological behavior of carbon-nanotube-filled PTFE composites. Tribol. Lett. **15**, 275–278 (2003)
50. Li, F., Hu, K., Li, J., Zhao, B.: The friction and wear characteristics of nanometer ZnO filled polytetrafluoroethylene. Wear. **249**, 877–882 (2001)
51. Wang, Q., Xue, Q., Liu, H., Shen, W., Xu, J.: The effect of particle size of nanometer ZrO_2 on the tribological behaviour of PEEK. Wear. **198**, 216–219 (1996)
52. Wang, Q., Xue, Q., Shen, W.: The friction and wear properties of nanometre SiO_2 filled polyetheretherketone. Tribol. Int. **30**, 193–197 (1997)
53. Bhimaraj, P., Burris, D.L., Action, J., Sawyer, W.G., Toney, C.G., Siegel, R.W., Schadler, L.S.: Effect of matrix morphology on the wear and friction behavior of alumina nanoparticle/poly (ethylene) terephthalate composites. Wear. **258**, 1437–1443 (2005)
54. Higgs, C.F., Marinack, M., Mpagazehe, J., Pudjoprawoto, R.: Particle tribology: granular, slurry, and powder tribosystems. In: Tribology for Scientists and Engineering, pp. 391–445. Springer, New York (2013). https://doi.org/10.1007/978-1-4614-1945-7_12
55. Schmid, G. (ed.) Nanoparticles: From Theory to Application, 2nd Completely Revised and Updated Edition. Wiley-VCH Verlag GmbH & Co. KGaA (2010)
56. Sun, L.-H., Yang, Z.-G., Li, X.-H.: Study on the friction and wear behavior of POM/Al_2O_3 nanocomposites. Wear. **264**, 693–700 (2008)
57. Zhao, L., Zheng, L., Zhao, S.: Tribological performance of nano-Al_2O_3 reinforced polyamide 6 composites. Mater. Lett. **60**, 2590–2593 (2006)
58. Zhang, G., Wetzel, B., Jim, B., Österle, W.: Impact of counterface topography on the formation mechanisms of nanostructured tribofilm of PEEK hybrid nanocomposites. Tribol. Int. **83**, 156–165 (2015)

59. Burris, D.L., Santos, K., Lewis, S.L., Liu, X., Perry, S.S., Blanchet, T.A., Schadler, L.S., Sawyer, W.G.: Polytetrafluoroethylene matrix nanocomposites for tribological applications. In: Developments of Nanocomposites/Coatings for Special Applications, pp. 403–438. Elsevier, Amsterdam (2008). https://doi.org/10.1016/S1572-3364(08)55017-8
60. Wang, Y., Lim, S., Luo, J.L., Xu, Z.H.: Tribological and corrosion behaviors of Al_2O_3/polymer nanocomposite coatings. Wear. **260**, 976–983 (2006)
61. Song, H.-J., Zhang, Z.-Z., Men, X.: Effect of nano-Al_2O_3 surface treatment on the tribological performance of phenolic composite coating. Surf. Coatings Technol. **201**, 3767–3774 (2006)
62. Wetzel, B., Haupert, F., Friedrich, K., Zhang, M.Q., Rong, M.Z.: Impact and wear resistance of polymer nanocomposites at low filler content. Polym. Eng. Sci. **42**, 1919–1927 (2002)
63. Luo, T., Wei, X., Zhao, H., Cai, G., Zheng, X.: Tribology properties of Al_2O_3/TiO_2 nanocomposites as lubricant additives. Ceram. Int. **40**, 10103–10109 (2014)
64. Shi, G., Zhang, M.Q., Rong, M.Z., Wetzel, B., Friedrich, K.: Sliding wear behavior of epoxy containing nano-Al_2O_3 particles with different pretreatments. Wear. **256**, 1072–1081 (2004)
65. Bahadur, S., Tabor, D.: Role of fillers in the friction and wear behavior of high-density polyethylene. In: Polymeric Wear and Its Control, pp. 253–268. ACS Publications, New York (1985). https://doi.org/10.1021/bk-1985-0287.ch017
66. Kato, K.: Wear in relation to friction – a review. Wear. **241**, 151–157 (2000)
67. Bahadur, S., Gong, D., Anderegg, J.W.: The role of copper compounds as fillers in transfer film formation and wear of nylon. Wear. **154**, 207–223 (1992)
68. Vande Voort, J., Bahadur, S.: Effect of PTFE Addition on the Transfer Film, Wear and Friction of PEEK-CuO Composite. American Society of Mechanical Engineers, New York (1995)
69. Yu, L., Yang, S., Liu, W., Xue, Q.: An investigation of the friction and wear behaviors of polyphenylene sulfide filled with solid lubricants. Polym. Eng. Sci. **40**, 1825–1832 (2000). https://doi.org/10.1002/pen.11314
70. Bahadur, S., Zhang, L., Anderegg, J.W.: The effect of zinc and copper oxides and other zinc compounds as fillers on the tribological behavior of thermosetting polyester. Wear. **203**, 464–473 (1997)
71. Bahadur, S., Tabor, D.: The wear of filled polytetrafluoroethylene. Wear. **98**, 1–13 (1984)
72. Kapoor, A., Bahadur, S.: Transfer film bonding and wear studies on CuS-nylon composite sliding against steel. Tribol. Int. **27**, 323–329 (1994)
73. Vande Voort, J., Bahadur, S.: The growth and bonding of transfer film and the role of CuS and PTFE in the tribological behavior of PEEK. Wear. **181**, 212–221 (1995)
74. Yu, L., Bahadur, S.: An investigation of the transfer film characteristics and the tribological behaviors of polyphenylene sulfide composites in sliding against tool steel. Wear. **214**, 245–251 (1998)
75. Schwartz, C.J., Bahadur, S.: The role of filler deformability, filler–polymer bonding, and counterface material on the tribological behavior of polyphenylene sulfide (PPS). Wear. **251**, 1532–1540 (2001)
76. Cho, M.H., Bahadur, S.: Study of the tribological synergistic effects in nano CuO-filled and fiber-reinforced polyphenylene sulfide composites. Wear. **258**, 835–845 (2005)
77. Song, H.-J., Zhang, Z.-Z., Men, X.-H., Luo, Z.-Z.: A study of the tribological behavior of nano-ZnO-filled polyurethane composite coatings. Wear. **269**, 79–85 (2010)
78. Bahadur, S., Sunkara, C.: Effect of transfer film structure, composition and bonding on the tribological behavior of polyphenylene sulfide filled with nano particles of TiO_2, ZnO, CuO and SiC. Wear. **258**, 1411–1421 (2005)
79. Zhang, Z., Breidt, C., Chang, L., Haupert, F., Friedrich, K.: Enhancement of the wear resistance of epoxy: short carbon fibre, graphite, PTFE and nano-TiO_2. Compos. Part A Appl. Sci. Manuf. **35**, 1385–1392 (2004)
80. Chang, L., Zhang, Z., Zhang, H., Friedrich, K.: Effect of nanoparticles on the tribological behaviour of short carbon fibre reinforced poly (etherimide) composites. Tribol. Int. **38**, 966–973 (2006)

81. Chang, L., Zhang, Z., Zhang, H., Schlarb, A.K.: On the sliding wear of nanoparticle filled polyamide 66 composites. Compos. Sci. Technol. **66**, 3188–3198 (2006)
82. You, Y.-L., Li, D.-X., Si, G.-J., Deng, X.: Investigation of the influence of solid lubricants on the tribological properties of polyamide 6 nanocomposite. Wear. **311**, 57–64 (2014)
83. Su, F., Zhang, Z., Liu, W.: Mechanical and tribological properties of carbon fabric composites filled with several nano-particulates. Wear. **260**, 861–868 (2006)
84. Shao, X., Tian, J., Liu, W., Xue, Q., Ma, C.: Tribological properties of SiO_2 nanoparticle filled–phthalazine ether sulfone/phthalazine ether ketone (50/50 mol%) copolymer composites. J. Appl. Polym. Sci. **85**, 2136–2144 (2002)
85. Zhang, M.Q., Rong, M.Z., Yu, S.L., Wetzel, B., Friedrich, K.: Effect of particle surface treatment on the tribological performance of epoxy based nanocomposites. Wear. **253**, 1086–1093 (2002)
86. Wang, Z.Z., Gu, P., Zhang, Z.: Indentation and scratch behavior of nano-SiO_2/polycarbonate composite coating at the micro/nano-scale. Wear. **269**, 21–25 (2010)
87. Li, Y., Ma, Y., Xie, B., Cao, S., Wu, Z.: Dry friction and wear behavior of flame-sprayed polyamide1010/n-SiO_2 composite coatings. Wear. **262**, 1232–1238 (2007)
88. Moniruzzaman, M., Winey, K.I.: Polymer nanocomposites containing carbon nanotubes. Macromolecules. **39**, 5194–5205 (2006)
89. Kumar, S., Doshi, H., Srinivasarao, M., Park, J.O., Schiraldi, D.A.: Fibers from polypropylene/nano carbon fiber composites. Polymer (Guildf). **43**, 1701–1703 (2002)
90. De Zhang, W., Shen, L., Phang, I.Y., Liu, T.: Carbon nanotubes reinforced nylon-6 composite prepared by simple melt-compounding. Macromolecules. **37**, 256–259 (2004)
91. Nobile, M.R., Valentino, O., Morcom, M., Simon, G.P., Landi, G., Neitzert, H.-C.: The effect of the nanotube oxidation on the rheological and electrical properties of CNT/HDPE nanocomposites. Polym. Eng. Sci. **57,** 665–673 (2017). https://doi.org/10.1002/pen.24572
92. Lai, S., Yue, L., Li, T., Liu, X., Lv, R.: An investigation of friction and wear behaviors of polyimide/attapulgite hybrid materials. Macromol. Mater. Eng. **290**, 195–201 (2005)
93. Ambrosio-Martin, J., Fabra, M.J., López-Rubio, A., Gorrasi, G., Sorrentino, A., Lagaron, J. M.: Assessment of ball milling as a compounding technique to develop nanocomposites of poly (3-Hydroxybutyrate-co-3-Hydroxyvalerate) and bacterial cellulose nanowhiskers. J. Polym. Environ. **24**, 241–254 (2016)
94. Vertuccio, L., Gorrasi, G., Sorrentino, A., Vittoria, V.: Nano clay reinforced PCL/starch blends obtained by high energy ball milling. Carbohydr. Polym. **75**, 172–179 (2009). https://doi.org/10.1016/j.carbpol.2008.07.020
95. Dolmatov, V.Y.: Detonation nanodiamonds in oils and lubricants. J. Superhard Mater. **32**, 14–20 (2010)
96. Dubkova, V.I., Korzhenevskii, A.P., Krut, N.P., Komarevich, V.G., Kul, L.V.: Detonation-synthesis nanodiamonds in compositions of ultrahigh-molecular-weight polyethylene. J. Eng. Phys. Thermophys. **89**, 1024–1033 (2016)
97. Jurkowska, B., Jurkowski, B., Kamrowski, P., Pesetskii, S.S., Koval, V.N., Pinchuk, L.S., Olkhov, Y.A.: Properties of fullerene-containing natural rubber. J. Appl. Polym. Sci. **100**, 390–398 (2006)
98. Wang, J., Gu, M., Songhao, B., Ge, S.: Investigation of the influence of MoS_2 filler on the tribological properties of carbon fiber reinforced nylon 1010 composites. Wear. **255**, 774–779 (2003). https://doi.org/10.1016/S0043-1648(03)00268-0
99. Suresha, B., Chandramohan, G., Renukappa, N.M.: Mechanical and tribological properties of glass–epoxy composites with and without graphite particulate filler. J. Appl. Polym. Sci. **103**, 2472–2480 (2007)
100. Khun, N.W., Zhang, H., Lim, L.H., Yue, C.Y., Hu, X., Yang, J.: Tribological properties of short carbon fibers reinforced epoxy composites. Friction. **2**, 226–239 (2014)
101. Quan, H., Zhang, B., Zhao, Q., Yuen, R.K.K., Li, R.K.Y.: Facile preparation and thermal degradation studies of graphite nanoplatelets (GNPs) filled thermoplastic polyurethane (TPU) nanocomposites. Compos. Part A Appl. Sci. Manuf. **40**, 1506–1513 (2009)

102. Song, F., Wang, Q., Wang, T.: High mechanical and tribological performance of polyimide nanocomposites reinforced by chopped carbon fibers in adverse operating conditions. Compos. Sci. Technol. **134**, 251–257 (2016)
103. Larsen, T.Ø., Andersen, T.L., Thorning, B., Horsewell, A., Vigild, M.E.: Changes in the tribological behavior of an epoxy resin by incorporating CuO nanoparticles and PTFE microparticles. Wear. **265**, 203–213 (2008)
104. Qian, F., Melhachat, B., Chen, C., Jiang, K., Zhao, Z., Yang, X.: A Mössbauer study of iron/polytetrafluoroethylene nanocomposites prepared by high-energy ball milling. Nucl. Sci. Tech. **17**, 139–142 (2006). https://doi.org/10.1016/S1001-8042(06)60027-4
105. Rong, M.Z., Zhang, M.Q., Shi, G., Ji, Q.L., Wetzel, B., Friedrich, K.: Graft polymerization onto inorganic nanoparticles and its effect on tribological performance improvement of polymer composites. Tribol. Int. **36**, 697–707 (2003)
106. Xing, X.S., Li, R.K.Y.: Wear behavior of epoxy matrix composites filled with uniform sized sub-micron spherical silica particles. Wear. **256**, 21–26 (2004)
107. Friedrich, K., Zhang, Z., Schlarb, A.: Effects of various fillers on the sliding wear of polymer composites. Compos. Sci. Technol. **65**, 2329–2343 (2005). https://doi.org/10.1016/j.compscitech.2005.05.028
108. Dai, H.: Carbon nanotubes: opportunities and challenges. Surf. Sci. **500**, 218–241 (2002). https://doi.org/10.1016/S0039-6028(01)01558-8
109. Gorrasi, G., Sorrentino, A.: Photo-oxidative stabilization of carbon nanotubes on polylactic acid. Polym. Degrad. Stab. **98**, 963–971 (2013). https://doi.org/10.1016/j.polymdegradstab.2013.02.012
110. De Vivo, B., Lamberti, P., Tucci, V., Guadagno, L., Vertuccio, L., Vittoria, V., Sorrentino, A.: Comparison of the physical properties of epoxy-based composites filled with different types of carbon nanotubes for aeronautic applications. Adv. Polym. Technol. **31**, 205–218 (2012). http://www.scopus.com/inward/record.url?eid=2-s2.0-84864683182&partnerID=40&md5=de0bac503009e539f5488443837fb5e5
111. Wang, C., Xue, T., Dong, B., Wang, Z., Li, H.-L.: Polystyrene–acrylonitrile–CNTs nanocomposites preparations and tribological behavior research. Wear. **265**, 1923–1926 (2008)
112. Al-Kawaz, A., Rubin, A., Badi, N., Blanck, C., Jacomine, L., Janowska, I., Pham-Huu, C., Gauthier, C.: Tribological and mechanical investigation of acrylic-based nanocomposite coatings reinforced with PMMA-grafted-MWCNT. Mater. Chem. Phys. **175**, 206–214 (2016)
113. Dasari, A., Yu, Z.-Z., Mai, Y.-W.: Fundamental aspects and recent progress on wear/scratch damage in polymer nanocomposites. Mater. Sci. Eng. R Reports. **63**, 31–80 (2009). https://doi.org/10.1016/j.mser.2008.10.001
114. Yang, Z., Dong, B., Huang, Y., Liu, L., Yan, F.-Y., Li, H.-L.: Enhanced wear resistance and micro-hardness of polystyrene nanocomposites by carbon nanotubes. Mater. Chem. Phys. **94**, 109–113 (2005)
115. Liu, S., Hsu, W., Chang, K., Yeh, J.: Enhancement of the surface and bulk mechanical properties of polystyrene through the incorporation of raw multiwalled nanotubes with the twin-screw mixing technique. J. Appl. Polym. Sci. **113**, 992–999 (2009)
116. Martínez-Hernández, A.L., Velasco-Santos, C., Castano, V.: Carbon nanotubes composites: processing, grafting and mechanical and thermal properties. Curr. Nanosci. **6**, 12–39 (2010)
117. Jacobs, O., Xu, W., Schädel, B., Wu, W.: Wear behaviour of carbon nanotube reinforced epoxy resin composites. Tribol. Lett. **23**, 65–75 (2006)
118. Chen, H., Jacobs, O., Wu, W., Rüdiger, G., Schädel, B.: Effect of dispersion method on tribological properties of carbon nanotube reinforced epoxy resin composites. Polym. Test. **26**, 351–360 (2007)
119. Zoo, Y.-S., An, J.-W., Lim, D.-P., Lim, D.-S.: Effect of carbon nanotube addition on tribological behavior of UHMWPE. Tribol. Lett. **16**, 305–309 (2004)
120. Kanagaraj, S., Varanda, F.R., Zhil'tsova, T.V., Oliveira, M.S.A., Simões, J.A.O.: Mechanical properties of high density polyethylene/carbon nanotube composites. Compos. Sci. Technol. **67**, 3071–3077 (2007). https://doi.org/10.1016/j.compscitech.2007.04.024

121. Lee, J., Kathi, J., Rhee, K.Y., Lee, J.H.: Wear properties of 3-aminopropyltriethoxysilane-functionalized carbon nanotubes reinforced ultra high molecular weight polyethylene nanocomposites. Polym. Eng. Sci. **50**, 1433–1439 (2010)
122. Bin Ali, A., Abdul Samad, M., Merah, N.: UHMWPE hybrid nanocomposites for improved tribological performance under dry and water-lubricated sliding conditions. Tribol. Lett. **65**, 102 (2017). https://doi.org/10.1007/s11249-017-0884-y
123. Samad, M.A., Sinha, S.K.: Effects of counterface material and UV radiation on the tribological performance of a UHMWPE/CNT nanocomposite coating on steel substrates. Wear. **271**, 2759–2765 (2011)
124. Kim, J., Im, H., Cho, M.H.: Tribological performance of fluorinated polyimide-based nanocomposite coatings reinforced with PMMA-grafted-MWCNT. Wear. **271**, 1029–1038 (2011)
125. Vail, J.R., Burris, D.L., Sawyer, W.G.: Multifunctionality of single-walled carbon nanotube–polytetrafluoroethylene nanocomposites. Wear. **267**, 619–624 (2009)
126. May, B., Hartwich, M.R., Stengler, R., Hu, X.G.: The influence of carbon nanotubes on the tribological behavior and wear resistance of a polyamide nanocomposite. In: Advance Tribology, pp. 515–515, Springer, Berlin/Heidelberg (2009). https://doi.org/10.1007/978-3-642-03653-8_163
127. Meng, H., Sui, G.X., Xie, G.Y., Yang, R.: Friction and wear behavior of carbon nanotubes reinforced polyamide 6 composites under dry sliding and water lubricated condition. Compos. Sci. Technol. **69**, 606–611 (2009)
128. Giraldo, L.F., López, B.L., Brostow, W.: Effect of the type of carbon nanotubes on tribological properties of polyamide 6. Polym. Eng. Sci. **49**, 896–902 (2009)
129. Armstrong, G., Ruether, M., Blighe, F., Blau, W.: Functionalised multi-walled carbon nanotubes for epoxy nanocomposites with improved performance. Polym. Int. **58**, 1002–1009 (2009)
130. Li, J., Zhang, L.Q.: The effects of adding carbon nanotubes to the mechanical and tribological properties of a carbon fibre reinforced polyether ether ketone composite. Proc. Inst. Mech. Eng. Part C J. Mech. Eng. Sci. **223**, 2501–2507 (2009)
131. Cai, H., Yan, F., Xue, Q.: Investigation of tribological properties of polyimide/carbon nanotube nanocomposites. Mater. Sci. Eng. A. **364**, 94–100 (2004)
132. Endo, M., Kim, Y.A., Hayashi, T., Fukai, Y., Oshida, K., Terrones, M., Yanagisawa, T., Higaki, S., Dresselhaus, M.S.: Structural characterization of cup-stacked-type nanofibers with an entirely hollow core. Appl. Phys. Lett. **80**, 1267–1269 (2002)
133. Liu, Q., Ren, W., Chen, Z.-G., Yin, L., Li, F., Cong, H., Cheng, H.-M.: Semiconducting properties of cup-stacked carbon nanotubes. Carbon N. Y. **47**, 731–736 (2009)
134. Endo, M., Kim, Y.A., Ezaka, M., Osada, K., Yanagisawa, T., Hayashi, T., Terrones, M., Dresselhaus, M.S.: Selective and efficient impregnation of metal nanoparticles on cup-stacked-type carbon nanofibers. Nano Lett. **3**, 723–726 (2003)
135. Choi, Y.-K., Gotoh, Y., Sugimoto, K., Song, S.-M., Yanagisawa, T., Endo, M.: Processing and characterization of epoxy nanocomposites reinforced by cup-stacked carbon nanotubes. Polymer (Guildf). **46**, 11489–11498 (2005)
136. Yokozeki, T., Iwahori, Y., Ishiwata, S.: Matrix cracking behaviors in carbon fiber/epoxy laminates filled with cup-stacked carbon nanotubes (CSCNTs). Compos. Part A Appl. Sci. Manuf. **38**, 917–924 (2007)
137. Yokozeki, T., Iwahori, Y., Ishiwata, S., Enomoto, K.: Mechanical properties of CFRP laminates manufactured from unidirectional prepregs using CSCNT-dispersed epoxy. Compos. Part A Appl. Sci. Manuf. **38**, 2121–2130 (2007)
138. Werner, P., Altstädt, V., Jaskulka, R., Jacobs, O., Sandler, J.K.W., Shaffer, M.S.P., Windle, A. H.: Tribological behaviour of carbon-nanofibre-reinforced poly (ether ether ketone). Wear. **257**, 1006–1014 (2004)
139. Zhang, L.C., Zarudi, I., Xiao, K.Q.: Novel behaviour of friction and wear of epoxy composites reinforced by carbon nanotubes. Wear. **261**, 806–811 (2006)

140. Yang, Z., Dong, B., Huang, Y., Liu, L., Yan, F.-Y., Li, H.-L.: A study on carbon nanotubes reinforced poly (methyl methacrylate) nanocomposites. Mater. Lett. **59**, 2128–2132 (2005)
141. Elinski, M.B., Liu, Z., Spear, J.C., Batteas, J.D.: 2D or not 2D? The impact of nanoscale roughness and substrate interactions on the tribological properties of graphene and MoS_2. J. Phys. D. Appl. Phys. **50**, 103003 (2017). http://stacks.iop.org/0022-3727/50/i=10/a=103003
142. Pan, B., Tan, J., Jia, H., Chen, J., Tai, Y., Liu, J., Zhang, Y., Niu, Q.: Tribological behavior of phenolic nanocomposites reinforced by 2D atomic crystal of boron nitride. J. Polym. Mater. **33**, 567 (2016)
143. Uddin, F.: Clays, nanoclays, and montmorillonite minerals. Metall. Mater. Trans. A. **39**, 2804–2814 (2008). https://doi.org/10.1007/s11661-008-9603-5
144. Alexandre, M., Dubois, P.: Polymer-layered silicate nanocomposites: preparation, properties and uses of a new class of materials. Mater. Sci. Eng. R Reports. **28**, 1–63 (2000). https://doi.org/10.1016/S0927-796X(00)00012-7
145. Yu, Y., Gu, J., Kang, F., Kong, X., Mo, W.: Surface restoration induced by lubricant additive of natural minerals. Appl. Surf. Sci. **253**, 7549–7553 (2007)
146. Lange, J., Wyser, Y.: Recent innovations in barrier technologies for plastic packaging? A review. Packag. Technol. Sci. **16**, 149–158 (2003). https://doi.org/10.1002/pts.621
147. Sorrentino, A., Pantani, R., Brucato, V.: Injection molding of syndiotactic polystyrene/clay nanocomposites. Polym. Eng. Sci. **46**, 1768–1777 (2006)
148. Gorrasi, G., Milone, C., Piperopoulos, E., Lanza, M., Sorrentino, A.: Hybrid clay mineral-carbon nanotube-PLA nanocomposite films. Preparation and photodegradation effect on their mechanical, thermal and electrical properties. Appl. Clay Sci. **71**, 49–54 (2013). https://doi.org/10.1016/j.clay.2012.11.004
149. Raka, L., Sorrentino, A., Bogoeva-Gaceva, G.: Isothermal crystallization kinetics of polypropylene latex-based nanocomposites with organo-modified clay. J. Polym. Sci. Part B Polym. Phys. **48**, 1927–1938 (2010). https://doi.org/10.1002/polb.22069
150. Hussain, F.: Review article: polymer-matrix nanocomposites, processing, manufacturing, and application: an overview. J. Compos. Mater. **40**, 1511–1575 (2006). https://doi.org/10.1177/0021998306067321
151. Dasari, A., Yu, Z.-Z., Mai, Y.-W., Hu, G.-H., Varlet, J.: Clay exfoliation and organic modification on wear of nylon 6 nanocomposites processed by different routes. Compos. Sci. Technol. **65**, 2314–2328 (2005)
152. Jawahar, P., Gnanamoorthy, R., Balasubramanian, M.: Tribological behaviour of clay–thermoset polyester nanocomposites. Wear. **261**, 835–840 (2006)
153. Yuan, Q., Ramisetti, N., Misra, R.D.K.: Nanoscale near-surface deformation in polymer nanocomposites. Acta Mater. **56**, 2089–2100 (2008). https://doi.org/10.1016/j.actamat.2007.12.051
154. Srinath, G., Gnanamoorthy, R.: Effect of nanoclay reinforcement on tensile and tribo behaviour of Nylon 6. J. Mater. Sci. **40**, 2897–2901 (2005)
155. Srinath, G., Gnanamoorthy, R.: Two-body abrasive wear characteristics of Nylon clay nanocomposites – effect of grit size, load, and sliding velocity. Mater. Sci. Eng. A. **435**, 181–186 (2006)
156. Peng, Q.-Y., Cong, P.-H., Liu, X.-J., Liu, T.-X., Huang, S., Li, T.-S.: The preparation of PVDF/clay nanocomposites and the investigation of their tribological properties. Wear. **266**, 713–720 (2009)
157. Fan, B., Yang, Y., Feng, C., Ma, J., Tang, Y., Dong, Y., Qi, X.: Tribological properties of fabric self-lubricating liner based on organic montmorillonite (OMMT) reinforced phenolic (PF) nanocomposites as hybrid matrices. Tribol. Lett. **57**, 22 (2015)
158. Landi, G., Sorrentino, A., Fedi, F., Neitzert, H.C., Iannace, S.: Cycle stability and dielectric properties of a new biodegradable energy storage material. Nano Energy. **17**, 348–355 (2015). https://doi.org/10.1016/j.nanoen.2015.09.006

159. Li, X., Cai, W., An, J., Kim, S., Nah, J., Yang, D., Piner, R., Velamakanni, A., Jung, I., Tutuc, E.: Large-area synthesis of high-quality and uniform graphene films on copper foils. Science (80). **324**, 1312–1314 (2009)
160. Choi, W., Lahiri, I., Seelaboyina, R., Kang, Y.S.: Synthesis of graphene and its applications: a review. Crit. Rev. Solid State Mater. Sci. **35**, 52–71 (2010)
161. Allen, M.J., Tung, V.C., Kaner, R.B.: Honeycomb carbon: a review of graphene. Chem. Rev. **110**, 132–145 (2009)
162. Landi, G., Fedi, F., Sorrentino, A., Neitzert, H.C., Iannace, S.: Gelatin/graphene systems for low cost energy storage. In: AIP Conference Proceedings, vol. 1599(1), pp. 202–205. AIP Publishing, Naples (2014). https://doi.org/10.1063/1.4876813
163. Dreyer, D.R., Park, S., Bielawski, C.W., Ruoff, R.S.: The chemistry of graphene oxide. Chem. Soc. Rev. **39**, 228–240 (2010)
164. Wei, D., Grande, L., Chundi, V., White, R., Bower, C., Andrew, P., Ryhänen, T.: Graphene from electrochemical exfoliation and its direct applications in enhanced energy storage devices. Chem. Commun. **48**, 1239–1241 (2012)
165. Shen, X.-J., Pei, X.-Q., Fu, S.-Y., Friedrich, K.: Significantly modified tribological performance of epoxy nanocomposites at very low graphene oxide content. Polymer (Guildf). **54**, 1234–1242 (2013)
166. Landi, G., Sorrentino, A., Iannace, S., Neitzert, H.C.: Differences between graphene and graphene oxide in gelatin based systems for transient biodegradable energy storage applications. Nanotechnology. **28**, 54005 (2016). https://doi.org/10.1088/1361-6528/28/5/054005
167. Furio, A., Landi, G., Altavilla, C., Sofia, D., Iannace, S., Sorrentino, A., Neitzert, H.C.: Light irradiation tuning of surface wettability, optical, and electric properties of graphene oxide thin films. Nanotechnology. **28**, 54003 (2016)
168. Berman, D., Erdemir, A., Sumant, A.V.: Graphene: a new emerging lubricant. Mater. Today. **17**, 31–42 (2014). https://doi.org/10.1016/j.mattod.2013.12.003
169. Pan, B., Peng, S., Song, S., Chen, J., Liu, J., Liu, H., Zhang, Y., Niu, Q.: The adaptive tribological investigation of polycaprolactam/graphene nanocomposites. Tribol. Lett. **65**, 9 (2017)
170. Tai, Z., Chen, Y., An, Y., Yan, X., Xue, Q.: Tribological behavior of UHMWPE reinforced with graphene oxide nanosheets. Tribol. Lett. **46**, 55–63 (2012)
171. Min, C., Nie, P., Song, H.-J., Zhang, Z., Zhao, K.: Study of tribological properties of polyimide/graphene oxide nanocomposite films under seawater-lubricated condition. Tribol. Int. **80**, 131–140 (2014)
172. Pan, B., Xu, G., Zhang, B., Ma, X., Li, H., Zhang, Y.: Preparation and tribological properties of polyamide 11/graphene coatings. Polym. Plast. Technol. Eng. **51**, 1163–1166 (2012)
173. Huang, T., Xin, Y., Li, T., Nutt, S., Su, C., Chen, H., Liu, P., Lai, Z.: Modified graphene/polyimide nanocomposites: reinforcing and tribological effects. ACS Appl. Mater. Interfaces. **5**, 4878–4891 (2013)
174. Song, H., Wang, Z., Yang, J., Jia, X., Zhang, Z.: Facile synthesis of copper/polydopamine functionalized graphene oxide nanocomposites with enhanced tribological performance. Chem. Eng. J. **324**, 51–62 (2017). https://doi.org/10.1016/j.cej.2017.05.016
175. Kalin, M., Zalaznik, M., Novak, S.: Wear and friction behaviour of poly-ether-ether-ketone (PEEK) filled with graphene, WS_2 and CNT nanoparticles. Wear. **332**, 855–862 (2015)
176. Landi, G., Altavilla, C., Ciambelli, P., Neitzert, H.C., Iannace, S., Sorrentino, A.: Preliminary investigation of polystyrene/MoS2-Oleylamine polymer composite for potential application as low-dielectric material in microelectronics. In: AIP Conference Proceedings, p. 20044. AIP Publishing, Naples (2015). https://doi.org/10.1063/1.4937322
177. Singer, I.L., Pollock, H.: Fundamentals of Friction: Macroscopic and Microscopic Processes. Springer Netherlands, Dordrecht (1992). https://doi.org/10.1007/978-94-011-2811-7

178. Balendhran, S., Deng, J., Ou, J.Z., Walia, S., Scott, J., Tang, J., Wang, K.L., Field, M.R., Russo, S., Zhuiykov, S.: Enhanced charge carrier mobility in two-dimensional high dielectric molybdenum oxide. Adv. Mater. **25**, 109–114 (2013)
179. Kalantar-Zadeh, K., Tang, J., Wang, M., Wang, K.L., Shailos, A., Galatsis, K., Kojima, R., Strong, V., Lech, A., Wlodarski, W.: Synthesis of nanometre-thick MoO_3 sheets. Nanoscale. **2**, 429–433 (2010)
180. Radisavljevic, B., Radenovic, A., Brivio, J., Giacometti, V., Kis, A.: Single-layer MoS_2 transistors. Nat. Nanotechnol. **6**, 147–150 (2011). https://doi.org/10.1038/nnano.2010.279
181. Kumar, A., Ahluwalia, P.K.: Electronic structure of transition metal dichalcogenides monolayers 1H-MX2 (M= Mo, W; X= S, Se, Te) from ab-initio theory: new direct band gap semiconductors. Eur. Phys. J. B. **85**, 186 (2012)
182. Bissessur, R., Gallant, D., Brüning, R.: Novel nanocomposite material consisting of poly [oxymethylene-(oxyethylene)] and molybdenum disulfide. Mater. Chem. Phys. **82**, 316–320 (2003). https://doi.org/10.1016/S0254-0584(03)00310-9
183. Bissessur, R., White, W.: Novel alkyl substituted polyanilines/molybdenum disulfide nanocomposites. Mater. Chem. Phys. **99**, 214–219 (2006). https://doi.org/10.1016/j.matchemphys.2005.10.012
184. Lin, B.-Z., Ding, C., Xu, B.-H., Chen, Z.-J., Chen, Y.-L.: Preparation and characterization of polythiophene/molybdenum disulfide intercalation material. Mater. Res. Bull. **44**, 719–723 (2009). https://doi.org/10.1016/j.materresbull.2008.09.031
185. Wang, T., Liu, W., Tian, J., Shao, X., Sun, D.: Structure characterization and conductive performance of polypyrrol-molybdenum disulfide intercalation materials. Polym. Compos. **25**, 111–117 (2004). https://doi.org/10.1002/pc.20009
186. Naffakh, M., Díez-Pascual, A.M., Remškar, M., Marco, C.: New inorganic nanotube polymer nanocomposites: improved thermal, mechanical and tribological properties in isotactic polypropylene incorporating INT-MoS_2. J. Mater. Chem. **22**, 17002 (2012). https://doi.org/10.1039/c2jm33422d
187. Basavaraj, E., Ramaraj, B.: Polycarbonate/molybdenum disulfide/carbon black composites: physicomechanical, thermal, wear, and morphological properties. Polym. Compos. **33**, 619–628 (2012). https://doi.org/10.1002/pc.22179
188. Basavaraj, E., Ramaraj, B.: A study on mechanical, thermal, and wear characteristics of nylon 66/molybdenum disulfide composites reinforced with glass fibers. Polym. Compos. **33**, 1570–1577 (2012). https://doi.org/10.1002/pc.22293
189. Benavente, E., González, G.: Microwave activated lithium intercalation in transition metal sulfides. Mater. Res. Bull. **32**, 709–717 (1997). https://doi.org/10.1016/S0025-5408(97)00037-8
190. Najmaei, S., Zou, X., Er, D., Li, J., Jin, Z., Gao, W., Zhang, Q., Park, S., Ge, L., Lei, S., Kono, J., Shenoy, V.B., Yakobson, B.I., George, A., Ajayan, P.M., Lou, J.: Tailoring the physical properties of molybdenum disulfide monolayers by control of interfacial chemistry. Nano Lett. **14**, 1354–1361 (2014). https://doi.org/10.1021/nl404396p
191. Divigalpitiya, W.M.R., Morrison, S.R., Frindt, R.F.: Thin oriented films of molybdenum disulphide. Thin Solid Films. **186**, 177–192 (1990). https://doi.org/10.1016/0040-6090(90)90511-B
192. Zhou, X., Wu, D., Shi, H., Fu, X., Hu, Z., Wang, X., Yan, F.: Study on the tribological properties of surfactant-modified MoS_2 micrometer spheres as an additive in liquid paraffin. Tribol. Int. **40**, 863–868 (2007). https://doi.org/10.1016/j.triboint.2006.09.002
193. Altavilla, C., Sarno, M., Ciambelli, P.: A novel wet chemistry approach for the synthesis of hybrid 2D free-floating single or multilayer nanosheets of MS_2 @oleylamine (M═Mo, W). Chem. Mater. **23**, 3879–3885 (2011). https://doi.org/10.1021/cm200837g
194. Altavilla, C., Ciambelli, P., Sarno, M.: "One-pot" synthesis of 2D, 1D, e 0D nano crystals of tungsten and molybdenum chalcogenides (WS_2,MoS_2) functionalized with long chain amine and/or carboxylic acid and/or thiol, WO/2012/042511. http://patentscope.wipo.int/search/en/detail.jsf?docId=WO2012042511&recNum=3&docAn=IB2011054334&queryString=NONOTUBE*or%22NANOTUBE*%22&maxRec=1363 (2012). Accessed 14 Oct 2014

195. Altavilla, C., Sarno, M., Ciambelli, P., Senatore, A., Petrone, V.: New "chimie douce" approach to the synthesis of hybrid nanosheets of MoS_2 on CNT and their anti-friction and anti-wear properties. Nanotechnology. **24**, 125601 (2013). https://doi.org/10.1088/0957-4484/24/12/125601
196. Sorrentino, A., Altavilla, C., Merola, M., Senatore, A., Ciambelli, P., Iannace, S.: Nanosheets of MoS_2-oleylamine as hybrid filler for self-lubricating polymer composites: thermal, tribological, and mechanical properties. Polym. Compos. **36**, 1124–1134 (2015)
197. Altavilla, C., Fedi, F., Sorrentino, A., Iannace, S., Ciambelli, P.: Polystyrene/MoS2@oleylamine nanocomposites. In: AIP Conference Proceedings, Naples, pp. 194–197 (2014). https://doi.org/10.1063/1.4876811
198. Hu, K.H., Wang, J., Schraube, S., Xu, Y.F., Hu, X.G., Stengler, R.: Tribological properties of MoS_2 nano-balls as filler in polyoxymethylene-based composite layer of three-layer self-lubrication bearing materials. Wear. **266**, 1198–1207 (2009)
199. Hu, K.H., Schraube, S., Xu, Y.F., Hu, X.G., Stengler, R.: Micro-tribological behavior of polyacetal-based self-lubrication composite materials modified with MoS_2. Tribology. **30**, 38–45 (2010)
200. Hu, K.H., Hu, X.G., Wang, J., Xu, Y.F., Han, C.L.: Tribological properties of MoS_2 with different morphologies in high-density polyethylene. Tribol. Lett. **47**, 79–90 (2012)
201. Wang, J., Hu, K.H., Xu, Y.F., Hu, X.G.: Structural, thermal, and tribological properties of intercalated polyoxymethylene/molybdenum disulfide nanocomposites. J. Appl. Polym. Sci. **110**, 91–96 (2008)
202. Yang, J.-F., Parakash, B., Hardell, J., Fang, Q.-F.: Tribological properties of transition metal dichalcogenide based lubricant coatings. Front. Mater. Sci. **6**, 116–127 (2012). https://doi.org/10.1007/s11706-012-0155-7
203. Xin, Y., Li, T., Gong, D., Xu, F., Wang, M.: Preparation and tribological properties of graphene oxide/nano-MoS_2 hybrid as multidimensional assembly used in the polyimide nanocomposites. RSC Adv. **7**, 6323–6335 (2017). https://doi.org/10.1039/C6RA27108A

Recent Progress in Self-Lubricating Ceramic Composites

5

Guangyong Wu, Chonghai Xu, Guangchun Xiao, and Mingdong Yi

Contents

Abstract

Structural ceramic composites have received increasing attention over the past few decades for their potential applications in various fields. Lubrication is usually required for moving ceramic parts because of their high coefficient of friction under dry sliding conditions. Self-lubricating ceramic composites have been applied in severe operating conditions where conventional lubrication method, such as liquid lubrication, is unavailable. The solid lubricants added in

G. Wu
School of Mechanical Engineering, Shandong University, Jinan, China
e-mail: gywu168@sina.com

C. Xu (✉)
School of Mechanical Engineering, Shandong University, Jinan, China

School of Mechanical and Automotive Engineering, Qilu University of Technology, Jinan, China

Key Laboratory of Advanced Manufacturing and Measurement and Control Technology for Light Industry in Universities of Shandong, Qilu University of Technology, Jinan, China
e-mail: xch@qlu.edu.cn

G. Xiao · M. Yi
School of Mechanical and Automotive Engineering, Qilu University of Technology, Jinan, China

Key Laboratory of Advanced Manufacturing and Measurement and Control Technology for Light Industry in Universities of Shandong, Qilu University of Technology, Jinan, China

P. L. Menezes et al. (eds.), *Self-Lubricating Composites*,
https://doi.org/10.1007/978-3-662-56528-5_5

self-lubricating ceramic composites can reduce the coefficient of friction. However, they decrease mechanical properties and then weaken antiwear property of the ceramic composites, which consequently restricts self-lubricating ceramic composites' application scope. Therefore, there is a contradiction between the antifriction and antiwear properties of self-lubricating ceramic composites and many efforts from researchers have been devoted to resolve it. In this chapter, two new types of self-lubricating ceramic composites were elaborated. Graded self-lubricating ceramic composites were developed by adopting the design concept of functionally graded materials (FGMs). Their characteristics are that the solid lubricant content decreases with a gradient from the surface to the center and thermal residual compressive stresses exist in the surface after the sintering process. The gradient distribution of solid lubricant and the thermal residual compressive stresses are used to improve the mechanical properties of the ceramic composites. Another new type of self-lubricating ceramic composites is those with the addition of coated solid lubricants. The solid lubricant powders are firstly coated by metal or metallic oxide, etc., to form core-shell structured composite powders and then mixed with the ceramic matrix powders to prepare self-lubricating ceramic composites by sintering. The shell substance is used to protect the solid lubricant core from reacting with the ceramic matrix during the sintering process and promote the relative density of the ceramic composites. The two new types of self-lubricating ceramic composites showed superior mechanical properties and tribological properties to the traditional self-lubricating ceramic composites.

5.1 Introduction

Nowadays, structural ceramic composites have been paid attention increasingly for their distinctive properties, such as high hardness, high wear resistance, high-temperature resistance, and good chemical inertness [1]. They have been widely used for many applications, for instance, cutting tools, bearing parts, valve seats, etc. However, the friction coefficient of moving ceramic parts, especially of those made of alumina based ceramic composites, is relatively high [2]. Higher friction coefficient causes more cost and energy waste. The traditional oil or grease lubrication not only leads to environmental pollution, but also loses efficacy under harsh conditions, such as elevated temperature. Besides, due to poor thermal shock resistance of ceramic composites, inappropriate cooling will cause hot cracks and breakage. Therefore, development and application of ceramic composites with self-lubricating function is an effective and eco-friendly solution to improve the antifriction properties.

So far there are three main methods to make ceramic composites possess self-lubricating function: (1) make use of tribochemical reaction under high working temperature to get in situ formed tribofilm with lubricating function on the surface of ceramic composites, (2) adopt coating, impregnation, or implantation technologies

to enable the surface of ceramic composites to have lubricating function, and (3) fabricate self-lubricating ceramic composites which contain solid lubricants. Compared with the other two methods, the third one can make ceramic composites possess self-lubricating function during their whole service life because there are always solid lubricants in the composites. Besides, it can make the self-lubricating function be available in a wide working temperature range.

The traditional self-lubricating ceramic composites are homogeneous materials with the addition of pristine solid lubricants. Many researches revealed that the added solid lubricants can produce both positive and negative effects on properties of ceramic composites [3, 4]. On the one hand, the solid lubricant can reduce the friction coefficient by forming a tribofilm in the working areas. However, on the other hand, the dispersed solid lubricants can cause a decline in mechanical properties of the ceramic matrix, especially the hardness and fracture toughness, and thus reduce the wear resistance of the ceramic composite [5]. Thus, the traditional self-lubricating ceramic composites are not available to possess rational combination of antifriction and antiwear properties, which consequently restricts their application scope. It is urgent and significant to develop new type of self-lubricating ceramic composites.

In the past few years, we proposed and developed two new types of self-lubricating ceramic composites by modifying the traditional self-lubricating ceramic composites at macroscopic and microscopic level, respectively. The first type is graded self-lubricating ceramic composites [6–8]. It is macrostructural modification to the traditional self-lubricating ceramic composites. The second type is self-lubricating ceramic composites with the addition of metal coated solid lubricants [9]. It is microstructural modification to the traditional self-lubricating ceramic composites.

This chapter introduced the two new types of self-lubricating ceramic composites. Their microstructures, mechanical properties, and tribological properties were studied in detail.

5.2 Graded Self-Lubricating Ceramic Composites

Graded self-lubricating ceramic composites were proposed in terms of macrostructural modification to the traditional self-lubricating ceramic composites. This new type of self-lubricating ceramic composite is characterized by gradually decreasing distribution of solid lubricants from the composite's working surface to its interior and the residual compressive stresses existing in the working surface. There are two design criteria for the graded self-lubricating ceramic composites. Firstly, the solid lubricants should be gradually reduced from the working surface to the interior. Secondly, the thermal expansion coefficient of the composite should gradually increase from the working surface to the inside in order to form residual compressive stresses in the working surface after the sintering process [10].

CaF_2 is well known as a high-temperature solid lubricant and Al_2O_3/(W,Ti)C ceramic is a kind of widely used ceramic material, thus Al_2O_3/(W,Ti)C and CaF_2 were chosen to be the matrix material and solid lubricant, respectively. The starting

Table 5.1 Physical properties of the starting powders

Starting powder	Density ρ ($g{\cdot}cm^{-3}$)	Young's modulus E (GPa)	Poisson's ratio ν	Thermal expansion coefficient α ($\times 10^{-6}\ K^{-1}$)	Thermal conductivity k ($W{\cdot}m^{-1}\ K^{-1}$)
α-Al_2O_3	3.99	380	0.26	8.5	40.37
(W,Ti)C	9.56	550	0.194	5.8	26.74
CaF_2	3.18	75.8	0.26	18.85	9.71

powders were commercial Al_2O_3, (W,Ti)C, and CaF_2 and their physical properties are listed in Table 5.1.

Al_2O_3/(W,Ti)C/CaF_2 graded self-lubricating ceramic composite was designed in disk shape with its compositional distribution changing along the thickness direction. In order that the top and bottom surfaces of the composite can be used as work surfaces with the same self-lubricating performance, a symmetrically laminated structure with seven layers was adopted. Because the graded self-lubricating ceramic composite consists of three components which are Al_2O_3, (W,Ti)C, and CaF_2, a multicomponent gradient distribution model was proposed [7, 8]. The distribution model uses symmetrical power-law functions containing two compositional distribution exponents n_1 and n_2 which are for CaF_2 and (W,Ti)C, respectively.

The geometry model of Al_2O_3/(W,Ti)C/CaF_2 graded self-lubricating ceramic composite is a cylinder in a Cartesian coordinate system. The cylinder's bottom surface is in the X-Y plane and its axis coincides with the Z axis. The diameter and height of the cylinder are D and H, respectively. Because of their very small amounts, pores and sintering additives are not taken into account in the multicomponent distribution model. By regarding α-Al_2O_3 and (W,Ti)C as a matrix component, the volume fraction of CaF_2 in Al_2O_3/(W,Ti)C/CaF_2 material along the thickness of the material is given as:

$$V_{CaF_2} = f_1(\xi) = \begin{cases} \left(f_1^{CF} - f_0^{CF}\right)\left[\frac{0.5-\xi}{0.5}\right]^{n_1} + f_0^{CF} & 0 \le \xi \le 0.5 \\ \left(f_1^{CF} - f_0^{CF}\right)\left[\frac{\xi-0.5}{0.5}\right]^{n_1} + f_0^{CF} & 0.5 \le \xi \le 1 \end{cases} \tag{5.1}$$

Where ξ is the ratio of arbitrary coordinate value along the thickness direction (z) to the total thickness of the Al_2O_3/(W,Ti)C/CaF_2 material (H), i.e., z/H, and the range of ξ is [0,1]; ${f_1}^{CF}$ and ${f_0}^{CF}$ are volume fractions of CaF_2 in the Al_2O_3/(W,Ti)C/CaF_2 material of the surface layers and the middle layer, respectively; n_1 is the compositional distribution exponent for CaF_2 distributing in the Al_2O_3/(W,Ti)C/CaF_2 material.

Then the composition profile of the Al_2O_3/(W,Ti)C matrix component is determined as $V_{Al_2O_3/(W,Ti)C} = 1 - V_{CaF_2}$.The volume fraction of (W,Ti)C in the matrix along the thickness of the Al_2O_3/(W,Ti)C/CaF_2 material is given as:

$$V^*_{(W,Ti)C} = f_2(\xi) = \begin{cases} \left(f_1^{WT} - f_0^{WT}\right)\left[\frac{0.5-\xi}{0.5}\right]^{n_2} + f_0^{WT} & 0 \le \xi \le 0.5 \\ \left(f_1^{WT} - f_0^{WT}\right)\left[\frac{\xi-0.5}{0.5}\right]^{n_2} + f_0^{WT} & 0.5 \le \xi \le 1 \end{cases} \tag{5.2}$$

Where ξ is the same as in Eq. (5.1); ${f_1}^{WT}$ and ${f_0}^{WT}$ are volume fractions of (W,Ti)C in the Al_2O_3/(W,Ti)C matrixes of the surface layers and the middle layer, respectively; n_2 is the compositional distribution exponent for (W,Ti)C distributing in the Al_2O_3/(W,Ti)C matrix.

The volume fraction of (W,Ti)C in Al_2O_3/(W,Ti)C/CaF_2 material along the thickness of the material should be given as:

$$V_{(W,Ti)C} = (1 - f_1(\xi))f_2(\xi) \tag{5.3}$$

And the volume fraction of Al_2O_3 in Al_2O_3/(W,Ti)C/CaF_2 material along the thickness of the material should be given as:

$$V_{Al_2O_3} = (1 - f_1(\xi))(1 - f_2(\xi)) = 1 - V_{CaF_2} - V_{(W,Ti)C} \tag{5.4}$$

The combinations of nonnegative values of n_1 and n_2 can determine the compositional distributions of Al_2O_3/(W,Ti)C/CaF_2 material and then its gradients of microstructure as well as properties. According to values of n_1 and n_2, Al_2O_3/(W,Ti)C/CaF_2 material can be categorized into five general types:

(a) $n_1 = n_2 = 0$. Volume fraction of CaF_2 in the whole material and volume fraction of (W,Ti)C in the matrix are constant to form homogeneous material.
(b) $n_1 = 0$, $n_2 \neq 0$. Volume fraction of CaF_2 in the whole material is constant and volume fraction of (W,Ti)C in the matrix is varying to form the first kind of graded material.
(c) $n_1 \neq 0$, $n_2 = 0$. Volume fraction of CaF_2 in the whole material is varying and volume fraction of (W,Ti)C in the matrix is constant to form the second kind of graded material.
(d) $n_1 = n_2 \neq 0$. Volume fraction of CaF_2 in the whole material and volume fraction of (W,Ti)C in the matrix are varying with the same rate to form the third kind of graded material.
(e) $n_1 \neq n_2 \neq 0$. Volume fraction of CaF_2 in the whole material and volume fraction of (W,Ti)C in the matrix are varying with different rates to form the fourth kind of graded material.

In order to conform the two design criteria and use a simpler structure, the compositional distribution exponents were chosen to be $n_1 = n_2 = 2.0$. The detailed design procedure was presented in [7]. Table 5.2 lists the compositions of each layer and their physical properties which were calculated by the formulae in [10].

The Al_2O_3/(W,Ti)C/CaF_2 graded self-lubricating ceramic composite was prepared using a layer stacking method and powder metallurgical process. The detailed preparation process and measurement method of mechanical properties were described in [7]. An Al_2O_3/(W,Ti)C/CaF_2 homogeneous self-lubricating ceramic composite was also made from the same ingredients with the surface layers of the graded composite. Phase identification was made by X-ray diffraction (XRD) using an X-ray diffractometer (Bruker D8 ADVANCE). XRD patterns were recorded from

Table 5.2 Compositions and physical properties of graded layers

Layer number	Content of CaF_2 (Vol. %)	Volume ratio of (W,Ti)C: α-Al_2O_3 in matrix (Vol %)	Young's modulus E (GPa)	Poisson's ratio ν	Thermal expansion coefficient α ($\times 10^{-6}$ K^{-1})	Thermal conductivity k ($W \cdot m^{-1}$ K^{-1})
4th	0	30:70	424.710	0.242	7.660	35.156
3rd;5th	3.3	40:60	420.602	0.235	7.516	32.275
2nd;6th	6.7	50:50	415.416	0.229	7.386	29.643
1st;7th	10	60:40	410.367	0.223	7.262	27.303

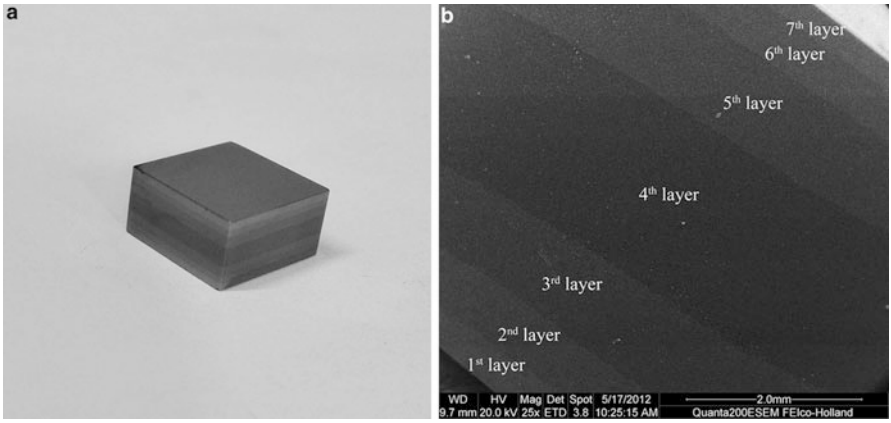

Fig. 5.1 (**a**) Optical photograph and (**b**) SEM micrograph of Al_2O_3/(W,Ti)C/CaF_2 graded composite

20° to 80° with a step of 0.02° under the condition of 40 kV and 20 mA. The componential distribution of Al_2O_3/(W,Ti)C/CaF_2 graded composite was analyzed by line scanning technique with energy dispersive spectrometer (EDS, Oxford INCAx-act). The microstructures were observed on polished cross section and fracture surfaces by environmental scanning electron microscope (ESEM, model FEI-quanta 200).

Optical photograph of Al_2O_3/(W,Ti)C/CaF_2 graded ceramic composite is shown in Fig. 5.1a. It can be seen that the layers are perpendicular to the thickness direction. SEM micrograph of the cross section surface is shown in Fig. 5.1b. A symmetrical seven-layer structure can be easily observed. The higher the (W,Ti)C content of a layer is, the brighter the layer looks like. The layer interfaces are straight and parallel to each other, which is in accord with the design objective.

The microstructural changes which agree with the gradient variation of the components are shown in Fig. 5.2. The darker phase in the micrographs is identified by EDS to be Al_2O_3 and the brighter phase is (W,Ti)C and CaF_2. From the first layer (surface layer) to the fourth layer (middle layer), because the content of Al_2O_3

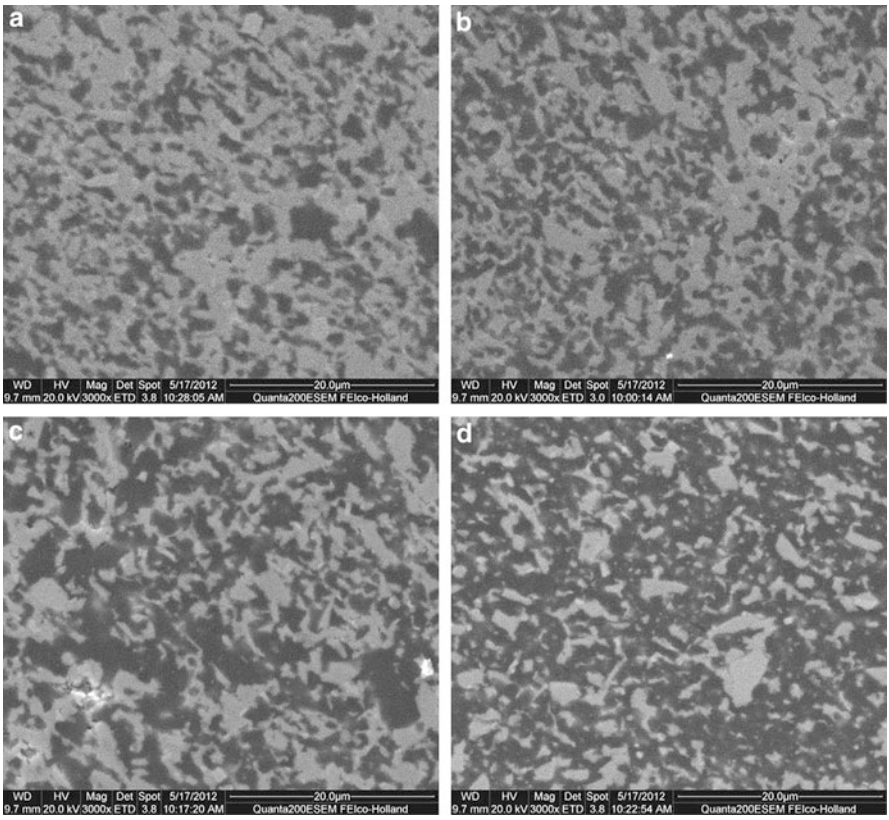

Fig. 5.2 SEM micrographs of the polished surface of Al_2O_3/(W,Ti)C/CaF_2 graded composite: (**a**) the 1st layer, (**b**) the 2nd layer, (**c**) the 3rd layer, and (**d**) the 4th layer

increases meanwhile the content of (W,Ti)C and CaF_2 decreases layer by layer, the proportion of darker areas in the micrographs increases and brighter areas follow the opposite variation trend. Furthermore, the phases in each layer are uniformly distributed and form relatively dense microstructures.

The SEM micrographs of the fractured surface of the Al_2O_3/(W,Ti)C/CaF_2 graded self-lubricating ceramic composite are shown in Fig. 5.3. It can be seen that each phase in the different layers has small and uniform grains. The cavities that are left after grains were pulled out can be observed. This sign indicates typical intergranularc fracture. The wavy or stepped features formed after grains were fractured can also be observed, which indicates typical transgranular fracture. Therefore, mixed intergranular fracture and transgranular fracture are fracture modes of the graded self-lubricating ceramic composite.

Figure 5.4 illustrates XRD pattern of surface layer of the Al_2O_3/(W,Ti)C/CaF_2 graded self-lubricating ceramic composite. It can be seen that Al_2O_3, (W,Ti)C, and CaF_2 phases well exist in the composite.

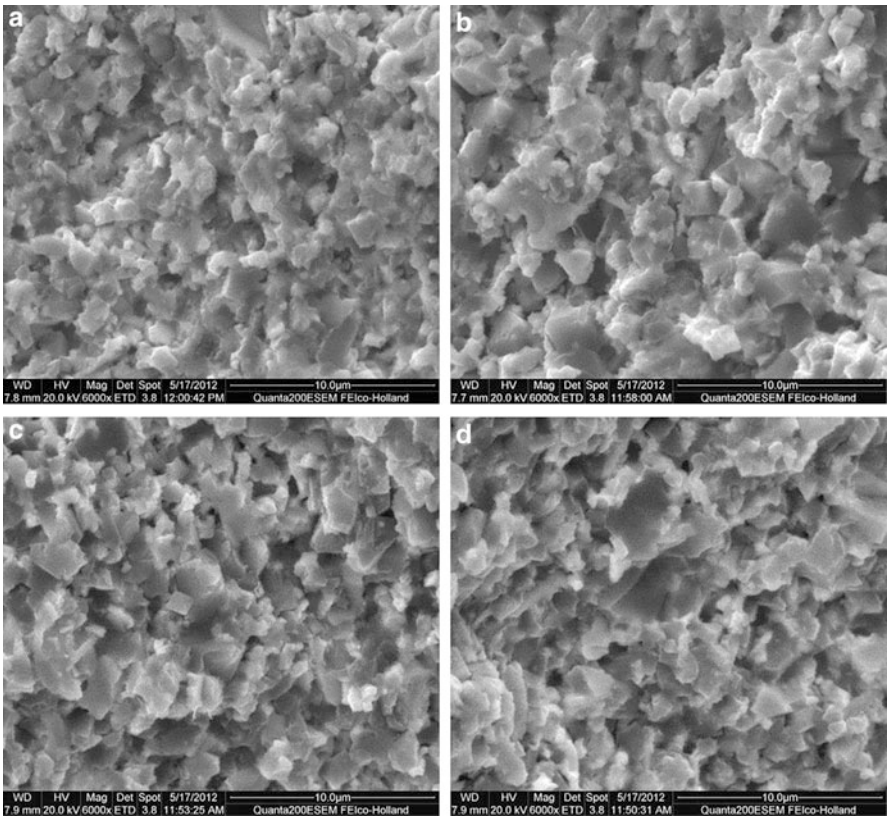

Fig. 5.3 SEM micrographs of the fractured surface of Al_2O_3/(W,Ti)C/CaF_2 graded composite: (**a**) the 1st layer, (**b**) the 2nd layer, (**c**) the 3rd layer, and (**d**) the 4th layer

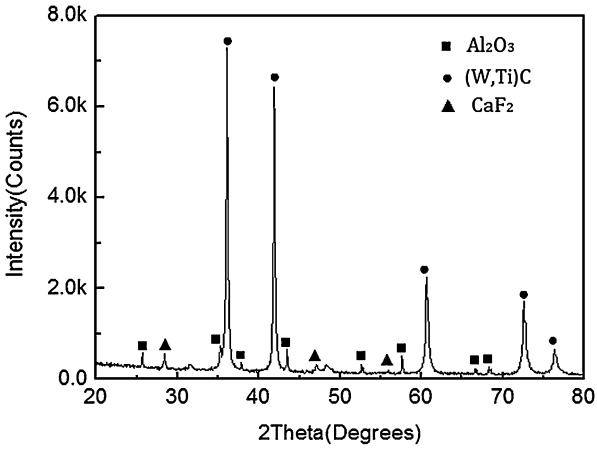

Fig. 5.4 XRD pattern of surface layer of Al_2O_3/(W,Ti)C/CaF_2 graded composite

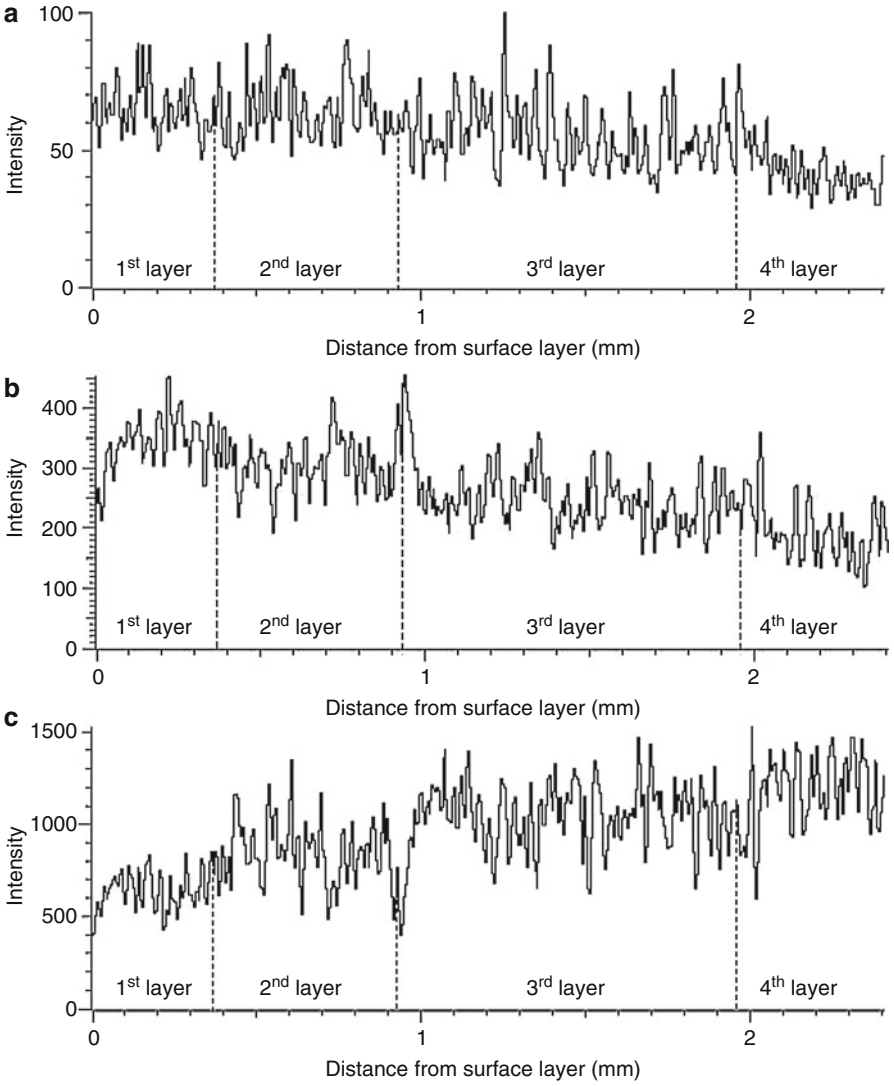

Fig. 5.5 Line scanning patterns for elemental distributions along the compositional gradient direction: (**a**) Ca element, (**b**) Ti element, and (**c**) Al element

Elemental gradient distributions from a surface layer (first layer) to the middle layer (fourth layer) are shown in Fig. 5.5. It can be seen that the concentrations of Ca and Ti elements decrease from the surface layer to the middle layer in the graded composite, whereas the Al concentration follows the opposite trend. It is indicated that the graded distributions of Al_2O_3, (W,Ti)C, and CaF_2 conform to the design scheme shown in Table 5.2. It should be noticed that a small amount of elemental Ca is detected in the middle layer of the material where no CaF_2 was added. The

Table 5.3 Mechanical properties of the self-lubricating ceramic composites

Specimen	Flexural strength (MPa)	Vickers hardness (GPa)	Fracture toughness ($MPa \cdot m^{1/2}$)
Graded composite	769±22[a]	15.36 ± 0.3[b]	4.02 ± 0.2[b]
Homogeneous composite	617 ± 31	12.89 ± 0.5	3.81 ± 0.3

[a]The testing forces were loaded perpendicularly with respect to the layers
[b]The data were from measurements taken on the surface layers

concentration of elemental Ca sharply decreases from the boundary of the fourth layer and the third layer to the interior of the fourth layer. This result could be attributed to the melting point of CaF_2, which is lower than the sintering temperature. Some CaF_2 may have melted during the sintering process and diffused into the middle layer from the adjacent layers.

The mechanical properties of Al_2O_3/(W,Ti)C/CaF_2 graded self-lubricating ceramic composite and the homogeneous composite are listed in Table 5.3. The flexural strength, Vickers hardness, and fracture toughness of the Al_2O_3/(W,Ti)C/CaF_2 graded composite are respectively 25%, 19%, and 6% higher than those of the Al_2O_3/(W,Ti)C/CaF_2 homogeneous composite. The significant improvement in the mechanical properties can be attributed to the two design criteria. Firstly, the decreasing gradient of the CaF_2 content from the surface layers to the middle layer of the graded composite can ensure excellent self-lubricating properties in the surface layers because of its relatively high CaF_2 content, and improve the flexural strength of the whole material due to substantially higher flexural strength of the middle layer where no CaF_2 had been added. Secondly, residual compressive stresses in the surface layers were caused by the mismatched thermal coefficients of expansion between adjacent layers. The presence of these stresses can effectively improve the mechanical properties of the surface layers, especially the fracture toughness and hardness [11].

The thermal residual stresses were calculated by the indentation method [12]. The indentation was produced by a Vickers indenter on central line of each layer of a cross section of the composite, using a load of 49 N. The indents were aligned in the way that their diagonals and possible radial cracks were parallel and perpendicular to the graded layers. As shown in Fig. 5.6a, the indentation cracks that are perpendicular to the layers are clearly shorter and narrower than those parallel to the layers, which indicates the presence of compressive stresses in the surface layers. It can be seen from Fig. 5.6b that the exterior layers are subjected to compressive stresses while tensile stresses are found in the interior layers. The profile of residual stresses satisfactorily conforms to the design objective.

The dry friction and wear test took pin-on-disk type and was carried out on a MMW-1A multipurpose friction and wear testing machine. The pin specimen (10 mm × 10 mm × 5 mm, Ra 0.1 μm) was made of the self-lubricating ceramic composites by cutting, grinding, and polishing. The disk was a hardened 45# carbon steel ring (Φ54mm × Φ38mm × 10 mm, HRC 45, Ra 0.08 μm). The pin and disk were ultrasonically cleaned for 10 min in acetone and then completely dried in a

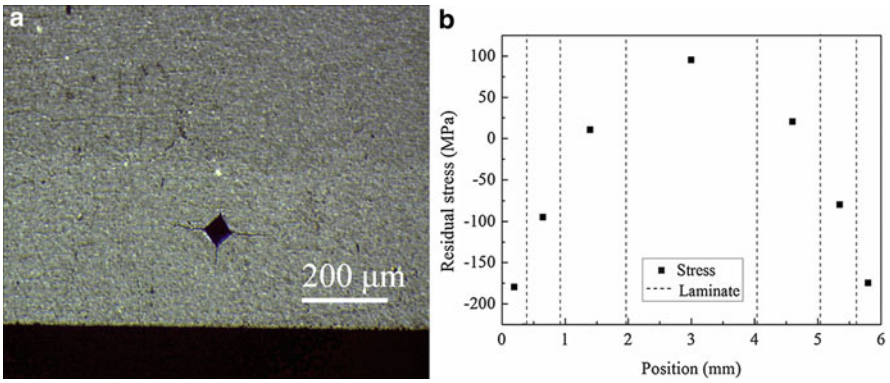

Fig. 5.6 (**a**) Optical micrograph of an indentation on the surface layer, and (**b**) profile of residual stresses measured by the indentation method

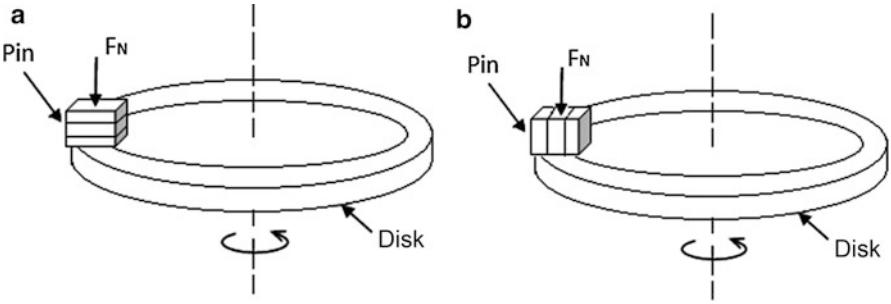

Fig. 5.7 Schematic diagrams of the testing device and clamping mode of pin specimen

vacuum drying oven. The schematic diagrams of the friction and wear testing device and clamping mode of pin specimen are shown in Fig. 5.7. During the dry friction and wear test, the pin specimen of Al_2O_3/(W,Ti)C/CaF_2 graded composite was clamped in the way shown as Fig. 5.7a and was sliding on the disk with a rotational speed of 100–300 r/min under a normal load of 100 N.

The friction coefficient μ of the ceramic composite was calculated by the formula:

$$\mu = F/P = M/(\mathrm{R} \cdot P) \tag{5.5}$$

where F is the fiction force (N); P is the normal load (N); M is the friction torque (N·m); R is intermediate radius of the steel ring (m). The friction coefficient was acquired directly from the friction and wear machine.

The wear rate W (mm^3/N·m) of the ceramic composite was calculated by the formula:

$$W = V/(L \cdot P) = m/(2\pi \cdot \mathrm{R} \cdot n \cdot t \cdot \rho \cdot P) \tag{5.6}$$

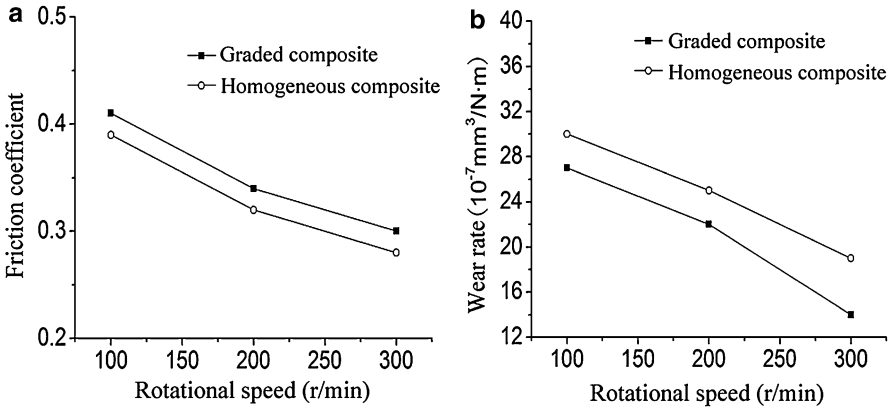

Fig. 5.8 Effect of rotational speed on (**a**) friction coefficient and (**b**) wear rate

where V is the volume loss (mm^3); L is the sliding distance (m); m is the mass loss (g); n is the rotational speed (r/min); t is the friction duration (min); ρ is the density (g/mm^3) and was measured by Archimedes method.

As shown in Fig. 5.8a, the friction coefficient of the two ceramic composites decreases with the increase of rotational speed from 100 r/min to 300 r/min. It is indicated that their antifriction property at relatively high speed is better than that at lower speed. It can also be seen that the fiction coefficient of Al_2O_3/(W,Ti)C/CaF_2 graded ceramic composite is slightly higher than that of the homogeneous one. The homogeneous ceramic composite and the surface layer of the graded ceramic composite were made from the same combined powders. They have the same CaF_2 content and other constituent content. Thus the antifriction property of Al_2O_3/(W,Ti)C/CaF_2 graded ceramic composite is comparable to that of the homogeneous one. As shown in Fig. 5.8b, the wear rate of the two ceramic composites decreases as the rotational speed increases from 100 r/min to 300 r/min. Besides, the wear rate of Al_2O_3/(W,Ti)C/CaF_2 graded ceramic composite is lower than that of Al_2O_3/(W,Ti)C/CaF_2 homogeneous composite. It means that the graded composite has better antiwear property than the homogeneous composite. According to the research of Evans et al. [5], the improvement in antiwear property should be attributed to the enhancement of mechanical properties of the graded ceramic composite, which was caused by the residual compressive stresses existing in the surface layer.

The pin specimen of the graded self-lubricating ceramic composite was clamped in the way shown as Fig. 5.7b. The cross section was used as the rubbing surface to make all layers sliding against the disk at the same time. The effect of CaF_2 content on the wear property of the ceramic composite was analyzed by observing the wear morphologies of graded layers with different composition. Figure 5.9 shows wear morphologies of graded layers with different composition under the normal load of 100 N and rotational speed of 200 r/min. It is shown that the worn surface of the fourth layer, where no CaF_2 was added, is rough and abounds with furrow-like

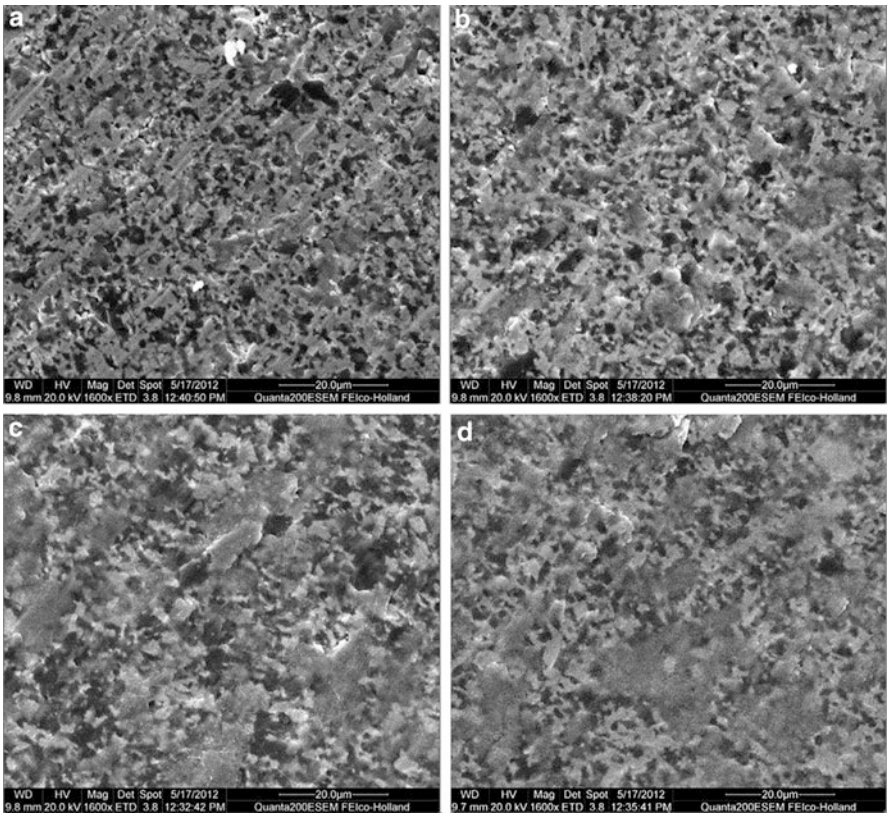

Fig. 5.9 SEM micrographs of wear morphologies of different layers: (**a**) 4th layer with 0 Vol.% CaF_2, (**b**) 3rd layer with 3.3 Vol.% CaF_2, (**c**) 2nd layer with 6.7 Vol.% CaF_2, (**d**) 1st layer with 10 Vol.% CaF_2

scratches, which is a typical sign of abrasive wear. With the increase of CaF_2 content, tribofilm with increasing coverage area was formed and abrasive wear was alleviated layer by layer. It indicates that the CaF_2 solid lubricant was released and smeared on the worn surfaces, because CaF_2 has planes of perfect crystal cleavage in its crystal structure suggesting low-shear strength [13]. Relatively complete tribofilm was formed on the wear surface of the surface layer containing 10Vol.% CaF_2. The tribofilm played a major role in antifriction and wear resistance.

5.3 Self-Lubricating Ceramic Composites with Metal Coated Solid Lubricants

Self-lubricating ceramic composites with the addition of metal coated solid lubricants were proposed in terms of microstructural modification to the traditional self-lubricating ceramic composites. Metal coated solid lubricants are composite

Table 5.4 Composition and parameters of the electroless nickel plating bath

Role in the bath	Chemical	Parameter
Main salt	Nickel sulfate ($NiSO_4 \cdot 6H_2O$)	25 g/L
Reducing agent	Sodium hypophosphite ($NaH_2PO_2 \cdot H_2O$)	25 g/L
Complexing agent	Tri-sodium citrate ($C_6H_5Na_3O_7 \cdot 2H_2O$)	50 g/L
Buffering agent	Ammonium chloride (NH_4Cl)	30 g/L
pH adjuster	Aqueous ammonia ($NH_3 \cdot H_2O$)	Proper amount
pH of solution		9.5–10.0
Plating temperature		45–50 °C
Loading ratio		2–10 g/L

powders with a solid lubricant core and metallic shell. There are many methods to synthesize core-shell composite powders with metallic shell, such as precipitation [14], chemical vapor deposition [15], electroplating [16], electroless plating [17], displacement plating [18], thermo-chemistry co-reduction [19], and gas suspension spray coating [20]. Among these methods, electroless plating has been recognized as one of the most convenient and effective techniques [21]. It is an autocatalytic chemical reduction process in which the reducing agent is oxidized and metallic ions are reduced and then deposited on the substrate surface.

In the study, metal coated solid lubricant powders were firstly prepared by ultrasonic assisted electroless plating process, and then the as-prepared coated powders were mixed with ceramic matrix powders to prepare self-lubricating ceramic composites by hot pressing.

Al_2O_3/(W,Ti)C, CaF_2, and Ni were chosen to be the matrix material, solid lubricant, and metal for coating, respectively. The starting powders were commercially available α-Al_2O_3, (W,Ti)C, and CaF_2 with average particle size of 0.5 μm, 2.5 μm, and 5 μm, respectively. Before electroless nickel plating process, the raw CaF_2 powders were cleaned, coarsened, sensitized, and activated [9]. After that, the CaF_2 powders were dispersed in distilled water and then poured into an electroless nickel plating bath with ultrasonic agitation. The composition and parameters of the plating bath are listed in Table 5.4 [9]. The overall reaction in the electroless plating can be expressed as follows [22]:

$$2Ni^{2+} + 8H_2PO_2^- + 2H_2O \rightarrow 6H_2PO_3^- + 2H^+ + 3H_2 \uparrow + 2P + 2Ni \qquad (5.7)$$

Because $NaH_2PO_2 \cdot H_2O$ was used as reductant in the plating bath, phosphorus element was electroless co-deposited with nickel atoms on CaF_2 powders to form core-shell structure. After electroless plating, the nickel coated CaF_2 powders (CaF_2@Ni) were rinsed with distilled water for several times and then dried in a vacuum oven at 100–110 °C for 8–10 h.

Figure 5.10 shows SEM micrographs of pristine CaF_2 powders and CaF_2@Ni powders with different CaF_2 loading ratios. It can be seen from Fig. 5.10a that the pristine CaF_2 powders have irregular and polyhedral shape with clean and smooth

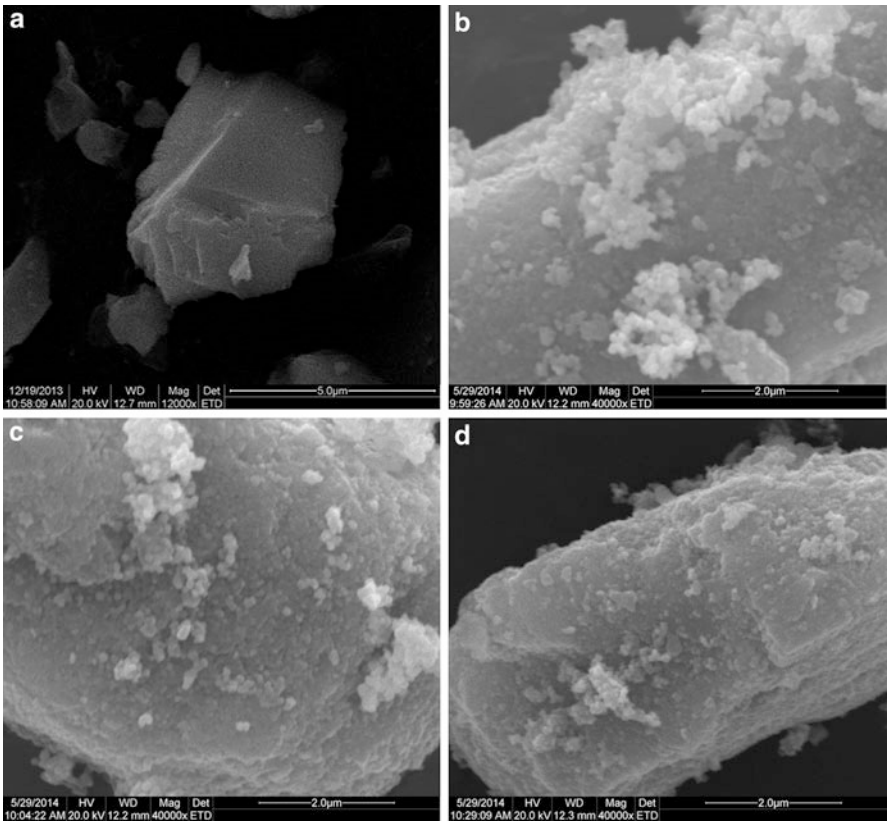

Fig. 5.10 SEM micrographs of (**a**) pristine CaF_2 powders and CaF_2@Ni powders with different CaF_2 loading ratios: (**b**) 2 g/L, (**c**) 5 g/L, (**d**) 10 g/L

surfaces. By contrast, the CaF_2@Ni powders exhibit coarse surfaces with regular nanometric spheres, as shown in Fig. 5.10b–d. When CaF_2 loading ratio is 2 g/L, the nickel coating is complete but has a lot of free Ni aggregates. When CaF_2 loading ratio is 10 g/L, the nickel coating is incompact and incomplete. The nickel coating with CaF_2 loading ratio of 5 g/L is uniform, compact, and complete. Therefore, CaF_2@Ni powders prepared when CaF_2 loading ratio was 5 g/L were used to prepare Al_2O_3/(W,Ti)C/CaF_2@Ni ceramic composite.

Figure 5.11 shows XRD pattern of CaF_2@Ni composite powders when CaF_2 loading ratio of electroless plating was 5 g/L. Besides sharp diffraction peaks belonging to CaF_2, noncrystalline background appears and there is a hillock-like peak (shown in dashed frame) near $2\theta = 45°$. EDS was used to further confirm the coating composition, as shown in Fig. 5.12. It is obviously seen that Ni and P peaks appear at the EDS spectrum besides Ca and F peaks. The XRD and EDS analysis evidently confirm that CaF_2 powders were covered by amorphous Ni-P alloy.

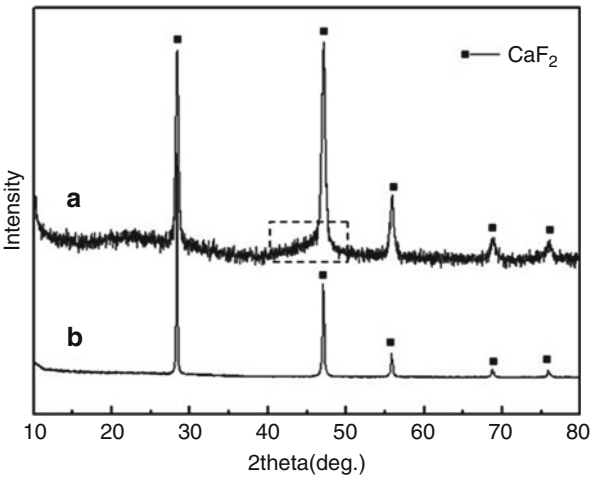

Fig. 5.11 XRD patterns of (**a**) CaF_2@Ni composite powders and (**b**) pristine CaF_2 powders

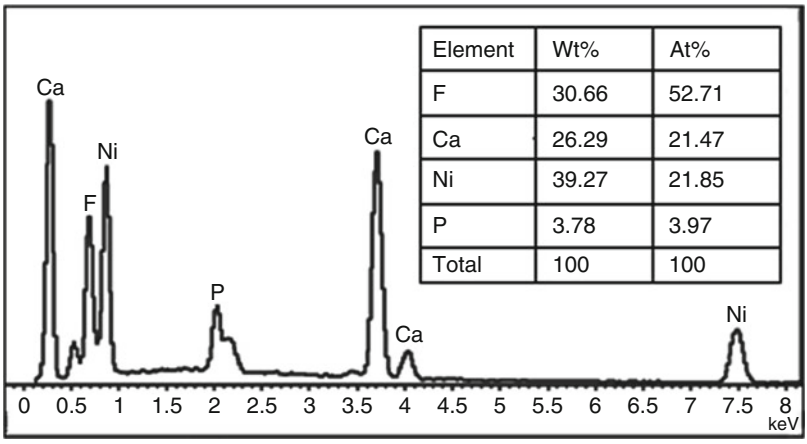

Element	Wt%	At%
F	30.66	52.71
Ca	26.29	21.47
Ni	39.27	21.85
P	3.78	3.97
Total	100	100

Fig. 5.12 EDS spectrum of CaF_2@Ni composite powders

The as-prepared CaF_2@Ni powders were mixed with the raw α-Al_2O_3 and (W,Ti)C powders (α-Al_2O_3:(W,Ti)C = 55:45, v/v) and hot pressed to produce Al_2O_3/(W,Ti)C/CaF_2@Ni ceramic composite containing 10 vol.% CaF_2@Ni powders. The detailed preparation process and measurement method of mechanical properties were described in [9]. An Al_2O_3/(W,Ti)C/CaF_2 ceramic composite with 10 vol.% uncoated CaF_2 was also prepared by using the same technical process.

Figure 5.13 shows SEM micrographs of the polished surfaces of the two ceramic composites. The light gray phase is identified by EDS to be (W,Ti)C and CaF_2, and the deep gray phase is Al_2O_3. It can be seen that the (W,Ti)C phase of Al_2O_3/(W,Ti)C/CaF_2@Ni composite is uniformly distributed in the Al_2O_3 matrix and has smoother grains than Al_2O_3/(W,Ti)C/CaF_2 composite. It is deduced that the

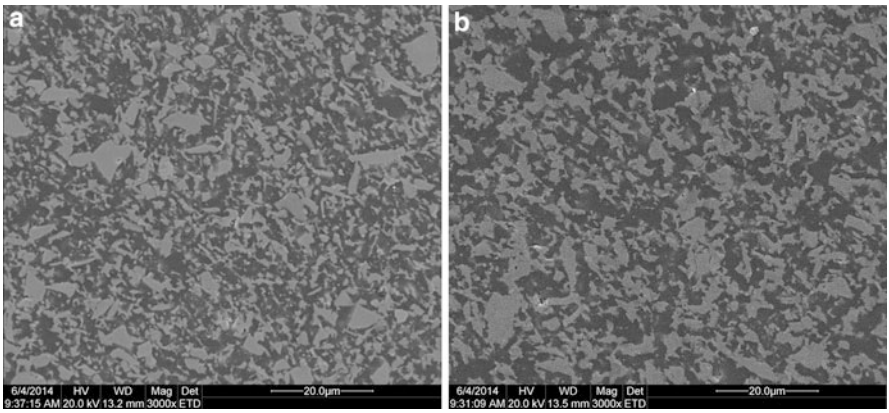

Fig. 5.13 SEM micrographs of polished surfaces: (**a**) Al_2O_3/(W,Ti)C/CaF_2 and (**b**) Al_2O_3/(W,Ti)C/CaF@Ni.

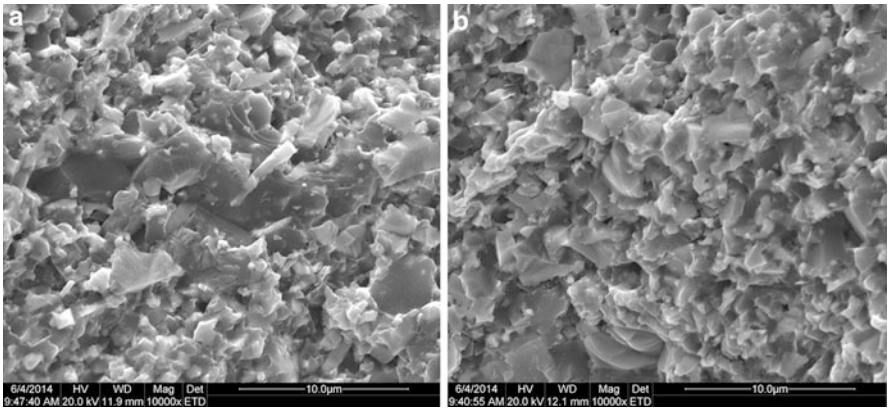

Fig. 5.14 SEM micrographs of fracture surfaces: (**a**) Al_2O_3/(W,Ti)C/CaF_2 and (**b**) Al_2O_3/(W,Ti)C/CaF_2@Ni

pointedness of (W,Ti)C in Al_2O_3/(W,Ti)C/CaF_2@Ni composite fused during the sintering process due to the addition of CaF_2@Ni powders.

Figure 5.14 presents SEM micrographs of the fracture surface of the two ceramic composites. The microstructure of Al_2O_3/(W,Ti)C/CaF_2 composite is not so homogeneous and some grains with abnormal growth can be seen. By contrast, the microstructure of Al_2O_3/(W,Ti)C/CaF_2@Ni composite is compact and the grain size of each phase is uniform. The addition of CaF_2@Ni powders leads to the improvement in microstructure. For one thing, adding the coated powders enhanced dispersity of the solid lubricants in the ceramic composite. For another, the nickel was in fluid phase at the sintering temperature and played a role in promoting densification and preventing grains from abnormally growing. Furthermore, fracture modes of the both ceramic composites are mixed transgranular fracture and intergranular fracture.

The measured flexural strength of the Al_2O_3/(W,Ti)C/CaF_2@Ni composite was 582 ± 27 MPa, which is 15% higher than that of the Al_2O_3/(W,Ti)C/CaF_2 composite (506 ± 21 MPa). The Vickers hardness of the Al_2O_3/(W,Ti)C/CaF_2@Ni composite was 14.1 ± 0.4 GPa, which was increased by 5% compared to that of the Al_2O_3/(W,Ti)C/CaF_2 composite (13.4 ± 0.3 GPa). The fracture toughness measured on the surface layers of the Al_2O_3/(W,Ti)C/CaF_2@Ni composite was 4.3 ± 0.3 MPa·$m^{1/2}$, which is 19% higher than that of the Al_2O_3/(W,Ti)C/CaF_2 composite (3.6 ± 0.2 MPa·$m^{1/2}$). The enhancement of the mechanical properties can be attributed to two reasons: firstly, the inhomogeneous distribution of a second phase and abnormally grown grains can act as the fracture origin and then do harm to mechanical properties [23], so the enhanced flexural strength and hardness of Al_2O_3/(W,Ti)C/CaF_2@Ni composite may be caused by its more homogeneous microstructure refined by adding CaF_2@Ni powders. Secondly, ceramic materials can be toughened by incorporating ductile metal particles in terms of sintering metal coated ceramic powders [24, 25]. The main toughening mechanisms are the bridging effect and the deflection of cracks by the metal particles. So the addition of CaF_2@Ni powders should account for the notable fracture toughness improvement of Al_2O_3/(W,Ti)C/CaF_2@Ni composite.

The dry friction and wear test took pin-on-disk type and was carried out on the MMW-1A multipurpose friction and wear testing machine. The pin specimen (10 mm × 10 mm × 5 mm, Ra 0.1 μm) was made of the self-lubricating ceramic composites by cutting, grinding, and polishing. The disk was a hardened 45# carbon steel ring (Φ54mm × Φ38mm × 10 mm, HRC 45, Ra 0.08 μm). The pin and disk were ultrasonically cleaned for 10 min in acetone and then completely dried in a vacuum drying oven. During the dry friction and wear test, the pin specimen was sliding on the disk with a rotational speed of 100–400 r/min under a normal load of 20 N.

The effect of the rotational speed on the friction coefficient is illustrated in Fig. 5.15a. It can be seen that with the increase of rotational speed from 100 r/min to 400 r/min, the friction coefficient of the two composites shows a downward trend. In addition, the friction coefficient of Al_2O_3/(W,Ti)C/CaF_2@Ni composite is smaller than that of Al_2O_3/(W,Ti)C/CaF_2 composite at each rotational speed. This phenomenon can be attributed to the different addition methods of CaF_2. For Al_2O_3/(W,Ti)C/CaF_2 composite, a chemical reaction between CaF_2 and Al_2O_3 may occur during the sintering process [26]:

$$3CaF_2(s) + Al_2O_3(s) \rightarrow 3CaO(s) + 2AlF_3(g) \tag{5.8}$$

The reaction results in loss of some CaF_2 and weakens the self-lubricating property of the ceramic composite. For Al_2O_3/(W,Ti)C/CaF_2@Ni composite, the metal shell of the CaF_2@Ni powders can prevent or reduce the reaction between CaF_2 and Al_2O_3. Thus Al_2O_3/(W,Ti)C/CaF_2@Ni composite exhibits better anti-friction property than Al_2O_3/(W,Ti)C/CaF_2 composite.

Figure 5.15b illustrates the effect of the rotational speed on the wear rate of the two composites. Firstly, the wear rate of the two composites decreases as the rotational speed increases from 100 r/min to 400 r/min. Secondly, the wear rate of Al_2O_3/(W,Ti)C/CaF_2@Ni composite is lower than that of Al_2O_3/(W,Ti)C/CaF_2 composite. It

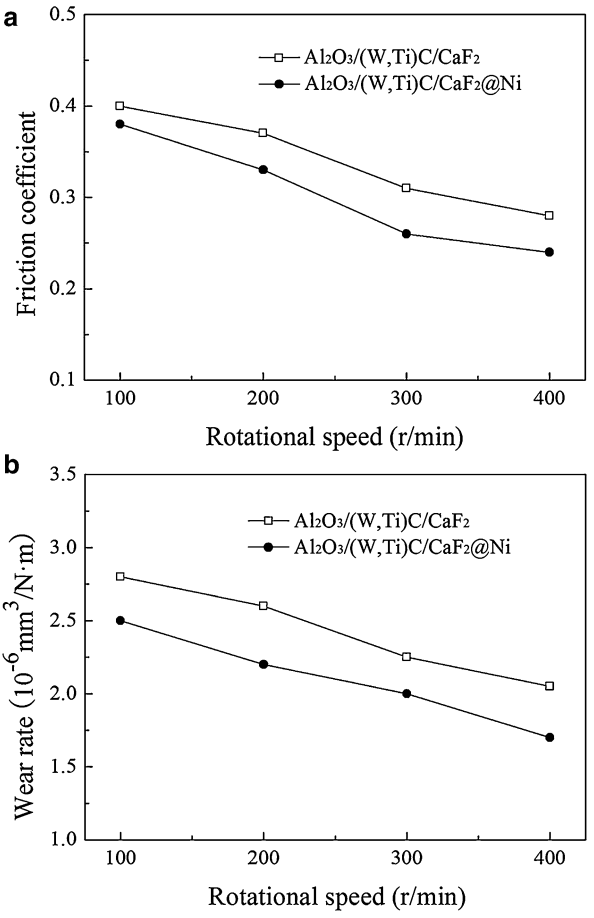

Fig. 5.15 Effect of rotational speed on (**a**) friction coefficient and (**b**) wear rate

indicates that the antiwear property of the composite with the addition of CaF_2@Ni powders is superior to that of the composite with the addition of pristine CaF_2 powders. Evans et al. reported that the wear rate of ceramic material is inversely proportional to the product of its fracture toughness and hardness, i.e., $K_{IC}^{3/4}H^{1/2}$ [5]. Therefore, the better antiwear property of Al_2O_3/(W,Ti)C/CaF_2@Ni composite can be ascribed to the higher mechanical properties especially the hardness and fracture toughness.

The worn surfaces of the two composites under the rotational speed of 200 r/min are presented in Fig. 5.16a and c, respectively. It can be seen that the worn surface of Al_2O_3/(W,Ti)C/CaF_2 composite is rougher than that of Al_2O_3/(W,Ti)C/CaF_2@Ni composite, which verifies the wear resistance of the latter is higher than the former. In addition, EDS analysis reveals that more Ca and less Fe exist on the worn surface of Al_2O_3/(W,Ti)C/CaF_2@Ni composite in comparison to Al_2O_3/(W,Ti)C/CaF_2 composite, as shown in Fig. 5.16b and d. It is indicated that the ceramic composite with

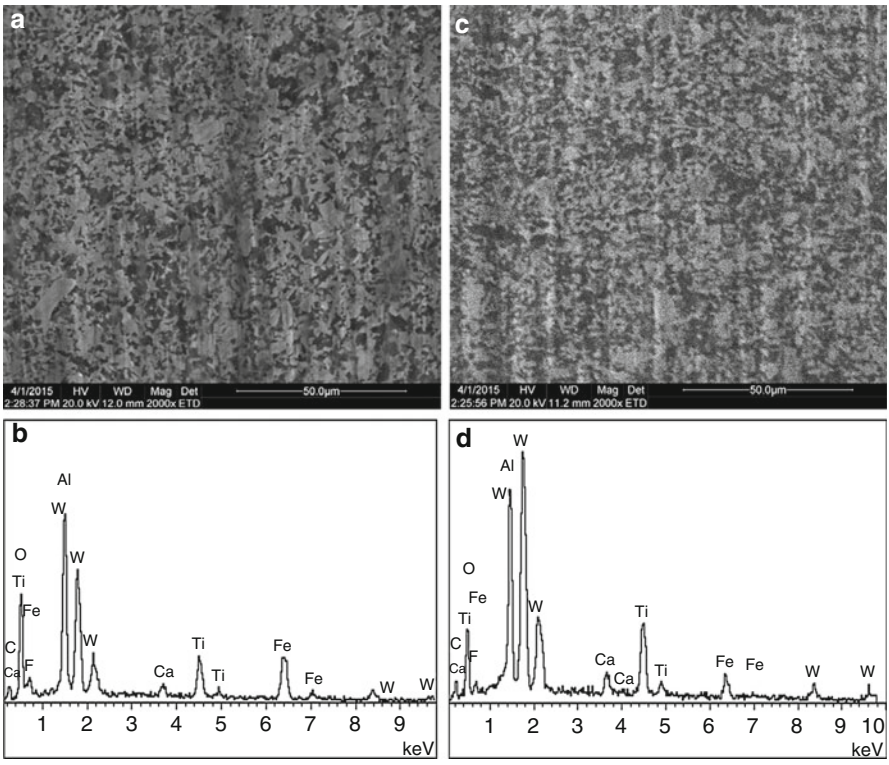

Fig. 5.16 (**a**) SEM micrograph and (**b**) EDS analysis of worn surface of Al_2O_3/(W,Ti)C/CaF_2; (**c**) SEM micrograph and (**d**) EDS analysis on worn surface of Al_2O_3/(W,Ti)C/CaF_2@Ni.

the addition of CaF_2@Ni powders has better antiadhesive property than the ceramic composite with the addition of pristine CaF_2 powders.

5.4 Summary

Aiming at the difficult problem that the traditional self-lubricating ceramic composites are not available to possess rational combination of antifriction and antiwear properties, two new types of self-lubricating ceramic composites were developed in recent years. They modified the traditional self-lubricating ceramic composites at macroscopic and microscopic levels, respectively.

Al_2O_3/(W,Ti)C/CaF_2 graded self-lubricating ceramic composite was developed in terms of macrostructural modification. The microstructures changed layer by layer, which agreed with the gradient variation of the components. The exterior layers were subjected to compressive stresses and the interior layers were subjected to tensile stresses. The flexural strength, Vickers hardness, and fracture toughness of the Al_2O_3/(W,Ti)C/CaF_2 graded composite were respectively 25%, 19% and 6% higher than those of the homogeneous Al_2O_3/(W,Ti)C/CaF_2 composite. The dry friction and

wear test showed that the graded self-lubricating ceramic composite had comparable antifriction properties and superior antiwear properties to the homogeneous composite. The evident improvement in the mechanical and tribological properties can be attributed to the fulfillment of the two design criteria. For one thing, the gradually decreasing distribution of CaF_2 from the composite's surface layers to middle layer ensured good self-lubricating property of the surface layers and enhanced the flexural strength of the graded composite. For another, the existing residual compressive stresses increased hardness, fracture toughness, and antiwear properties of the surface layers of the graded composite.

Al_2O_3/(W,Ti)C/CaF_2@Ni self-lubricating ceramic composite with the addition of metal coated solid lubricants was developed in terms of microstructural modification. As compared with the Al_2O_3/(W,Ti)C/CaF_2 composite, the microstructure of Al_2O_3/(W,Ti)C/CaF_2@Ni composite was more uniform. The flexural strength, Vickers hardness, and fracture toughness were increased by about 15%, 5%, and 19%, respectively. The dry friction and wear test showed that Al_2O_3/(W,Ti)C/CaF_2@Ni composite had obviously better antifriction and antiwear properties than Al_2O_3/(W,Ti)C/CaF_2 composite. The addition of CaF_2@Ni powders led to the improvement in the microstructure, mechanical properties, and tribological behaviors. Firstly, the nickel shell of CaF_2@Ni powders promoted dispersity of CaF_2 in the ceramic composite and protected CaF_2 from reacting with the Al_2O_3 matrix, which enhanced antifriction property. Secondly, the nickel shell promoted the ceramic composite's densification, prevented grains from abnormally growing, and toughened the ceramic composite, which improved the microstructure, mechanical properties, and antiwear property.

Acknowledgments This research work was supported by the National Natural Science Foundation of China, Grant No. 51075248 and Grant No. 51575285.

References

1. Reis, P., Filho, V., Davim, J.P., Xu, X., Ferreira, J.M.F.: Wear behavior on advanced structural ceramics: α-sialon matrix reinforced with b-sialon fibers. Mater. Design. **26**, 417–423 (2005)
2. Deng, J., Cao, T.: Self-lubricating mechanisms via the in situ formed tribofilm of sintered ceramics with CaF_2 additions when sliding against hardened steel. Int. J. Refract. Met. Hard Mater. **25**, 189–197 (2007)
3. Carrapichano, J.M., Gomes, J.R., Silva, R.F.: Tribological behaviour of Si_3N_4-BN ceramic materials for dry sliding applications. Wear. **253**, 1070–1076 (2002)
4. Deng, J., Cao, T., Ding, Z., Liu, J., Sun, J., Zhao, J.: Tribological behaviors of hot-pressed Al_2O_3/TiC ceramic composites with the additions of CaF_2 solid lubricants. J. Eur. Ceram. Soc. **26**, 1317–1323 (2006)
5. Evans, A.G., Wilshaw, T.R.: Quasi-static solid particle damage in brittle solids – I. Observations analysis and implications. Acta Metall. **24**, 939–956 (1976)
6. Wu, G., Xu, C., Zhang, Y., Yi, M.: State of the art of graded self-lubricating ceramic cutting tool materials. Appl. Mech. Mater. **66–68**, 1598–1604 (2011)
7. Xu, C.H., Wu, G.Y., Xiao, G.C., Fang, B.: Al_2O_3/(W,Ti)C/CaF_2 multi-component graded self-lubricating ceramic cutting tool material. Int. J. Refract. Met. Hard Mater. **45**, 125–129 (2014)
8. Xu, C., Wu, G., Zhang, Y., Yi, M., Xiao, G., Fang, B.: Development of multicomponent graded self-lubricating ceramic cutting tool materials. J. Mech. Eng. **50**(7), 94–101 (2014)

9. Wu, G., Xu, C., Xiao, G., Yi, M., Chen, Z., Xu, L.: Self-lubricating ceramic cutting tool material with the addition of nickel coated CaF_2 solid lubricant powders. Int. J. Refract. Met. Hard Mater. **56**, 51–58 (2016)
10. Ai, X., Zhao, J., Huang, C., Zhang, J.: Development of an advanced ceramic tool material – functionally gradient cutting ceramics. Mater. Sci. Eng. A. **248**(1–2), 125–131 (1998)
11. Mehrali, M., Wakily, H., Metselaar, I.H.S.C.: Residual stress and mechanical properties of Al_2O_3/ZrO_2 functionally graded material prepared by EPD from 2-butanone based suspension. Adv. Appl. Ceram. **110**, 35–40 (2011)
12. Hvizdoš, P., Jonsson, D., Anglada, M., Anné, G., Biest, O.V.D.: Mechanical properties and thermal shock behaviour of an alumina/zirconia functionally graded material prepared by electrophoretic deposition. J. Eur. Ceram. Soc. **27**, 1365–1371 (2007)
13. Shuaib, M., Davies, T.J.: Wear behaviour of a REFEL SiC containing fluorides up to 900 °C. Wear. **249**, 20–30 (2001)
14. Li, G., Huang, X., Guo, J.: Fabrication of Ni-coated Al_2O_3 powders by the heterogeneous precipitation method. Mater. Res. Bull. **36**, 1307–1315 (2001)
15. Chen, C.-C., Chen, S.-W.: Nickel and copper deposition on Al_2O_3 and SiC particulates by using the chemical vapour deposition-fluidized bed reactor technique. J. Mater. Sci. **32**, 4429–4435 (1997)
16. Chen, L., Yu, G., Chu, Y., Zhang, J., Hu, B., Zhang, X.: Effect of three types of surfactants on fabrication of Cu-coated graphite powders. Adv. Powder Technol. **24**, 281–287 (2013)
17. Amirjan, M., Zangeneh Madar, K., Parvin, N.: Evaluation of microstructure and contiguity of W/Cu composites prepared by coated tungsten powders. Int. J. Refract. Met. Hard Mater. **27**, 729–733 (2009)
18. Zhang, R., Gao, L., Guo, J.: Preparation and characterization of coated nanoscale Cu/SiCp composite particles. Ceram. Int. **30**, 401–404 (2004)
19. Li, J., Chen, W., Tao, W., Shao, F., Ding, B.: Nano-composite powder of tungsten coated copper produced by thermo-chemistry co-reduction. Rare Met. Mater. Eng. **41**, 2091–2094 (2012)
20. Choi, W.C., Byun, D., Lee, J.K., Cho, B.W.: Electrochemical characteristics of silver- and nickel-coated synthetic graphite prepared by a gas suspension spray coating method for the anode of lithium secondary batteries. Electrochim. Acta. **50**, 523–529 (2004)
21. Xu, X., Cui, Z.D., Zhu, S.L., Liang, Y.Q., Yang, X.J.: Preparation of nickel-coated graphite by electroless plating under mechanical or ultrasonic agitation. Surf. Coating Technol. **240**, 425–431 (2014)
22. Hu, B., Sun, R., Yu, G., Liu, L., Xie, Z., He, X., et al.: Effect of bath pH and stabilizer on electroless nickel plating of magnesium alloys. Surf. Coating Technol. **228**, 84–91 (2013)
23. Oh, S.-T., Sando, M., Niihara, K.: Mechanical and magnetic properties of Ni-Co dispersed Al_2O_3 nanocomposites. J. Mater. Sci. **36**, 1817–1821 (2001)
24. Mao, D.S., Liu, X.H., Li, J., Guo, S.Y., Zhang, X.B., Mao, Z.Y.: A fine cobalt-toughened Al_2O_3-TiC ceramic and its wear resistance. J. Mater. Sci. **33**, 5677–5682 (1998)
25. Zhu, L., Luo, L., Li, J., Wu, Y.: The influence of powder characteristics on mechanical properties of Al_2O_3-TiC-Co ceramic materials prepared by Co-coated Al_2O_3/TiC powders. Int. J. Refract. Met. Hard Mater. **34**, 61–65 (2012)
26. Wang, Q., Ge, Y., Cui, W., Chen, K., Ferreira, J.M.F., Xie, Z.: Carbothermal synthesis of micro-scale spherical AlN granules with CaF_2 additive. J. Alloy Compd. **663**, 823–828 (2016)

Polymeric Solid Lubricant Transfer Films: Relating Quality to Wear Performance

6

Jiaxin Ye, Diana Haidar, and David Burris

Contents

Abstract

Polymers and polymer composites are often described as solid lubricants because they provide relatively low friction coefficients and wear rates in unlubricated and other extreme tribological conditions. However, few, if any, are inherently lubricious or wear resistant. These materials achieve useful tribological properties by depositing a layer of debris onto the mating counterface; this sacrificial layer is called a transfer film and it shields the polymer from damage by the harder counterface. The friction and wear performance of these systems depend as much on the formation, evolution, and stability of the transfer film as they do on the structure and composition of the solid lubricant itself. Although it is understood that transfer films are essential for high tribological performance of polymers and polymer composites, the causal relationship between transfer film

J. Ye
Institute of Tribology, Hefei University of Technology, Hefei, China

D. Haidar · D. Burris (✉)
Department of Mechanical Engineering, University of Delaware, Newark, DE, USA
e-mail: dlburris@udel.edu

P. L. Menezes et al. (eds.), *Self-Lubricating Composites*,
https://doi.org/10.1007/978-3-662-56528-5_6

qualities and wear resistance remains uncertain due largely to the difficulty in quantitatively measuring their properties. There have been increased efforts, particularly in the last 10 years, to develop quantitative methods to assess the topographical, adhesive, mechanical, and chemical properties of polymer transfer films. This chapter reviews the latest efforts to measure transfer film qualities and quantitatively relate them to the tribological performance of solid lubricant polymers.

6.1 Background

Certain polymer blends and composites achieve low friction coefficients ($\mu < 0.2$) and low wear rates ($k < 10^{-6}$ mm^3/Nm) without intentional external lubrication of the contact area [1–3]; as such, these materials are known as solid lubricants. Unfortunately, no general rules exist to guide the design of such materials, and solid lubricant materials discovery almost always involves substantial trial and error. Fillers, depending on their properties, can affect the tribology of polymers by preferentially supporting load [4], arresting subsurface cracks [5], and modifying interfacial shear strength [6] to name a few mechanisms. However, none of these functions explains the orders of magnitude effects some small changes in filler composition [2, 7], loading [2, 8], or environment [9, 10] are known to have on the wear rate of the system. Normally, the polymer produces wear debris during sliding against a hard metallic counterface, most commonly steel. These debris particles are dragged through the contact and are eventually ejected from the wear track in most cases. In special cases, the debris can adhere to the counterface to initiate the formation of a layer called the transfer film. Regardless of the materials used, low wear sliding of polymeric materials always leaves a thin and continuous transfer film on the steel counterpart. Likewise, high wear sliding of polymers always leaves a thick and patchy transfer film. The studies of polymer solid lubricants in the literature provide strong evidence that the properties of transfer films and the measured wear rates are related [11–20].

Briscoe [13] first recognized the relationship between transfer film properties and polymer wear rate and concluded that the primary role of the filler is to help adhere the debris to the counterface. He suggested that active fillers degrade the relatively inert polymer chains thereby creating new opportunities for bonding with the counterface. Bahadur and Gong [21] asserted that the role of a filler is to enhance counterface adhesion by having the active filler itself create the bond between the polymer debris and counterface. Both theories support the need for a tribochemically adhered transfer film that reduces wear by protecting the polymer from the hard and high energy counterface. Bahadur and Tabor [22] conducted a clever experiment to test this idea. They used low wear polymers to form high quality transfer films and then measured the wear rates of traditionally high wear polymers against presumably protective predeposited transfer films. Interestingly, these high quality predeposited films had no effect on the wear rate of the high wear polymers. On further inspection, they found that the predeposited transfer film was removed almost immediately

during sliding against the new polymer pin. Based on this observation, they concluded that the high-quality transfer films must be a consequence of the small debris generated during low wear sliding and not the cause of low wear. This is supported by evidence from Ricklin [23], Tanaka and Kawakami [24], Blanchet and Kennedy [5], and Burris and Sawyer [2], all of whom concluded that effective fillers reduced the wear of polytetrafluoroethylene (PTFE) by disrupting subsurface damage and thereby reducing debris size.

PTFE-based polymer systems have been the subject of numerous studies of the relationship between tribochemistry, transfer film adhesion, and tribological performance. Gong et al. [25] and Blanchet et al. [26] used XPS (X-ray photoelectron spectroscopy) to study the effects of tribochemistry on transfer film adhesion and wear reduction of PTFE-based materials. Although they observed clear evidence of tribochemistry in the form of metal fluorides, these reaction products occurred in both low and high wear systems. Furthermore, because fluorine is monovalent, metal-fluorides represent the transfer of fluorine from the polymer to the counterface and not a bond between them. Both studies concluded that tribochemically induced transfer film adhesion was not the primary means of wear reduction in the PTFE system.

Although much of the recent literature suggests that tribochemistry is simply a consequence of bond-breaking during tribological contact, other studies have shown clear evidence that it can play a critical role in wear reduction. During studies of a particularly low wear alumina-PTFE system in environments of variable humidity, Krick et al. [9] found that the wear rate increased by orders of magnitude as the availability of gaseous water was systematically removed. This observation provides strong evidence that tribochemistry plays an important role in the wear reduction of PTFE and, potentially, polymers in general [9, 10, 27]. To date, however, the link between tribochemistry, transfer film adhesion, and wear reduction remains uncertain.

The way in which transfer films develop may have equally important implications for elucidating causation between transfer film qualities, adhesion, and wear rate. Based on XPS studies, Gong et al. [28] concluded that PTFE-based transfer films grow over time. They interpreted their result as evidence of a thickening process in which new layers deposit onto old layers; the role of the filler, they proposed, is to strengthen the bond at these internal interfaces within the transfer film. Blanchet et al. [26] found similar evidence of growth but concluded that transfer film growth was the result of new debris adhering to remaining areas of exposed counterface. Ye et al. [29] used in situ optical microscopy to study the development of a transfer film in real time. Their results showed that the transfer film developed as new debris adhered to remaining areas of exposed counterface. The results also showed that existing transfer films thickened with increased sliding. More importantly, they showed that the transfer film of a low wear PTFE-based system was very stable; many of the debris particles deposited early in the test could be identified at the end of the test. The results demonstrated that the transfer films of this very wear resistant polymer are themselves very wear resistant. Ye et al. [6] studied the wear rate of this transfer film directly and found it to be exceedingly resistant to removal with an

effective wear rate orders of magnitude lower than that of the parent polymer. Interestingly, the wear rate increased by many orders of magnitude when the surface energy of the wear probe increased beyond a threshold value, thus demonstrating that a low wear condition simply reflects the presence of a single weak interface to accommodate sliding.

There is little doubt based on the literature that transfer films play one or more critical roles in governing the wear response of polymeric solid lubricants. Nonetheless, the specific way in which fillers, polymers, stresses, and environments govern the development and properties of the transfer films remain unclear. This chapter reviews the most recent advancements in this field that have helped to shape our understanding of the cause-effect relationships between materials design, transfer film properties, and tribological performance of these polymer systems.

6.2 Properties of Transfer Films

6.2.1 Topography

Transfer films and their properties are central to most hypothesized mechanisms of polymer wear reduction. The reason is well-illustrated by Fig. 6.1. Two 5 wt% alumina-PTFE nanocomposites were prepared identically and tested under the same tribological conditions (50 mm/s, 6.4 MPa). The only known differences were the size, morphology, and phase of the alumina filler particles. The Δ-Γ phase alumina-PTFE composite produced a moderate wear rate of 10^{-5} mm^3/Nm, while the α phase alumina-PTFE composite produced a low wear rate of 10^{-7} mm^3/Nm. There are marked visual differences between the transfer films produced by these materials. The transfer film of the moderate wear rate composite is thicker and patchier, while the transfer film of the low wear rate composite is thinner and more complete. It is logical to conclude that the 100X difference in wear rates is somehow related to the

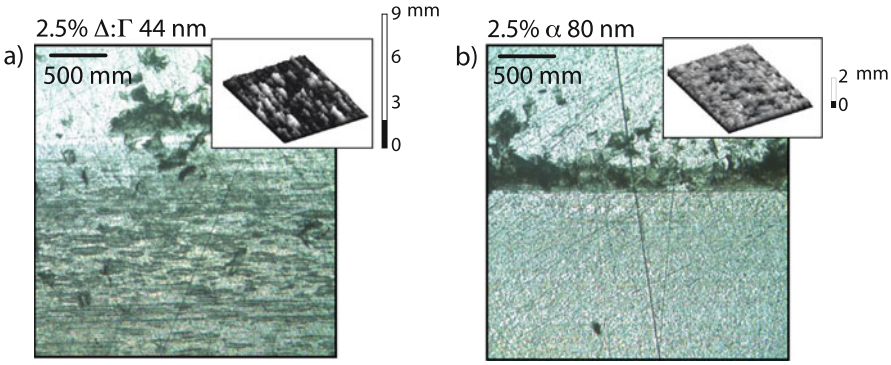

Fig. 6.1 Two types of transfer films of PTFE nanocomposites: (**a**) transfer film of a moderate wear system (K~ 10^{-5} mm^3/Nm, 44 nm Δ: Γ alumina) and (**b**) transfer film of an ultra-low-wear system (K~10^{-7} mm^3/Nm, 80 nm α alumina)

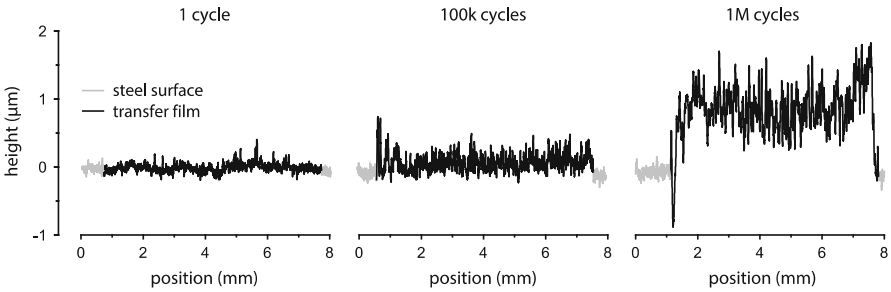

Fig. 6.2 Stylus profilometry measurements of transfer film thickness. (Image reprinted from [27] with permission)

obvious visual differences between the transfer films formed by these similar composite materials.

There are numerous examples in the literature for which improved wear resistance of a filled polymer is accompanied by comparable visual improvements in the appearance of the transfer film [5, 14–17, 21, 22, 30–33]. Wang et al. [7] found that nanoscale ZrO_2 significantly reduced the wear of polyetheretherketone (PEEK). Scanning electron microscopy revealed that the transfer film of unfilled PEEK was "thick, lumpy, and incoherent" while that of ZrO_2-PEEK nanocomposite was "thin, uniform, and coherent." They obtained similar results from a study of nanoscale SiC in PEEK [8] and described the transfer films as "thin, uniform, and tenacious" based on similar post-test visual observations of transfer films. The authors attributed the tribological benefits of nanofillers in PEEK to improvements in quality of the transfer films. Li et al. [9] found that the addition of nanoscale ZnO to polytetrafluoroethylene (PTFE) reduced its wear rate while improving the "uniformity and tenacity" of the transfer films. Sawyer et al. [10] described the transfer films of low wear nanoscale alumina reinforced PTFE as "well adhered, smooth, and continuous." Bhimaraj et al. [11] found that alumina filled polyethylene terephthalate (PET) nanocomposites produced more "coherent and uniform" transfer films with increasing nanoparticle loading. McCook et al. [12] noted that more "uniform" transfer films accompanied improved friction and wear performance of their epoxy nanocomposites.

Although there is clearly a ubiquitous relationship between wear rate and transfer film quality, it is difficult to assess the state of the art in general due to a lack of standard definitions for the terms used to describe these properties. "Thinness" can be quantified and is the obvious place to begin defining transfer film quality. A traditional 1-D thickness measurement is illustrated in Fig. 6.2. In these measurements, a sharp stylus is lightly loaded and dragged across the width of the transfer film, while a displacement transducer tracks the deflection of the tip. The height of the transfer film was determined here using the bare counterface as a baseline for subtraction. The average height of the transfer film was defined as the difference between the *average height* within the wear track and the average height outside the wear track [27]. Blanchet and Kennedy [5] were among the first to use this method to

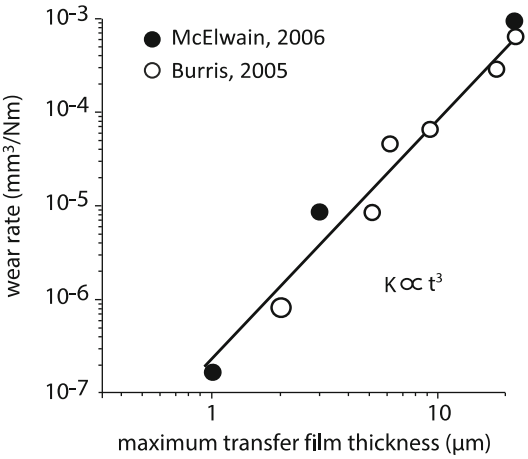

Fig. 6.3 Observed correlation between transfer film thickness and wear rates of various PTFE-based systems. (Image reprinted from [19, 34] with permission)

determine the thickness of unfilled PTFE transfer films, which they reported to be in the range from 4 to 20 μm. Pitenis et al. [27] used this method to show that the transfer films of alumina-PTFE nanocomposites thickened with increased sliding distance and approached ~1 μm at steady state (Fig. 6.2). When they removed environmental moisture, the transfer films thickened and wear rates increased [10].

Many transfer films are discontinuous or patchy. In these cases, the thickness from the method described above will depend on thickness and coverage (the output thickness will be half the transfer film thickness at 50% coverage). A different approach is necessary if the goal is to assess thickness directly. Burris and Sawyer [34] used optical profilometry to obtain the same type of surface profile information, but instead of quantifying the average thickness as described above, they quantified the maximum thickness, which depends only on heights of the transferred debris particles. McElwain [35] used mapping stylus profilometry to quantify maximum transfer film thickness for similar materials. Despite differences in the techniques used, their data suggest that the wear rate of this system is proportional to the cube of the maximum transfer film thickness (Fig. 6.3).

Laux and Schwartz [36] proposed a robust method to quantify average thickness that is independent of the coverage; their method is illustrated in Fig. 6.4. When the transfer film is statistically distinct from the roughness, two peaks will emerge in the probability density function of surface height; the lower elevation peak is associated with the counterface and the higher elevation peak is associated with the transfer film. Laux and Schwartz fit two Gaussian curves to the data set and used the distance between the fitted peaks to quantify the most probable thickness of the transfer film. Using this method, they found no strong correlation between wear and transfer films thickness for unfilled PEEK tested at varying conditions [36, 37]. The correlation between transfer film thickness and wear rate appears to be system specific.

Transfer film coverage is similarly intuitive as a potential driver of wear protection; many researchers have used adjectives like complete, uniform, and continuous to describe them [30, 31, 33, 38–40]. In theory, the film area fraction (X), which is

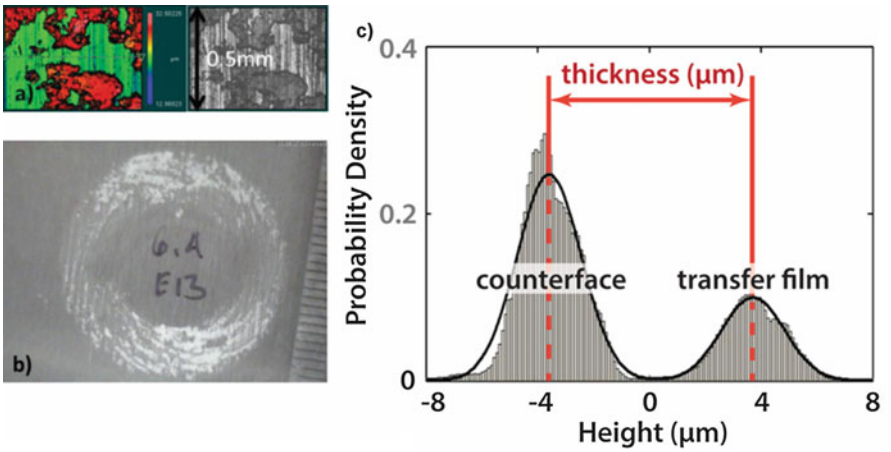

Fig. 6.4 Laux and Schwartz's method of measuring transfer film thickness using the counterface's surface height histogram: (**a**) scanning white light interferometry image of the wear track, (**b**) optical image of the wear track, and (**c**) probability density of the wear track height distribution. (Image reprinted from [36] with permission)

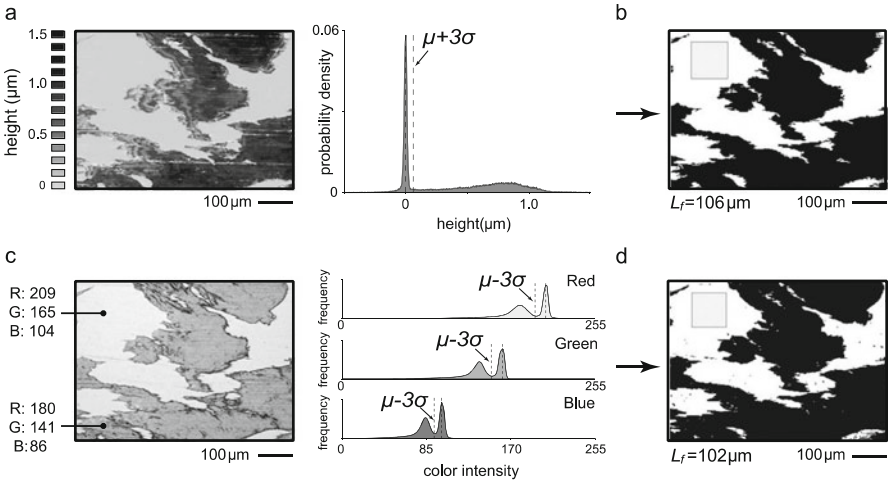

Fig. 6.5 Example of converting color images or height profiles to pixel representations of transfer film (black) and exposed counterface (white) to measure (**a**) area fraction and (**b**) free-space length. (Image reprinted from [41] with permission)

the ratio of film coverage area to total area, is easy to quantify using optical microscopy, electron microscopy, or profilometry images. In some cases, by simply applying a threshold pixel value, transfer film images can be converted into binary maps from which area fraction is readily calculated, as illustrated by Fig. 6.5. Images size is also critical to the differentiation between the film and the counterface as

shown by Ye et al. [41]. Bhimaraj et al. [42] studied the wear and transfer film coverage of polyethylene terephthalate (PET) nanocomposites with different filler loadings and although transfer film area fraction increased with increased filler loading, area fraction and wear were not well correlated. Laux and Schwartz [36] used the same method to quantify transfer film area fraction and studied the effect of sliding direction on the wear of PEEK. They found that the wear rate decreased by 60% with a 100% increase in the transfer film area fraction when the sliding direction changed from single direction to reciprocating. Similarly, Ye et al. [41] found that the transfer film area fraction of a PTFE nanocomposite increased with decreased wear rate throughout a single wear test.

Transfer film thickness and coverage likely play an important role in wear mitigation but neither factor alone appears to be a reliable predictor of wear rate. Laux and Schwartz [37] suggested that transfer film heterogeneity/discontinuity is likely to be more directly relatable to the wear rate. This effect of nonuniformity is consistent with observations from Blanchet et al. [26] that transfer films developed by gradually filling in remaining areas of exposed counterface.

Because covered areas are theoretically protected, future transfer and wear are more likely governed by the nature of the uncovered areas than by the nature of the covered areas; this is consistent with the transfer films in Fig. 6.1. The high quality transfer film is thinner and covers more area, but the visual impression of "uniformity" comes from the fact that the characteristic size of the "gaps"/transfer film-free space/areas of exposed counterface have been substantially reduced. Thus, we propose that heterogeneity should be defined by the characteristic size of the uncovered areas or the free-spaces and not by their total area or area fraction.

Ye et al. [41] proposed that the free-space length (L_f), or the size of the characteristic free-space, limits the size of the wear fragment and may therefore serve as a more reliable topographical predictor of wear rate. The method used to measure free-space length begins with a representative image of the surface, which is then converted into a black and white image; black represents transfer film and white free-space. Their custom Matlab script used Monte Carlo simulation to identify the smallest randomly placed square for which the most probable number of intersecting transfer film pixels is zero; this length is the free-space length. The method is illustrated in Fig. 6.5 using optical and stylus based measurements of the same region. In theory, decreased free-space lengths should produce smaller debris; smaller debris consume less volume while producing thinner and more stable transfer films. Ye et al. [41] studied the relationship between free-space length and wear rate using low wear alumina-PTFE during the transition from high wear during run-in to low wear at steady state. Optical observations showed that the free space decreased with sliding distance as new debris gradually filled in the gaps in the transfer film as described previously by Blanchet et al. [26]. Changes in the free-space length were accompanied by changes in the wear rate as shown in Fig. 6.6a. Wear rate is plotted versus free-space length in Fig. 6.6b; the results suggest that reduced free-space

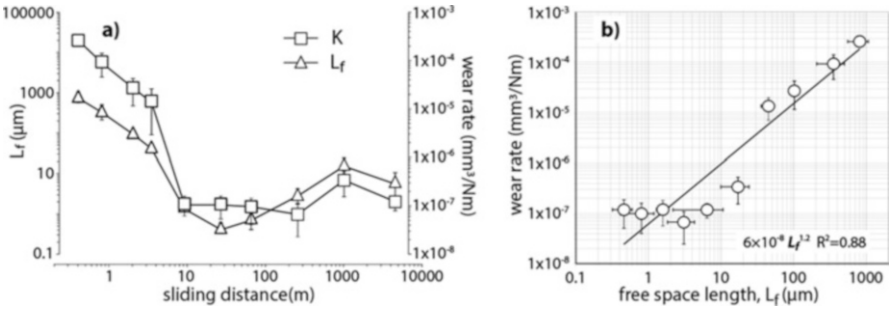

Fig. 6.6 (**a**) Transfer film free-space length and wear rate of an alpha-alumina PTFE nanocomposite during the course of a single wear test. (**b**) In-situ wear rate plotted against transfer film free-space length. (Image reprinted from [41] with permission)

length reduces wear down to a minimum value below which the wear rate remains constant at a value associated with the polymer on a perfect transfer film.

The relationship between free-space length and wear rate in Fig. 6.6a suggests that changes in free-space length ***caused*** changes in wear rate, particularly since increased wear rate at 1 km of sliding was preceded by an increase in free-space length. This fact combined with the ubiquitous observation that transfer films of all polymers become thinner and more continuous with reduced wear rates suggests that there may be some universal relationship between transfer film topography and polymer wear. Haidar et al. (manuscript under review by the journal *Wear*) tested the generality of the relationship between wear rate and transfer film topography using 10 different but representative polymers and polymer composites to determine the strength of correlation between wear rate and transfer film thickness, area fraction, and free-space length; the results are shown in Fig. 6.7. Although there is no reason to believe there should be a universal relationship between wear rate and transfer film properties, the data generally reflect the expected relationships; wear rate tended to decrease with increased coverage, decreased thickness, and decreased free-space length. The best fits to the data are shown as dashed lines. The variation between the data and the bet-fit model was used as an indicator of uncertainty when using the model fit to independently predict wear rate; the grey region represents the mean plus and minus one uncertainty. The uncertainty in the predicted wear rate is 8x based on the free-space length alone, 17x based on the area fraction alone, and 21x based on the thickness alone.

The existing studies show that transfer film topography has limited utility as an independent predictor of wear rate. Nonetheless, despite enormous variations in the material properties of the polymers, their wear properties, and the characteristics of their transfer films, there was a remarkably strong correlation between wear rate and free-space length. Future efforts by other investigators to quantify the topographical qualities of transfer films and relate them to wear rates of polymers will clarify

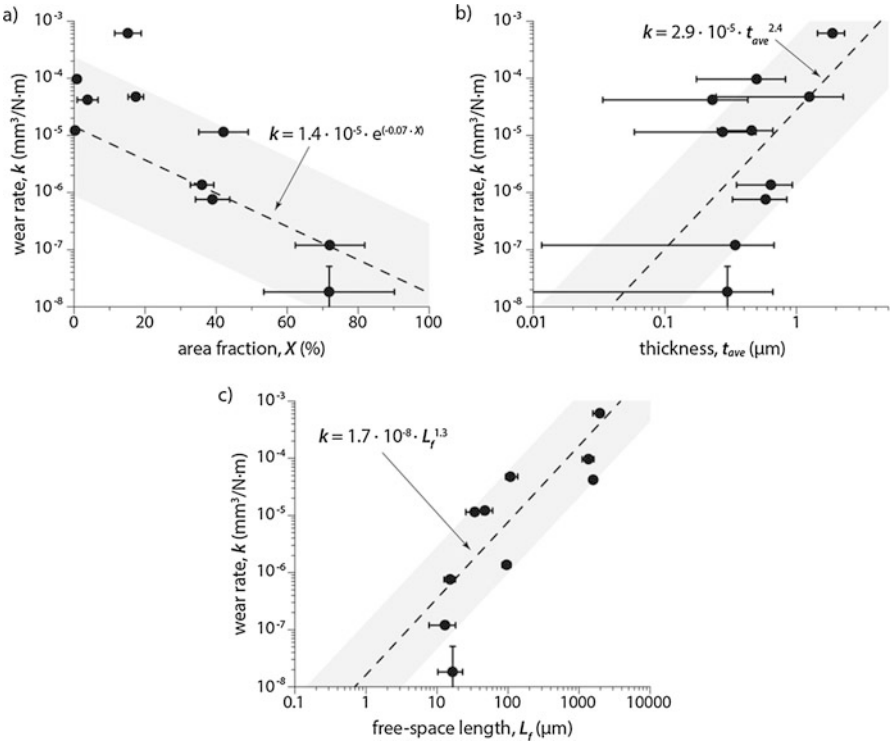

Fig. 6.7 A case study of correlation comparison between three transfer film quantifiers and the composite pin's wear rate. Materials studied by Haidar et al. (manuscript submitted to the journal *Wear*) include: PTFE, PEEK, PET, PPS, Epoxy, 5% wt. γ-Al_2O_3 + PTFE, 5% wt. α-Al_2O_3 + PTFE, 5% wt. γ-Al_2O_3 + PEEK, 5% wt. α-Al_2O_3 + PEEK and 32% wt. PEEK + PTFE

whether any general relationship exists between the topographical properties of transfer films and the wear of polymers.

6.2.2 Adhesion

Most hypotheses of polymer wear resistance are rooted in transfer film adhesion. Many have suggested the adhesion strength at the film-counterface interface determines the tenacity of the transfer film and the wear rate of the polymer. Bahadur and Tabor first showed evidence that transfer films are most likely adhered by mechanical engagement of the debris with the topographical features of the counterface [22]. While studying the effect of counterface finish on the transfer and wear of various PTFE composites, Burris and Sawyer [34] showed that while even extreme roughness and smoothness failed to affect transfer and wear of these materials at steady state, scratches oriented in the direction of sliding disrupted the formation of

the transfer film and increased wear rates by orders of magnitude. They concluded that debris was simply pushed from the contact because the surface lacked the features necessary to entrap the debris. Harris et al. [43] systematically studied the wear of the same material system against surfaces with a unidirectional finish. The lowest wear rates and best transfer films were observed when the surface roughness was aligned against the sliding direction. Wear resistance and transfer film quality degraded as the orientation approached the sliding direction. Laux and Schwartz studied the effect of roughness orientation on the transfer of polyetheretherketone (PEEK) using unidirectional surface finishes with a circular wear path. They found that the transfer films were thickest and patchiest when the sliding direction approached the roughness orientation [36]. TEM studies of the transfer films of a low wear epoxy nanocomposite [44] showed evidence that the transfer film initiated in the scratches. In sum, these results suggest strongly that polymer transfer films initiate by some form of mechanical engagement with topographical features of the counterface.

In cases of random surface finish, recent studies have shown that the low wear alumina-PTFE system can only achieve low wear and quality transfer films if there is sufficient water available to fuel a particular tribochemical pathway [9]. During sliding in humid environments, chain scission of the polymer backbone led to the formation of carboxylates, which directly linked degraded polymer chains to the counterface and filler particles. [27, 45]. Thus, both mechanical and chemical factors are necessary but neither sufficient for the formation of quality transfer films.

Transfer films only protect the polymer from contacting the counterface if they persist. Many have used the fact that transfer films are thin and continuous during low wear as evidence that they are also "tenacious," which implies persistence, longevity, and resistance to removal. However, Bahadur and Tabor showed that even high quality transfer films were quickly removed when the parent low wear polymer was replaced with a high wear polymer [22]. The preexisting transfer film had no wear reducing effect on the high wear polymer because the transfer film lacked tenacity. To date the relationship between wear rate, quality, persistence, and adhesive strength remains unresolved.

In 2013, Ye et al. [29] set out to determine the extent to which the transfer films of low wear alumina-PTFE persisted during sliding. Fig. 6.8 shows images of the transfer film after ~500 m of sliding. This point in the experiment is particularly interesting because it shows how the steady state transfer film initiates. At 485 m, the transfer film consists of a sparse collection of micron and even submicron debris fragments. After 20 m of additional sliding, it is clear that many of the fragments remain. As sliding continues, these debris fragments grow, merge, and homogenize into larger domains that can easily be identified after tens of thousands of additional sliding cycles. This study provides direct insight into the formation mechanisms of a specific transfer film and demonstrates, despite prior evidence to the contrary, that persistence is likely a necessary component of ultra-low-wear sliding of polymeric solid lubricants [40, 46, 47].

Persistence is almost certainly a function of the adhesive strength between the film or debris fragments and the counterface. Unfortunately, transfer film adhesion has proven difficult to quantify. The most common means to quantify coating adhesion is

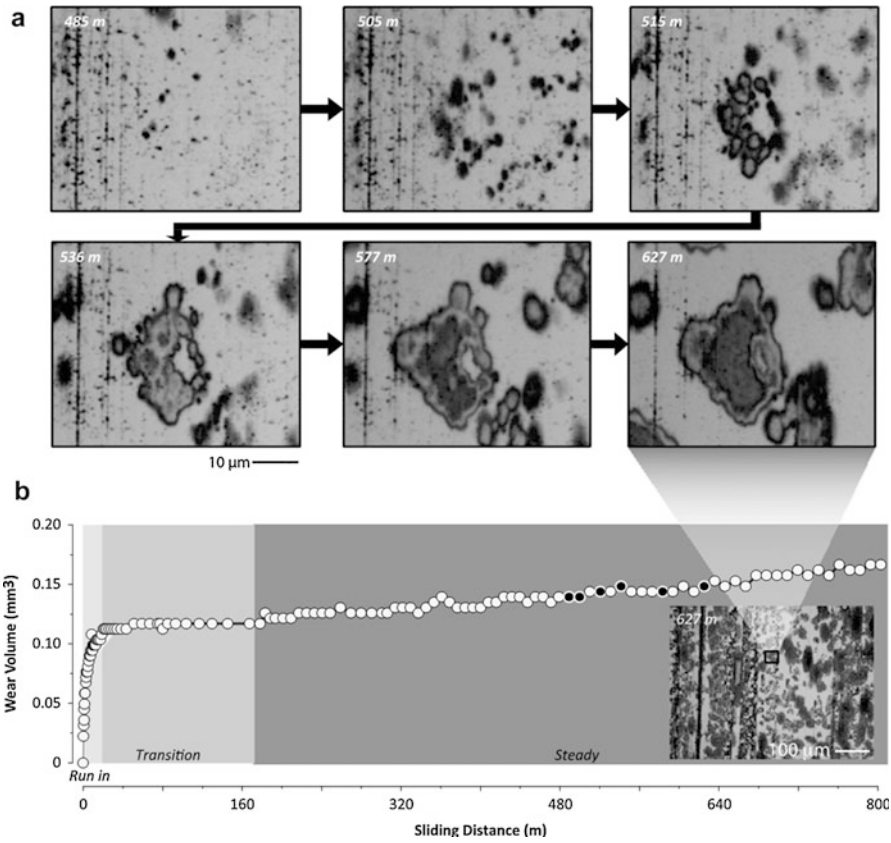

Fig. 6.8 Images of transfer film development in an ultra-low-wear alumina–PTFE nanocomposite: (**a**) images illustrating the evolution of the steady state transfer film as a function of distance slid; (**b**) wear volume as a function of distance slid. (Image reprinted from [29] with permission)

the scratch test. Typically, the normal force is ramped as an indenter slides across the coating surface; the load at which coating failure occurs provides an indirect measure of adhesion strength [48]. A more direct method is the peel test [49, 50]. Schwartz and Bahadur [33] bonded a copper tab to predeposited alumina-PPS nanocomposite transfer films and measured the peel strength as a function of alumina loading. They found that transfer film adhesion strength increased with increased filler loading (up to 2%) and counterface roughness. The results were consistent with debris size regulation and improved engagement of smaller debris fragments with the rough surface. In a subsequent paper, Bahadur and Sunkara [16] measured the wear rates and the transfer film adhesion strength of PPS nanocomposites of different filler types and loadings. Although the wear rates of the composites were both higher and lower than that of the unfilled polymer, their values correlated strongly with the adhesive strength of the transfer film (Fig. 6.9).

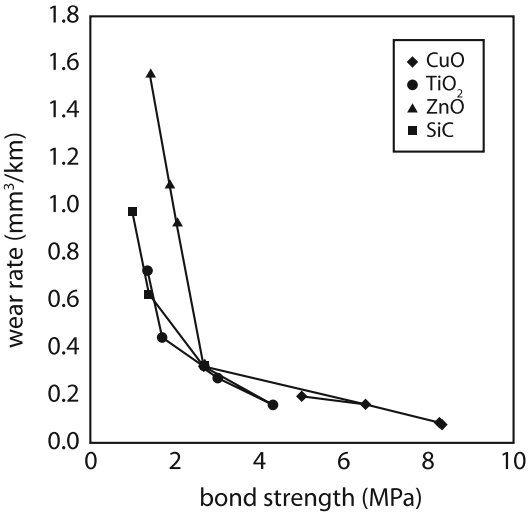

Fig. 6.9 Measured transfer film counterface bond strength versus composite's wear rates. (Image reprinted from [16] with permission)

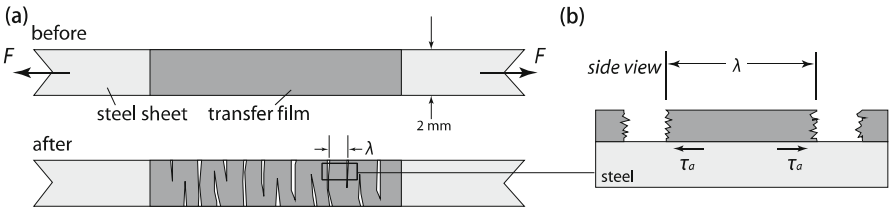

Fig. 6.10 Thin-film stretch method for measuring transfer film adhesion strength by (**a**) pulling a sample with a predeposited transfer film in tension along the sliding direction in the native wear tests until transverse cracks within the film initiated and (**b**) observing the transverse cracks, which have an average crack spacing of λ. This value was found to be inversely proportional to the adhesion shear strength at the film-substrate interface. (Image reprinted from [41] with permission)

The scratch and peel tests have important practical limitations. Neither test provides a useful measure of adhesion strength when the interfacial shear strength exceeds the shear strength of the film [48]. Furthermore, free-spaces from heterogeneity confound the measurements by providing direct bond sites between the adhesive and the counterface in peel tests and by nucleating failure in scratch tests. Lastly, the measurements are confounded by potential contributions from the addition of a second contact interface (adhesive-transfer film and indenter-transfer film). Agrawal and Raj [51, 52] solved these issues with the thin-film stretch test illustrated in Fig. 6.10. The film and counterface are loaded in tension until cracks form and stabilize or until the counterface fails. Mathematically, they showed that the ratio of the crack spacing to coating thickness is proportional to the *normalized* adhesive strength, which is defined as the ratio of adhesive shear strength to cohesive shear strength. This method requires no additional interface and provides spatial specificity for statistical evaluation. One potentially significant downside of the method is

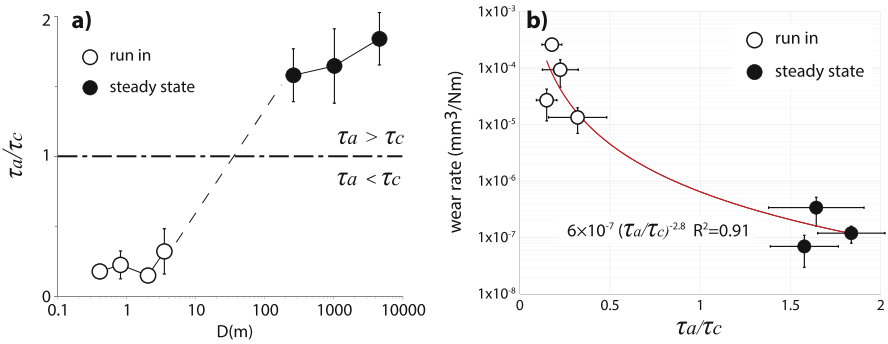

Fig. 6.11 (**a**) Normalized transfer film adhesion strength plotted against the sliding distance of an ultra-low wear PTFE nanocomposite. (**b**) Composite wear rate plotted against the normalized film adhesion strength. (Image reprinted from [6] with permission)

that it only measures the ratio of adhesive strength to cohesive strength; measurements of absolute adhesive strength require knowledge of the absolute cohesive strength of the transfer film. The other downside of the method is that the substrate must have a larger ultimate strain than the transfer film.

Although the normalized adhesive strength is often viewed as a limitation of the stretch method, it is likely a better predictor of transfer film persistence than adhesive strength alone. One could argue that delamination is favored if the cohesive strength significantly exceeds the adhesive strength. Delamination is an undesirable failure route because it leaves the surface completely unprotected. Cohesive failure would be expected when the adhesive strength exceeds the cohesive strength. Cohesive failure leaves the counterface protected and is therefore the preferred failure mode. For this reason, the normalized adhesive strength is likely a more valuable metric of coating adhesion than the adhesive strength.

Ye et al. [6] used the thin-film stretch method to study the evolution of the normalized adhesive strength of the low wear alumina-PTFE transfer film from run-in to steady state; the results are shown in Fig. 6.11a. In the beginning of the test, wear rates were high and the cohesive strength of the transfer film exceeded its adhesive strength, which suggests that delamination was the favored failure mode. In situ studies of the thick flaky transfer films of this material during run-in have shown that they were removed and replenished on each pass of the pin [29]; this fact implies that transfer films failed to protect the polymer during the run-in. This is supported by recent experiments, which showed that removing the transfer film by replacing the counterface with a fresh counterface had no detectable effect on the wear volume produced by the pin (Fig. 6.12) [53]. In this case, visual improvements in the transfer film during the run-in period were caused by reduced wear not the cause of reduced wear [22].

The transition to low wear was accompanied by the first observations of adherent debris (20 m of sliding in Fig. 6.8). Unfortunately, the fragments were too small

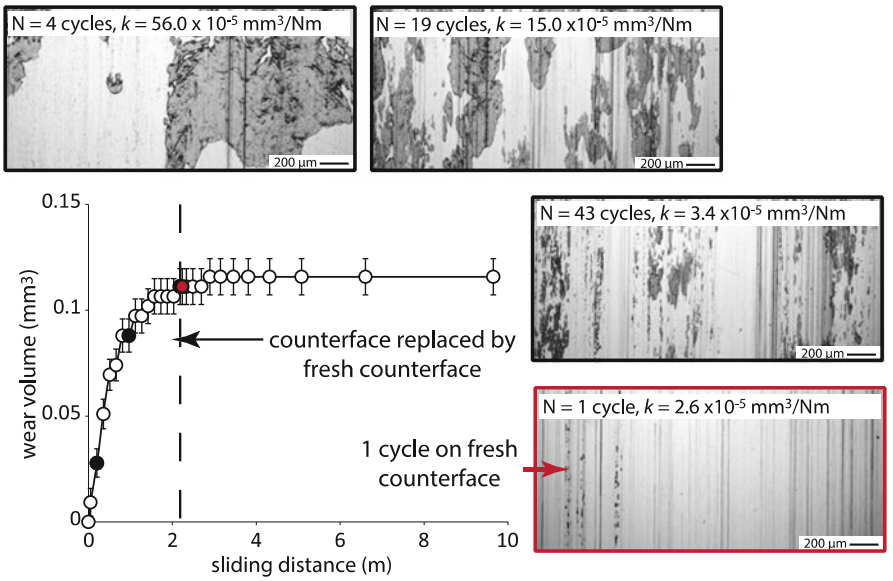

Fig. 6.12 Wear volume plotted against sliding distance for a test in which the developing transfer film was removed after cycle 43 and replaced with a fresh counterface. The results show that the transfer film and wear rate develop as they would in an uninterrupted test, which suggests that the transfer film develops in response to the developing surface properties of the pin. (Image reprinted from [53] with permission)

during this transition period to produce detectable cracking patterns [29]. However, as Fig. 6.8 demonstrates, these debris fragments merged and homogenized with increased sliding to create larger domains with detectable cracking patterns. The first possible measurement in the steady state sliding period revealed clear evidence that the bond between the transfer film and the counterface significantly exceeded the strength of the film itself, which suggests that cohesive failure was favored over delamination. This transition in normalized adhesive strength accompanies improved topographical quality of the transfer film (Fig. 6.6), the onset of transfer film persistence (Fig. 6.8), and dramatically reduce wear rate (Fig. 6.11), all of which is consistent with the expected transition from delamination to cohesive failure. The wear rate decreased as the normalized adhesive strength increased with sliding distance, which suggests that improved bonding of the transfer film contributes as a cause of wear reduction.

Another way to measure the transfer film persistence is through a direct transfer film wear rate measurement. From a simple control-volume analysis, this value represents the minimum possible wear rate of the solid lubricant system at steady state as noted by Blanchet and Kennedy [5]. Wang et al. [54–56] used bare steel spheres to quantify the wear resistance of predeposited transfer films. Standard gravimetric and volumetric wear measurements are difficult due to the fact that

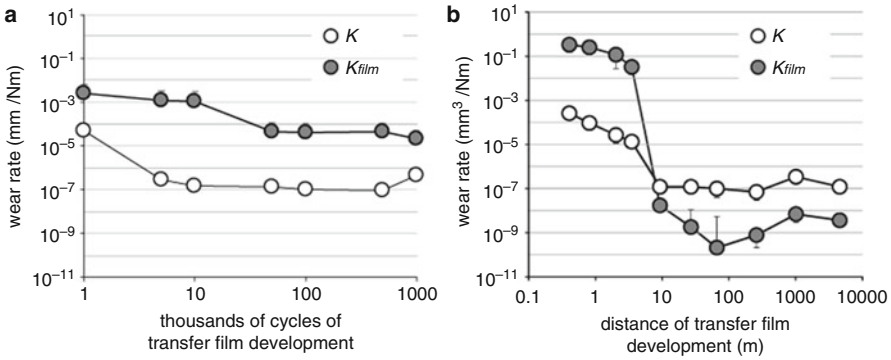

Fig. 6.13 Comparison of wear rates of an alumina-PTFE nanocomposite (K) and the corresponding transfer film (K_{film}) at predefined cycles of development in the native wear test: (**a**) Result from Urueña et al. [58] using a steel sphere to measure transfer film wear rates, (**b**) Result from Ye et al. [6] using a polyethylene sphere to measure transfer film wear rates. All error bars represent 95% confidence intervals. (Image reproduced from [6, 58] with permission)

transfer films are thin and discontinuous. Because increased friction is expected when metal first contacts metal, the friction coefficient provides a useful indicator of coating failure. Wang et al. [55, 56] used this friction coefficient transition method to show that PTFE composite transfer films persisted 10X longer distances than those of unfilled PTFE. Using similar methods, Li et al. [57] showed that the wear lives of their transfer films were sensitive to the load, speed, and the counterface roughness used in creating the transfer film. Urueña et al. [58] used the same friction-based steel ball-on-film configuration to study wear rates of the low-wear alumina–PTFE transfer films described previously as persistent and well adhered. They used mean film thickness measurements with reasonable geometric assumptions to estimate the worn volume and wear rate at failure. As expected, the wear rate of the transfer film decreased as the wear rate of the polymer decreased during the development of the transfer film (Fig. 6.13a). Surprisingly, however, the wear rates of the transfer films were orders of magnitude larger than the wear rate of the parent system. This result implies that the transfer film was worn immediately and played no role in wear reduction, which is unlikely based on the observations and reasoning discussed previously. The alternative is that the test itself had artificially increased the wear rate of the transfer film, which is more likely given the differences in the contacting materials and pressures.

Ye et al. [6] tested the wear rates of the same transfer films using a high-density polyethylene sphere to provide a better mechanical surrogate to the original polymer pin. The transfer film wear rate and the original solid lubricant pin wear rate are plotted against the accumulated sliding distance used to generate the transfer film in Fig. 6.13b. During running-in, the transfer film wear rate is much larger than the pin's wear rate; the transfer films were easily/immediately removed, which is

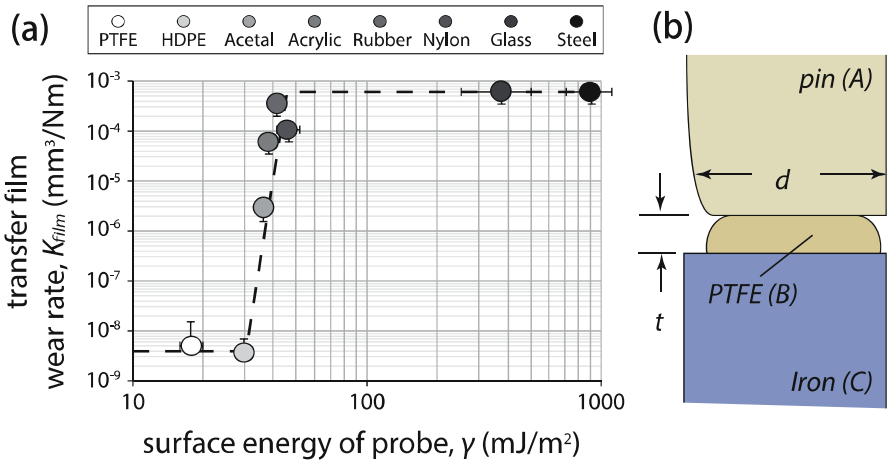

Fig. 6.14 (**a**) Surface energies of the probes versus ultra-low-wear Al_2O_3/PTFE transfer film wear rates in microtribometry experiments. Error bars represent the 95% confidence interval; and (**b**) three-body wear model involving a pin (A), transfer film (B), and counterface (C) (Reprinted with permission from [6])

consistent with the results of direct optical observations of the transfer film evolution [29]. After the transition (~7 m of accumulated sliding distance in this case), the transfer film wear rate decreased sharply and stayed well below the pin's wear rate; this is consistent with the persistence observed from direct optical observations [29] and the transition from weak to strong normalized adhesion strength (Fig. 6.11).

Despite significant potential for differences in the source materials, preparation procedures, and testing conditions between these independent studies, the steady state wear behaviors of the polymer nanocomposites were indistinguishable (Fig. 6.13a, b). Clearly, the wear behavior of this material is robust and insensitive to these differences. The strong agreement in polymer wear rates makes the orders of magnitude disagreements in transfer film wear rates that much more remarkable.

Ye et al. [6] repeated the measurements with spherical probes of varying material to clarify the cause of the enormous differences in the wear response of the same transfer film to different probes. Ultimately, the wear rate of the ultra-low wear transfer film did not vary systematically with contact pressure, friction coefficient, or shear stress during sliding. It did vary systematically as a function of probe surface energy as shown in Fig. 6.14a. Both PTFE and HDPE promoted ultra-low wear behavior of the transfer films. When tested against polymer probes of higher surface energy, the wear rate increased by orders of magnitude. They proposed that low surface energy probes reduced wear by 5 orders of magnitude by setting up a preferred slip system for which pure interfacial sliding becomes favorable over adhesive wear. For this system, interfacial sliding became favorable when the surface energy of the probe was less ~30 mJ/m^2, which is comparable to estimates of that of the film. These results reinforce the fact that the wear resistance of a material,

particularly a transfer film, can depend as strongly on the properties of the countersurface as it does on the properties of the wear surface.

6.2.3 Mechanical Properties

Mechanical properties are also believed to be important contributors to the stability of transfer films and the wear resistance of polymers. Gong et al. [28] first proposed that increased transfer film cohesive strength discourages transfer film failure at internal interfaces and thereby stabilizes the film. However, as illustrated previously, stronger transfer films may be more likely to delaminate without a corresponding increase in strength at the counterface. Mechanical properties can also provide useful information about filler accumulation and polymer degradation, both of which change mechanical properties like hardness, toughness, and modulus.

The primary challenge to measuring the mechanical properties of thin films is isolating the properties of the film from those of the much stiffer and harder substrate [59, 60]. Friedrich et al. [61] used micro-indentation and measured transfer film hardness of two fiber-reinforced PEEK composites with different fiber orientations (normal vs. parallel) relative to the sliding surface. They found that composites produced lower wear rates and harder transfer films when fibers were oriented normally to the sliding interface. Randall et al. [62, 63] studied the correlation between transfer film hardness and wear of several ceramic coatings. They found the most wear resistant coating had transfer films that were ~30% harder than either the sliding counterpart suggesting a possible metal alloying effect. Ye [64] measured transfer film hardness and modulus of the low-wear alumina-PTFE system using AFM-based nanoindentation and found that the transfer film hardens and stiffens during sliding. However, Chang et al. [65] showed that the indentation hardness of thin (200 nm) epoxy transfer films had been artificially increased by contributions from the substrate. When transfer films thin and harden, it becomes difficult to differentiate between hardening of the film material and the effect of the substrate [61–63].

The substrate effect may be avoided by indenting on the running film, which forms on the sliding surface of the bulk solid lubricant. McCook et al. [18] measured hardness and modulus for running films of low wear PTFE-epoxy composites and found that the hardness and modulus of the worn surface were uniformly reduced. The results suggested that the running film was PTFE rich, which likely contributed to the low measured values of friction coefficient and wear rate. Krick et al. [66] measured the mechanical properties of running films from a low wear alumina-PTFE nanocomposite as a function of sliding distance. The film hardened and stiffened with increased sliding distance and decreased wear rate (Fig. 6.15). They concluded that filler accumulation and PTFE degradation were both likely contributors. Their results indicate that the cohesive strength of the running film increased by >2X. If we assume the transfer film is identical to the mated running film, then the absolute adhesive strength of these transfer films increased by >10X from run-in to steady state based on the results from Fig. 6.11.

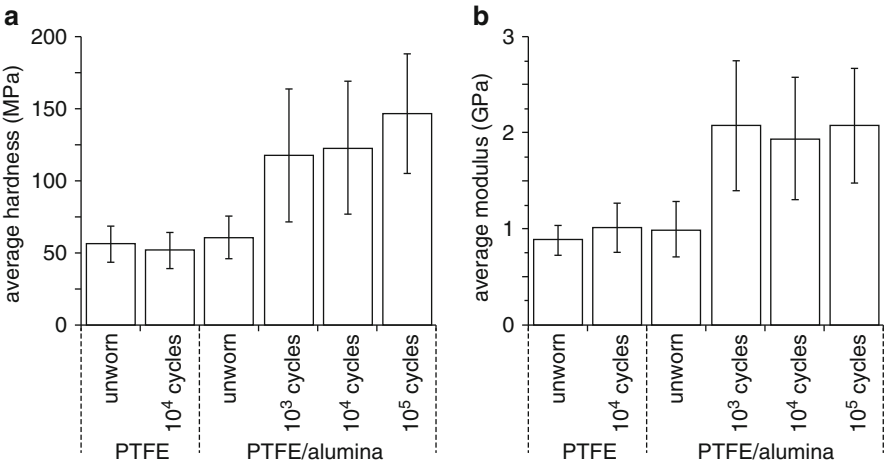

Fig. 6.15 Average (**a**) hardness and (**b**) reduced modulus of worn and unworn PTFE and PTFE–Al_2O_3 nanocomposites, for indentation contact depths in the range of 100–150 nm. Error bars represent ±1 standard deviation from the mean. (Image reprinted from [66] with permission)

6.2.4 Tribochemistry

Tribochemistry is an important factor governing the adhesion and mechanical properties of transfer films. Briscoe [13] first proposed that effective fillers reduce wear by promoting polymer degradation and thereby increasing the adhesive strength of the transfer film. Bahadur and Tabor [22] found that even high quality transfer films did not stick around long after the parent pin was replaced and concluded that transfer film adhesion must be primarily mechanical in nature. Studies on PTFE-based solid lubricants have shown that ultra-low wear sliding is consistently accompanied by small wear debris, thin transfer films, and brown discoloration of both sliding surfaces [7, 9, 10, 19, 27, 29, 45, 66, 67]. This discoloration indicates tribochemical degradation, which is particularly remarkable for PTFE given its unique resistance to chemical attack.

A recent study by Krick et al. [9] provided the most compelling evidence to date that a specific chemistry is required for ultra-low wear sliding of the low wear α phase alumina-PTFE nanocomposite system. As they removed water from the environment, the wear rate of the system increased by two orders of magnitude from 10^{-7} mm^3/Nm to 10^{-5} mm^3/Nm, the latter of which is more typical of PTFE composites. This increase in wear rate in dry environments was accompanied by the loss of the brown discoloration and a transition toward large flaky debris fragments. The inability of this low wear material to achieve low wear in dry environments has been reproduced independently by Pitenis et al. [10] and Khare et al. [53]. Since the environmental constituents have no obvious effects on the mechanical or structural properties of the composite, the most reasonable conclusion is that wear rates

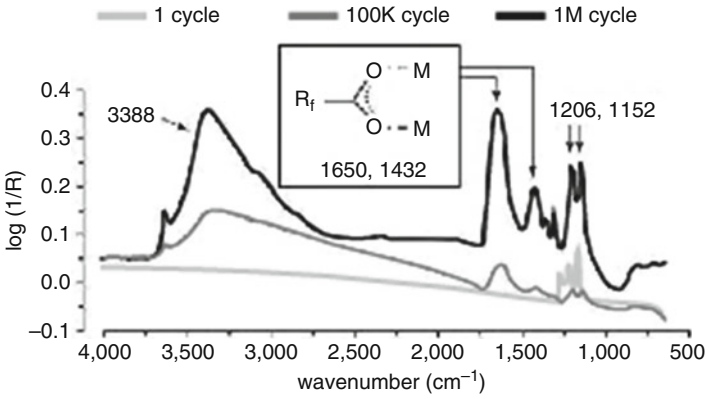

Fig. 6.16 Infrared reflectance results from the metal surface after one cycle of sliding (light grey line), 100 k (gray line) and 1 M (black line) cycles. (Reprinted with permission from [27, 45])

increased due to the loss of favorable tribochemistry at the sliding interface; thus, a specific tribochemistry appears necessary for ultra-low wear of this system.

XPS studies of the transfer films of this low wear alumina-PTFE system by Burris et al. [68] revealed an unexpected peak at 288 eV, which they attributed to a tribochemical degradation product. Computational modeling by Onodera et al. [69, 70] showed that end-chain carboxyl groups formed in humid environments and suggested that they help bond PTFE transfer films to metal counterfaces. Experimental infrared spectroscopic (IR) studies by Pitenis et al. [10] and Harris et al. [45] showed that the new tribochemical product was a metal chelate salt of perfluorinated carboxylic acid (Fig. 6.16). Harris et al. [45] proposed a realistic reaction route that involved mechanical rupture of PTFE chains and fibrils, reaction of chain ends with oxygen and then water to form carboxylic acid, and, finally, chelation of the acid at the chain end to metal atoms in the counterface and filler particles. The reaction products increase with sliding distance (Fig. 6.16), which helps explain why these transfer films become more persistent, better adhered, stronger, and more wear resistant with increased sliding distances.

6.3 Causes and Consequences: A Case Study with a Low Wear Composite

Despite the compelling evidence from Pitenis et al. [10] and Harris et al. [45] that tribochemistry is necessary to anchor transfer films, recent studies of the run-in period of this particular PTFE nanocomposite provides further insights into the timing of favorable tribochemistry and its role in low wear sliding of polymers. Ye et al. [29] showed that the transfer films were compositionally and mechanically

identical to the unworn composite and Pitenis et al. [10] found a comparable lack of carboxylates during run-in. Furthermore, Khare et al. [53] showed that, unlike at steady state, the run-in and transition behaviors of this material are completely independent of environment. Thus, the transition to low wear during run-in appears to occur without the benefit of favorable tribochemistry. Ye et al. [29] showed that the wear rate and the transfer film of these low wear alumina-PTFE composites were indistinguishable from those of unfilled PTFE initially, which suggests that the crack arresting role of the filler is negligible initially. With each pass, however, they observed reduced wear rate and thinner transfer films of characteristically smaller debris. Although the transfer films were immediately dislodged throughout run-in, Khare et al. [53] showed that the transfer film had no effect on the wear rate of the polymer during run-in; they did this by interrupting the test and replacing the transfer film with a fresh steel counterface. If anything, the wear rate of the pin was lower when the transfer film was removed from the contact, which demonstrates that the perceived improvements in transfer film quality during the run-in period are consequences of an increasingly wear resistant running surface and not the cause of progressively reduced wear rates. The result suggests that filler accumulation and mechanical conditioning of the running surface (e.g., filler accumulation, polymer orientation, polymer crazing) are responsible for the transition from large debris and high wear to small debris and low wear.

During the run-in phase, wear continues to decrease until effectively stopping at a critical point Ye et al. [29] defined as the transition. The system wear rate is well below 10^{-6} mm^3/Nm and Ye et al. [29] report the first compositional evidence of polymer degradation at this point. Interestingly, Khare et al. [53] observed indistinguishable run-in and transition features when they removed ambient moisture to preclude favorable tribochemistry. This is not entirely surprising given that the run-in is independent of tribochemistry [10, 29] and suggests that low wear of this system does not require favorable tribochemistry, at least initially. These results suggest that mechanical debris size regulation is the first step toward low wear in this particular system. These debris fragments can become so small that they automatically adhere to produce stable low energy surfaces. Mechanical stability must precede tribochemical stability because the products of improbable chemical events take time to accumulate [10]. As low wear sliding continues, adhered debris fragments grow by scavenging material from the pin (Fig. 6.8). As debris fragments grow, adhesion energy becomes less competitive with elastic energy until they destabilized at a critical thickness Ye et al. [6] estimates to be on the order of ~1 μm for PTFE. However, if the humidity is sufficient, tribochemical reactions begin to link the polymer chemically to the counterface, thus increasing the critical thickness for instability as the film grows. This, we propose, explains why run-in is independent of environment, why low wear was achievable but unstable in dry nitrogen [53], and why the system can sustain low wear indefinitely in humid environments [9]. The cross-linking effect of tribochemistry is consistent with the substantial increases in adhesion strength [6, 29, 58], hardness [64, 66], and modulus [64, 66] for this system from run-in to steady state.

6.4 Summary

This chapter reviews the latest methods to quantify the topographical, adhesive, mechanical, and chemical properties of polymeric transfer films. Topographical features of interest, including thickness, area fraction, and free-space length, have been quantified primarily with profilometry and microscopy. Both thickness and area fraction tend to correlate strongly with wear rate for specific systems but less so across systems. Based on limited studies, the free-space length appears to be the best of the three for predicting wear rates in general. It is interesting to note that the free-space length is most closely related to the visual cues that have motivated use of the terms "uniform," "coherent," and "continuous" [31, 38, 71–74]. Nonetheless, despite consistent evidence that transfer film properties correlate strongly with wear rate, no universal function is likely to emerge.

Although peel and scratch tests are typical for qualifying coating adhesion, such measurements are confounded by the discontinuous nature of transfer films. The tensile cracking test eliminates the need for a second interface and is not affected by discontinuity in the transfer film. Additionally, it provides a direct measure of adhesion strength per unit cohesion strength; since adhesive failure is far more detrimental to tribopolymer wear than cohesive failure, this property is perhaps the most direct measure of transfer film adhesion performance. Lastly, although a wear test appears to be the most direct measure of tenacity, we have shown that the measured wear rates of transfer films can vary by many orders of magnitude depending on the surface properties of the probe material used; caution is necessary when interpreting the results of transfer film wear tests in an absolute sense for this reason.

Hardness and modulus are the most common mechanical metrics of transfer film performance and both are typically quantified with micro and nano-indentation. Because transfer films are thin and soft, the results are confounded by effects from the counterface, which effectively converts an inherently quantitative measurement into a qualitative assessment. Some have quantified the mechanical properties of the running film on the soft polymer surface as a way to address this issue of transfer film characterization. However, caution must be exercised when using running films as surrogates for transfer films because there is some evidence that the films are compositionally distinct despite developing at the same tribological interface.

Finally, we have used a particularly well-studied alumina-PTFE system as a case study for wear reduction. Based on the methods described throughout, its transfer films are thin, well-covered, persistent, well-adhered, chemically distinct, and mechanically stronger than the unworn composite. These changes are strongly associated with a favorable tribochemical reaction; polymer chains break mechanically during sliding, react with gaseous oxygen and water from the environment to form carboxylic acid, then chelate to metal surfaces to strengthen the film and bond it to the counterface. The end result is a stable and protective film that minimizes the wear rate of the system.

The mechanisms of wear mitigation in this system, particularly the tribochemical aspects, are likely unique given that the four order of magnitude wear reducing effect of fillers appears to be limited to fluoropolymers [2, 67]. Nonetheless, it is interesting that transfer film uniformity, thickness, coverage, bond strengthening, chemical

degradation, and mechanical strengthening are recurring themes in the tribopolymer literature. Although the exact mechanisms are likely system-specific, the quantitative methods described here may be used broadly to expose common trends and elucidate general causation relationships. Ultimately, knowledge of these causation relationships will be critical to materials discovery by design rather than the more traditional trial and error-based approaches.

Acknowledgments The authors are very grateful for the financial support from the Air Force Office of Scientific Research (FA9550-10-1–0295), the National Science Foundation Graduate Research Fellowship (1247394), the National Natural Science Foundation of China (51505117), and the Anhui Provincial Natural Science Foundation (1608085QE98).

References

1. Burris, D.L., Sawyer, W.G.: A low friction and ultra low wear rate PEEK/PTFE composite. Wear. **261**(3–4), 410–418 (2006)
2. Burris, D.L., Sawyer, W.G.: Improved wear resistance in alumina-PTFE nanocomposites with irregular shaped nanoparticles. Wear. **260**(7–8), 915–918 (2006)
3. McCook, N.L., et al.: Epoxy, ZnO, and PTFE nanocomposite: friction and wear optimization. Tribol. Lett. **22**(3), 25–257 (2006)
4. Lancaster, J.K.: Polymer-based bearing materials: the role of fillers and fibre reinforcement. Tribology. **5**(6), 249–255 (1972)
5. Blanchet, T.A., Kennedy, F.E.: Sliding wear mechanism of polytetrafluoroethylene (PTFE) and PTFE composites. Wear. **153**(1), 229–243 (1992)
6. Ye, J., Moore, A.C., Burris, D.L.: Transfer film tenacity: a case study using ultra-low-wear alumina–PTFE. Tribol. Lett. **59**(3), 1–11 (2015)
7. Burris, D.L.: Wear-Resistance Mechanisms in Polytetrafluoroethylene (PTFE) Based Tribological Nanocomposites. University of Florida, Gainesville (2006)
8. Burris, D.L., et al.: A route to wear resistant PTFE via trace loadings of functionalized nanofillers. Wear. **267**(1–4), 653–660 (2009)
9. Krick, B.A., et al.: Environmental dependence of ultra-low wear behavior of polytetrafluoroethylene (PTFE) and alumina composites suggests tribochemical mechanisms. Tribol. Int. **51**(0), 42–46 (2012)
10. Pitenis, A.A., et al.: In Vacuo Tribological behavior of polytetrafluoroethylene (PTFE) and alumina nanocomposites: the importance of water for ultralow wear. Tribol. Lett. **53**, 1–9 (2014)
11. Lancaster, J.K.: Lubrication by transferred films of solid lubricants. A S L E Trans. **8**(2), 146–155 (1965)
12. Briscoe, B.J., Pogosian, A.K., Tabor, D.: The friction and wear of high density polythene: the action of lead oxide and copper oxide fillers. Wear. **27**(1), 19–34 (1974)
13. Briscoe, B.: Wear of polymers: an essay on fundamental aspects. Tribol. Int. **14**(4), 231–243 (1981)
14. Bahadur, S., Gong, D., Anderegg, J.W.: The role of copper compounds as fillers in transfer film formation and wear of nylon. Wear. **154**(2), 207–223 (1992)
15. Briscoe, B.J., Sinha, S.K.: Wear of polymers. Proc. Inst. Mech. Eng. J J. Eng. Tribol. **216**(6), 401–413 (2002)
16. Bahadur, S., Sunkara, C.: Effect of transfer film structure, composition and bonding on the tribological behavior of polyphenylene sulfide filled with nano particles of TiO2, ZnO, CuO and SiC. Wear. **258**(9), 1411–1421 (2005)
17. Friedrich, K., Zhang, Z., Schlarb, A.K.: Effects of various fillers on the sliding wear of polymer composites. Compos. Sci. Technol. **65**(15–16), 2329–2343 (2005)

18. McCook, N.L., et al.: Wear resistant solid lubricant coating made from PTFE and epoxy. Tribol. Lett. **18**(1), 119–124 (2005)
19. Burris, D.L., et al.: Polymeric nanocomposites for Tribological applications. Macromol. Mater. Eng. **292**(4), 387–402 (2007)
20. Ye, J., Burris, D.L., Xie, T.: A review of transfer films and their role in ultra-low-wear sliding of polymers. Lubricants. **4**(1), 4 (2016)
21. Bahadur, S., Gong, D.: The action of fillers in the modification of the tribological behavior of polymers. Wear. **158**(1–2), 41–59 (1992)
22. Bahadur, S., Tabor, D.: The wear of filled polytetrafluoroethylene. Wear. **98**(0), 1–13 (1984)
23. Ricklin, S.: Review of Design Parameters for Filled PTFE Bearing Materials. Lubrication Engineering. **33**(9), 487–490 (1977)
24. Tanaka, K., Kawakami, S.: Effect of various fillers on the friction and wear of polytetrafluoroethylene-based composites. Wear. **79**(2), 221–234 (1982)
25. Gong, D., Qunji, X., Hongli, W.: ESCA study on tribochemical characteristics of filled PTFE. Wear. **148**(1), 161–169 (1991)
26. Blanchet, T.A., Kennedy, F.E., Jayne, D.T.: XPS analysis of the effect of fillers on PTFE transfer film development in sliding contacts. Tribol. Trans. **36**(4), 535–544 (1993)
27. Pitenis, A.A., et al.: Ultralow wear PTFE and alumina composites: it is all about Tribochemistry. Tribol. Lett. **57**(2), 1 (2015)
28. Gong, D., Qunji, X., Hongli, W.: Physical models of adhesive wear of polytetrafluoroethylene and its composites. Wear. **147**(1), 9–24 (1991)
29. Ye, J., Khare, H.S., Burris, D.L.: Transfer film evolution and its role in promoting ultra-low wear of a Ptfe nanocomposite. Wear. **297**(1–2), 1095–1102 (2013)
30. Chen, W.X., et al.: Tribological behavior of carbon-nanotube-filled PTFE composites. Tribol. Lett. **15**(3), 275–278 (2003)
31. Sawyer, W.G., et al.: A study on the friction and wear behavior of PTFE filled with alumina nanoparticles. Wear. **254**(5–6), 573–580 (2003)
32. Bahadur, S.: The development of transfer layers and their role in polymer tribology. Wear. **245** (1–2), 92–99 (2000)
33. Schwartz, C.J., Bahadur, S.: Studies on the tribological behavior and transfer film–counterface bond strength for polyphenylene sulfide filled with nanoscale alumina particles. Wear. **237**(2), 261–273 (2000)
34. Burris, D.L., Sawyer, W.G.: Tribological sensitivity of PTFE/alumina nanocomposites to a range of traditional surface finishes. Tribol. Trans. **48**(2), 147–153 (2005)
35. McElwain, S.: Wear Resistant PTFE Composites Via Nano-scale Filler Particles. Rensselaer Polytechnic Institute, Troy/New York (2006)
36. Laux, K.A., Schwartz, C.J.: Influence of linear reciprocating and multi-directional sliding on PEEK wear performance and transfer film formation. Wear. **301**(1), 727–734 (2013)
37. Laux, K.A., Schwartz, C.J.: Effects of contact pressure, molecular weight, and supplier on the wear behavior and transfer film of polyetheretherketone (PEEK). Wear. **297**(1), 919–925 (2013)
38. Li, F., et al.: The friction and wear characteristics of nanometer ZnO filled polytetrafluoroethylene. Wear. **249**(10–11), 877–882 (2001)
39. Blanchet, T.A., Kandanur, S.S., Schadler, L.S.: Coupled effect of filler content and Countersurface roughness on PTFE nanocomposite wear resistance. Tribol. Lett. **40**(1), 11–21 (2009)
40. Zhang, G., et al.: Role of monodispersed nanoparticles on the tribological behavior of conventional epoxy composites filled with carbon fibers and graphite lubricants. Wear. **292**, 176–187 (2012)
41. Ye, J., Khare, H.S., Burris, D.L.: Quantitative characterization of solid lubricant transfer film quality. Wear. **316**(1–2), 133–143 (2014)
42. Bhimaraj, P., et al.: Tribological investigation of the effects of particle size, loading and crystallinity on poly (ethylene) terephthalate nanocomposites. Wear. **264**(7), 632–637 (2008)
43. Harris, K.L., et al.: Wear debris mobility, aligned surface roughness, and the low wear behavior of filled polytetrafluoroethylene. Tribol. Lett. **60**(1), 1–8 (2015)

44. Zhang, G., et al.: Formation and function mechanisms of nanostructured tribofilms of epoxy-based hybrid nanocomposites. Wear. **342–343**, 181–188 (2015)
45. Harris, K.L., et al.: PTFE tribology and the role of Mechanochemistry in the development of protective surface films. Macromolecules. **48**(11), 3739–3745 (2015)
46. Kandanur, S.S., et al.: Suppression of wear in graphene polymer composites. Carbon. **50**(9), 3178–3183 (2012)
47. Kandanur, S.S., et al.: Effect of activated carbon and various other nanoparticle fillers on PTFE wear. Tribol. Trans. **57**(5), 821–830 (2014)
48. Bull, S.J., Berasetegui, E.G.: An overview of the potential of quantitative coating adhesion measurement by scratch testing. Tribol. Int. **39**(2), 99–114 (2006)
49. Committee, D.: Test Method for Peel or Stripping Strength of Adhesive Bonds. ASTM International, West Conshohocken, PA (2010)
50. Committee, D.: Test Method for Strength Properties of Adhesives in Cleavage Peel by Tension Loading (Engineering Plastics-to-Engineering Plastics). ASTM International, West Conshohocken, PA (2012)
51. Agrawal, D.C., Raj, R.: Measurement of the ultimate shear strength of a metal-ceramic interface. Acta Metall. **37**(4), 1265–1270 (1989)
52. Agrawal, D.C., Raj, R.: Ultimate shear strengths of copper-silica and nickel-silica interfaces. Mater. Sci. Eng. A. **126**(1–2), 125–131 (1990)
53. Khare, H.S., et al.: Interrelated effects of temperature and environment on wear and Tribochemistry of an ultralow wear PTFE composite. J. Phys. Chem. C. **119**(29), 16518–16527 (2015)
54. Wang, Y., Yan, F.: Tribological properties of transfer films of PTFE-based composites. Wear. **261**(11–12), 1359–1366 (2006)
55. Wang, Y., Yan, F.: A study on tribological behaviour of transfer films of PTFE/bronze composites. Wear. **262**(7–8), 876–882 (2007)
56. Wang, Y., Wang, H., Yan, F.: Investigation of transfer film of PTFE/bronze composites on 2024Al surface. Surf. Interface Anal. **41**(9), 753–758 (2009)
57. Li, H., et al.: A study of the tribological behavior of transfer films of PTFE composites formed under different loads, speeds and morphologies of the counterface. Wear. **328–329**, 17–27 (2015)
58. Urueña, J.M., et al.: Evolution and wear of fluoropolymer transfer films. Tribol. Lett. **57**(2), 1–8 (2015)
59. Pharr, G.M., Oliver, W.C.: Measurement of thin film mechanical properties using nano-indentation. MRS Bull. **17**(07), 28–33 (1992)
60. Oliver, W.C., Pharr, G.M.: Measurement of hardness and elastic modulus by instrumented indentation: advances in understanding and refinements to methodology. J. Mater. Res. **19**(01), 3–20 (2004)
61. Friedrich, K., et al.: Experimental and numerical evaluation of the mechanical properties of compacted wear debris layers formed between composite and steel surfaces in sliding contact. Wear. **251**(1–12), 1202–1212 (2001)
62. Randall, N.X., Bozet, J.L.: Nanoindentation and scanning force microscopy as a novel method for the characterization of tribological transfer films. Wear. **212**(1), 18–24 (1997)
63. Randall, N.X., Harris, A.: Nanoindentation as a tool for characterising the mechanical properties of tribological transfer films. Wear. **245**(1–2), 196–203 (2000)
64. Ye, J.: Characterizing PTFE Transfer Film Properties to Elucidate Transfer Film's Role in Ultra-low Wear Sliding of Polymer Nanocomposites, p. 173. University of Delaware, Newark (2014)
65. Chang, L., et al.: Tribological properties of epoxy nanocomposites: III. Characteristics of transfer films. Wear. **262**(5–6), 699–706 (2007)
66. Krick, B.A., Ewin, J.J., McCumiskey, E.J.: Tribofilm formation and run-in behavior in ultra-low-wearing polytetrafluoroethylene (PTFE) and alumina nanocomposites. Tribol. Trans. **57**(6), 1058–1065 (2014)
67. Sidebottom, M.A., et al.: Ultralow wear Perfluoroalkoxy (PFA) and alumina composites. Wear. **362–363**, 179–185 (2016)

68. Burris, D.L., et al.: Polytetrafluoroethylene matrix nanocomposites for tribological applications. In: Tribology of Polymeric Nanocomposites. Elsevier, Amsterdam (2008)
69. Onodera, T., et al.: Chemical reaction mechanism of polytetrafluoroethylene on aluminum surface under friction condition. J. Phys. Chem. C. **118**(10), 5390–5396 (2014)
70. Onodera, T., et al.: Effect of Tribochemical reaction on transfer-film formation by poly (tetrafluoroethylene). J. Phys. Chem. C. **118**(22), 11820–11826 (2014)
71. Wang, Q., et al.: The effect of particle size of nanometer ZrO2 on the tribological behaviour of PEEK. Wear. **198**(1–2), 216–219 (1996)
72. Wang, Q., Xue, Q., Shen, W.: The friction and wear properties of nanometre SiO 2 filled polyetheretherketone. Tribol. Int. **30**(3), 193–197 (1997)
73. Wang, Q.-H., et al.: The effect of nanometer SiC filler on the tribological behavior of PEEK. Wear. **209**(1–2), 316–321 (1997)
74. Wang, Q.-H., et al.: The friction and wear characteristics of nanometer SiC and polytetrafluoroethylene filled polyetheretherketone. Wear. **243**(1), 140–146 (2000)

7 In Situ Generated Turbostratic 2D Graphite: A New Way to Obtain High-Performance Self-Lubricating Iron-Based Composites

Jose Daniel Biasoli de Mello, Cristiano Binder, Sonia Maria Hickel Probst, and Aloisio Nelmo Klein

Contents

Abstract

The production of self-lubricating composites containing second phase particles is one of the most promising choices for controlling friction and wear in energy efficient modern systems. Initially, we present a new microstructural model/processing route able to produce a homogeneous dispersion of in situ generated, discrete, solid lubricant particles in the volume of sintered composites. The high mechanical and tribological performances of the composites are a result of the combination of matrix mechanical properties and structural parameters, such as the degree of continuity of the metallic matrix, the nature, the amount, and the lubricant particle size and shape which determine the mean free path between solid lubricant particles and the active area covered by each lubricant particles.

J. D. B. de Mello (✉) · C. Binder · S. M. H. Probst · A. N. Klein
Laboratório de Materiais, Departamento de Engenharia Mecânica, Universidade Federal de Santa Catarina, Florianópolis, SC, Brazil
e-mail: ltm-demello@ufu.br

P. L. Menezes et al. (eds.), *Self-Lubricating Composites*,
https://doi.org/10.1007/978-3-662-56528-5_7

This new route was achieved by in situ formation of graphite nodules due to the dissociation of a precursor (SiC particles) mixed with metallic matrix powders during the feedstock preparation. Thermal debinding and sintering were performed in a single thermal cycle using a plasma-assisted debinding and sintering (PADS) process. Nodules of graphite (size $\leq$20 μm) presenting a nanostructured stacking of graphite foils with thickness of a few nanometers were obtained. Micro-Raman spectroscopy indicated that the graphite nodules are composed of a so-called turbostratic 2D graphite which has highly misaligned graphene planes separated by large interlamellae distance. The large interplanar distance and misalignment among the graphene foils has been confirmed by transmission electron microscopy and is, probably, the origin of the remarkably low dry friction coefficient (0.06). The effects of precursor content (0 to 5 wt% SiC) and of sintering temperature (1100 °C, 1150 °C and 1200 °C) on tribolayer durability and average friction coefficient in the lubricious regime ($\mu < 0.2$) are presented and discussed. In addition, the effect of the metallic matrix composition (Fe-C; Fe-C-Ni; Fe-C-Ni-Mo) is presented. Friction coefficient decreased and durability drastically increased with the amount of graphite formed during sintering, whereas friction coefficient was little affected by sintering temperature. However, the durability of the tribolayer was greatly increased when lower sintering temperatures were used. The addition of alloying elements considerably reduced wear rate and friction of specimens and counter-bodies. Friction coefficient values as low as 0.04 were obtained for the Fe-C-Ni-Mo composites. We also analyzed the effect of precursor content and of sintering temperature on the tribological behavior under constant normal load sliding tests. Again, the presence of graphite nodules significantly reduced the friction coefficients and wear rates, whereas the sintering temperature hardly affected these parameters. The results were compared with those caused by other forms of graphite (nodules in nodular cast iron and powder graphite) and were discussed in terms of the crystalline structure of the analyzed graphite using micro-Raman spectroscopy. Chemical analyses of the wear scars using scanning electron microscopy (SEM – EDX) and Auger electron spectroscopy (AES) showed a tribolayer that was composed predominantly of carbon and oxygen. This tribolayer is removed and restored during sliding and is continuously replenished with graphite. Finally, the strong effect of surface finishing is presented and discussed.

7.1 Introduction

The crucial need for more energy efficient mechanical systems exacted the change in the severity of the tribological contacts, increasing operational failure for traditional designs. In this context, the tribology of critical contacts and possible new contact materials are under intense research investigation [1–3]. Furthermore, the interfaces in contact in these modern systems must be able to withstand severe operating conditions caused by the tendency of using smaller clearances and increased speeds

to achieve higher efficiency [4]. In addition, the state of lubrication in many components is unknown and usually operates in the boundary and mixed lubrication regimes [5].

In particular, solid lubrication and solid lubricants are one of the most promising choices for controlling friction and wear in energy efficient modern systems. A combination of solid and liquid lubrication is also feasible and may have a beneficial synergistic effect on the friction and wear performance of sliding surfaces, in particular in the elasto-hydrodynamic regime of lubrication [6].

Several inorganic materials (e.g., transition-metal, graphite, hexagonal boron nitride, boric acid) can provide excellent lubrication [7–10]. Most of these solids owe their lubricity to a lamellar or layered crystal structure. A few others (e.g., soft metals, polytetrafluoroethylene, polyimide, certain oxides and rare-earth fluorides, diamond and diamond-like carbons (DLC), fullerenes) can also provide lubrication although they do not have a layered crystal structure [8–10].

In spite of considerable research development, through more than 2000 published papers during the past 25 years, there exists no single solid lubricant that can provide both low friction and low wear over broad operational conditions [11]. In order to achieve a combination of high wear resistance, high load support, and low friction coefficient, a multifunctional production process combining purpose-oriented phases can be applied [12, 13].

The increasingly multifunctional needs and more stringent operating conditions envisioned for future mechanical systems will certainly make solid tribological materials and advanced coatings far more important. [14].

To meet the increasing tribological needs of these advanced systems, researchers are constantly exploring new materials and developing novel coatings. As a result, great strides have been made in recent years in the fabrication and diverse utilization of new tribomaterials and coatings that are capable of satisfying the multifunctional needs of more advanced mechanical systems [14].

Accordingly to Erdemir [15], solid lubricants can be applied to a tribological surface in a variety of forms. The oldest and simplest method is to sprinkle, rub, or burnish the fine powders of solid lubricants. Certain solid lubricants have been blended in an aerosol carrier and sprayed directly onto the surfaces to be lubricated. Solid lubricant powders can be strongly bonded to a surface by appropriate adhesives and epoxy resins to provide longer wear life [12]. Powders and nanoparticles made of solid lubricants have been mixed with oils and greases to achieve improved lubrication under extreme pressure and high temperature conditions [16–21]. In most modern applications, thin films of solid lubricants, generally deposited onto surfaces by advanced vacuum deposition processes, are preferred to powders or bonded forms. In this case, the durability of the lubricious effect is limited due to the finite lubricant film thickness. To increase durability of these films, a self-replenishment or resupply mechanism is needed but is very difficult to obtain [15].

In this context the production of self-lubrication composites containing second phase particles incorporated into the volume of the material appears to be a promising solution [11, 22, 23]. Indeed, self-lubricating composites have been available

for a long time and are used rather extensively by industry to combat friction and wear in a variety of sliding, rolling, and rotating bearing applications [15].

Composite self-lubricating components have been used for several decades in household and office light equipments such as printers, electric shavers, drills, blenders, and others. The most used metallic matrices materials are copper, ferrous, and Niguel alloys. Compounds like MoS_2, WS_2, $MoSe_2$, NbS_2, $TaSe_2$, $MoTe_2$, h-BN, low melting metals like Ag, Sn and Pb, graphite and polytetrafluorethylene (PTFE) are the most used as solid lubricants [11, 23–25]. The majority of the composites developed contain a high percentage of solid lubricant particles (15–40%) in order to obtain a low friction coefficient. This results in a largely discontinuous metallic matrix that exhibits poor mechanical properties.

The production of new high-performance self-lubricating composites containing second phase particles incorporated into a continuous matrix and having a low friction coefficient combined with high mechanical strength and wear resistance appears to be a promising solution for controlling friction and wear in energy efficient modern systems and points to an engineered microstructure.

7.2 Microstructural Model

The high mechanical and tribological performance is a consequence of the combination of matrix mechanical properties and structural parameters such as the degree of continuity of the metallic matrix, the shape, amount, and the size of solid lubricant particles and the resulting mean free path between them. In addition, it is clear that the development of high-quality composites demands improved mechanical resistance.

Figure 7.1 presents a schematic drawing of the ideal microstructure of a self-lubricating composite. The microstructure must consist of a continuous matrix containing regularly dispersed solid lubricant particles and take into account the mean free path between them and the active area to be covered by each one of them.

The solid lubricant dispersed in the volume of the composite material should be a completely discontinuous phase and many aspects such as the content of solid lubricant [26]; the size and size distribution of solid lubricant particles [27, 28] and the mean free path between the solid lubricant particles [29] have to be considered for microstructural optimization of the composite. To further minimize the interruption of the metallic matrix, the amount of the dispersed solid lubricant must be kept as low as possible. In this context, in addition to the traditional characteristics of the metallic matrix and of the solid lubricant powder particles such as type, amount, and shape, special attention must be paid to the relative size of particles (d_m/d_{sl}) since this parameter has a great influence on the degree of continuity of the matrix which, in turn, as already said, is determinant in the mechanical and tribological behavior of the composite. In fact, as illustrated in Fig. 7.1b, insoluble particles much smaller than those of the matrix tend to be located in the interstices occupying almost the entire interface between the metallic particles with a

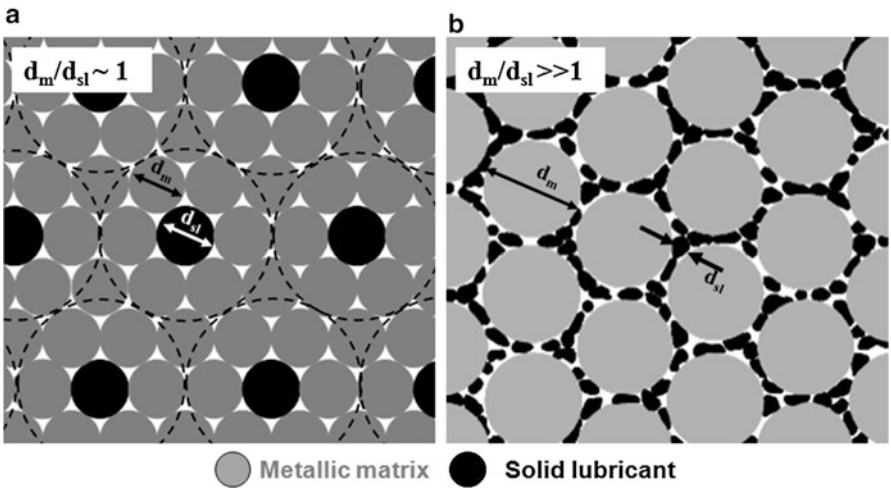

Fig. 7.1 Microstructural model (schematic). (**a**) Desirable distribution of the solid lubricant particles in the volume of the matrix and the corresponding area to be lubricated by each particle. (**b**) Continuity of the matrix

strong tendency to be the continuous phase which does not happen when they have equivalent sizes, Fig. 7.1a.

The metallic matrix which is the continuous phase that gives strength to the composite must be hard and tough enough to avoid the occurrence of micro-plastic deformation by friction and wear. The mass flow that occurs by plastic deformation may gradually cover the solid lubricant reservoirs and block the self-replenishment or resupply of solid lubricant to the interface. Further, it is important that the metallic matrix does not chemically react with the solid lubricant phase.

There are several possible manufacturing routes for producing such composites, in polymeric, metallic, or even ceramic matrices [30–32]. For the particle reinforced metallic matrix composites the methods to synthesize them are generally classified into (1) solid state processing, (2) liquid state processing, and (3) vapor deposition [33]. The most frequently used metallic matrix materials are copper [34], nickel [35], and ferrous alloys [36, 37]. Powder metallurgy techniques are especially suitable for the production of such composites.

7.3 Powder Metallurgy

For the development of metal-matrix composites, powder metallurgy (PM), widely used in industry, is a competitive and attractive technique because of its low cost when applied to large-volume production and because of its great versatility due to the suitability of the technique for tailoring the microstructure according to the requirements imposed by a given application. In addition, PM processes are very advantageous for developing complex shape parts or even small-size components,

which have been increasingly required due to the miniaturization of modern mechanical systems.

The high porosity of sintered components leads to reduced mechanical strength and load capacity when compared with fully dense materials. However, they have the potential to store lubricant that can be released during the use of the component [38, 39]. Also, the pores could eventually play an important role in the removal of wear debris from the sliding interfaces, as suggested by some authors [40]. Therefore, powder metallurgists are continuously searching for new alternatives and mechanisms to improve mechanical resistance and load support. In this sense, several processing parameters must be strictly controlled such as temperature and time of sintering, compression method, and techniques for the dispersion of the solid lubricant particles in the volume of the composite. Sintering is the most important step in the production of the composite. The variables in sintering are atmosphere, heating rate, temperature, dwelling time, and cooling rate. The sintering temperature should be lower than the decomposition temperature of solid lubricant. Reactions among the matrix, alloying elements and solid lubricant, which result in loss of solid lubricant, should also be avoided.

Special attention should be devoted to the compression technique. Several compaction techniques, like uniaxial die pressing, extruding, rolling, 3D prototyping, and powder injection molding, must be considered depending on the geometry and properties desired for the composite material. Uniaxial mechanical pressing, due to its low manufacturing costs, is still the most traditional processing route. It also produces the closest tolerances in the finished parts, thus nearly eliminating post-sintering operations such as machining [41]. However, depending on the configuration (single or double action), this technique presents gradients of porosity that may eventually be very high [42–44].

Recently [45], we presented a potential alternative for improving the mechanical strength of self-lubricating sintered composites: the use of the double pressing/double sintering (DPDS) technique [46] originally developed by Hoeganaes [47] and used in the automotive industry. The goal of this method is to increase the density of composites by twofold pressing. According to German [48], reductions of 2–3% in porosity would result in up to a 20% increase in mechanical strength. Although more expensive, MIM has the advantage of flexibility of the processing parameters, which allows the production of very small parts presenting high geometric complexity, refined microstructure, and elevated final density [49]. That is not feasible with the current uniaxial die cold pressing process. For the case of self-lubricating composites, the metal injection molding method is particularly indicated due to the small powder size which induces more homogeneous tribolayers covering the whole interface, Fig. 7.1a.

Roughly speaking, in MIM process, metal powders are premixed with polymeric binders. The mixture is heated and forced under pressure into a die cavity, where it cools and is subsequently ejected. The polymer is then removed (debinding stage) and the component sintered to the required density, Fig. 7.2.

The debinding stage, during which polymer is removed, can greatly influence the mechanical properties of the sintered component [49, 50]. In our case, the debinding

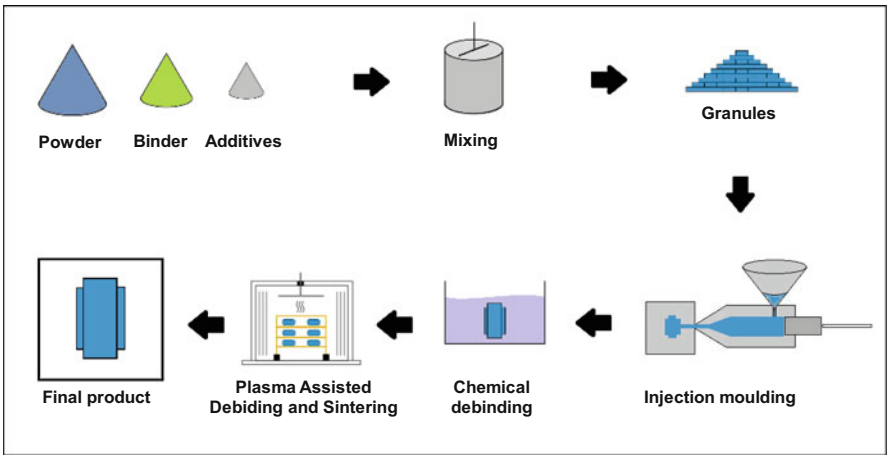

Fig. 7.2 Metal injection mold processing route

was carried out in a stepwise process: chemical debinding was followed by plasma-assisted thermal debinding. The chemical step consisted of the dissolution in hexane of the low molecular weight components of the binder system, forming an open pore network within the injected parts.

The thermal debinding, as well as the sintering, was performed in a single thermal cycle (plasma-assisted debinding and sintering – PADS) [50]. In summary, its advantages are short processing time (debinding and sintering in about 10 h versus 90 h for the thermochemical classical processes) and no binder residues after debinding. This process allows sintering in a single cycle and eliminates a cleaning procedure after every cycle. In the plasma-assisted debinding process, the polymer macromolecules are dissociated by bombardment of energetic electrons (inelastic collision) resulting in hydrocarbon radicals (C_xH_y) whose recombination is prevented by the presence of atomic hydrogen present in the hydrogen plasma, Fig. 7.3b. The reaction of atomic hydrogen with hydrocarbon radicals results in hydrocarbon gas that is removed from the reactor chamber via the vacuum pump.

The plasma reactor, developed in [51], was specially designed for the PADS process and described in [50–52] allows the control of the processing temperatures and the heating rates independently of the plasma parameters. The vacuum chamber, shown schematically in Fig. 7.3a, contains electrodes for the generation of plasma DC and electrical heaters for heating control. The samples were set on ceramic plates supported by the structure of the anode and were initially processed in floating potential plasma. Abnormal hydrogen glow discharge was then generated and the power supply voltage was biased to the cathode during the isothermal sintering.

As already pointed out (Fig. 7.1a), the ideal microstructure of a self-lubricating composite must consist of a continuous matrix containing regularly dispersed solid lubricant particles. Unfortunately, such an ideal distribution of the solid lubricant particles is not obtained simply by blending metallic and solid lubricant powders.

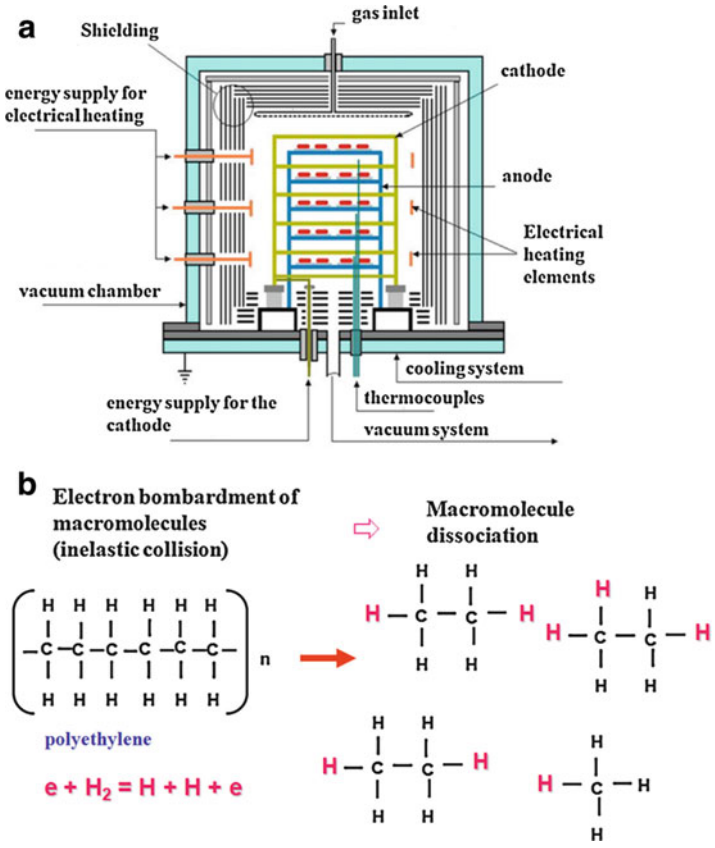

Fig. 7.3 Plasma-assisted debinding and sintering process. (**a**) Hybrid reactor [50]. (**b**) Macromolecule dissociation principle

In order to produce a self-lubricating sintered composite, there are basically two ways of dispersing the solid lubricant particles in the volume of the metal matrix [53, 54]:

(i) Mixing the solid lubricant particles with matrix powders
(ii) "In situ" generation of the solid lubricant particles during the sintering by dissociation of a precursor mixed to the powders of the metallic matrix

In the first method, where the composite is obtained by mixing the metallic matrix powders with the solid lubricant particles, the shear stresses that occur during mixing and compacting spread the solid lubricant by shearing between the powder particles of the metal matrix. This leads to an undesirable arrangement in which the solid lubricant covers the metallic particles to a large extent [55]. The presence of these layers of insoluble solid lubricant hampers the formation of contacts between the

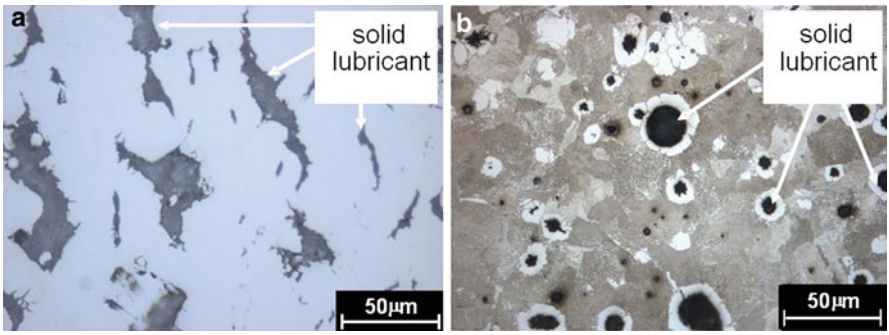

Fig. 7.4 Solid lubricant particles dispersion. (**a**) Mixing of powders prior to compaction. (**b**) In situ generated by decomposition of a precursor

particles during sintering. This results in a metallic matrix with a high degree of discontinuity, Fig. 7.4a, and leads to a composite material with reduced mechanical strength.

There are two possibilities to overcome these difficulties. The first one is to rearrange the solid lubricant phase in discrete agglomerates by the capillary action of a liquid phase. The liquid phase spreads and penetrates the interfaces between the metal and the lubricant, thus pushing the solid lubricant and rearranging it in agglomerates. The second one is to produce the solid lubricant phase in situ during sintering by decomposition or dissociation of a precursor, giving rise to a more continuous and sound matrix, Fig. 7.4b.

Preliminary studies evidenced that the in situ generation of the solid lubricant phase particles during the sintering by the dissociation of a precursor was the most promising production route.

7.4 In Situ Generated Graphite

Silicon carbide (SiC), molybdenum carbide (Mo_2C), chromium carbide (Cr_3C_2), etc., are potential precursors to generate graphite nodules in ferrous matrix [56, 57]. Among them, those inducing the stabilization of the body-centered cubic phase of iron (α-Fe) are the most indicated in order to produce iron-based self-lubricating composites. SiC is particularly appropriate since it features a high carbon content, and silicon is a strong alpha phase stabilizer in addition to being one of the most effective hardening elements of ferrite [58].

Figure 7.5 shows typical aspects of the microstructure of the composites.

The reference alloy (Fe + 0.6 C + 4 Ni) presented a microstructure constituted of perlite (P) + ferrite (α), Fig. 7.5a, whereas the addition of SiC to the feedstock powder induced the formation of graphite nodules. The graphite nodules (G) are always surrounded by ferrite (α) rings, Fig. 7.5b.

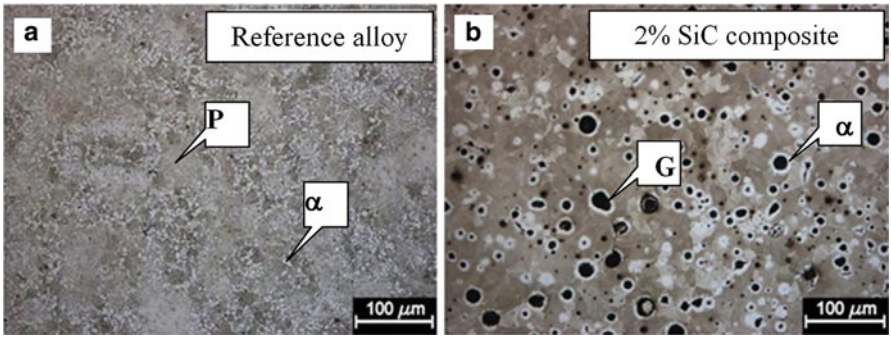

Fig. 7.5 Typical aspects of the microstructure. (**a**) Reference alloy (matrix alloy – Fe-0.6%C-4% Ni). (**b**) 2 wt% SiC composite. Sintering temperature 1150 °C

The evolution of the microstructure depends on precursor (SiC) content, sintering parameters (temperature, time, and atmosphere), and the previous composition (other alloying elements) of the ferrous matrix. [53]. For example, the presence of carbon in the matrix prior to the startup of SiC dissociation reduces the dissolution of the carbon originated from the dissociation of SiC and increases the size and the amount of the graphite nodules formed [36, 59]. The presence of Ni, a strong stabilizer of the face-centered cubic phase of iron (γ-phase) of the iron matrix, positively influences the morphology of the graphite nodules [36].

Such microstructure formation was expected from thermodynamic considerations as evidenced by the Ellingham diagram presented in Fig. 7.6a and its evolution depends on sintering time and temperature, as well as on the amount of SiC added to the ferrous matrix. This is well described in a recent paper [53].

Roughly, during the sintering, at the initial stage of the dissociation of the SiC particles, silicon and carbon atoms diffused into the ferrous matrix, Fig. 7.6b. However, the continuous enrichment of the ferrous matrix with Si around the former silicon carbide particles leads to stabilization of the body-centered cubic structure of the ferrous matrix (ferrite) in which the solubility for the carbon atoms is very low (solubility $\leq$0,022 wt%), [60], drastically reducing the dissolution of graphite. The dissolution of silicon, in contrast, is maintained [60]. As a consequence ferrite rings are formed around the former SiC particles, Fig. 7.7a [53, 54, 61].

The remaining carbon forms graphite nodules (size $\leq$20 μm), Fig. 7.7b which present a nanostructured stacking of graphite layers a few tenths of nanometers thick, Fig. 7.7c, d. The evolution of such microstructure depended on the amount of SiC, as well as on sintering temperature and time and is fully described in a recent paper [59]. The precipitation of graphite nodules started at temperatures higher than 1100 °C. At this temperature the precipitation is important for times superior to 1 h as evidenced by XRD analysis [61].

Finally, Fig. 7.8 presents line profiles of C and Si throughout a graphite nodule and a ferrite ring evidencing the low solubility of carbon in the ferrite and the depletion of silicon in the former SiC particle.

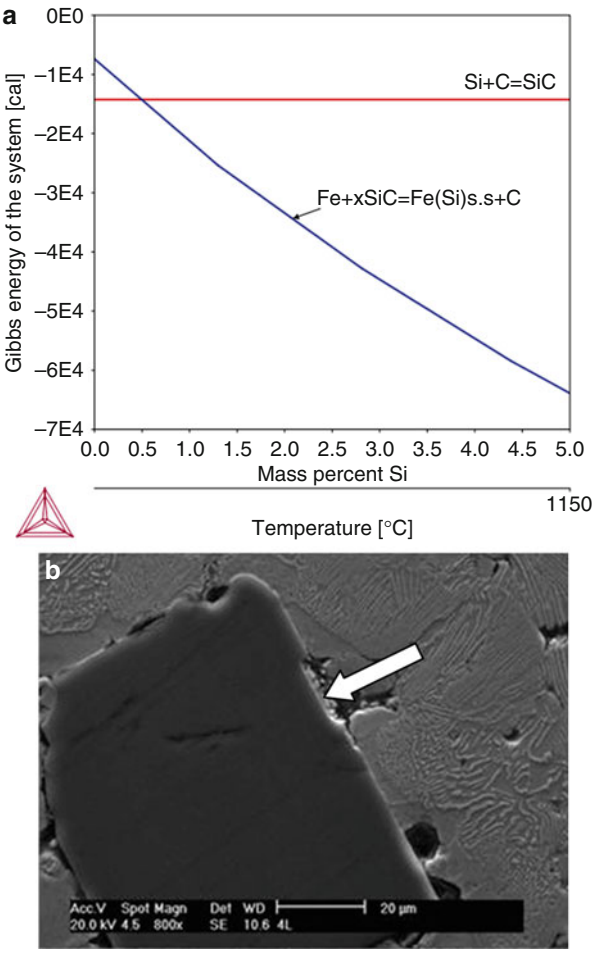

Fig. 7.6 Thermodynamic equilibrium. (**a**) Ellingham diagram. (**b**) Initial stage of SiC dissociation, SEM

The nodules are composed mostly of carbon, whereas the ferrite ring around the nodule has an almost constant high concentration of silicon, and the carbon concentration is greatly reduced. Outside the ferrite ring, the silicon concentration decreases, and the carbon concentration in the matrix increases. This interface is the separation between the ferritic (α-Fe) phase and pearlitic (γ-Fe) regions, thus confirming the formation of the carbon nodules by the SiC dissociation and the formation of a diffusion barrier due to α-Fe phase stabilization by silicon.

7.5 Tribological Characterization

The tribological behavior was evaluated using two types of experiments schematized in Fig. 7.9:

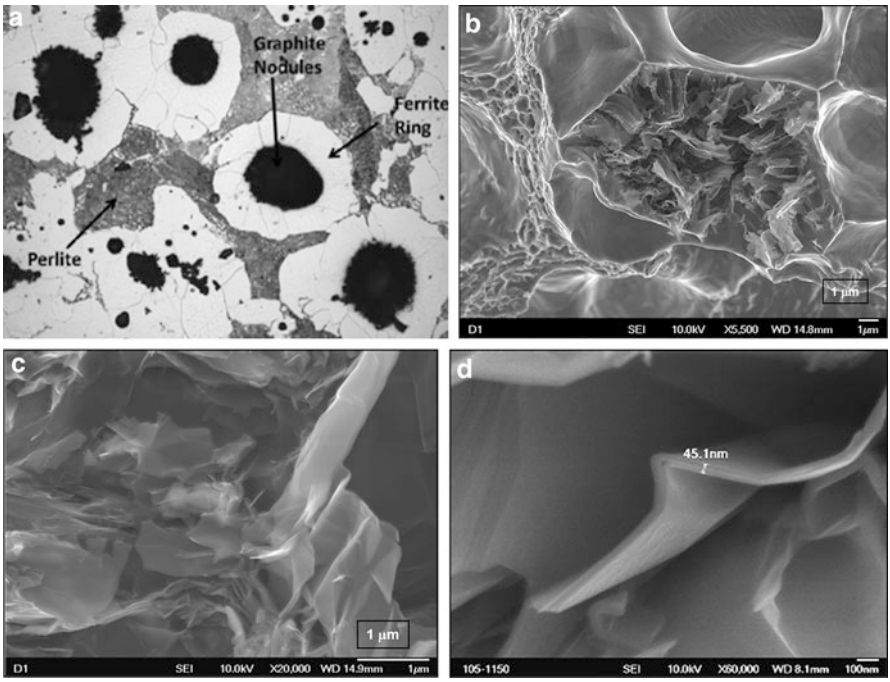

Fig. 7.7 Typical aspects of the microstructure. Composite Fe-0.6C-4 Ni-2 SiC. (**a**) Ferrite ring. (**b**–**c**) Graphite nodule (fractography). (**d**) Graphite layer

(a) Reciprocating sliding tests were conducted at constant normal load to access the friction coefficient and wear rates of specimens and counter-bodies.
(b) Reciprocating sliding tests were carried out in an incremental loading mode. In this case, by increasing the normal load in increments of 7 N at 10 min. intervals, the scuffing resistance was determined. The scuffing resistance was defined as the work (N m) at which the value of the friction coefficient first rose above 0.20 (lubricity effect) [12].

In both kind of experiments, a hard steel AISI 52100 ball (diameter 5 or 10 mm) was fixed on a pivoted arm and rested against the specimen surface under constant stroke (5 mm) and frequency (2 Hz). The tests were conducted under controlled relative humidity (50%) and temperature (22 ± 4 °C).

Wear scars were analyzed by using SEM-EDX as well as FEG-SEM, micro-Raman spectroscopy, Auger electron spectroscopy, and laser interferometry.

7.6 Mechanical Properties

The evolution of the mechanical properties with precursor content and sintering temperature is illustrated in Fig. 7.10.

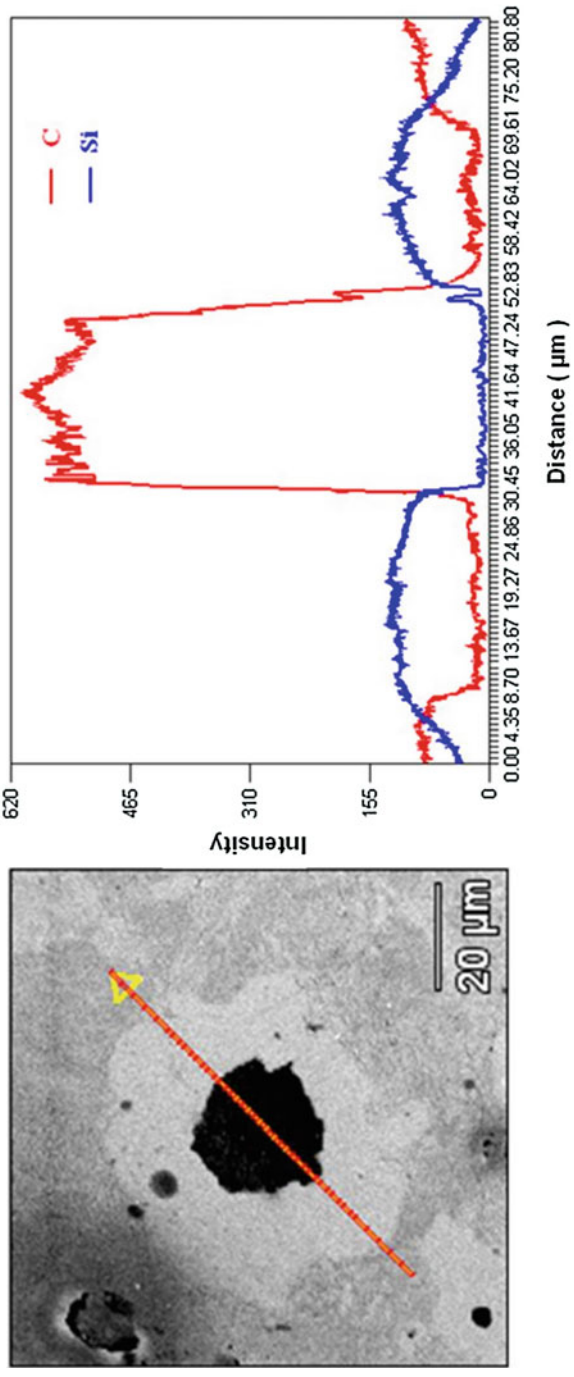

Fig. 7.8 Line profile showing the concentration of silicon and carbon along the graphite nodule and the surrounding metal matrix

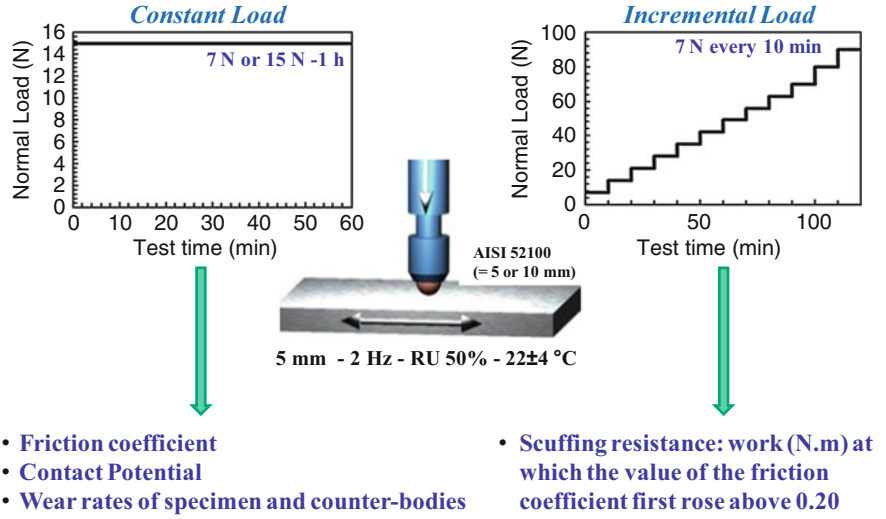

Fig. 7.9 Tribological characterization

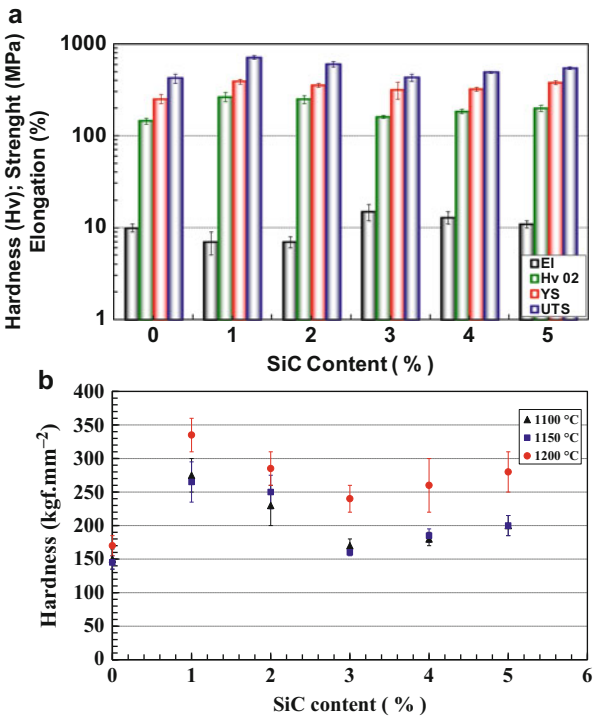

Fig. 7.10 Typical evolution of the mechanical properties. (**a**) Effect of SiC content on mechanical properties for composites sintered 1150 °C. (**b**) Influence of SiC content and sintering temperature on hardness

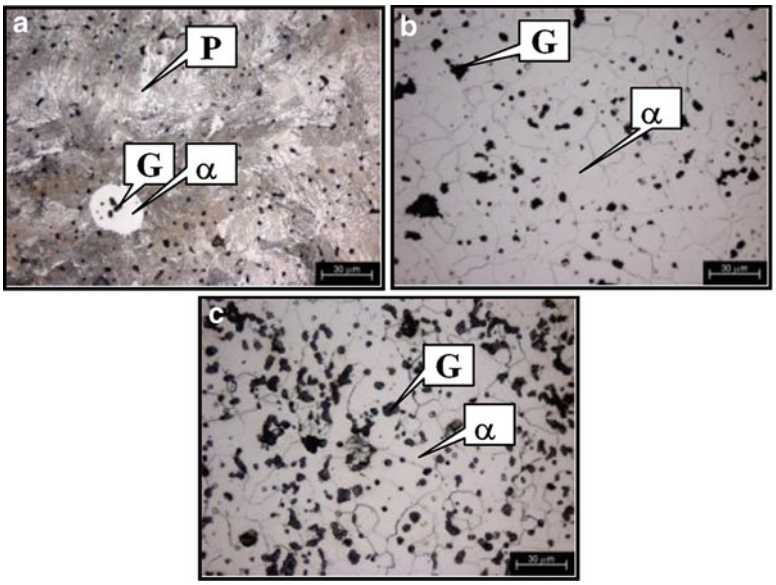

Fig. 7.11 Typical microstructures. Sintering temperature 1150 °C. (**a**) 1% SiC; (**b**) 3% SiC; (**c**) 5% SiC

The addition of SiC induced a quite complex evolution of the mechanical properties, Fig. 7.10a. There is a sharp increase up to a maximum for additions of 1% SiC. Then the hardness decreased to a minimum at 3% SiC and afterwards gradually increased. The strength of the composites follows the same behavior whereas, of course, the elongation behaved in the opposite sense.

In terms of hardness, Fig. 7.10b, the dissociation of SiC particles produced harder composites than those of the metallic matrix alone. There is a sharp increase up to a maximum for additions of 1% SiC. Then the hardness decreased to a minimum at 3% SiC and afterwards gradually increased. Indeed, for composites presenting 3% SiC the metallic matrix is mainly constituted of ferrite (α), Fig. 7.11b, whereas for smaller SiC contents the microstructure presents a certain amount of perlite (P), Fig. 7.11a. For higher SiC amounts, Fig. 7.11c, it is reasonable to suppose that the great availability of silicon induces a larger hardening of the matrix (ferrite).

The mechanical properties of the composites are a compromise between the two different effects of the dissolution of the SiC particles [53, 61]:

(i) An increase in the mechanical resistance caused by the strengthening of the metallic matrix due to the dissolution of Si
(ii) A decrease in the mechanical resistance as a consequence of the formation of graphite nodules during the sintering process, which decreases the degree of continuity of the metallic matrix.

Silicon is known to be one of the most efficient promoters of the hardening of ferrous matrix by the formation of substitutional solid solution [62, 63].

On the other hand, the sintering temperature produced a strong effect on the mechanical properties as illustrated by hardness, Fig. 7.10b. The high sintering temperature produced harder (up to 50%) composites whereas the variation from 1100 °C to 1150 °C produced almost no effect. The higher values presented by the samples sintered at 1200 °C are supposed to be mainly due to the higher degree of the homogeneity of the composites (in particular the distribution of Si and pearlitic regions in the matrix) sintered in this higher temperature. However, for composites with 4% and 5% SiC sintered at 1200 °C, values of yield and tensile stress decrease, which was related to the formation or "line structures" reducing matrix continuity and affecting the material properties [59].

7.7 Tribological Behavior

7.7.1 Introduction

In this section, the tribological behavior of self-lubricating composites produced taking advantage of the powder injection molding process, the recently introduced plasma-assisted debinding and sintering (PADS) process, and the in situ formation solid lubricant particles is presented and discussed. In this case, we obtained the in situ formation of graphite nodules in the volume of the sintered composites during sintering simply by dissociation of particles of silicon carbide (SiC) mixed to the metallic matrix powders prior to the compaction.

Recent studies concluded that a transfer film is found on the sliding surfaces [53]. The formation of such a film on the sliding interfaces seems to be the key for achieving low friction and long wear life in most solid-lubricated surfaces [13]. It was found that, initially, transfer films were not present but were formed as a result of surface wear and subsurface deformation. These films are continuously replenished by embedded graphite particles dispersed in the matrix [64].

The effects of precursor content (0 to 5 wt% SiC) and of sintering temperature (1100 °C, 1150 °C and 1200 °C) on tribolayer durability, average friction coefficient in the lubricious regime ($\mu < 0.2$), and wear rate of the specimens and counter-bodies are presented and discussed. In addition, the effect of the metallic matrix composition (Fe-C; Fe-C-Ni; Fe-C-Ni-Mo) and surface finishing are also presented. Special emphasis is given to the protective tribolayer.

7.7.2 Materials

Sintered composites with different chemical compositions were produced by mixing carbonyl iron powder (Carbonyl BASF grade OM) with elemental powder of the alloying elements. The carbonyl iron used had a particle size of 7.8 μm and

contained 0.8% carbon. Different contents of silicon carbide (Cobral) powder (1%, 2%, 3%, 4%, and 5% SiC) having particle size of 10 μm were added to the carbonyl iron powder. The feedstock for injection was prepared in a Haake Sigma mixer (180 °C, 70 rpm, 90 min) using 8% of an organic binder system containing paraffin wax, polypropylene, stearic acid (surfactant), ethylene vinyl acetate copolymer (EVA), and amide wax.

Samples with the appropriate geometry for performing tensile and tribological tests were injected (injection pressure of 100 MPa) using an Arbourg 320S injection molding machine. The debinding was performed in two steps: a chemical debinding followed by plasma-assisted thermal debinding. The thermal debinding, as well as the sintering, was performed in a single thermal cycle in a plasma reactor, i.e., using the plasma-assisted debinding and sintering (PADS).

A hydrogen abnormal glow discharge was generated at a pressure of 133 Pa (1 Torr) and the gas flow was adjusted to $3.33.10^{-6}$ m^3 s^{-1} (200 sccm). The power supply voltage biased to the cathode was fixed at 500 V. A heating rate of 0.7 °C/min was fixed up to 500 °C for the plasma-assisted thermal debinding step. Then, the heating rate was increased to 5 °C/min up to the sintering temperature. The isothermal sintering was processed at 1100 °C, 1150 °C, and 1200 °C for 60 min.

In order to analyze the effect of the metallic matrix, three compositions of sintered composites (Fe–Si–C, Fe–Si–C–Ni, and Fe–Si–C–Ni–Mo) were also produced. The same iron powder was used (Carbonyl BASF grade OM). The alloying elements Ni and Mo were mixed to the feedstock in the form of elemental Ni (Vale Inco Type 123) and elemental Mo (H.C. Starck Type) powder. Silicon was added in the form of 3 wt% silicon carbide powder (Cobral) aiming at its dissociation during sintering. The same processing route was used but just one sintering temperature and time (Ts = 1150 °C- 60 min) were used.

7.7.3 Tribological Evaluation

7.7.3.1 Incremental Load Tests (Scuffing Resistance)

Typical results are shown in Fig. 7.12.

All results present similar behavior. There is a transient associated with the onset of contact between specimen and counter-body at the beginning of tests before a high lubricity steady state is reached. The reasons for the difference in the evolution of the friction coefficient within the transient period are not yet well understood and will not be treated in the present chapter. However, it is reasonable to suppose that the stabilization of the friction coefficient is related to the generation of a protective tribolayer, where the transient corresponds to the kinetics of formation of the layer. As long as the formation rate of the tribolayer is different from the degradation rate, friction coefficient will vary. Once this formation rate is equal to or greater than the degradation rate, a steady state is reached.

All specimens behaved in a similar manner in the lubricious regime. However, low SiC content composites (e.g., 1% SiC) presented higher friction coefficient which gradually increases with the sliding distance associated with a shorter and

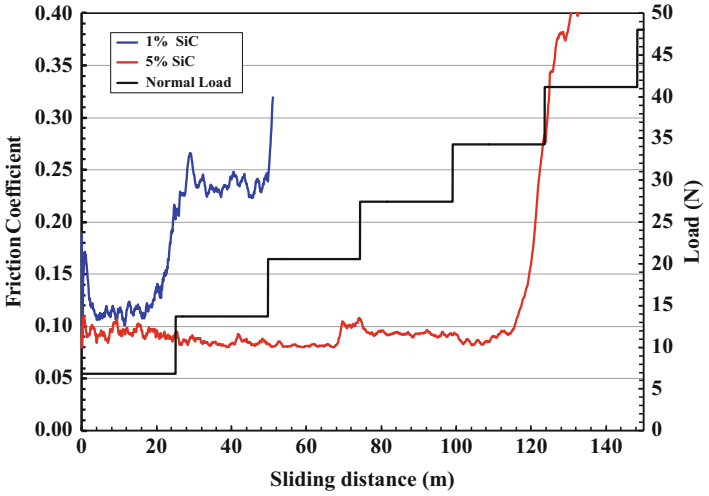

Fig. 7.12 Typical evolution of friction coefficient with sliding distance and applied normal load

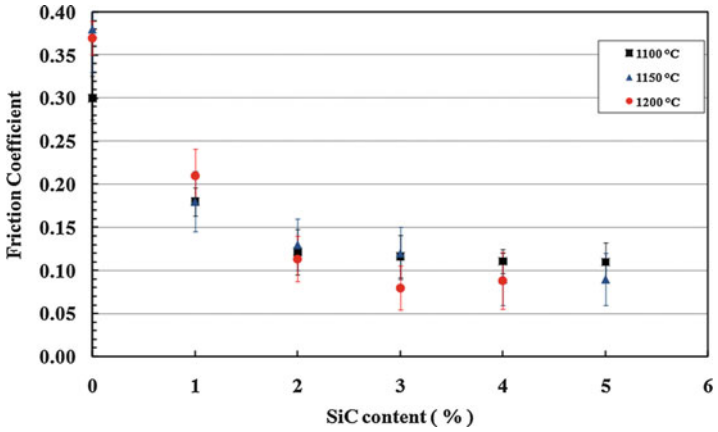

Fig. 7.13 Effect of SiC content and of sintering temperature on the average friction coefficient during the lubricious regime

almost equivalent scuffing resistance, whereas the high SiC content (e.g., 5% SiC) composites exhibited lower friction coefficients coupled with much longer period in the lubricious regime signalized by a rapid increase in the friction coefficient. The friction coefficient values for each test were computed by averaging the lubricious steady-state values.

The influence of the precursor content and of the sintering temperature on the friction coefficient behavior is synthesized in Fig. 7.13.

Independently of the sintering temperature, increasing the precursor content and, as a consequence, the number of graphite nodules produced a reduction of the

average friction coefficient. In general, the reduction was substantial, up to 3% SiC. For higher values of SiC content, the friction coefficient was almost constant. It is reasonable to suppose that graphite foils are removed from the in situ generated graphite nodules and remain at the interface thus contributing to the formation of a protective tribolayer. Due to the small size of the powders, the mean free path between graphite nodules is also small and the complete "coverage" of the surface between nodules is easily reached. As a consequence, the number of graphite foils generated in composites containing more than 3% of SiC is sufficient to produce the protective layer and low friction coefficients. Additionally, there is almost no effect of the sintering temperature on the average friction coefficient.

A comparison between Figs. 7.10 and 7.13 shows that there is, definitely, no correlation associating the friction coefficient with mechanical properties of the composites.

Figure 7.14 presents typical aspects of the wear scars. The test was interrupted at the normal load of 14 N which is within the lubricious regime ($\mu < 0.2$).

At low magnifications, Fig. 7.14a, the wear scar appears quite homogeneous. It presents flat and smooth regions where contact with the counter-body occurred. It seems that there is a protective layer on the active interface (brown/gray areas, confirmed, by using back scattered electrons, to be composed of elements presenting low atomic number). It is reasonable to suppose that graphite foils are removed from the in situ generated graphite nodules and remain at the interface (Fig. 7.14b) thus contributing to the formation of the protective tribolayer. Due to the small size of the powders, the mean free path between graphite nodules is also small and the complete "coverage" of the surface between nodules is easily reached. As a consequence, the number of graphite foils generated in composites containing more than 3% of SiC is sufficient to produce the protective layer and low friction coefficients thus explaining the saturation of the friction coefficient variation with precursor content, Fig. 7.13.

On the other hand, since the tribolayers also degrade under the action of the sliding (Fig. 7.14c).

Figure 7.14d presents a typical Raman spectra obtained in the central region of the wear scar. It clearly presents a widened G band (associated with the sp^2 hybridization) and a D band (associated with crystallinity disorder). The widening of the bands, the ID/IG ratio, and the size of the graphite crystallites are, accordingly to literature [61, 65–68], clear evidence of disorder in the material. They are also a strong indication of the presence of the so-called turbostratic 2D graphite which presents longer interlamellae distances among the graphene foils when compared to the highly oriented 3D graphite coupled with a strong misalignment of the graphene foils. Moreover, the analysis of the second-order band G′ confirms the greater contribution of the 2D graphite to the formation of the D band.

The increase in distance may induce low interaction between these atomic planes and is, probably, the origin of the low friction coefficient [69].

To further understand this point, a few other types of graphite were analyzed under the same tribological configuration: They are graphite nodules in a nodular cast iron, and the contact was submerged in graphite in powder. The matrix alloy (graphite-free – Fe 0.6 wt% C) was also tested as a reference.

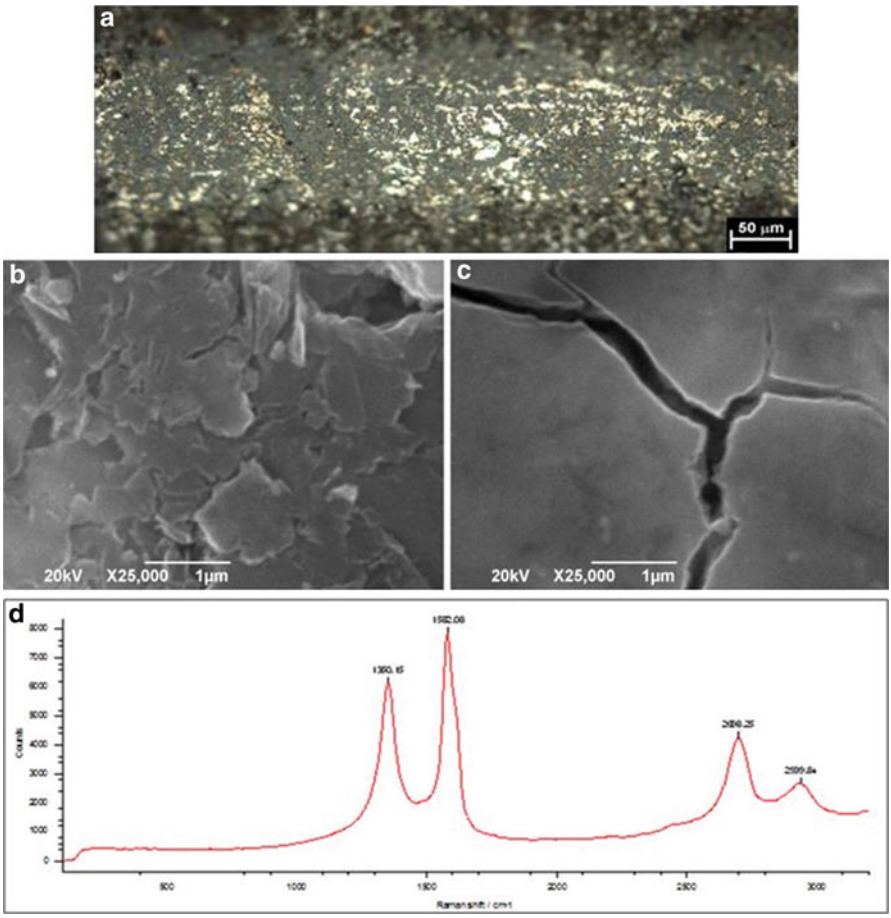

Fig. 7.14 Typical wear scars produced in the lubricious regime ($\mu < 0.2$). Fe + 0.6C + 5SiC. (**a**) General aspect, optical microscopy; (**b**, **c**) FEG-SEM; (**d**) Raman spectra

Figure 7.15 shows the average friction coefficient (steady state) of different materials.

The reference alloy presented the highest friction coefficient. The presence of graphite (nodules in nodular cast iron and graphite in powder) strongly reduced the friction coefficient (170% and 290%, respectively). The addition of 3 wt% SiC further reduced the friction coefficient (530%) and induced a remarkably low value (0.06).

Figure 7.16 presents the typical Raman spectra of different graphite types.

They clearly show a G band at approximately 1580 cm^{-1}. The spectrum of the graphite nodules produced by the SiC decomposition (Fig. 7.16a) clearly presents a D and a D′ band both associated with crystallinity disorder. The analysis of the spectra shows many evidence (the widening of the bands, the I_D/I_G ratio, the size of

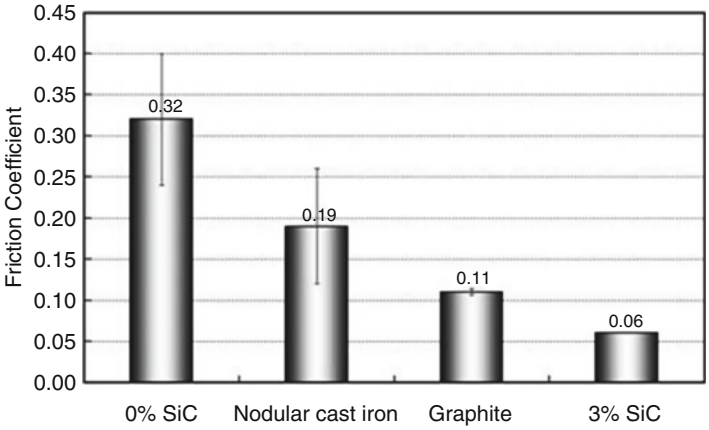

Fig. 7.15 Effect of graphite type on friction coefficient

the graphite crystallites, and the shape of the second-order G′ band) of the presence of the so called turbostratic graphite (2D graphite). Moreover, the analysis of the second-order G′ band (very sensitive to the stacking order of the graphene sheets along the c axis [70, 71]) confirms the greater contribution of 2D graphite to the formation of the D band. Graphite associated with graphite powders, Fig. 7.16b, and nodular cast iron, Fig. 7.16c, is characterized as 3D graphite and is highly aligned according to the literature [65–67].

According to the literature [61–68, 72], the widening of the bands, the ID/IG ratio (widely used for characterizing the defect quantity in graphitic materials) [70–73] and the size of the graphite crystallites (La) are clear evidence of disorder in the graphite nodules in the composite Fe-0.6 wt% C + 3 wt% SiC. They also strongly indicate the presence of the so-called turbostratic 2D graphite, which has highly misaligned graphene planes separated by larges paces. A recent paper presents the main aspects of the 2D turbostratic graphite including a comprehensive analysis of the Raman spectra of the different graphite types [72] clearly evidencing that major contribution to the G′ band stems from graphite 2D, not from 3D graphite.

Transmission electron microscopy, Fig. 7.17, confirmed the large interplanar distance, Fig. 7.17b ($\geq$3.499 Å against 3354 Å for the high aligned 3D graphite), among the graphene foils and the misorientation of the graphene foils, inset in Fig. 7.17c.

Figure 7.17a, b show bright field images of graphite sheets obtained from the graphite nodules of a Fe +0.6C + 3SiC composite and the corresponding SAED. Figure 7.17c presents high-resolution (HRTEM) image with fringes representing individual carbon layers and the SAED pattern (inset) taken from this region. Moreover, the increased interlayer spacing could be correlated to the stacking fault disorder, inherent of turbostratic graphite [74, 75].

These large spaces associated with the misalignment among the graphene planes drastically decreased the interaction among the planes, which results in a low shear

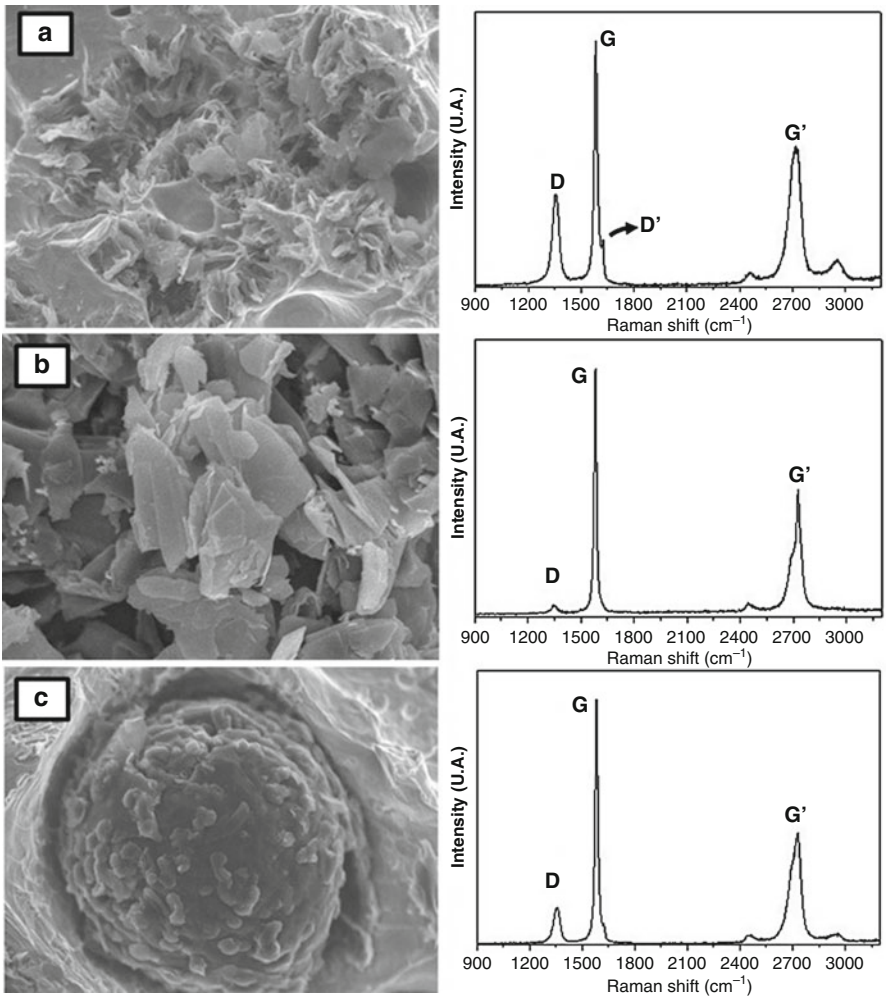

Fig. 7.16 Typical Raman spectra. (**a**) Graphite nodule obtained via SiC dissociation, (**b**) graphite in powder, (**c**) graphite nodule in nodular cast iron [72]

strength. Thus, it is reasonable to suppose that during the reciprocating sliding, the graphite planes easily shear and maintain a constantly lubricated contact interface.

There is almost no effect of the sintering temperature on the lubricious average friction coefficient. On the contrary, the sintering temperature strongly influences scuffing resistance, Fig. 7.18. The low sintering temperature induces significantly higher scuffing resistance (5×).

For the extreme sintering temperatures, increasing SiC content up to 2% induced a strong increase in scuffing resistance and then it remained almost constant, Fig. 7.18. In this case, the saturation effect is reached at 2% of SiC indicating that the self-replenishment provided by the graphite nodules is already active at this

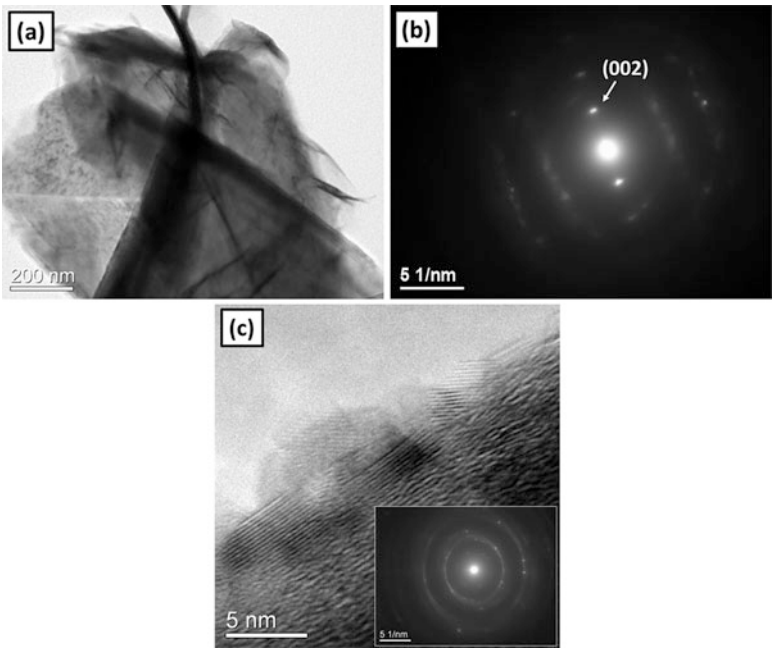

Fig. 7.17 (**a**) Bright field TEM micrograph, (**b**) the corresponding SAED pattern, and (**c**) high-resolution TEM image of graphite sheets obtained from graphite nodules for a Fe + 0.6C + 3SiC sample. The inset in (**c**) shows a typical SAED pattern recorded from this region (graphite sheets) [72]

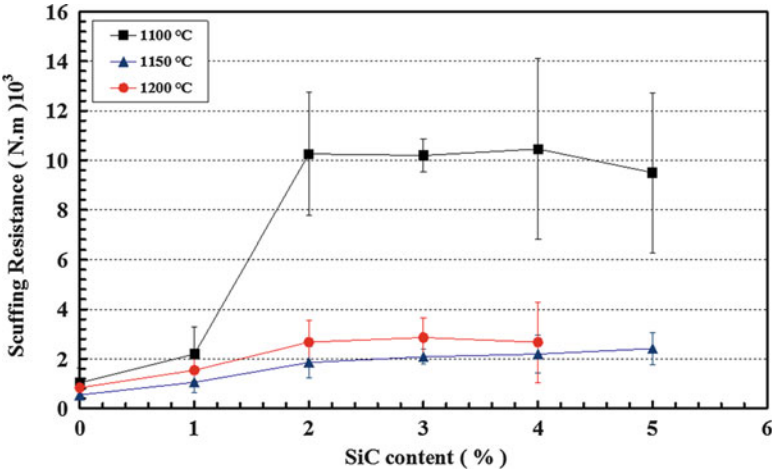

Fig. 7.18 Effect of SiC content and of sintering temperature on scuffing resistance

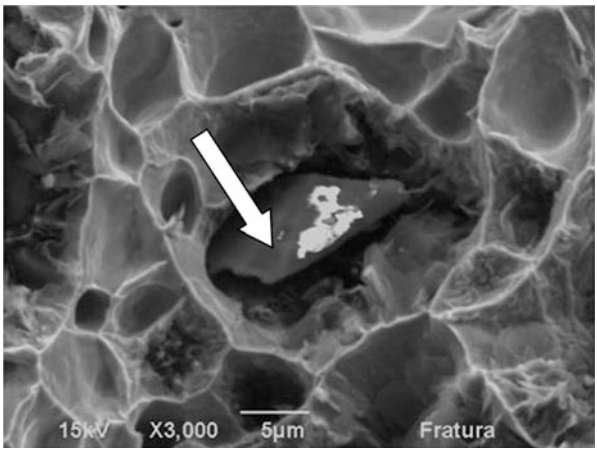

Fig. 7.19 Typical undissociated SiC particle. Fe + 0.6C + 3SiC, 1100 °C, 60 min

lower value. However, for the intermediate sintering temperature there is an almost monotonous increase of scuffing resistance after this threshold is reached.

Again, there is definitely no correlation associating the scuffing resistance with mechanical properties of the composites. In order to further understand why the low sintering temperature induced higher scuffing resistance, Fig. 7.18, the samples sintered at 1100 °C were cryogenically fractured and then the surfaces were analyzed using SEM. A typical aspect of the graphite nodules present in Fe + 0.6C + 3SiC composite is illustrated in Fig. 7.19.

The white arrow points to a partially dissolved SiC particle. EDS point analysis showed that there is, probably, a ring of ferrite around the nodule since the chemical composition was higher than 2.1 wt% Si.

Taking into account that the metallic matrix is continuous, it is reasonable to suppose that the solid lubricant, or its precursor, does not contribute to the mechanical resistance of the composite as already illustrated and discussed in the hardness/SiC content relationship. However, the presence of undissociated particles of SiC may produce a greater load-bearing capacity and the protection of the matrix/tribolayer, thus inducing higher scuffing resistance.

7.7.3.2 Constant Load Tests

Effect of Precursor Content and Sintering Temperature

In this section, the effect of the sintering temperature (1100 °C, 1150 °C, and 1200 °C) and SiC content (0–5 wt%) on the tribological behavior (friction coefficients and wear rates of specimens and counter bodies) is presented and discussed.

In all cases, the evolution of the friction coefficient with time exhibited a transient state at the beginning of the tests; then, a steady state with similar fluctuations from the start to the end of the test was attained, Fig. 7.30. The evolution of the average steady-state fiction coefficient with precursor content and sintering temperature is presented in Fig. 7.20.

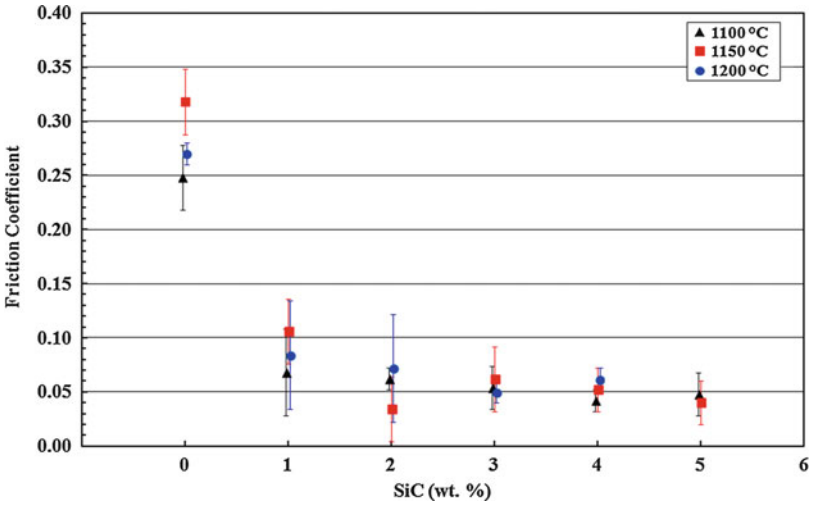

Fig. 7.20 Effect of the silicon carbide content and sintering temperature on the steady-state friction coefficient. *The x values were slightly shifted* (±0.02) *to the left and to the right in order to separate overlapping symbols*

Independently of the sintering temperature, an increase of the precursor content, which increased the number of 2D turbostratic graphite nodules, reduced the average friction coefficient. In general, the reduction was substantial (up to 3 wt% SiC).

For higher SiC contents, the friction coefficient was almost constant. It is also noticeable that the friction coefficient was hardly affected by the sintering temperature. All composites showed a considerably smaller friction coefficient (one order of magnitude) than the matrix alloys (carbide-free alloys). Again, there is, definitely, no correlation associating the friction coefficient with the mechanical properties of the composites and the outstanding tribological behavior may be attributed to the presence of the so-called turbostratic 2D graphite.

Figure 7.21a shows the effect of the silicon carbide content and sintering temperature on the wear rate of the specimens.

The addition of SiC, which creates 2D turbostratic graphite nodules, clearly enhances the tribological behavior. The matrix alloy showed a considerably higher (one order of magnitude higher) wear rate than the composites. When the SiC content increased, there was a decrease to a minimum at 3 wt% SiC; then, the wear rate gradually increased. The wear rate of the counter-bodies had an equivalent behavior. It is also noticeable that despite the higher hardness, the counter bodies had a much higher wear rate than the specimens (one order of magnitude), Fig. 7.21b.

There is a complex competition among different phenomena:

(i) During the silicon carbide dissociation, the matrix hardened because of the Si diffusion, which increased the strength of the composite. However, the mechanical strength decreased because graphite nodules and pores (4–12% [59])

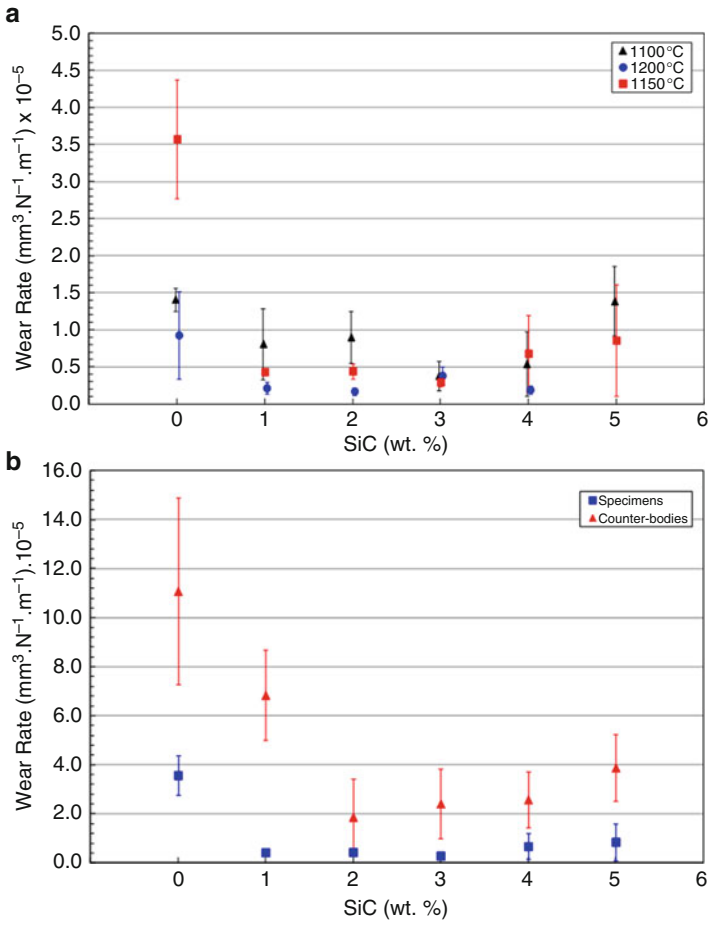

Fig. 7.21 Wear rate. (**a**) Effect of the SiC content and sintering temperature on the wear rate of the specimens. *The x values were slightly shifted* (±0.02) *to the left and to the right in order to separate overlapping symbols*). (**b**) Evolution of the wear rate of the specimens (sintering temperature = 1150 °C) and counter-bodies as a function of the SiC content

formed during the sintering process, which decreased the degree of continuity of the metallic matrix [69].

(ii) The graphite nodules formed a protective tribolayer at the interface, which led to the better tribological behavior of the composites.

Composites with SiC amounts exceeding 4 wt% featured an increased wear rate, which may be associated with a decreased mechanical strength due to the large amount of pores/graphite nodules (large discontinuity of the matrix) [59], as illustrated in Fig. 7.11b, c. In this case, the graphite nodules decreased the hardness and increased wear despite the presence of a rich carbon-based protective layer in the contact interface, which is responsible for the low friction coefficient (Fig. 7.20).

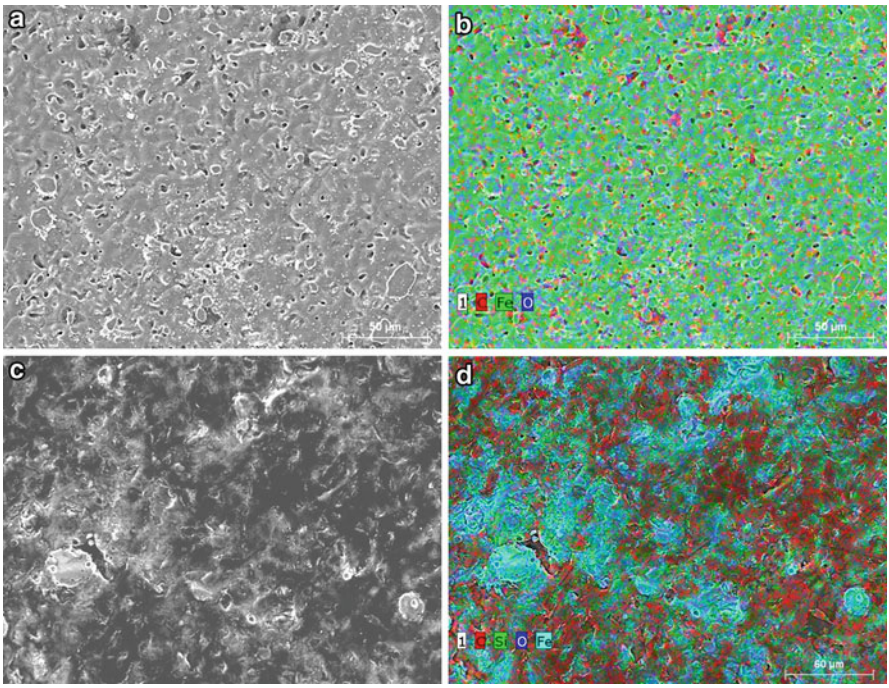

Fig. 7.22 Typical SEM images and elemental mapping of specimen surfaces before the tests. (**a**, **b**) Matrix alloy (Fe-0.6 wt% C); (**c**, **d**) composite Fe-0.6 wt% C + 3 wt% SiC

Figure 7.22 shows the typical SEM and elemental mapping images of the specimen surfaces before the tests. It is noticeable that the matrix alloy exhibited a slightly higher porosity. Moreover, the use of SiC as a precursor for the graphite nodules was notably efficient. In fact, the elemental mapping images clearly show large amounts of carbon (red regions) well distributed on the composites surfaces.

Figure 7.23 shows typical aspects of the surfaces after the tests and illustrates the wear mechanisms that acted on the specimens and counter-bodies. For the matrix alloy (Fig. 7.23a), the wear marks have smoother surfaces where third-body "islands" (arrow) are observed. Moreover, third-body islands are also visible in notably smooth and even counter-body worn surface, which are indicated with an arrow in Fig. 7.23b. The EDX analysis of these regions [76] shows that they are rich in oxygen.

Surprisingly, unlike the observation in the reference sample, composites with graphite nodules in the microstructure (3 and 5 wt% SiC) show strong evidence of plastic deformation, Fig. 7.23c, which is characterized by the presence of grooves parallel to the sliding direction, which indicates abrasive wear as the dominant wear mechanism. This aspect is even more evident in the wear marks of the counter-bodies, Fig. 7.23d.

A great quantity of wear debris was observed on the wear marks. Figure 7.24 shows the general aspect, morphology, and dimensions of the produced particles.

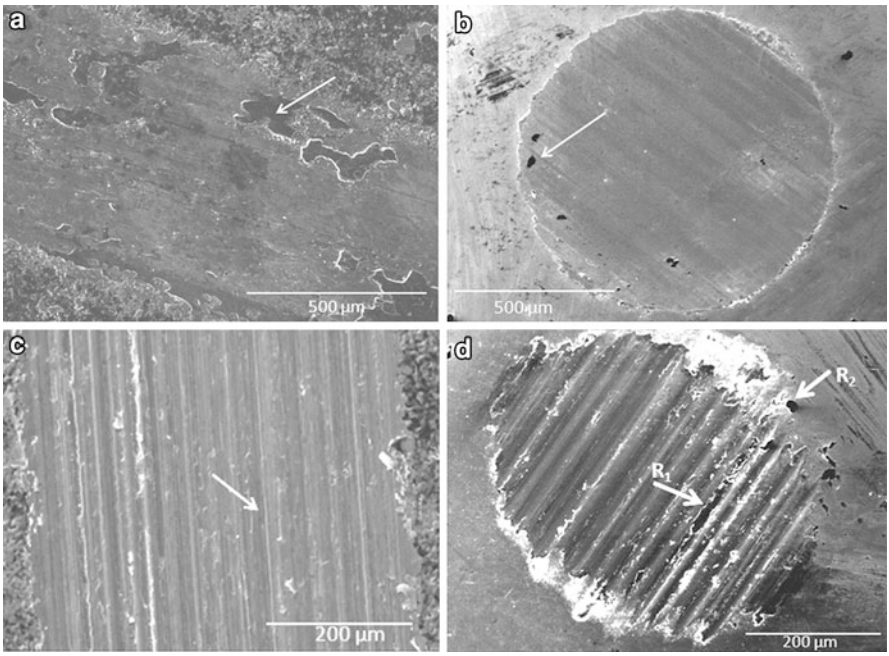

Fig. 7.23 Typical wear mechanisms. (**a**) Matrix alloy, specimen; (**b**) matrix alloy, counter-body; (**c**) 3 wt% SiC composite, specimen; (**d**) 3 wt% SiC composite, counter-body

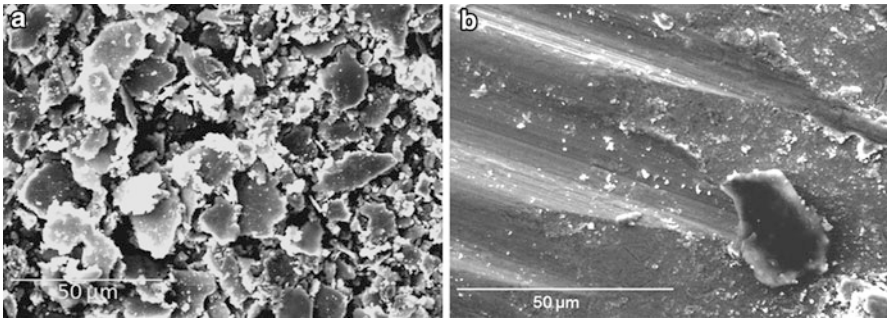

Fig. 7.24 Wear debris. (**a**) General aspect; (**b**) producing abrasion on the counter-body. Composite Fe-C- 3 wt% SiC

They consist primarily of carbon and oxygen, as evidenced by EDX. It is reasonable to assume that these particles actively operate in the abrasion process, as clearly shown in Fig. 7.24b.

The chemical composition analysis using EDX [76] in the regions indicated with arrows in Fig. 7.23 shows the presence of oxygen and an important carbon content in the wear mark of the samples. Even if the strong abrasion apparently does not allow for tribolayer formation, a significant amount of carbon (approximately 20 wt%) was

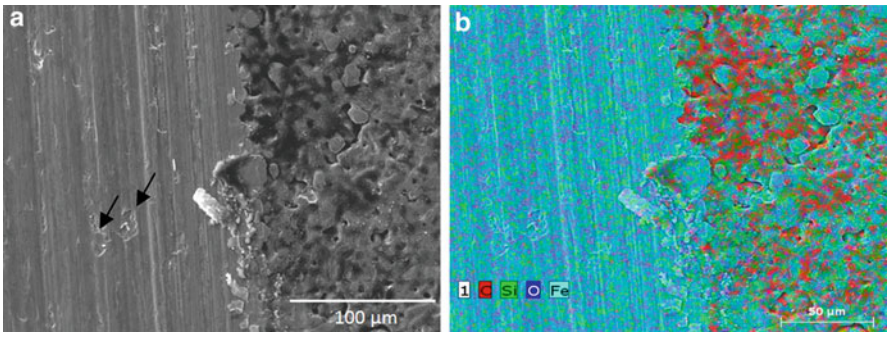

Fig. 7.25 Wear scar. (**a**) Typical aspect at the boundary; (**b**) X-ray map obtained using EDS. Composite Fe-C- 3 wt% SiC

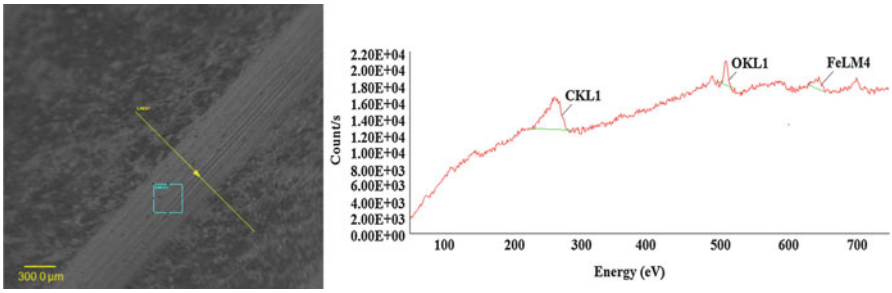

Fig. 7.26 Typical AES analysis. Fe-C- 3 wt% SiC composite

found in the wear mark of the counter-body (regions R_1 and R_2, Fig. 7.23d), which proves the existence of a carbon-rich material.

A high magnification analysis (Fig. 7.25a) shows a tenuous tribolayer that is fractured at various points.

By associating this image with the map of elements obtained using EDX (Fig. 7.25b), it is possible to verify that the contact is fuelled by carbon from the graphite nodules. Furthermore, oxygen is observed (dark blue region), which was expected because the tribological tests were performed in air.

To further understand this point, the wear scar of the 3 wt% SiC composite was analyzed using Auger electron spectroscopy (AES), Fig. 7.26.

Analyses in the wear scar confirmed that the tribolayer, which was formed during sliding, was composed of oxygen and predominantly carbon. In contrast, a similar analysis performed on the wear marks of the reference sample (matrix alloy) [76] showed the predominance of oxygen in the worn surface, which indicates the presence of oxides in the tribolayer.

To further understand the formation and degradation of the tribolayer, using the 3 wt% SiC composite as specimens, sliding tests were conducted and interrupted at predefined moments, corresponding to 100, 1000, and 2000 cycles.

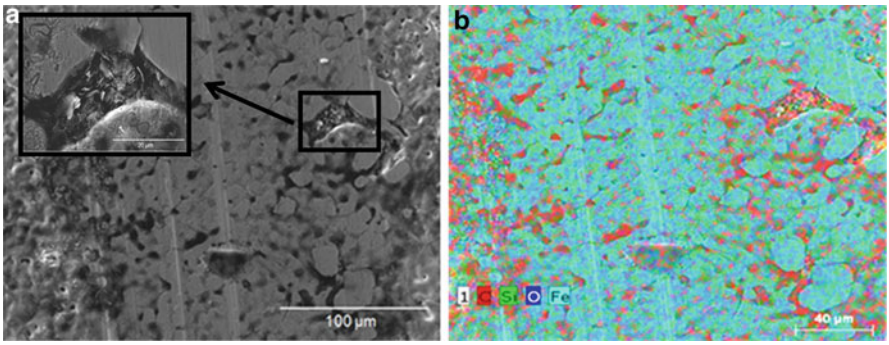

Fig. 7.27 Wear scar after 100 cycles: (**a**) SEM images and (**b**) elemental analyses

Figure 7.27 shows the typical aspects of the wear scar after 100 cycles.

The pores in the samples were filled with lamellar structures, as shown in the high-magnification inset in Fig. 7.27a. The elemental map shows that this material is rich in carbon, which was confirmed using the EDX analysis (~31 wt% C). It is reasonable to suppose that the graphite foils are removed from the in situ-generated graphite nodules and remain at the interface, which contributes to the formation of the protective tribolayer interface.

However, despite the presence of a few scratches, the surface of the counter-body had a large amount of carbon (~30 wt%), which indicates material transfer during the test and the early formation of a graphite-rich tribolayer at the contact interface, which maintained the region lubricated and reduced the coefficient of friction at the end of 100 sliding cycles.

The main features associated with longer test times (1000 and 2000 cycles) were pore closure and tribolayer degradation. Figure 7.28 illustrates the typical aspects of the wear scars after 1000 cycles.

The strong plastic deformation that led to the pore closure at the center of the wear scar was evidently associated with the tribolayer spalling. Additionally, EDS chemical analyses showed the presence of carbon and oxygen. Furthermore, the oxidation processes associated with tribochemical reactions contributed to the formation of oxide regions on the counter-body surface.

Effect of Surface Finishing

In this section, the influence of surface finishing (as sintered and polished) on the tribological behavior of MIM self-lubricating composites sintered at 1150 °C with (3 and 5% wt%) and without SiC additions is presented. The tribological behavior was analyzed using linear reciprocating sliding tests (constant load of 7 N, 60 min duration). Polishing of the specimens was performed manually with sand paper #1200, #2400, and #4000 in a polishing machine with automatic controls of time and rotation, for 10 min and 150 rpm. After polishing, the surface topography was characterized.

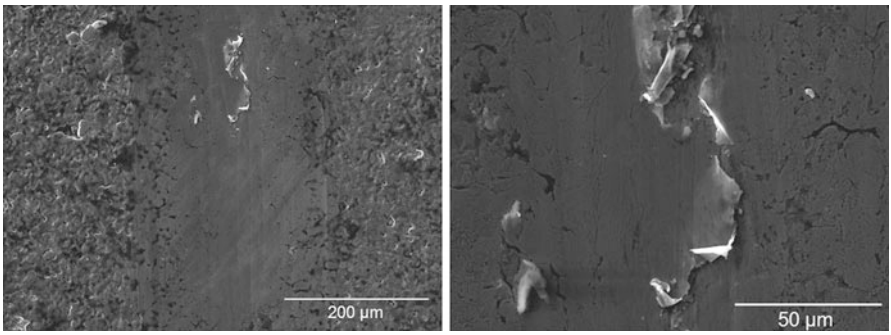

Fig. 7.28 Wear scar after 1000 cycles

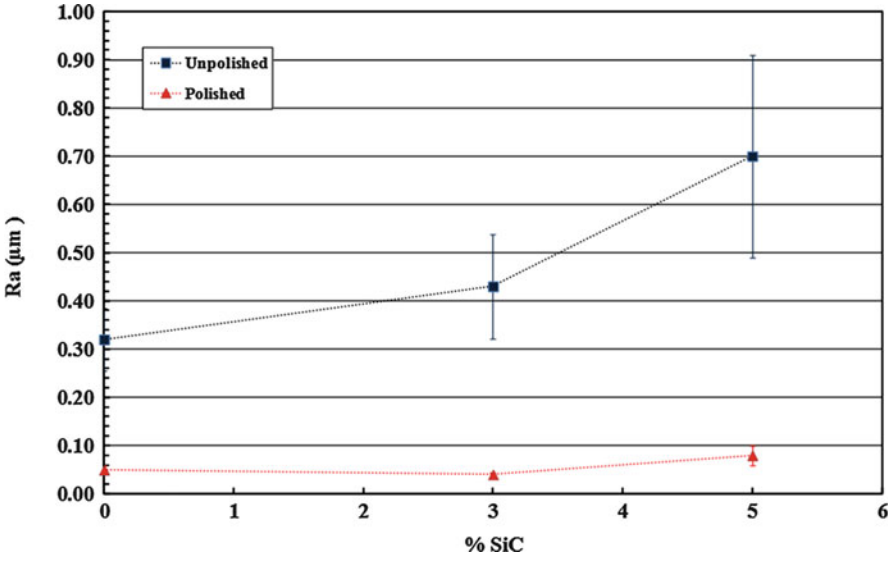

Fig. 7.29 Average surface roughness according to SiC content before and after polishing

The effect of SiC content on surface topography before and after polishing is illustrated in Fig. 7.29.

The mean surface roughness of unpolished samples increases significantly when the SiC content increases. Such behavior can be observed also for polished samples, but in a more subtle way. As already mentioned, the reference alloy presented a microstructure constituted of perlite + ferrite whereas the addition of SiC induces the formation of 2D turbostratic graphite nodules which in turn induced increased surface roughness. Thus, higher SiC contents increase the quantity of graphite nodules and, therefore, increase surface roughness. After polishing, a significant reduction of the average values of Ra is observed when compared with the values obtained for the unpolished samples.

Typical aspects of the surfaces before and after polishing are presented in Fig. 7.30.

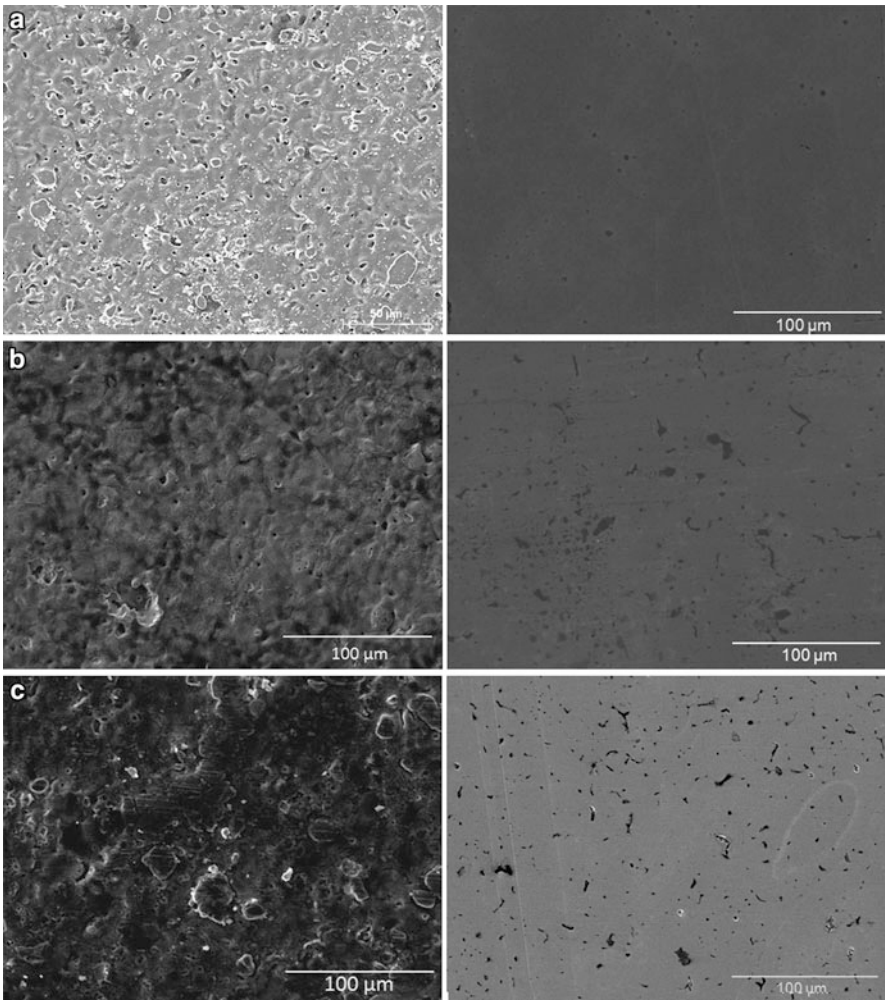

Fig. 7.30 Typical surfaces of unpolished surfaces (left) and polished (right) specimens. (**a**) 0 wt% SiC; (**b**) 3 wt% SiC and (**d**) 5 wt% SiC

It is clearly observed that after polishing the surfaces are smoother and feature dark regions constituted of graphite nodules and pores. From now on, these dark regions will be called lubricant reservoirs. Due to limitations of the technique used for image analysis already reported in the literature [59, 61], it was not possible to distinguish between pores and graphite nodules. The dark regions were previously identified as turbostratic 2D graphite. Compared with the polished surface of the reference sample (0 wt% SiC), the polished surfaces of specimens containing 3 and 5 wt% SiC presented increasing amounts of dark regions (pores + graphite nodules) evenly distributed on the surface.

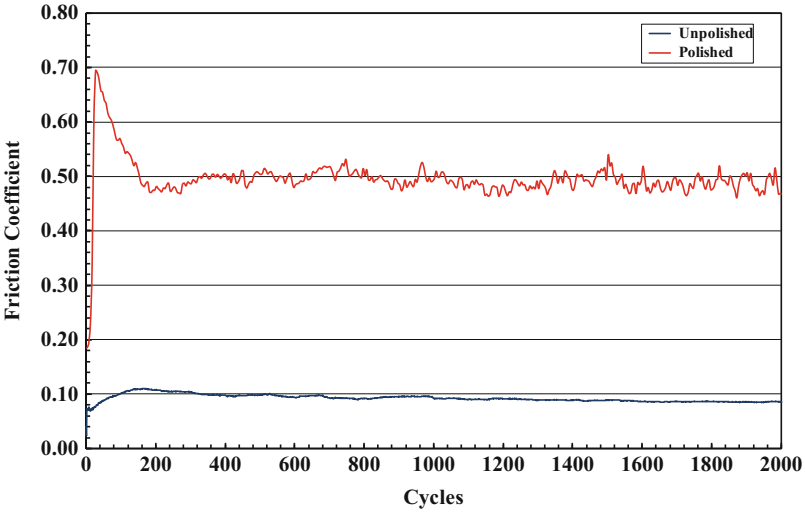

Fig. 7.31 Typical evolution of friction coefficient with number of cycles. 3 wt% SiC

Figure 7.31 shows how the evolution of the friction coefficient during the test duration is influenced by surface finishing.

All results present similar behavior. There is a transient associated with the onset of contact between specimen and counter-body at the beginning of tests before a steady state is reached. For the unpolished specimens, friction coefficient showed a rapid increase and stayed nearly constant during the rest of the test, i.e., a steady state was reached. For the polished specimens, after a rapid initial increase, friction coefficient starts to gradually decrease to a lower steady-state value.

As already discussed the reasons for the difference in the evolution of the friction coefficient within the transient period will not be treated in the present chapter. However, it is reasonable to suppose that the stabilization of the friction coefficient is related to the generation of a protective tribolayer, where the transient corresponds to the kinetics of formation of the layer. The values of the friction coefficient for each test were computed by averaging the steady-state values. The results are summarized in Fig. 7.32.

Increasing the precursor content and, as a consequence, the number of turbostratic 2D graphite nodules produced a reduction of the average friction coefficient. In general, the reduction was substantial, up to 3% SiC. For higher values of SiC content, the friction coefficient was almost constant. As already stated, the graphite foils are removed from the in situ-generated graphite nodules and remain at the interface thus contributing to the formation of the protective tribolayer.

Additionally, it is observed that the friction coefficient is strongly influenced by surface finish. Polished specimens exhibit significantly higher friction coefficients ($\mu > 0.4$) suggesting that the 2D turbostratic graphite nodules do not actively participate in the tribolayer formation. In fact, multielemental X-ray maps obtained

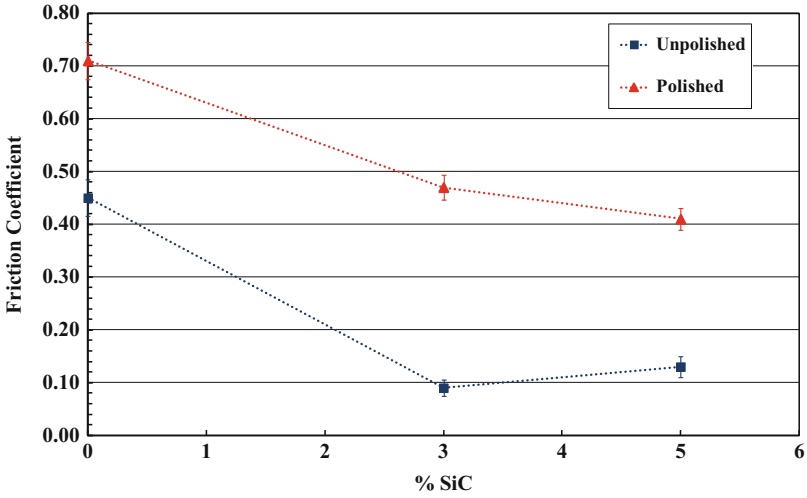

Fig. 7.32 Steady-state friction coefficient

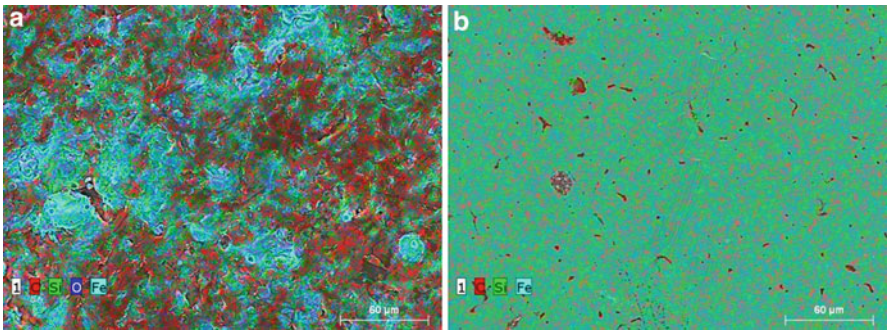

Fig. 7.33 Multielemental X-ray map obtained by EDS. Composite Fe-0.6% C-3% SiC. (**a**) Unpolished. (**b**) Polished

by EDS (Fig. 7.33), in which the red color is associated with carbon, clearly show a large decrease in the amount of graphite nodules for the polished surface.

Besides significantly reducing the surface roughness, as illustrated in Figs. 7.29 and 7.30, polishing also affected the availability of solid lubricant reservoirs in the active sliding interface. It is well known the paramount role played by pores (in our case pores + solid lubricant reservoirs) in the tribological behavior of sintered materials [39, 78].

In addition to a reduction in strength and, as a consequence, in load bearing capacity, the presence of porosity alone might influence the wear mechanisms acting on the surfaces of powder metallurgy parts in a number of ways. In particular, open pores in the active interface are reported to act as foci for the generation and trapping

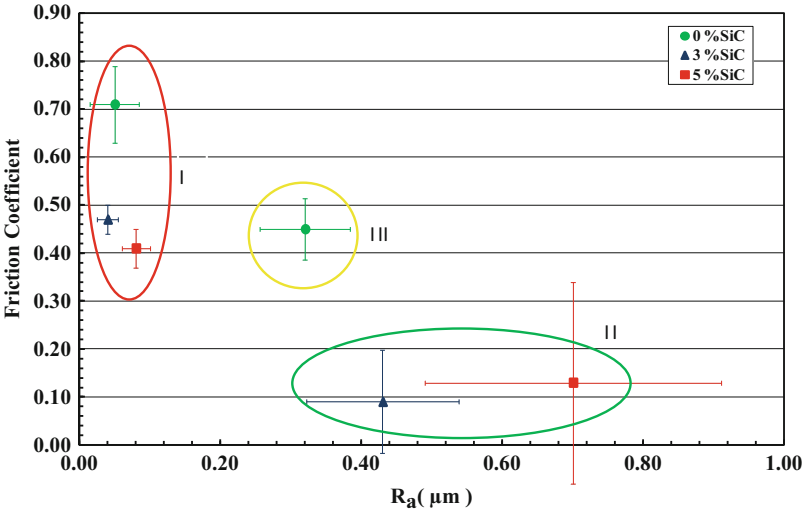

Fig. 7.34 Friction coefficient in function of surface roughness and SiC content

of wear debris during sliding wear [77]. If the reservoirs remain active (open), there will be a continuous self-replenishment of solid lubricants to the contact area and, as a consequence, the maintenance of a protective tribolayer [45]. The plastic deformation imposed by polishing induces the closure of pore + solid lubricants reservoirs, which significantly reduces the lubricant supply into the active interface. This justifies the high friction coefficient presented by the polished composites. Without a doubt, the closure of the reservoirs is an important factor in increasing friction coefficient of the composites containing SiC. On the other hand, it would not justify the increased friction coefficient also observed for the reference composites alloys (without SiC) since they do not contain graphite nodules. In this case, it is reasonable to suppose that the variation in friction coefficient is mainly due to changes in surface topography during polishing.

In addition, friction coefficient decreased when the amount of precursor (SiC) increased for both surface finishing routes. The reference specimen (0% SiC) presented a mean friction coefficient significantly higher than those of the samples containing 3% and 5% SiC. It is remarkable the positive influence of turbostratic 2D graphite nodules on the tribological behavior of these composites. For the case of the unpolished specimens, the addition of 3% SiC induced a remarkable 80% reduction in friction coefficient.

There is a compromise between surface topography and solid lubricant availability in the active interface. Figure 7.34 shows the average friction coefficient as a function of roughness. Three regions are highlighted in Fig. 7.34: The first region (I) consists of the polished samples (0%, 3%, and 5% SiC); the second region (II) is associated with unpolished samples containing 2D turbostratic graphite nodules (3% and 5% SiC), and finally, the third region (III) concerns the unpolished reference alloy (0% SiC).

The polished samples, regardless of the chemical composition, showed higher friction coefficients and obviously low roughness when compared with the unpolished ones. On the other hand, the unpolished composites (region II) presented higher roughness associated with lower friction coefficient. Also noteworthy is the unpolished reference alloy behavior (region III): It presents intermediate values for both roughness and friction coefficient, suggesting the already mentioned compromise between surface topography and solid lubricant availability in the active interface suggesting that the presence of 2D turbostratic graphite nodules affects the surface topography of the samples and has a great influence on the dynamics of the formation of protective tribolayers, and consequently on wear mechanisms [69, 78]. In fact, the polished samples, regardless of the chemical composition, presented very low values of reduced valley height (Rv) (0.1–0.18 μm) when compared with the unpolished ones (0.67–1.51 μm). Since Rv is related to the distribution of valleys or pores in a surface [79], this evidences the closure of pores + solid lubricant reservoirs during polishing.

According to Keller et al. the difference in surface topography has an important impact on wear mechanisms and building up of tribolayers [79]. A rough surface, i.e., small real contact area or high real contact pressure, leads to higher friction coefficients and wear [79]. However, despite being considerably rougher than the polished specimens, the unpolished specimens presented significantly lower friction coefficients, pointing to an important participation of the turbostratic graphite nodules in the lubrication process. It appears that during sliding, due to the high contact pressure, the formation of the protective tribolayer occurs rapidly in the initial cycles, preventing direct metal-metal contact, and thus maintaining low friction coefficients. If the reservoirs remain active (open), there will be a continuous self-replenishment of solid lubricants to the contact area and, as a consequence, the maintenance of a protective tribolayer as illustrated in Fig. 7.35 which shows a kind of self-healing feature of the tribolayer. Whenever the normal force is increased (black curve) there is a partial destruction of the tribolayer as indicated by the sharp decrease in electrical potential of the contact. Immediately, the tribolayer is reestablished as clearly indicated by the rapid increase in electrical potential of the contact.

Figure 7.36 presents the influence of the precursor content and of the specimen surface finish on the wear rates of the specimens and their respective counter-bodies.

The influence of surface finish was marginal for the reference alloys (0% SiC). However, for the composites (3% and 5% SiC), the unpolished specimens exhibited significantly lower wear rates compared to the polished samples, Fig. 7.36a.

The counter-bodies (Fig. 7.36b) presented much higher wear rates when siding against the polished surfaces, being this even more significant for the reference alloy (0% SiC). The absence of graphite nodules associated with the smooth surface topography of the reference samples promoted an increased wear of the specimen and respective counter-bodies. Polishing, besides modifying the surface topography of the sample, promoted the closure of the pores and of the graphite reservoirs as already described. This resulted in increased friction coefficient and wear rates for both sides of the tribo pair.

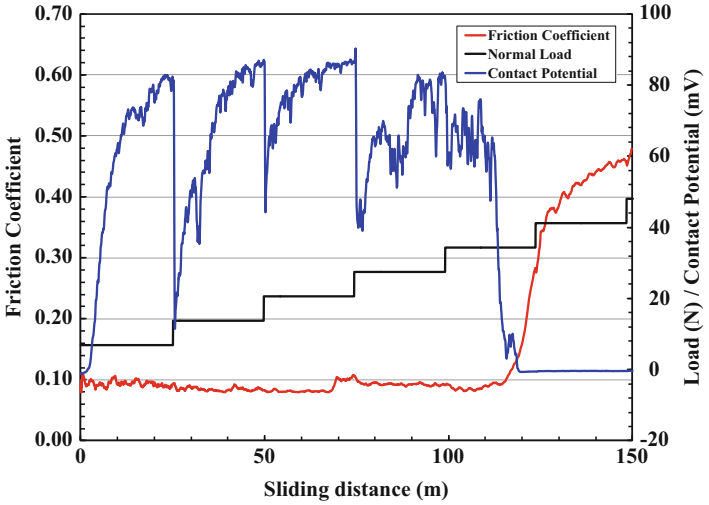

Fig. 7.35 Self-healing of the tribolayer

Typical aspects of the wear scars of specimens and counter-bodies associated with polished specimens are shown in Fig. 7.37. In both cases, there are clear indications of abrasive wear. For the reference alloy, analysis by EDX in selected areas indicated a strong presence of oxygen in the active interface of both specimens (30%) and counter-bodies (14%), a clear evidence of oxidative wear [76].

Abrasive wear evidence is even more visible in wear scars associated with specimens rich in 2D turbostratic graphite, Fig. 7.38.

Moreover, EDX analysis indicated the presence of a protective tribolayer in the wear scars of both specimen and counter-body, as indicated by the higher amounts of carbon (specimen: 9%; counter-body: 14%) in relation to the reference alloy.

Again, a great quantity of wear debris was observed on the wear marks. Elemental analysis by EDX of the wear debris [76] showed that the debris generated for the reference alloy have higher oxygen content than the debris produced by the composites containing 2D turbostratic graphite nodules which, in turn, are richer in carbon. During sliding in air, oxygen reacts at the contact interface giving rise to a tribolayer that forms and breaks down cyclically. For the reference alloys, the rupture of this tribolayer gives rise to wear debris consisting mainly of iron and oxygen. The debris originated from the composites, in addition to iron and oxygen, also present, as expected, a significant amount of carbon, since the graphite nodules actively participate in lubrication of the contact interface, thereby justifying the low friction coefficients and wear rates measured for the unpolished samples.

Effect of the Metallic Matrix

Apart from contributing to the formation and degradation of the tribolayer, the microstructure of the metallic matrix always has large influence on the tribological

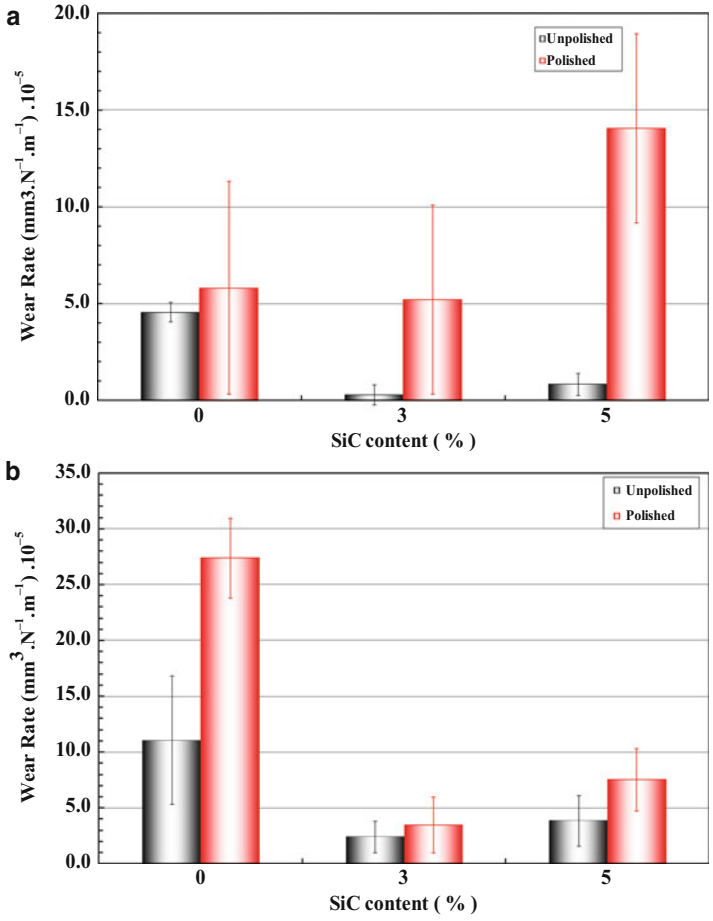

Fig. 7.36 Wear rate. (**a**) Specimens. (**b**) Counter-bodies

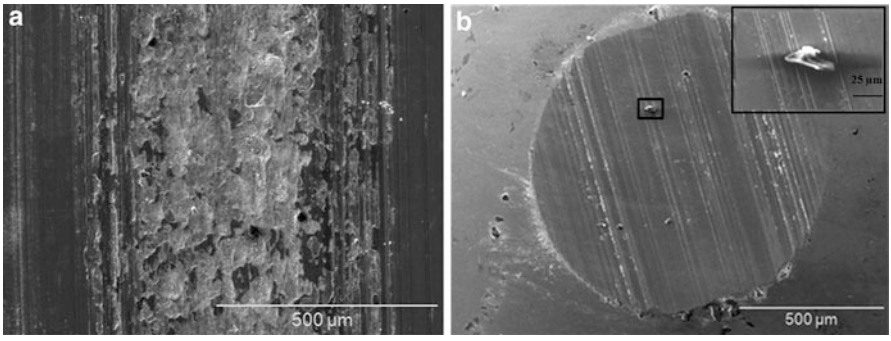

Fig. 7.37 Typical aspects of the wear scars. Reference alloy (0% SiC) (**a**) polished specimen. (**b**) Counter-body

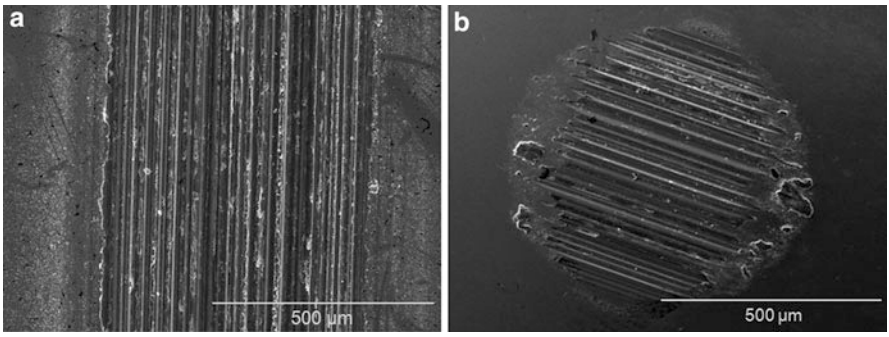

Fig. 7.38 Typical aspects of the wear scars. 3% SiC composite (**a**) polished specimen. (**b**) Counterbody

behavior of any material. According to Zum Gahr [80], when considering wear, the best tribological behavior of a metallic material is reached by combining the most appropriate combination of strength, ductility, and fracture toughness.

In this section, the effect of the metallic matrix composition on the formed microstructural constituents, as well as their effect on the tribomechanical behavior of plasma-assisted debinded and sintered MIM self-lubricating composites is presented and discussed. Three different metal matrices containing embedded 2D turbostratic graphite nodules were obtained by adding alloying elements (Ni and Ni + Mo) to the initial composition of the Fe-C-SiC composite.

Figure 7.39 illustrates the typical microstructures of the studied composites.

All composites were prepared by mixing 3% SiC to the feedstock and were sintered at 1150 °C for 1 h. All three microstructures have in common the presence of graphite nodules (arrows), induced by the addition of SiC to the feedstock powder, whereas for the present imposed conditions, the metallic matrix varies from ferrite to martensite. Addition of Nickel did not substantially change the microstructural constituents (ferrite + small fractions of perlite), Fig. 7.39b, but it seems that the graphite nodules are a little larger and in greater quantities than in the standard Fe-C-composites. For the Ni + Mo containing composite, the metallurgical constituents changed from ferrite/perlite to martensite even under the low cooling rates imposed by the PADS reactor (7 °C/min). The addition of these elements probably dislocated the TTT curve of this steel, favoring the formation of martensite [81].

Figure 7.40 summarizes the mechanical properties of the composites.

They were evaluated by measuring the micro-hardness of the metallic matrix and the tensile resistance of the composite (elongation, yield strength, and ultimate strength). It is possible to observe that even with the presence of solid lubricant nodules in the metallic matrices, the level of resistance for the composites is very high. This occurs because the nodules of graphite are very small (less than 20 µm) and they are homogeneously dispersed throughout the ferrous matrix thus preserving the matrix continuity.

As expected, the addition of alloying elements produced a strong effect on the hardness and mechanical strength of the matrices. Nickel increases the resistance of

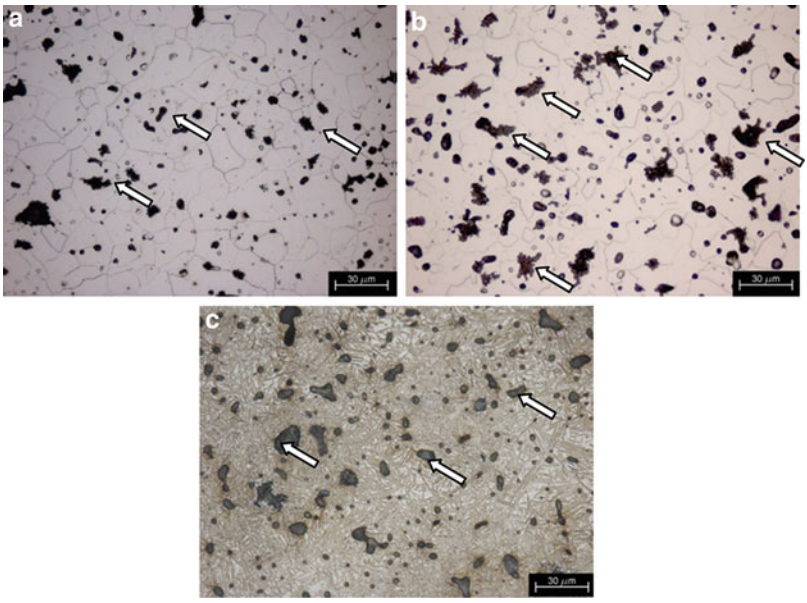

Fig. 7.39 Typical microstructure of self-lubricating composites produced by adding 3% SiC. (**a**) Fe + 0.6%C. (**b**) Fe + 0.6%C + 4.0%Ni. (**c**) Fe + 0.6%C + 4.0%Ni + 1.0%Mo

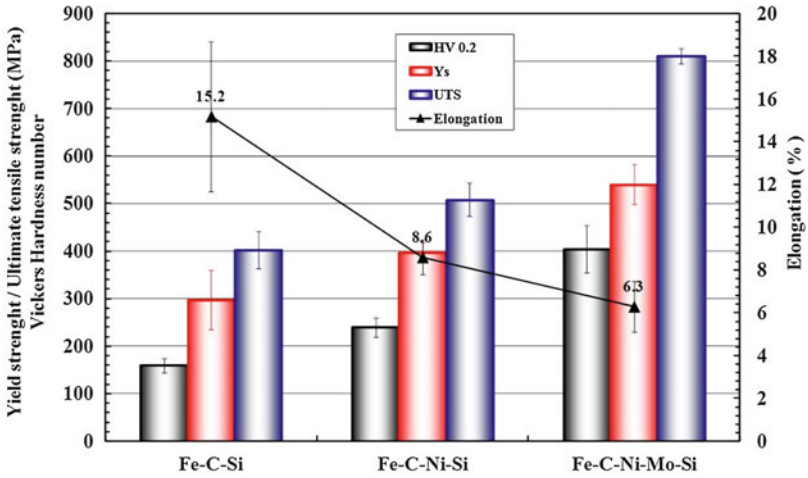

Fig. 7.40 Mechanical properties

the composites by solid solution and partially reduces its ductility in relation to the standard Fe-C composite. The combination of Ni + Mo induces a large increase in mechanical resistance because it changes the metallurgical microstructure from ferrite/perlite to martensite. As explained earlier, the martensite transformation

occurs for the Fe-C-Ni-Mo even under low cooling rates. As expected, the elongation behaved in a contrary manner.

It is worth noting that UTS values as high as 1000 MPa were reported for the Ni + Mo containing composite when sintered at 1200 °C [61]. A possible factor for such an increase in mechanical properties was the higher homogenization obtained at higher temperatures. It is very well known that the diffusion rates are enhanced with temperature. Furthermore, at 1200 °C, liquid phase sintering may occur, thus producing a better chemical homogenization and densification.

It might also be interesting to point out that the UTS of self-lubricating composites available on the market do not normally exceed 300 MPa. This is a result of the large discontinuity of the metallic matrix produced by the addition of up to 40% of large solid lubricant particles which are necessary to keep friction at low levels.

The friction coefficient of the reference composite (Fe-C) gradually increases with the sliding distance until, at about 100 m, it evolves in a more uniform and constant way. For the composites containing nickel and molybdenum, the friction coefficient evolves in a more stable way from the beginning of the test. Although presenting a significantly lower average value, the evolution alternates low and high intensities periods. Furthermore, a higher oscillation of the contact potential was verified, indicating instability of the insulating tribolayer. The Ni-containing composites presented a similar evolution at values in between those of the reference composite and that of the Ni-Mo composites [82].

The effect of metallic matrix composition on the steady-state friction coefficient is presented in Fig. 7.41.

The reference composite, Fe-C, presented the highest friction coefficient (0.11). The addition of alloying elements considerably reduced the friction coefficient (45% reduction for the Ni composites) and values as low as 0.04 (65% reduction) for the Fe-C-Ni-Mo composites. This remarkably low value may be considered superlubricity in the real world.

Figure 7.42 illustrates the general appearance of the wear scars produced in both specimens and counter-bodies.

Wear scars associated with the specimens presented different widths and the general appearance of the wear marks also varied. The wear volume was reduced by the introduction of the alloying elements. Inside the wear scar there is a clear evidence of abrasive wear, as evidenced by the presence of multiple parallel scratches. The intensity and number of scratches varied according to the material. The wear loss of the counter-bodies (AISI 52100 steel ball) presented the same behavior as the specimens. The wear rate of specimens and counter-bodies is summarized in Fig. 7.43.

The lowest wear rate value determined was 8.29×10^{-6} mm^3 N^{-1} m^{-1} for the Fe-C-Ni-Mo composites whereas the highest wear rate was measured for the reference composite (Fe-C), 34.5×10^{-6} mm^3 N^{-1} m^{-1}. This corresponded to a 420% reduction. For the nickel composites (14.5×10^{-6} mm^3 N^{-1} m^{-1}), the reduction was 240% in relation to the reference composite. In all cases, the wear rate of the ball was almost identical [(9.47; 19.31 and 37.22) $\times 10^{-6}$ mm^3 N^{-1} m^{-1}, respectively] which induced the same order of magnitude in wear reduction.

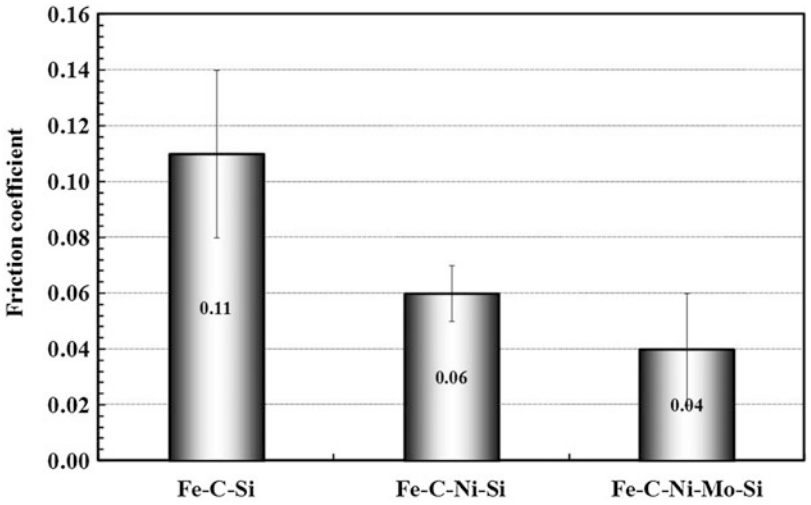

Fig. 7.41 Steady-state friction coefficient

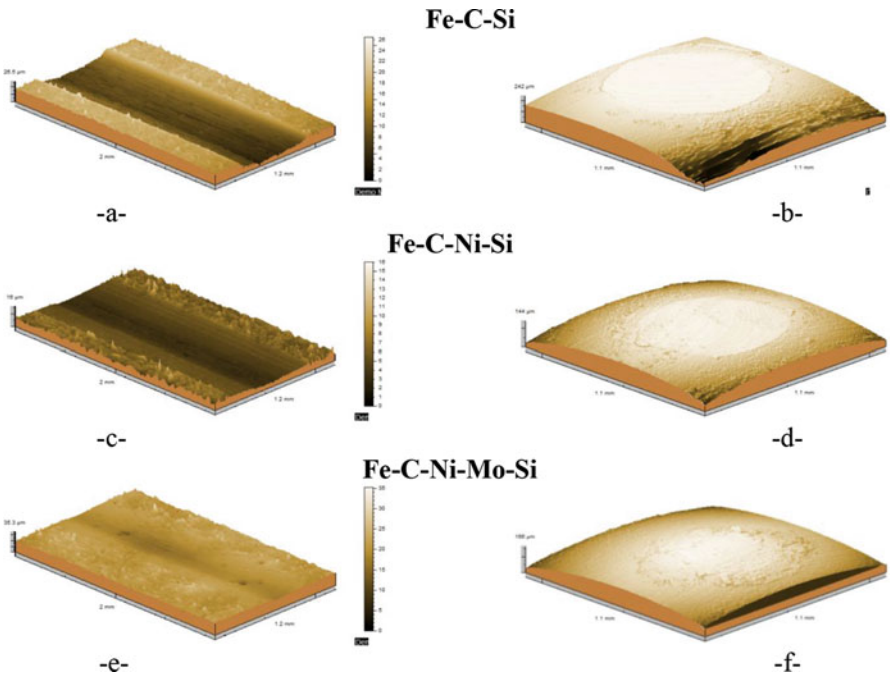

Fig. 7.42 Typical aspects of the wear scars obtained by laser interferometry. Composite Fe-C-Si, (**a**) specimen, (**b**) counter-body. Composite Fe-C-Ni-Si, (**c**) specimen, (**d**) counter-body. Composite Fe-C-Ni-Mo-Si, (**e**) specimen, (**f**) counter-body

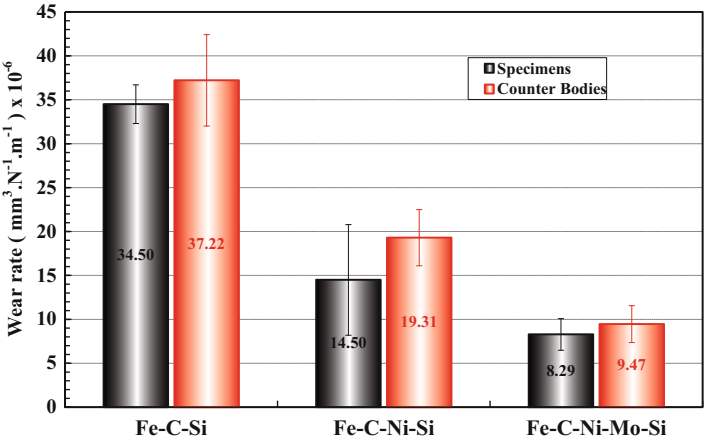

Fig. 7.43 Wear rate of the self-lubricating composite and AISI 52100 steel ball

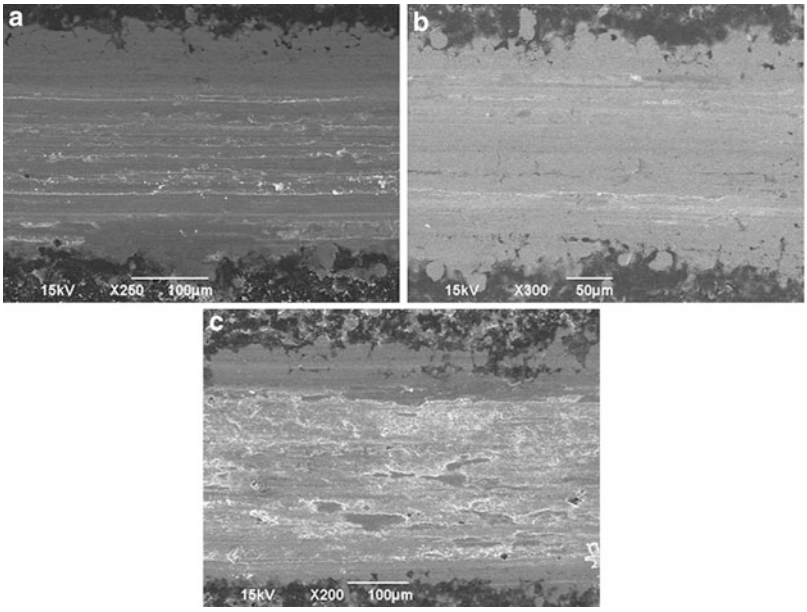

Fig. 7.44 General appearance of the wear scars. (**a**) Fe-C. (**b**) Fe-C-Ni. (**c**) Fe-C-Ni-Mo

Figure 7.44 illustrates the general appearance of the wear scars produced.

Wear mechanisms acting on the reference composite and on the nickel-containing composite are quite similar: Abrasive wear is present as indicated by the fine scratches in the sliding direction. The intensity and number of scratches varies according to the material. The shallow, thinner, and less numerous scratches are present in Fe-C-Ni specimens. They are probably caused by the abundant hard,

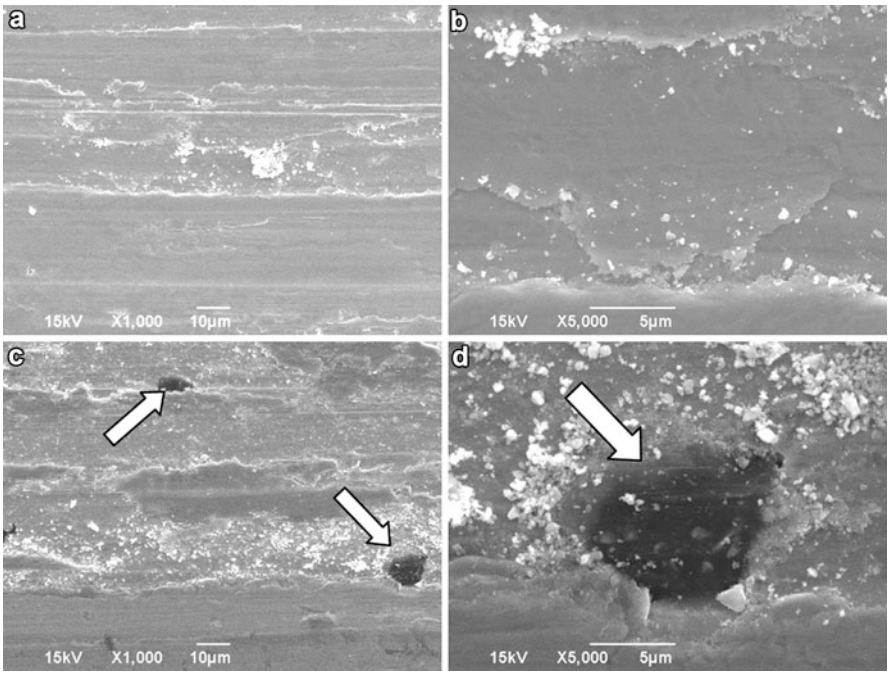

Fig. 7.45 Selected appearance of the wear scars. (**a**, **b**) Fe-C-Si composite. (**c**, **d**) Fe-C-Ni-Mo-Si composite

oxidized wear debris generated at the interface. On the other hand, for the nickel-molybdenum composite the tribological conditions produced smoother surfaces where third-body "islands" were observed.

This behavior might be linked to the resistance of the metallic matrix to plastic deformation and consequently, to the sealing of lubricant reservoirs, Fig. 7.45.

For the higher friction coefficient and wear rate specimens (Fe-C composites, Fig. 7.45a, b), the intense plastic deformation produces the complete closure of the solid lubricant reservoirs, whereas for the lower friction coefficient and wear rates (Fe-C-Ni-Mo composites, Fig. 7.45c, d), the solid lubricant reservoirs remains open and active (white arrow).

If the solid lubricant particles do not reach the surface, the self-replenishment mechanism of the tribofilm is partially restrained and the friction coefficient remains relatively high.

In order to further understand the effect of the metallic matrix on the tribolayer (and, as a consequence, on the tribological behavior), the wear scars present on the specimens and counter-bodies were analyzed by micro-Raman spectroscopy. Figure 7.46 synthesizes these results.

Again, only the borderline results are presented: Fe-C samples (higher friction coefficient and wear rates) and Fe-C-Ni-Mo composites (lower friction coefficient and wear rates).

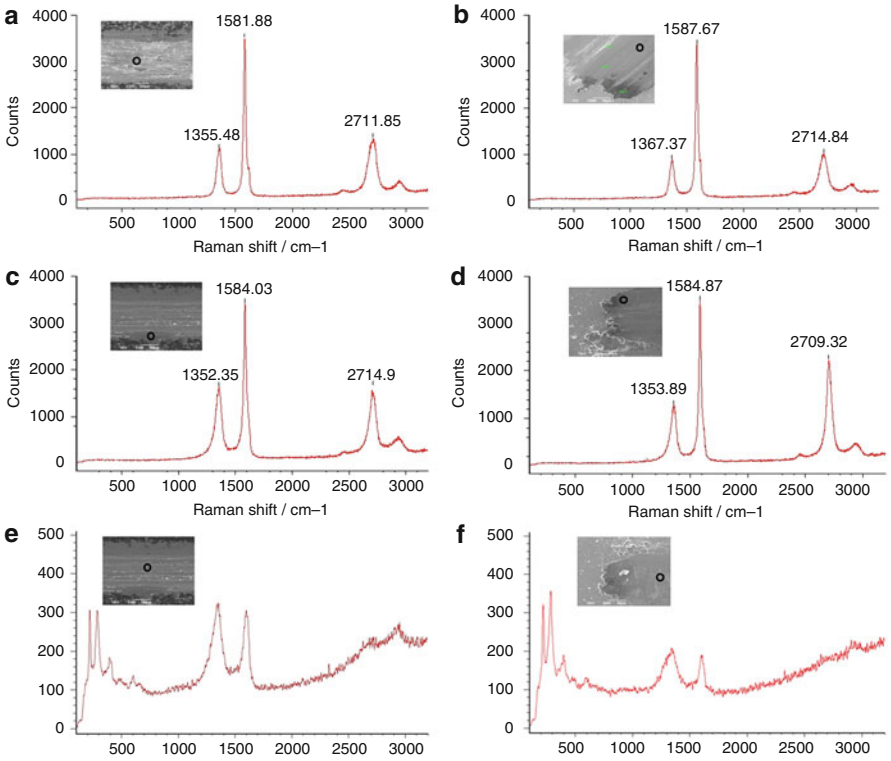

Fig. 7.46 Typical Raman spectra. (**a**) Fe-C-Ni-Mo specimen. (**b**) Fe-C-Ni-Mo counter-body. (**c**) Fe-C specimen, border of the scar. (**d**) Fe-C counter-body, border of the scar. (**e**) Fe-C specimen, center of the scar. (**f**) Fe-C counter-body, center of the scar

Figure 7.46a, b present the dominant spectra found in the wear scar of the Fe-C-Ni-Mo composite. All spectra clearly show the presence of the so-called turbostratic 2D graphite as evidenced by the typically widened G band and the presence of a D band which is associated with crystallinity disorder. The measured widening of the bands, the ID/IG ratio, the size of the graphite crystallites, and the analysis of the second-order band G′ also confirm the disorder in the material. It is also noticeable that the spectra of tribolayers presented in the wear scars of the specimens or in the counter-bodies are almost identical and indicate the beneficial presence of the turbostratic 2D graphite on both sides of the tribo pair.

On the contrary, the spectra found in the wear track of the reference composite changed according to their position in the wear scar. Spectra similar to those found in the previous case were measured near the border of the wear scars, Fig. 7.46c, d whereas those found in the center of the scar were a little different, Fig. 7.46e, f. Despite presenting lower intensities of the 2D graphite characteristic bands and a certain amount of fluorescence, the spectra also presented other smaller bands at lower frequencies. The origin of these bands was attributed [13] to the formation of

Table 7.1 Relevant properties

Property		MIM + PADS + In situ
Scuffing resistance [N m]		8000
Friction coefficient		0.04
Wear rate $[mm^3\ N^{-1}\ m^{-1}] \cdot 10^{-6}$	Specimen	8.28
	Counter-body	9.47
Ultimate tensile strength [Mpa]		500
Elongation [%]		6.3

iron oxide by tribochemical reaction caused by the surrounding atmosphere and is, probably, a consequence of the high energy availability associated with high friction coefficients. The positions of the bands in the range of 225–650 cm^{-1} match fairly well those observed for iron oxide phases [83].

The bands at 290, 408, 497, and 607 cm^{-1} indicated the presence of hematite Fe_2O_3 whereas the band at 667 cm^{-1} was assigned to magnetite Fe_3O_4 [84–86]. It is reasonable to suppose that the presence of iron oxides associated with the smaller intensities of the graphitic phase is likely to induce inferior tribological performance.

7.8 Concluding Remarks

We introduced a new microstructural model/processing route (metal injection molding followed by a single thermal cycle using a plasma-assisted debinding and sintering process and in situ formation of graphite nodules due to the dissociation of a precursor (SiC particles)). The results clearly show the great tailoring ability of the proposed microstructural model/processing routes applied to the development of innovative, low-cost, self-lubricating composites presenting low friction coefficient associated with high mechanical strength and wear resistance. Moreover, the optimized processing parameters produced outstanding new iron-based self- lubricating composites as illustrated in Table 7.1.

References

1. Cannaday, M.L., Polycarpou, A.A.: Tribology of unfilled and filled polymeric surfaces in refrigerant environment for compressor application. Tribol. Lett. **19**, 249–262 (2005)
2. Demas, N.G., Polycarpou, A.A.: Tribological investigation of cast iron air-conditioning compressor surfaces in CO_2 refrigerant. Tribol. Lett. **22**(3), 271–278 (2006)
3. Lee, Y.Z., Oh, S.D.: Friction and wear of the rotary compressor vane–roller surfaces for several sliding conditions. Wear. **255**, 1168–1173 (2003)
4. Solzak, T.A., Polycarpou, A.A.: Tribology of WC/C coatings for use in oil-less piston-type compressors. Surf. Coat. Technol. **201**, 4260–4265 (2006)
5. Pergande, S.R., Polycarpou, A.A., Conry, T.F.: Nanomechanical properties of aluminum 390-T6 rough surfaces undergoing tribological testing. J. Tribol. Trans. ASME. **126**, 573–582 (2004)

6. Oliveira Jr., M.M., Hammes, G., Binder, C., Klein, A.N., de Mello, J.D.B.: Solid lubrication in fluid film lubrication. Lubrication Science. **30**, 102–115 (2018)
7. Lancaster, J.K.: Solid lubricants. In: Booser, E.R. (ed.) CRC Handbook of Lubrication: Theory and Practice of Tribology Theory and design, vol. II, pp. 269–290 (1). CRC Press, Boca Raton (1984)
8. Sliney, H.E.: Solid lubricant materials for high temperatures: a review. Tribol. Int. **15**, 293–302 (1982)
9. Lansdown, A.R. Molybdenum disulphide lubrication. In: Dowson, D. (Ed.) Tribology series, vol. 35. Elsevier, Amsterdam (1999)
10. Brookes, C.A., Brookes, E.J.: Diamond on perspective. A review of mechanical properties of natural diamond. Diamond Relat. Mater. **1**, 13–17 (1991)
11. Donnet, C., Erdemir, A.: Historical developments and new trends in tribological and solid lubricant coatings. Surf. Coat. Technol. **180/181**, 76–84 (2004)
12. De Mello, J.D.B., Binder, R.: A methodology to determine surface durability in multifunctional coatings applied to soft substrates. Tribol. Int. **39**, 769–773 (2006)
13. De Mello, J.D.B., Binder, R., Demas, N.G., Polycarpou, A.A.: Effect of the actual environment present in hermetic compressors on the tribological behaviour of a Si rich multifunctional DLC coating. Wear. **267**, 907–915 (2009)
14. Bhushan, B. (ed.): Modern Tribology Handbook, vol. II. CRC Press, Boca Raton (2001)
15. Erdemir, A.: In: Bhushan, B. (ed.) Modern Tribology Handbook, vol. II, pp. 787–825. CRC Press, Boca Raton (2001)
16. Kimura, Y., Wakabayashi, T., Okada, K., Wada, T., Nishikawa, H.: Boron nitride as a lubricant additive. Wear. **232**, 199–206 (1999)
17. Erdemir, A.: Review of engineered tribological interfaces for improved boundary lubrication. Tribol. Int. **38**(3), 249–256 (2005)
18. Rapoport, L., Feldman, Y., Homyonfer, M., Cohen, H., Sloan, J., Hutchison, J.L., Tenne, R.: Inorganic fullerene-like material as additives to lubricants: structure-function relationship. Wear. **225–229**, 975–982 (1999)
19. Joly-Pottuz, L., Dassenoy, F., Belin, M., Vacher, B., Martin, J.M., Fleischer, N.: Ultralow-friction and wear properties of IF-WS_2 under boundary lubrication. Tribol. Lett. **18**(4), 477–485 (2005)
20. Tontini, G., Semione, G.D.L., Bernardi, C., Binder, R., de Mello, J.D.B., Drago, V.: Synthesis of nanostructured flower-like MoS_2 and its friction properties as additive in lubricating oils. Indust. Lubr. Tribol. **68**(6), 658–664 (2016)
21. Pacheco, F.G., Oliveira Jr, M.M., Santos, A.P., Costa, H.L., de Mello, J.D. B., Furtado, C.A.: Tribological evaluation of carbon nanotubes as additives in palm biolubricants. Submitted to Lubricants (2017)
22. Pauleau, Y., Thièry, F.: Deposition and characterization of nanostructured metalycarbon composite films. Surf. Coat. Technol. **180–181**, 313–322 (2004)
23. Erdemir, A.: Review of engineered tribological interfaces for improved boundary lubrication. Tribol. Int. **38**, 249–256 (2005)
24. Kato, H., Takama, M., Iwai, Y., Washida, K., Sasaki, Y.: Wear and mechanical properties of sintered copper–tin composites containing graphite or molybdenum disulfide. Wear. **255**, 573–578 (2003)
25. Dangsheng, X.: Lubrication behaviour of Ni–Cr-based alloys containing MoS_2 at high temperature. Wear. **251**, 1094–1099 (2001)
26. Huang, C., Du, L., Zhang, W.: Effects of solid lubricant content on the microstructure and properties of NiCr/Cr_3C_2–BaF_2·CaF_2 composite coatings. J. Alloys Compd. **479**, 777–784 (2009)
27. Zhu, S., Bi, Q., Yang, J., Liu, W., Xue, Q.: Effect of particle size on tribological behaviour of Ni_3Al matrix high temperature self-lubricating composites. Tribol. Int. **44**, 1800–1809 (2011)
28. Reeves, C.J., Menezes, P.L., Lovell, M.R., Jen, T.C.: The influence of surface roughness and particulate size on the tribological performance of bio-based multi-functional hybrid lubricants. Tribol. Int. **88**, 40–55 (2015)

29. Zhang, D., Lin, P., Dong, G., Zen, Q.: Mechanical and tribological properties of self-lubricating laminated composites with flexible design. Mater. Des. **50**, 830–838 (2013)
30. Burris, D.L., Sawyer, W.G.: A low friction and ultra-low wear rate PEEK/PTFE composite. Wear. **261**, 410–418 (2006)
31. Ouyang, J.H.: Microstructure and tribological properties of $ZrO_2(Y_2O_3)$ matrix composites doped with different solid lubricants from room temperature to 800 °C. Wear. **267**, 1353–1360 (2009)
32. Chen, B., Bi, Q., Yang, J., Xia, Y., Hao, J.: Tribological properties of solid lubricants (graphite, h-BN) for Cu-based P/M friction composites. Tribol. Int. **41**, 1145–1152 (2008)
33. Moghadam, A.D., Omrani, E., Menezes, P.L., Rohatgi, P.K.: Mechanical and tribological properties of self-lubricating metal matrix nanocomposites reinforced by carbon nanotubes (CNTs) and graphene: a review. Compos. Part B Eng. **77**, 402–420 (2015)
34. Tsuya, Y., Shimura, H., Umeda, K.: A study of the properties of copper and copper- tin base self-lubricating composites. Wear. **22**, 143–162 (1972)
35. Liu, E.R., Wang, W., Gao, Y., Jia, J.: Tribological properties of Ni-based self-lubricating composites with addition of silver and molybdenum disulfide. Tribol. Int. **57**, 235–241 (2013)
36. Binder, C., Hammes, G., Schroeder, R.M., Klein, A.N., de Mello, J.D.B., Binder, R.: 'Fine tuned' steels point the way to focused future. Met. Powder Rep. **65**, 29–37 (2010)
37. Mahathanabodee, S., Palathai, T., Raadnui, S., Tongsri, R., Sombatsompop, N.: Effects of hexagonal boron nitride and sintering temperature on mechanical and tribological properties of SS316L/h-BN composites. Mater. Des. **46**, 588–597 (2013)
38. de Mello, J.D.B., Binder, R., Klein, A.N., Hutchings, I.M.: Effect of compaction pressure and powder grade on microstructure and hardness of steam oxidised sintered iron. Powder Metall. **44**, 53–61 (2001)
39. de Mello, J.D.B., Hutchings, I.M.: Effect of processing parameters on the surface durability of steam-oxidized sintered iron. Wear. **250**, 435–448 (2001)
40. Ahn, H.S., Kim, J.Y., Lim, D.S.: Tribological behaviour of plasma-sprayed zirconia. Wear. **203**, 77–87 (1997)
41. PM Design Center of Metal Powder Industries Federation: Conventional Powdered Metal Components, 17 p (2012)
42. Tamura, S., Aizawa, T., Mitzuno, T., Kihara, J.: Steel powder compaction analysis. Int. J. Powder Metall. **34**, 50–59 (1998)
43. Al-Qureshi, H.A., Galiotto, A., Klein, A.N.: On the mechanics of cold die compaction for powder metallurgy. J. Mater. Process. Technol. **166**, 135–143 (2005)
44. Pavanati, H.C., Maliska, A.M., Klein, A.N., Muzart, J.L.R.: Comparative study of porosity and pores morphology of unalloyed iron sintered in furnace and plasma reactor. Mater. Res. **10**(1), 87–93 (2007)
45. Hammes, G., Schroeder, R.M., Binder, C., Klein, A.N., de Mello, J.D.B.: Effect of double pressing/double sintering on the sliding wear of self-lubricating sintered composites. Tribol. Int. **70**, 119–127 (2014)
46. Milligan, D., et al.: Materials properties of heat treated double pressed/sintered P/M steels in comparison to warm compacted/sinterhardened materials. In: PM^2TEC Advances in Powder Metallurgy and Particulate Materials, vol. 4, pp. 130–137 (2002)
47. James, B., et al.: Optimized double press-double sinter powder metallurgy method. US Patent 5,080,712, 1992
48. German, R.M.: Powder Metallurgy and Particulate Materials Processing, 1st edn, p. 528. Metal Powder Industries Federation, Princeton (2005)
49. German, R.M.: Powder Injection Molding, p. 521. Metal Powder Industries Federation, Princeton (1990)
50. Machado, R., Ristow, Jr., W., Klein, A.N., Muzart, J.L.R., et al.: Industrial plasma reactor for plasma assisted thermal debinding of powder injection molded parts. US Patent US7,718,919B2, PCT (WO 2006012718) and INPI (PI-0403536-4), 2010

51. Wendhausen, P.A.P., Fusao, D., Klein, A.N., Muzart, J.L.R., et al.: Plasma assisted debinding and sintering: process and equipment. In: Proceeding of the Powder Metallurgy World Congress & Exhibition, EURO PM2004, Vienna, vol. 4, pp. 37–142 (2004)
52. Klein, A.N., Muzart, J.L.R, et al.: Process for removal of binders from parts produced by powder injection moulding. US Patent US 6,579,493 B1, 2003
53. Klein, A.N., Binder, C., Hammes, G., de Mello, J.D.B., Ristow, W., Binder, R.: Self lubricating sintered steels with high mechanical resistance obtained via in situ formation of solid lubricant particles during sintering. In: Proceedings of EURO PM2009, vol. 1, pp. 191–196 (2009)
54. Binder, R., Klein, A.N., Binder, C., Hammes, G., Parucker, M.L., Ristow Jr., W.: Composicao metalurgica de materiais particulados, produto sinterizado autolubrificante e processo de obtencao de produtos sinterizados autolubrificantes. Patent application, PI 0803956-9, INPI, Brazil, 2008
55. Binder R., Binder, C., Ristow Jr., W., Klein, A.N.: Composition of particulate materials for forming self-lubricating products in sintered steels, product in self- lubricating sintered steel and process for obtaining self-lubricating products in sintered steel, PI0805606-Brazil; US 20110286873A1-USA; International Number: WO 2010/069020 A2-Europe; CN102497948A-China; JP 2012-512320-Japan; 10-2011-0110179-South Korea; SG 172168 A1-Singapore, TW 201034773 A1-Taiwan 2008
56. Lancaster, J.K.: Solid lubricants. In: Booser, E.R. (ed.) CRC Handbook of Lubrication, Theory and Practice of Tribology Theory and design, vol. II. CRC Press, Boca Raton (1984)
57. Xua, J., Zhang, R., Chena, P., Shena, D., Yea, X., Ge, S.: Mechanism of formation and electrochemical performance of carbide-derived carbons obtained from different carbides. Carbon. **64**, 444–455 (2013)
58. Totten, G. (ed.): Steel Heat Treatment: Metallurgy and Technologies, p. 191. CRC Press, Boca Raton (2007)
59. Binder, C., Bendo, T., Pereira, R. V., Hammes, G., de Mello, J.D.B, Klein, A.N.: Influence of the SiC content and sintering temperature on the microstructure, mechanical properties and friction behaviour of sintered self-lubricating composites. Powder Metallurgy. **59**, 1–10 (2016). https://doi.org/10.1080/00325899.2016.1250036
60. Callister Jr., W.D.: Fundamentals of Materials Science and Engineering, p. 552. Wiley, New York (2001)
61. Binder, C.: Desenvolvimento de novos tipos de aços sinterizados autolubrificantes a seco com elevada resistência mecânica aliada a baixo coeficiente de atrito via moldagem de pós por injeção. Ph.D. Thesis, Federal University of Santa Catarina, Brazil, 178 p. In Portuguese (2009)
62. ASM: ASM Handbook, Volume 1: Properties and Selection: Irons, Steels, and High-Performance Alloys, vol. 1. ASM International, Materials Park. 1063 p (1990)
63. Thelning, K.E: Steels and its heat treatment, 2nd edn. Butterworths, London. 450 p (1984)
64. Rohatgi, P.K., Ray, S., Liu, Y.: Tribological properties of metal matrix graphite particle composites. Int. Mater. Rev. **37**, 129–149 (1992)
65. Matthews, M.J., Pimenta, M.A., Dresselhaus, G., Dresselhaus, M.S., Endo, M.: Origin of dispersive effects of the Raman D-band in disordered carbon materials. Phys. Rev. B. **59**, R6585 (1999)
66. Cançado, L.G., Pimenta, M.A., Saito, R., et al.: Stokes and anti-stokes double resonance Raman scattering in two-dimensional graphite. Phys. Rev. B. **66**, 035415 (2002)
67. Ferrari, A.C., Meyer, V., Scardaci, C., et al.: Raman spectrum of graphene and graphene layers. Phys. Rev. Lett. **97**, 187401 (2006)
68. Ferrari, A.C.: Raman spectroscopy of graphene and graphite: disorder, electron–phonon coupling, doping and non adiabatic effects. Solid State Commun. **143**, 47–57 (2007)
69. de Mello, J.D.B., Binder, C., Binder, R., Klein, A.N.: Effect of precursor content and sintering temperature on the scuffing resistance of sintered self-lubricating steel. Wear. **271**, 1862–1867 (2011)
70. Ferrari, A.C., Robertson, J.: Interpretation of Raman spectra of disordered and amorphous carbon. Phys. Rev. B. **61**, 14095–14107 (2000)

71. Lespade, P., Marchand, A., Couzi, M., Cruege, F.: Caracterisation de materiaux carbones par microspectrometrie Raman. Carbon. **22**, 375–385 (1984)
72. Binder, C., Bendo, T., Hammes, G., Neves, G.O., de Mello, J.D.B, Klein, A.N., Binder, R.: Structure and properties of in situ generated 2D turbostratic graphite nodules. Carbon. **124**, 685–692 (2017)
73. Pimenta, M.A., Dresselhaus, G., Dresselhaus, M.S., Cançado, L.G., Jorio, A., Saito, R.: Studying disorder in graphite-based systems by Raman spectroscopy. Phys. Chem. Chem. Phys. **9**, 1276–1291 (2007)
74. Le Roux, H.: An electron diffraction analysis of turbostratic graphite in cemented carbides. Acta Metall. **33**, 309–315 (1985)
75. Karthik, C., Kane, J., Butt, D.P., Windes, W.E., Ubic, R.: Microstructural characterization of next generation nuclear graphites. Microsc. Microanal. **18**, 272–278 (2012)
76. Campos, K.R.: Caracterização tribológica da lubrificação sólida. Ph.D. Thesis, Universidade Federal de Uberlândia, Brazil, 2012, 162 p. In Portuguese (2012)
77. Lim, S.C., Brunton, J.H.: The unlubricated wear of sintered iron. Wear. **113**, 371–382 (1986)
78. Campos, K.R., Kapsa, P., Binder, C., Binder, R., Klein, A.N., de Mello, J.D.B.: Tribological evaluation of self-lubricating sintered steels. Wear. **332–333**, 932–940 (2015)
79. Keller, J., Fridrici, V., Kapsa, P.H., Huard, J.F.: Surface topography and tribology of cast iron in boundary lubrication. Tribol. Int. **42**, 1011–1018 (2009)
80. Zum Gahr, K.H.: Microstructure and Wear of Materials Tribolology Series, vol. 10. Elsevier, Amsterdam (1987.) 560 pp
81. Babu, S.S.: Acicular ferrite and bainite in steels. Ph.D. Thesis, University of Cambridge, UK (1992)
82. de Mello, J.D.B., Binder, C., Hammes, G., Klein, A.N.: Effect of the metallic matrix on the sliding wear of plasma assisted debinded and sintered MIM self-lubricating steel. Wear. **301**, 648–655 (2013)
83. Beattie, I.R., Gibson, T.R.J.: J. Chem. Soc. A. **6**, 980 (1970)
84. Oh, S.J., Cook, D.C., Townsend, H.E.: Characterization of iron oxides commonly formed as corrosion product on steel. Hyperfine Interact. **112**, 59–65 (1998)
85. Crockett, R.M., Derendinger, M.P., Hug, P.L., Roos, S.: Wear and electrical resistance on diesel lubricated surfaces undergoing reciprocating sliding. Tribol. Lett. **16**, 187–194 (2004)
86. Ouyang, M., Hiraoka, H.: Structure and magnetic properties of iron oxide films deposited by excimer laser ablation of a metal-containing polymer. Mater. Res. Bull. **32**, 1099–1107 (1997)

Surface Engineering Design of Alumina-Matrix Composites

8

Yongsheng Zhang, Hengzhong Fan, Litian Hu, Yuan Fang, and Junjie Song

Contents

Abstract

The three-dimensional lubricating layer on a ceramic surface realizes the integration of the structure and lubricating function in ceramic materials, which can achieve outstanding lubricating properties and maintain the excellent mechanical properties of ceramics, solving the special lubrication and wear failure in mechanical systems under extreme conditions (e.g., corrosive environment and wide-temperature range condition). In this chapter, two kinds of surface-lubricating structural-laminated ceramics with high reliability were designed and prepared based on experiment research and theoretical simulation. These ceramics can achieve stable and effective lubrication in a water environment and wide-temperature range condition. These materials are Al_2O_3/Ni- and

Y. Zhang (✉) · L. Hu · Y. Fang
State Key Laboratory of Solid Lubrication, Lanzhou Institute of Chemical Physics, Chinese Academy of Sciences, Lanzhou, China
e-mail: zhysh@licp.cas.cn

H. Fan · J. Song
State Key Laboratory of Solid Lubrication, Lanzhou Institute of Chemical Physics, Chinese Academy of Sciences, Lanzhou, China

University of Chinese Academy of Sciences, Beijing, China

P. L. Menezes et al. (eds.), *Self-Lubricating Composites*,
https://doi.org/10.1007/978-3-662-56528-5_8

Al_2O_3/Mo-laminated composites suitable for use in a water environment and in wide-temperature range conditions, respectively. The relation between the surface microstructure of the prepared materials and their properties (mechanical and tribological) was investigated. Results indicated that the integration of the structure and lubricating function of the ceramic composites is realized through the bionic, surface microstructure, and three-dimensional self-lubricating design of the materials, further improving their lubricating and practical properties. Factors that can influence the tribological behavior and wear failure of the above materials were proposed through the systematic study of the tribological behavior under different environments and test conditions, as well as the relation among the structure, composition, and properties of these two kinds of materials. In addition, theoretical models of the relation between the structural parameters and performance of the materials were built. These methods provided theories and technologies for the preparation and application of high performance lubricating materials that can be used in corrosive and wide-temperature range environments.

8.1 Introduction

Lubrication in extreme environment is a key factor that affects the security, high efficiency, and stable operation of a mechanical system. This factor also restricts the development of high-end equipment. During the past decades, various self-lubricating materials have been developed for different machineries. These developments were geared toward improving the properties of materials, allowing them to surmount severe challenges under extreme conditions. The lubricating materials for different fields must be capable of working in corrosive environments or other extreme conditions (e.g., wide-temperature range condition requires continuous and complex multienvironment lubrications) for a long time. In the current science and technology development context, high-performance ceramic lubricating materials are the most promising candidates for the harsh environment application of wear-resistant components because of their excellent mechanical properties, such as high strength, resistance to corrosion, and oxidation stability under extreme conditions, and insensitivity to defects. Moreover, ceramic lubricating composites are the only material that can work above 1000 °C and in complex harsh environments [1–6]. Nevertheless, the high friction coefficient of this kind of material under dry sliding, boundary lubrication conditions, and brittleness of the ceramic matrix itself limit their practical application in tribological and high-end equipment areas. Therefore, the design and fabrication of high-performance lubricating materials must be geared toward improving both the mechanical and lubricating properties. This can also solve the limited application of ceramic lubricating materials.

Laminating composites is one of the new strategies. The method integrates strong or weak interfaces with ceramics inspired by bionic multilayer structures, such as shells, lignum, and teeth. It has attracted significant research attention because of the excellent mechanical properties of structured ceramics. These materials possess

noncatastrophic fracture behavior and damage tolerance that exhibit much higher fracture toughness and work of fracture than monolithic ceramics [7–9]. The pioneering work of Clegg et al. successfully fabricated SiC/graphite-laminated composites using SiC as the strong layers and graphite as the weak interface. These materials exhibited great mechanical properties with a fracture toughness and work of fracture of 15 MPa · $m^{1/2}$ and 4625 J · m^{-2}, respectively. Moreover, the laminated composites also showed excellent lubricating property and wear resistance because of their special weak interfacial graphite layer [10]. According to previous studies, Al_2O_3/Ni and Al_2O_3/Mo are typical laminated composites. Al_2O_3/Ni and Al_2O_3/Mo are promising candidates in corrosive environment and high temperature condition applications, respectively. The two typical laminated composites exhibit excellent mechanical properties that can achieve security, high efficiency, and stable operation for mechanical systems as structural materials [11, 12]. Nevertheless, the friction coefficient and wear rate of Al_2O_3/Ni-laminated composites are high and unstable under boundary lubricating conditions. The room and medium-temperature friction coefficients of Al_2O_3/Mo-laminated composites are high under dry sliding conditions. Thus, these factors limit the application of these two laminated composites in lubricating areas.

Laser surface texturing (LST), which forms regular micro-patterns on the sliding surface, is generally recognized as an effective means to improve the tribological property of moving part surfaces. Previous studies showed that the introduction of specific texturing on sliding surfaces can effectively alleviate the friction and wear of materials, increase the lifetime of the sliding contacts by trapping wear debris, or promote the retention of a lubricant film between mating surfaces [13–18]. This method combined with laser surface texture and solid lubricant films can significantly improve the tribological performance of materials. The mechanism of such composition-lubrication structure involves the use of textured microdimples on the material surface to store lubricants. Lubricants are squeezed on the friction surface to form a lubricating film during friction. This method improves the contact states between the friction pair. This process leads to reduced frictional wear and increased service life of materials. The method of forming a composite lubricating layer on a textured surface mainly includes burnishing, sputtering, and hot press sintering. Lubricants stored in textured micropatterns can supply the friction surface continuously, prolonging the service life of materials [19–24]. Therefore, the integration of LST and lubricants on the surface of materials is an effective means to achieve outstanding lubricating properties for the materials. However, few in-depth and systematic studies are available on the combination of laser surface texturing and bionic-laminated ceramics. These studies are necessary to investigate and improve the application limits of these laminated ceramic composites systematically.

On the basis of this background, two kinds of surface-lubricating structural-laminated ceramics with high reliability were designed and prepared. The three-dimensional lubricating layer fabricated on the ceramic surface realizes the integration of structure and lubricating function in laminated ceramic materials. This method can achieve outstanding lubricating properties and maintain the excellent mechanical properties of the ceramic. This process can also address the special

lubrication and wear failure in mechanical system under corrosive environment and wide-temperature range conditions, respectively. These materials are surface textured integrated with diamond-like carbon (DLC) film, LaF_3-doped MoS_2 composite coating of alumina/nickel-laminated composites, and surface textured integrated with solid lubricants of alumina/molybdenum-laminated composites. These are suitable for use in a water environment and wide-temperature range conditions, respectively. The relation between the surface microstructure of the prepared materials and their properties (mechanical and tribological) was investigated.

8.2 Laser Surface Texturing and Tribological Properties of Ceramic Composites

Zirconia toughened alumina (ZTA) ceramic nanocomposites are potential candidates for the application of wear-resistant components because of their excellent properties, such as superior strength and fracture toughness, high wearability and hardness, low specific density, and antioxidation effect. Nevertheless, the friction coefficient and wear rate of ZTA nanocomposites are high under dry sliding conditions, which limit the application of these nanocomposites in tribological areas. LST is the basis for the integration of structured and lubricating functions in ceramics. The friction reduction mechanisms of surface texturing with different shapes and dimensions were investigated in several research works. The mechanisms mainly contain preventing stiction during start-up in magnetic storage industry, trapping wear debris in the texture micropatterns to reduce friction and wear, improving load capacity by enhancing hydrodynamic and hydrostatic lubrications, and acting as reservoirs to enhance lubricant retention and provide continuous lubrication to sliding surfaces [15, 25, 26]. The method is simple and effective in achieving antifriction and reduces the coefficient friction on the surface of ceramics by laser surface texturing. This part aims to reveal the microtexture mechanism that affects the tribological properties of ZTA nanocomposites and provide guidance for the optimum design of a composition-lubrication structure on the surface of laminated ceramic materials.

By controlling the sintering temperature properly, ZTA nanocomposites with excellent mechanical properties were prepared by hot pressing. The microhardness and bending strength of the sintered nanocomposites were approximately 17.01 GPa and 470 MPa, respectively. A commercial pulsed Nd:YAG laser was employed to produce the texture on the surface of the ZTA nanocomposites [27].

The scanning electron microscopy (SEM) photographs of the surface morphology of the ZTA nanocomposites with laser textures are presented in Fig. 8.1a. The 3D characteristic profiles of the textured surface for the nanocomposites are exhibited in Fig. 8.1b. A size-controlled microdimpled texture with a regular pattern was successfully fabricated on the surface of the ZTA nanocomposites by a pulsed Q-switch Nd:YAG solid-state laser. Through the optimized design of the laser texturing parameters, the tribological performance of the ZTA nanocomposites was significantly improved [27]. Figure 8.2 shows the curves of the friction coefficients of the

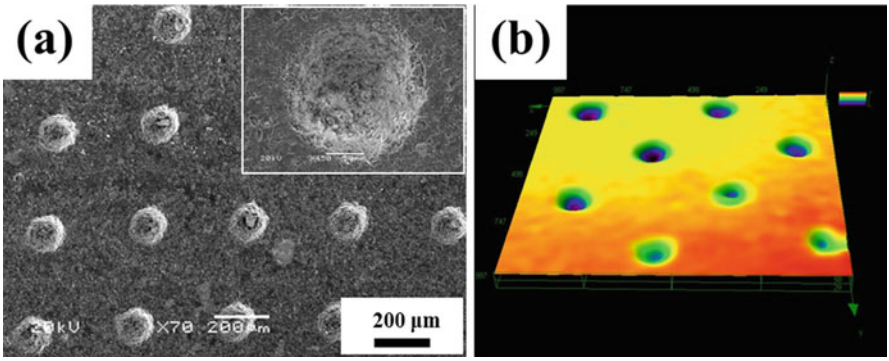

Fig. 8.1 SEM photographs (**a**) and 3D characteristic profiles (**b**) of the textured surface for the nanocomposites

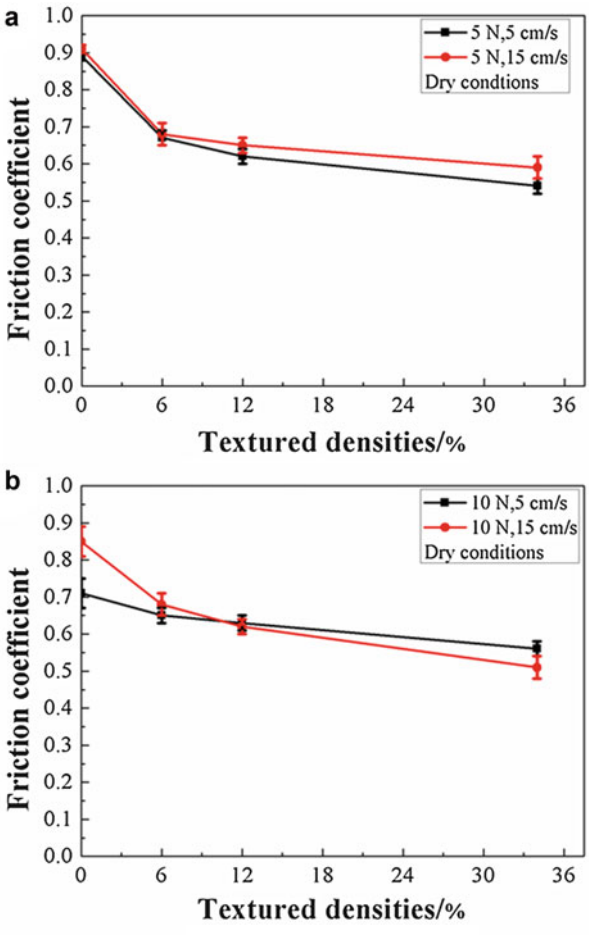

Fig. 8.2 Friction coefficient under dry contact for untextured and textured surfaces with different densities [27]

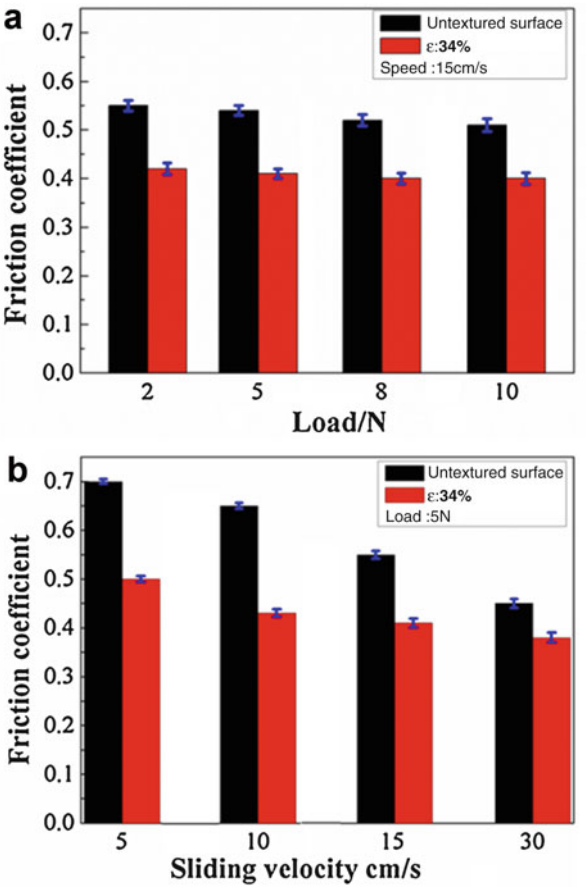

Fig. 8.3 Average values of friction coefficient for the untextured and textured surfaces under different loads (**a**) and sliding velocities (**b**) under water lubrication [27]

untextured and textured surfaces of the ZTA nanocomposites under dry contact. The results indicated that the textured ZTA nanocomposite surface exhibited a low coefficient under dry friction conditions, especially under a relatively high load and sliding speed. Moreover, the texture density has an important effect on the property of the materials. The dense micro-dimples were advantageous in improving the tribological properties of the material. When the texture density is 34%, the friction coefficient of the textured ZTA nanocomposites can be reduced to 0.5. This value was approximately 44% lower than that of the untextured ZTA nanocomposite surface.

Figure 8.3 shows the average values of the friction coefficients of the untextured and textured ZTA nanocomposite surfaces at different loads and sliding speeds in a water environment. The increase in texture density resulted in an increase in water storage capacity. Thus, the reduction of the friction coefficient was primarily

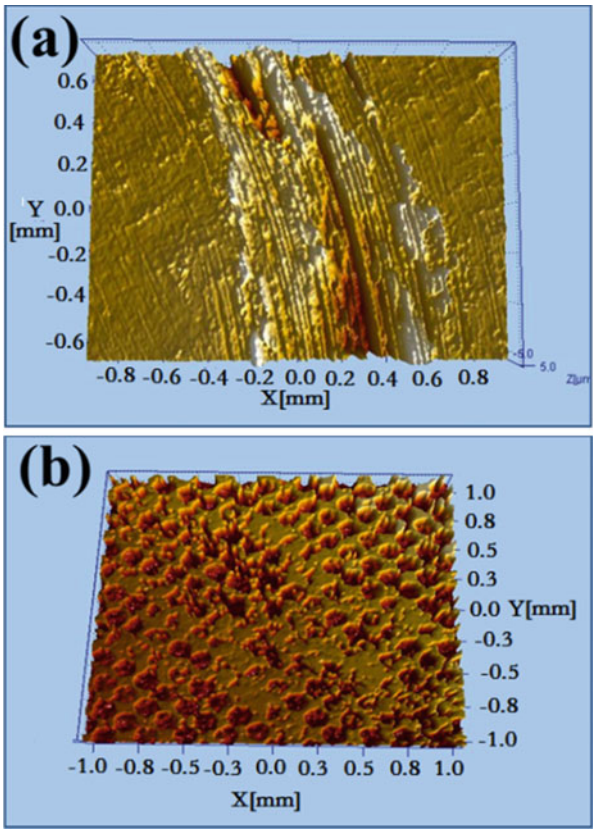

Fig. 8.4 3D topographical of the wear scars of the untextured (**a**) and textured $\varepsilon = 34\%$ (**b**) surfaces

attributed to the secondary lubricating effect produced by the lubricant (water) stored in the microdimples of the ZTA nanocomposite surfaces.

Figure 8.4 shows the typical 3D topographical structure of the worn surfaces of the untextured (Fig. 8.4a) and textured (Fig. 8.4b) samples. As shown in Fig. 8.4a, the untextured surfaces exhibited serious plough and adhesion wear under dry condition. By contrast, the textured surfaces exhibited excellent antiwear ability. The wear debris was effectively trapped and stored by the produced microdimples. This phenomenon can prevent abrasive wear and reduce plowing of the friction surfaces.

The understanding of such mechanisms provides guidance for the optimized design of a composition-lubrication structure on the ceramic surface. The process also provides theoretical guidance and technology support for the application of new ceramic materials in the high-technology fields. Therefore, the following laser surface texturing technology is used to design the surface composition-lubrication structure of alumina-matrix-laminated composites.

8.3 Surface Lubricating Design, Fabrication, and Tribological Properties in a Water Environment of Al_2O_3/Ni-Laminated Composites

The chemical resistance of lubricating ceramics is the ability of a material to resist the destructive effect of an aggressive environment. In addition to the properties of the corrosive medium, this ability depends also on the microstructure of the lubricating ceramic material and conditions of the corrosion process, especially in medium-material contact [28–30]. High-performance alumina-matrix lubricating ceramics are potential candidates for the application of wear-resistant components because of their high wearability and hardness, low specific density, and anti-oxidation effect. However, the ability to resist the corrosive environment, such as liquids (solution of acid, alkaline, salts, molten salts, glasses, slags and metals, water, and so on), is one of the most limited properties of materials in many industrial applications. Therefore, designing and fabricating alumina-matrix-laminated composites with excellent mechanical and tribological properties that are adapted to the corrosive environment is significant. The combination of the bionic design with corrosion-resistant weak interface and surface lubricating design suitable for corrosive environment of ceramic-matrix-laminated composites is a promising way to achieve the optimal integration of mechanical and tribological properties. In this section, a surface lubricating structural Al_2O_3/Ni-laminated ceramics was designed and fabricated with high reliability and suitable for use in a water environment; the material can achieve stable and effective lubrication under water-based corrosive environments [31, 32].

First, Al_2O_3/Ni-laminated composites with excellent mechanical properties were successfully fabricated through layer-by-layer pressing and hot-press sintering method. Their bending strength, fracture toughness, and work of fracture can reach up to 470 MPa, 9.6 $MPa \cdot m^{1/2}$, and 1952 $J \cdot m^{-2}$, respectively [31]. On the basis of the Al_2O_3/Ni-laminated composites, two types of surface composition-lubrication structures were fabricated through the laser texturing and deposition/spraying technologies [31, 32]. These methods improved the surface tribological performance of the Al_2O_3/Ni-laminated composites under water environment remarkably. The regularity of the internal relationships between the surface texture micropattern and the microstructure, chemical composition, and properties of the lubricating films was systematically investigated. This process provided an important theoretical and experimental basis for the design of materials for water-based corrosive environments. The schematic and design concept of the surface composition-lubrication structure on the surface of Al_2O_3/Ni-laminated composites is shown in Fig. 8.5.

The microstructures of typical Al_2O_3/Ni-laminated composites are illustrated in Fig. 8.6, where the dark layer is the Al_2O_3 layer and the light layer is the Ni, which is markedly thinner than the Al_2O_3 layer. The laminated composites present a relatively straight obvious multilayer structure. The boundary between the strong/weak layer was sharp and without clear delamination (Figs. 8.6a, b). Moreover, the Al_2O_3 and Ni layers in the composites were all fully densified because of their good sinterability. Thus, Ni and Al_2O_3 presented compact-crystallized structures with no obvious

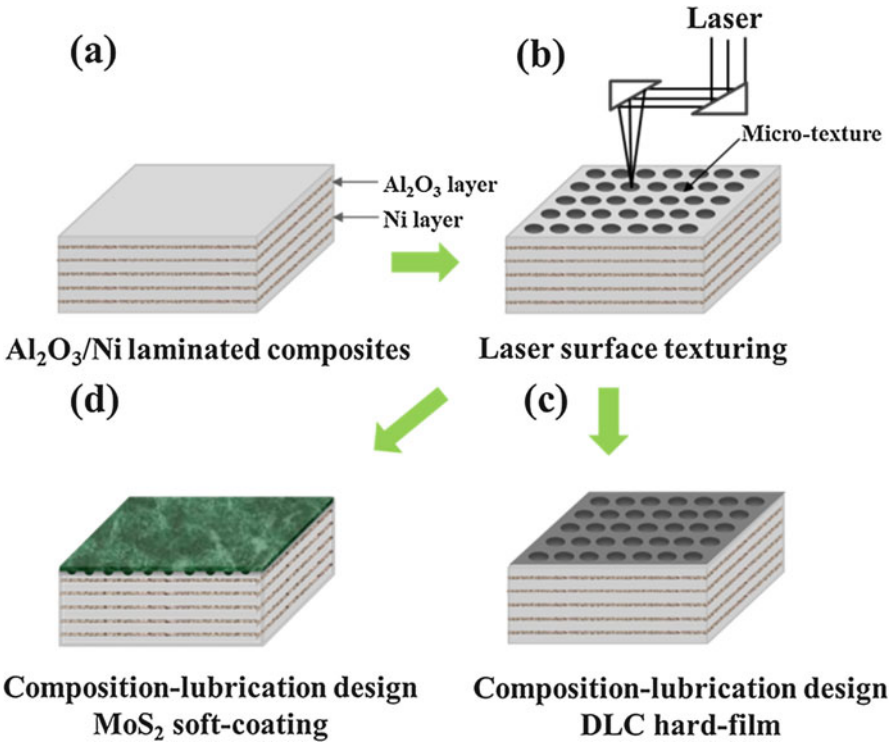

Fig. 8.5 The schematic and surface lubricating design concept of Al_2O_3/Ni-laminated composites

flaws (Fig. 8.6c). These special weak interfacial layers played an important role in improving the mechanical and tribological properties of the laminated composites.

The SEM microtexture photographs of DLC films and LaF_3-doped MoS_2 composite coatings of the Al_2O_3/Ni-laminated composites are presented in Fig. 8.7a and b, respectively. As seen from Fig. 8.7a, the microdimples of DLC films are uniform. The surface around the microdimples is smooth, indicating the absence of notable cracks or other morphological discontinuities. As seen from Fig. 8.7b, the LaF_3-doped MoS_2 composite coatings on the textured surfaces are composed of closely packed powder particles. No obvious microcracks, holes, or other defects can be observed on the textured LaF_3-doped MoS_2 composite coatings. The LaF_3-doped MoS_2 composite coatings on the textured surface exhibit a relatively rough surface morphology.

Fig. 8.8a shows the different surface types of friction behaviors of Al_2O_3/Ni-laminated composites. The textured DLC films with different microdimple area densities are illustrated in Fig. 8.8b. The synergistic effect of a surface texture and DLC film in a water environment is a dominant cause of the decrease of the surface friction coefficient of the material. When friction against a stainless steel pin occurs in a water environment, the friction coefficient of the composition-lubrication structure can decrease to 0.06. This value is nearly one order of magnitude lower

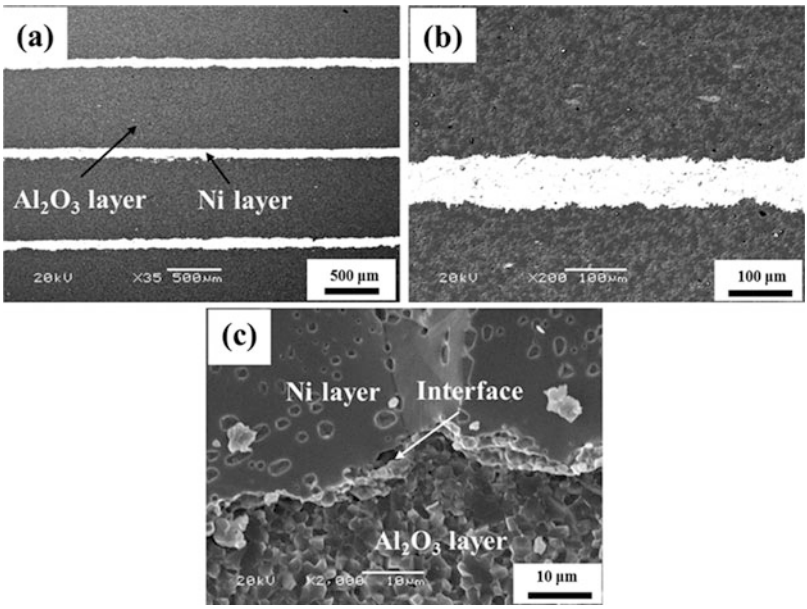

Fig. 8.6 Multilayer and cross-section microstructure of the Al_2O_3/Ni-laminated composites

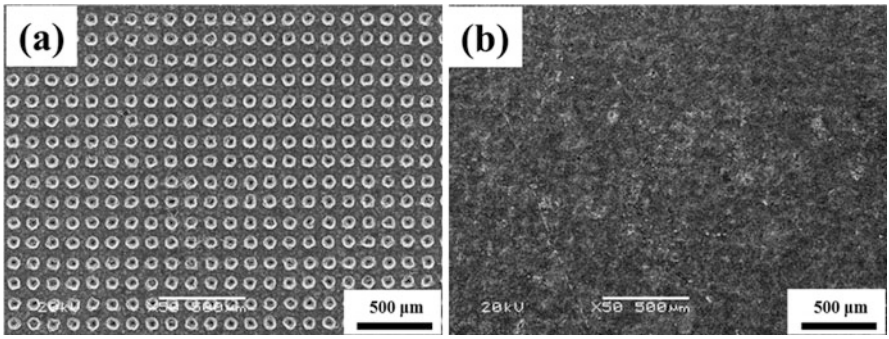

Fig. 8.7 Textured surface lubricating structure with (**a**) DLC films and (**b**) LaF_3-doped MoS_2 composite coating of the Al_2O_3/Ni-laminated composites

than that of the uncoated smooth ceramic surface (0.51). Moreover, the microdimple density of the texture with DLC film plays a key role in improving the tribological properties. When the texture density is low, the tribological properties of the composition-lubrication structure primarily depend on the synergistic lubrication of the surface texture and the DLC thin film because of the low storage of lubricant in the microdimples and the low viscosity feature of water. For high-density textured surfaces, the increase of texture density decreases with DLC content on the surface. This phenomenon indicates that the lubrication effect of DLC decreases. Meanwhile,

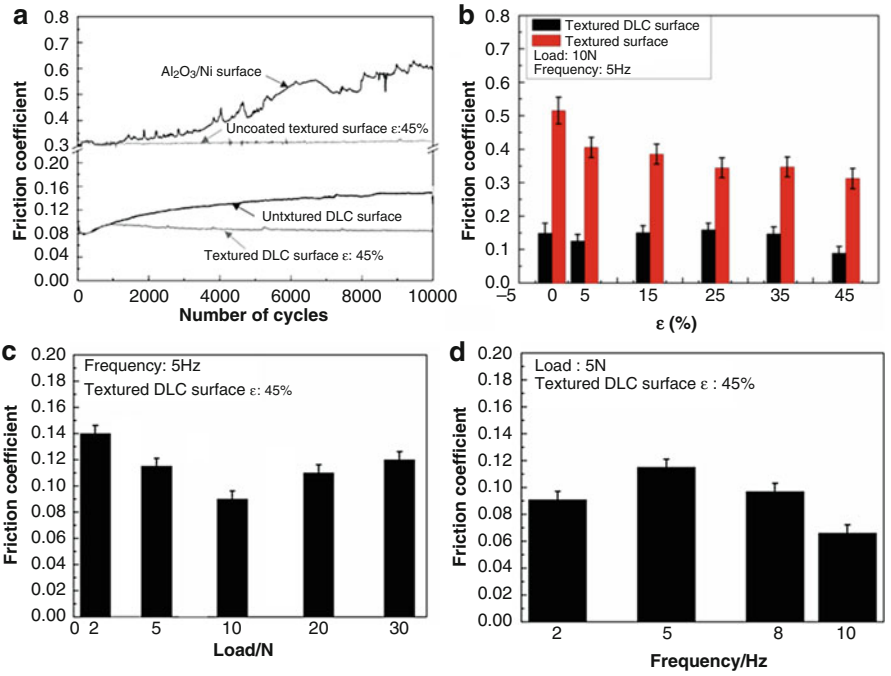

Fig. 8.8 Friction coefficient curves (**a**) and the average values friction coefficients (**b**, **c**, **d**) of samples [31]

the increase of the texture density increases the storage volume of the lubricant that facilitates the formation of lubricating films on the friction surface. When the texture density is 5% or 45%, the composition-lubrication structure exhibits optimal tribological properties and adequate environmental adaptability. Figure 8.8c and d shows the average evolution values of the friction coefficients of the high-density (45%) textured DLC films at different loads and sliding frequencies under water lubrication. As shown in the figure, the textured DLC surface with a microdimple density of 45% exhibits excellent tribological properties in these working conditions. The friction coefficient of the textured surfaces is in the range of 0.06–0.14. The test conditions exhibited a significant effect on the tribological properties of the materials. The effect of sliding frequency on the friction coefficients was larger than the effect of the load.

Figure 8.9 shows the typical SEM micrographs of the worn surfaces of the untextured surface of DLC films (Fig. 8.9a) and textured surface of DLC films (Fig. 8.9b). As shown in Fig. 8.9a, the DLC films on the untextured substrate are severely worn out and flaked off, whereas the textured DLC films are intact and merely exhibit a very small abrasion at the edge of the microdimples (Fig. 8.9b). Therefore, the textured surfaces effectively prevented the peeling of DLC films and exhibited excellent antiwear ability. The performance of the Al_2O_3/Ni-laminated composites can be improved significantly by introducing a regular texture and DLC

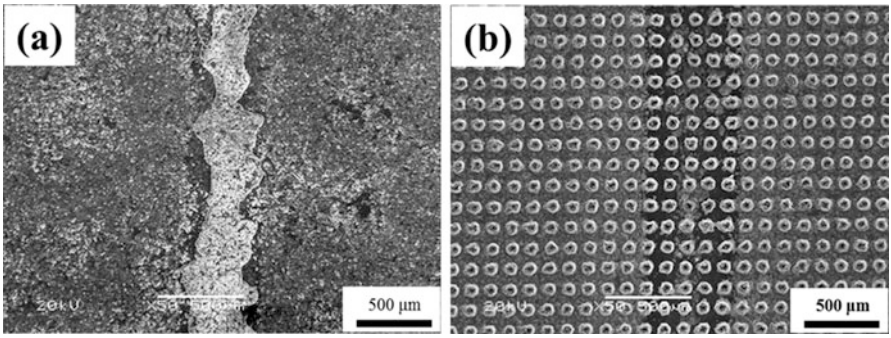

Fig. 8.9 SEM morphologies of the wear tracks of untextured (**a**) and textured DLC films

films on the surface of the materials. Thus, low and stable friction coefficients can be obtained on the sliding surface.

For the soft composition-lubrication layers of LaF_3-doped MoS_2 composite coatings on the surface of Al_2O_3/Ni-laminated composites, the following results were can be determined through the systematic investigation of the tribological behavior and fatigue failure mechanism in a water environment. Surface texture can significantly reduce the contact angle between the surfaces of Al_2O_3/Ni-laminated composites. The lubricant of water promoting the formation of water film and reducing the friction coefficient of the friction pair surfaces effectively. The friction coefficient of the soft composite lubrication surface can be reduced to 0.08, which is less than one-sixth of that of the smooth surface. The sliding lifetime of the lubricating coating can be increased by a factor of more than 10^5 cycles because of the self-locking function of the surface microtexture on the adhesive coating and its secondary lubrication effect, as shown in Fig. 8.10.

The typical SEM morphologies of the wear tracks of untextured and textured LaF_3-doped MoS_2 composite coatings are shown in Fig. 8.11. The untextured LaF_3-doped MoS_2 composite coating surface has flaked off completely resulting in severe wear off. However, for the sample with textured LaF_3-doped MoS_2 composite coating surface, some LaF_3-doped MoS_2 composite lubricants still exist in the sliding area and in microdimples though the coating has flaked off of local region. The LaF_3-doped MoS_2 lubricants in microdimples can be continually replenished into the sliding surface when the coating on the wear scar is quickly worn off. This phenomenon will provide further lubrication.

8.4 Surface Lubricating Design, Fabrication, and Tribological Properties Under a Wide-Range Temperature of Al_2O_3/Mo-Laminated Composites

The rapid development in aerospace, military industry, and other high-tech fields has resulted in the increasing demands for high-temperature wear-resistant materials and high-temperature self-lubricating technology. Self-lubricating composites with

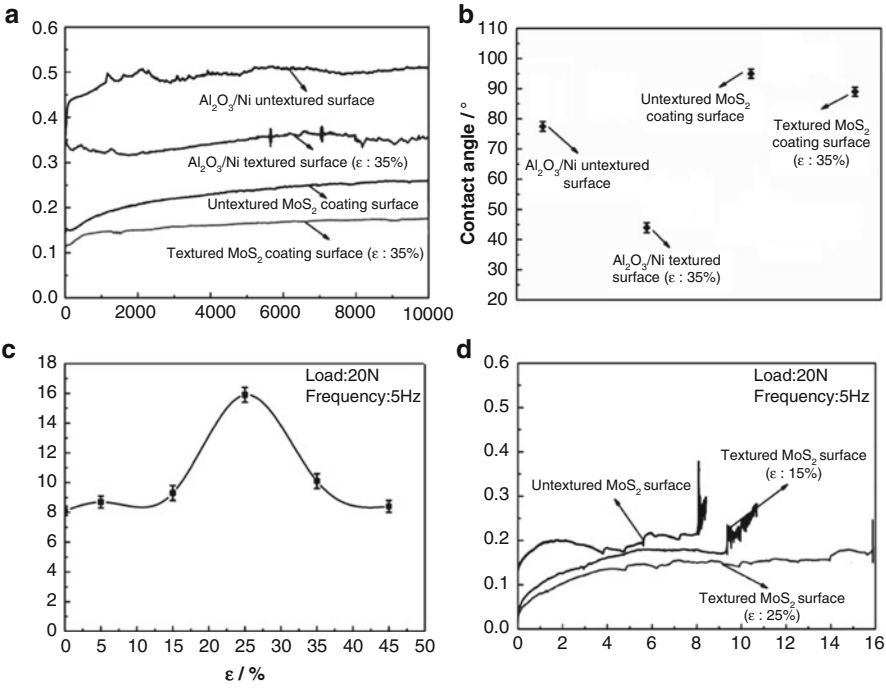

Fig. 8.10 The friction curves (**a**) and the contact angles of water droplets (**b**) on material surface at a normal load of 10 N and the sliding frequency of 5 Hz; the wear life (**c**) and typical friction curves (**d**) of LaF_3-doped MoS_2 composite coatings with different microdimpled densities at a normal load of 20 N and the sliding frequency of 5 Hz [32]

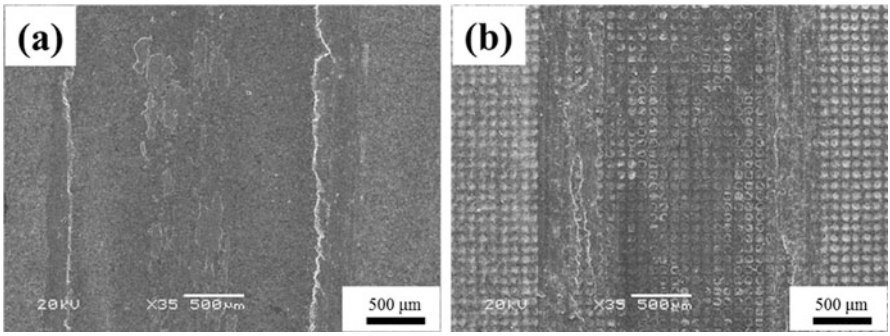

Fig. 8.11 The typical SEM morphologies of the wear tracks of LaF_3-doped MoS_2 composite coatings for untextured surface (**a**) and textured surface (**b**) after worn-out

excellent tribological performance in a wide-temperature range are urgently needed. However, lubricating materials are highly sensitive to temperature. The preparation of self-lubricating composites with wide-temperature range lubrication is very challenging and meaningful. Mechanical lubrication at temperatures above 400 °C

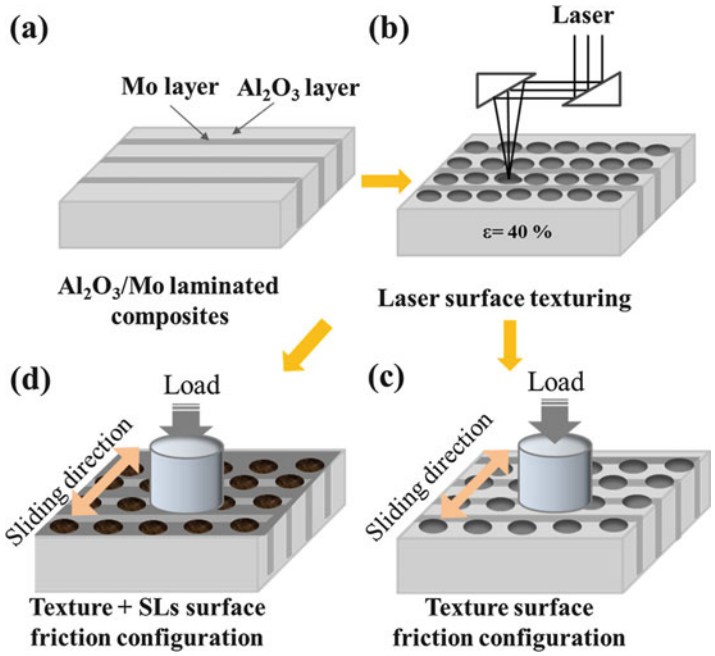

Fig. 8.12 The schematic and surface lubricating design concept of Al_2O_3/Mo-laminated composites

can only depend on solid lubricants (SLs). Thus, two or three SLs are usually combined. Moreover, their synergy lubrication effect is fully utilized to achieve materials with wide-temperature range lubrication. In this part, we developed a three-dimensional lubricating layer by combining the optimized surface textures and SLs. Texture patterns were used as storage carrier of SLs. This structure can realize continuous lubrication from room temperature to 800 °C by fully utilizing the synergy effect and antifriction of the surface texture and SLs stored in the micro-dimples. Two types of different textured density surfaces and the three-dimensional lubricating layer with combined laser surface texture and solid film lubricant of Al_2O_3/Mo-laminated composites were fabricated. The synergy lubrication effect and mechanism of different lubricants from room temperature to 800 °C were discussed [33, 34]. The schematic and surface wide range lubricating design concept of Al_2O_3/Mo-laminated composites are shown in Fig. 8.12.

Using the LST technology, different microdimple densities and microgroove textures were fabricated on the surface of the Al_2O_3/Mo-laminated composites. Figure 8.13 shows the surface morphology of Al_2O_3/Mo-laminated composites with two types of microtextures and composite SLs. Clear and uniform micro-dimples and microgrooves with smooth edges are observed. The shape of the microdimples is not influenced by the metal Mo layer (Figs. 8.13a, b). As shown in Fig. 8.13c, the textured microdimples are all filled with SLs after repeated wiping.

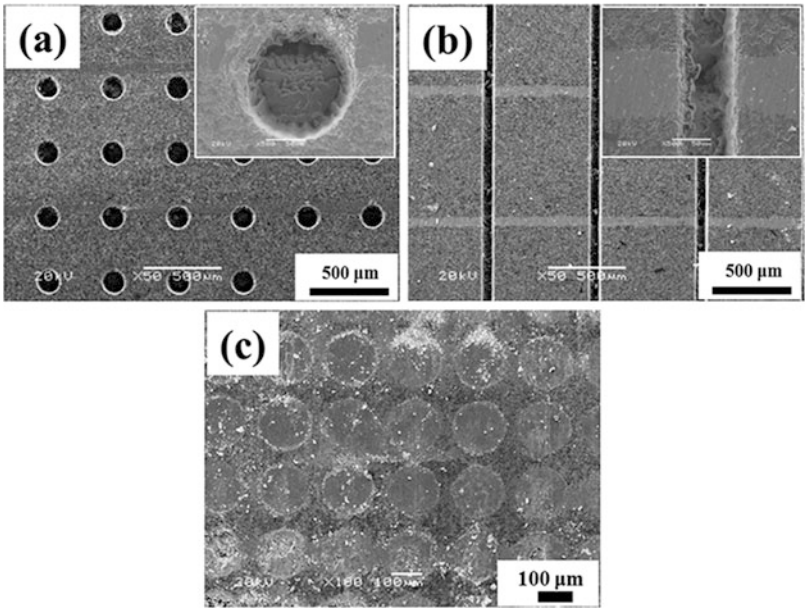

Fig. 8.13 The surface morphology with microdimples (**a**), microgrooves (**b**), and burnished composite SLs (**c**) of Al_2O_3/Mo-laminated composites

Figure 8.14 shows the friction coefficients of laser textured surfaces with different microdimple densities (a) and different microgroove densities (b) at room temperature and 800 °C. Considering the following advantages of the microtexture that increases the contact pressure of the friction surface, traps wear debris, and promotes the formation of lubricating film at high temperatures, the friction coefficients of Al_2O_3/Mo-laminated composites at 800 °C and at room temperature can be further reduced. Meanwhile, the friction coefficient of the material decreases with the increase in the texture surface density. At room temperature, the surface texture trapped wear debris. The friction coefficient of the surface texture can be decreased to as low as 0.5, which is 39% less than that of the untextured surface. Furthermore, the surface with a microdimpled texture exhibited a lower friction coefficient than that with a microgrooved texture. The surface texture facilitated an increase in the contact pressure of the friction pair and the contact area of the material surface with air at 800 °C. Thus, the formation and transfer of the lubricating film of MoO_3 are facilitated. The friction coefficient can be reduced to as low as 0.22. This value is 55% less than that of the untextured surface.

Then, applying composite lubricants on the surface of optimized textured Al_2O_3/Mo-laminated composites and forming a surface three-dimensional lubricating layer can achieve the continuous lubrication of the material from room temperature to 800 °C. Surface texture plays a key role in storing lubricants that can constantly lubricate the sliding surface during the friction process to form a continuous, uniform

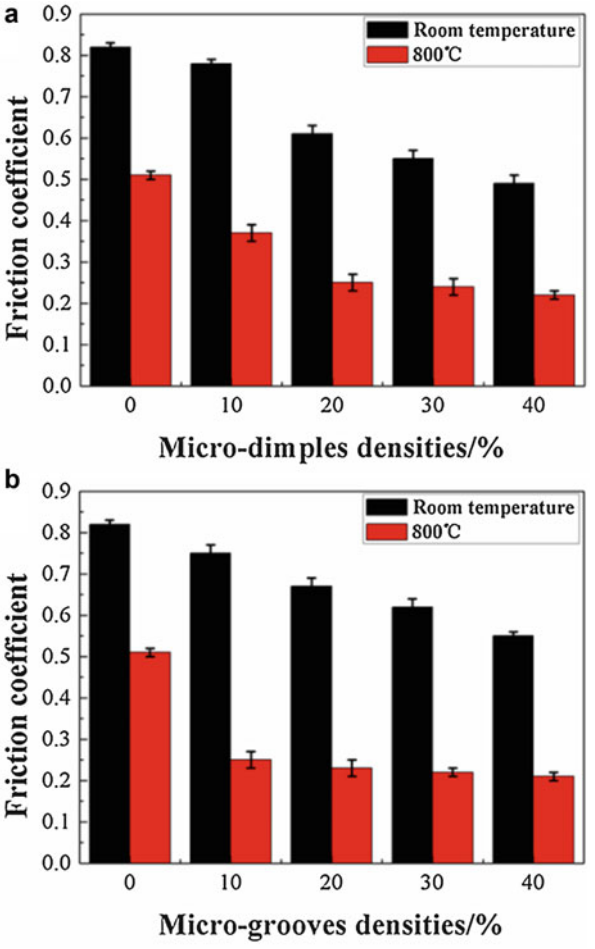

Fig. 8.14 Friction coefficients of laser textured surfaces with different microdimples densities (**a**) and different microgrooves densities (**b**) at room temperature and 800 °C [33]

lubricating film. Therefore, the friction coefficient and wear of the sliding surface can be decreased, and the lifetime of the material can be effectively increased.

Herein, the three-dimensional structure combined with excellent antifriction and antiwear properties of solid lubricants with unique structural characteristics of microtexture effectively improved the tribological performance of materials at room temperature and up to increased temperatures. Therefore, the continuous lubrication of materials in a wide-temperature range can be sufficiently realized. For the surface of the MoS_2/CaF_2-BaF_2 composite lubricants, the friction coefficients were below 0.50 throughout the entire temperature range. The lubrication effect was provided by MoS_2 at a temperature range from room temperature to 600 °C. From 600 °C to 800 °C, the synergetic effects of CaF_2-BaF_2 eutectic, $CaMoO_4$, and $BaMoO_4$ effectively provided the lubrication effect. Composite graphite/$BaSO_4$/CaF_2-BaF_2 lubricants maintained the friction coefficient of

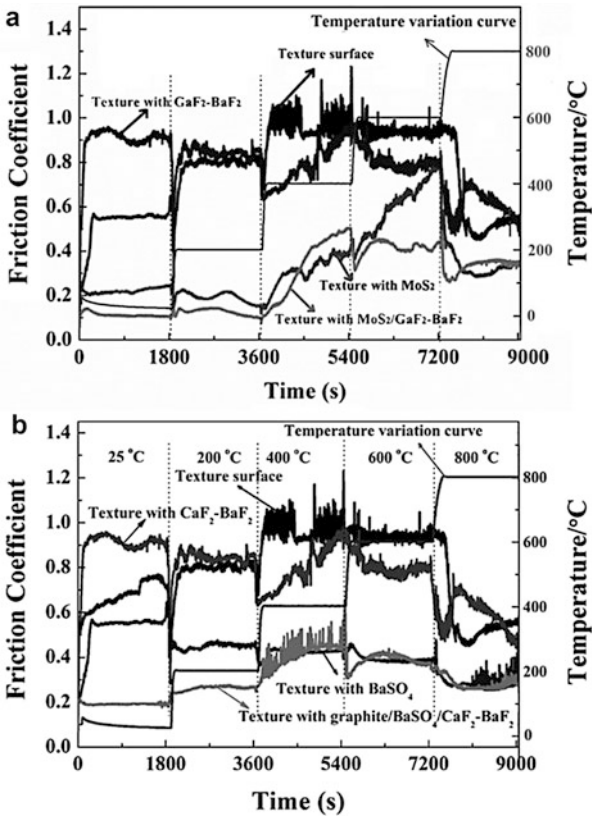

Fig. 8.15 Friction coefficients of surface burnished with different solid lubricants from room temperature to 800 °C [34, 35]

materials below 0.45 in the entire tested temperature range from room temperature to 800 °C. The lubrication effect was provided by graphite, $BaSO_4$, and the synergy effect of $BaMoO_4$ and $CaMoO_4$ at room, medium and high temperatures, respectively (Fig. 8.15).

Figure 8.16 shows the typical wear tracks of the untextured surface (Fig. 8.16a), textured without burnishing SLs (Figs. 8.16b, c), and textured surface with burnishing SLs at 800 °C under the same conditions. The untextured surface exhibited serious wear and plastic deformation mainly because of the temperature increase in the friction experiment. However, for the textured surface without burnishing SLs, trapping wear debris in the microgrooves and microdimples can be clearly observed. The texture also maintained relatively intact morphology. For the textured surface burnished with SLs, microdimples maintained relatively intact morphology. A mild wear surface was also produced after a long friction experiment. The SLs stored in microdimples were squeezed to the friction surface during friction process forming a continuous lubricating film.

In summary, Al_2O_3/Ni and Al_2O_3/Mo-laminated composites with surface composition-lubrication structure realize the integration of mechanical and lubricating properties. The performance of the surface composition-lubrication layers can be

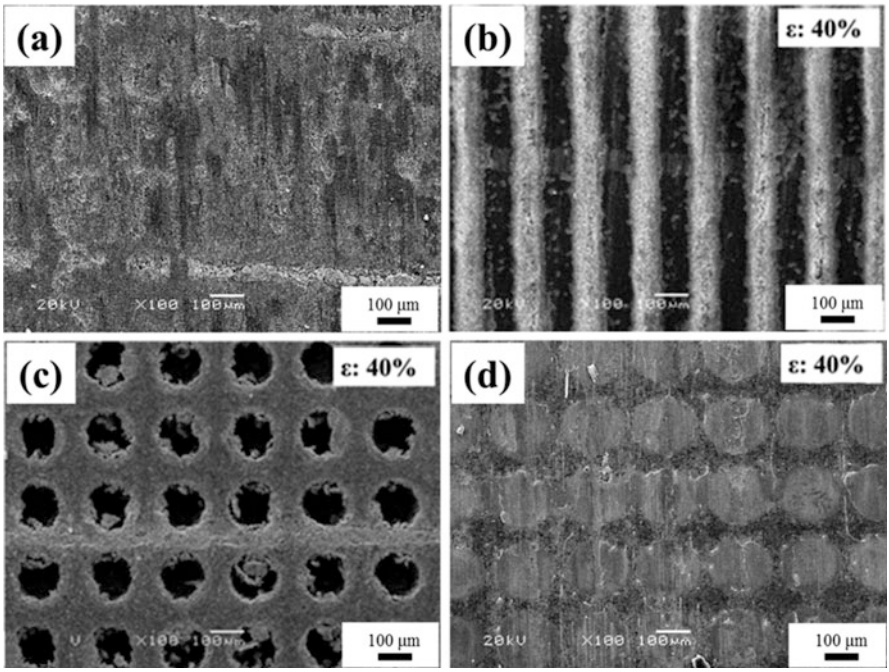

Fig. 8.16 Worn surfaces of untextured surface (**a**), textured surfaces with microgrooves (**b**), microdimples (**c**) and textured surface with burnished SLs (**d**) at 800 °C

facility controlled by the design of the texture micropattern, film/coating characteristics and compound of solid lubricants. The excellent mechanical and tribological properties of the optimal laminated and surface composition-lubrication structure enable them to be used in a wide range of applications. These methods also provided theories and technologies for the preparation and application of high performance lubricating materials that can be used in corrosive and wide-temperature range environments.

Acknowledgment This work was supported by the National Natural Science Foundation of China (51775534) and the Youth Innovation Promotion Association CAS (2013272).

References

1. Zhang, Y.S., Hu, L.T., Chen, J.M., Liu, W.M.: Lubrication behavior of Y-TZP/Al_2O_3/Mo nanocomposites at high temperature. Wear. **268**(9–10), 1091–1094 (2010)
2. Hu, T.C., Zhang, Y.S., Hu, L.T.: Mechanical and wear characteristic of Y-TZP/Al_2O_3 nanocomposites. Ind. Lubr. Tribol. **66**(2), 209–214 (2014)
3. Qi, Y.E., Zhang, Y.S., Hu, L.T.: High-temperature self-lubricated properties of Al_2O_3/Mo laminated composites. Wear. **280–281**, 1–4 (2012)

4. Fang, Y., Zhang, Y.S., Song, J.J., Fan, H.Z., Hu, L.T.: Design and fabrication of laminated-graded zirconia self-lubricating composites. Mater. Des. **49**, 421–425 (2013)
5. Qi, Y.E., Zhang, Y.S., Fang, Y., Hu, L.T.: Design and preparation of high-performance alumina functional graded self-lubricated ceramic composites. Compos. Part B Eng. **47**, 145–149 (2013)
6. Fang, Y., Zhang, Y.S., Song, J.J., Fan, H.Z., Hu, L.T.: Influence of structural parameters on the tribological properties of Al_2O_3/Mo laminated nanocomposites. Wear. **320**, 152–160 (2014)
7. Wang, C.A., Huang, Y., Zan, Q.F., Zou, L.H., Cai, S.Y.: Control of composition and structure in laminated silicon nitride/boron nitride composites. J. Am. Ceram. Soc. **85**(10), 2457–2461 (2002)
8. Hwu, K.L., Derby, B.: Fracture of metal/ceramic laminates-II. Crack growth resistance and toughness. Acta Mater. **47**(2), 545–563 (1999)
9. Wang, C.A., Huang, Y., Zan, Q.F., Guo, H., Cai, S.Y.: Biomimetic structure design-a possible approach to change the brittleness of ceramics in nature. Mater. Sci. Eng. C. **11**(1), 9–12 (2000)
10. Clegg, W.J., Kendall, K., Alford, N.M., Button, T.W., Birchall, J.D.: A simple way to make tough ceramics. Nature. **347**(6292), 455–457 (1990)
11. Zuo, K.H., Jiang, D.L., Lin, Q.L.: Mechanical properties of Al_2O_3/Ni laminated composites. Mater. Lett. **60**(9–10), 1265–1268 (2006)
12. Song, J.J., Zhang, Y.S., Fang, Y., Fan, H.Z., Hu, L.T., Qu, J.M.: Influence of structure parameters and transition interface on the fracture property of Al_2O_3/Mo laminated composite. J. Eur. Ceram. Soc. **35**, 1581–1591 (2015)
13. Ryk, G., Kligerman, Y., Etsion, I.: Experimental investigation of laser surface texturing for reciprocating automotive components. Tribol. Trans. **45**(4), 444–449 (2002)
14. Yu, X.Q., He, S., Cai, R.L.: Frictional characteristics of mechanical seals with a laser-textured seal face. J. Mater. Process. Technol. **129**(1–3), 463–466 (2002)
15. Etsion, I., Halperin, G., Brizmer, V., Kligerman, Y.: Experimental investigation of laser surface textured parallel thrust bearings. Tribol. Lett. **17**(2), 295–300 (2004)
16. Kawasegi, N., Sugimori, H., Morimoto, H., Morita, N., Hori, I.: Development of cutting tools with microscale and nanoscale textures to improve frictional behavior. Precis. Eng. J. Int. Soc. Precis. Eng. Nanotechnol. **33**(3), 248–254 (2009)
17. Baumgart, P., Krajnovich, D.J., Nguyen, T.A., Tam, A.C.: A new laser texturing technique for high-performance magnetic disk drives. IEEE Trans. Magn. **31**(6), 2946–2951 (1995)
18. Varenberg, M., Halperin, G., Etsion, I.: Different aspects of the role of wear debris in fretting wear. Wear. **252**(11–12), 902–910 (2002)
19. Etsion, I., Halperin, G.: A laser surface textured hydrostatic mechanical seal. Tribol. Trans. **45**(3), 430–434 (2002)
20. Kovalchenko, A., Ajayi, O., Erdemir, A., Fenske, G., Etsion, I.: The effect of laser surface texturing on transitions in lubrication regimes during unidirectional sliding contact. Tribol. Int. **38**(3), 219–225 (2005)
21. Hu, T.C., Zhang, Y.S., Hu, L.T.: Tribological investigation of MoS_2 coatings deposited on the laser textured surface. Wear. **278–279**, 77–82 (2012)
22. Uehara, Y., Wakuda, M., Yamauchi, Y., Kanzaki, S., Sakaguchi, S.: Tribological properties of dimpled silicon nitride under oil lubrication. J. Eur. Ceram. Soc. **24**(2), 369–373 (2004)
23. Wang, X., Adachi, K., Otsuka, K., Kato, K.: Optimization of the surface texture for silicon carbide sliding in water. Appl. Surf. Sci. **253**(3), 1282–1286 (2006)
24. Schreck, S., Zum Gahr, K.H.: Laser-assisted structuring of ceramic and steel surfaces for improving tribological properties. Appl. Surf. Sci. **247**(1–4), 616–622 (2005)
25. Etsion, I., Kligerman, Y., Halperin, G.: Analytical and experimental investigation of laser-textured mechanical seal faces. Tribol. Trans. **42**(3), 511–516 (1999)
26. Etsion, I., Sher, E.: Improving fuel efficiency with laser surface textured piston rings. Tribol. Int. **42**(4), 542–547 (2009)
27. Fan, H.Z., Hu, T.C., Zhang, Y.S., Fang, Y., Song, J.J., Hu, L.T.: Tribological properties of micro-textured surfaces of ZTA ceramic nanocomposites under the combined effect of test conditions and environments. Tribol. Int. **78**, 134–141 (2014)

28. Hnatko, M., Galusek, D., Šajgalík, P.: Low cost preparation of Si_3N_4-SiC micro/nano composites by in-situ carbothermal reduction of silica in silicon nitride matrix. J. Eur. Ceram. Soc. **24**(2), 189–196 (2004)
29. Křesťan, J., Šajgalík, P., Pánek, Z.: Carbothermal reduction and nitridation of powder pyrophyllite raw material. J. Eur. Ceram. Soc. **24**(5), 791–796 (2004)
30. Balog, M., Šajgalík, P., Lenčéš, Z., Kečkéš, J., Huang, J.T.: Liquid phase sintering of SiC with AlN and rare-earth oxide additives, silicon-based structural ceramics for the new millennium. Brito ME, Lin HT, Plucknett K (Eds.) Ceram. Trans. **142**, 191–202 (2003)
31. Fan, H.Z., Zhang, Y.S., Hu, T.C., Song, J.J., Ding, Q., Hu, L.T.: Surface composition-lubrication design of Al_2O_3/Ni laminated composites–Part I: tribological synergy effect of micro-dimpled texture and diamond-like carbon filmsin a water environment. Tribol. Int. **84**, 142–151 (2015)
32. Fan, H.Z., Hu, T.C., Wan, H.Q., Zhang, Y.S., Song, J.J., Hu, L.T.: Surface composition-lubrication design of Al_2O_3/Ni laminated composites – Part II: tribological behavior of LaF_3-doped MoS_2 composite coating in a water environment. Tribol. Int. **96**, 258–268 (2016)
33. Fang, Y., Zhang, Y.S., Fan, H.Z., Hu, T.C., Song, J.J., Hu, L.T.: Surface composition-lubrication design of Al_2O_3/Mo laminated composites – Part I: influence of laser surface texturing on the tribological behavior at 25 and 800 °C. Wear. **334–335**, 23–34 (2015)
34. Fang, Y., Fan, H.Z., Song, J.J., Zhang, Y.S., Hu, L.T.: Surface engineering design of Al_2O_3/Mo laminated composites – Part II: continuous lubrication effects of a three-dimensional lubricating layer at temperatures from 25 to 800 °C. Wear. **360–361**, 97–103 (2016)
35. Fang, Y., Fan, H.Z., Zhang, Y.S., Song J.J., Hu, L.T.: Preparation and tribological performance of three-dimensional lubricating layer on the surface of Al_2O_3/Mo self-lubricating structural ceramics. Tribol. **37**(3), 395–401 (2017 in Chinese)

9 Molecular Dynamics Simulation of Friction in Self-Lubricating Materials: An Overview of Theories and Available Models

Ali Bakhshinejad, Marjan Nezafati, Chang-Soo Kim, and Roshan M D'Souza

Contents

Abstract

In this chapter, an overview of theories and investigated computational models is presented. Among all available theoretical models, Quantum Mechanics (QM), Molecular Mechanics (MM), Monte Carlo (MC), and Molecular Dynamics (MD) are the most used models. MD was selected as the focus of this chapter, because of its high accuracy in predicting the molecular level motions while keeping the computational costs relatively low as well as availability of well-established modeling softwares (i.e., LAMMPS). MD models have been used to investigate mechanical and chemical behaviors of different phenomena, including friction and self-lubrication. The authors further reviewed available MD models in previous literatures with focus on self-lubricating materials. These models direct the contribution of different self-lubricating agents including graphite, graphene, MoS_2, and poly tetra-fluoro ethylene (PTFE) on the friction behavior

A. Bakhshinejad (✉) · M. Nezafati · C.-S. Kim · R. M. D'Souza
University of Wisconsin-Milwaukee, Milwaukee, WI, USA
e-mail: Bakhshi3@uwm.edu; nezafati@uwm.edu; kimcs@uwm.edu; dsouza@uwm.edu

P. L. Menezes et al. (eds.), *Self-Lubricating Composites*,
https://doi.org/10.1007/978-3-662-56528-5_9

of different composites. This review was conducted in order to show the power of computational modeling to predict the molecular level behaviors of different physical models.

9.1 Introduction

Friction, the force resisting relative motion between contacting surfaces and generating heat by converting kinetic energy, can be formulated as a function of normal load and coefficient of friction (COF).

$$F = \mu P \tag{9.1}$$

COF (expressed by μ) is a dimensionless scalar which is directly related to the material property and P is the normal load pressing the surfaces together. This theory was first formulated by Amontons (1699) and advanced by Coulomb (1785), and the equation is well known as Amontons-Columb law.

Wear is another phenomenon that happens in case of contact. In this process, one or both in-contact surfaces will lose material under mechanical and/or chemical processes [1]. The wear rate of the materials can be evaluated using two commonly used methods: (1) weight loss and (2) volume loss [2].

In most of the applications, liquid- or greased-based lubricants are used to reduce the effects of friction and wear. Lubricants are made of materials with lower shear strength compare to sliding surfaces [1]. Therefore, this layer of material between two sliding surfaces reduces friction during relative motion. Under extreme conditions, such as vacuum, extreme temperatures (low or high), and pressure contact and radiation, using the liquid lubricants becomes challenging. Under these circumstances, solid lubricants are the alternatives. These lubricants are made of low shear strength materials and functions same as liquid-based lubricants [3–5].

As opposed to the liquid-lubricants, a constant supply of solid-lubricants can be challenging. The most avant-garde solution to this challenge was the introduction of self-lubricating materials. A self-lubricating material is a composite with its matrix reinforced using solid lubricants such as graphite, MoS_2, (Fig. 9.1). These materials facilitate the relative motion by incorporating a self-dispensed and self-regulated solid-lubricant delivery system. Since the initial development of self-lubricating

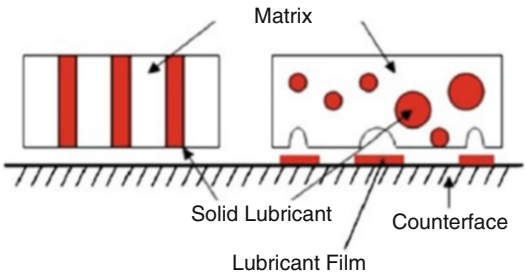

Fig. 9.1 Schematic of self-lubricating composites and its mechanism [15]. (With permission of Springer)

materials, different groups researched and developed a variety of self-lubricating materials [3–11].

As shown in the Fig. 9.1, the solid-lubricant particles continuously will be exposed to the surface due to wear against the contact surface. These solid-lubricant particles then form a thin layer of lubricants which reduces the friction and wear effect of sliding. These layers are not present initially and form as results of worn surface and subsurface deformation [2, 12]. Different industries can benefit from self-lubricating effect, from atomistic scale (i.e., atomic force microscopy [13]) up to macro scale (i.e., bearing [14]).

As mentioned earlier, Amontons-Columb law can estimate the COF as a function of friction and applied normal forces. Despite the great success of this theory in bulk models, the Amontons-Columb law fails to predict the micro−/nanoscale behavior of the friction. The micro−/nanoscale behavior can be well described as a many-body system. In order to simulate a many-body system, a suitable molecular model of the system is formulated and the molecular trajectories are calculated using different numerical schemes.

These trajectories then are used to calculate the properties of the system. Different methods have been developed over the years. Quantum Mechanical (QM), Molecular Mechanics (MM), Monte Carlo (MC), and Molecular Dynamics (MD) are the most commonly used models. Each of these methods has their own advantages and disadvantages. Based on the application and the requirements of the problem, one can select the most appropriate approach.

In the next section, the most used theoretical models are introduced briefly and MD is described in more details. After that, a summary of investigated MD simulation of dry friction and a few self-lubricating materials are presented.

9.2 Methods

The Quantum Mechanical (QM) method solves a simplified Schrodinger's equation for a many-particle system where particles are treated as wave functions. The equations describe the spatial probability distributions corresponding to the energy states and are solved to obtain saddle points or minima on the potential energy surface. The Schrodinger wave equation describing the motions of electrons and nuclei in a molecular system is:

$$H\psi = E\psi \tag{9.2}$$

where H is the Hamiltonian and calculates as:

$$H = E_k \ + E_p \tag{9.3}$$

Here E_k is the kinetic energy and E_p represents the potential energy. For a *3D* system, the wave function ψ depends on the 3N coordinates of all the particles and therefore even for a relatively small number of particles, it is extremely difficult to

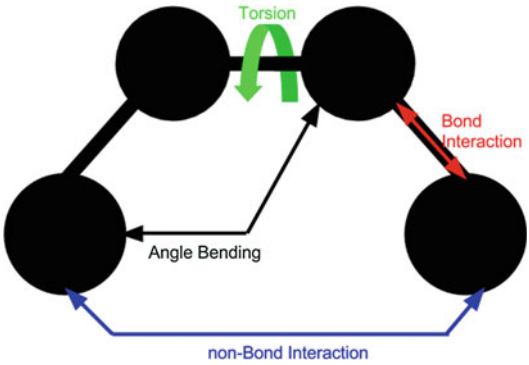

Fig. 9.2 Schematic representation of applied forces

solve the equation without simplifications or approximations. Despite the accuracy of the model which calculations match experimental data or a theoretical prediction, the exponential increment of computation time with the number of particles makes this method un-practical for more complicated models.

The Molecular Mechanics (MM) method is based on classical mechanics where atoms in the molecules are treated as particles with mass, which interact in a force field. The force field functions are obtained from quantum mechanics calculations. The bonds between the atoms are treated as springs and spring deformation is used to characterize bond stretching (E_{bond}), bending (E_{angle}), and torsion (E_{tor}) (Fig. 9.2). To mimic nonbonded atoms, van der Waals and electrostatic interaction are used ($E_{\text{non - bond}}$) (Fig. 9.2). Again, the aim is to find saddle points or minima on the potential energy surface using appropriate mathematical algorithms. The potential energy is typically the sum of all the energies associated with bonded and nonbonded interactions. A typical functional form of the potential energy function is:

$$E = E_{\text{bond}} + E_{\text{angle}} + E_{\text{tor}} + E_{LJ} + E_{\text{coul}} \tag{9.4}$$

$$E_{\text{bond}} = \sum_{\text{bonds}} \frac{1}{2} k_b \left(b - b_0\right)^2 \tag{9.5}$$

$$E_{\text{angle}} = \sum_{\text{angles}} \frac{1}{2} k_{\varnothing} \left(\varnothing - \varnothing_0\right)^2 \tag{9.6}$$

$$E_{\text{tor}} = \sum_{\text{tor}} \frac{1}{2} \tau [1 \pm \cos\left(n\alpha - \beta\right)] \tag{9.7}$$

$$E_{\text{non-bond}} = \sum_{\text{atomic pairs}} 4\varepsilon_{ij} \left[\left(\frac{\sigma_{ij}}{r_{ij}}\right)^{12} - \left(\frac{\sigma_{ij}}{r_{ij}}\right)^{6} \right] + k \frac{q_i q_j}{r_{ij}} \tag{9.8}$$

The bond stretching equation (Eq. 9.5) and bending energy equation (Eq. 9.6) are based on Hook's law. Here k_b represents the stiffness of the bond, b_0 stands for the equilibrium length which both are depends on type of the bond (e.g., C–C, O–C,

etc.), and b is the length of bond. Same as the bond stretching equation, in bending equation (Eq. 9.6), $k_{\varnothing}$ represents the stiffness of the angle, $\varnothing_0$ is the equilibrium angle, and $\varnothing$ stands for the angle of the bond. In order to correct the calculated energy (bond stretching energy + bending energy + non-bonded energy) and make it to agree with experimental measurements, the torsion energy (Eq. 9.7) was added to the energy equation as a periodic function. In this function (Eq. 9.7), τ controls the amplitude of the function and β shifts the function along the rotation angle axis (α). All parameters from torsion equation are assigned based on bond type (e.g., C-C-C-C, C-O-C-N). As mentioned before, van der Waals attraction, repulsion, and electrostatic interactions are taken into account as nonbonded energy (Eq. 9.8). The repulsion/attraction effect is modeled using Lennard–Jones potential where r_{ij} is the distance between two atoms and σ_{ij} and ε_{ij} are Lennard-Jones parameters depending on interacting atoms (e.g., C-O, C-H). The second term of Eq. 9.8 is Coulomb electrostatic potential where q is the partial charge of each atom and k is Coulomb's constant.

The Monte Carlo (MC) method is used to simulate systems with fixed N number of particles in a fixed volume V, at absolute temperature T. For such a system, MC as an iterative method tries to minimize the system's potential by randomly moving atoms into a new position. As the number of random numbers increases to infinity, the solutions get closer to the correct solution. In order to decrease the randomness and consequentially decreasing the computational time, since the Boltzmann factor causes the possible configurations to make non-uniform contributions, a sampling method can be implemented in the Metropolis method. Despite the MC's simplicity of implementation, it cannot be used to study time-dependent properties and is applicable only for configurations near equilibrium systems.

9.2.1 Molecular Dynamics

The Molecular Dynamics (MD) models can be categorized into two groups based on their formulation as classical and first-principles. In the classical approach, molecules are modeled as classical objects, something like "ball and stick" model. In this model, atoms are considered as soft balls and bonds model as elastic sticks, and the laws of classical mechanics define the dynamics of the system. The first-principles or quantum MD simulations take the quantum nature of chemical bonds into account explicitly. Despite its important improvement over the classical model, the computational cost of this model makes it impractical to implement. Therefore, in this section the classical MD model will be described and referred to as MD.

In MD simulation, the time evolution of a set of interacting particles is solved based on Newton's second law or the equation of motion for a many-body system as

$$F_i = m_i \frac{d^2 r_i(t)}{dt^2} \tag{9.9}$$

where F_i is the force acting on ith particle at time t and m_i is the mass of the particle. And $r_i(t)$ represents the position vector of ith particle at time t as $r_i(t) = (x_i(t),y_i(t), z_i(t))$. In MD, "Particles" usually refer to atoms, although they may represent any district entities that can be conveniently described in terms of a certain interaction law. To integrate the second-order differential equation of the equation of motion, the forces acting on each particle at each time step as well as their initial position and velocities need to be specified. Then the integration of the equations yields a trajectory that describes the position, velocities, and accelerations of the particles as they marching forward in time. As the particles move, their trajectories may be analyzed in order to calculate their average properties. Once the positions and velocities of each atom are known, the state of the system can be predicted at any time.

Interaction between particles can be calculated using force field or quantum chemical models, or via mixing force fields and quantum chemical models. The atomic force field model describes physical system as collection of atoms kept together by interatomic forces. The interaction law is specified by the potential $E(r_1,\ldots,r_N)$ (Eq. 9.4), which represents the potential energy of N interacting atoms as a function of their positions $r_i = (x_i,y_i,z_i)$. Given the potential, the force acting upon ith atom is determined by the gradient with respect to atomic displacements as:

$$F_i = -\nabla_{r_i} E(r_1,\ldots,r_N) = -\left(\frac{\partial E}{\partial x_i}, \frac{\partial E}{\partial y_i}, \frac{\partial E}{\partial z_i}\right) \tag{9.10}$$

Having the force fields as a function of particles location, one can calculate each particles position ($r_i(t + \Delta t)$) at time $t + \Delta t$ by integrating the Newton's equation of motion in time by knowing the positions at time t. Numerous numerical algorithms have been developed for integration. Some of the most used ones are: Verlet algorithm, Leap-frog algorithm, Velocity Verlet, and Beeman's algorithm. All the integration algorithms assume the position can be approximated by a Taylor series expansions. The basic formula for the Verlet algorithm can be expressed by writing two third-order Taylor expansion of the position $r(t)$, one forward and one backward in time:

$$r_i(t+\Delta t) = r_i(t) + v_i(t)\Delta t + \frac{1}{2}\frac{F_i(t)}{m_i}\Delta t^2 + \frac{1}{6} b_i(t)\Delta t^3 + O\left(\Delta t^4\right) \tag{9.11}$$

$$r_i(t-\Delta t) = r_i(t) - v_i(t)\Delta t + \frac{1}{2}\frac{F_i(t)}{m_i}\Delta t^2 - \frac{1}{6} b_i(t)\Delta t^3 + O\left(\Delta t^4\right) \tag{9.12}$$

where $v_i(t)$ represents the velocity and $b_i(t)$ the third derivative of position of the ith particle with respect to time. Adding the two expressions gives:

$$r_i(t+\Delta t) \cong 2r_i(t) - r_i(t-\Delta t) + \frac{F_i(t)}{m_i}\Delta t^2 \tag{9.13}$$

The truncation error of the algorithm when evolving the system by Δt is of the order of Δt^4. A problem with this version of the Verlet algorithm is that velocities are not directly calculated. While they are not needed for time evolution, their comprehension is sometimes necessary. Moreover, they are required to compute the kinetic energy K, whose evaluation is necessary to test the conservation of the total energy $E = K + V$. One simple way to calculate the velocity is by using the position as:

$$v_i(t) = \frac{r_i(t + \Delta t) - r_i(t + \Delta t)}{2\Delta t} \tag{9.14}$$

As one can immediately see, the error is not an order of Δt^4 anymore but Δt^2. To overcome this problem, different variations of the Verlet algorithm have been developed. The *leap-frog* and *velocity* Verlet scheme are two of many [16]. One cloud calculates the velocity using the *velocity* Verlet scheme as following:

$$r_i(t + \Delta t) = r_i(t) + v_i(t)\Delta t + \frac{1}{2}\, a_i(t)\Delta t^2 \tag{9.15}$$

$$v_i\left(t + \frac{\Delta t}{2}\right) = v_i(t) + \frac{1}{2}a_i(t)\Delta t \tag{9.16}$$

$$a_i(t + \Delta t) = -\frac{1}{m_i}\nabla_{r_i} E_i(r(t + \Delta t)) \tag{9.17}$$

$$v(t + \Delta t) = v\left(t + \frac{\Delta t}{2}\right) + \frac{1}{2}a(t + \Delta t)\Delta t \tag{9.18}$$

These equations can be solved in an iterative fashion. By setting the initial values of positions and velocities, one can numerically solve the above equations to obtain the new position and velocities. Once all the trajectories are obtained, they can be used to calculate other static and dynamic properties as well as system temperature.

As it can be observed, MM and MD are both based on classical mechanics and have some fundamental similarities. Both methods are computationally fast, can handle large number of atoms, and are using potentials obtained by QM. However, the advantage of MD compare to MM is that this method is capable of capturing the dynamic of the system and therefore ease of calculating non-equilibrium state of the system.

9.3 Simulating Friction Using Molecular Dynamics

Different research groups were trying to develop an equipment to measure the friction phenomena in the atomic level and validate the theory. The first atomic friction measurements were reported by Mate et al. [17]. Development of the atomic force microscope (AFM) enabled researchers to quantitatively measure friction forces. Since the first measurement, the AFM experiment setup has not changed a

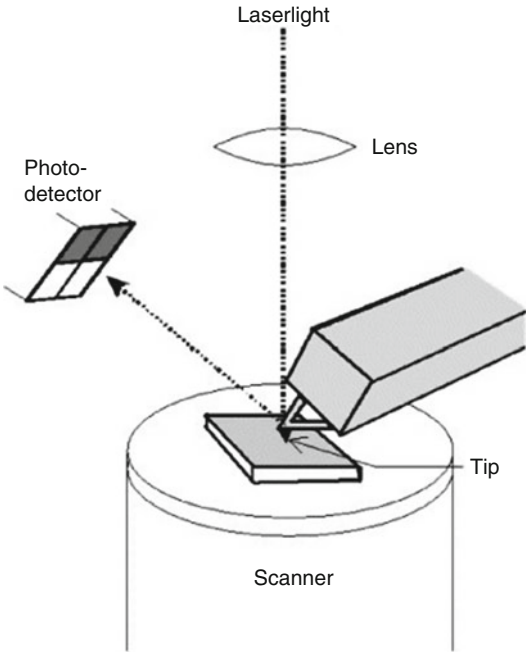

Fig. 9.3 Schematic of an atomic force microscope (AFM). (Reprinted from [18], Copyright 2005, with permission from Elsevier)

lot. An AFM setup consists of a nanoscale tip mounted on a microscale cantilever as well as a fixed substrate as schematically shown in Fig. 9.3. Moving the tip against the substrate under a small normal load of a few nano-Newton causes a torsion twisting in the cantilever. The torsional twisting is caused by the lateral force recorded by an optical technique. Moving the tip back and forth generates a force contrast pattern called a lateral force image (friction image), or a lateral trace (friction trace) which shows the resistance of the substrate to sliding tip. The variation of the friction trace is often not smooth due to the atomic discreteness of the surface, but it is more like a saw-tooth pattern refer to as stick-slip friction. It is called stick-slip since the tip sticks at some position for a while and then slips forward in the direction of the lateral forces. The stick-slip pattern can be used for friction-related quantities such as frictional resistance of the surface.

It has been shown that in dry surface contact, only a small number of micro- and nano size asperities come into contact. The friction between each asperity and the substrate called atomic friction. The process of how these asperities come into contact has a significant influence on the frictional characterization of the sliding surfaces. Taking advantage of computer experiment, one can predict the friction forces using different available models such as MD by calculating atom trajectories by computing Newton's Second law. Since predicting and modeling this level of complexity requires a large amount of computational power and effort, many researchers simplified their study by focusing on the sliding of single micro−/nanoscale asperity surface. This fundamental understanding becomes even more

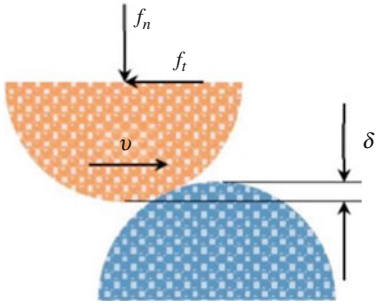

Fig. 9.4 Schematic asperity-asperity interaction [20]

relevant when we are looking at small-scale applications like Micro-electromechanical systems (MEMS) and Nanoelectromechanical systems (NEMS).

For better understanding, a single asperity-asperity interaction is described here (Fig. 9.4). In this model, an asperity on a moving base slides past on a stationary-based asperity under controlled velocity and normal load. The atoms on these asperities are initially at equilibrium where the attraction and repulsive forces from other atoms are balanced. As soon as the interaction starts, atoms in contact are no longer in balance. Under the influence of the interaction and the amount of forces applied on atoms, these atoms are moving away from their original position and may or may not return. Depending on the movement distance, if it is smaller than the bond length, by removing the forces atoms are able to get back to their original position. Otherwise, the atoms are displaced to the new positions. This model is the basis of different phenomena such as adhesion, plastic deformation, wear, and energy dissipation. As Gao et al. [19] showed, the number of atomic or molecular bonds that are broken or formed are directly proportional to the adhesion. Therefore, better understanding of this interaction can help with advancing the understanding of the other phenomena.

Bhavin et al. [21] developed a three dimensional geometrical model consists of two asperities each connected to a base in order to investigate the effect of different variables on friction coefficient. With moving one of the bases, the asperity-asperity interaction was modeled. Copper was chosen as the material in a lattice with the size of $3.615A^{\circ}$ with different orientation angles. The effect of different velocities was investigated as 10 *m/s* and 100 *m/s*. The time-step size was chosen as 0.002 ps. And the boundary condition was set to periodic at x and z-direction and shrink-wrapped in y-direction. In periodic directions, atoms can interact across the boundary, and they can exit from one end and enter from another end of the domain. As the shrink wrapping direction, the position of the face is set so as to encompass the atoms, no matter how far they move. As the result of the sliding (Fig. 9.5), they have studied effects of changing dimensions (radius of asperities (R) and interference (δ) as shown in Fig. 9.4), forces, sliding velocity, and lattice size for asperity-asperity interaction.

Using MD simulation other researchers were able to investigate different friction models. The atomic-scale friction of two diamond surfaces was modeled by Harrison et al. [22]. In this study as one of the early MD studies, they analyzed the friction as a

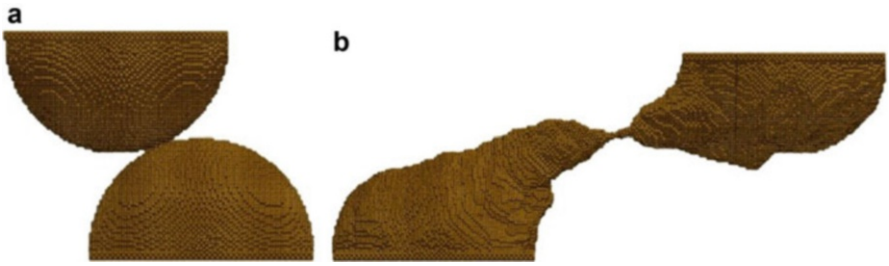

Fig. 9.5 Copper asperities before (**a**) and after (**b**) sliding process for $R = 7.5\ nm$, $v = 10\ m/s$ and $\delta/R = 0.1$ [20]

function of applied load, temperature, and sliding velocity. Zhang and Tanaka [23] showed four different deformation regimes as no-wear, adhering, plowing, and cutting of the surface by sliding a diamond tip on a flat copper. Song and Srolovitz [24] studied the effect of loading and unloading of forces between a single asperity surface and a flat surface. During repetitive contact, they observed the transformation from face-centered cubic into hexagonal close packed structure. Liu et al. [25] studied the effect of scratch direction on the friction coefficient. Zhang et al. [26] used MD to investigate the effect of stiffness of graphene on its friction behavior. The nanoscale friction between diamond-structure silicon (Si) and diamond was investigated by Bai et al. [27]. They have divided the friction into two stages: the static friction and the kinetic friction. The effective friction coefficient in a granular material was studied by Hurley and Andrade [28]. Hu et al. [29] studied the effect of adding Cu nanoparticles to the solid contact between friction surfaces. They have found that the friction forces are decreasing by increasing the sliding velocity. The atomic-scale friction of diamond (111) surface with boron doped diamond (111) surface was modeled by Wang et al. [30]. The effect of temperature and its relationship with roughness in dry sliding was studied by Spijker et al. [31]. Yang et al. [32] studied the nanoscale friction forces between hemisphere sphere sliding on rectangular solid plane. They have shown that with increasing the depth of the contact, the atoms close-packed accumulation increases.

9.4 Molecular Dynamics Simulation for Self-Lubricant Materials

MD simulations [13] have shown that the self-lubrication mechanism in two sliding surfaces is due to stabilization of the atomic cluster adsorbed from one surface to the other and the ability of the cluster structure adjustment. The self-lubricating ability of the material can be achieved by modifying the composition of the matrix with graphite [2, 9], graphene [33, 34], carbon nanotubes [35, 36], or inert polymeric molecules such as poly tetra-fluoro ethylene (PTFE) [10, 13]. Although the general influences of these components are similar, they each obey specific mechanism to result in self-lubricating effect.

9.4.1 Graphite and Graphene

The layered structure of graphite is a result of strong electronic σ-bonds between carbon atoms within a layer and weak electronic π-bonds between carbon atoms in adjacent layers. In this atomic structure, π-electrons play a dominant role in the intercalation among the carbon atoms and interactional atoms and facilitate the sliding process and reduce the friction between layers [9]. Yin et al. [37] modeled the sliding process and self-lubricating mechanism in alumina-graphite composite coating using MD simulation. Their model presents the preferred orientation for the hexagonal structure of graphite under shear forces during sliding of friction pairs. Figure 9.6 demonstrates the MD model, as two alumina surface glide under shear forces and the graphite shows significant stratification in the Z-direction. Over the simulation time the layers of graphite are adsorbed to the surfaces of the friction pair and decrease the chemical affinity between the contacting surfaces. Formation of layered structure of graphite with weak forces in c-direction and low adhesion explains the self-lubricating mechanism in the alumina-graphite composite.

As a two-dimensional material of sp2 carbon network, graphene has been introduced as an efficient solid lubricant [33]. Xu et al. [34] applied MD models to describe the "stick-slip" mechanism in few-layer (3–8) graphene (FLG). They divided the process to three stages including the initial stage, the developing stage, and the stable sliding stage to develop stable sliding interfaces. Their model contained 3–8 AB stacked graphene layers while each layer was composed of 3200 carbon. The top view of their system has been demonstrated in Fig. 9.7. The bottom layer shown in white has been fixed, and a constant velocity was applied to the two top layers in the shear direction, while they had constraints in other two orthogonal directions.

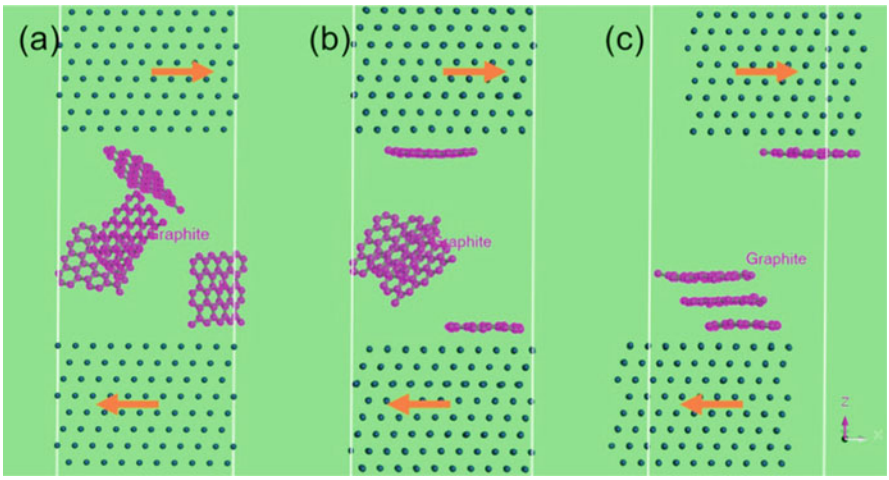

Fig. 9.6 MD model of sliding pair interface containing random graphite sheets after (**a**) 0 ps, (**b**) 30 ps, (**c**) 90 ps. (Reprinted from [37], Copyright 2016, with permission from Elsevier)

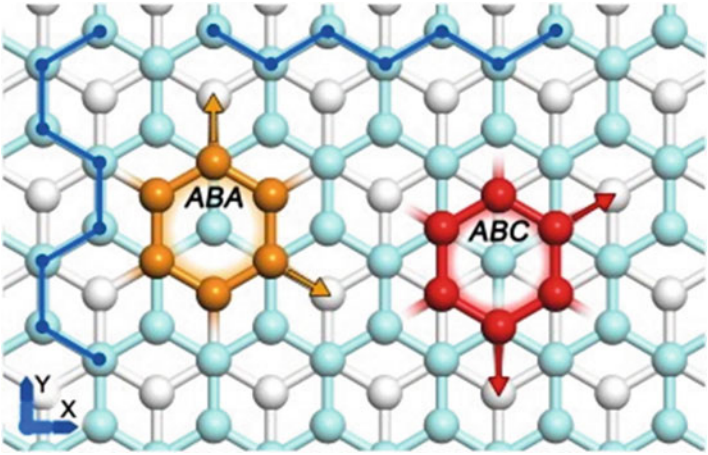

Fig. 9.7 Possible slip directions for the top layer in a three-layer graphene. The bottom layer and middle layer atoms are demonstrated in white and cyan, respectively, while the atoms of top layer with ABA and ABC stacking configurations have been presented in orange and red, respectively. (Reprinted from [34], Copyright 2012, with permission from Elsevier)

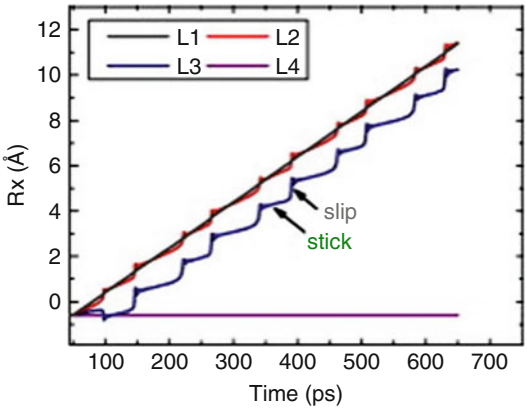

Fig. 9.8 Slip and stick during the motion of four graphene layers sliding in x-direction. (Reprinted from [34], Copyright 2012, with permission from Elsevier)

A sudden slip is observed after stick period in Fig. 9.8. The lateral stiffness of sliding body, which is greatly reduced by the existence of multiple weak interlayer interfaces, is always smaller than the lateral contact stiffness at the sliding interface, resulting in stick-slip system according to PT model (Prandtl-Tomlinson model) [38]. PT model suggests that the stick-slip feature is inevitable for systems containing more than three layers of graphene. This model confirms that the friction forces drop dramatically with decreasing the number of graphene layers, and they vanish as the number of layers decreases to three or two layers. Nanolubrication and self-lubricating materials can benefit from this mechanism of sliding in layers of graphene.

Graphene is also known to potentially control the nanowear on some substrates. The MD model by Zhang et al. [39] proves that during C_{60} intrusion, graphene can control nanowear. This MD Model consists of one lower and one upper substrates of Si (100) containing 4145 and 716 atoms, respectively. Depending on the position of the graphene layer covering each of these substrates, four different cases were compared as demonstrated in Fig. 9.9. In all the cases, the two surfaces made an angle (α) where the lower substrate was horizontal and a C_{60} intruding through the sliding substrates. The nanowear for the contact surface was evaluated by the number of dropped atoms (Si atoms that displaced more than the cutoff distance of 0.27 nm from the substrate). Figure 9.9 displays four different conditions for the nanowear test. In Fig. 9.9a the highest amount of wear is observed during intrusion of C_{60} between Si surfaces. Figure 9.9b shows the system when the upper substrate is layered by graphene. In this case the interactions among the C_{60} and two substrates are smaller than the first case. The upper substrate still bends during sliding and some of the Si atoms were pulled off from the bottom of the upper substrate. The third case is when only the lower substrate is layered by graphene as demonstrated in Fig. 9.9c. The MD calculations showed that in this case and also in a system including two graphene layers on both upper and lower substrates (Fig. 9.9d), no Si atom is pulled off from either of the substrates and only a slight bending is observed on the upper substrate. This MD model showed that through layering graphene on the substrate surfaces nanowear can be controlled in the system and no-wear of the sliding substrates can be realized.

9.4.2 Carbon Nanotubes (CNT)

Carbon nanotubes (CNTs) can be described as a rolled sheet/s of carbon atoms. Depending on the number of sheets, it can be single-walled carbon nanotubes (SWCNTs) with diameter of 1–2 nm or double- and multiwalled carbon nanotubes with diameter ranging from 4 to 20 nm (Fig. 9.10) [35].

Yao and Lordi [40] measured the SWCNTs stiffness using MD simulation as 1 TPa. Despite better mechanical property of SWCNTs compared to multiwalled carbon nanotubes (MWNTs), due to their higher production expenses, SWCNTs are less employed as a reinforcement. One of the limitations of MWNTs is telescoping effect where inner tubes can be pulled out from outer tubes due to tensile stresses. Interfacial friction and sliding of SWCNTs and MWCNTs embedded in an amorphous carbon matrix were modeled using MD by Li et al. [36]. Pavia and Curtin [41] also studied the interfacial sliding effect in ceramic composites using MD.

The mechanical behavior of individual single and multiwalled carbon nanotubes has been exclusively modeled and studied by different groups using MD. Zhao et al. [42] estimated the binding energy of two parallel SWCNTs as well as two cross MWCNTs using MD. The self-assembly process of edge-unpassivated graphene nanoribbons with defects using SWNCT was modeled by Zhang and Chen [43]. The vibration characterization of single and double carbon nanotubes was studied using MD models by Ansari et al. [44]. Ghosh and Padmanabhan [45] modeled the effect

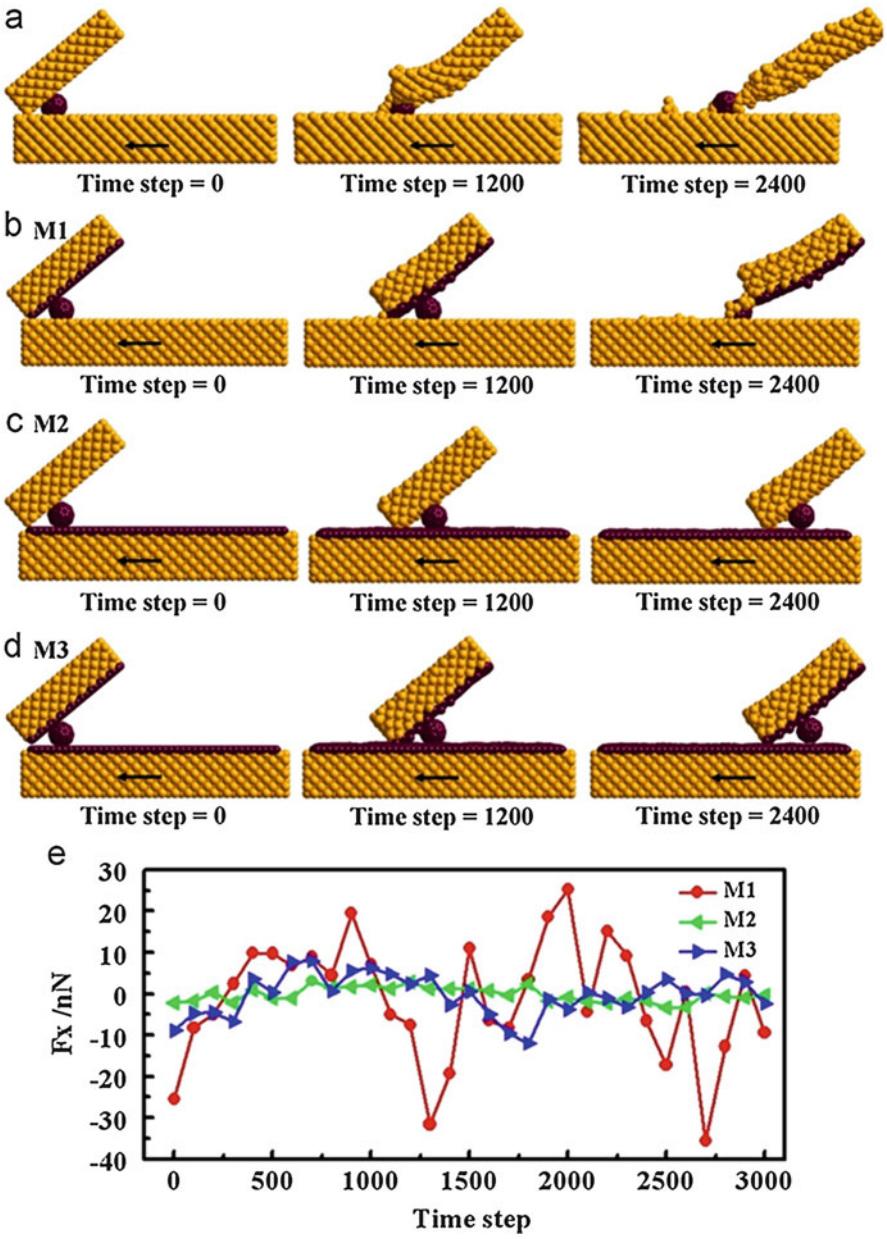

Fig. 9.9 MD model snapshots during *C*60 ball intrusion (**a**) for two sliding Si substrates, (**b**) upper substrate layered by grapheme, (**c**) lower substrate layered by graphene, (**d**) both upper and lower substrates layered by graphene. (Reprinted from [39], Copyright 2012, with permission from Elsevier)

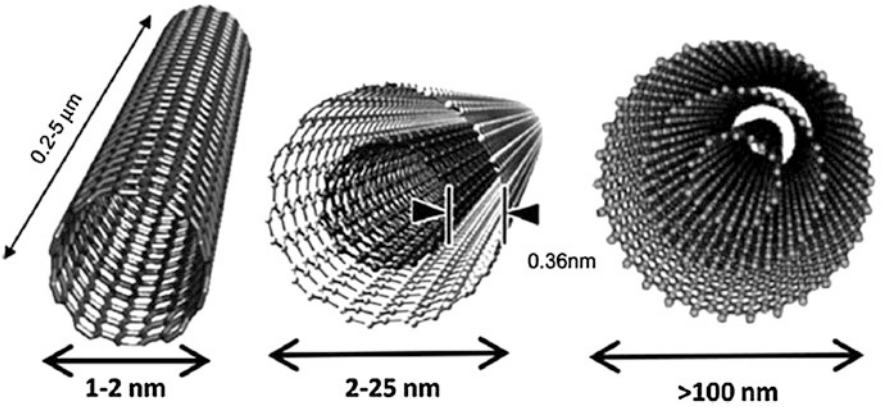

Fig. 9.10 Single-, double-, and multiwalled carbon nanotubes (CNTs). (Reprinted from [35], Copyright 2015, with permission from Elsevier)

of different types of defection on SWCNTs capacity of hydrogen adsorption using both MD and density functional theory (DFT). These publications are just a few of so many of available studies in the literature on the behavior of carbon nanotubes.

Despite exclusive studies using MD simulation of individual SWCNTs and MWCNTs in the literature, to the best of authors' knowledge, there is no specific MD study, addressing the lubricating behavior of composites using carbon nanotubes as reinforcement.

9.4.3 MoS_2-Based Nanostructures

D-transition metal dichalcogenides (TmS_2, Tm = Mo, W, Nb, and Ta) not only reduce the friction coefficient as lubricant materials, but also they maintain their lubricating capability at higher loads compared to the traditional lubricants. The tribological properties of these materials can even enhance if they are applied in the form of spherical or cylindrical nanostructures. The "bearing effect" is known to be responsible for this enhancement. Due to this effect the nanoparticles enter the intersurface area and act as a ball bearing during the sliding of the two surfaces against each other [46]. Among this group of materials, MoS_2 has been the center of attention in recent studies. Dallavalle et al. [47] introduced an MD model to describe the lubrication effect of MoS_2 nanotubes. They simulated the sliding of the top layers by keeping the velocities of the top sulfur atoms constant in the a-direction and unrestricted in the b- and c-directions. The sliding direction was kept constant during the simulation, while a normal load was applied on the top surface as demonstrated in Fig. 9.11. The model studies the sliding process in both a- and b-directions for an armchair double-wall nanotube, indices pairs such as (29,29)@(36,36). Constant number, volume, and temperature (NVT) ensemble at 298 K was used for all the calculations with sliding velocity of 100 m/s. The sliding of the double walled

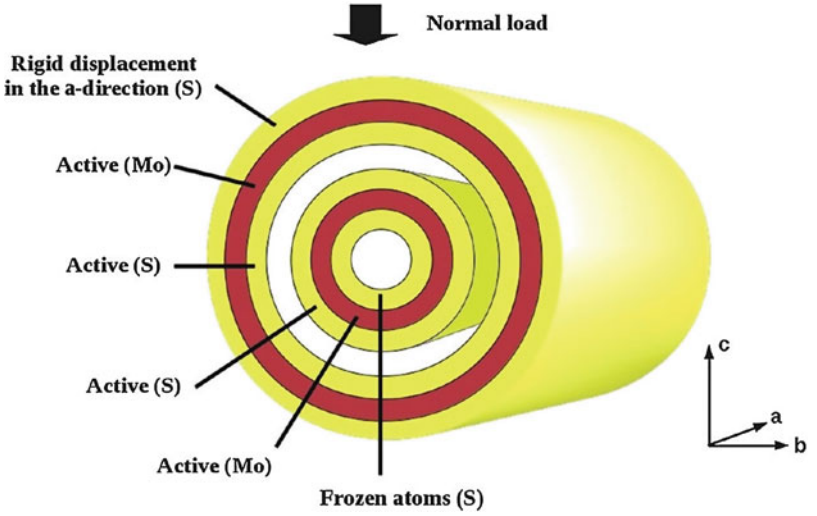

Fig. 9.11 Schematic of DWNT during the sliding modeled with MD simulation. A normal load is applied in the c-direction and the motion of the DWNT is rigid in a-direction. (Reprinted with permission from [47]. Copyright 2012 American Chemical Society)

nanotube (DWNT) in a-direction showed that the top layer slides along a sinusoidal, zigzag rout, because the sulfur atoms avoid each other and try to stay close to molybdenum atoms. For sliding in b-direction, the top layer has a random motion with an occasional large diagonal movement.

This model averages the frictional coefficient over the forces of the sulfur atoms, from auto-correlation function (ACF) of the forces using Green-Kubo equation (Eq. 9.19) and the friction coefficient from classical physics Amonton's laws (Eq. 9.20).

$$K = c \int_0^{\infty} < A(t)d(t) > \tag{9.19}$$

where K is the friction coefficient, A are the forces experienced by the system in the friction process, and in Eq. 9.20, F is the lateral friction force and L is the normal, externally applied load.

$$\mu = \frac{F}{L} \tag{9.20}$$

They showed that the friction differs for sliding in a- and b-direction because of the smaller oscillations observed during the dynamics and sudden diagonal displacement of MoS_2 layer in b-direction. The microscopic model based on the Green-Kubo equation demonstrates a high lubricating performance of MoS_2 in optimal conditions. They also showed a reverse relationship between the friction coefficient and

force, which can be explained by increase in repulsive contribution of the Lennard-Jones potential at higher loads. This contribution results in better sliding and lower friction coefficient in MoS_2 DWNTs.

9.4.4 Poly Tetra-Fluoro Ethylene (PTFE) (Polymeric Agents)

Poly tetra-fluoro ethylene (PTFE) can be applied in metal-, ceramic-, and carbon-based composites to improve the mechanical and thermal properties and more importantly to decrease the friction [6–8]. This resin has excellent antiwear performance. It is chemically stable and naturally softer than conventional metals, so; it can reduce the friction if applied as sliding parts between sliding metallic surfaces. It has been suggested that the formation of transfer films is responsible for the friction reduction [48]. Although the thickness of this film is only few nanometers, its presence between sliding PTFE and metallic surface reduces the friction and results in self-lubricating effect in the composite. Here we will go over some atomistic models covering both formation of the nanoscale transfer film and also the self-lubrication mechanism in corresponding composites.

Onodera et al. [10] evaluated the friction behavior of aluminum surface considering the chemical reaction with Polytetrafluoroethylene. Their model benefited from quantum chemical molecular dynamics (QCMD) method and considered aluminum oxide to represent a typical surface of aluminum alloy. α-Al_2O_3 and three layers of PTFE chains aligned parallel to the α-Al_2O_3 surface form the geometry of the model. The topmost surface of α-Al_2O_3 was fully terminated by the OH groups to represent the chemisorption of water vapor from the atmosphere in contact with the aluminum surface. Mechanical forces on the α-Al_2O_3 layer consist of vertical pressure of 500 MPa forcing the oxide toward the polymeric layers and the shear velocity of 100 m/s resulting in the sliding of the α-Al_2O_3 over the polymer. One bottom layer of the crystalline PTFE was fixed to represent the bulk material. This model suggested that the formation of the transfer film is conditional to elimination of the interfacial electrostatic repulsion between two sliding surfaces. Such repulsive forces are the result of formation of aluminum fluoride due to reaction of the aluminum atom from the surface oxide with the fluorine from the PTFE chain during the sliding. In another model [11], they showed that the tribological performance of the surface can be enhanced by the chemical reaction of the aluminum surface with water vapor in the atmosphere. The carboxyl group that forms as a product of such reaction results in increasing the amount of transfer film on aluminum surface and consequently improving the self-lubrication behavior of the surface. They used classical MD method to study the sliding of the PTFE/aluminum interface with three different structures as demonstrated in Fig. 9.12. The first configuration in Fig. 9.12a represents the interface between OH-terminated α-Al_2O_3 and genuine PTFE prior to their tribochemical reaction, Fig. 9.12b shows the tribochemical reaction on the α-Al_2O_3/*PTFE* interface and the F-terminated α-Al_2O_3/*genuine* PTFE interface. Figure 9.12c also models the F-terminated α-Al_2O_3/*genuine* PTFE interface where the top layer of PTFE contains

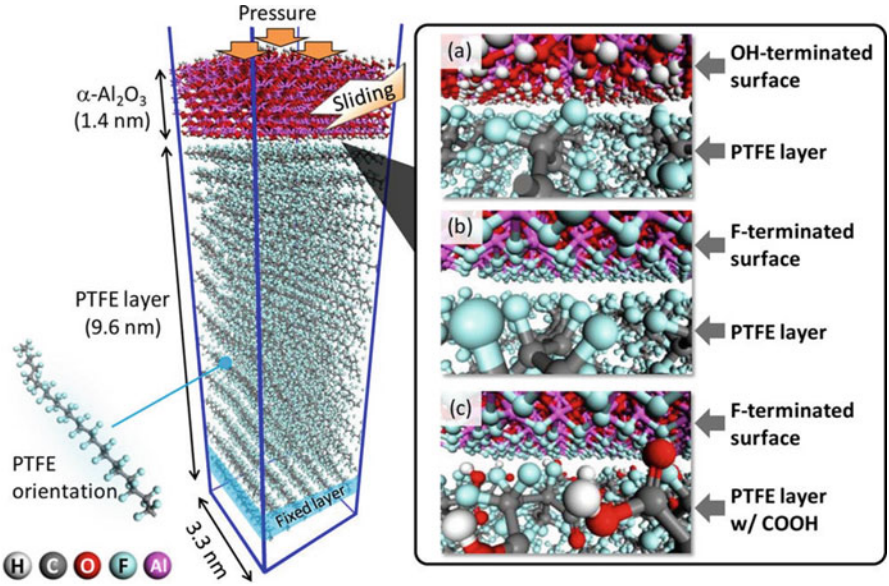

Fig. 9.12 Transfer film formation on PTFE α-Al_2O_3 (**a**) PTFE/OH-terminated α-Al_2O_3 (**b**) PTFE/F-terminated α-Al_2O_3 and (**c**) PTFE with carboxyl group/F-terminated α-Al_2O_3. (Reprinted with permission from [11]. Copyright 2014 American Chemical Society)

several carboxyl groups as a product of chemical reaction between PTFE and water vapor. A periodic boundary condition was applied to the system for the MD model at temperature of 300 K. The topmost layer of α-Al_2O_3 was under vertical pressure in such way that on a real contact area of PTFE/Al system, the pressure was set to a few hundred mega-pascals (500 MPa) in the molecular-level because on a real contact area of PTFE/Al system, the pressure is much higher than a macroscopic contact pressure which is typically in the mega-pascal order. The bottom layer of the PTFE was fixed and sliding parallel to PTFE chains with velocity of 10 m/s was applied to the α-Al_2O_3 as demonstrated in Fig. 9.13. In the first model in Fig. 9.13a, the PTFE transfer film was generated on the OH-terminated surface and the sliding interface appeared between the PTFE layers and not in the *PTFE*/α-Al_2O_3 interface. The second model in Fig. 9.13b, which represents an F-terminated α-Al_2O_3 surface only two of the PTFE layers form the transfer film. The chemical reaction between PTFE and α-Al_2O_3 is responsible for the difference between these two models. When the hydroxyl group stays on the α-Al_2O_3 surface, the electrostatic attraction between the hydrogen atoms and fluorine atoms in PTFE facilitates the transfer of PTFE. On the other hand when the α-Al_2O_3 is terminated by fluorine atoms, the electrostatic repulsion between PTFE and the F-terminated α-Al_2O_3 inhibits the transfer of PTFE layer. The third model is when the carboxyl group forms as a product of interaction with water vapor. In such case as shown in Fig. 9.13c although the surface was terminated by fluorine atoms, three or four layers of PTFE were transferred.

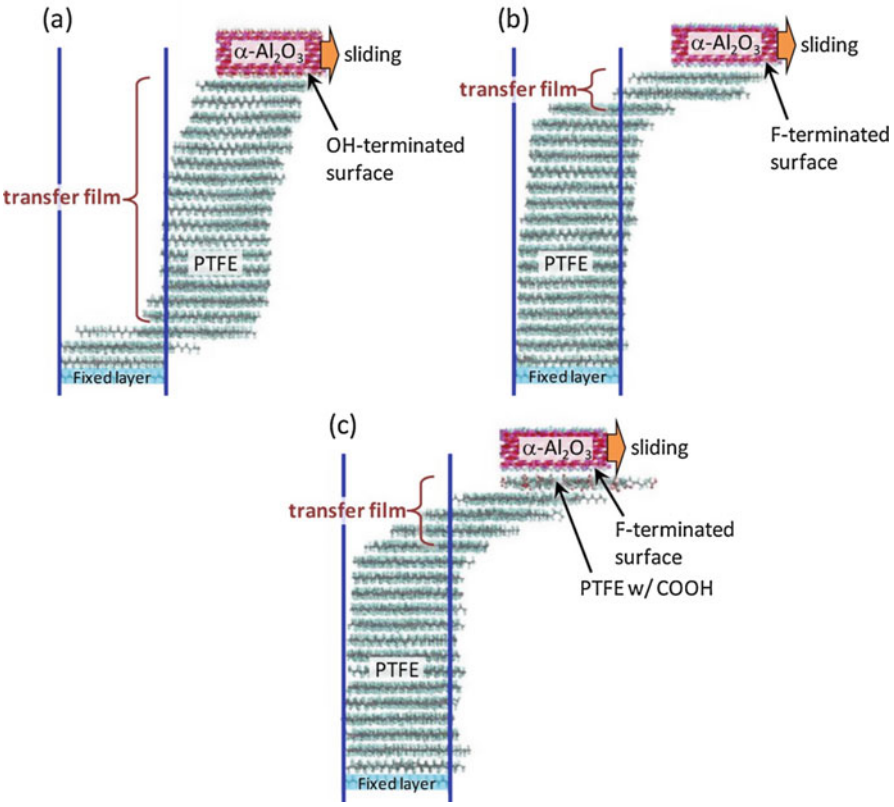

Fig. 9.13 Final structure of the three different PTFE/α-Al_2O_3 interface of Fig. 9.12 from MD simulation with sliding distance of 5 *nm* for all the models. (Reprinted with permission from [11]. Copyright 2014 American Chemical Society)

9.5 Conclusion

In this chapter, the commonly used theoretical and MD models describing the friction behavior of self-lubricating materials have been discussed. Different mechanisms have been reported to be responsible for friction reduction in such materials including the bearing effect in MoS_2 and carbon nanotubes, and the anisotropic forces between carbon atoms facilitating the sliding of graphite sheets.

These mechanisms were studied using MD models over the last three decades. It has been shown and validated by different groups that computational models are accurate methods to enhance the understanding of such phenomena. Despite the exclusive number of MD researches on different materials, there are only a few studies with focus on self-lubricant materials. The main reason is the complexity of self-lubricating systems which is a drawback for researchers to develop such models. Another limiting factor is the computational expense of these studies which growth

exponentially with increase in the number of modeled atoms. Therefore, the computational models of self-lubricating materials require more research in MD model implementation.

References

1. Menezes, P.L., Reeves, C.J., Lovell, M.R.: Fundamentals of Lubrication, pp. 295–340. Springer, New York (2013). https://doi.org/10.1007/9781-4614-1945-7-10
2. Omrani, E., Moghadam, A.D., Menezes, P.L., Rohatgi, P.K.: Influences of graphite reinforcement on the tribological properties of self-lubricating aluminum matrix composites for green tribology, sustainability, and energy efficiencya review. Int. J. Adv. Manuf. Technol. **83**(1–4), 325–346 (2016)
3. Dorri Moghadam, A., Schultz, B.F., Ferguson, J.B., Omrani, E., Rohatgi, P.K., Gupta, N.: Functional metal matrix composites: self-lubricating, self-healing, and nanocomposites-an outlook. JOM. **66**(6), 872–881 (2014.) http://link.springer.com/10.1007/s11837-014-0948-5
4. Shankara, A., Menezes, P.L., Simha, K.R.Y., Kailas, S.V.: Study of solid lubrication with MoS_2 coating in the presence of additives using reciprocating ball-on-flat scratch tester. Sadhana. **33** (3), 207–220 (2008.) http://link.springer.com/10.1007/s12046-008-0014-5
5. Omrani, E., Dorri Moghadam, A., Menezes, P.L., Rohatgi, P.K.: New Emerging Self-lubricating Metal Matrix Composites for Tribological Applications, pp. 63–103. Springer, Cham (2016). https://doi.org/10.1007/9783-319-24007-7-3
6. Chen, W.X., Li, F., Han, G., Xia, J.B., Wang, L.Y., Tu, J.P., Xu, Z.D.: Tribological behavior of carbon-nanotube-filled PTFE composites. Tribol. Lett. **15**(3), 275–278 (2003)
7. Krick, B.A., Ewin, J.J., Blackman, G.S., Junk, C.P., Gregory Sawyer, W.: Environmental dependence of ultra-low wear behavior of polytetrafluoroethylene (PTFE) and alumina composites suggests tribochemical mechanisms. Tribol. Int. **51**, 42–46 (2012). https://doi.org/10.1016/j.triboint.2012.02.015
8. Ye, J., Khare, H.S., Burris, D.L.: Transfer film evolution and its role in promoting ultralow wear of a PTFE nanocomposite. Wear. **297**(1–2), 1095–1102 (2013)
9. Chung, D.D.L.: Review: graphite. J. Mater. Sci. **37**(8), 1475–1489 (2002)
10. Onodera, T., Kawasaki, K., Nakakawaji, T., Higuchi, Y., Ozawa, N., Kurihara, K., Kubo, M.: Chemical reaction mechanism of polytetrafluoroethylene on aluminum surface under friction condition. J. Phys. Chem. C. **118**(10), 5390–5396 (2014)
11. Onodera, T., Kawasaki, K., Nakakawaji, T., Higuchi, Y., Ozawa, N., Kurihara, K., Kubo, M.: Effect of Tribochemical reaction on transfer-film formation by poly(tetrafluoroethylene). J. Phys. Chem. C. **118**(22), 11820–11826 (2014). https://doi.org/10.1021/jp503331e
12. Rohatgi, P.K., Ray, S., Liu, Y.: Tribological properties of metal matrix-graphite particle composites. Int. Mater. Rev. **37**(1), 129–152 (1992). https://doi.org/10.1179/imr.1992.37.1.129
13. Livshits, A.I., Shluger, A.L.: Self-lubrication in scanning-force-microscope image formation on ionic surfaces. Phys. Rev. B. **56**(19), 12482 (1997)
14. Orkin, S., Hudacko, V.: Self-lubricating bearing. US Patent 3,428,374, 18 Feb 1969. [Online]. Available: https://www.google.com/patents/US3428374
15. MacKerell, J.A.D., Bashford, D., Bellott, M., Dunbrack, J.R.L., Evanseck, J.D., Field, M.J., Fischer, S., Gao, J., Guo, H., Ha, S., Joseph-McCarthy, D., Kuchnir, L., Kuczera, K., Lau, F.T. K., Mattos, C., Michnick, S., Ngo, T., Nguyen, D.T., Prodhom, B., Reiher, W.E., Roux, B., Schlenkrich, M., Smith, J.C., Stote, R., Straub, J., Watanabe, M., Wiorkiewicz-Kuczera, J., Yin, D., Karplus, M.: All-atom empirical potential for molecular modeling and dynamics studies of proteins. J. Phys. Chem. B. **102**(18), 3586–3616 (1998). https://doi.org/10.1021/jp973084f
16. Allison, T.C., Coskuner, O., Gonzalez, C.A.: Metallic Systems: A Quantum Chemist's Perspective. CRC Press, Boca Raton (2011)

17. Mate, C.M., McClelland, G.M., Erlandsson, R., Chiang, S.: Atomic-scale friction of a tungsten tip on a graphite surface. Phys. Rev. Lett. **59**(17), 1942–1945 (1987). https://doi.org/10.1103/PhysRevLett.59.1942
18. Butt, H.-J., Cappella, B., Kappl, M.: Force measurements with the atomic force microscope: technique, interpretation and applications. Surf. Sci. Rep. **59**(1), 1–152 (2005)
19. Jianping Gao, Luedtke, W.D., Gourdon, D., Ruths, M., Israelachvili, J.N., Landman, U.: Frictional forces and Amontons' law: from the molecular to the macroscopic scale. J. Phys. Chem. B. **108**(11), 3410–3425 (2004). https://doi.org/10.1021/jp036362l
20. Vadgama, B.N.: Molecular Dynamics Simulations of Dry Sliding Asperities to Study Friction and Frictional Energy Dissipation. Ph.D. dissertation, Auburn University (2014)
21. Vadgama, B.N., Jackson, R.L., Harris, D.K.: Molecular scale analysis of dry sliding copper asperities. Appl. Nanosci. **5**(4), 469–480 (2015.) http://link.springer.com/10.1007/s13204-014-0339-9
22. Harrison, J.A., White, C.T., Colton, R.J., Brenner, D.W.: Molecular-dynamics simulations of atomic-scale friction of diamond surfaces. Phys. Rev. B. **46**(15), 9700–9708 (1992). https://doi.org/10.1103/PhysRevB.46.9700
23. Zhang, L., Tanaka, H.: Towards a deeper understanding of wear and friction on the atomic scalea molecular dynamics analysis. Wear. **211**(1), 44–53 (1997.) http://linkinghub.elsevier.com/retrieve/pii/S0043164897000732
24. Song, J., Srolovitz, D.J.: Atomistic simulation of multicycle asperity contact. Acta Mater. **55** (14), 4759–4768 (2007)
25. Liu, X., Liu, Z., Wei, Y.: Ploughing friction and nanohardness dependent on the tip tilt in nano-scratch test for single crystal gold. Comput. Mater. Sci. **110**, 54–61 (2015)
26. Zhang, H., Guo, Z., Gao, H., Chang, T.: Stiffness-dependent interlayer friction of graphene. Carbon. **94**, 60–66 (2015)
27. Bai, L., Sha, Z.-D., Srikanth, N., Pei, Q.-X., Wang, X., Srolovitz, D.J., Zhou, K.: Friction between silicon and diamond at the nanoscale. J. Phys. D Appl. Phys. **48**(25), 255303 (2015)
28. Hurley, R.C., Andrade, J.E.: Friction in inertial granular flows: competition between dilation and grain-scale dissipation rates. Granul. Matter. **17**(3), 287–295 (2015). https://doi.org/10.1007/s10035-015-0564-2
29. Hu, C., Bai, M., Lv, J., Liu, H., Li, X.: Molecular dynamics investigation of the effect of copper nanoparticle on the solid contact between friction surfaces. Appl. Surf. Sci. **321**, 302–309 (2014)
30. Wang, L., Shen, B., Sun, F.: Investigation of the atomic-scale friction of boron doped diamond using molecular dynamics. J. Comput. Theor. Nanosci. **11**, 1550 (2014)
31. Spijker, P., Anciaux, G., Molinari, J.-F.: Relations between roughness, temperature and dry sliding friction at the atomic scale. Tribol. Int. **59**, 222–229 (2013)
32. Yang, X.J., Zhan, S.P., Chi, Y.L.: Molecular dynamics simulation of nanoscale sliding friction process between sphere and plane. Appl. Mech. Mater. **268–270**, 1134–1142 (2012.) http://www.scientific.net/AMM.268-270.1134
33. Lee, C., Li, Q., Kalb, W., Liu, X.-Z., Berger, H., Carpick, R.W., Hone, J.: Frictional characteristics of atomically thin sheets. Science. **328**(October 2016), 76–80 (2010)
34. Xu, L., Ma, T.B., Hu, Y.Z., Wang, H.: Molecular dynamics simulation of the interlayer sliding behavior in few-layer graphene. Carbon. **50**(3), 1025–1032 (2012)
35. Dorri Moghadam, A., Omrani, E., Menezes, P.L., Rohatgi, P.K.: Mechanical and tribological properties of self-lubricating metal matrix nanocomposites reinforced by carbon nanotubes (CNTs) and graphene – a review. Compos. Part B. **77**(July 2016), 402–420 (2015)
36. Li, L., Niu, J.B., Xia, Z.H., Yang, Y.Q., Liang, J.Y.: Nanotube/matrix interfacial friction and sliding in composites with an amorphous carbon matrix. Scr. Mater. **65**(11), 1014–1017 (2011)
37. Yin, B., Peng, Z., Liang, J., Jin, K., Zhu, S., Yang, J., Qiao, Z.: Tribological behavior and mechanism of self-lubricating wear-resistant composite coatings fabricated by one-step plasma electrolytic oxidation. Tribol. Int. **97**, 97–107 (2016). https://doi.org/10.1016/j.triboint.2016.01.020

38. Xu, L., Ma, T.-B., Hu, Y.-Z., Wang, H.: Vanishing stick-slip friction in few-layer graphenes: the thickness effect. Nanotechnology. **22**(28), 285708 (2011)
39. Zhang, Q., Diao, D.: Potential of graphene layer controlling nano-wear during C60 intrusion by molecular dynamics simulation. Wear. **306**(1–2), 248–253 (2012). https://doi.org/10.1016/j.wear.2012.09.003
40. Yao, N., Lordi, V.: Young's modulus of single-walled carbon nanotubes. J. Appl. Phys. **84**(i), 1939 (1998.) http://scitation.aip.org/content/aip/journal/jap/84/4/10.1063/1.368323
41. Pavia, F., Curtin, W.: Interfacial sliding in carbon nanotube/diamond matrix composites. Acta Mater. **59**(17), 6700–6709 (2011)
42. Zhao, J., Jia, Y., Wei, N., Rabczuk, T.: Binding energy and mechanical stability of two parallel and crossing carbon nanotubes. Proc. R. Soc. Lond. A. **471**(2180), 20150229 (2015)
43. Zhang, C., Chen, S.: Defect- and dopant-controlled carbon nanotubes fabricated by self-assembly of graphene nanoribbons. Nano Res. **8**(9), 2988–2997 (2015.) http://link.springer.com/10.1007/s12274-015-0804-0
44. Ansari, R., Ajori, S., Ameri, A.: On the vibrational characteristics of singleand double-walled carbon nanotubes containing ice nanotube in aqueous environment. Appl. Phys. A. **121**(1), 223–232 (2015.) http://link.springer.com/10.1007/s00339-015-9413-8
45. Ghosh, S., Padmanabhan, V.: Adsorption of hydrogen on single-walled carbon nanotubes with defects. Diam. Relat. Mater. **59**, 47–53 (2015)
46. Stefanov, M., Enyashin, A.N., Heine, T., Seifert, G.: Nanolubrication: how do MoS_2-based nanostructures lubricate? J. Phys. Chem. C. **112**(46), 17764–17767 (2008)
47. Dallavalle, M., Sandig, N., Zerbetto, F.: Stability, dynamics, and lubrication of MoS_2 platelets and nanotubes. Langmuir ACS J. Surf. Colloid. **28**(19), 7393–7400 (2012.) http://www.ncbi.nlm.nih.gov/pubmed/22530739
48. Wang, Y., Yan, F.: Tribological properties of transfer films of PTFE-based composites. Wear. **261**(11–12), 1359–1366 (2006)

Environmental Analysis of Self-Lubricating Composites: A Review

10

Mohammad Hasan Balali, Narjes Nouri, and Wilkistar Otieno

Contents

Abstract

Human activities have affected the balance in the eco-system and put the habitant surrounding us in a catastrophic danger. Most of these wrecking effects which had been strengthened or emerged recently would also last for a long period of time. Taking immediate thoughtful actions are necessary to prevent high risk human activities. Based on the data collected for global surface mean temperature and CO_2 emission, it has been shown that a huge discrepancy in climate is already occurring. There are various reasons which are causing climate change, specifically global warming, which most of those would be discussed in this study. The negative effects of different materials on the eco-system have one of the biggest

M. H. Balali (✉)
Department of Industrial and Manufacturing Engineering, College of Engineering & Applied Science, University of Wisconsin-Milwaukee, Milwaukee, WI, USA
e-mail: mbalali@uwm.edu

N. Nouri
Lubar School of Business, University of Wisconsin-Milwaukee, Milwaukee, WI, USA

W. Otieno
Industrial and Manufacturing Engineering Department, University of Wisconsin-Milwaukee, Milwaukee, WI, USA

P. L. Menezes et al. (eds.), *Self-Lubricating Composites*,
https://doi.org/10.1007/978-3-662-56528-5_10

shares in environmental concerns. Emerging Eco-tribology science helped design products and processes for the environment. The design of products has been significantly modified to be more environmental friendly and sustainable. A brief review of tribology and different definitions, which had been changed during the time, will be discussed in this study. Furthermore, eco-tribology has a positive effect in reducing energy consumption and increasing the lifetime of the products. Lubricant is an example of the materials which produce environment destructive waste. In the recent decades, researchers improved the lubricant materials to be less destructive for the environment. Self-lubricant composites, for instance, significantly reduced the drawbacks of lubricant materials. The advantage is not only improving wear resistance and reduced COF, but also the elimination of the need for external lubricants. Aluminum/graphite (Al/Gr) composites have been used as self-lubricating materials due to the superior lubricating effect of graphite during sliding process. This study reviews the environmental concerns and advances of eco-tribological, lubricant and self-lubricant composites.

10.1 Introduction

Environmental effects of different materials that are used in human activities are one of the most concerning issues for scientists, environmental researchers, and policy makers. Global warming, climate change, and environmental pollutions are getting more tangible for everyone in every corner of the world [1]. Finding a better substitute for hazardous materials would improve the life's quality for the next generations. "Fig. 10.1" shows the progress in global mean surface temperature of earth since 1880. Some actions should be taken to stop or slow down this increasing trend of temperature. Carbon emission is always an important factor in environmental analysis since the negative effects of carbon on environment are usually irreparable. "Fig. 10.2" shows the global carbon emission from fossil fuels since 1900. The growing trend of global carbon emission from fossil fuels is as concerning as increasing trend of global mean surface temperature.

Derek Markham [4] summarized the top 10 causes and effects for global warming as follow:

Causes:

- Carbon dioxide emissions from burning fossil fuel in power plants
- Carbon dioxide emissions from burning gasoline for transportation purposes
- Methane emissions from animals, agriculture such as rice paddies, and from Arctic seabed
- Deforestation, especially tropical forests for wood, pulp, and farmland
- Increase in usage of chemical fertilizers on croplands

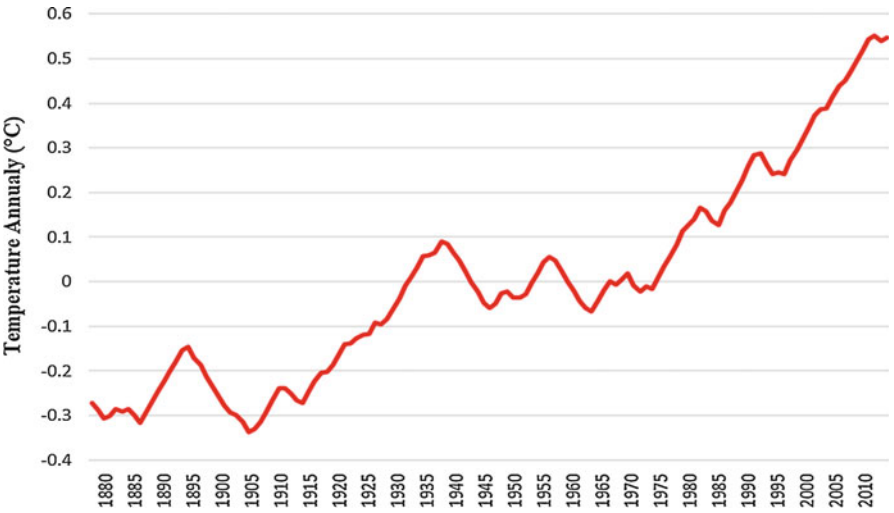

Fig. 10.1 Global mean surface temperature, 5-year annual running mean Earth Observatory, NASA [2]

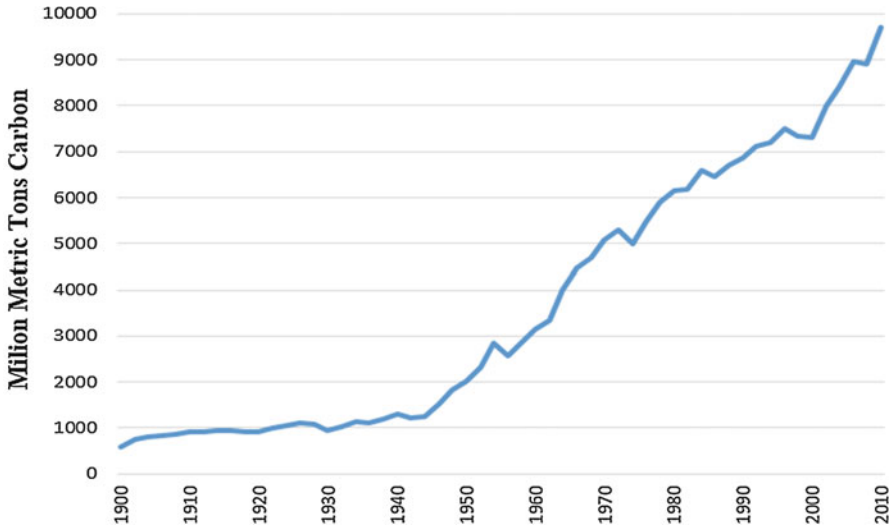

Fig. 10.2 Global Carbon emission from fossil fuels, United States Environmental Protection Agency [3]

Effects:

- Rise in sea levels in worldwide scale
- More killer storms all around the world

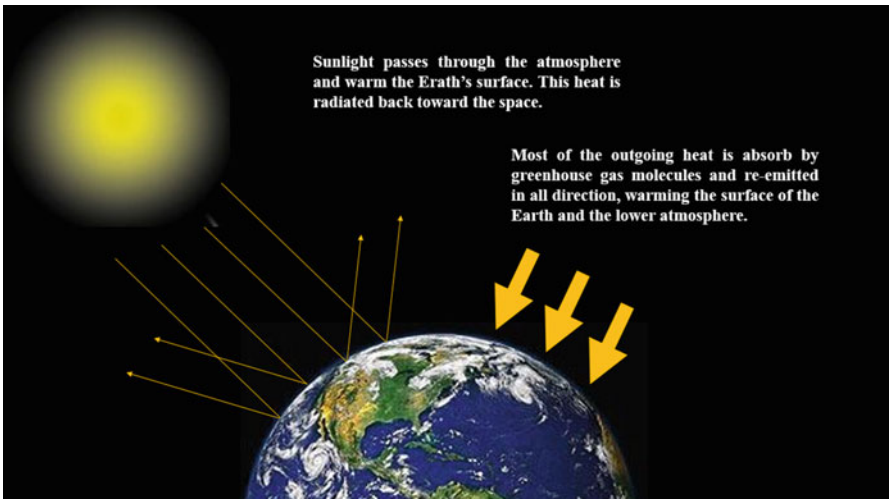

Fig. 10.3 A layer of greenhouse gases, primarily water vapor, including small amounts of carbon dioxide, methane, and nitrous oxide [5]

- Massive crop failures
- Widespread extinction of species of animals, plants and other creatures
- Disappearance of coral reefs

Based on IPCC Fourth Assessment Report 2007 [5], most of the climate scientists agree that the main cause of the current level of temperature which leads to global warming has been done by human activities. "Fig. 10.3" shows a schematic view of a layer of greenhouse gases around earth. Water vapor (H_20), nitrous oxide (N_2O), carbon dioxide (CO_2), and methane (CH_4) have the largest shares in green-house gases [6].

Based on NASA report [7], the possible consequences following climate change are as follows:

- Change will continue in this century and after that
- Global temperature will continue to rise
- Frost-free season will be lengthening
- Precipitation patterns will be changed
- More droughts and heat waves
- Hurricanes will become stronger and more intense
- Sea level will be raised 1–4 feet by 2100
- Arctic likely to become ice-free

Human activities should be modified to minimize their negative effects on the environment. Tribology is playing an important role in this cycle to help the environment deal with all those problems and reduce the negative effects of some

materials on it. But how tribology works to benefit the environment is a question that is being frequently asked. Tribology can help various technologies such as energy efficiency and durability of vehicles, household appliances, industrial machines, and plants to become more mature and productive. Tribology also supports the societal ideas to decrease substances from products that would be a menace to the environment, which has included abolishing asbestos from vehicle brake systems, replacing refrigerants with CFC-substitutes, and controlling the lead used in bearings [8, 9]. Therefore, reducing the usage of some destroying materials and substituting them with less wrecking materials would significantly help the environment.

Although, from an economic standpoint, enforcing law to fix or reduce environmental issues is not profitable for policy makers at this point but, these matters usually create huge costs in the long term that will justify its expenditure. Moreover, most of the damages caused by human activities are irrecoverable or it takes a long time to be mended in the environment. It means that using more sustainable and environmental friendly materials is an economically justified plan in the long term. A good design of sustainable materials would have positive impact on both economic and environment at the same time.

This study is a review of the development of the tribology and lubricating materials starting with a brief review of environmental problems associated with lubricating materials and their effects on eco-system and energy sector. This chapter places extra emphasis on the role of advanced lubricating materials on energy sector since energy became the most concerning issues of societies in recent decades. Different definition and applications of tribology have been presented. In addition to the tribology aspects of environmental friendly materials, some economic benefits have been mentioned as well. Using the advanced tribological materials could save millions of dollar in global scale. For instance, car industries could reduce the fuel consumption of the produced car which leads to saving both money and energy. Different advantages of using self-lubricating composites have been reported in this study. Applying more advanced self-lubricating composites can improve the environmental issues while have positive impacts on economics.

10.2 Eco-Tribology

Tribology is assisting societies to be more sustainable and productive and it is not only human but all the living creatures can benefit from tribology since it can reduce negative effects of some materials and make their habitat more sustainable. Although global economic is still an important matter in eco-tribology, environmental effects are more crucial to decide about the value of a product [8].

Through time, objectives of the tribology have been expanded gradually, tribology for energy conservation (1997), environmental friendly tribology (2000), ecological tribology or eco-tribology (2000), green tribology (2003), and lifecycle tribology (2004) [10]. Controlling friction, reducing wear, and improving lubrication have extended to save energy and materials, reducing emissions, shock absorption, decreasing noise pollution, developing bio- and eco-lubrication, and improving

quality of life and to become the basics of the tribology in the recent decades [10, 11].

Green tribology should be able to provide the full technical support for the preservation of energy, resources, environmental protection, and improvement of quality of life and to decrease the natural disasters. Certainly, it is an important way forward to be a more sustainable society [10, 12]. Green tribology has been emerged to keep both sides of the sustainable developments and society and it meant as a new way of thinking which shows views on ecological balance and environmental protection and so embodies the ideology of the sustainable developments of nature and society perfectly at a same time. The main objectives of green tribology can be summarized into 3L + 1H, namely, respectively, low energy consumption, low discharge (CO_2), low environmental cost, and high quality of life [12].

As it has been mentioned above, saving energy resources and reducing the destructive environmental impact of the sources are the most important goals of eco-tribology. Using environmental friendly lubricant materials in energy sector can significantly reduce the negative environmental impacts. Using renewable energy resources coupled with energy storage systems has been more developed during recent years [13, 14]. Eco-friendly materials which are used in energy storage systems can significantly reduce environmental effects. Therefore, eco-tribology plays an important role in energy consumption saving sector and affect societies and quality of life [15].

Useful lifetime of products can be extended by using materials with less wear and friction, better design, and advanced lubrication. The main results of using the useful lifetime of products are the reduction in energy consumption, required energy for replacing the worn or failed components, and the time and resources for machinery.

From the economic point of view, using renewable and recycled materials has direct and indirect savings of raw materials and sources and saving the energy since less energy is needed for the extraction and production of raw materials [16].

Wilfried J. Bartz [16] classified the tribologically appropriate selection of materials as follow:

- Materials with easy machinability and deformability consume less energy and less man power needed for components production.
- For longer lifetime of products, low wear materials should be used to save man power, energy and raw materials.
- Tribological contacts with low friction resulting in reduced wear which leads to more usable lifetime.

Designers should attempt to create a balance between desire usage of energy sources and the adverse environmental effects which can last forever. A main goal of this is decreasing the inefficient systemic losses through the wear and friction. Durability and sustainability are the main characteristics of a mechanical system. It is necessary to control the frictional and wear losses to achieve durability and sustainability [17].

S. Zhang [18] stated that the main objectives of tribology are mostly controlling friction, reducing wear, and improving lubrication. Tribology should be able to meet

the demands of a sustainable society. The ecological balance and environmental impact at that time owing to the restrictions of the times did not consider as it was expected. Thereupon, green tribology has been emerged to keep abreast of the sustainable developments of societies. Green is a new concept that represents the views on ecological balance and environmental effects and so embodies the ideology of the sustainable developments of nature and society perfectly.

10.3 Lubricants

All waste lubricants can easily destroy soil's microflora and make it infertile in the long term. Even very low doping in water makes it unsuitable for drinking because of the smell, taste, and health hazards. Millions of tons of waste lubricants are released in the world every year. Consequently, more severe regulations and rules are needed to protect the environment and decrease the harmful effects of these products. Saving nonrenewable resources and reducing the harmful environmental effects of lubricants are the two main missions of these regulations [19].

M. Stojilković et al. [19] concluded that lubricants can be considered environmentally acceptable if they meet some requirements which rapid biodegradability, nontoxicity to humans, marines, or even bacteria are the most important ones.

Biodegradability means the tendency of lubricants to be decomposed by microorganisms. Eco-toxicity implies a toxic effect on plants and animals and not on the human health. Substances with a Lethal Dose LD 50 $>$ 1000 ppm/kg are barely considered toxic. [19].

W.J. Bartz [16] determined the important aspects for a reduced impairment of environment by lubricants as follow:

- Less outflows to reduce the pollution
- Extended lubricant change periods or even fill for life lubrication
- avoiding lubricant consumption side effects to save energy
- Treatments, recycling and disposal

L.A. Bronshteyna and J.H. Kreiner [20] estimated that approximately 11% of the total energy annually consumed in the USA in the four sections of transportation, turbomachinery, power generation, and industrial processes can be saved through new developments in lubrication and tribology.

In 1994, 500 million vehicles were registered for use globally with an additional 40 to 50 million cars produced in the world every year [16] (International Organization of Motor Vehicle Manufacturers. See: http://www.worldometers.info/cars/). About 10% reduction in the mechanical losses due to effective tribology leads to a 1.5% drop in the fuel consumption equating to about 340 liter of petrol during car's lifetime (about 125.000 miles) apart from the environmental gains due to reduced emissions and durability [15] (Taylor CM. Automobile engine tribology – design considerations for efficiency). Thus, it becomes clear that if you integrate these small

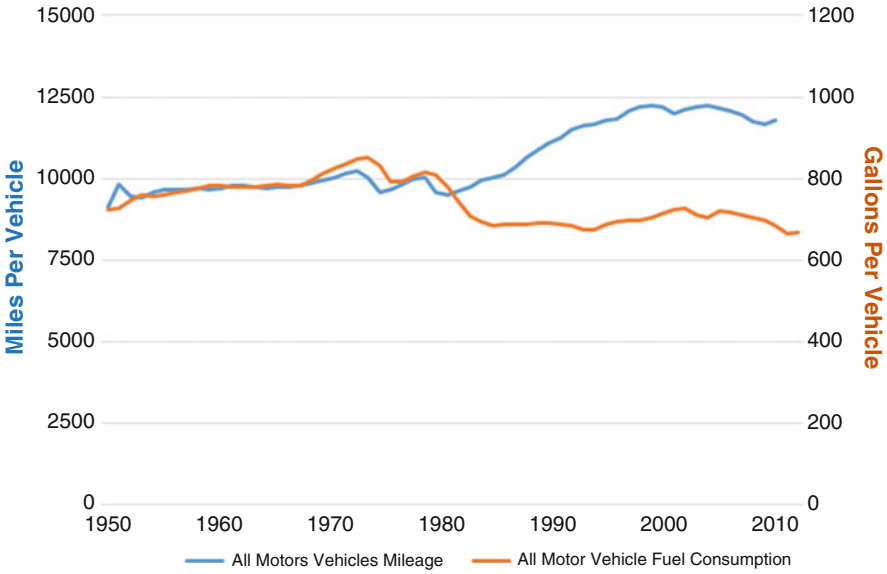

Fig. 10.4 Motor Vehicle Mileage, Fuel Consumption, and Fuel Economy, 1949–2010 [21]

savings ($350) per car to the vast number of cars currently in use, the economic savings and environmental benefits are huge.

Based on the 2016 data from http://www.worldometers.info/cars/ and International Organization of Motor Vehicle Manufacturers (OICA), it is estimated that for the first time in 2010 the number of passenger cars traveling the streets and roads of the world was reached to 1 billion-unit mark. In this scale, the effects of tribology in fuel consumption reduction are completely tangible. "Fig. 10.3" shows that motor vehicles mileage (miles per vehicles) had been significantly increased from 1949 to 2010 while the vehicles fuel consumption (gallon per vehicle) had been decreased. Although Tribology is not the only reason and there are different substitutions for fuel, positive effects of tribology are undeniable (Fig. 10.4).

G. Howarth and M. Hadfield [22] have generated a model assessing the sustainable development aspects of a product from a design perspective depicting the environmental, social, and economic impact.

Kenneth Holmberg and Ali Erdemir [23] reported the followings in their studies. One-fifth of all energy produced worldwide that is about 100 million terajoule is used annually to overcome friction. The largest quantities of energy are used by industry (29%) and transportation (27%) sections. Based on our recent studies on energy use in passenger cars, trucks, and buses, it has been concluded that it is possible to save as much as 17.5% of the energy use in road transports in a short period of time, about 5–9 years by effective implementation of new tribological solutions. This equals to annual energy savings of 11.6 oxyjoules, fuel savings of 330 billion liters, and 860 million tons reduction in CO_2 emissions. In a paper mill, 15–25% of the energy used is spent to overcome friction. The electrical energy used

by a paper machine is distributed as 32% to overcome friction, 36% for the paper production and mass transportation, and 32% is lost in other sectors. In paper machines, 11% of the total energy used to overcome friction can be saved by the implementation of new tribological technologies.

Energy is a key resource in a lot of sectors today and will be crucial for the sustainability of our society in the future. As it was stated above, considerable amount of energy is consumed to overcome friction, especially in the transportation, industrial, and power-generation sectors, and major economic losses are also due to wear of products and components and their replacement [23].

It is necessary to take actions, if possible, using machine element types processing higher efficiencies, e.g., spur gears instead of worm gears, roller bearings, instead of mixed film lubricated journal bearings and the result is less consumption of energy.

Reduced consumption of lubricants can be realized by:

- Optimum-design seals which reduces leakage
- Lubricants with higher stability against oxidation and thermal degradation and contamination by liquid and solid matters

A reduction of energy consumption can be achieved by different types of savings, as defined below:

- Direct savings: Primary savings reduction of mechanical friction losses such as operating cost
- Secondary savings: less frequent replacement of worn and failed parts and less necessity to reproduce them such as metal working and maintenance cost
- Tertiary savings: less expenditure for extraction and reproduction of raw materials required for the production of parts which have to be replaced such as cost of energy content of materials
- Indirect savings: reduction of investment cost by extended useful lifetime of machines and machine elements and selecting smaller machines
- Short-term savings: characterized by the fact that no additional cost for research and development is needed and only the consequent application of available knowledge is enough
- Medium-term savings: research and development cost for, e.g., 5 years have to be spent in order to transform basic and scientific knowledge into practical usable forms.
- Long-term savings: using solutions which at present are not yet conceivable.

I. Tzanakisa, M. Hadfield, et al. [17] reported that lubricants greatly contribute to decreasing frictional losses in mechanical systems. It is expected that low-viscosity, long life oils will be developed with advanced additives such as friction modifiers and antiwear and antioxidation agents. Research on decreasing the detrimental impacts of lubricants on the environment now encompasses such topics as halogen-free and biodegradable oils, carbon-neutral vegetable oils, the minimum

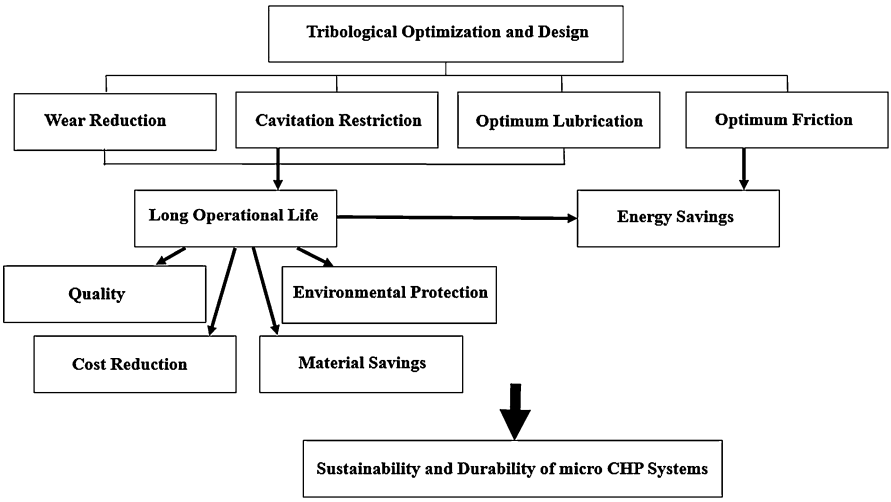

Fig. 10.5 Schematic representation of the tribological optimization of the scroll expander [17]

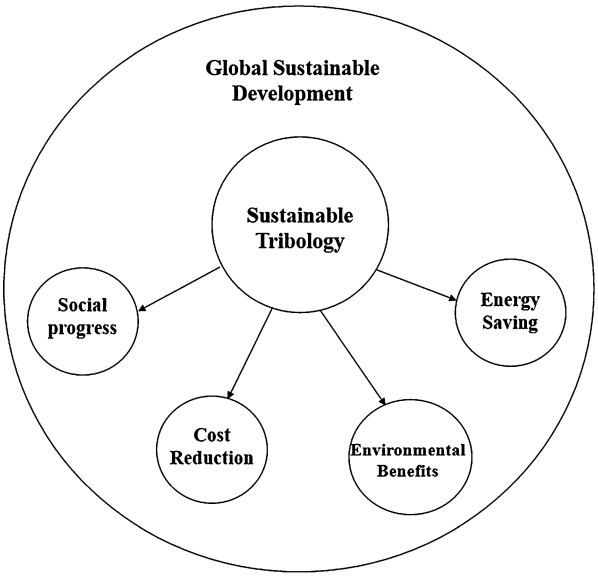

Fig. 10.6 The impact of sustainable tribology to sustainable development [17]

quantity of lubrication (MQL) [24], and process fluid lubrication such as water lubrication [25, 8] (Fig. 10.5).

I. Tzanakisa, M. Hadfield, et al. [17] indicated that frictional losses, sliding wear, cavitation, and oil degradation are the critical damage mechanisms of the scroll

expander which can seriously affect the performance and the lifespan of the scroll and the micro-CHP unit. A number of recommendations provided to industry after the completion of the research project in order for the durability and sustainability of the scroll to be improved. These were successfully adapted by industry and applied to their new generation scroll expander systems alleviating any undesirable effects (Fig. 10.6).

A novel fullerene-like hydrogenated carbon film was prepared by pulse bias-assisted plasma enhanced chemical vapor deposition, and its mechanical and tribological properties were investigated. This film displayed super-low friction and wear in both dry inert and humid ambient atmospheres and less sensitivity to H_2O and O_2 molecules in air [18, 26].

V. Rodriguez et al. [27] reported that graphite, molybdenum disulfide (MoS_2), and polytetrafluoroethylene (PTFE) are a few examples of predominant materials which used as solid lubricants. Other examples of lubricants include boron nitrite, talc, calcium fluoride, cerium fluoride, and tungsten disulfide. These lubricants are less common but in some cases can outperform graphite and MoS_2.

V. Rodriguez et al. [27] and Rudnick [28] concluded that applications involving high-temperature and high load carrying requirements have their highest efficiency using Graphite. In contrast, PTFE does not have layered structure. It has an exceptionally low coefficient of friction. Both static and dynamic coefficients are smaller than that of any other solid lubricant and the lubrication properties are at least partially the result of its high softening point [27, 28].

The most recent iridologists result investigating the lubricant behavior of unexplored or even of new materials proved that PEEK with fiber reinforcement and lubricant additives are very efficient. As an example, Briscoe et al. [29] investigated the friction and wear properties of 10% PTFE in a PEEK matrix. A significant reduction in the coefficient of friction and an improved wear resistance was the outcome of this experiment. Other investigations also showed an optimum of increase in wear resistance and minimum frictional coefficient [27, 30].

According to a study by A.D. Moghadam et al. [31], development of advanced metal matrix nanocomposites for structural engineering and functional devices could be consequence of rapid innovation in nanotechnology in past few years. Carbonous materials, such as graphite, carbon nanotubes (CNTs), have attracted the attention of researchers to synthesize lightweight self-lubricating metal matrix nanocomposites with superior tribological properties for various applications in automotive and aerospace industries based on their unique properties and lubricious nature. Adding CNT and graphene to metals decreases both coefficient of friction and wear rate while increases the tensile strength.

The results of A.D. Moghadam et al. [32] show that reducing energy consumption and improving heat dissipation between two moving solids can be reached through designing advanced tribological materials. Self-lubricating MMCs have advantages of improving wear resistance, reducing COF, and eliminating the need for external lubricants to avoid seizing. Bidaki and Akhlaghi [33] concluded that self-lubricating materials are characterized by their capability for transferring microscopic amounts of lubricant material, which creates a film that shows the lubrication and reduces

friction over the contact surface. MMCs reinforced with graphite particles are self-lubricating and have superior wear resistance and reduced COF since the graphite particles work as a solid lubricant between contact surfaces.

E. Omrani et al. [34] stated that aluminum/graphite (Al/Gr) composites are examples of self-lubricating materials which have been used because of their superior lubricating effects of graphite during sliding process. The effects of different parameters such as (a) material properties, graphite size, and volume fraction and (b) mechanical factors, applied load, and sliding speed on the tribological properties of self-lubricating aluminum composites are important. To reduce the external use of petroleum-based lubricants in sliding contacts, self-lubricating composites can be used into different operating systems is a solution in a way to help the environment and reduce energy dissipation in industrial components in order to increase sustainability and energy efficiency. Self-lubrication is one of the capabilities of materials to transfer embedded solid lubricants, such as graphite to the contact surface to decrease wear rate and COF while there is not any external lubricant. Solid self-lubricating composites are usually solid carbon (carbon fibers graphite particles, CNTs, graphene), molybdenum disulfide, and hexagonal boron nitride [34, 35].

10.4 Conclusion

Recently, human activities changed the balance in the eco-system and caused several environment dangers which last for centuries. Environmental hazards are effecting the human, animal wildlife, plants, and our planet as a whole. Immediate thoughtful actions are necessary more than ever to help decreasing destructive human activities. Climate change is occurring right now, and there is no more time to waste for taking actions. Some materials have negative impact on the eco-system which should be redesigned and modified. Currently there are lots of products which design has been significantly modified to be more environmental friendly and sustainable. For instance, lubricant materials have been improved based on latest science to reduce their discharging wastes. The positive effects of eco-tribological materials in reducing energy consumption and increasing the lifetime of the products have been also discussed. Self-lubricant composites such as aluminum/graphite (Al/Gr) composites which have been mentioned in this study have significantly less drawbacks than some common lubricants. This study was a comprehensive review of the environmental concerns and advances of eco-tribological, lubricant, and self-lubricant composites.

References

1. Balali, M.H., Nouri, N., Rashidi, M., Nasiri, A., Otieno, W.: A multi-predictor model to estimate solar and wind energy generations. Int. J. Energy Res. (2017). https://doi.org/10.1002/er.3853
2. N. Earth Observatory, (2015)
3. United States Environmental Protection Agency. (2011)
4. Markham, D.: Global Warming Effects and Causes: A Top 10 List. planetsave.com. (2009)
5. Report, IPCC Fourth Assessment, (2007)

6. N. Report, A blanket around the Earth
7. NASA, Vital Signs of Planet Blobal Climate Change
8. Sasaki, S.: Environmentally friendly tribology (Eco-tribology). J. Mech. Sci. Technol. **24**, 67–71 (2010)
9. Zarandi, M.A.F., Pillai, K.M.: "Spontaneous imbibition of liquid in glass fiber wicks, Part II: Validation of a diffuse-front model," Transport Phenomena and Fluid Mechanics. AlChe. (2017). https://doi.org/10.1002/aic.15856
10. Zhang, S.-W.: Green tribology: fundamentals and future development. Short Commun. **1**, 186–194 (2013)
11. Shafiee, S., McCay, M.H.: A Hybrid energy storage system based on metal hydrides for solar thermal power and energy systems. In: Proceedings of ASME 2016 10th International Conference on Energy Sustainability, Charlotte (2016)
12. Zhang, S.W.: Current industrial activities of tribology in China. In: Plenary Lecture to the 5th China International Symposium. Beijing, China (2008)
13. Balali, M.H., Nouri, N., Nasiri, A., Seifoddini, H.: Development of an economical model for a hybrid system of grid, PV and energy storage systems. In: International Conference on Renewable Energy Research and Applications (ICRERA), Palermo, pp. 1108–1113 (2015) https://doi.org/10.1109/ICRERA.2015.7418582
14. Balali, M.H.: An Economical Model Development for a Hybrid System of Grid Connected Solar PV and Electrical Storage System. Theses and Dissertations, University of Wisconsin Milwaukee UWM Digital Commons (2015)
15. Balali, M.H., Pichka, K., Nouri, N., Seifoddini, H., Yue, X.: Classifying US states for facility location decisions using clustering algorithm. Int. Res. J. Appl. Basic Sci. **10**(2), 166–172 (2016)
16. Bartz, W.J.: Ecotribology: environmentally acceptable tribological practices. Tribol. Int. **39**, 728–733 (2006)
17. Tzanakisa, I., Hadfield, M., Thomas, B., Noya, S., Henshaw, I., Austen, S.: Future perspectives on sustainable tribology. Renew. Sust. Energ. Rev. **16**, 4126–4140 (2012)
18. Zhang, S.-W.: Green tribology: fundamentals and future development. Friction. **1**(2), 186–194 (2013)
19. Stojilković, M., Golubović, D., Ješić, D.: Ecotribology aspects in the lubricants application. 6th International Symposium on Exploitation of Renewable Energy Sources. EXPRES (2014)
20. Bronshteyna, L., Kreiner, J.: Energy efficiency of industrial oils. Tribol. Trans. **771–776**(4), 42 (1999)
21. U. E. I. A. EIA. http://www.eia.gov/totalenergy/data/annual/showtext.cfm?t=ptb0208
22. Howarth, G., Hadfield, M.: A sustainable product design model. Mater. Des. **27**, 1128–1133 (2006)
23. Holmberg, K., Erdemir, A.: Global impact of friction on energy consumption, economy and environment. FME Trans. **43**, 181–185 (2015)
24. Suda, S.: Developments in cutting fluids for MQL cutting. Tribologist. **47**(7), 550–556 (2002)
25. Sassaki, S.: The effects of surrounding atmosphere on the friction and wear of alumina, zirconia, silicon carbide and silicon nitride. Wear. **134**, 134–185 (1989)
26. Ji, L., Li, H., Zhou, F., Quan, W., Chen, J., Zhou, H.: Fullerene-like hydrogenated carbon films with super-low friction and wear, and low sensitivity to environment. J. Phy. D Appl. Phys. **43**, 015404 (2010)
27. Rodriguez, V., Sukumaran, J., Schlarb, A.K., DeBaets, P.: Influence of solid lubricants on tribological properties of polyetheretherketone (PEEK). Tribol. Int. **103**, 45–57 (2016)
28. Rudnick, L.: Lubricant Additives in Chemistry and Applications. CRC Press, Boca Raton (2009)
29. Briscoe, B., Lin Heng Yao, J., Stolarski, T.A.: The friction and wear of poly (tetrafluoroethylene)-poly (etheretherketone) composites: An initial appraisal of the optimum composition. Wear. **108**(4), 357–374 (1986)
30. Schroeder, R.: Failure mode in sliding wear of PEEK based composites. Wear. **301**, 717 (2013)

31. Moghadam, A.D., Schultz, B.F., Ferguson, J.B., Omrani, E., Rohatgi, P.K., Gupta, N.: Functional metal matrix composites: self-lubricating, self-healing, and nanocomposites-an outlook. JOM. **66**, 872 (2014)
32. Moghadam, A.D., Omrani, E., Menezes, P.L., Rohatgi, P.K.: Mechanical and tribological properties of self-lubricating metal matrix nanocomposites reinforced by carbon nanotubes (CNTs) and graphene – a review. Compos. Part B. **77**, 402–420 (2015)
33. Akhlaghi, F., Zare-Bidaki, A.: Influence of graphite content on the dry sliding and oil impregnated sliding wear behavior of Al 2024–graphite composites produced by in situ powder metallurgy method. Wear. **266**(1–2), 37–45 (2009)
34. Omrani, E., Moghadam, A.D., Menezes, P.L., Rohatgi, P.K.: Influences of graphite reinforcement on the tribological properties of self-lubricating aluminum matrix composites for green tribology, sustainability, and energy efficiency – a review. Int. J. Adv. Manuf. Technol. **85**, 325–346 (2016)
35. Balali, M.H., Nouri, N., Omrani, E., Nasiri, A., Otieno, W.: An overview of the environmental, economic, and material developments of the solar and wind sources coupled with the energy storage systems. Int. J. Energy Res. (2017). https://doi.org/10.1002/er.3755

Retraction Note to: Self-Lubricating Composites

Pradeep L. Menezes, Pradeep K. Rohatgi, and Emad Omrani

Retraction Note to:
Chapter "Fundamentals of Solid Lubricants" in: P. L. Menezes et al. (eds.) *Self-Lubricating Composites*,
https://doi.org/10.1007/978-3-662-56528-5_1

The authors have retracted this chapter [1] because it significantly overlaps with a previously published article by Scharf and Prasad [2]. All authors agree with this retraction. [1] Prajapati A.K., Omrani E., Menezes P.L., Rohatgi P.K.: Fundamentals of Solid Lubricants. In: Menezes P., Rohatgi P., Omrani E. (eds.) Self-Lubricating Composites. Springer, Berlin, Heidelberg (2018) [2] Scharf, T.W., Prasad, S.V.: Solid lubricants: a review. J. Mater. Sci. 48, 511–531 (2013). https://doi.org/10.1007/s10853-012-7038-2

Retraction Note to:
Chapter "Self-Lubricating Polymer Composites" in: P. L. Menezes et al. (eds.) *Self-Lubricating Composites*,
https://doi.org/10.1007/978-3-662-56528-5_3

The authors have retracted this chapter [1] because it significantly overlaps with a previously published article by Fusaro [2]. All authors agree with this retraction. [1] Prajapati A.K., Omrani E., Menezes P.L., Rohatgi P.K.: Self-Lubricating Polymer Composites. In: Menezes P., Rohatgi P., Omrani E. (eds.) Self-Lubricating

The retracted version of this chapter can be found at
https://doi.org/10.1007/978-3-662-56528-5_1
https://doi.org/10.1007/978-3-662-56528-5_3

P.L. Menezes et al. (eds.), *Self-Lubricating Composites*,
https://doi.org/10.1007/978-3-662-56528-5_11

Composites. Springer, Berlin, Heidelberg (2018) [2] Fusaro, R.L.: Self-lubricating polymer composites and polymer transfer film lubrication for space applications, Tribology International, Volume 23, Issue 2, 105–122 (1990). https://doi.org/10.1016/0301-679X(90)90043-O